



2017

# SELF-SENSING CEMENTITIOUS MATERIALS

Alexander Nicholas Houk

University of Kentucky, alex.houk2015@hotmail.com

Author ORCID Identifier:

 <https://orcid.org/0000-0001-7392-5539>

Digital Object Identifier: <https://doi.org/10.13023/ETD.2017.430>

**[Click here to let us know how access to this document benefits you.](#)**

---

## Recommended Citation

Houk, Alexander Nicholas, "SELF-SENSING CEMENTITIOUS MATERIALS" (2017). *Theses and Dissertations--Civil Engineering*. 58.

[https://uknowledge.uky.edu/ce\\_etds/58](https://uknowledge.uky.edu/ce_etds/58)

This Master's Thesis is brought to you for free and open access by the Civil Engineering at UKnowledge. It has been accepted for inclusion in Theses and Dissertations--Civil Engineering by an authorized administrator of UKnowledge. For more information, please contact [UKnowledge@lsv.uky.edu](mailto:UKnowledge@lsv.uky.edu).

**STUDENT AGREEMENT:**

I represent that my thesis or dissertation and abstract are my original work. Proper attribution has been given to all outside sources. I understand that I am solely responsible for obtaining any needed copyright permissions. I have obtained needed written permission statement(s) from the owner(s) of each third-party copyrighted matter to be included in my work, allowing electronic distribution (if such use is not permitted by the fair use doctrine) which will be submitted to UKnowledge as Additional File.

I hereby grant to The University of Kentucky and its agents the irrevocable, non-exclusive, and royalty-free license to archive and make accessible my work in whole or in part in all forms of media, now or hereafter known. I agree that the document mentioned above may be made available immediately for worldwide access unless an embargo applies.

I retain all other ownership rights to the copyright of my work. I also retain the right to use in future works (such as articles or books) all or part of my work. I understand that I am free to register the copyright to my work.

**REVIEW, APPROVAL AND ACCEPTANCE**

The document mentioned above has been reviewed and accepted by the student's advisor, on behalf of the advisory committee, and by the Director of Graduate Studies (DGS), on behalf of the program; we verify that this is the final, approved version of the student's thesis including all changes required by the advisory committee. The undersigned agree to abide by the statements above.

Alexander Nicholas Houk, Student

Dr. Lindsey Sebastian Bryson, Major Professor

Dr. Yi-Tin Wang, Director of Graduate Studies

---

# SELF-SENSING CEMENTITIOUS MATERIALS

---

## THESIS

---

A thesis submitted in partial fulfillment of the  
requirements for the degree of Master of Science in  
Civil Engineering in the College of Engineering at the  
University of Kentucky

By

Alexander Nicholas Houk

Lexington, Kentucky

Director: Dr. L. Sebastian Bryson, Professor of Civil Engineering

Lexington, Kentucky

2017

Copyright © Alexander Nicholas Houk 2017

ORCID: 0000-0001-7392-5539

## ABSTRACT OF THESIS

### SELF-SENSING CEMENTITIOUS MATERIALS

The study of self-sensing cementitious materials is a constantly expanding topic of study in the materials and civil engineering fields and refers to the creation and utilization of cement-based materials (including cement paste, cement mortar, and concrete) that are capable of sensing (i.e. measuring) stress and strain states without the use of embedded or attached sensors. With the inclusion of electrically conductive fillers, cementitious materials can become truly self-sensing. Previous researchers have provided only qualitative studies of self-sensing material stress-electrical response. The overall goal of this research was to modify and apply previously developed predictive models on cylinder compression test data in order to provide a means to quantify stress-strain behavior from electrical response. The Vipulanandan and Mohammed (2015) stress-resistivity model was selected and modified to predict the stress state, up to yield, of cement cylinders enhanced with nanoscale iron(III) oxide ( $\text{nanoFe}_2\text{O}_3$ ) particles based on three mix design parameters:  $\text{nanoFe}_2\text{O}_3$  content, water-cement ratio, and curing time. With the addition of a nonlinear model, parameter values were obtained and compiled for each combination of  $\text{nanoFe}_2\text{O}_3$  content and water-cement ratio for the 28-day cured cylinders. This research provides a procedure and lays the framework for future expansion of the predictive model.

**KEYWORDS:** Self Sensing, Iron Oxide Nanoparticle, Conductive Filler, Compressive Strength, Predictive Model, Piezoresistivity

---

Alexander N. Houk

---

October 23, 2017

---

# SELF-SENSING CEMENTITIOUS MATERIALS

By

Alexander Nicholas Houk

---

Dr. Lindsey Sebastian Bryson

Director of Thesis

---

Dr. Yi-Tin Wang

Director of Graduate Studies

---

October 23, 2017

### Dedication

I would like to dedicate this thesis to my parents, Paul and Janice, who have always pushed me to be the best version of myself.

## ACKNOWLEDGEMENTS

There are many people that played important roles in helping me to complete this thesis. First and foremost, I would like to thank my parents, Paul and Janice, and my brother, Adam, who have always been supportive of me throughout my life. They always knew when I needed encouragement and extra motivation.

I would like to thank the University of Kentucky Civil Engineering Department faculty and staff for providing an innovative and encouraging atmosphere that allowed me to grow as an aspiring engineer. I want to thank Sheila Williams for always providing assistance and a welcoming environment from the office whenever I needed it. I would like to thank Floyd Taylor and his entire team at the University of Kentucky machine shop for developing many pieces of equipment that I used in this research. Their fabrication expertise greatly enhanced the efficiency of my research. There are also many other people that assisted at various times during the testing phase of the research and I would like to recognize their efforts: undergraduate researchers Cam Sayre and Lucien Whaley; graduate researcher Macy Purcell; and Ph.D. candidates Faisal Shakib Ahmed, Wisam Muttashar, and Majid Mahmoodabadi.

I would like to thank my advisor, Dr. Sebastian Bryson, for guiding and challenging me as a student, a researcher, and a young engineer over the past four years in both the undergraduate and graduate programs. His vast knowledge and expertise has allowed me to get closer to reaching my overall potential as a student and civil engineer. He has always pushed me to succeed, to make the most of every available opportunity for expanding my skills, and to explore new areas outside of my comfort zone. His approach has led me to become a well-rounded engineer, and his instruction and lessons have been greatly appreciated.

I would also like to thank the other members of my committee, Dr. Issam Harik, Dr. Kamyar Mahboub, and Dr. Michael Kalinski, for their willingness to evaluate my research and offer their recommendations for improving my thesis.

## TABLE OF CONTENTS

Acknowledgements.....	iii
List of Tables .....	vi
List of Figures .....	vii
1 Introduction.....	1
1.1 Problem Synopsis.....	1
1.2 Research Objectives .....	2
1.3 Relevance of Research .....	2
1.4 Contents of Thesis.....	4
2 Technical Background .....	5
2.1 General Theory of Self-Sensing Materials.....	5
2.1.1 Composition of Self-Sensing Materials.....	5
2.1.2 Obtaining Electrical Measurements from Self-Sensing Materials.....	7
2.1.3 Sensing Characteristic of the Composite Material.....	9
2.2 Relevant Testing.....	9
2.2.1 Using Fibrous Fillers.....	10
2.2.2 Using Particle Fillers.....	15
2.3 Selection of NanoFe <sub>2</sub> O <sub>3</sub> as a Functional Filler.....	18
2.4 Predictive Models.....	19
2.5 Testing and Parameters Established for this Research.....	24
3 Materials and Methods.....	25
3.1 Materials Used.....	25
3.2 Mixing and Sample Preparation.....	25
3.3 Sample Curing.....	32
3.4 Static Electrical Measurements .....	35
3.4.1 Effect of Defoamer on Resistivity of DI-water.....	35
3.4.2 Frequency Sweeps .....	38
3.5 Electrical Response During Curing.....	41
3.6 Electrical and Stress-Strain Response During Compression Test (ASTM C39).....	44
4 Analysis.....	53
4.1 Static Electrical Testing Analysis .....	53



4.1.1	Analysis of Defoamer Effects on Resistivity of DI-water .....	53
4.1.2	Analysis of Frequency Sweeps .....	55
4.2	Resistivity Index Testing Analysis.....	60
4.3	Stress-Strain Predictive Model Analysis.....	64
4.3.1	Comparison of Accuracy of Stress-Strain Predictive Models .....	64
4.3.2	Effects of Parameters on Stress-Strain Predictive Models .....	66
4.3.3	Analysis of Stress-Strain Values Sorted by Mix Design Parameters .....	68
4.4	Stress-Resistivity Predictive Model Analysis .....	70
4.4.1	Effects of Parameters on Stress-Resistivity Predictive Model .....	71
4.4.2	Analysis of Stress-Resistivity Values Sorted by Mix Design Parameters..	73
4.5	Proposal of New Model to Predict Stress-Electrical Response.....	74
4.6	Resolution Analysis of Proposed Model.....	80
5	Summary and Conclusions .....	84
Appendix A	Batch Mix Design.....	87
Appendix B	Frequency Sweeps .....	107
Appendix C	Resistivity Index Testing.....	140
Appendix D	Stress-Strain Testing .....	157
Appendix E	Stress-Electrical Testing .....	231
Appendix F	Predictive Model.....	271
References	.....	276
Vita	.....	279

## LIST OF TABLES

Table 2.1: Electrical resistivity of cement pastes containing electrically conductive admixtures (after Chung 2004). .....	14
Table 4.1: Effects of Defoamer on Sample Resistivity.....	54
Table 4.2: Average Resistivity and Conductivity Based on Defoamer Content.....	54
Table 4.3: Average RI Testing Values for Samples Sorted by NanoFe <sub>2</sub> O <sub>3</sub> Content. ....	63
Table 4.4: Average RI Testing Values for Samples Sorted by Water-Cement Ratio.....	63
Table 4.5: 28-day curing time data to be used for new predictive model.....	76
Table 4.6: Nonlinear model parameter values for determining $\sigma_f$ . ....	77
Table 4.7: Average contributions of Equations 4.2 and 4.3 to overall parameter values. ....	79
Table 4.8: Proposed model values for Cylinder #36.....	80
Table 4.9: Measured vs. Predicted data using proposed model for Cylinder #36. ....	81
Table 4.10: Proposed model values for Cylinder #51.....	82
Table 4.11: Measured vs. Predicted data using proposed model for Cylinder #51. ....	83

## LIST OF FIGURES

Figure 2.1: Overall makeup of the self-sensing composite material (Han et al. 2015). ....	6
Figure 2.2: Typical electrode layouts for self-sensing materials testing (Han et al. 2015). 8	
Figure 2.3: Response of cement mortar under cyclic compressive loading (after Chung 1998). .....	11
Figure 2.4: Sensor specimen (Azhari and Banthia 2012). .....	12
Figure 2.5: Effect of loading rate on electrical response of the specimen (Azhari and Banthia 2012). .....	13
Figure 2.6: Uniaxial compression testing of using nickel powder as a filler (after Han et al. 2008). .....	15
Figure 2.7: Scanning electron microscope 2000x photos of (a) Type 123, (b) Type 287, and (c) Type 255 nickel powder (after Han et al. 2010). .....	16
Figure 2.8: Hognestad (1951) model for unconfined concrete (Kasarin et al. 2014). ....	21
Figure 2.9: Analysis of the stress-strain predictive models on the Vipulanandan and Mohammed (2015) data. ....	23
Figure 3.1: Hobart® C-100 Mixer. Necessary components pictured include (a) mixing bowl, (b) flat beater, (c) lever, (d) bowl slideway, (e) speed handle, (f) mixing timer. ...	26
Figure 3.2: Mixing of ingredients in bowl at beginning (left) and end (right) of mixing process. ....	28
Figure 3.3: Smooth metal rod is used to tamp the mixture after a lift has been poured. ..	29
Figure 3.4: Details of plastic cap used for mixing molds .....	30
Figure 3.5: 2 kg weights placed on top sample molds during 24 hour hardening phase. ..	31
Figure 3.6: Samples after a full 24 hours of hardening. ....	31
Figure 3.7: Telescoping and straight PVC pieces connected to humidifier. ....	32
Figure 3.8: Outer (left) and inside (right) view of threaded elbow PVC connection to plastic container. ....	33
Figure 3.9: Fully assembled curing chamber and settings used during curing process. ....	33
Figure 3.10: PVC rack in the curing chamber. ....	34
Figure 3.11: Unassembled resistivity cell used to measure electrical properties of DI-water and defoamer mixture. Parts pictured include: (a) bottom plate, (b) top plate, (c) acrylic cylinder, (d) sprockets, and (e) O-rings. ....	36

Figure 3.12: Alligator clips connected to bolts on resistivity cell plates. ....	36
Figure 3.13: Agilent® LCR Meter Model 4285A and attached Agilent® Test Leads Model 16048A. Display screen and settings also pictured. ....	37
Figure 3.14: Concrete cylinder top surface sanded smooth by the disc sander. ....	39
Figure 3.15: Elevation view of stainless steel electrode. ....	39
Figure 3.16: Frequency sweep setup. Anode (red) attached to top electrode and cathode (black) attached to bottom electrode. A weight produces a 6.895 kPa load on the cylinder cap. ....	40
Figure 3.17: Resistivity index testing mold details. ....	42
Figure 3.18: Electrode glued to top of PVC mold. Glue was also placed around screw on outside face of electrode. ....	43
Figure 3.19: Resistivity index testing electrical measurement cantilever with connection to LCR meter. ....	43
Figure 3.20: Cylinder configuration on compression testing machine. ....	45
Figure 3.21: Controller used for compression testing. Pictured: (a) Frame panel and (b) Control console. ....	46
Figure 3.22: Partner™ program display screen during compression testing. ....	47
Figure 3.23: Graph of Cylinder #46 Stress-Strain data with relevant factors displayed. .	48
Figure 4.1: Capacity vs. Frequency (left) and Resistance vs. Frequency (right) graphs for Cylinder #2. ....	56
Figure 4.2: Resistance Tangent Intersection vs. Curing Time for 5 percent NanoFe <sub>2</sub> O <sub>3</sub> . ....	57
Figure 4.3: Capacitance vs. Frequency Graph for Batch #11 (Cylinder #31-33). ....	58
Figure 4.4: Capacitance vs. Frequency Graph for Batch #11 (Cylinder #31-33). ....	59
Figure 4.5: Resistivity vs. Curing Time Behavior for Batch 2 Sample over 24 Hours. ....	61
Figure 4.6: RI <sub>24hr</sub> vs. Water-Cement Ratio ....	62
Figure 4.7: RI <sub>24hr</sub> vs. NanoFe <sub>2</sub> O <sub>3</sub> Content. ....	62
Figure 4.8: Comparison of Vipulanandan and Mohammed vs. Ezeldin and Balaguru prediction accuracy based on R <sup>2</sup> values. ....	65
Figure 4.9: Effect of Vipulanandan and Mohammed <i>q</i> parameter value on stress-strain predictive model with constant <i>p</i> value. ....	66

Figure 4.10: Effect of Vipulanandan and Mohammed $p$ parameter value on stress-strain predictive model with constant $q$ value. ....	67
Figure 4.11: Effect of $\beta$ parameter value on Ezeldin and Balaguru stress-strain predictive model.....	68
Figure 4.12: Tangent modulus sorted by curing time for individual cylinders. ....	69
Figure 4.13: Effect of Vipulanandan and Mohammed $q$ parameter value on stress-resistivity model with constant $p$ value for Cylinder #21.....	72
Figure 4.14: Effect of Vipulanandan and Mohammed $p$ parameter value on stress-resistivity model with constant $q$ value for Cylinder #21.....	73
Figure 4.15: Measured vs. Predicted data using proposed model for Cylinder #36.....	81
Figure 4.16: Measured vs. Predicted data using proposed model for Cylinder #51.....	83

---

## **1 Introduction**

### **1.1 Problem Synopsis**

As structures age or become damaged by natural or man-made events, rehabilitation or even replacement may become a necessity in certain instances. Presently in the United States, a growing number of aging structures are in critical need of such repair in order to comply with current strength and serviceability standards. Through extensive research and testing, design guides created by organizations such as ASCE and AASHTO are constantly updated to allow engineers to perform efficient and accurate calculations that ensure safer designs. This advancement in design codes and standards combined with an increasing need for structural repair has created an opportunity for researchers to explore innovative materials that benefit future engineers.

Concrete is the most widely used construction material worldwide and cementitious materials have been used for centuries due to their abundance, cost, and reliability. Over time, different admixtures and additives have been included in concrete mixes to enhance certain qualities such as workability or compressive strength. An emerging area of research is the study of “smart” self-sensing cementitious materials.

Self-sensing cementitious materials refers to the creation and utilization of cement-based materials (including cement paste, cement mortar, and concrete) that are capable of sensing (i.e. measuring) stress and strain states without the use of embedded or attached sensors. It has been observed that changes in the stress state of most materials correlate to changes in the measured electrical responses of those materials. Thus, the ability of a cementitious material to be self-sensing refers to the possibility that the stress state (from the elastic regime through yield and up to failure) can be directly correlated to the electrical response of the material. Cementitious materials alone are not intrinsically conductive, and therefore the self-sensing process requires the inclusion of some type of electrically conductive filler into the cement matrix to enhance the electrical response (Han et al. 2007; Hou and Lynch 2005).

This research will investigate the effectiveness of using a filler that will be evenly dispersed within the cement matrix and will develop a quantitative methodology which will facilitate the obtainment of stress-strain behavior from electrical response.

## **1.2 Research Objectives**

The intent of this research is to develop and analyze a cementitious material possessing true self-sensing capabilities. Thus, one objective is to perform fundamental research that will enable the development of a cement mortar capable of real-time stress sensing based on electrical response. The overall goal of this research is to modify and apply previously developed predictive models on cylinder compression test data in order to provide a means to obtain stress-strain behavior from electrical response. In this manner, internal stresses can be determined through non-contact methods.

The specific objectives of this research include:

- Conduct a technical review of existing literature to investigate which conductive fillers, which mixing methods, and what quantities of such fillers could be utilized to produce the most effective electrical response of the cement matrix.
- Determine what types of testing will be conducted to most effectively analyze and evaluate the electrical response of the cement specimens.
- Find and evaluate the effectiveness of multiple predictive formulas that could potentially predict the stress-electrical behavior of the specimens.
- Analyze the data after testing in order to define potential correlations that exist in the stress-strain and stress-electrical response of the specimens.
- Use the data obtained through testing to develop a new predictive model capable of quantifying the stress-electrical response of the specimens.

## **1.3 Relevance of Research**

With the prevalence of natural and man-made disasters and aging infrastructure, structural health monitoring has an ever-increasing importance in the way engineers approach future infrastructure designs. Currently, engineers are able to visually observe structures on-site

for deficiencies such as cracking and spalling of concrete. Many of these deficiencies are relatively harmless to the integrity of the structure, but others could signify the onset of much more severe problems if not properly addressed. Presently, the common methods of monitoring the more critical deficiencies involve optic sensors and electric-resistance strain gauges among other equipment (Han and Ou 2007). The problem with these types of monitoring devices is that they must be mounted, and could become dislodged or damaged during significant events. Therefore, it is beneficial to develop a means of assessing internal stresses through non-contact methods.

Some researchers have shown that damage sensing from electrical response is possible using conductive fillers in cement mix designs (Chung 1998). Different types of conductive fillers from carbon fibers to powders such as carbon black, nickel powder, and nanoscale iron oxide ( $\text{Fe}_2\text{O}_3$ ) have been used to enhance the electrical sensing abilities of plain concrete (Han et. al 2010; Li et. al 2004). While these studies provide useful insight into the abilities of electrically enhanced cement to sense an electrical response, they only show a qualitative response of the material to external loading. The goal of this research is to expand on those studies and develop a quantitative model capable of predicting the internal stresses on a self-sensing cementitious material from the electrical response based on mix design parameters such as water-cement ratio, curing time, and conductive filler content.

With the rapid advancement of technology, self-sensing materials have the potential to become a standard for infrastructure design. As new design codes are constantly updated with the expansion of research, self-sensing materials could become prevalent in future designs. These materials would have the ability to remediate and improve the constantly aging and deteriorating infrastructure in the United States in an efficient and cost-effective manner. Quantifying damage of cementitious materials simply by determining the electrical response could have a significant opportunity to impact all sectors of infrastructure.



## **1.4 Contents of Thesis**

Chapter 2 will present a technical review of existing literature covering topics discussed within this research.

Chapter 3 will detail the materials used during the research as well as the methods and procedures followed.

Chapter 4 will analyze the data that was obtained through the various tests and will seek to determine if there are any correlations or conclusions that can be derived from the results. Then, a new model to predict the stress-resistivity behavior based on mix design parameters will be proposed.

Chapter 5 will conclude the research and discuss any significant findings that were observed through testing and analysis.

---

## **2 Technical Background**

A technical review of existing research was conducted in order to obtain knowledge regarding self-sensing materials. This review will cover materials and procedures used in previous research as well as conclusions that could be pertinent for this research.

### **2.1 General Theory of Self-Sensing Materials**

Interest in structural health monitoring has rapidly increased over the past few decades and, as a result, the study of self-sensing cementitious materials has become an evolving field of research for upwards of 25 years beginning in the early 1990s. The effectiveness of using self-sensing cementitious materials on infrastructure has even recently been studied in China (Ou and Li 2010). A spectrum of conductive fillers, from fibers to nanotubes to powders, have been included in research papers. Different studies have observed how adding these fillers can enhance the electrical response of the cement matrix. Variations in mix design properties such as filler content, curing time, and loading rate as well as different procedures have been followed in order to determine the contributions of factors to the electrical response of cement specimens under loading. So far, many qualitative relationships have been established between the electrical behavior of a cement specimen and its strain, stress, or damage state under loading. However, the field of structural health monitoring using self-sensing cementitious materials is starting to incorporate the use of predictive models as a means of correlating and quantifying the electrical and stress states of these materials. This research will seek to expand the scope of the existing studies regarding this correlation between the stress and electrical states, and will look to provide additional quantifiable data through analysis.

#### **2.1.1 Composition of Self-Sensing Materials**

There are two main phases of intrinsically self-sensing materials illustrated by Figure 2.1: the matrix material and the conductive filler. The matrix material forms the bulk of the matrix-filler composite and typically has little or no sensing abilities. The important purpose of the matrix material is to provide the overall mechanical properties of the composite and to hold the conductive filler together. Portland cement has been a common

matrix material used in previous studies due to its cost, availability, and effectiveness as a binder.

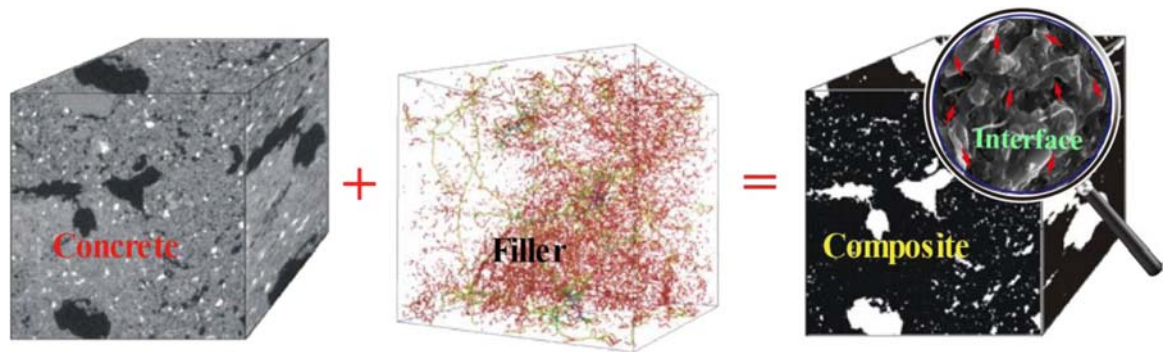


**Figure 2.1: Overall makeup of the self-sensing composite material (Han et al. 2015).**

The second main component is the conductive filler which, as its name implies, significantly enhances the electrical conductivity of the composite material and provides the sensing property. These fillers are usually microscale or nanoscale size and should be dispersed well throughout the mix. The self-sensing ability of the filler can be dependent on several factors: material component (carbonaceous vs. metallic); filler shape (fibrous vs. particle); filler size; conductive capability; and surface state (natural vs. modified) among several other factors (Han et al. 2015). It is important to understand the overall goals, scope of research, and cost effectiveness when selecting a particular conductive filler for research applications.

In some instances, additives may be added to a composite in order to disperse the filler material more effectively throughout the matrix. Both surfactant and mineral admixtures have been applied in testing to provide homogeneity to the overall composite material (Han et al. 2011; Vaisman et al. 2006).

At the microscopic level, the interfaces between the matrix material and the conductive filler act as a third phase to the overall composite material. These filler-matrix and filler-filler interfaces provide areas of electrical contact between matrix and filler materials and between the fillers themselves. The quality of the electrical conductivity is directly influenced by the interface effectiveness. Thus, it is imperative that the filler is well-dispersed in the matrix material in order to produce a continuous electrical pathway

throughout the composite. Some researchers have also experimented with manipulating the interfaces by treating or coating the fillers (Li et al. 2007; Fu et al. 1998).

The mixing and dispersing of the matrix material and the fillers is unquestionably the most important step in the process of developing an effective self-sensing composite. These steps contribute to the homogeneity and sensing ability of the composite. There are two types of methods for mixing/dispersing: (1) physical and (2) chemical. Physical methods include shear mixing, ball milling, and ultrasonication. Chemical means usually involve altering the filler surface structures to enhance the solubility and dispersibility of those fillers throughout the composite (Catalá et al. 2010). However, some chemical treatments may have the negative effect of decreasing the mechanical or electrical properties of the composite (Vaisman et al. 2006).

After the mixing process, molding of the specimens takes place. Molding the composite after mixing increases the compaction of the material, thus providing better mechanical properties for the specimen. Once the composite has been in the molding process for typically 24 hours, it is removed from the mold and then cured, or hydrated, for an extended period of time. This curing process influences not only the mechanical properties of the composite, but it also enhances the interface bonding between the matrix material and the fillers. Other researchers have elaborated on the role of the molding and curing processes on the composite (Fu and Chung 1997; Xin et al. 2011).

### **2.1.2 Obtaining Electrical Measurements from Self-Sensing Materials**

In order to obtain electrical measurements from the self-sensing composite, electrodes must be fabricated. These electrodes can be manufactured in several fixing styles such as attachments, embedded mesh, and metal plates among other options. Many previous studies used the attachment or embedment methods, but it is possible to use other means as long as the electrodes have low electrical resistance so that they are competently conductive. Copper and stainless steel plates are two practical plate materials that can be utilized as alternatives to attached or embedded electrodes (Han et al. 2015).

In addition to choosing the type of electrode used for experimentation, the researcher must choose how to lay out the electrodes on or in the composite material. Variations of the

two-probe and four-probe layouts, as shown in Figure 2.2, have been studied by multiple researchers as the most logical options.

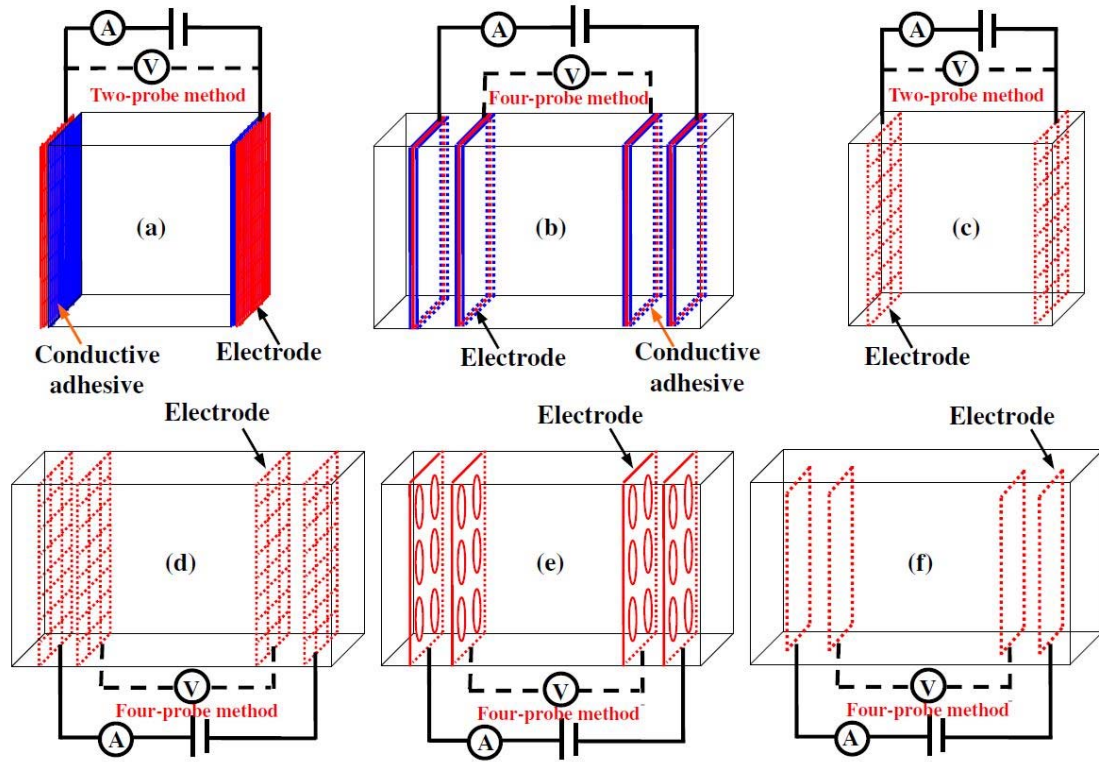


**Figure 2.2: Typical electrode layouts for self-sensing materials testing (Han et al. 2015).**

Attached electrodes have been applied to specimens using a conductive adhesives such as silver paint, which was used in many studies (Azhari and Banthia 2012; Wen and Chung 2006). The main issue with using attached electrodes is that they have the potential to debond from the composite during testing. Embedded electrodes, on the contrary, are protected by the surrounding composite material, thus keeping the electrodes intact during practical testing. Han et al. (2007) concluded that the embedded electrodes perform better than the attached electrodes in certain situations.

Choosing between a two-probe and a four-probe layout has been discussed at length as well. While the two-probe method is a much simpler setup for obtaining electrical readings, the four-probe method is able to eliminate contact resistance between the composite and the electrode where the two-probe method cannot. This causes the measured resistance obtained from the two-probe approach to be slightly higher than the

actual resistance value. However, according to Reza et al. (2003), the two-probe system was still able to detect changes in resistance of the composite under compressive loading. Therefore, the two-probe method is still widely used due to its ease of assembly. Researchers have used both direct current (DC) and alternating current (AC) in their studies.

### **2.1.3 Sensing Characteristic of the Composite Material**

Han et al. (2015) summarized that the sensing behavior of the composite can be observed by the relationship between the fractional change in resistivity  $\Delta\rho/\rho_o$ , with  $\Delta\rho = \rho_i - \rho_o$  where  $\rho_i$  is the resistivity at the  $i$ th increment and  $\rho_o$  is the initial resistivity, and an external force, stress, or strain. Due to the limitations of scope and resources for this research, only the sensing behavior under monotonic compression will be studied.

As concluded by several researchers, the fractional change in resistivity of the composite under monotonic compressive loading starts by decreasing, balances, and then abruptly increases corresponding to the compaction, crack germination, and crack extension, respectively. During the pressure compaction stage, the fillers are pushed closer together, which then improves the conductive interface network. While gradually increasing the loading on the sample, cracking will inevitably initiate. These cracks lead to deconstruction and then reconstruction of the conductive pathways as the material is separated and then pushed back together continuously. After excessive loading, these cracks will continue to expand and then eventually lead to permanent damage of the conductive network as well as physical failure of the composite specimen. Due to the inconsistent stress-strain behavior that arises after the specimen has reached peak loading, it may be useful for future quantitative studies to only analyze the electrical response up to failure of the test specimens.

## **2.2 Relevant Testing**

As mentioned in Chapter 2.1, researchers have used various procedures and different types of fillers to observe the electrical response of their composite materials. Some studies and their results will be discussed in more detail to provide a basis for this research project.

### 2.2.1 Using Fibrous Fillers

The utilization of conductive fillers within a cement mix design has been studied by several researchers. Carbon fibers were among the earliest types of fillers used for testing the effectiveness of self-sensing cementitious materials. Chen and Chung (1993) used short carbon fibers (0.2–0.4 volume percent) along with methylcellulose and latex as dispersants in a cement mortar mix. The goal was to observe how adding these conductive fillers would alter the electrical properties of the mixture. Silver paint was applied to the 50.8 x 50.8 x 50.8 mm mortar cubes in four parallel planes around the perimeter of the cube to serve as electrodes for electrical sensing. Under compressive loading, it was found that the resistivity of the mortar containing fibers and methylcellulose increased by 1040 percent whereas the resistivity of the mortar containing fibers and latex increased by 385 percent. Conversely, the plain mortar resistivity remained constant during loading and unloading. Thus, it could be established that short carbon fibers did have an observable impact on the specimens' electrical properties.

Chung (1998) researched short carbon fibers once again in a cement matrix to sense internal strains for structural control applications and damage for structural health monitoring. In the study, the researcher determined that cement containing short carbon fibers as filler material enhanced the electrical response of the specimens. The ability of the filler to sense reversible strain and damage was confirmed. Tensile and compressive cyclic loading was performed on the mortar specimens to monitor the electrical response. The electrical response of the cement paste to cyclic compressive loading using ozone treated carbon fibers is exemplified in Figure 2.3.

The fractional change in resistance,  $\Delta R/R_0$ , with  $\Delta R = R_i - R_0$  where  $R_i$  is the resistance at the  $i$ th increment and  $R_0$  is the initial resistance, was shown to decrease during compressive loading and then subsequently increase during the unloading phase. It was stated in this research that the self-monitoring ability of the concrete enhanced with carbon fiber fillers was due to slight fiber-pull out during strain and fiber and matrix fracture during damage.

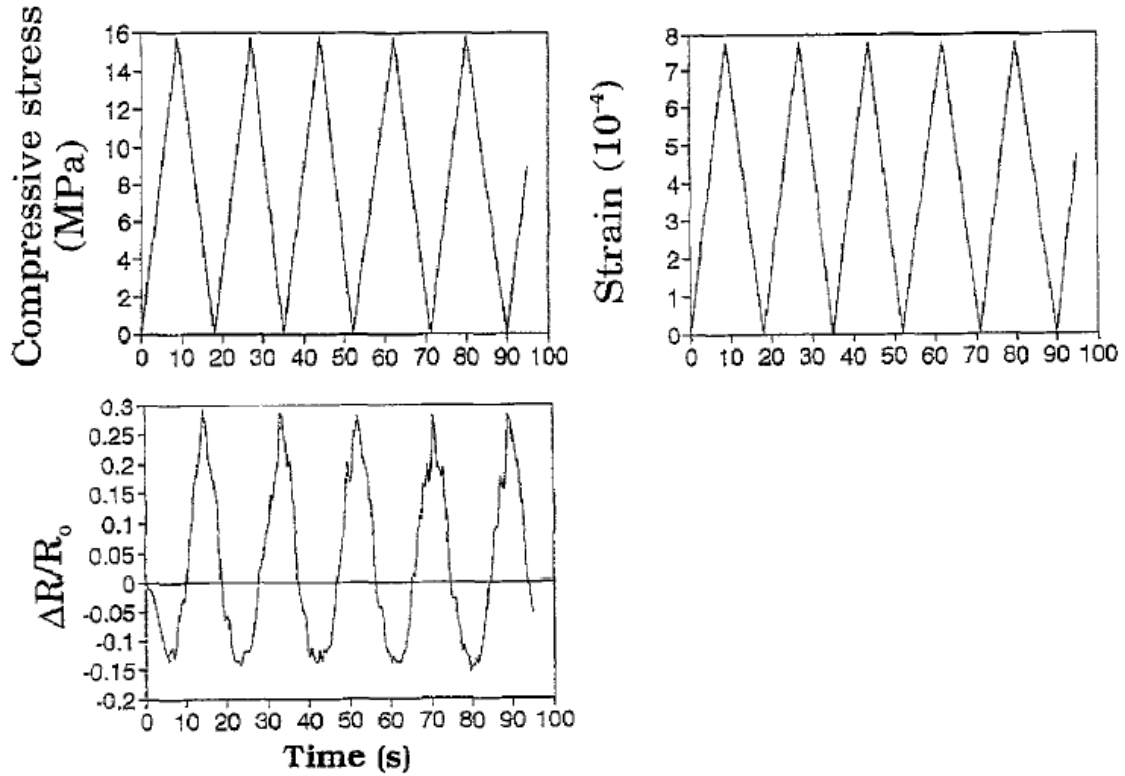


**Figure 2.3: Response of cement mortar under cyclic compressive loading (after Chung 1998).**

Among other discussion, Chung (1998) concluded that using short carbon fiber fillers was an effective method for sensing the strain and damage in cement mortar. Strain and damage sensing using short carbon fibers was studied extensively in additional research articles (Chung 2000; Wang and Chung 2006).

Azhari and Banthia (2012) continued with the study of structural health monitoring using carbon fibers and carbon nanotubes. Testing was performed on cement cylinders containing carbon fibers and carbon nanotubes to study the electrical response due to compressive loading. The cylinder specimens were fitted with a strain gauge and silver paste to serve as the electrodes. As evidenced by Figure 2.4, a four-probe method was used for gathering resistance measurements. From the bottom of the 100 mm cylinder, the electrodes were placed at 10 mm, 20 mm, 80 mm, and 90 mm.



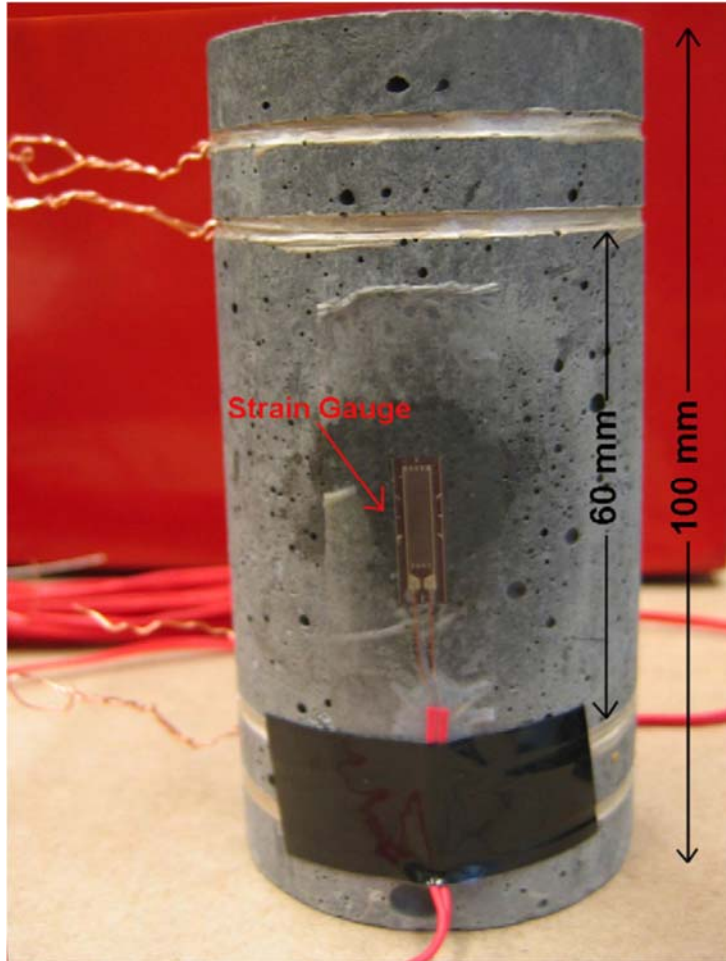


**Figure 2.4: Sensor specimen (Azhari and Banthia 2012).**

It was found that under cyclic compressive loading up to 30 kN, the fractional change in resistivity decreased as the load on the cylinder increased. In the same study, it was also shown that the loading rate on the cylinder was a factor in the fractional change in resistivity under loading, as shown in the graph in Figure 2.5. From the graph, it was determined that fractional change in resistivity response under cyclic compressive loading was rate-dependent.

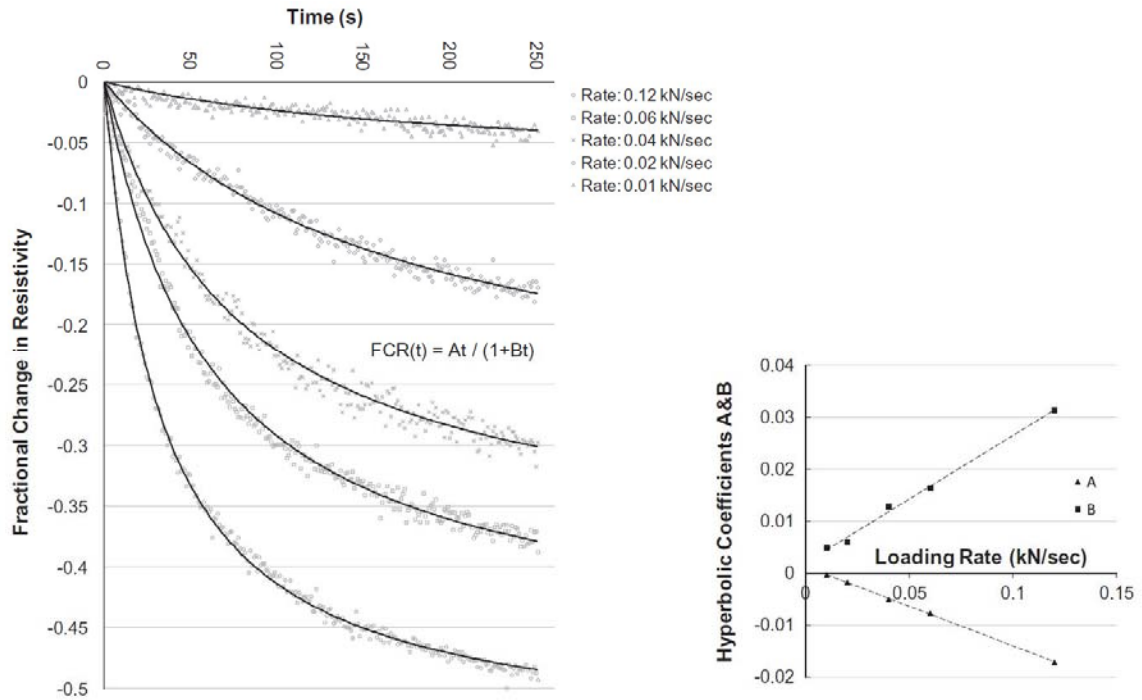


**Figure 2.5: Effect of loading rate on electrical response of the specimen (Azhari and Banthia 2012).**

From the graph, it was discovered that the fractional change in resistivity increased with increasing load rate. This could be due to the fact that the compaction pressure on the cylinders occurs at a much faster rate, moving the fillers closer together. Quickly forcing the fillers closer to each other improves the conductive network of the composite, thus creating a much sharper increase in the magnitude of the fractional change in resistivity. The fractional change in resistivity had a nonlinear response to changing stress states. This response was modeled using a hyperbolic model with variables based on the load rate of the specimens.

Chung (2004) compiled the resistivity, and therefore the conductive effectiveness, of various electrically conductive admixtures. At the time of this study, it was well-known that adding conductive admixtures could lower the resistivity, and thus raise the conductivity, of cement-based materials. The resistivity and volumetric content measurements of steel fibers, carbon fibers, coke powder, and graphite powder among other fillers from various studies were examined in the research and are shown in Table 2.1.

**Table 2.1: Electrical resistivity of cement pastes containing electrically conductive admixtures (after Chung 2004).**

Conductive admixture	Vol. %	Resistivity ( $\Omega\cdot\text{cm}$ )
None	0	6.1E+05
None, but with graphite powder ( $< 1\ \mu\text{m}$ ) coating		
Steel fiber (8 $\mu\text{m}$ diameter)	0.09	4.5E+03
Steel fiber (60 $\mu\text{m}$ diameter)	0.10	5.6E+04
Steel fiber (8 $\mu\text{m}$ diameter)	0.18	1.4E+03
Steel fiber (60 $\mu\text{m}$ diameter)	0.20	3.2E+00
Steel fiber (8 $\mu\text{m}$ diameter)	0.27	9.4E+02
Steel fiber (60 $\mu\text{m}$ diameter)	0.28	8.7E+03
Carbon fiber (10 $\mu\text{m}$ diameter) (crystalline, intercalated)	0.31	6.7E+03
Steel fiber (8 $\mu\text{m}$ diameter)	0.36	57
Steel fiber (60 $\mu\text{m}$ diameter)	0.40	1.7E+03
Carbon fiber (10 $\mu\text{m}$ diameter) (crystalline, pristine)	0.36	1.3E+04
Steel fiber (8 $\mu\text{m}$ diameter)	0.54	23
Steel fiber (60 $\mu\text{m}$ diameter)	0.50	1.4E+03
Carbon fiber (15 $\mu\text{m}$ diameter) (amorphous, pristine)	0.48	1.5E+04
Carbon filament (0.1 $\mu\text{m}$ diameter)	0.5	1.3E+04
Graphite powder ( $< 1\ \mu\text{m}$ )	0.46	2.3E+05
Coke powder ( $< 75\ \mu\text{m}$ )	0.51	6.9E+04
Steel fiber (8 $\mu\text{m}$ diameter)	0.72	16
Steel fiber (8 $\mu\text{m}$ diameter)	0.9	40
Carbon fiber (15 $\mu\text{m}$ diameter) (amorphous, pristine)	1.0	8.3E+02
Carbon fiber (10 $\mu\text{m}$ diameter) (crystalline, intercalated)	1.0	7.1E+02
Carbon filament (0.1 $\mu\text{m}$ diameter)	1.0	1.2E+04
Graphite powder ( $< 1\ \mu\text{m}$ )	0.92	1.6E+05
Coke powder ( $< 75\ \mu\text{m}$ )	1.0	3.8E+04
Coke powder ( $< 75\ \mu\text{m}$ )	6.1	2.9E+04
Steel dust (0.55 mm)	6.6	
Graphite powder ( $< 45\ \mu\text{m}$ )	37	4.8E+02

From the table, it was deduced that 8  $\mu\text{m}$  steel fibers were the most effective for lowering electrical resistivity followed by carbon fiber. In addition, the fibers were shown to be more effective than the coke powder or the graphite powder. The conductivity of a self-sensing material was determined by three main components: (1) the inherent conductivity of the admixture itself; (2) the degree of dispersion of the admixture within the cement matrix; and (3) the contact electrical resistivity of the interface between the admixture and the cement matrix. By these properties, fibers would be more practical for creating a more effective continuous interface between the conductive filler and the cement matrix. On the other hand, powders can be dispersed much more readily throughout a mix without need

for additional dispersing admixtures that could potentially alter the electrical properties of the material. Therefore, finding a highly conductive filler could offset the relative disadvantages experienced by either fibers or powders. Providing the proper amount of filler used in a mix design is also worth consideration. Too much filler (especially with larger fibers) could lead to workability issues, while too little filler may not provide enough of an interface between the filler and the surrounding cement for effective electrical sensing to occur.

### 2.2.2 Using Particle Fillers

Like fibrous fillers, particles fillers have been shown in other studies to be fully capable of adding self-sensing properties to a composite material (Han et al. 2008; Han et al. 2010; Li et al. 2004; Vipulanandan and Mohammed 2015).

Han et al. (2008) conducted research using nickel powder combined with Type I Portland cement, silica fume, and a water-reducing agent. A 40 x 20 x 20 mm composite specimen was created and was equipped with embedded copper electrodes arranged in a four-probe layout. A uniaxial compressive force was applied along the specimen's longitudinal axis and measurements were taken using both a wired and a wireless acquisition system. Some of the test results can be viewed in Figure 2.6.

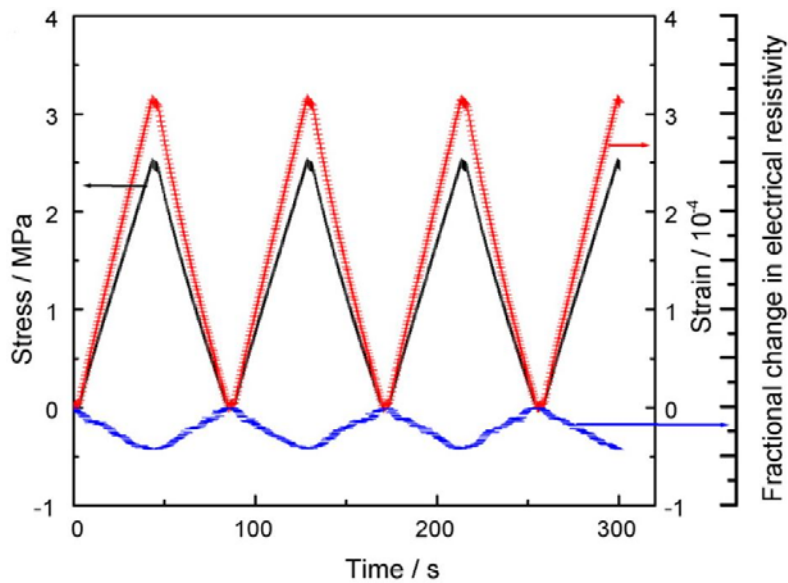


**Figure 2.6: Uniaxial compression testing of using nickel powder as a filler (after Han et al. 2008).**

From the graph in Figure 2.6, the fractional change in resistivity decreased up to a maximum of 42.719 percent at  $\sigma = 2.5$  MPa and  $\varepsilon = 311.5$   $\mu\epsilon$ . In this regard, the nickel powder composite produced the same general qualitative stress-electrical behavior as other studies like Azhari and Banthia (2012) and Chung (1998). This research also demonstrated the strong capability of wireless sensors to perform well in structural health monitoring applications.

The effect of nickel powder content as well as nickel powder particle size on the piezoelectric properties of composites has been examined as well by Han et al. (2010). Three different types of nickel powder, shown in Figure 2.7, were used during experimentation.

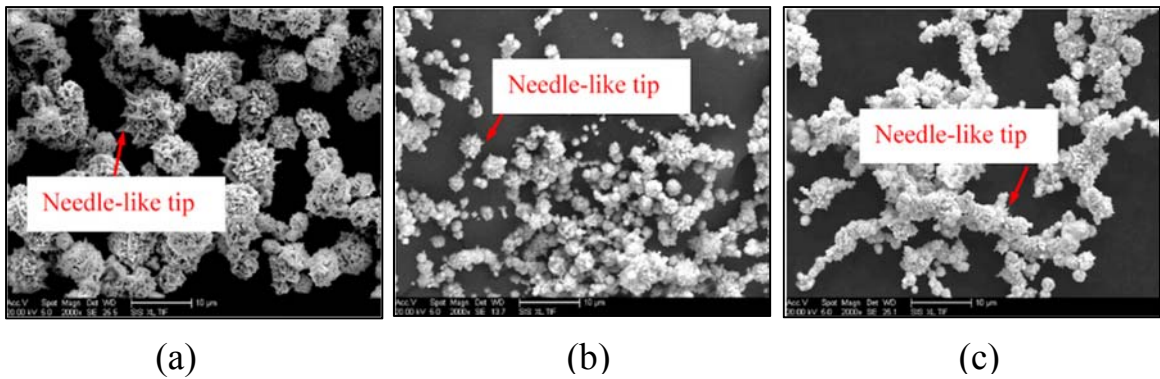


**Figure 2.7: Scanning electron microscope 2000x photos of (a) Type 123, (b) Type 287, and (c) Type 255 nickel powder (after Han et al. 2010).**

The sizes between the Type 123 (3-7  $\mu\text{m}$ ), Type 287 (2.6-3.3  $\mu\text{m}$ ), and Type 255 (2.2-2.8  $\mu\text{m}$ ) varied, but each type of nickel powder had a spiky spherical shape. The sharp surface protrusions of the nickel powder allow for an effective production of field emission, which is the quantum mechanical tunneling of electrons out of metal surfaces under a high electric field condition (Chen 2007). The nickel powder was used in conjunction with Type I Portland cement, silica fume, and a high performance water-reducing agent. The same four-probe layout with embedded copper electrodes that was chosen in Han et al. (2008) was used once again for this research. Nickel powder quantity was added into the composite at either 20, 22, or 24 percent by volume of mix.

Using the Type 123 particles, it was found that the 22 percent by volume had the highest sensitivity of the three volume percentage mixes. The 22 percent specimen had a maximum

fractional change in resistivity of approximately  $-(79.28 \pm 7.66)$  percent at 32.5 MPa of compressive stress. The effect of particle size was studied by holding the volume percentage of nickel powder at a constant 24 percent while changing the type of particle. It was discovered that the Type 123 (3-7  $\mu\text{m}$ ) particle samples had the highest electrical sensitivity of the three. In fact, the fractional change in resistivity of the Type 123 sample at 12.5 MPa (in the elastic range) was significantly higher than the second-highest fractional change in resistivity experienced by the Type 287 sample at -62.61 percent and -37.63 percent, respectively. This study concluded that the piezoresistive sensing property of the composite is partially dependent on the conductive filler's content and particle size.

Nanoscale iron oxide was another capable particle filler that has been intensively researched. Li et al. (2004) used nanoFe<sub>2</sub>O<sub>3</sub> in combination with Portland cement, water-reducing admixtures, and a defoamer. A water-cement ratio of 0.50 was used, and the quantities of fillers and admixtures were varied to observe their effects on the electrical response. It was found that the plain Portland cement was virtually nonconductive under loading, while the fractional change in resistance,  $\Delta R/R_0$ , decreased approximately linearly under increased loading for 3 and 5 percent nanoFe<sub>2</sub>O<sub>3</sub> composites by weight of cement. The  $\Delta R/R_0$  value decreased by 20 percent at peak stress for the 3 percent nanoFe<sub>2</sub>O<sub>3</sub> content specimen, while the 5 percent nanoFe<sub>2</sub>O<sub>3</sub> specimen experienced a  $\Delta R/R_0$  decrease of approximately 45 percent. Logically, it could be derived that adding more nanoFe<sub>2</sub>O<sub>3</sub> to a specimen will enhance the composite's conductivity, leading to a sharper decrease in  $\Delta R/R_0$  (and therefore  $\Delta \rho/\rho_0$ ) with increasing stress in specimens containing higher concentrations of conductive fillers.

NanoFe<sub>2</sub>O<sub>3</sub> was also used in Vipulanandan and Mohammed (2015) as a filler. Unlike the other studies that have been discussed, this study sought to *quantify* the piezoresistive and compressive strength of the composite under loading using predictive models. Class H well cement was used in addition to 0.1 percent of conductive fillers. Three series of mixes were grouped by additional nanoFe<sub>2</sub>O<sub>3</sub> content: 0, 0.5, and 1 percent by weight of cement. Cylinders specimens with a diameter of 2 inches and a height of 4 inches were developed and then cured for either 1 day, 7 days, or 28 days. Commercial 10 mm resistance strain gauges were used to measure strain and sulfur capping was performed on the specimen surfaces to provide a smooth plane for compressive testing.

A resistivity index test (to be explained in Chapter 3) was performed to study the piezoresistive behavior of the cement slurry over the first 24 hours of curing time. It was found that adding nanoFe<sub>2</sub>O<sub>3</sub> lowered the initial resistivity and the resistivity after 24 hours, signifying an increase in conductivity of the composite.

In addition, a compressive strength test (ASTM C39) was conducted on the cylinders to analyze the effects of the nanoFe<sub>2</sub>O<sub>3</sub> on the piezoresistive and stress-strain behaviors. Predictive formulas in conjunction with a nonlinear model that predicts the formula parameters' values from preparation variables (curing time and nanoFe<sub>2</sub>O<sub>3</sub> content) were utilized to model the stress-resistivity response of the cylinders under loading. These predictive models will be highlighted in Chapter 2.4 and discussed in greater detail in Chapters 3 and 4. It was concluded that the nonlinear models were very capable of predicting the stress-resistivity behavior of the modified cement.

### **2.3 Selection of NanoFe<sub>2</sub>O<sub>3</sub> as a Functional Filler**

Selecting a capable functional filler was one of the most essential aspects of the research planning phase. The studies presented in Chapter 2.2 have highlighted the effectiveness of all types of different fillers.

One method of narrowing down the filler options was to choose a filler shape: fibrous or particle. From Chapter 2.2, it was demonstrated that both types of filler shapes performed adequately when providing conductivity to a composite material. From Chung (2004), it was shown that the steel and carbon fibers reduced the resistivity of the composite more effectively than any of the powders that were included. It was suggested that the larger size of the fibers was responsible for the effectiveness. Therefore, it would take a lower effective concentration of fibrous fillers to achieve adequate electrical sensitivity. However, an important observation to take away from the Chung (2004) study is that all of the particle fillers that were observed were carbonaceous rather than metal.

Nickel powder and nanoFe<sub>2</sub>O<sub>3</sub> were two of the particle fillers that were not included in the Chung (2004) study because of their more recent history of being included in self-sensing composites. Particle fillers also have some benefits over fibrous fillers. One of the main difficulties of using fibrous fillers is that they are harder to disperse homogeneously

throughout the composite due to their size and shape. It was determined in Azhari and Banthia (2012) that carbon nanotubes tended to cluster together during mixing due to van der Waals forces. Therefore, chemical admixtures are oftentimes required in order to achieve composite homogeneity. The problem with using chemical admixtures is that they have the potential to introduce structural defects by altering the filler properties (i.e. decrease in mechanical property, electrical property, etc.) (Han et al. 2015).

Due to the limited scope of this research, it was decided that physical mixing would be used rather than chemical dispersion. Particle fillers also have a distinct advantage when it comes to physical mixing as well. While shear mixing can separate fibrous fillers from each other, it could also damage the fillers and lower their aspect ratio, which in turn would decrease their sensing effectiveness. Even after the composites have been mixed effectively, fibrous fillers such as carbon nanotubes have the potential to buckle under large strains during testing (Falvo et al. 1997; Lourie et al. 1998).

From the factors that were discussed, the decision was made to use particle fillers in this research. The particle filler options were divided into two material groups: carbonaceous or metal. After considering the results of Chung (2004) combined with the knowledge of the effectiveness of metal particles fillers in Han et al. (2008) and Vipulanandan and Mohammed (2015), it was deduced that a metal particle filler would provide the better opportunity for the research goals. Nickel powder and nanoFe<sub>2</sub>O<sub>3</sub> were discussed in depth as two of the more effective and widely-used metal particle fillers that were shown to aid in enhancing the piezoresistive properties of the composite material. Both could work as fully capable fillers, but it was ultimately decided that nanoFe<sub>2</sub>O<sub>3</sub> would be used for this research partially because some predictive quantitative analysis had already been performed for this conductive filler. The predictive analysis presented in Vipulanandan and Mohammed (2015) would serve as a starting point for this research to build from.

## **2.4 Predictive Models**

A few predictive models were considered for use in this research and would be utilized to predict the stress state on the test specimens based on the obtained electrical data.



The first two models are presented in Vipulanandan and Mohammed (2015). The first formula models the stress-strain behavior:

$$\sigma = \left( \frac{\frac{\varepsilon}{\varepsilon_f}}{q + (1 - p - q) \frac{\varepsilon}{\varepsilon_f} + p \left( \frac{\varepsilon}{\varepsilon_f} \right)^{\frac{p+q}{p}}} \right) \times \sigma_f \quad (2.1)$$

where  $\sigma$  (MPa) is the predicted stress,  $\varepsilon$  (percent) is corresponding strain,  $\sigma_f$  (MPa) is the peak stress,  $\varepsilon_f$  (percent) is the peak strain, and  $p$  and  $q$  are model parameters.

The second formula predicts the stress-resistivity data:

$$\sigma = \left( \frac{\frac{x}{x_f}}{q + (1 - p - q) \frac{x}{x_f} + p \left( \frac{x}{x_f} \right)^{\frac{p}{p-q}}} \right) \times \sigma_f \quad (2.2)$$

where  $\sigma$  (MPa) is the predicted stress,  $x = \left| \Delta\rho/\rho_0 \right|$  is the fractional change in electrical resistivity at which  $\sigma$  is being predicted,  $\sigma_f$  (MPa) is the peak stress,  $x_f = \left| \Delta\rho/\rho_0 \right|_f$  is the fractional change in electrical resistivity corresponding to  $\sigma_f$ , and  $p$  and  $q$  are model parameters.

For both formulas, the  $q$  is the ratio of the secant modulus to the tangent modulus of the graphed data and  $p$  is an iterated value. Both Equations 2.1 and 2.2 were utilized in research and they were adept at predicting piezoresistive and stress-strain behaviors.

Another stress-strain model was presented in Ezeldin and Balaguru (1992). Unlike the Vipulanandan and Mohammed model, the Ezeldin and Balaguru model does not account for the tangent modulus and secant modulus, which enhance the Vipulanandan and Mohammed model's effectiveness at shaping the actual curvature of the graph. Additionally, this model only has one material parameter  $\beta$  as seen in the model formula:

$$\sigma = \left( \frac{\beta \left( \frac{\varepsilon}{\varepsilon_f} \right)}{\beta - 1 + \left( \frac{\varepsilon}{\varepsilon_f} \right)^\beta} \right) \times \sigma_f \quad (2.3)$$

where  $\sigma$  (MPa) is the predicted stress,  $\varepsilon$  (percent) is corresponding strain,  $\sigma_f$  (MPa) is the peak stress,  $\varepsilon_f$  (percent) is the peak strain, and  $\beta$  is a model parameter.

Upon initial observation, this equation seems like a simplified version of the Vipulanandan stress-strain formula. According to Ezeldin and Balaguru (1992), the  $\beta$  term was based on the modulus of elasticity which was in turn determined by the reinforcing index  $RI$ . The reinforcing index was dependent on the fiber content in weight fraction, the fiber length, and the fiber diameter. The Ezeldin and Balaguru model was used for calculating a composite with steel fiber reinforcement, hence the importance of the reinforcing index. However, for the scope of this current research,  $\beta$  will be considered an iterated parameter similar to the Vipulanandan  $p$  parameter rather than a material-based value. The Ezeldin and Balaguru model was not used for predicting piezoresistive behavior, so its capability will be tested by changing the strain variables to fractional change in resistivity variables.

One of the stress-strain models that is widely used to this day is the Hognestad Model. Hognestad (1951) created a model, shown in Figure 2.8, to develop the stress-strain behavior of unconfined normal strength concrete.

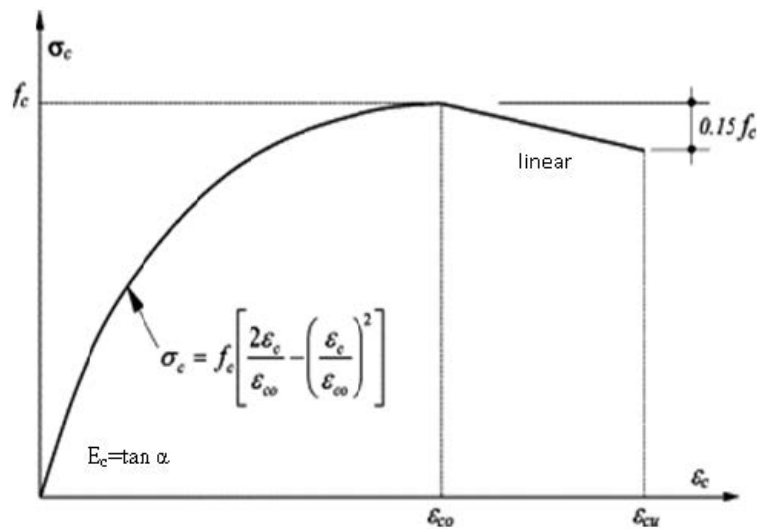


**Figure 2.8: Hognestad (1951) model for unconfined concrete (Kasarin et al. 2014).**

This model has been proven as a satisfactory stress-strain model. This research is only concerned with the piezoresistive behavior up to peak stress, and the Hognestad (1951) model is considered to be a second-order parabola up to the peak stress using the formula

$$\sigma_c = f_c \left[ \frac{2\varepsilon_c}{\varepsilon_{co}} - \left( \frac{\varepsilon_c}{\varepsilon_{co}} \right)^2 \right] \quad (2.4)$$

where  $\sigma_c$  is the predicted stress,  $\varepsilon_c$  is the strain corresponding to the predicted stress,  $f_c$  is the maximum compressive stress, and  $\varepsilon_{co}$  is the peak strain. After reaching peak stress, the model becomes linear down to the ultimate stress which is typically taken as 85 percent of the peak stress.

Kent and Park (1971) further simplified the Hognestad model by altering the  $\varepsilon_{co}$  value to remain a constant 0.002:

$$\sigma_c = f_c \left[ \frac{2\varepsilon_c}{0.002} - \left( \frac{\varepsilon_c}{0.002} \right)^2 \right] \quad (2.5)$$

The post-peak stress state was modified to account for both confined and unconfined concrete. For the scope of this research, the post-peak stress state will be disregarded.

Many other examples of stress-strain models that account for the strain hardening and softening of the specimen under loading can be found in Ozbakkaloglu et al. (2013). Many of these other stress-strain equations are based off the Hognestad Model up to the peak stress, so they will not be discussed in additional detail at this point.

In order to evaluate the stress-strain predictive properties of the models in question, data from Vipulanandan and Mohammed (2015) was analyzed using the four models that were discussed. The stress-strain graph of a 28-day cured specimen with 1 percent nanoFe<sub>2</sub>O<sub>3</sub> content was digitized using GetData Graph Digitizer Version 2.26 ©. Each of the four models were utilized with the measured data up to the peak stress as displayed in Figure 2.9 and then examined for accuracy.

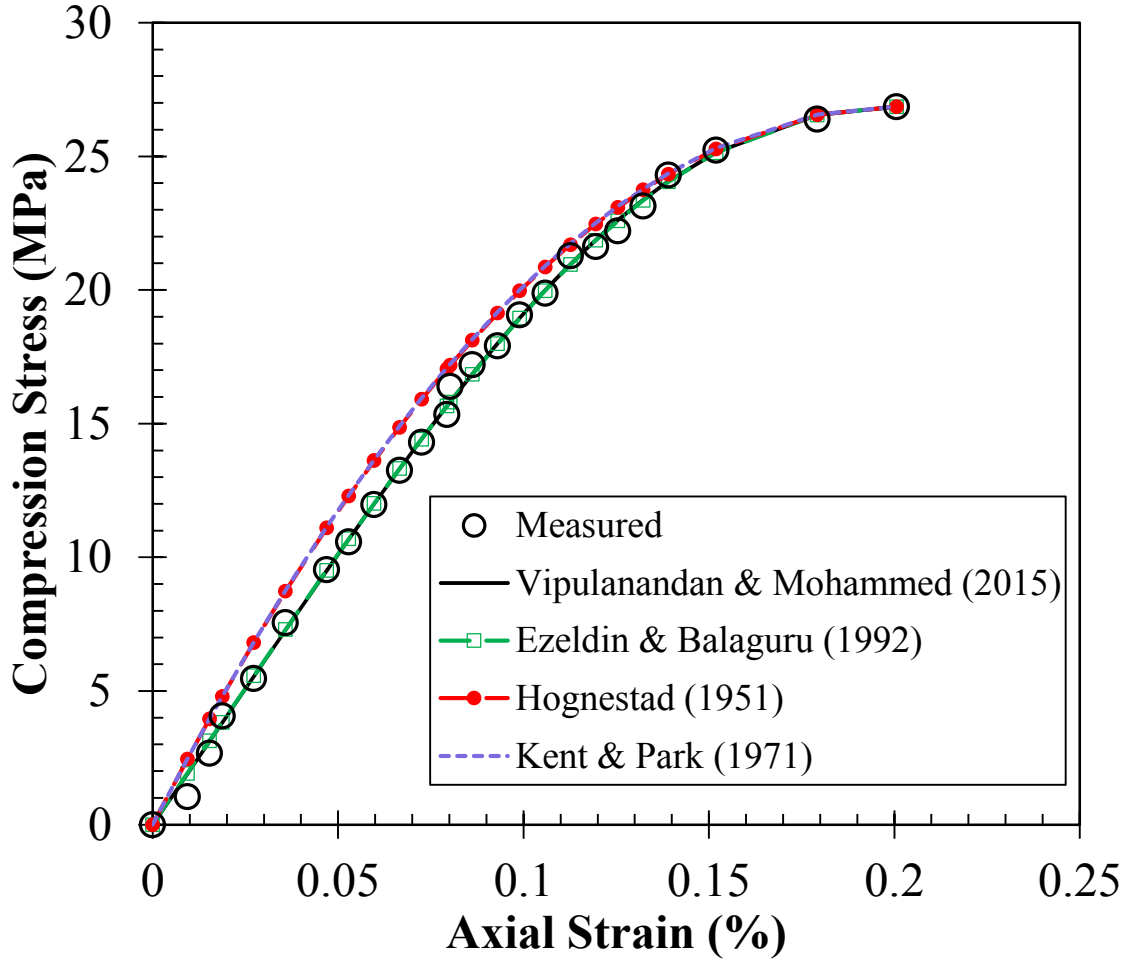


**Figure 2.9: Analysis of the stress-strain predictive models on the Vipulanandan and Mohammed (2015) data.**

Upon observation of the four graphs, the Vipulanandan and Mohammed and the Ezeldin and Balaguru models were able to outperform the Hognestad and the Kent and Park models for this specific dataset due to the iterated parameter capabilities. Having parameter values that are iterated allows the Vipulanandan and Mohammed and Ezeldin and Balaguru models to adapt to irregularities in the curvature due to irregular hardening behavior under compression. Many curvature irregularities are likely to occur in the raw data considering that this research will involve a large number of samples. Therefore, in order to better account for this phenomenon and to reduce test time, only the Vipulanandan and Mohammed and the Ezeldin and Balaguru models will be used in this research. The Ezeldin and Balaguru model has not yet been used to predict piezoresistive behavior, thus its applicability will be examined in Chapter 4.

## 2.5 Testing and Parameters Established for This Research

After completing a technical review of the existing literature on the topics covered in this research, the final design details were chosen. Many of these decisions were based on availability and cost effectiveness of materials as well as limitations of the project scope.

NanoFe<sub>2</sub>O<sub>3</sub> will be used as the conductive filler (Chapter 2.3). The Vipulanandan and Mohammed and Ezeldin and Balaguru models will be used to predict the stress-strain and piezoresistive behavior of the specimens (Chapter 2.4). Portland cement will be used as the matrix material. In addition, a defoamer will be used to increase the mechanical properties of the mix as well as to minimize the air voids within the specimens that could interfere with the conductive network.

A total of 60 composite cylinders will be developed using mixing procedures discussed in Chapter 3. A combination of 5 different nanoFe<sub>2</sub>O<sub>3</sub> contents, 4 water-cement ratios, and 3 curing times will be used in the mix designs.

The following tests/procedures will be conducted and will be further elaborated on in Chapter 3:

- Static Electrical Testing – Includes test of the defoamer's effect on conductivity as well as a Frequency Sweep on each hardened cylinder before the compression test.
- Resistivity Index (RI) Testing for examining piezoresistive behavior of each mix design over the first 24 hours of curing.
- Compressive Strength Test (ASTM C39) with simultaneous LCR meter readings to correlate the electrical response with the stress state.
- Prediction of the measured stress-strain and piezoresistive data using the Vipulanandan and Mohammed and Ezeldin and Balaguru models.
- Creation of a new model to predict the piezoresistive behavior based on the mix design parameters.
- Resolution analysis to demonstrate the procedure and effectiveness of the new model.

---

### **3 Materials and Methods**

This chapter will discuss the materials used throughout the research and the procedures followed to obtain the desired results.

#### **3.1 Materials Used**

The materials used in this research were reflective of materials that would be used in typical construction applications. Quikrete® Type I/II Portland Cement was used exclusively and was compatible with ASTM C-150 and Federal Specifications for Portland cement. Iron (III) oxide nanopowder / nanoparticles ( $\text{nanoFe}_2\text{O}_3$ ) were used to enhance the electrical properties of the mixture and were obtained from US Research Nanomaterials, Inc. in Houston, Texas. Particle size varied between 20-40 nm. Air voids presented problems in preliminary testing by creating discontinuities in the concrete cylinder samples and thus providing a possibility for less accurate electrical readings. Therefore, a defoamer was required in order to minimize the amount of air bubbles created during mixing and reduce trapped air in the composite mix. C-64 Concrete Defoamer and Densifying Admixture from Fishstone® in Crystal Lake, Illinois was used throughout the entirety of testing. Deionized (DI) water was used in place of tap water in order to significantly limit the amount of ionic impurities that could potentially alter the electrical readings.

#### **3.2 Mixing and Sample Preparation**

In addition to the mix ingredients, molds and mixing instruments were acquired. Plastic cylindrical molds, each having a 50.8 mm diameter and 101.6 mm height, were purchased from Forney® located in Zelienople, Pennsylvania. The 2:1 height-to-diameter aspect ratio was considered standard for compression testing. A Hobart® Model C-100 mixer, as shown in Figure 3.1, was used to fully mix the materials.

Twenty unique batch mix designs were developed, having different quantities of cement, DI-water, defoamer, and  $\text{nanoFe}_2\text{O}_3$ . Four different water-cement ratios (0.40, 0.45, 0.50, and 0.60) and five different  $\text{nanoFe}_2\text{O}_3$  contents (0, 2.5, 5, 7.5, and 10 percent) were included in the mix designs. Water-cement ratio was defined as the ratio of the weight of water to the weight of cement in the mix, and  $\text{nanoFe}_2\text{O}_3$  content was defined as the weight

of iron oxide nanoparticles divided by the weight of cement expressed as a percentage. For each batch, 4 cylinders were desired: one each for a 1-day, 7-day, and 28-day curing time, along with an extra cylinder in case of unintended errors during curing or testing. Developing the batches in this manner allowed the three mix design parameters to be analyzed more extensively: water-cement ratio, nanoFe<sub>2</sub>O<sub>3</sub> content, and curing time.

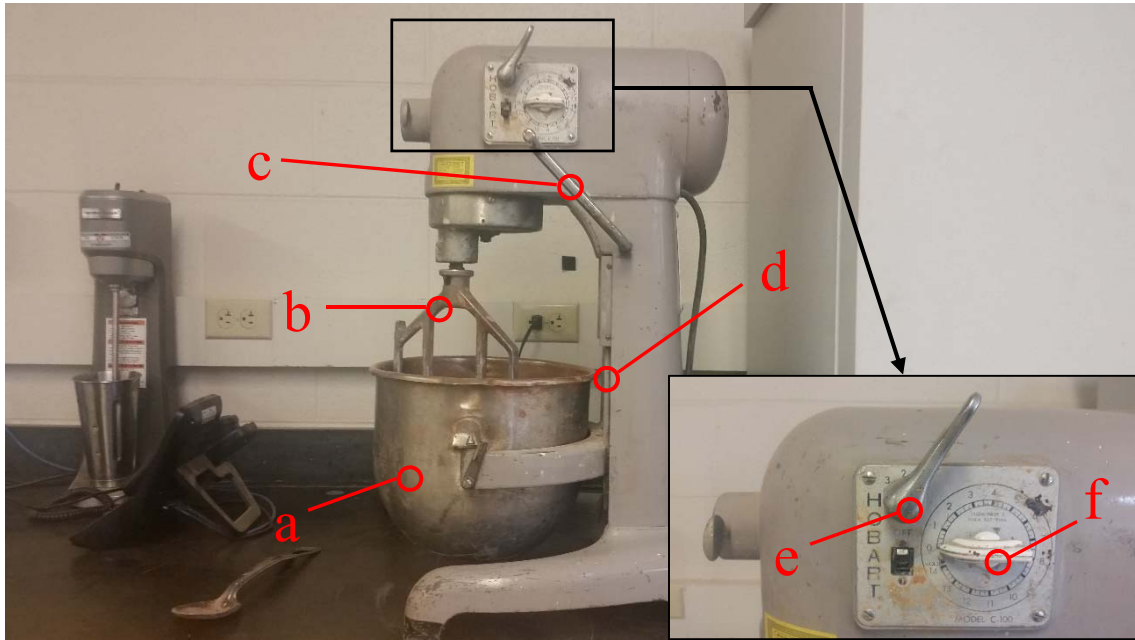


**Figure 3.1: Hobart® C-100 Mixer. Necessary components pictured include (a) mixing bowl, (b) flat beater, (c) lever, (d) bowl slideway, (e) speed handle, (f) mixing timer.**

Calculations for exact quantities were performed before mixing commenced. As an example, the full mix ingredient quantities for Cylinder #13 in Batch 5 (0.40 water-cement ratio and 2.5 percent nanoFe<sub>2</sub>O<sub>3</sub>) will be calculated. To begin, the volume of a single 50.8 mm diameter by 101.6 mm tall cylinder was calculated from the diameter  $d$  and the height  $h$  using Equation 3.1:

$$V_{\text{cyl}} = \frac{\pi \cdot d^2}{4} \times h = \frac{\pi \cdot (5.08\text{cm})^2}{4} \times 10.16\text{cm} = 204.308\text{cm}^3 \quad (3.1)$$

This volume was multiplied by 4 to account for all cylinders in the batch, producing a total volume of 817.23 cm<sup>3</sup>. A 0.4 water-cement ( $wc$ ) ratio was used in Batch 5, meaning that for every 1 gram of cement there will be 0.4 grams of water. The unit weights of each material were calculated using a VWR® Model 5002B Balance and a Pyrex® 600 mL

glass beaker. The unit weight of the cement  $\gamma_c$  was found to be 1.506 gram/cm<sup>3</sup>, the unit weight of DI-water  $\gamma_w$  was approximately 1 gram/cm<sup>3</sup>, and the unit weight of the defoamer  $\gamma_{def}$  was measured to be 0.93 gram/cm<sup>3</sup>. Knowing these values, the required weight of cement to produce 4 cylinders was calculated using Equation 3.2:

$$W_{\text{cement}} = \frac{V_{\text{cyl.total}}}{\left( \frac{1}{\gamma_c} + \frac{wc}{\gamma_w} \right)} = \frac{817.23 \text{ cm}^3}{\left( \frac{1}{1.506 \text{ g/cm}^3} + \frac{0.40}{1 \text{ g/cm}^3} \right)} = 768.1 \text{ grams} \quad (3.2)$$

In order to account for possible material loss elimination of air bubbles during testing, the required weight of cement was doubled and then rounded up to approximately 1560 grams. With a water-cement ratio of 0.40, the weight of water was then determined from Equation 3.3:

$$W_{\text{water}} = W_{\text{cement}} \times wc = 1560 \text{ grams} \times 0.40 = 624 \text{ grams} \quad (3.3)$$

The instructions for the defoamer stated that 10 to 20 mL of defoamer per gallon of water should be used in the mix. In order to get the maximum desired effect of reducing the air bubbles during mixing, the higher end of the range 20 mL/gallon was used throughout. The volume of defoamer was calculated using Equation 3.4:

$$V_{\text{defoamer}} = 624 \text{ g water} \times \frac{\text{mL}}{1 \text{ g}} \times \frac{1 \text{ gal water}}{3785.412 \text{ mL}} \times \frac{20 \text{ mL}}{\text{gal water}} = 3.297 \text{ mL} \quad (3.4)$$

The nanoFe<sub>2</sub>O<sub>3</sub> content was simply calculated by multiplying the weight of cement by the percentage of nanoFe<sub>2</sub>O<sub>3</sub>, which in the case of Cylinder #13 was 2.5 percent. Therefore, the weight of nanoFe<sub>2</sub>O<sub>3</sub> was determined to be 39 grams. The remaining cylinder mix designs were calculated in the same manner by changing the water-cement ratio and nanoFe<sub>2</sub>O<sub>3</sub> content as needed. A full batch mix design can be found in Appendix A.

The mixing procedure was set to begin after the batch mix designs were developed. The mix ingredients were sorted and weighed using the balance according to the previously developed batch mix designs. The cement and iron oxide nanoparticle quantities were measured out and then the two materials were combined into a metal mixing bowl. A metal spoon was used to consistently mix the cement and nanoFe<sub>2</sub>O<sub>3</sub> particles together. Next, the beaker was used to measure the volume of DI-water required to produce the desired



water-cement ratio. The appropriate volume of the defoamer was then measured and then combined with the DI-water in the glass beaker. A clean metal rod with a hemispherical tip was used to mix the DI-water and the defoamer for 30 seconds to ensure that the defoamer was fully dispersed throughout the mixture.

With the mixing bowl of the Hobart® Model C-100 mixer placed in the lowest position along the bowl slideway, the DI-water and defoamer mixture was poured into the mixing bowl, coating the bottom and sides. The cement and nanoFe<sub>2</sub>O<sub>3</sub> mixture was poured into the mixing bowl next. Once all of the ingredients were poured in to the mixing bowl, the lever was turned to raise the bowl to the top of the slideway, at which point the flat beater was in contact with the ingredients. The speed handle was set to the number 1, the low speed setting. The bowl was fastened to the mixer and the timer was set to 7 minutes to allow the ingredients enough time to fully mix. At this point, the mixer began to automatically mix and it was left alone to let the mixing process proceed, as displayed in Figure 3.2.



**Figure 3.2: Mixing of ingredients in bowl at beginning (left) and end (right) of mixing process.**

While the ingredients were mixing, 4 plastic cylinder molds as well as a metal spoon and a smooth metal rod were arranged next to the mixer for sample preparation. After the mixing had finished at the end of the 7 minutes, the lever was turned to lower the bowl down the slideway. The cementitious mixture was removed from the bowl using the spoon and poured into one of the molds in three lifts. Each lift was approximately one-third of the mold height, or 33.87 mm. After the first lift was poured, the metal rod was used to tamp the layer 25 times evenly distributed across the entire top surface area of the mold. Tamping the sample with a vertical up and down motion of the rod, shown in Figure 3.3, consolidated the sample by reducing the air voids. The rod was then used to lightly tap around the outer casing of the mold for 30 seconds to 1 minute, depending on the water cement ratio, in order to cause air bubbles near the surface of the mixture to rise and be removed. Air bubbles were able to rise more efficiently through the wetter batches with higher water-cement ratios. Thus, the higher the water-cement ratio of the batches was, the less tapping time was required to eliminate surface air bubbles.



**Figure 3.3: Smooth metal rod is used to tamp the mixture after a lift has been poured.**

Once the cement had been poured to the top of the mold, the metal rod was rolled across the top of the plastic mold to strike off the mix in order to produce a flat top surface of the composite specimen. The bottom surface of the specimens were optimally smooth due the

mix ingredients gravitating towards the bottom of the mold. However, from practice mixing it was found that using the cap connected to the plastic mold allowed excessive space at the top of the closed mold, which caused air bubbles to form an irregular top surface on the sample after 24 hours of hardening. This presented a problem because the electrodes used to gather electrical data during the later compression testing required a smooth surface to provide more accurate readings. Irregularities in the top surface could cause incorrect or inconsistent electrical measurements. Thus, a 50.8 mm diameter indented plastic cap was fabricated to produce a much smoother top surface for the sample during the hardening phase and is detailed in Figure 3.4.

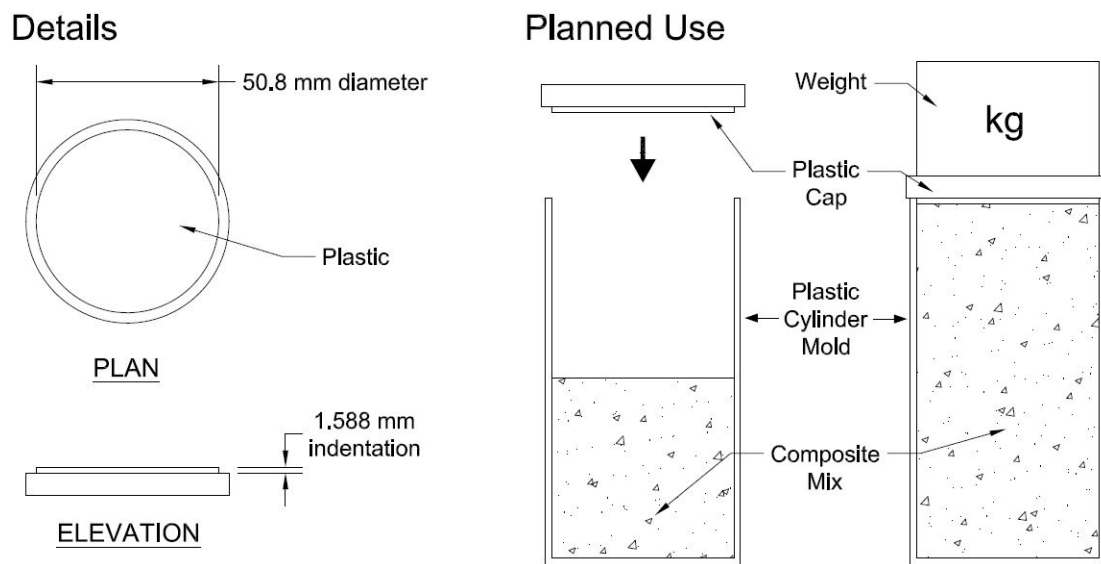


**Figure 3.4: Details of plastic cap used for mixing molds**

The plastic cap was fabricated in the University of Kentucky Machine Shop, and its significant feature was the 1.588 mm indentation. The indentation allowed the plastic cap to fit snugly within the mold and minimized the space for air and liquid to escape the mold. Therefore, utilizing the fabricated plastic cap provided much smoother top surface for the cylinder samples.

After the caps had been placed on top of the molds, a 2 kg steel weight was placed on top of two sealed molds for the 24 hour hardening duration, as shown in Figure 3.5. The purpose of the added weight on top of the sample during hardening was to ensure that the mixture did not expand and displace the plastic cap and also to keep the plastic cap sealed tightly on top of the sample during the hardening process.



**Figure 3.5: 2 kg weights placed on top sample molds during 24 hour hardening phase.**

The molds were left to harden in place for 24 hours, after which the weights and plastic caps were removed from the molds. Under these conditions, some cylinders with water cement-ratios greater than or equal to 0.50 had not fully hardened after 24 hours. For consistency of the preparation method, all cylinders were left out of the curing chamber for additional 24 hours to continue hardening as shown in Figure 3.6. This added time was not considered as part of the curing time.



**Figure 3.6: Samples after a full 24 hours of hardening.**



At the end of the 48 hours of sample hardening, the molds were stripped using a box cutter. A small incision was made at the top of the plastic mold before a shallow vertical cut was formed down the side of the plastic. The vertical cut was deep enough to split the mold, but not deep enough to scratch the surface of the sample. The plastic mold was then pulled apart by hand and the curing process could commence.

### **3.3 Sample Curing**

The concrete curing began immediately after the samples had been stripped from the molds, and its purpose was to keep the samples moist in order to prevent shrinkage cracks and other disturbances while the cement was hydrating. In order to effectively cure the cylinders, a makeshift curing chamber was created that remained fully enclosed while moisture was cycled through it. The components of the curing chamber consisted of a plastic container with a lid, PVC pipes, and a PureGuardian® Ultrasonic Humidifier Model H1510.

The curing chamber was built in a manner such that it would be simple to both build and disassemble. First, a 25.4 mm diameter commercially available telescoping PVC pipe was inserted snugly into the top of the humidifier. A 355.6 mm long and 25.4 mm diameter PVC pipe was then connected to the top of the telescoping PVC, as seen in Figure 3.7.



**Figure 3.7: Telescoping and straight PVC pieces connected to humidifier.**

A 25.4 mm diameter hole was drilled in the front of the plastic container approximately 38.1 mm from the bottom on the container. A threaded 90° 25.4 mm PVC elbow was worked into the drilled hole and then sealed with caulk on the inside of the container to prevent moisture from escaping, as displayed in Figure 3.8.



**Figure 3.8: Outer (left) and inside (right) view of threaded elbow PVC connection to plastic container.**

The bottom of the elbow was then connected to the top of the straight PVC. The plastic container was placed on top of a 96.5 cm tall table, and a 22.9 cm tall stand was built to support the humidifier, shown in Figure 3.9. A small hole was drilled in both the top lid and the bottom of the plastic container to allow some of the moisture to dissipate by exiting the chamber.

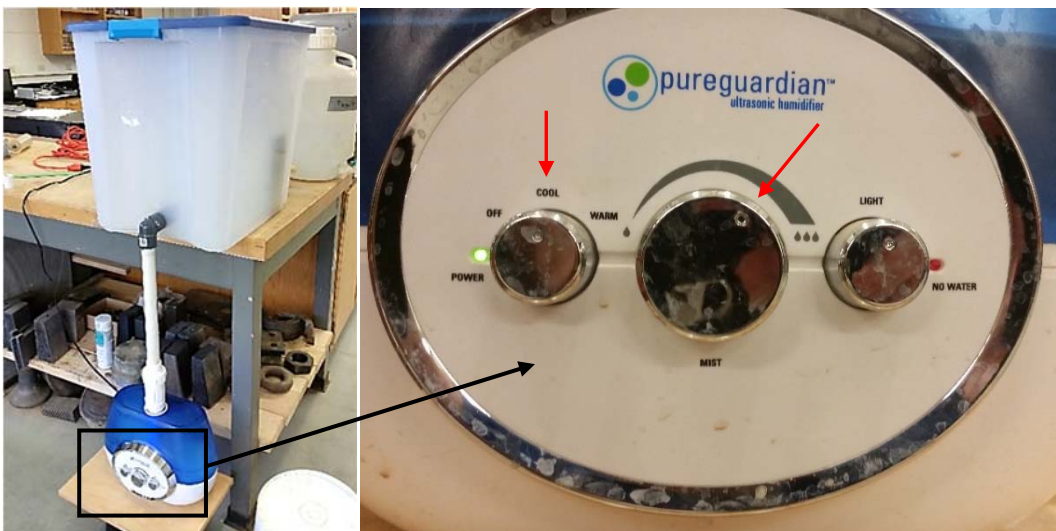


**Figure 3.9: Fully assembled curing chamber and settings used during curing process.**

The concrete cylinders could be cured after the chamber had been fully assembled. Tap water from the laboratory sink was used to fill the humidifier, which was refilled with new water once daily throughout the curing process. The moisture temperature was manipulated using the left knob, and it was set to the “Cool” setting for the curing duration. The middle knob controlled the amount of vapor produced by the humidifier and was turned to produce approximately one-third of the maximum output. The goal was to obtain a chamber internal temperature of around 73°F and humidity of 95 percent or higher, both of which were achieved.

An AcuRite® Model 00592W2 Indoor/Outdoor Temperature and Humidity Sensor was used to obtain measurements of the inside of the curing chamber. The sensor was placed on the inside of the chamber and the battery case was sealed to ensure that moisture would not corrode the sensor’s batteries. Temperature and humidity measurements were wirelessly transmitted to the display monitor outside of the chamber, where readings were updated in real time. A 5-gallon paint bucket was placed under the pre-drilled hole in the bottom of the plastic container to catch any excess moisture escaping the curing chamber. Shortly after batch production began, it became evident that more space would be required inside of the chamber to store all of the samples. Rather than finding a larger plastic container, a rack was created using PVC pipes, shown in Figure 3.10, to increase the capacity of the chamber.



**Figure 3.10: PVC rack in the curing chamber.**

The PVC rack was covered by 6.35 mm wide strips of acrylic that provided a flat surface for the concrete cylinders while simultaneously allowing the moisture to reach the cylinders above the rack. By utilizing the PVC rack, an additional 24 cylinders could be placed inside the chamber at a time. The added capacity significantly reduced the experimentation time and improved the efficiency of the research.

Cylinders were left in the curing chamber for either 1 day, 7 days, or 28 days depending on the curing time specified for the cylinder. A chart and a calendar were created in order to keep track of where each cylinder was located in the chamber and when that cylinder's specific curing time had elapsed. Once the curing time for a cylinder had expired, the cylinder was removed from the chamber before being subjected to further testing.

### **3.4 Static Electrical Measurements**

Before any compression testing was conducted, static electrical measurements were obtained from two separate procedures – (1) Analysis of defoamer content on electrical resistivity of DI-water and defoamer mixture and (2) Frequency Sweeps of each cylinder. These tests were conducted on samples in a static state in which conditions were kept constant throughout the entirety of testing.

#### **3.4.1 Effect of Defoamer on Resistivity of DI-water**

Static electrical testing was performed to study the effects of defoamer content on the electrical conductivity of the DI-water and defoamer mixture. A resistivity cell capable of obtaining electrical readings from this mixture, shown unassembled in Figure 3.11, was fabricated by the University of Kentucky machine shop. This device consisted of 5 main components: a bottom plate with 4 threaded rods extending upwards, a top plate, a 50.8 mm inner diameter by 25.4 mm tall acrylic cylinder, 4 threaded sprockets, and two 50.8 mm diameter rubber O-rings. Both the top and bottom plates held an embedded 50.8 mm diameter copper electrode that protruded approximately 2.38 mm from the circular indentation in the plastic on both plates.





**Figure 3.11: Unassembled resistivity cell used to measure electrical properties of DI-water and defoamer mixture. Parts pictured include: (a) bottom plate, (b) top plate, (c) acrylic cylinder, (d) sprockets, and (e) O-rings.**

Four screws and 1 central bolt held the copper electrodes in place on each plate, and the bolt extended through the outer face of each plate. A washer and a hex nut were placed on the end of each bolt and the hex nut was tightened with a wrench to minimize liquid leakage around the bolt. Alligator clips could then be attached to the ends of the bolts on both the top and bottom plates, as shown in Figure 3.12.

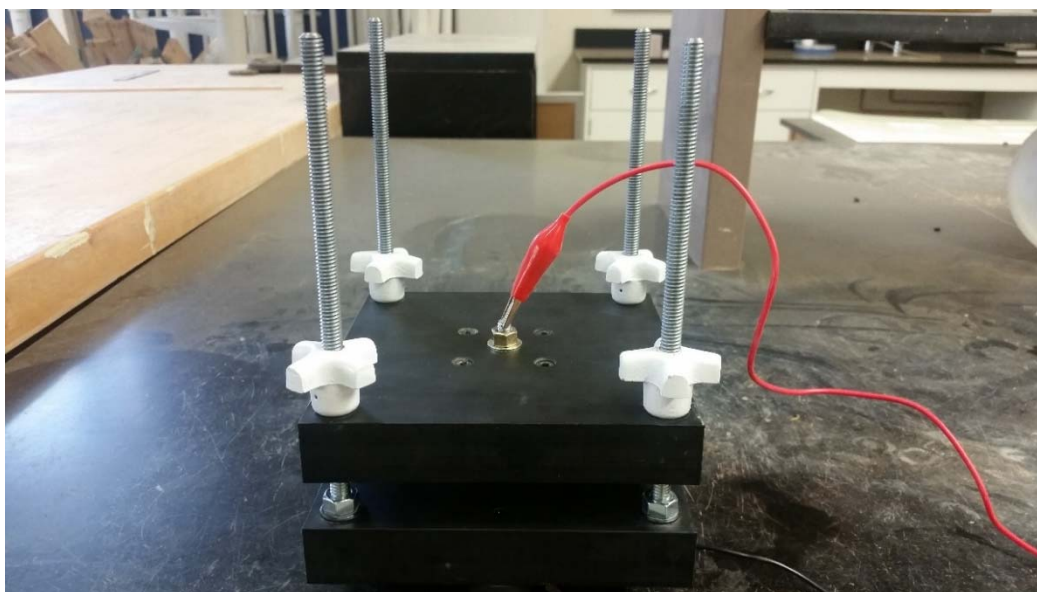


**Figure 3.12: Alligator clips connected to bolts on resistivity cell plates.**

An Agilent® Model 4285A Precision LCR Meter was acquired and was used to measure inductance (L), capacitance (C), and resistance (R) of samples for this test and all of the future electrical testing. Agilent® Model 16048A Test Leads were connected to the front of the LCR meter, as shown in Figure 3.13, and alligator clips were then clipped to the end of the test leads. The red alligator clip (anode) was connected to the red and orange test leads while the black alligator clip (cathode) was attached to the black and gray test leads. Once these clips were attached to electrodes on either end of a sample, current flowed from the anode to the cathode, and the corresponding electrical measurements would be transmitted back to the LCR meter's display screen where they would then be recorded. The voltage was set at 1.00 V for the entirety of all electrical testing conducted in this research. The frequency was set at 100.0 kHz for all testing unless otherwise noted. The LCR was set to measure capacitance and resistance,  $C_p$  and  $R_p$ , respectively.



**Figure 3.13: Agilent® LCR Meter Model 4285A and attached Agilent® Test Leads Model 16048A. Display screen and settings also pictured.**

The LCR meter was connected to a power source and the alligator clips were connected to the bolts on the top and bottom plates of the resistivity cell. The anode was connected to the top plate bolt and the cathode was connected to the bottom plate bolt. Rubber O-rings were placed inside of the top and bottom plate circular indentations. Next, the acrylic

cylinder was placed in the bottom plate indentation and was held down by hand while DI-water was poured to the top of the cylinder. The top plate was aligned with the threaded rods and was lowered until the plastic cylinder fit inside of the top plate indentation. Pressure was applied to the top plate by hand to avoid leakage while the four sprockets were adequately tightened to hold the plastic cylinder in place. Electrical readings were then obtained from the DI-water contained in the plastic cylinder. The capacitance and resistance read from the display on the LCR meter and the dimensions of the plastic cylinder were converted to metric. For resistivity calculations, the height of the resistivity cell was considered to be 25.4 mm minus the indentation of the copper electrodes on the top and bottom plates, which produced a total height of 20.64 mm. The dimensions and resistance were used to determine the resistivity of the DI-water using Equation 3.5:

$$\rho = \frac{R \times A}{L} \quad (3.5)$$

where  $\rho$  ( $\Omega \cdot m$ ) is the resistivity,  $R$  is the resistance ( $\Omega$ ),  $A$  is the area of the copper electrode ( $m^2$ ), and  $L$  is the height of the resistivity cell (m).

After measurements had been collected for the DI-water, the resistivity cell was disassembled and cleaned thoroughly. A DI-water and defoamer mix was produced consisting of 20 mL of defoamer per gallon of DI-water as previously specified for the batch mix designs. The same procedure was repeated to determine the resistivity of the DI-water and defoamer mix. The test was conducted again on the DI-water both with and without the defoamer to provide additional data for analysis. The results and analysis are discussed in Chapter 4.1.1.

### 3.4.2 Frequency Sweeps

A frequency sweep was conducted on each concrete cylinder before compression testing. After a cylinder was removed from the curing chamber, it was dried using a paper towel. As previously mentioned, the tops of the cylinders were susceptible to surface irregularities due to air bubbles. The top surfaces were sanded smooth using a Sears/Craftsman® 6 inch Disc Sander equipped with a 60 grit Gator-Grit® sanding disc. The guide on the disc sander was aligned perpendicular to the sanding disc surface. The cylinder was slowly

pushed into the sanding wheel in order to smooth out any major surface irregularities, as demonstrated in Figure 3.14.



**Figure 3.14: Concrete cylinder top surface sanded smooth by the disc sander.**

The cylinder was slowly rotated clockwise while being pressed against the sanding disc to ensure that the sanding was evenly distributed across the entire top surface. After initial sanding, the cylinder top surface was examined with a level. If the top surface was not flat, additional sanding was performed until a flat surface was achieved.

Two stainless steel electrodes were used for the frequency sweeps and compression tests and were fabricated by the University of Kentucky Machine Shop, with dimensions shown in Figure 3.15.

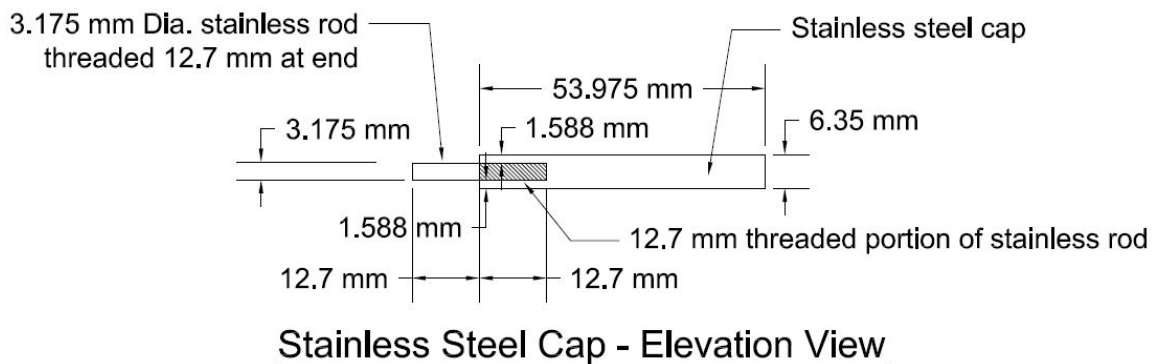


**Figure 3.15: Elevation view of stainless steel electrode.**



The stainless steel electrode consisted of a 53.975 mm diameter by 6.35 mm thick cap and a 3.175 mm diameter by 25.4 mm long threaded stainless steel rod. The caps were sufficiently thick to allow the rod to be threaded 12.7 mm into the caps. Additionally, the caps were sufficiently thick to withstand the stresses that would be encountered during compression testing.

To initiate the frequency sweep process, a concrete cylinder was placed between the two stainless steel electrodes. Acrylic plates were placed below the bottom electrode and above the top electrode. The anode and cathode alligator clips that were connected to the LCR meter were then attached to the top and bottom electrodes, respectively. A weight equivalent to 6.895 kPa loading to the top electrode cap was found and was placed on top of the acrylic plate. The acrylic plate served to eliminate contact between the stainless steel electrode and the metallic weight which could have slightly altered the electrical readings. Once the setup was completed as shown in Figure 3.16, the test could commence.

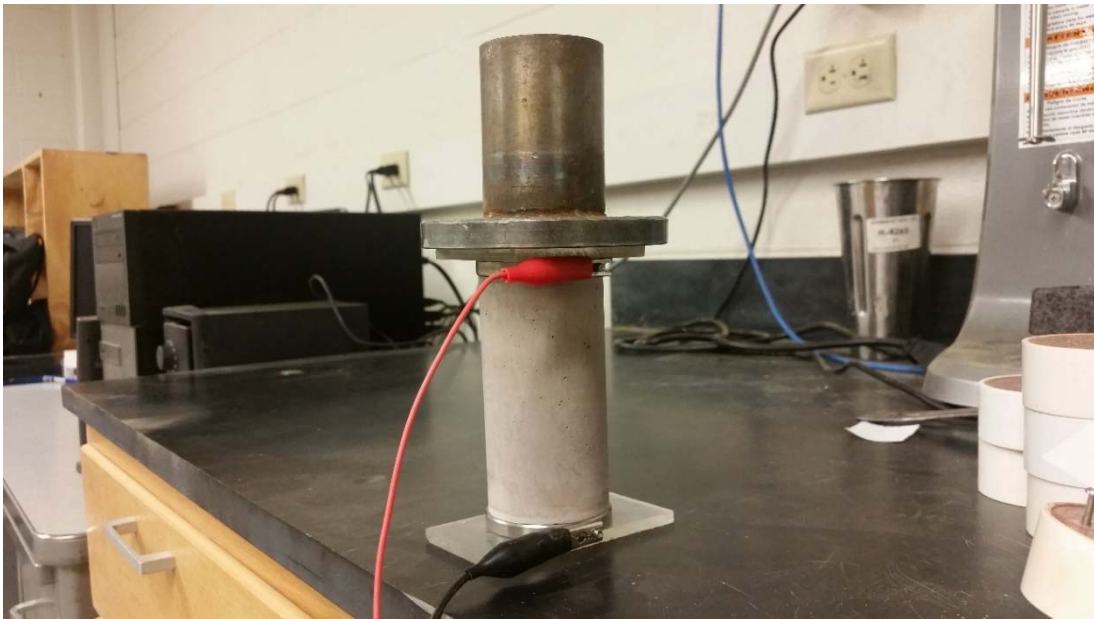


**Figure 3.16: Frequency sweep setup. Anode (red) attached to top electrode and cathode (black) attached to bottom electrode. A weight produces a 6.895 kPa load on the cylinder cap.**

With the LCR meter turned on, the frequency was set to the lowest possible increment, or 75 kHz. The capacitance and resistance of the concrete cylinder was recorded, and then the LCR meter was set to the next frequency increment. The capacitance and resistance

were recorded for this frequency and the cycle continued until the final frequency increment, 30 MHz, was reached. Graphs of Capacitance vs. Frequency and Resistance vs. Frequency were compiled for each cylinder and are included in Appendix B, and continued analysis of the frequency sweep results is discussed further in Chapter 4.1.2.

### 3.5 Electrical Response During Curing

Resistivity index (RI) testing was conducted during the curing phase for each of the 20 batch mixes to examine the change in resistivity over a 24 hour curing cycle. The resistivity index was defined in Vipulanandan and Mohammed (2015) as the percentage of maximum change in resistivity in 24 hours and was calculated for each batch using Equation 3.6:

$$RI_{24hr} = \left( \frac{\rho_{24} - \rho_{min}}{\rho_{min}} \right) \times 100 \quad (3.6)$$

where  $\rho_{min}$  is the minimum resistivity recorded over the 24-hour period and  $\rho_{24}$  is the sample resistivity recorded after 24 hours of curing. The goal of the RI testing was to observe any correlations between the resistivity index and the batch design mix parameters, nanoFe<sub>2</sub>O<sub>3</sub> and water-cement ratio.

New PVC cylindrical molds were fabricated by the University of Kentucky machine shop for the RI testing. A 50.8 mm inner diameter PVC pipe was cut individual 25.4 mm lengths for each mold. A 0.1588 mm indentation was cut into the top and bottom surfaces of the PVC to hold the electrodes. Circular 53.975 mm diameter pieces were cut from a square foot sheet of 1.016 mm thick C101 oxygen free copper purchased from OnlineMetals.com and functioned as the electrodes. Using a 2.35 mm drill bit, a hole was drilled into each copper disc approximately 10 mm from the edge. A 25.4 mm long steel screw approximately 3.175 mm in diameter was worked into the drilled hole with a screwdriver until it extended through to the other side of the disc. Then, a hex nut was fastened to the screw using a wrench on the underside of the disc to hold it in place. Once two electrodes had been created, they could be placed at the top and bottom of the 25.4 mm PVC section to form the RI testing mold, as detailed in Figure 3.17.

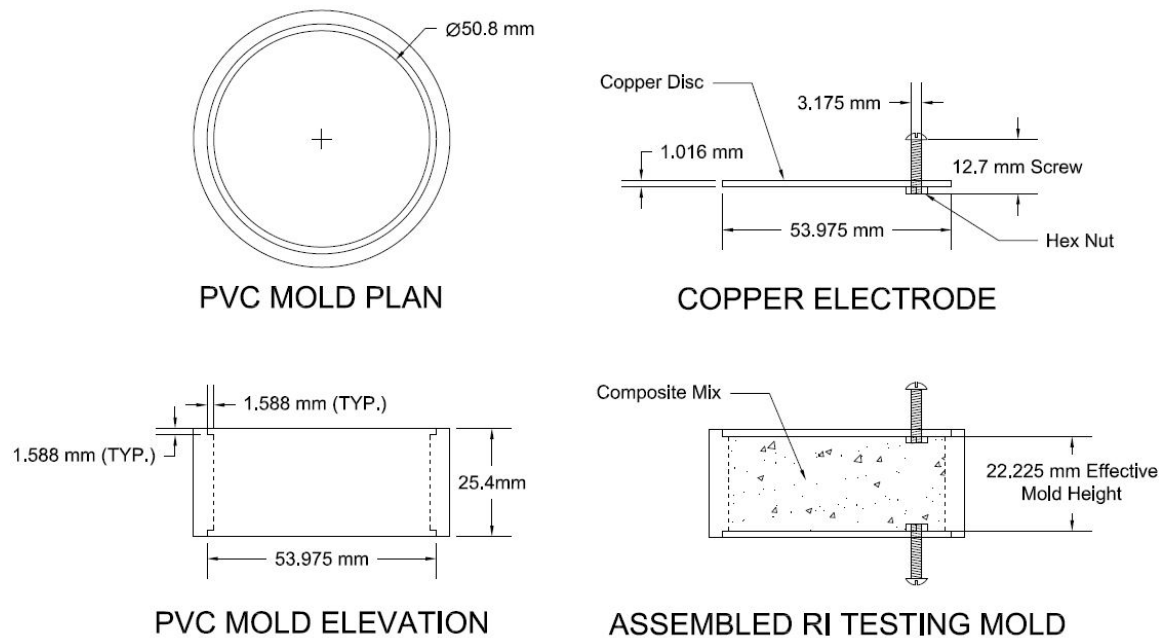


**Figure 3.17: Resistivity index testing mold details.**

One electrode was placed inside of the PVC indentation and was glued in place using HDX™ Super Glue, as shown in Figure 3.18. The glue was placed all around the edge of the electrode to provide a leak-proof seal. A bead of glue was also placed around the screw on the outer face of the electrode to prevent leaks. The same batch mix designs that were discussed in Chapter 3.2 were scaled down to 1:16 proportions to fill the RI testing molds. The mixing was performed in the same manner as previously discussed. The mold was placed with the glued electrode face down and the screw overhanging the edge of a counter to keep the mold flat. The cementitious mixture was poured, in 1 lift rather than 3, up to the bottom of the indentation in the mold. The other copper electrode was then placed within the mold's upper indentation, but was not glued.



**Figure 3.18: Electrode glued to top of PVC mold. Glue was also placed around screw on outside face of electrode.**

A makeshift cantilever, shown in Figure 3.19, was created to accommodate for the shape of the RI testing mold. Two 30.5 cm long by 25.4 mm wide wooden planks were placed on a countertop with an approximately 10 cm overhang. Two 2 kg weights were placed on the back end of the planks to support the cantilever.

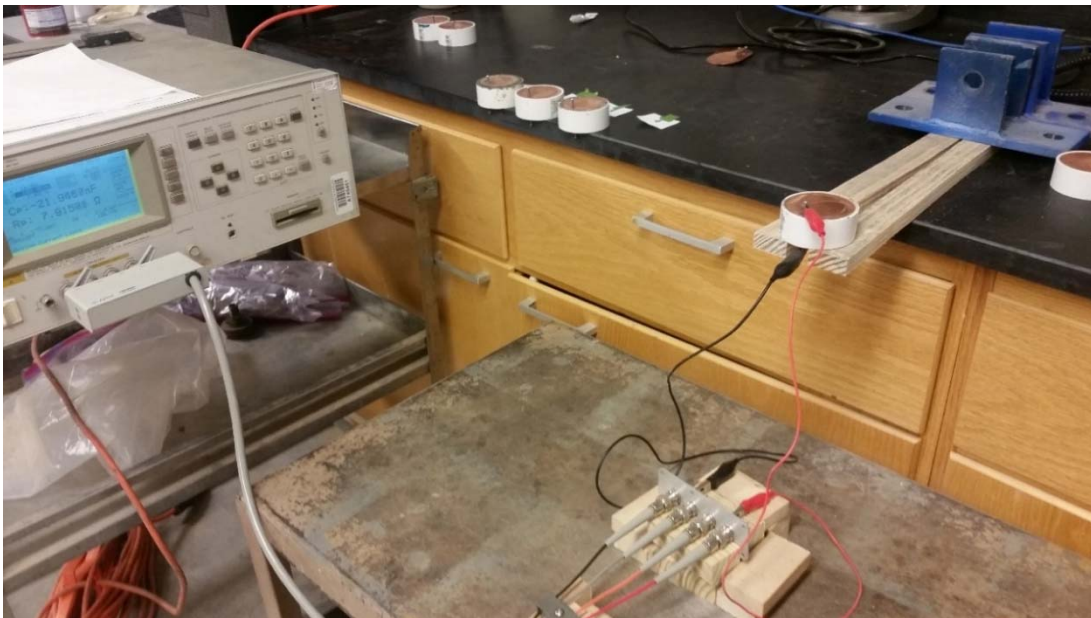


**Figure 3.19: Resistivity index testing electrical measurement cantilever with connection to LCR meter.**



The ends of the planks at the cantilever were moved 25.4 mm apart to provide space for the bottom electrode screw. The LCR meter was set to a frequency of 100 kHz and the anode and cathode clips were attached to the top and bottom electrodes, respectively.

In order to model the resistivity behavior of each sample over the 24 hour curing time, resistance readings were recorded at several time increments. Resistance readings were recorded at a minimum: one time immediately after sample pouring; once every 10 minutes from initial pour until 2 hours of curing; once every 15 minutes from 2 hours until 3 hours; and once at 24 hours of curing. Additional readings were taken for other samples solely to observe further softening/hardening behavior during curing. However, the overall purpose of the RI testing was to record the minimum resistance and the resistance at 24 hours of each sample rather than to model the behavior during curing. Therefore, the extra readings were not performed on all samples. Further analysis of the resistivity index testing will be discussed in Chapter 4.2.

In order to clean out the molds for re-use after 24 hours, the top electrode disc was removed by hand. The super glue on the edge of the bottom electrode was cut into using a box cutter so that the bottom electrode could be removed by hand. A hammer was used to break up the hardened cement and eventually push it out of the mold. Any remaining cementitious material was cleaned off of the PVC casing with a wet rag. After drying the PVC, the bottom electrode disc was re-glued to the PVC indentation before repeating the procedure for the next sample.

### **3.6 Electrical and Stress-Strain Response During Compression Test (ASTM C39)**

Compression testing was conducted on each cylinder after the frequency sweep was finished. By performing compression testing on each cylinder, stress-strain response could be obtained. Using the LCR meter to simultaneously measure the electrical response under loading would allow for an observation of the stress-electrical response of each cylinder.

A 300,000 pound capacity Southwark Emery Universal Testing Machine manufactured by Baldwin Locomotive Works in Philadelphia in 1944 was used to conduct the compression testing. This machine was equipped with a Celesco® Position Sensor (Extensometer) Model DPT250-0025-111-1230 to measure changes in displacement of the crosshead

during compression testing. This change in position will then be used to calculate the strain of the concrete cylinders during testing. The machine was recently upgraded with a SATEC™ Series controller and an Instron® hydraulics system.

First, the test cylinder diameter was measured using a Mitutoyo® Absolute Digimatic Caliper at the bottom, middle, and top of the cylinder and then the average of the three readings was recorded as the diameter. The height of the cylinder was also measured using the caliper. The stainless steel electrodes were placed on the bottom and top of the cylinder which had been recently sanded down by the disc sander as mentioned in Chapter 3.4.2. Acrylic squares were placed on the outer faces of the electrodes in to prevent the metallic surfaces of the compression testing machine from coming into contact with the metal electrodes and potentially altering the electrical measurements. The configuration was then placed on the compression testing machine load plate as shown in Figure 3.20. The cylinder was centered underneath the crosshead.

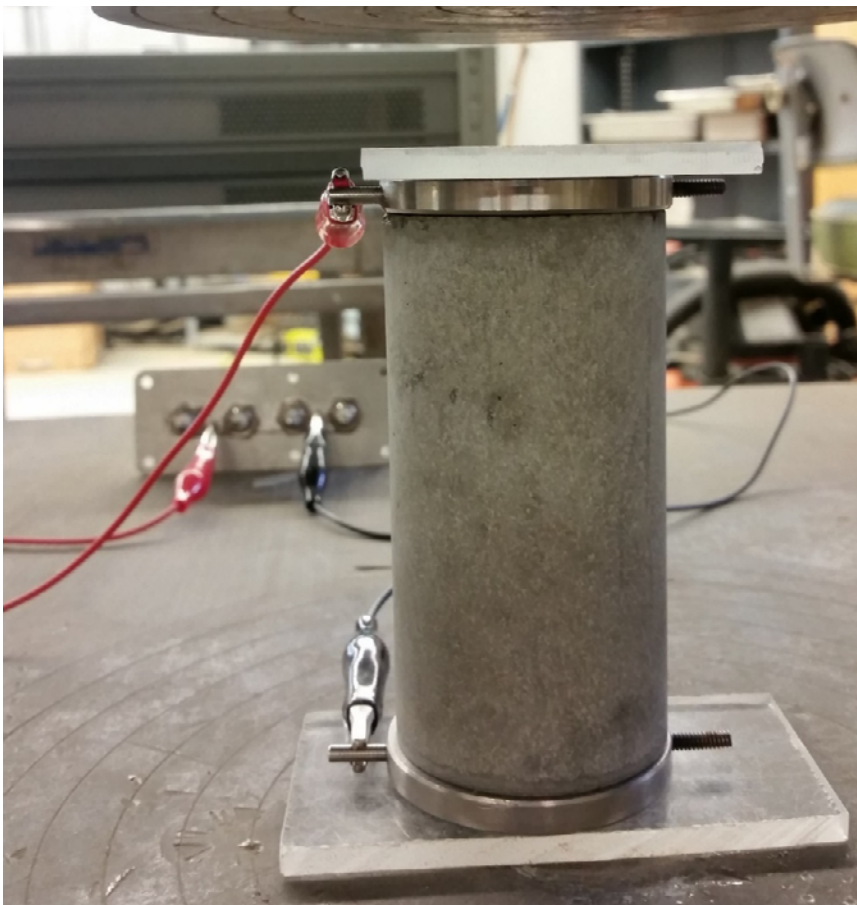


**Figure 3.20: Cylinder configuration on compression testing machine.**

Partner™ software was used to obtain measurements from the testing machine. The step-by-step Partner™ procedure is explained in detail in Appendix D. From the setup, the crosshead speed was set to 0.635 mm/min (0.025 in/min setting) to provide ample time to obtain the electrical readings manually. The rate was set to a position/time increment rather than a load/time increment as in ASTM in order to facilitate the alignment of the Partner™ compression test data with the LCR meter data. The Partner™ procedure was loaded onto the computer.

The controller shown in Figure 3.21 was used to maneuver the crosshead over the cylinder specimen before the test began.

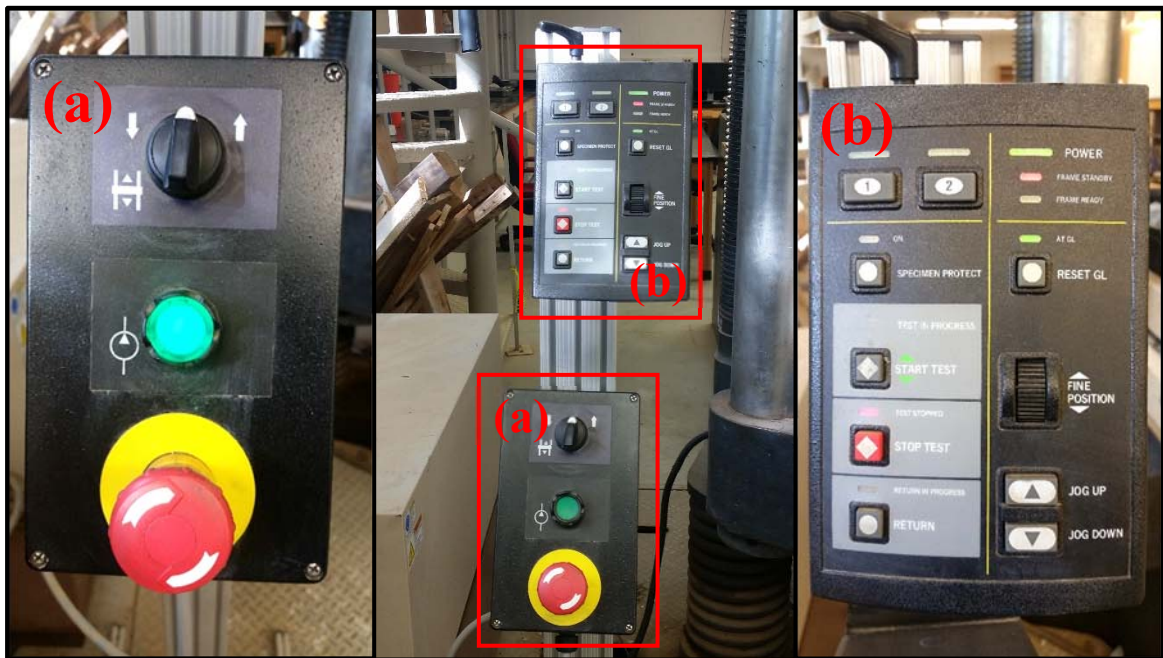


**Figure 3.21: Controller used for compression testing. Pictured: (a) Frame panel and (b) Control console.**

First, the machine was turned on by depressing the green power button on the frame panel. With the power turned on, the crosshead could be positioned onto the sample. The JOG UP button on the control console was initially pressed to lower the crosshead. Once the crosshead was moved to about 3 mm above the sample, the FINE POSITION thumbwheel was scrolled up to lower the crosshead at a slow rate until it met the top acrylic square. After the load readout on the computer became approximately zero, the top electrode was considered to be in full contact with the top of the cylinder. The RESET GL (Gage Length

Reset) button was then pressed to reset the position of the gage to 0 inches. After both the load and position were zeroed, the test was started.

Electrical readings, capacitance and resistance, of the cylinder were recorded simultaneously during the compression testing. A Samsung Galaxy S5 cell phone was used to video the LCR meter screen during the entirety of the test. A picture of the screen was manually taken at every 0.127 mm (converted from 0.005 inch) increment of position change, which was continuously updated in the bottom right panel on the Partner™ display screen as shown in Figure 3.22.

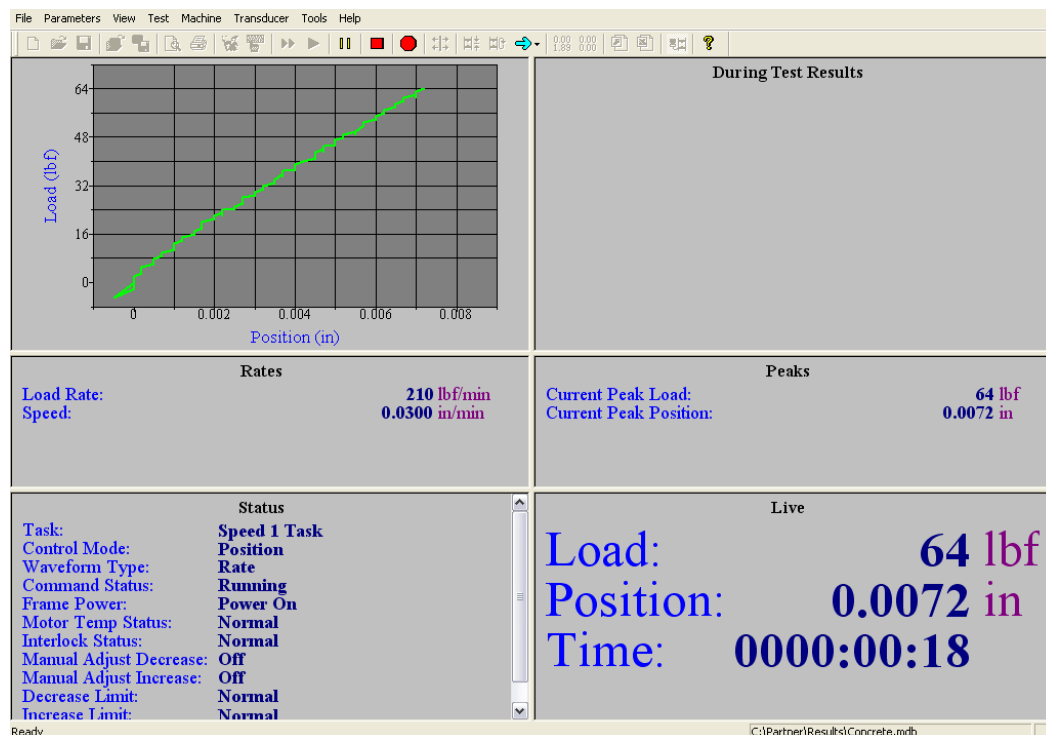


**Figure 3.22: Partner™ program display screen during compression testing.**

At the conclusion of the compression test, the pictures were used to manually record the resistance measurements taken at each position increment. The measurements were compiled into a table on a Microsoft® Excel. The raw data from the compression test was also exported into a separate Excel spreadsheet at this time.

A macro used to produce the stress-strain data, found in Appendix D, was developed using Visual Basic for Application (VBA) in Excel to convert raw data into final results. The macro first prompted the user to type in the diameter and height of the cylinder which

would be carried through all of the calculations for determining the stress and strain on the cylinder. The diameter was used to calculate the cross sectional area, and was converted to metric units. The individual stresses were calculated using the Partner™ measured loads and then converted to metric units as illustrated by Equation 3.7:

$$\sigma(\text{MPa}) = \frac{\text{Load}(\text{lbf})}{\text{Area}(\text{m}^2)} \times \frac{4.44822\text{kN}}{1000\text{lbf}} \times \frac{1\text{MN}}{1000\text{kN}} \quad (3.7)$$

The extensometer position measurements were used to calculate the strain as a percentage as displayed in Equation 3.8:

$$\text{Strain}(\%) = \frac{\text{Position}(\text{in})}{\text{CylinderLength}(\text{m})} \times \frac{0.0254\text{m}}{1\text{in}} \times 100\% \quad (3.8)$$

The measured stress-strain data was calculated before the two predictive models, Vipulanandan and Mohammed and Ezeldin and Balaguru, were used to predict the stress on the cylinder for each strain measurement. Figure 3.23 shows the four properties that were used to enable the Vipulanandan and Mohammed model parameters: tangent modulus ( $E_o$ ), secant modulus ( $E_s$ ), peak (or failure) stress ( $\sigma_f$ ), and the peak strain ( $\epsilon_f$ ).

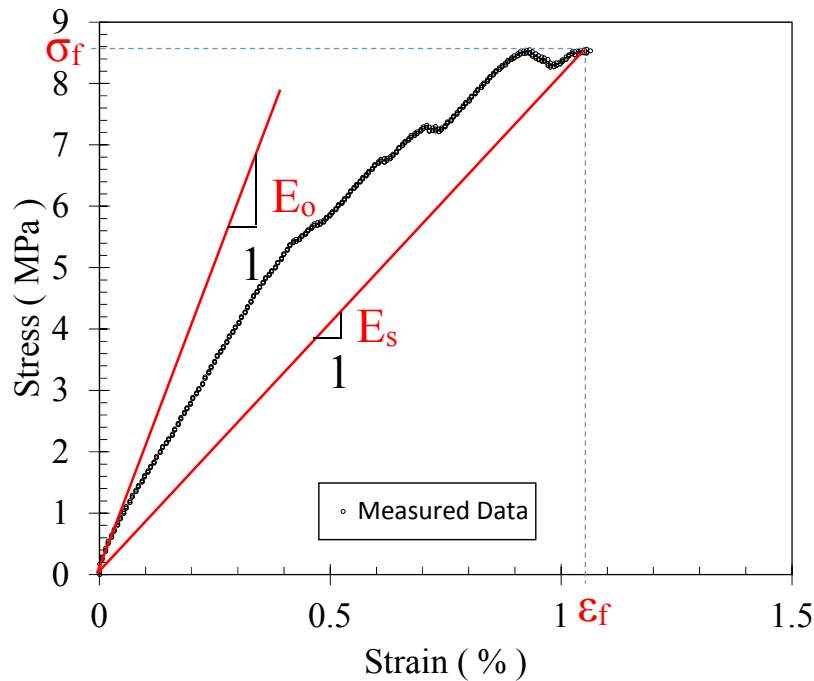


**Figure 3.23: Graph of Cylinder #46 Stress-Strain data with relevant factors displayed.**

All stress-strain measurements after the peak stress were removed as the predictive models were only desired to predict up to failure. The failure stress and the corresponding strain were recorded. The secant modulus was calculated by dividing the peak stress by the corresponding peak strain. The tangent modulus was determined by visually selecting two points that approximated the tangent slope, and then calculating the slope of a line between these two points.

The Vipulanandan  $q$  parameter was calculated by dividing the secant modulus by the tangent modulus. The  $p$  parameter was initially set to a value of 1.0 and would later be determined by using the Solver function on Excel. Predicted stress values were obtained using the Vipulanandan and Mohammed (2015) stress-strain predictive formula that was presented as Equation 2.1 in Chapter 2 and is repeated here as Equation 3.9:

$$\sigma = \left( \frac{\frac{\varepsilon}{\varepsilon_f}}{q + (1-p-q)\frac{\varepsilon}{\varepsilon_f} + p\left(\frac{\varepsilon}{\varepsilon_f}\right)^{\frac{p+q}{p}}} \right) \times \sigma_f \quad (3.9)$$

where  $\sigma$  (MPa) is the predicted stress and  $\varepsilon$  (percent) is the strain percentage measurement at which  $\sigma$  is being predicted. This equation was used to predict a stress for each strain measurement up to the peak strain for the cylinder.

In order to produce effective prediction data, the  $p$  parameter was changed by using the Solver Excel function to produce a close curve fit. This was achieved by minimizing the sum of square error,  $e^2$ , in the same manner as Mebarkia and Vipulanandan (1992) calculated by Equation 3.10:

$$e^2 = \sum_{i=1}^N \left( \frac{\sigma_{ip} - \sigma_{ie}}{\sigma_c} \right)^2 \quad (3.10)$$

where  $N$  represents the overall number of measured strain values,  $\sigma_{ip}$  is the  $i$ th predicted stress,  $\sigma_{ie}$  is the  $i$ th experimental stress, and  $\sigma_c$  is the peak stress. In order to allow for a better prediction of the data, the constraints on the  $p$  and  $q$  values in Mebarkia and

Vipulanandan (1992) were modified. The  $p$  parameter was confined to a minimum value of 0.01 to a maximum value of 5. The minimum  $p$  value was set to 0.010 to avoid letting the parameter converge to 0 since doing so would create a “cannot divide by zero” error in Excel. Once, the constraints were established, the Solver function was run with a “GRG Nonlinear” (Generalized Reduced Gradient) engine to solve for the final  $p$  parameter that produced the lowest  $e^2$  value.

In addition to the sum of square error, the coefficient of determination,  $R^2$ , was simultaneously calculated for each data set using Equation 3.11:

$$R^2 = \left( \frac{\sum_i (x_i - \bar{x})(y_i - \bar{y})}{\sqrt{\sum_i (x_i - \bar{x})^2} \times \sqrt{\sum_i (y_i - \bar{y})^2}} \right)^2 \quad (3.11)$$

where  $y_i$  is the  $i$ th measured value,  $x_i$  is the  $i$ th predicted value,  $\bar{y}$  is the mean of the measured values, and  $\bar{x}$  is the mean of the predicted values. The lower the  $e^2$  value and the higher the  $R^2$  value of the data, the better the model was considered at predicting the measured stress-strain data for each sample.

In order to set up the Ezeldin and Balaguru predictive model, only the peak stress and peak strain were required along with an iterated  $\beta$  value (discussed in Chapter 2.4). The predicted stresses were calculated using the previously presented Equation 2.3 from Chapter 2, repeated here as Equation 3.12:

$$\sigma = \left( \frac{\beta \left( \frac{\epsilon}{\epsilon_f} \right)}{\beta - 1 + \left( \frac{\epsilon}{\epsilon_f} \right)^\beta} \right) \times \sigma_f \quad (3.12)$$

There were no constraints placed on the  $\beta$  parameter, and the Solver function was utilized again to obtain a  $\beta$  value that produced the lowest sum of square error. Like the Vipulanandan and Mohammed prediction data, the  $e^2$  and  $R^2$  values were calculated for the Ezeldin and Balaguru stress-strain data. The  $e^2$  and  $R^2$  values and other relevant model parameters for both the Vipulanandan and Mohammed and Ezeldin and Balaguru models were compiled for each cylinder in a database for further analysis.

In order to analyze the stress measurements based on electrical response, stress vs. change in resistivity graphs similar to those in Vipulanandan and Mohammed (2015) were developed. The manually recorded electrical resistance measurements along with a second VBA macro that continued where the stress-strain macro ended were used to produce the stress-electrical predictive data. A lookup table was used to search the stress-strain measured values for the strain values closest to the corresponding 0.127 mm increments at which the resistance readings were taken. The stresses associated with the strains were then obtained. In this manner of combining the stress-strain with the strain-electrical data, the resistance readings could be related to the measured stresses. Resistivity values for each position increment were calculated using Equation 3.5. The change in resistivity from the initial resistivity was calculated using Equation 3.13:

$$\frac{\Delta\rho}{\rho_o} = \frac{\rho_i - \rho_o}{\rho_i} \quad (3.13)$$

where  $\rho_i$  is the resistivity at the  $i$ th position increment and  $\rho_o$  is the initial resistivity. Through compression testing, it was observed that resistance values decreased as the load increased. Therefore, it was decided that the absolute value of the change in resistivity data would be taken in order to avoid negative values. The stress vs. change in resistivity data was then graphed for each cylinder.

Only the Vipulanandan and Mohammed model was used to predict the stress-electrical data. Four properties were needed in addition to the  $p$  and  $q$  parameters to predict the stress vs. change in resistivity data: tangent modulus ( $E_o$ ), secant modulus ( $E_s$ ), peak stress ( $\sigma_f$ ), and the fractional change in resistivity corresponding to the peak stress ( $|\Delta\rho/\rho_o|_f$ ). All data points after the peak stress were excluded from the predictive model analysis.

The secant modulus was calculated by dividing the peak stress by its corresponding change in resistivity. The tangent modulus was taken as the slope of the line from the origin through either the first or second nonzero data point. The ratio of the tangent modulus to the secant modulus for the stress-resistivity data was much lower than that of the stress-strain data, which was attributed to the different curvature of the two graphs. While the stress-strain data generally had a concave down curvature up to the peak stress, the stress-resistivity data displayed an upward concavity. Therefore, the stress-strain predictive



equation would not be capable of effectively predicting the stress-resistivity data. The predicted stress values were obtained using the Vipulanandan and Mohammed (2015) stress-resistivity predictive formula noted first in Chapter 2 as Equation 2.2 and repeated here as Equation 3.14:

$$\sigma = \left( \frac{\frac{x}{x_f}}{q + (1 - p - q) \frac{x}{x_f} + p \left( \frac{x}{x_f} \right)^{\frac{p}{p - q}}} \right) \times \sigma_f \quad (3.14)$$

where  $\sigma$  (MPa) is the predicted stress and  $x = \left| \Delta\rho/\rho_0 \right|$  is the fractional change in electrical resistivity at which  $\sigma$  is being predicted. The Vipulanandan  $q$  parameter was once again calculated as the secant modulus divided by the tangent modulus, and the  $p$  parameter was iterated using the Solver function by minimizing the  $e^2$  value. The  $R^2$  value was also calculated for each cylinder, and the results were compiled for each cylinder in a database.

Analysis of the stress vs. strain and the stress vs. change in resistivity results will be discussed further in Chapters 4.3 and 4.4, respectively.

In addition to utilizing the Vipulanandan and Mohammed and Ezeldin and Balaguru models to predict stress-strain and stress-resistivity data, a new model will be proposed in Chapter 4.5 that will predict the stress on cylinders with different mix designs using the change in resistivity response.

---

## 4 Analysis

This chapter will discuss the analysis of the tests that were conducted and discussed in Chapter 3.

### 4.1 Static Electrical Testing Analysis

Data was compiled for the two static electrical tests described in Chapters 3.4.1 and 3.4.2. The analysis of the test results will be discussed in Chapters 4.1.1 (effects of defoamer of resistivity of DI-water) and 4.2.2 (frequency sweeps).

#### 4.1.1 Analysis of Defoamer Effects on Resistivity of DI-water

The purpose of the testing detailed in Chapter 3.4.1 was to determine the effects of adding defoamer to a mixture of DI-water. Since defoamer was included in each batch mix design, it was imperative to understand how adding the defoamer to DI-water could potentially impact the electrical response of the concrete samples.

As discussed in Chapter 3.4.1, the resistivity cell was used to measure the resistivity of DI-water and the DI-water and defoamer mixture. A total of four readings were taken: 2 readings for the DI-water without defoamer and 2 readings for the DI-water and 20 mL of defoamer per gallon mixture. Capacitance and resistance readings were recorded for each sample. The height of the resistivity cell was taken to be 22.225 mm after the electrode indentations were subtracted from the 25.4 mm acrylic cylinder, and the diameter was 50.8 mm. The electrode area was calculated using a simple circular area formula to be

$$\text{ElectrodeArea} = \frac{\pi \cdot d^2}{4} = \frac{\pi \cdot (0.051\text{m})^2}{4} = 0.00203\text{m}^2$$

The resistivity was calculated using Equation 3.5. For example, for the first mixture of DI-water without any defoamer, the measured resistance was 31.959 k $\Omega$ . Therefore, the resistivity was calculated to be

$$\rho = \frac{R \cdot A}{L} = \frac{31959\Omega \cdot 0.00203\text{m}^2}{0.022\text{m}} = 2914.531\Omega \cdot \text{m}$$

From the resistivity, the conductivity  $\kappa$  of the mixture could be determined. A sample's conductivity is the degree to it conducts electricity. The conductivity is simply the reciprocal of the resistivity, as shown by Equation 4.1:

$$\kappa = \frac{1}{\rho} \quad (4.1)$$

For the first DI-water without defoamer mixture, the conductivity was found to be

$$\kappa = \frac{1}{2914.531 \, \Omega \cdot \text{m}} = 3.431 \times 10^{-4} \text{ Siemens/m}$$

where 1 Siemen =  $1 \, \Omega^{-1}$ . The higher the conductivity of a sample, the more conductive to electricity a sample is. On the other hand, the higher the resistivity of a sample, the more resistant it is to conducting electric current. In the case of smart cementitious materials, it would be beneficial to have more conductive materials so that there would be less resistance for the electric current passing through the sample between electrodes. The calculations were repeated for the other 3 samples and were recorded in Table 4.1.

**Table 4.1: Effects of Defoamer on Sample Resistivity.**

	No Defoamer		20 mL Defoamer / gal	
Test Number	1	2	1	2
Capacitance, $C_p$ (pF)	116.220	112.620	102.840	92.378
Resistance, $R_p$ (k $\Omega$ )	31.959	32.020	33.978	40.706
Resistivity, $\rho$ ( $\Omega \cdot \text{m}$ )	2914.531	2920.094	3098.656	3712.222
Conductivity, $\kappa$ (S/m)	3.431E-04	3.425E-04	3.227E-04	2.694E-04

From this testing, it was determined that adding the defoamer to the DI-water increased the resistivity and conversely lowered the conductivity of the sample. In order to numerically quantify the effect of the defoamer, the results of the two samples of each defoamer content were averaged to produce Table 4.2.

**Table 4.2: Average Resistivity and Conductivity Based on Defoamer Content.**

Defoamer Content	0 mL/gal	20 mL/gal
Average $\rho$ , ( $\Omega \cdot \text{m}$ )	2917.313	3405.439
Average $\kappa$ , (S/m)	3.428E-04	2.961E-04

Ratios of both the average resistivity and conductivity between the defoamer contents were produced.

$$\rho \text{ Ratio (20mL/gal to 0mL/gal)} = \frac{3504.439 \, \Omega \cdot \text{m}}{2917.313 \, \Omega \cdot \text{m}} = 1.167$$

$$\kappa \text{ Ratio (20mL/gal to 0mL/gal)} = \frac{3.428 \times 10^{-4} \frac{\text{S}}{\text{m}}}{2.961 \times 10^{-4} \frac{\text{S}}{\text{m}}} = 0.864$$

From the ratios between defoamer contents, it was determined that adding 20 mL of defoamer per gallon of DI-water increased the mixture resistivity by 16.7 percent and decreased the conductivity by 13.6 percent. The decrease in conductivity from the added defoamer could be seen as detrimental to obtaining electrical readings from the concrete samples during compression testing. However, the main role of the defoamer was not to increase the conductivity of the concrete cylinders, but to minimize the amount of air bubbles created during the mixing process. Air voids within a hardened concrete cylinder could alter the flow of the electrical current through the solid cylinder and thus affect the electrical measurements. Because air bubbles often become trapped inside the cylinders during the hardening process, the defoamer was considered important to the mix design. While adding the defoamer slightly lowered the conductivity of the samples, it was surmised that the benefits of using it during mixing outweighed the potential risks.

#### 4.1.2 Analysis of Frequency Sweeps

Frequency sweeps were conducted for each cylinder according to the procedure discussed in Chapter 3.4.2. The capacitance and resistance were recorded at each frequency increment and then Capacitance vs. Frequency and Resistance vs. Frequency graphs were created for each cylinder with the exception of Cylinder #1 which was subjected to compression testing before a frequency sweep was conducted. For each cylinder, the three highest frequency increments – 20 MHz, 25 MHz, and 30 MHz – showed an “Unbalanced” message for both the capacitance and resistance on the LCR meter’s display screen, so there were no measurements taken at these frequencies. Using these graphs, such as the ones displayed for Cylinder #2 in Figure 4.1, were analyzed for any trends could show correlation to the nanoFe<sub>2</sub>O<sub>3</sub> content, water-cement ratio, or curing time.

One method of analyzing the data included examining tangent lines of each graph. Initial and final tangent lines were developed for each graph, and the frequency at which the two lines intersected was recorded in a table. Equations for the initial tangent line and the final tangent line were developed in Microsoft Excel and solved simultaneously in order to determine the point of intersection.

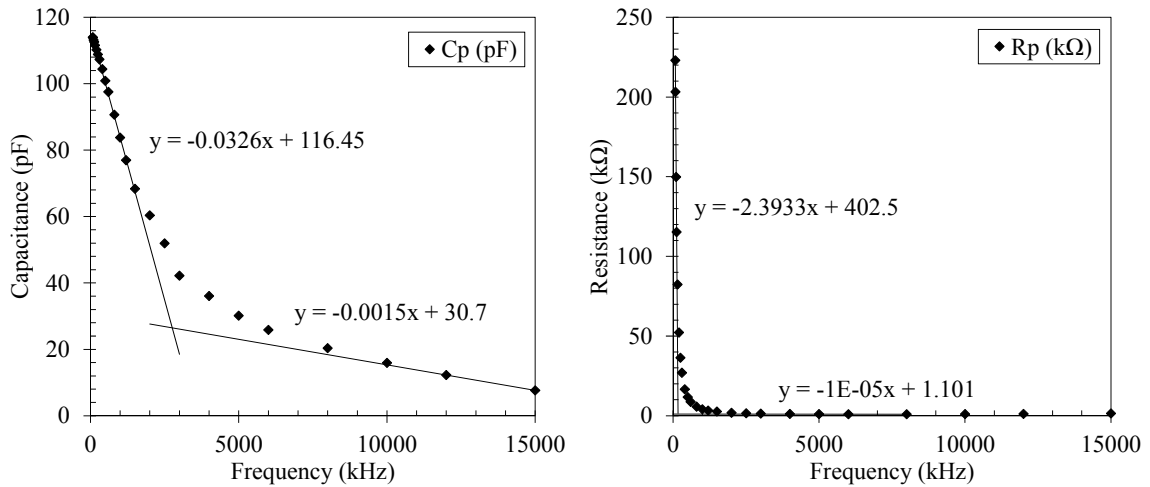


**Figure 4.1: Capacity vs. Frequency (left) and Resistance vs. Frequency (right) graphs for Cylinder #2.**

In the case of the Capacitance vs. Frequency graph for Cylinder #2, the intersecting frequency was calculated to be

$$-0.0326x + 116.45 = -0.0015x + 30.7 \rightarrow 0.0311x = 85.75 \rightarrow x = 2757.23 \text{ kHz}$$

Likewise, the intersecting frequency for the Resistance vs. Frequency graph was calculated to be

$$-2.3933x + 402.5 = -1 \cdot 10^{-5}x + 1.101 \rightarrow 2.39329x = 401.399 \rightarrow x = 167.72 \text{ kHz}$$

This method was reproduced for each cylinder and the final results were compiled in Table B.1 in Appendix B. After the tangent line frequency intersections were compiled for both the capacitance and resistance, the samples were sorted by both nanoFe<sub>2</sub>O<sub>3</sub> content and water-cement ratio and varied with curing time. Graphs of Capacitance Tangent Intersection vs. Curing Time and Resistance Tangent Intersection vs. Curing Time were created for each of the five nanoFe<sub>2</sub>O<sub>3</sub> contents and four water-cement ratios. Figure 4.2 presents the Resistance Tangent Intersection vs. Curing Time sorted data for all of the

cylinders with 5 percent nanoFe<sub>2</sub>O<sub>3</sub> and highlights some data inconsistencies that were discovered using this approach.

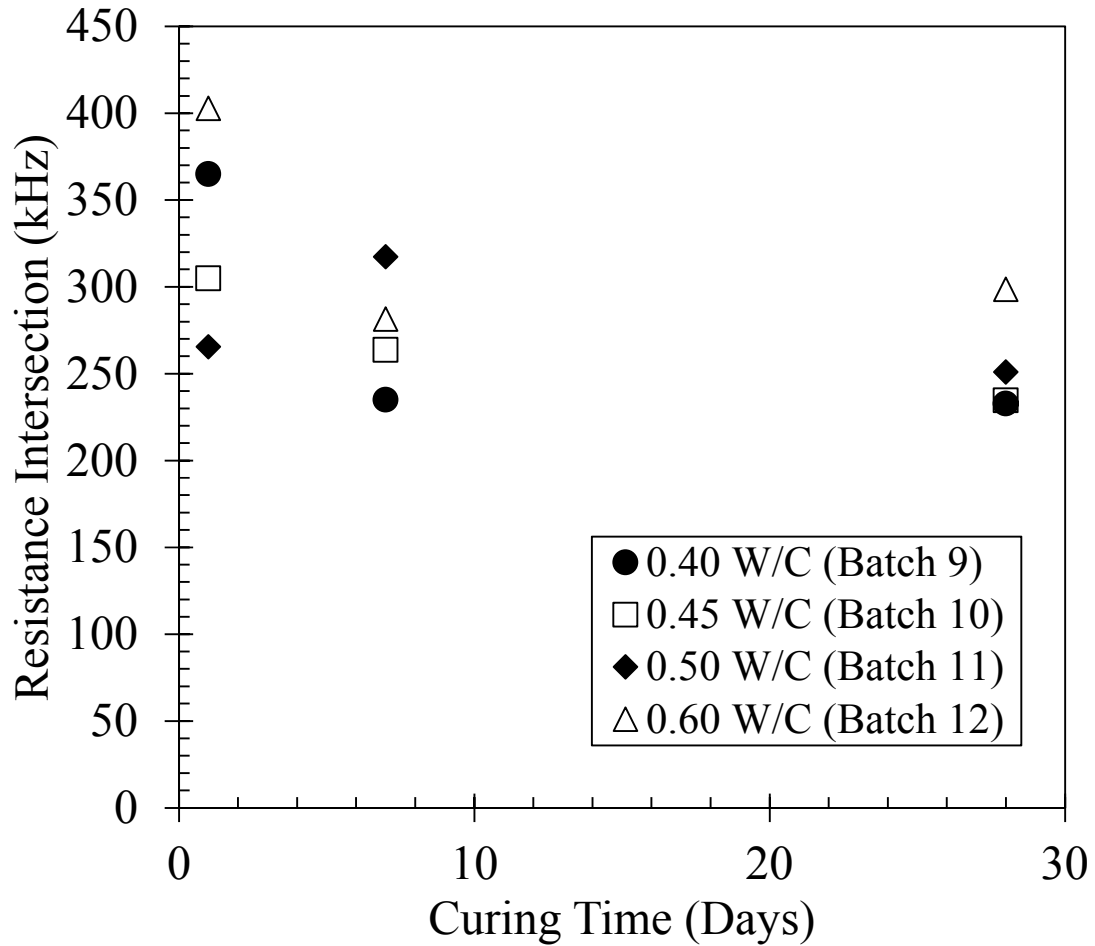


**Figure 4.2: Resistance Tangent Intersection vs. Curing Time for 5 percent NanoFe<sub>2</sub>O<sub>3</sub>.**

No apparent trends were discovered using the tangent line approach. From visual observation of Figure 4.2, it appears that there was no correlation between the resistance tangent intersection frequencies for 5 percent nanoFe<sub>2</sub>O<sub>3</sub> when sorted by water-cement ratio. For 1 day and 28 day curing times, the 0.60 water-cement ratio batch tangent lines intersected at a higher frequency than the other water-cement ratio batches. However, the 7 day curing data showed that the 0.50 water-cement ratio had the highest intersection frequency of all of the batches. Similar inconsistencies were found in most of the other sorted graphs. Additionally, based on observation of other tangent line intersection graphs, it was determined that the curing time had no effect on the tangent line intersection

frequency. The other tangent intersection graphs for capacitance and resistance are included in Appendix B. It was concluded that the tangent line intersection approach did not produce any consistent results and therefore no further judgments were made from these sorted tangent line intersection values or graphs.

In addition to taking a qualitative approach with the tangent line data, a qualitative observation of the Capacitance vs. Frequency and Resistance vs. Frequency graphs was performed. The intent was to determine on a batch-by-batch basis if the shapes of the graphs and values of capacitance and resistance varied by sample curing time as shown in Figures 4.3 and 4.4, respectively.

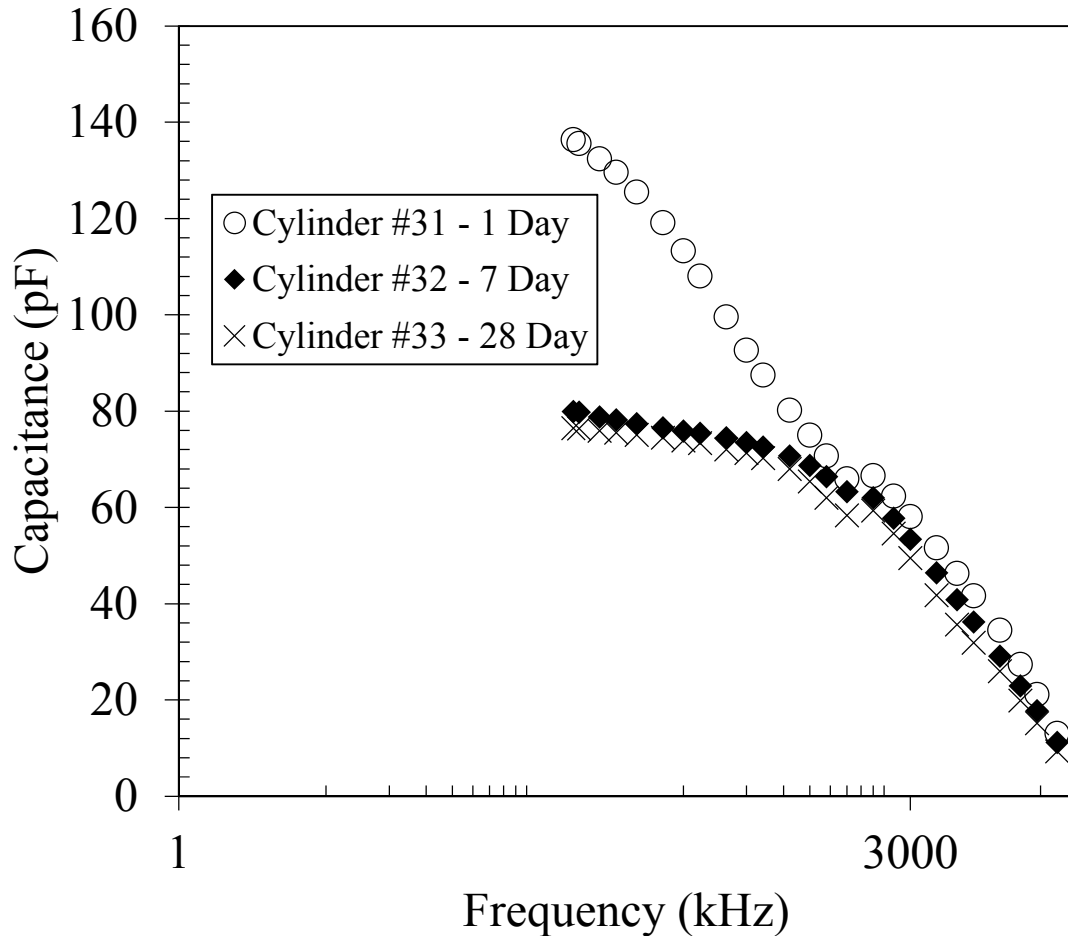


**Figure 4.3: Capacitance vs. Frequency Graph for Batch #11 (Cylinder #31-33).**

Upon visual observation of the Capacitance vs. Frequency in Figure 4.3, it can be seen that the three samples follow the same general curvature. For each frequency increment, it was

observed that the longer the sample's curing time, the lower the measured capacitance. Additionally, the capacitance readings between the three samples began to converge at higher frequencies.

The Resistance vs. Frequency graphs such as the one displayed in Figure 4.4 also demonstrated some qualitative trends. It was observed that samples with longer curing times had higher resistances measured at the same frequency increments. Like the capacitance, resistance values began to converge at higher frequencies. These trends were evident for other batches as well.

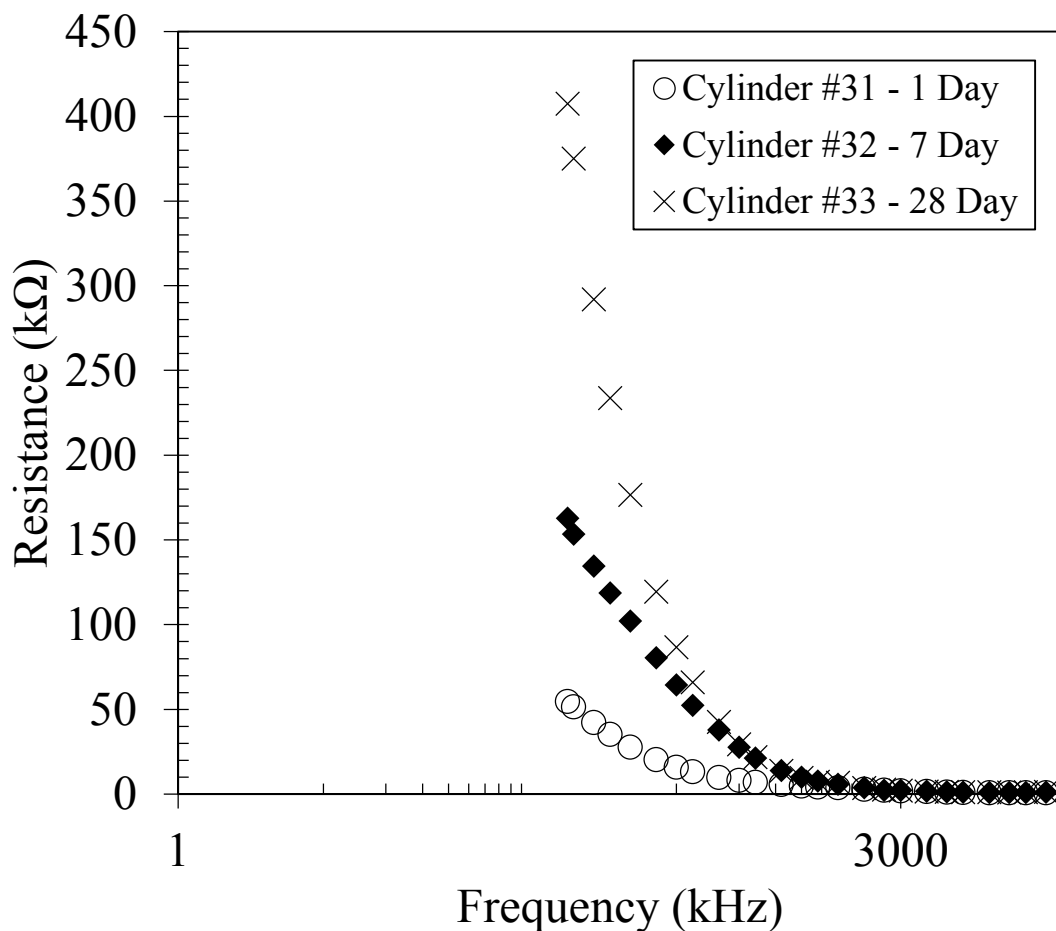


**Figure 4.4: Capacitance vs. Frequency Graph for Batch #11 (Cylinder #31-33).**

There was a reasonable explanation for the higher resistances measured for samples with longer curing times. The curing process functions to hydrate the concrete samples and as a result this increases the compressive strength, hardness, and density of the cylinder.



Additionally, porosity continues to decrease as the bonds between cement particles increase to pull them closer together. Therefore, cylinders that have been cured for 28 days will be harder and denser than cylinders with 1 day or 7 days of curing. The decrease in void space along with the close proximity of the cement particles makes it much more difficult for electrons to freely flow through the denser cylinders. Thus, the cylinders subjected to longer curing durations should have higher recorded resistance values than those with shorter curing times.

Another notable observation was made from the Capacitance vs. Frequency graphs. Generally for each cylinder, the capacitance decreased with each increasing frequency increment. However, many of the cylinders experienced a slight increase in capacitance at 2000 Hz. This phenomenon can be seen for all three of the cylinders in Figure 4.3 as well as many other batch Capacity vs. Frequency graphs which can be viewed in Appendix B. This could be due to either the equipment setup or the material properties of the composite. However, further capacitance analysis was not included in the scope of this research.

## **4.2 Resistivity Index Testing Analysis**

Resistivity index testing was conducted according to the procedure described in Chapter 3.4.2 for each of the 20 separate batches. Resistances were recorded at various times during curing and were converted to resistivity values using Equation 3.5. The resistivity index mold height, after subtracting out the indentations, was calculated to be 22.225 mm. A graph of resistivity vs. time was produced for each sample, and the minimum resistivity and the 24-hour resistivity were used to calculate  $RI_{24hr}$  using equation 3.6. The resistivity index testing values for each sample were arranged into Table C.1 in Appendix C.

The resistivity of each batch sample with relation to curing time was plotted in the graphs displayed in Appendix C. Every batch sample Resistivity vs. Curing Time graph, such as the one presented in Figure 4.5, resembled the same behavior of the 1 day resistivity test performed in Vipulanandan and Mohammed (2015). It was observed that the resistivity initially increased with time, or in some instances decreased slightly before beginning to increase, for the first 2.5 to 3 hours of curing. After approximately 3 hours of curing, the resistivity would begin to increase at a faster rate. The rate of resistivity change would

remain approximately constant from here up to the final 24 hour curing time. This general behavior was observed for every sample.

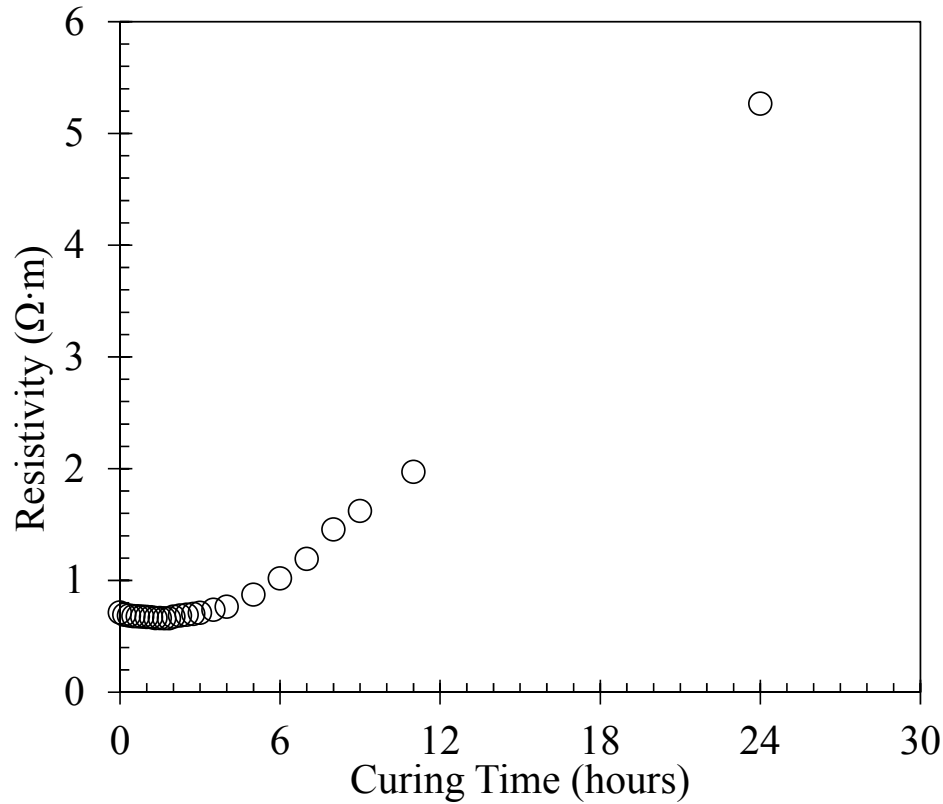


**Figure 4.5: Resistivity vs. Curing Time Behavior for Batch 2 Sample over 24 Hours.**

In addition to the qualitative resistivity vs. time behavioral analysis, a quantitative approach was conducted to understand the effect of the nanoFe<sub>2</sub>O<sub>3</sub> content or water-cement ratio parameters on the measured  $\rho_{\min}$ ,  $\rho_{24}$ , and  $RI_{24hr}$  values. Batch samples were sorted by nanoFe<sub>2</sub>O<sub>3</sub> content and water-cement ratio. Graphs of  $RI_{24}$  vs. Water-Cement Ratio, Figure 4.6, and  $RI_{24}$  vs. NanoFe<sub>2</sub>O<sub>3</sub> Content, Figure 4.7, which included data from all 20 batch samples were developed.

During the testing of the Batch 9 and 17 cylinders (both 0.40 water-cement ratios), swelling of the samples caused the top copper electrode to rise on the mold. It was estimated that air pockets underneath the top electrode may have lowered the resistance measurements. To be conservative, one-third of the electrode surface was estimated to have lost contact with the sample. Therefore, the recorded  $\rho_{24}$  value was multiplied by 1.5 to account for the lost electrode area for both of these batch samples.

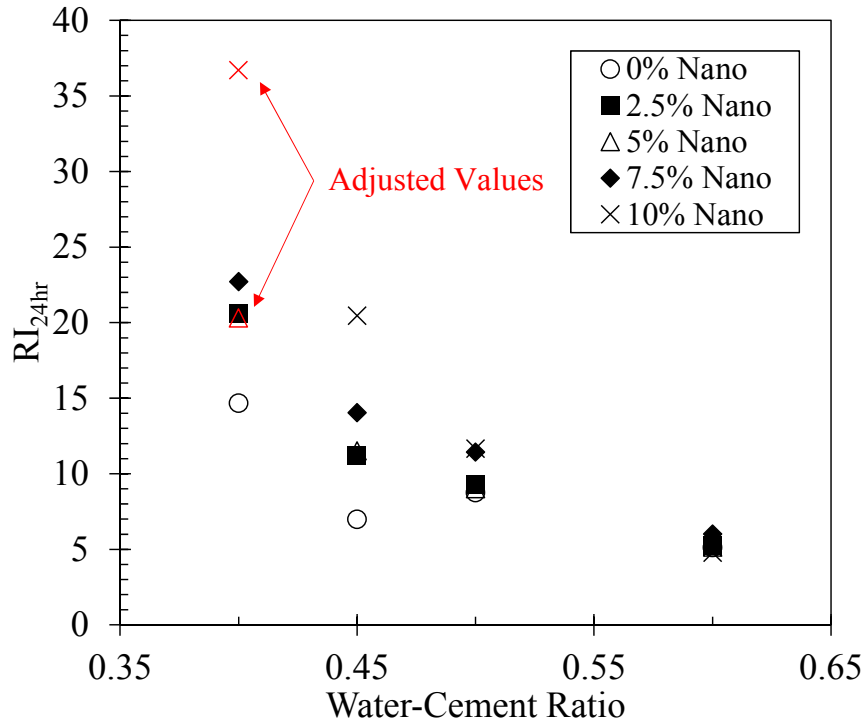


Figure 4.6:  $RI_{24hr}$  vs. Water-Cement Ratio

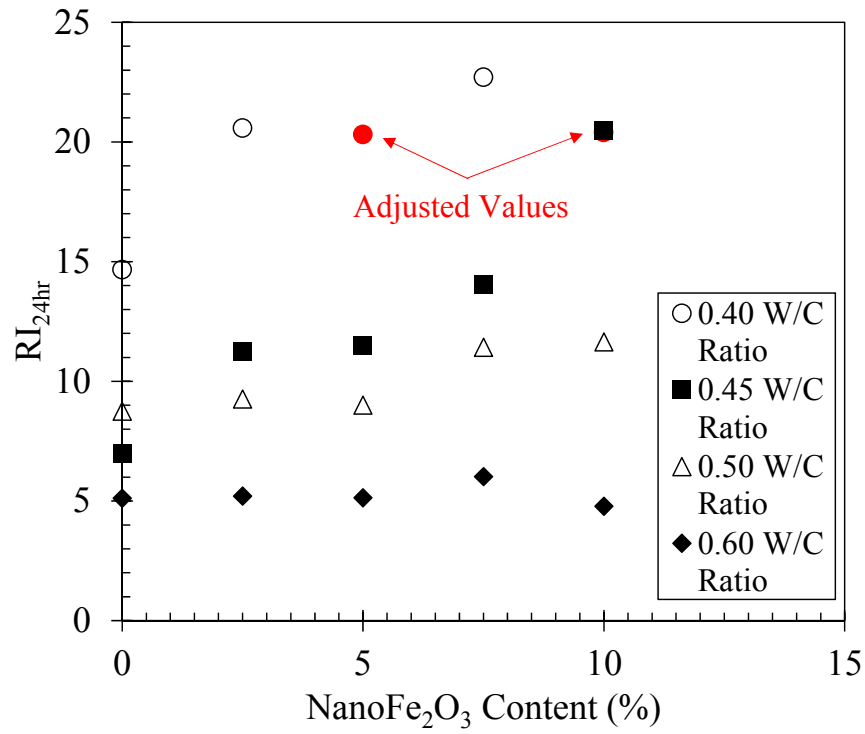


Figure 4.7:  $RI_{24hr}$  vs. Nano $Fe_2O_3$  Content

Figure 4.6 was used to examine the effects of the nanoFe<sub>2</sub>O<sub>3</sub> content on the resistivity index by sorting the batch samples by water cement ratio. Using this graph, trends for both the nanoFe<sub>2</sub>O<sub>3</sub> content and the water-cement ratio were observed. In general, the higher nanoFe<sub>2</sub>O<sub>3</sub> content samples had higher resistivity indices for each water-cement ratio. Additionally, the graph illustrated that the water-cement ratio and the resistivity index were inversely correlated. This trend is also highlighted in the RI<sub>24hr</sub> vs. NanoFe<sub>2</sub>O<sub>3</sub> Content graph in Figure 4.7. After the samples were sorted by nanoFe<sub>2</sub>O<sub>3</sub>, it was observed that the higher water-cement ratio mixes had lower resistivity indices. Furthermore, the resistivity index trends with respect to nanoFe<sub>2</sub>O<sub>3</sub> content were observed for each water-cement ratio. The resistivity index for 0.60 water-cement ratio samples remained approximately constant as nanoFe<sub>2</sub>O<sub>3</sub> content increased, while the resistivity indices increased slightly with increasing water-cement ratio for the remaining samples. Although Figure 4.7 did show that altering the  $\rho_{24}$  value allowed the 0.40 water-cement ratio samples to follow the trend of the other samples, future research should be conducted to confirm these findings.

After the samples had been analyzed on an individual level, the  $\rho_{min}$ ,  $\rho_{24}$ , and RI<sub>24hr</sub> values of each sorted nanoFe<sub>2</sub>O<sub>3</sub> content and water-cement ratio group were averaged and recorded in Tables 4.3 and 4.4, respectively.

**Table 4.3: Average RI Testing Values for Samples Sorted by NanoFe<sub>2</sub>O<sub>3</sub> Content.**

NanoFe <sub>2</sub> O <sub>3</sub> Content (%)	$\rho_{min}$ ( $\Omega \cdot m$ )	$\rho_{24}$ ( $\Omega \cdot m$ )	RI <sub>24hr</sub>
0	0.693	6.873	8.874
2.5	0.697	8.738	11.566
5	0.698	8.739	11.489
7.5	0.700	10.236	13.544
10	0.754	11.613	18.396

**Table 4.4: Average RI Testing Values for Samples Sorted by Water-Cement Ratio.**

Water-Cement Ratio	$\rho_{min}$ ( $\Omega \cdot m$ )	$\rho_{24}$ ( $\Omega \cdot m$ )	RI <sub>24hr</sub>
0.40	0.709	14.693	19.727
0.45	0.711	10.027	12.839
0.50	0.708	7.824	10.019
0.60	0.707	4.414	5.248

From Table 4.3, the average of the minimum resistivity values increased slightly with increasing nanoFe<sub>2</sub>O<sub>3</sub>, with the 10 percent nanoFe<sub>2</sub>O<sub>3</sub> content appearing to be a slight outlier. Likewise, the 24-hour resistivity values increased as the nanoFe<sub>2</sub>O<sub>3</sub> content increased, resulting in a directly proportional relationship between the nanoFe<sub>2</sub>O<sub>3</sub> content and the resistivity index. Conversely, Table 4.4 revealed an inverse correlation between the water-cement ratio and the resistivity index. The differences between the average  $\rho_{\min}$  values for the samples was negligible, but the average  $\rho_{24}$  values demonstrated an almost linear decrease with respect to water-cement ratio. As a result, the average RI<sub>24hr</sub> values decreased almost linearly with increasing water-cement ratio.

There is a logical explanation for the inverse relationship between the water-cement ratio and the resistivity index of each sample. Due to the higher proportion of water in the mixes with higher water-cement ratios, the samples take a longer time to harden and densify as the water-cement ratio increases. Therefore, extra water in the samples will prolong solidification and result in a lower resistance measurement after 24 hours. This leads to a lower calculated  $\rho_{24}$  value and, as a result, the final resistivity index will decrease accordingly.

### **4.3 Stress-Strain Predictive Model Analysis**

After compression testing was conducted on each cylinder in accordance with Chapter 3.6, the Vipulanandan and Mohammed and Ezeldin and Balaguru models were used to predict the measured stress-strain data. The tangent modulus, secant modulus, peak stress, and peak strain were recorded and compiled in Table D.2. The Vipulanandan and Mohammed  $p$  and  $q$  and the Ezeldin and Balaguru  $\beta$  values were recorded in Tables D.3 and D.4, respectively.

#### **4.3.1 Comparison of Accuracy of Stress-Strain Predictive Models**

The first method of analysis used was a comparison of the accuracy between the two models on predicting the measured stress-strain data of each individual cylinder. Through examination of the coefficient of determination values of both the Vipulanandan and Mohammed and Ezeldin and Balaguru models, it was found that both models effectively predicted the stress-strain behavior of the cylinders. A large majority of the coefficient of

determination values were above 0.95, indicating very strong predictive capabilities up to the peak stress in the data. Two cylinders had coefficient of determination values below 0.90 for the Vipulanandan and Mohammed predictive model, while three of the Ezeldin and Balaguru values were below 0.90, as displayed in Figure 4.8.

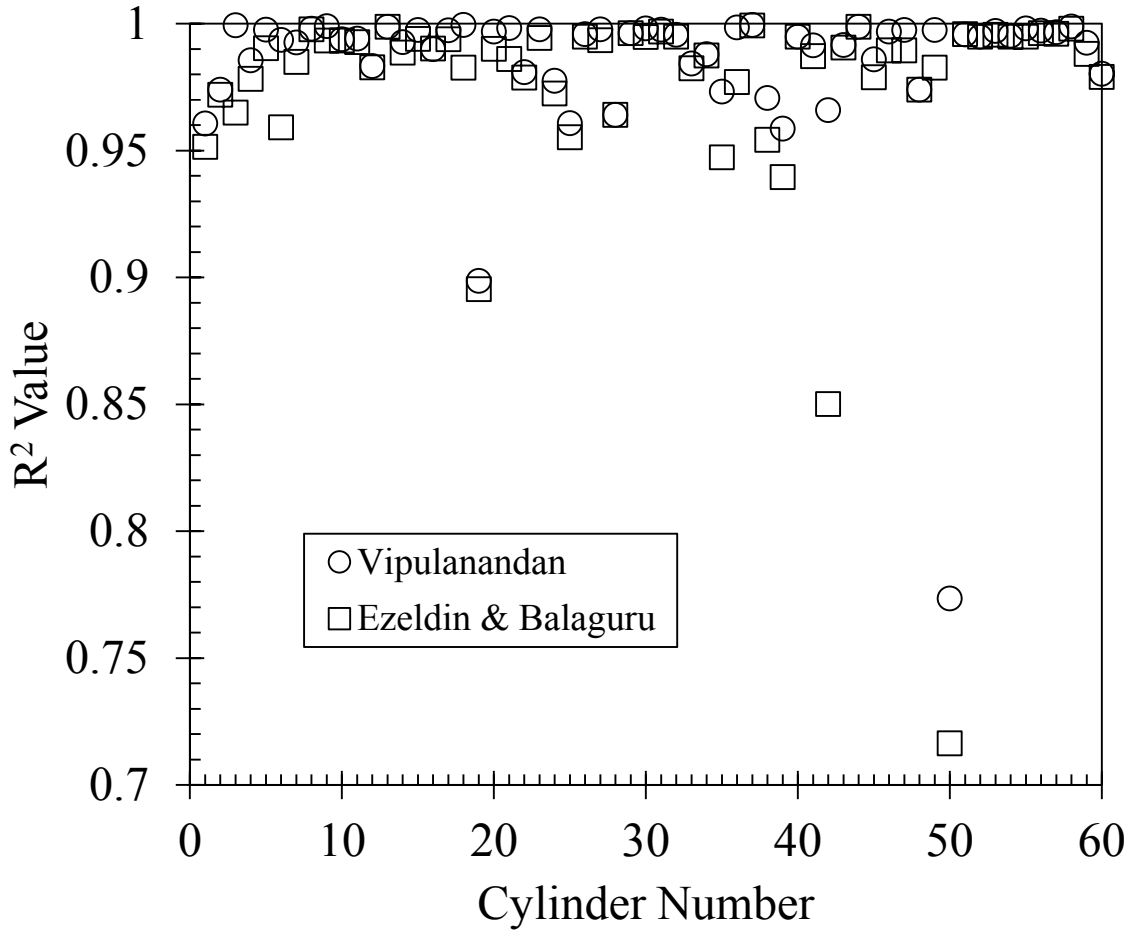


**Figure 4.8: Comparison of Vipulanandan and Mohammed vs. Ezeldin and Balaguru prediction accuracy based on  $R^2$  values.**

From Figure 4.8, it was determined that the accuracy of the Vipulanandan and Mohammed model was slightly higher than that of the Ezeldin and Balaguru model for predicting stress-strain behavior. This could potentially be due to the fact that the Vipulanandan and Mohammed model utilizes more parameters. While both models require the peak stress and strain and an iterated parameter (Vipulanandan and Mohammed  $p$  and Ezeldin and Balaguru  $\beta$ ), the Vipulanandan and Mohammed model also accounts for the tangent and secant modulus to shape the predictive model's curvature.

#### 4.3.2 Effects of Parameters on Stress-Strain Predictive Models

Figure 4.9 demonstrates how varying the Vipulanandan and Mohammed  $q$  parameter alters the curvature of the predictive model for Cylinder #59. The actual predictive parameter values for the test were 0.9120 and 0.7444 for  $p$  and  $q$ , respectively.

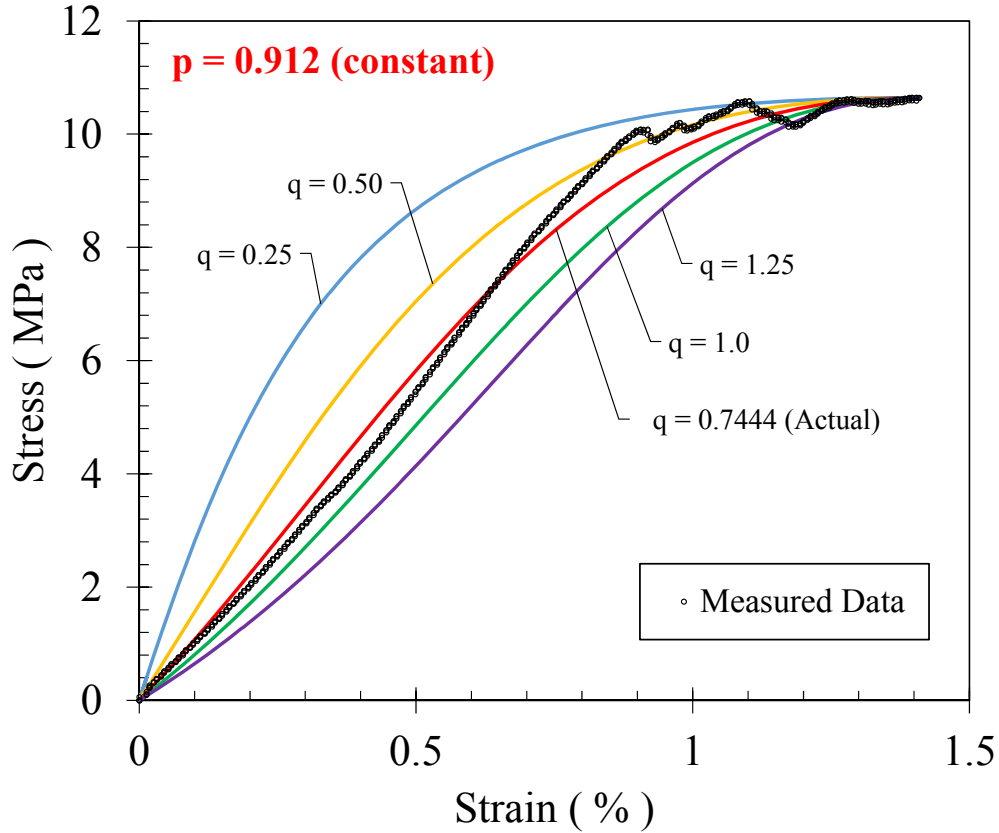


**Figure 4.9: Effect of Vipulanandan and Mohammed  $q$  parameter value on stress-strain predictive model with constant  $p$  value.**

Because the  $q$  parameter is the ratio of the secant modulus to the tangent modulus, a low value for  $q$  will create a graph with a steep initial slope before flattening out. A  $q$  value of 1.0 signifies that the tangent modulus and secant modulus are equal. Thus, that graph will have minimum curvature and will appear almost linear at the middle portion of the data. Graphs with  $q$  values greater than 1.0 will possess an initial upward concavity. In this manner, it is possible to obtain an adequate  $q$  value solely by visual observation of the tangent modulus and secant modulus.

Figure 4.10 displays the effects of the  $p$  value on the predictive model. Lower values of  $p$  produce an almost linear predictive model, while higher values allow for a greater amount of curvature in the model.

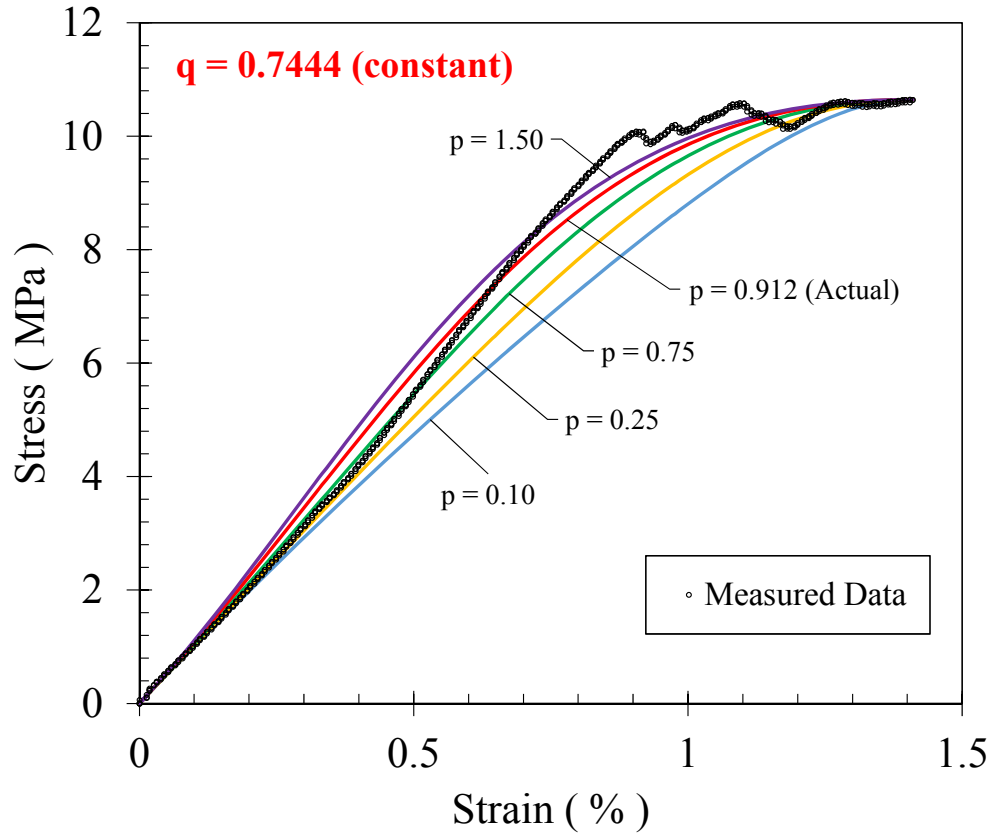


**Figure 4.10: Effect of Vipulanandan and Mohammed  $p$  parameter value on stress-strain predictive model with constant  $q$  value.**

The effect of the Ezeldin and Balaguru  $\beta$  parameter was also analyzed, as shown in Figure 4.11. Low  $\beta$  values create a predictive model similar to that of the Vipulanandan and Mohammed model with a low  $q$  value. Conversely, high  $\beta$  values produced a linear graph from 0 stress to peak stress. It was found that the Ezeldin and Balaguru formula was unable to predict a generally concave upwards set of data such as the stress-resistivity data that will be discussed in Chapter 4.4.



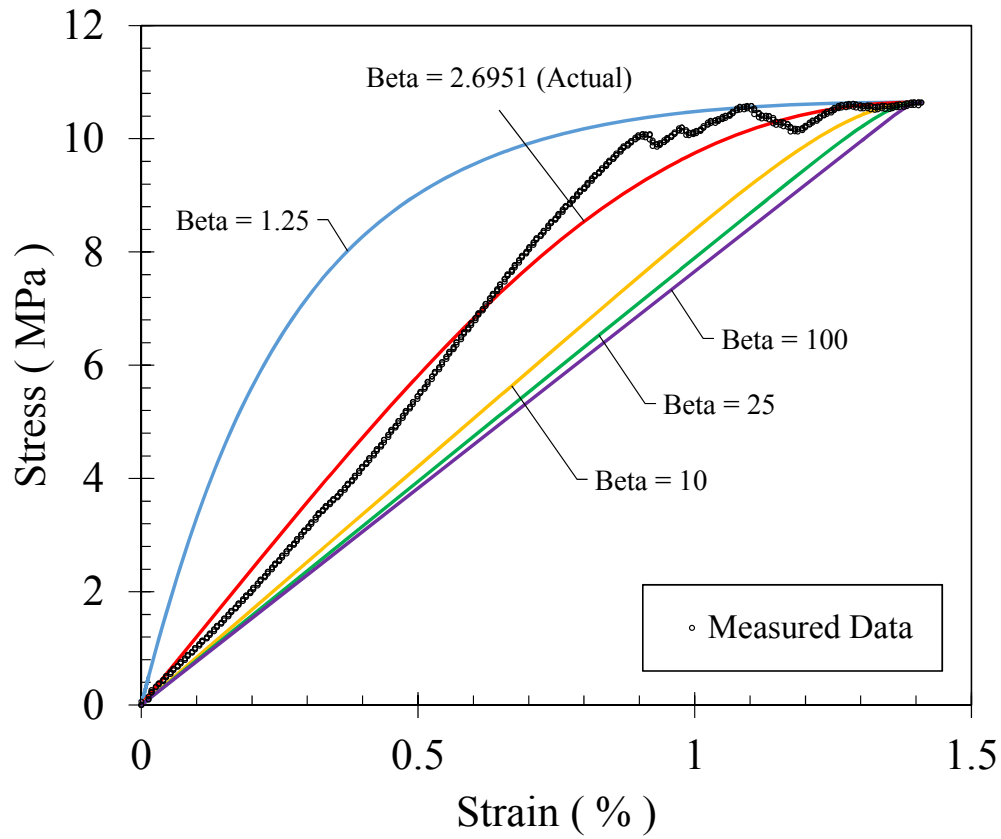


**Figure 4.11: Effect of  $\beta$  parameter value on Ezeldin and Balaguru stress-strain predictive model.**

From the graph and through experimentation with the model, it was discovered that raising the  $\beta$  value above 100 had very little effect on the predictive model. Therefore, it was decided that the Ezeldin and Balaguru model would be incapable of predicting the stress-resistivity data which possessed an upward concavity.

#### 4.3.3 Analysis of Stress-Strain Values Sorted by Mix Design Parameters

Additional analysis of the stress-strain parameters was performed for each cylinder. The tangent modulus, secant modulus, peak stress, peak strain,  $p$ ,  $q$ , and  $\beta$  values were sorted by the mix design parameters – water-cement ratio, nanoFe<sub>2</sub>O<sub>3</sub> content, and curing time – before being analyzed for potential correlations.

Figure 4.12 demonstrates one example of a stress-strain parameter (tangent modulus) that is sorted by a mix design parameter (curing time).

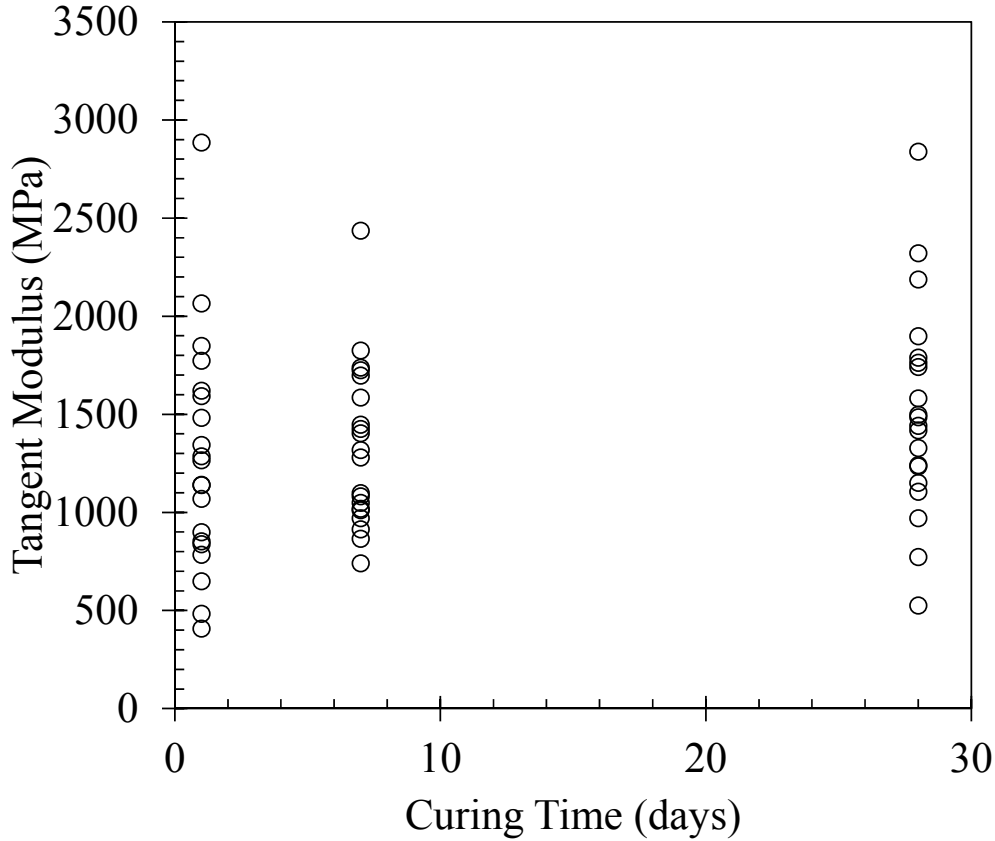


**Figure 4.12: Tangent modulus sorted by curing time for individual cylinders.**

From the graph in Figure 4.12 along with all of the other sorted graphs, it was evident that the distribution of individual cylinder data was too large. Therefore, averages were taken of each of the stress-strain model parameters after they were sorted by the mix design parameters before further analysis was conducted.

The stress-strain model parameters were averaged and sorted by each of the mix design parameters. From these graphs, displayed in Appendix D, correlations were observed. Both the tangent modulus and secant modulus increased as curing time increased due to cylinders with longer curing times having higher strength. As a result, the Vipulanandan  $q$  value also increased with increasing curing time. The Vipulanandan  $p$  value was observed to decrease almost linearly with respect to curing time. The Ezeldin and Balaguru  $\beta$  value showed no correlation when sorted by any of the mix design parameters. When sorted by water-cement ratio, both the tangent modulus and secant modulus decreased predictably due to the decreased compressive strength of the cylinders with higher water-

cement ratios. The average  $p$  values were very similar across all water-cement ratios with the exception of the 0.60 water-cement ratio average value. Likewise, the average  $q$  values were very close in value, with the 0.45 water-cement ratio behaving as a slight outlier. The effects of the nanoFe<sub>2</sub>O<sub>3</sub> content on the stress-strain parameter values were more difficult to interpret as there were more outliers. Both the tangent modulus and peak stress generally increased with increasing nanoFe<sub>2</sub>O<sub>3</sub> content, signifying that the nanoFe<sub>2</sub>O<sub>3</sub> may have slightly increased the compressive strength of the cylinders. However, a trend for the secant modulus and peak strain based on the nanoFe<sub>2</sub>O<sub>3</sub> content could not be established. The  $p$  and  $q$  values were likely affected because of the inconsistencies in these average parameter values. The average  $p$  values, when sorted by nanoFe<sub>2</sub>O<sub>3</sub> content, increased as the nanoFe<sub>2</sub>O<sub>3</sub> content increased. The average  $p$  value for the 2.5 percent nanoFe<sub>2</sub>O<sub>3</sub> was visually observed to be a major outlier, while the average  $p$  value for the 7.5 percent nanoFe<sub>2</sub>O<sub>3</sub> was determined to be a minor outlier. Inconsistencies in the peak strain occurred at these same two nanoFe<sub>2</sub>O<sub>3</sub> contents as well. Unlike the  $p$  values, the  $q$  values sorted by nanoFe<sub>2</sub>O<sub>3</sub> experienced a decrease as the nanoFe<sub>2</sub>O<sub>3</sub> content increased with only a minor outlier observed at 7.5 percent nanoFe<sub>2</sub>O<sub>3</sub>.

Based on the analysis of the stress-strain predictive models, the Vipulanandan and Mohammed model was slightly better than the Ezeldin and Balaguru model for the data for multiple reasons. Firstly, the Vipulanandan and Mohammed model accuracy was better than that of the Ezeldin and Balaguru model. Additionally, while Vipulanandan and Mohammed  $p$  and  $q$  parameters showed trends when sorted by mix design parameters, no trends were observed for the Ezeldin and Balaguru  $\beta$  parameter.

#### **4.4 Stress-Resistivity Predictive Model Analysis**

It was determined in Chapter 4.3 that the Ezeldin and Balaguru formula would not be capable of predicting the upwardly concave stress-resistivity data. Therefore, only the Vipulanandan and Mohammed model was used to analyze the electrical testing results.

Overall, the Vipulanandan and Mohammed formula for predicting the stress based on electrical properties was more slightly accurate than the formula for predicting stress-strain behavior. The stress-strain and stress-resistivity average of  $R^2$  values of the 60 cylinders

was 0.985 and 0.986, respectively. The average  $e^2$  values of the stress-strain and stress-resistivity predictive behavior was 0.914 and 0.015 respectively, indicating that both formulas were very effective at performing predictive tasks.

#### **4.4.1 Effects of Parameters on Stress-Resistivity Predictive Model**

The effects of the stress-resistivity Vipulanandan and Mohammed  $p$  and  $q$  parameters were analyzed in the same manner that the stress-strain parameters were studied in Chapter 4.3.2. Analyzing the effects of the  $q$  and  $p$  parameters individually on the Vipulanandan and Mohammed stress-resistivity predictive model will assist in the creation of a new theoretical model by highlighting the graphical properties and limitations that each parameter contributes to the model.

From the shape of the stress-resistivity graphs, it was found that the resistance initially decreased rapidly before continuously decreasing at a slower rate up until peak stress. It is also important to note that the peak stress used in the stress-resistivity model may not match the peak stress value for the corresponding cylinder's stress-strain data because the electrical readings were recorded at specific increments rather than continuously. Due to inconsistencies in resistivity change after the peak stress, electrical readings recorded after achieving the peak stress were removed.

The method of altering one parameter while keeping the other parameter constant was utilized to observe the effects that each individual parameter had on the predictive model. As an example, the stress-resistivity behavior of Cylinder #21 was studied in which the final predictive parameter values were 4.618 for  $q$  and 1.846 for  $p$ . Figures 4.13 displays the effects of changing the  $q$  value while keeping  $p$  constant.

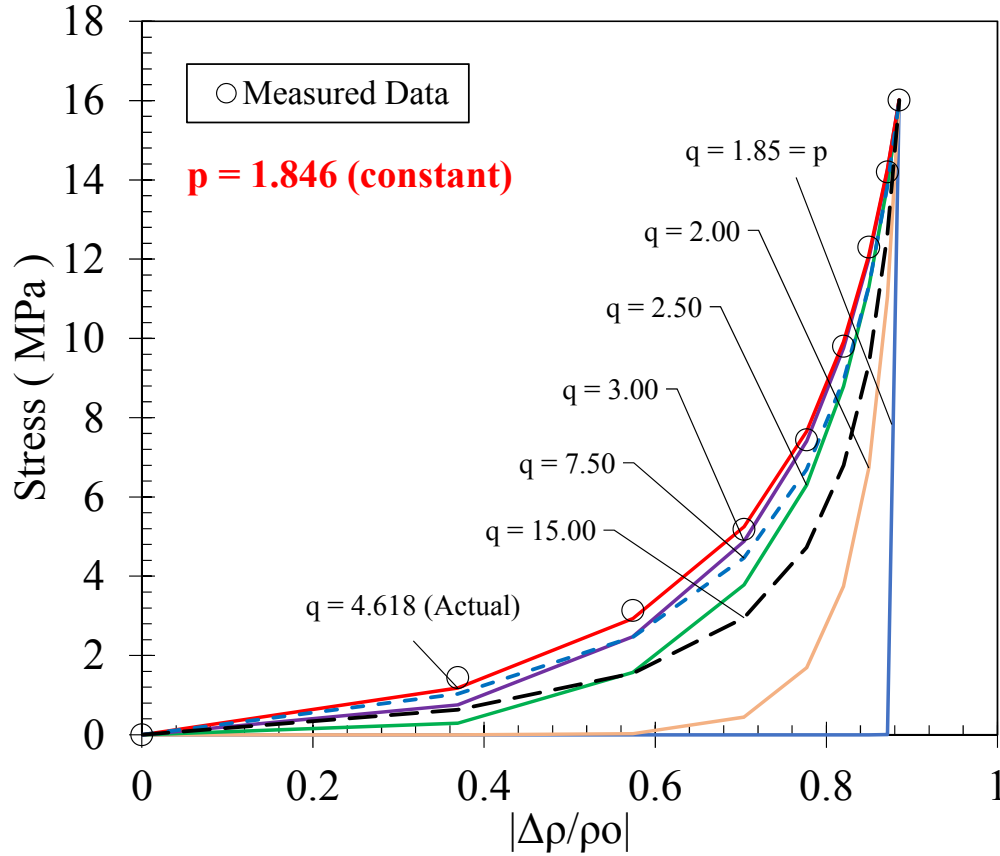


**Figure 4.13: Effect of Vipulanandan and Mohammed  $q$  parameter value on stress-resistivity model with constant  $p$  value for Cylinder #21.**

This graph, as well as every other stress-resistivity graph, possessed a greater secant modulus than tangent modulus. Therefore, each stress-resistivity  $q$  value must be greater than 1 due to the concave upwards curvature of these graphs. Upon altering the  $q$  value, it was determined that the  $q$  value must be greater than the  $p$  value in all cases. From Equation 3.14, setting  $q = p$  will cause a divide by zero error in an exponential denominator term, rendering the formula useless. Additionally, allowing the  $q$  to be less than the  $p$  will create negative stress predictive values. As the  $q$  value was steadily increased from 1.85 (approximately equal to  $p$ ) the predictive model got closer to the actual  $q$  value of 4.618. As  $q$  was increased past the optimum value, the predictive model rebounded further away from the optimized model.

The  $p$  parameter was also individually manipulated while keeping the  $q$  constant. Figure 4.14 illustrates the effect that the  $p$  parameter has on the predictive model while holding the  $q$  value constant.

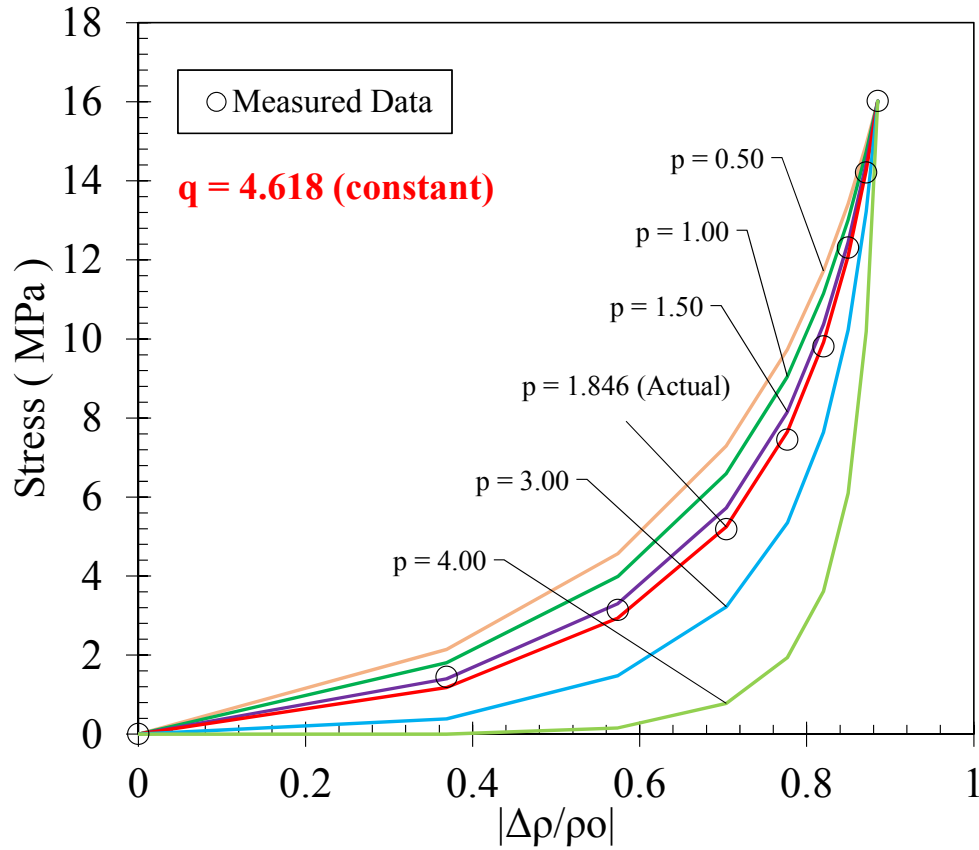


**Figure 4.14: Effect of Vipulanandan and Mohammed  $p$  parameter value on stress-resistivity model with constant  $q$  value for Cylinder #21.**

The effects of manipulating the  $p$  parameter were analyzed in Figure 4.14. By inputting different values of  $p$  into Equation 3.14 while holding all other terms constant, it was found that values of  $p$  below the optimized value increased the value of the denominator and thus overestimated the predicted stress values. Conversely, values of  $p$  above the optimum value decreased the denominator and resulted in an underestimation of the measured values. The  $p$  value was kept below the  $q$  value in order to avoid errors in Equation 3.14.

#### 4.4.2 Analysis of Stress-Resistivity Values Sorted by Mix Design Parameters

Similar to the stress-strain parameters, the distribution of the individual stress-resistivity parameters sorted by mix design parameters was too wide to derive any correlations. Thus, averages of the stress-resistivity parameters were taken after being sorted by the mix design parameters and then graphed in Appendix E.

Some expected correlations between the peak stress and the mix design parameters for the stress-resistivity graphs were observed. Higher nanoFe<sub>2</sub>O<sub>3</sub> contents provided slightly greater compressive strength to the cylinders. Likewise, longer curing times contributed to higher peak stresses, while higher water-cement ratios lowered the compressive strength of the cylinders. The secant moduli followed the same trends as the peak stress. The tangent moduli sorted by both nanoFe<sub>2</sub>O<sub>3</sub> content and water-cement ratio showed no correlation to the respective mix design parameters because there was too much variance in the initial change in resistivity values. The tangent modulus sorted by water-cement ratio was shown to have an inverse correlation, but this could likely be coincidence based on the reasoning for the nanoFe<sub>2</sub>O<sub>3</sub> content and water-cement ratio. When sorted by nanoFe<sub>2</sub>O<sub>3</sub> content, both the  $p$  and  $q$  average values increased with increasing nanoFe<sub>2</sub>O<sub>3</sub> content with only minor outliers in the average  $q$  values. The average  $p$  and  $q$  values appeared to decrease with increasing water-cement ratio, albeit with visible outliers. Lastly,  $q$  average values increased with increasing curing times and no discernible trend was discovered for the average  $p$  values sorted by curing time.

The effects of the individual Vipulanandan and Mohammed  $p$  and  $q$  parameters on the predictive model as well as the correlations between the stress-resistivity parameters and the mix design parameters were taken into account for the creation of a new predictive model.

#### **4.5 Proposal of New Model to Predict Stress-Electrical Response**

The goal of this research was not only to understand and interpret the correlations between the electrical response and the compressive stress on the cylinders, but to also develop a formula capable of predicting stress from resistivity based on the specific mix design of the individual cylinders. Extensive analysis was performed on two separate predictive formulas – (1) Vipulanandan and Mohammed and (2) Ezeldin and Balaguru – with the purpose of ultimately selecting one that could be modified for utilization as a predictive model for the collected data. After analysis of the capabilities and limitations of the two predictive formulas in Chapters 4.3 and 4.4, it was decided that the Vipulanandan and Mohammed model would be the most effective model to predict the stress-resistivity data and to serve as a starting point for a new empirical model.

From the scope of this research, it was decided that only one curing time should be used for creating the new model. The cylinders that were cured for 28 days were selected to develop the model because they would be most representative of an existing structure whose concrete had been cured for an extended amount of time.

Vipulanandan and Mohammed (2014) discussed a nonlinear model for predicting the stress-resistivity behavior based on the nanoFe<sub>2</sub>O<sub>3</sub> content and the curing time, as shown by the nonlinear power relationship in Equation 4.2:

$$\text{Parameter} = a \times (t)^b + c \times (t)^d \times (\text{NanoFe}_2\text{O}_3(\%))^e \quad (4.2)$$

where  $t$  is the curing time of the cylinder in days,  $\text{NanoFe}_2\text{O}_3$  is the content expressed in percentage by weight, and  $a$ ,  $b$ ,  $c$ ,  $d$ , and  $e$  are nonlinear model parameter values. Equation 4.2 would be used in order to determine the parameter values for  $\sigma_f$ ,  $|\Delta\rho/\rho_o|_f$ ,  $q$ , and  $p$  for the new predictive model. According to Vipulanandan and Mohammed (2014), multiple regression analysis using the least square method could be used on the measured stress-resistivity to obtain the nonlinear model parameter values for each of the four predictive model parameters. While this equation uses two out of the three mix design parameters, it does not account for the water-cement ratio of the mix. The effect of water-cement ratio has been analyzed in Chapter 4.4, and evaluation will be need to be conducted to determine the extent, if any, to which water-cement ratio affects the predictive model.

Initially, the nonlinear model parameter values found in Vipulanandan and Mohammed (2015) were used as starting point for the new predictive model to be created from. However, because the mix design used in that research differed from the mix designs used in this research, new nonlinear model parameter values would need to be developed.

First, a linear regression analysis of the 28-day curing data – 20 total cylinders – was conducted using Excel with a 95 percent confidence interval selected. Each of the four predictive model parameters  $\sigma_f$ ,  $|\Delta\rho/\rho_o|_f$ ,  $q$ , and  $p$  were considered the dependent variables while the curing time and nanoFe<sub>2</sub>O<sub>3</sub> content were representative of the independent variables. The data was sorted by water-cement ratio, thus dividing the data into four separate groups as shown in Table 4.5. Each group consisted of cylinders with the same water-cement ratio and curing time, but included all five nanoFe<sub>2</sub>O<sub>3</sub> contents.



**Table 4.5: 28-day curing time data to be used for new predictive model.**

Group	Batch	Cyl. #	NanoFe <sub>2</sub> O <sub>3</sub> (%)	Water-Cement	Curing Time (days)	Model Parameters			
						$\sigma_f$ (MPa)	$ \Delta\rho/\rho_o _f$	q	p
1	1	3	0	0.40	28	15.001	0.815	3.951	1.199
	5	15	2.5	0.40	28	15.201	0.811	3.813	1.303
	9	27	5	0.40	28	22.984	0.897	5.839	2.785
	13	39	7.5	0.40	28	27.368	0.920	6.088	3.755
	17	51	10	0.40	28	26.029	0.878	5.229	1.163
2	2	6	0	0.45	28	24.459	0.871	6.333	2.669
	6	18	2.5	0.45	28	16.233	0.883	4.204	1.698
	10	30	5	0.45	28	30.699	0.911	8.644	3.840
	14	42	7.5	0.45	28	12.367	0.911	4.437	3.326
	18	54	10	0.45	28	23.865	0.850	5.852	2.273
3	3	9	0	0.50	28	28.624	0.931	5.198	1.514
	7	21	2.5	0.50	28	16.011	0.885	4.618	1.846
	11	33	5	0.50	28	20.043	0.889	6.090	2.197
	15	45	7.5	0.50	28	16.087	0.810	4.065	2.130
	19	57	10	0.50	28	32.775	0.898	8.658	3.946
4	4	12	0	0.60	28	13.227	0.912	3.007	1.130
	8	24	2.5	0.60	28	15.585	0.864	5.096	2.629
	12	36	5	0.60	28	17.611	0.849	6.385	2.915
	16	48	7.5	0.60	28	14.839	0.880	5.403	2.681
	20	60	10	0.60	28	15.731	0.760	4.263	1.348

After performing the regression analysis on all four groups for each predictive model parameter, it was evident that the data was statistically insignificant. The standard deviations of the grouped data were too high, and the coefficient of determination values after regression analysis were too low to draw any conclusions. This was likely due to the fact that there were only five data points (different nanoFe<sub>2</sub>O<sub>3</sub> contents) for each group. An accurate regression analysis would require a much larger dataset which was outside of the research scope.

It was decided that Equation 4.2 would be used with the nonlinear model parameters  $a$ ,  $b$ ,  $c$ ,  $d$ , and  $e$  initially set to a value of 1. From there, each of the four predictive model parameters for each cylinder were predicted by using the GRG Nonlinear Solver function in Excel to simultaneously manipulate the nonlinear model parameter values to produce the value of the predictive model parameter. It is worth noting that using the Solver function provides only one of an infinite number of possible solutions. Therefore, it was imperative to start each of the cylinders with the same nonlinear model parameter values before running the Solver function. Table 4.6 shows the nonlinear model parameter values for the predictive model parameter  $\sigma_f$ .

**Table 4.6: Nonlinear model parameter values for determining  $\sigma_f$ .**

Water-Cement Ratio	NanoFe <sub>2</sub> O <sub>3</sub> (%)	a	b	c	d	e
0.40	0	0.716	0.039	1.000	1.000	1.000
	2.5	0.446	0.093	0.148	0.000	0.343
	5	0.519	0.018	0.294	0.011	0.077
	7.5	0.513	0.004	0.396	0.003	0.002
	10	0.402	0.004	0.461	0.004	0.003
0.45	0	0.724	0.056	1.000	1.000	1.000
	2.5	0.469	0.010	0.256	0.008	0.456
	5	0.521	0.022	0.296	0.013	0.078
	7.5	0.511	0.002	0.395	0.001	0.001
	10	0.241	0.000	0.457	0.058	0.040
0.50	0	0.731	0.073	1.000	1.000	1.000
	2.5	0.469	0.010	0.256	0.008	0.456
	5	0.518	0.016	0.293	0.010	0.076
	7.5	0.377	0.020	0.371	0.020	0.012
	10	0.404	0.007	0.464	0.009	0.006
0.60	0	0.729	0.067	1.000	1.000	1.000
	2.5	0.467	0.006	0.252	0.005	0.455
	5	0.512	0.006	0.286	0.004	0.073
	7.5	0.466	0.009	0.386	0.007	0.004
	10	0.226	0.000	0.443	0.038	0.026

It was observed that for all cases in which no nanoFe<sub>2</sub>O<sub>3</sub> was used, the values for  $c$ ,  $d$ , and  $e$  were 1 since a value of 0 percent for the nanoFe<sub>2</sub>O<sub>3</sub> content would cancel out the second half of Equation 4.2. The nonlinear model parameter values relating to the exponent on the curing time,  $b$  and  $d$ , were very low compared to the other values most likely because the curing time of 28 days was a high value to insert for  $t$ . The nonlinear model parameter  $a$ , a coefficient multiplier of the curing time, was the highest for the 0 percent nanoFe<sub>2</sub>O<sub>3</sub> content because the curing time was the only variable that had a role in calculating the  $\sigma_f$  value. Conversely, the value of  $c$ , a coefficient multiplier of the curing time in the second portion of Equation 4.2 increased with increasing nanoFe<sub>2</sub>O<sub>3</sub> content. The  $e$  value, dependent on the nanoFe<sub>2</sub>O<sub>3</sub> content, decreased with increasing curing time for the calculation of  $\sigma_f$ . Therefore, it was determined that with the exception of a few individual cases, the  $c$  and  $e$  values were inversely correlated for the calculation of  $\sigma_f$  in order to effectively balance the contribution of the second half of Equation 4.2 to the overall parameter value. A table displaying the nonlinear model parameter values for each of the predictive model parameters can be found in Appendix F.

In order to further interpret the results for each predictive model parameter, Equation 4.2 was divided into two parts, Equations 4.3 and 4.4:

$$\text{1st Half} = a \times (t)^b \quad (4.3)$$

$$\text{2nd Half} = c \times (t)^d \times (\text{NanoFe}_2\text{O}_3(\%))^e \quad (4.4)$$

By splitting Equation 4.1 into two separate equations, the relative contribution of the curing time and nanoFe<sub>2</sub>O<sub>3</sub> content to the overall parameter value could be analyzed. The first part of the nonlinear equation, Equation 4.3, was solely affected by the curing time, while Equation 4.4 was influenced by both the curing time and nanoFe<sub>2</sub>O<sub>3</sub> content. Calculations were performed on each individual cylinder to determine the percent contribution of Equations 4.3 and 4.4 to the total value of each of the predictive model parameters. The contribution percentages were then averaged by nanoFe<sub>2</sub>O<sub>3</sub> content, thus neglecting the effect of the water-cement ratio since it was not included in Equation 4.2. These contributions of Equations 4.3 and 4.4 to the overall predictive model parameter values are displayed in Table 4.7.

**Table 4.7: Average contributions of Equations 4.2 and 4.3 to overall parameter values.**

NanoFe <sub>2</sub> O <sub>3</sub> (%)	$\sigma_f$ (MPa)		$ \Delta\rho/\rho_o _f$		$q$		$p$	
	Average % Contribution		Average % Contribution		Average % Contribution		Average % Contribution	
	EQ. 4.2	EQ. 4.3	EQ. 4.2	EQ. 4.3	EQ. 4.2	EQ. 4.3	EQ. 4.2	EQ. 4.3
0	100.00%	0.00%	100.00%	0.00%	100.00%	0.00%	100.00%	0.00%
2.5	46.00%	54.00%	59.95%	40.05%	72.52%	27.48%	39.44%	60.56%
5	45.19%	54.81%	61.50%	38.50%	83.91%	16.09%	43.68%	56.32%
7.5	68.82%	31.18%	54.32%	45.68%	81.76%	18.24%	62.54%	37.46%
10	64.93%	35.07%	37.63%	62.37%	86.48%	13.52%	59.94%	40.06%

For the 0 percent nanoFe<sub>2</sub>O<sub>3</sub> case for each of the predictive model parameters, Equation 4.3 accounted for 100 percent of the overall parameter value since the nanoFe<sub>2</sub>O<sub>3</sub> content was negligible. For  $\sigma_f$ , it appeared that curing time actually played a greater role in the cylinders with the higher nanoFe<sub>2</sub>O<sub>3</sub> contents. The opposite was the case for  $|\Delta\rho/\rho_o|_f$ , where Equation 4.4 generally provided a larger contribution to the parameter value as the nanoFe<sub>2</sub>O<sub>3</sub> content increased. Since the  $|\Delta\rho/\rho_o|_f$  is an electrical property of the samples, it is plausible that more nanoFe<sub>2</sub>O<sub>3</sub> would have a greater effect on the overall parameter value. For the  $q$  value, it was evident that curing time had a greater influence than the nanoFe<sub>2</sub>O<sub>3</sub> content on the parameter value. This is logical because the  $q$  parameter is based on the tangent modulus and secant modulus of the cylinder, the latter of which is influenced by the peak stress of the cylinder. From the discussion in Chapter 4.4.2 and by visual observations of the graphs in Appendix E, it was evident that curing time influenced the peak stress more significantly than the nanoFe<sub>2</sub>O<sub>3</sub> content. Therefore, the effect of the curing time on the value of  $q$  will be greater than that of the nanoFe<sub>2</sub>O<sub>3</sub> content. Since the  $p$  parameter was an iterated value based on the other three parameters, it was difficult to make a definitive conclusion regarding the effect of the curing time and nanoFe<sub>2</sub>O<sub>3</sub> content on the overall  $p$  parameter value.

After analysis of the nonlinear model had been conducted for the 28-day cylinders, a resolution analysis was to be performed on two randomly selected cylinders from the dataset in order to confirm that the nonlinear model parameter values and Equations 4.2 and 3.14 could be used to predict the stress-resistivity behavior of those cylinders.

#### 4.6 Resolution Analysis of Proposed Model

Cylinder #36 and Cylinder #51 were randomly selected for a resolution analysis of the proposed model.

Cylinder #36 had a 28-day curing time, a 0.60 water-cement ratio, and a 5 percent weight of nanoFe<sub>2</sub>O<sub>3</sub> by weight of cement. The nonlinear model parameter values for each of the predictive model parameters were obtained from the tables in Appendix F and are shown in Table 4.8.

**Table 4.8: Proposed model values for Cylinder #36.**

	<b>a</b>	<b>b</b>	<b>c</b>	<b>d</b>	<b>e</b>
<b>σ<sub>f</sub> (MPa)</b>	0.941	0.800	0.763	0.207	0.616
<b> Δρ/ρ<sub>o</sub> <sub>f</sub></b>	0.512	0.006	0.286	0.004	0.073
<b>q</b>	1.195	0.457	0.533	0.000	0.332
<b>p</b>	0.702	0.039	0.699	0.085	0.512

Using Equation 4.2, the calculations for the predictive model parameters were made using 28 for *t* and 5 for *NanoFe<sub>2</sub>O<sub>3</sub>(%)*:

$$\sigma_f(\text{MPa}) = (0.941) \times (28)^{(0.800)} + (0.763) \times (28)^{(0.207)} \times (5)^{(0.616)} = 17.629 \text{ MPa}$$

$$|\Delta\rho/\rho_o|_f = (0.512) \times (28)^{(0.006)} + (0.286) \times (28)^{(0.004)} \times (5)^{(0.073)} = 0.848$$

$$q = (1.195) \times (28)^{(0.457)} + (0.533) \times (28)^{(0.000)} \times (5)^{(0.332)} = 6.389$$

$$p = (0.702) \times (28)^{(0.039)} + (0.699) \times (28)^{(0.085)} \times (5)^{(0.512)} = 2.915$$

These predictive model parameter values were inserted into Equation 3.14 to predict the stress on the cylinder from the measured electrical data. The results are displayed in Table 4.9 and a graphical display is shown in Figure 4.15.

**Table 4.9: Measured vs. Predicted data using proposed model for Cylinder #36.**

Measured Data		Prediction
Stress ( MPa )	$ \Delta\rho/\rho_o $	Stress ( MPa )
0.015	0.000	0.000
1.203	0.370	0.894
2.739	0.605	2.907
4.711	0.708	5.175
7.042	0.762	7.474
9.570	0.794	9.711
12.123	0.814	11.780
14.625	0.830	14.112
16.609	0.844	16.775
17.611	0.849	17.844

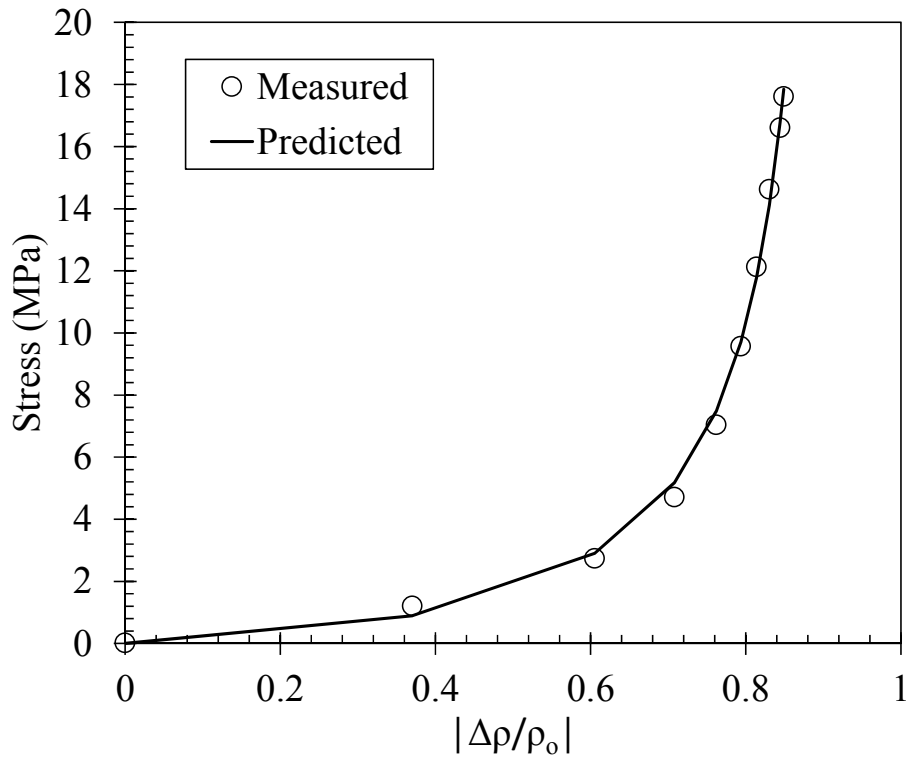


**Figure 4.15: Measured vs. Predicted data using proposed model for Cylinder #36.**

Using Equation 3.11, the coefficient of determination was calculated to be 0.997, indicating an excellent prediction of the measured data.

Cylinder #51 had the same 28-day curing time as well, but had a 0.40 water-cement ratio and a 10 percent nanoFe<sub>2</sub>O<sub>3</sub> content. The nonlinear model parameter values for each of the predictive model parameters were obtained from the tables in Appendix F and are shown in Table 4.10.

**Table 4.10: Proposed model values for Cylinder #51.**

	<b>a</b>	<b>b</b>	<b>c</b>	<b>d</b>	<b>e</b>
<b>σ<sub>f</sub> (MPa)</b>	0.980	0.932	0.761	0.202	0.449
<b> Δρ/ρ<sub>o</sub> <sub>f</sub></b>	0.402	0.004	0.461	0.004	0.003
<b>q</b>	0.914	0.472	0.594	0.000	0.139
<b>p</b>	0.605	0.012	0.507	0.010	0.007

Using Equation 4.2, the calculations for the predictive model parameters were made using 28 for *t* and 10 for *NanoFe<sub>2</sub>O<sub>3</sub>*(%):

$$\sigma_f(\text{MPa}) = (0.980) \times (28)^{(0.932)} + (0.761) \times (28)^{(0.202)} \times (10)^{(0.449)} = 26.071 \text{ MPa}$$

$$|\Delta\rho/\rho_o|_f = (0.402) \times (28)^{(0.004)} + (0.461) \times (28)^{(0.004)} \times (10)^{(0.003)} = 0.878$$

$$q = (0.914) \times (28)^{(0.472)} + (0.594) \times (28)^{(0.000)} \times (10)^{(0.139)} = 5.224$$

$$p = (0.605) \times (28)^{(0.012)} + (0.507) \times (28)^{(0.010)} \times (10)^{(0.007)} = 1.162$$

These predictive model parameter values were inserted into Equation 3.14 to predict the stress on the cylinder from the measured electrical data. The results are displayed in Table 4.11 and a graphical display is shown in Figure 4.16.

**Table 4.11: Measured vs. Predicted data using proposed model for Cylinder #51.**

Measured		Prediction
Stress ( MPa )	$ \Delta\rho/\rho_0 $	Stress ( MPa )
0.000	0.000	0.000
2.256	0.398	2.785
5.038	0.581	5.810
8.549	0.676	8.626
12.279	0.737	11.392
15.105	0.785	14.475
17.533	0.822	17.907
20.419	0.847	20.859
22.942	0.861	22.983
23.898	0.871	24.720
26.029	0.878	26.070

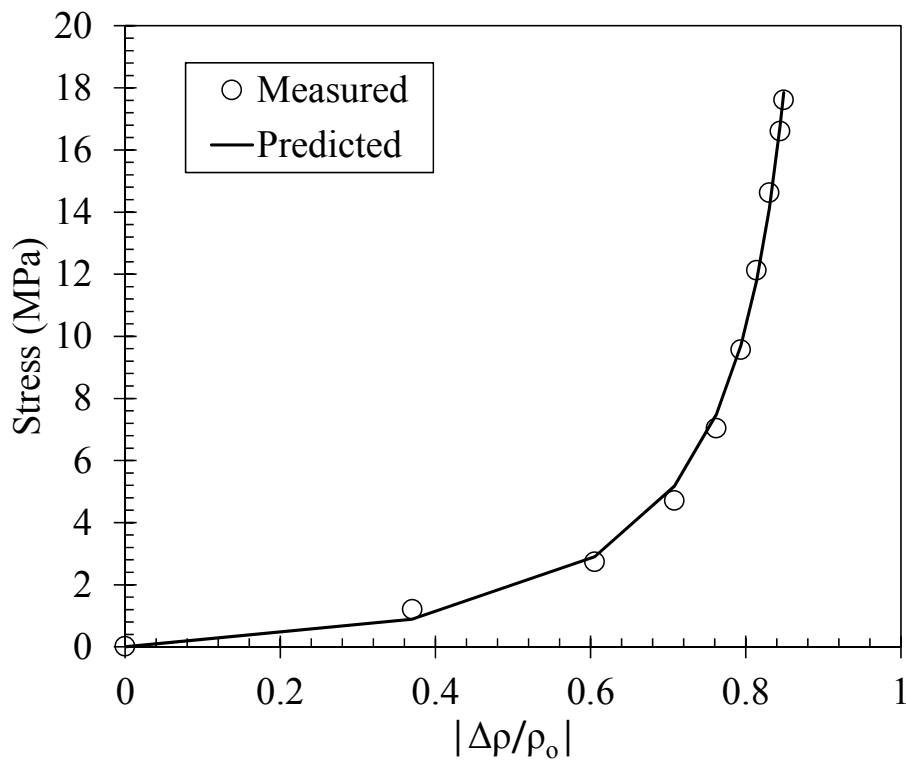


**Figure 4.16: Measured vs. Predicted data using proposed model for Cylinder #51.**

Using Equation 3.11, the coefficient of determination was also calculated to be 0.997, indicating a very strong prediction of the measured data.



---

## 5 Summary and Conclusions

Self-sensing composites containing nanoFe<sub>2</sub>O<sub>3</sub> particles as conductive fillers were produced and then tested. The Vipulanandan and Mohammed and Ezeldin and Balaguru models were utilized to predict the stress-strain and piezoresistive behavior of each specimen. The results of the analysis were then used to create a new model to predict the stress-resistivity behavior of 28-day cured cylinders. A resolution analysis was then performed on two random 28-day cylinders to demonstrate the model procedure and evaluate its effectiveness.

Through testing and analysis, several conclusions were formed:

- (1) It was found that adding defoamer to DI-water reduced the conductivity of the mixture by 13.6 percent. It was considered that the addition of nanoFe<sub>2</sub>O<sub>3</sub> would more than offset this loss in conductivity. Additionally, the defoamer was meant to minimize air voids in the composite that could harmfully affect the conductive network of the composite. The frequency sweep of each cylinder provided a qualitative view of the effects of varying the LCR meter frequency while subjecting the specimens to a 6.895 kPa load, but did not produce any meaningful results.
- (2) RI testing was conducted for each separate mix design parameter (nanoFe<sub>2</sub>O<sub>3</sub> content, water-cement ratio, and curing time) combination to observe the electrical response of the mix over the first 24 hours of curing. The resistivity of each mix was shown to slowly increase or even slightly decrease before steadily increasing at an almost linear rate up to 24 hours. It was determined that the RI<sub>24hr</sub> value increased with increasing nanoFe<sub>2</sub>O<sub>3</sub> content while the RI<sub>24hr</sub> value decreased with increasing water-cement ratio, proving that both mix design parameters influenced the resistivity (and conductivity) of the composite.
- (3) Monotonic compression testing was conducted simultaneously with LCR meter electrical readings and the data was aligned so that both the stress-strain and stress-resistivity behavior could be analyzed further. The Vipulanandan and Mohammed models and the Ezeldin and Balaguru model were applied to both the measured stress-strain and stress-resistivity data for each cylinder. For stress-strain predictions, both models performed adequately, but the Vipulanandan and

Mohammed model was slightly more accurate than the Ezeldin and Balaguru model. For stress-resistivity behavior, the Ezeldin and Balaguru model was not able to predict the data due to its concave upwards curvature. The Vipulanandan and Mohammed stress-resistivity model proved to be capable of accurately predicting the measured stress-resistivity data for each cylinder.

- (4) Using the Vipulanandan and Mohammed stress-resistivity model as a starting point, a new model was created to predict piezoresistive behavior of 28-day cured specimens. Predictive model parameter ( $\sigma_f$ ,  $|\Delta\rho/\rho_o|_f$ ,  $q$ ,  $p$ ) values were compiled for the 28-day specimens, and a nonlinear equation was utilized in conjunction with a nonlinear Generalized Reduced Gradient (GRG) Excel Solver function to produce empirical nonlinear model parameter ( $a$ ,  $b$ ,  $c$ ,  $d$ ,  $e$ ) values for each cylinder. The nonlinear model parameter values were sorted according to water-cement ratio and nanoFe<sub>2</sub>O<sub>3</sub> content for each of the predictive model parameters. The nonlinear equation was split into two separate equations to determine the extent to which the curing time and nanoFe<sub>2</sub>O<sub>3</sub> content contributed to the overall predictive model parameter values. Table 4.7 and the ensuing discussion concluded that the curing time and nanoFe<sub>2</sub>O<sub>3</sub> content influenced the  $\sigma_f$ ,  $|\Delta\rho/\rho_o|_f$ , and  $q$  parameter values to varying degrees, while no correlations were observed for the  $p$  parameter since it is only an iterated value.
- (5) The measured stress-resistivity data for two cylinders was to be selected at random to test the capability of the new predictive model. The nonlinear model parameter values were used to calculate the predictive model parameter values for Cylinders #36 and #51. A full resolution analysis was demonstrated for both cylinders, and the new model was used to predict the measured data. A coefficient of determination of 0.997 was calculated for both cylinders, indicating very strong accuracy of the predictive model.

At the conclusion of this research, a few suggestions could be considered for future research on this topic. Firstly, it is important to note that much more testing should be conducted to confirm the results of this research. Due to the limited research scope, only one cylinder was produced for each unique combination of nanoFe<sub>2</sub>O<sub>3</sub> content, water-

cement ratio, and curing time. It would be beneficial to increase the amount of cylinders tested as well as alter the mix designs to include different quantities or even different materials. With more data, a new nonlinear model could also be developed that incorporates the water-cement ratio in addition to the nanoFe<sub>2</sub>O<sub>3</sub> content and curing time. With additional cylinders for each mix design, additional statistical data such as standard deviation and variance can be applied to the data and enhance the overall effectiveness of the predictive model.

Quantifying the piezoresistive behavior of composites containing conductive fillers has the ability to greatly advance the fields of structural health monitoring and infrastructure materials science and engineering. The results of this research have the potential to lead to a new class of materials and innovative ways to quantify stress and damage on infrastructure from the material piezoelectric response without the need for externally attached sensors and gauges. This research represents just a beginning piece of what could ultimately become a much more significant topic of study in the future.

---

# **Appendix A**

## **Batch Mix Design**

**Table A.1: Cylinder Mix Design.**

Batch	Cylinder #	NanoFe <sub>2</sub> O <sub>3</sub> (%)	Water-Cement Ratio	Curing Time (days)
1	1	0	0.40	1
	2	0	0.40	7
	3	0	0.40	28
2	4	0	0.45	1
	5	0	0.45	7
	6	0	0.45	28
3	7	0	0.50	1
	8	0	0.50	7
	9	0	0.50	28
4	10	0	0.60	1
	11	0	0.60	7
	12	0	0.60	28
5	13	2.5	0.40	1
	14	2.5	0.40	7
	15	2.5	0.40	28
6	16	2.5	0.45	1
	17	2.5	0.45	7
	18	2.5	0.45	28
7	19	2.5	0.50	1
	20	2.5	0.50	7
	21	2.5	0.50	28
8	22	2.5	0.60	1
	23	2.5	0.60	7
	24	2.5	0.60	28
9	25	5	0.40	1
	26	5	0.40	7
	27	5	0.40	28
10	28	5	0.45	1
	29	5	0.45	7
	30	5	0.45	28
11	31	5	0.50	1
	32	5	0.50	7
	33	5	0.50	28
12	34	5	0.60	1
	35	5	0.60	7
	36	5	0.60	28
13	37	7.5	0.40	1
	38	7.5	0.40	7
	39	7.5	0.40	28

**Table A.1 (Continued): Cylinder Mix Design.**

Batch	Cylinder #	NanoFe <sub>2</sub> O <sub>3</sub> (%)	Water-Cement Ratio	Curing Time (days)
14	40	7.5	0.45	1
	41	7.5	0.45	7
	42	7.5	0.45	28
15	43	7.5	0.50	1
	44	7.5	0.50	7
	45	7.5	0.50	28
16	46	7.5	0.60	1
	47	7.5	0.60	7
	48	7.5	0.60	28
17	49	10	0.40	1
	50	10	0.40	7
	51	10	0.40	28
18	52	10	0.45	1
	53	10	0.45	7
	54	10	0.45	28
19	55	10	0.50	1
	56	10	0.50	7
	57	10	0.50	28
20	58	10	0.60	1
	59	10	0.60	7
	60	10	0.60	28

**W/C = 0.40 Batches (1, 5, 9, 13, 17):**

Volume of 2 in x 4 in Cylinder:  $V_{cyl} := \frac{\pi \cdot (2 \text{ in})^2}{4} \cdot 4 \text{ in} = 12.566 \text{ in}^3$

Water/Cement Ratio:  $wc := 0.40$

Unit weight of Type 1 Cement:  $\gamma_c := 94 \frac{\text{lb}}{\text{ft}^3}$

Unit Weight of Water:  $\gamma_w := 1 \frac{\text{gm}}{\text{cm}^3}$

Unit Weight of Defoamer:  $\gamma_{def} := \frac{46.51 \text{ gm}}{50 \text{ cm}^3} = 0.93 \frac{\text{gm}}{\text{cm}^3}$

\* Due to losses during mixing, a correction factor of 2 will be applied to final quantities.

---

**Useful Quantities:**

Weight of Cement w/c = 0.40:  $W_{cement} := \frac{V_{cyl}}{\left(\frac{1}{\gamma_c} + \frac{wc}{\gamma_w}\right)} = 193.516 \text{ gm}$

\* Multiply by 2 to account for loss:  $W_{cement,corr} := W_{cement} \cdot 2 = 387.033 \text{ gm} \rightarrow W_{cement,corr} := 390 \text{ gm}$

Weight of Water w/c = 0.40:  $W_{water} := W_{cement,corr} \cdot wc = 156 \text{ gm} \rightarrow W_{water} = 156 \text{ gm}$

We will be using four 2 in x 4 in cylinders for each batch (3 actual + 1 extra):

Total Weight of Cement Req'd:  $W_{cement,total1} := 4 \cdot W_{cement,corr} = 1560 \text{ gm}$

Total Weight of Water Req'd:  $W_{water,total1} := 4 \cdot W_{water} = 624 \text{ gm}$

Total Volume of Water:  $V_{water,total1} := \frac{W_{water,total1}}{\gamma_w} = 0.165 \text{ gal}$

**Double Check:**

Volume of Materials:  $V_{total} := \frac{W_{cement,total1}}{\gamma_c} + V_{water,total1} = 101.302 \text{ in}^3$

Volume of Cylinders:  $V_{cyl,total} := 4 \cdot 2 \cdot V_{cyl} = 100.531 \text{ in}^3$

--> Volume of Required Materials is slightly higher than the Volume of Cylinders, therefore OK

**W/C = 0.45 Batches (2, 6, 10, 14, 18):**

Volume of 2 in x 4 in Cylinder:  $V_{cyl} := \frac{\pi \cdot (2 \text{ in})^2}{4} \cdot 4 \text{ in} = 12.566 \text{ in}^3$

Water/Cement Ratio:  $wc := 0.45$

Unit weight of Type 1 Cement:  $\gamma_c := 94 \frac{\text{lb}}{\text{ft}^3}$

Unit Weight of Water:  $\gamma_w := 1 \frac{\text{gm}}{\text{cm}^3}$

Unit Weight of Defoamer:  $\gamma_{def} := \frac{46.51 \text{ gm}}{50 \text{ cm}^3} = 0.93 \frac{\text{gm}}{\text{cm}^3}$

\* Due to losses during mixing, a correction factor of 2 will be applied to final quantities.

---

**Useful Quantities:**

Weight of Cement w/c = 0.45:  $W_{cement} := \frac{V_{cyl}}{\left(\frac{1}{\gamma_c} + \frac{wc}{\gamma_w}\right)} = 184.832 \text{ gm}$

\* Multiply by 2 to account for loss:  $W_{cement,corr} := W_{cement} \cdot 2 = 369.663 \text{ gm} \rightarrow W_{cement,corr} := 375 \text{ gm}$

Weight of Water w/c = 0.45:  $W_{water} := W_{cement,corr} \cdot wc = 168.75 \text{ gm} \rightarrow W_{water} = 168.75 \text{ gm}$

We will be using four 2 in x 4 in cylinders for each batch (3 actual + 1 extra):

Total Weight of Cement Req'd:  $W_{cement,total2} := 4 \cdot W_{cement,corr} = 1500 \text{ gm}$

Total Weight of Water Req'd:  $W_{water,total2} := 4 \cdot W_{water} = 675 \text{ gm}$

Total Volume of Water:  $V_{water,total2} := \frac{W_{water,total2}}{\gamma_w} = 0.178 \text{ gal}$

**Double Check:**

Volume of Materials:  $V_{total} := \frac{W_{cement,total2}}{\gamma_c} + V_{water,total2} = 101.982 \text{ in}^3$

Volume of Cylinders:  $V_{cyl,total} := 4 \cdot 2 \cdot V_{cyl} = 100.531 \text{ in}^3$

--> Volume of Required Materials is slightly higher than the Volume of Cylinders, therefore OK



**W/C = 0.50 Batches (3, 7, 11, 15, 19):**

Volume of 2 in x 4 in Cylinder:  $V_{cyl} := \frac{\pi \cdot (2 \text{ in})^2}{4} \cdot 4 \text{ in} = 12.566 \text{ in}^3$

Water/Cement Ratio:  $wc := 0.50$

Unit weight of Type 1 Cement:  $\gamma_c := 94 \frac{\text{lb}}{\text{ft}^3}$

Unit Weight of Water:  $\gamma_w := 1 \frac{\text{gm}}{\text{cm}^3}$

Unit Weight of Defoamer:  $\gamma_{def} := \frac{46.51 \text{ gm}}{50 \text{ cm}^3} = 0.93 \frac{\text{gm}}{\text{cm}^3}$

\* Due to losses during mixing, a correction factor of 2 will be applied to final quantities.

---

**Useful Quantities:**

Weight of Cement w/c = 0.50:  $W_{cement} := \frac{V_{cyl}}{\left(\frac{1}{\gamma_c} + \frac{wc}{\gamma_w}\right)} = 176.893 \text{ gm}$

\* Multiply by 2 to account for loss:  $W_{cement,corr} := W_{cement} \cdot 2 = 353.786 \text{ gm} \rightarrow W_{cement,corr} := 360 \text{ gm}$

Weight of Water w/c = 0.50:  $W_{water} := W_{cement,corr} \cdot wc = 180 \text{ gm} \rightarrow W_{water} = 180 \text{ gm}$

We will be using four 2 in x 4 in cylinders for each batch (3 actual + 1 extra):

Total Weight of Cement Req'd:  $W_{cement,total3} := 4 \cdot W_{cement,corr} = 1440 \text{ gm}$

Total Weight of Water Req'd:  $W_{water,total3} := 4 \cdot W_{water} = 720 \text{ gm}$

Total Volume of Water:  $V_{water,total3} := \frac{W_{water,total3}}{\gamma_w} = 0.19 \text{ gal}$

**Double Check:**

Volume of Materials:  $V_{total} := \frac{W_{cement,total3}}{\gamma_c} + V_{water,total3} = 102.297 \text{ in}^3$

Volume of Cylinders:  $V_{cyl,total} := 4 \cdot 2 \cdot V_{cyl} = 100.531 \text{ in}^3$

--> Volume of Required Materials is slightly higher than the Volume of Cylinders, therefore OK

**W/C = 0.60 Batches (4, 8, 12, 16, 20):**

Volume of 2 in x 4 in Cylinder:  $V_{cyl} := \frac{\pi \cdot (2 \text{ in})^2}{4} \cdot 4 \text{ in} = 12.566 \text{ in}^3$

Water/Cement Ratio:  $wc := 0.60$

Unit weight of Type 1 Cement:  $\gamma_c := 94 \frac{\text{lb}}{\text{ft}^3}$

Unit Weight of Water:  $\gamma_w := 1 \frac{\text{gm}}{\text{cm}^3}$

Unit Weight of Defoamer:  $\gamma_{def} := \frac{46.51 \text{ gm}}{50 \text{ cm}^3} = 0.93 \frac{\text{gm}}{\text{cm}^3}$

\* Due to losses during mixing, a correction factor of 2 will be applied to final quantities.

---

**Useful Quantities:**

Weight of Cement w/c = 0.60:  $W_{cement} := \frac{V_{cyl}}{\left(\frac{1}{\gamma_c} + \frac{wc}{\gamma_w}\right)} = 162.9 \text{ gm}$

\* Multiply by 2 to account for loss:  $W_{cement,corr} := W_{cement} \cdot 2 = 325.799 \text{ gm} \rightarrow W_{cement,corr} := 330 \text{ gm}$

Weight of Water w/c = 0.60:  $W_{water} := W_{cement,corr} \cdot wc = 198 \text{ gm} \rightarrow W_{water} = 198 \text{ gm}$

We will be using four 2 in x 4 in cylinders for each batch (3 actual + 1 extra):

Total Weight of Cement Req'd:  $W_{cement,total4} := 4 \cdot W_{cement,corr} = 1320 \text{ gm}$

Total Weight of Water Req'd:  $W_{water,total4} := 4 \cdot W_{water} = 792 \text{ gm}$

Total Volume of Water:  $V_{water,total4} := \frac{W_{water,total4}}{\gamma_w} = 0.209 \text{ gal}$

**Double Check:**

Volume of Materials:  $V_{total} := \frac{W_{cement,total4}}{\gamma_c} + V_{water,total4} = 101.827 \text{ in}^3$

Volume of Cylinders:  $V_{cyl,total} := 4 \cdot 2 \cdot V_{cyl} = 100.531 \text{ in}^3$

--> Volume of Required Materials is slightly higher than the Volume of Cylinders, therefore OK

**Batch #1:**

$$Defoamer\_content := 20 \frac{mL}{gal}$$

$$NanoFe_2O_3\_content := 0\%$$

$$wc := 0.40$$

Mass of Cement Required:	$W_{cement.total1} = 1560 \text{ gm}$
Mass of Water Required:	$W_{water.total1} = 624 \text{ gm}$
Mass of $NanoFe_2O_3$ Required:	$W_{nano} := W_{cement.total1} \cdot NanoFe_2O_3\_content = 0 \text{ gm}$
Volume of Defoamer Required:	$V_{defoamer} := V_{water.total1} \cdot Defoamer\_content = 3.297 \text{ mL}$
Mass of Defoamer Required:	$W_{defoamer} := V_{defoamer} \cdot \gamma_{def} = 3.067 \text{ gm}$

**Batch #2:**

$$Defoamer\_content := 20 \frac{mL}{gal}$$

$$NanoFe_2O_3\_content := 0\%$$

$$wc := 0.45$$

Mass of Cement Required:	$W_{cement.total2} = 1500 \text{ gm}$
Mass of Water Required:	$W_{water.total2} = 675 \text{ gm}$
Mass of $NanoFe_2O_3$ Required:	$W_{nano} := W_{cement.total2} \cdot NanoFe_2O_3\_content = 0 \text{ gm}$
Volume of Defoamer Required:	$V_{defoamer} := V_{water.total2} \cdot Defoamer\_content = 3.566 \text{ mL}$
Mass of Defoamer Required:	$W_{defoamer} := V_{defoamer} \cdot \gamma_{def} = 3.317 \text{ gm}$

**Batch #3:**

$$Defoamer\_content := 20 \frac{mL}{gal}$$

$$NanoFe_2O_3\_content := 0\%$$

$$wc := 0.50$$

Mass of Cement Required:	$W_{cement.total3} = 1440 \text{ gm}$
Mass of Water Required:	$W_{water.total3} = 720 \text{ gm}$
Mass of $NanoFe_2O_3$ Required:	$W_{nano} := W_{cement.total3} \cdot NanoFe_2O_3\_content = 0 \text{ gm}$
Volume of Defoamer Required:	$V_{defoamer} := V_{water.total3} \cdot Defoamer\_content = 3.804 \text{ mL}$
Mass of Defoamer Required:	$W_{defoamer} := V_{defoamer} \cdot \gamma_{def} = 3.539 \text{ gm}$

**Batch #4:**

$$Defoamer\_content := 20 \frac{mL}{gal}$$

$$NanoFe_2O_3\_content := 0\%$$

$$wc := 0.60$$

Mass of Cement Required:	$W_{cement.total4} = 1320 \text{ gm}$
Mass of Water Required:	$W_{water.total4} = 792 \text{ gm}$
Mass of $NanoFe_2O_3$ Required:	$W_{nano} := W_{cement.total4} \cdot NanoFe_2O_3\_content = 0 \text{ gm}$
Volume of Defoamer Required:	$V_{defoamer} := V_{water.total4} \cdot Defoamer\_content = 4.184 \text{ mL}$
Mass of Defoamer Required:	$W_{defoamer} := V_{defoamer} \cdot \gamma_{def} = 3.892 \text{ gm}$

**Batch #5:**

$$Defoamer\_content := 20 \frac{mL}{gal}$$

$$NanoFe_2O_3\_content := 2.5\%$$

$$wc := 0.40$$

Mass of Cement Required:	$W_{cement.total1} = 1560 \text{ gm}$
Mass of Water Required:	$W_{water.total1} = 624 \text{ gm}$
Mass of $NanoFe_2O_3$ Required:	$W_{nano} := W_{cement.total1} \cdot NanoFe_2O_3\_content = 39 \text{ gm}$
Volume of Defoamer Required:	$V_{defoamer} := V_{water.total1} \cdot Defoamer\_content = 3.297 \text{ mL}$
Mass of Defoamer Required:	$W_{defoamer} := V_{defoamer} \cdot \gamma_{def} = 3.067 \text{ gm}$

**Batch #6:**

$$Defoamer\_content := 20 \frac{mL}{gal}$$

$$NanoFe_2O_3\_content := 2.5\%$$

$$wc := 0.45$$

Mass of Cement Required:	$W_{cement.total2} = 1500 \text{ gm}$
Mass of Water Required:	$W_{water.total2} = 675 \text{ gm}$
Mass of $NanoFe_2O_3$ Required:	$W_{nano} := W_{cement.total2} \cdot NanoFe_2O_3\_content = 37.5 \text{ gm}$
Volume of Defoamer Required:	$V_{defoamer} := V_{water.total2} \cdot Defoamer\_content = 3.566 \text{ mL}$
Mass of Defoamer Required:	$W_{defoamer} := V_{defoamer} \cdot \gamma_{def} = 3.317 \text{ gm}$

**Batch #7:**

$$Defoamer\_content := 20 \frac{mL}{gal}$$

$$NanoFe_2O_3\_content := 2.5\%$$

$$wc := 0.50$$

$$\text{Mass of Cement Required: } W_{cement.total3} = 1440 \text{ gm}$$

$$\text{Mass of Water Required: } W_{water.total3} = 720 \text{ gm}$$

$$\text{Mass of } NanoFe_2O_3 \text{ Required: } W_{nano} := W_{cement.total3} \cdot NanoFe_2O_3\_content = 36 \text{ gm}$$

$$\text{Volume of Defoamer Required: } V_{defoamer} := V_{water.total3} \cdot Defoamer\_content = 3.804 \text{ mL}$$

$$\text{Mass of Defoamer Required: } W_{defoamer} := V_{defoamer} \cdot \gamma_{def} = 3.539 \text{ gm}$$

**Batch #8:**

$$Defoamer\_content := 20 \frac{mL}{gal}$$

$$NanoFe_2O_3\_content := 2.5\%$$

$$wc := 0.60$$

$$\text{Mass of Cement Required: } W_{cement.total4} = 1320 \text{ gm}$$

$$\text{Mass of Water Required: } W_{water.total4} = 792 \text{ gm}$$

$$\text{Mass of } NanoFe_2O_3 \text{ Required: } W_{nano} := W_{cement.total4} \cdot NanoFe_2O_3\_content = 33 \text{ gm}$$

$$\text{Volume of Defoamer Required: } V_{defoamer} := V_{water.total4} \cdot Defoamer\_content = 4.184 \text{ mL}$$

$$\text{Mass of Defoamer Required: } W_{defoamer} := V_{defoamer} \cdot \gamma_{def} = 3.892 \text{ gm}$$

**Batch #9:**

$$Defoamer\_content := 20 \frac{mL}{gal}$$

$$NanoFe_2O_3\_content := 5\%$$

$$wc := 0.40$$

Mass of Cement Required:	$W_{cement.total1} = 1560 \text{ gm}$
Mass of Water Required:	$W_{water.total1} = 624 \text{ gm}$
Mass of $NanoFe_2O_3$ Required:	$W_{nano} := W_{cement.total1} \cdot NanoFe_2O_3\_content = 78 \text{ gm}$
Volume of Defoamer Required:	$V_{defoamer} := V_{water.total1} \cdot Defoamer\_content = 3.297 \text{ mL}$
Mass of Defoamer Required:	$W_{defoamer} := V_{defoamer} \cdot \gamma_{def} = 3.067 \text{ gm}$

**Batch #10:**

$$Defoamer\_content := 20 \frac{mL}{gal}$$

$$NanoFe_2O_3\_content := 5\%$$

$$wc := 0.45$$

Mass of Cement Required:	$W_{cement.total2} = 1500 \text{ gm}$
Mass of Water Required:	$W_{water.total2} = 675 \text{ gm}$
Mass of $NanoFe_2O_3$ Required:	$W_{nano} := W_{cement.total2} \cdot NanoFe_2O_3\_content = 75 \text{ gm}$
Volume of Defoamer Required:	$V_{defoamer} := V_{water.total2} \cdot Defoamer\_content = 3.566 \text{ mL}$
Mass of Defoamer Required:	$W_{defoamer} := V_{defoamer} \cdot \gamma_{def} = 3.317 \text{ gm}$



**Batch #11:**

$$Defoamer\_content := 20 \frac{mL}{gal}$$

$$NanoFe_2O_3\_content := 5\%$$

$$wc := 0.50$$

$$\text{Mass of Cement Required: } W_{cement.total3} = 1440 \text{ gm}$$

$$\text{Mass of Water Required: } W_{water.total3} = 720 \text{ gm}$$

$$\text{Mass of } NanoFe_2O_3 \text{ Required: } W_{nano} := W_{cement.total3} \cdot NanoFe_2O_3\_content = 72 \text{ gm}$$

$$\text{Volume of Defoamer Required: } V_{defoamer} := V_{water.total3} \cdot Defoamer\_content = 3.804 \text{ mL}$$

$$\text{Mass of Defoamer Required: } W_{defoamer} := V_{defoamer} \cdot \gamma_{def} = 3.539 \text{ gm}$$

**Batch #12:**

$$Defoamer\_content := 20 \frac{mL}{gal}$$

$$NanoFe_2O_3\_content := 5\%$$

$$wc := 0.60$$

$$\text{Mass of Cement Required: } W_{cement.total4} = 1320 \text{ gm}$$

$$\text{Mass of Water Required: } W_{water.total4} = 792 \text{ gm}$$

$$\text{Mass of } NanoFe_2O_3 \text{ Required: } W_{nano} := W_{cement.total4} \cdot NanoFe_2O_3\_content = 66 \text{ gm}$$

$$\text{Volume of Defoamer Required: } V_{defoamer} := V_{water.total4} \cdot Defoamer\_content = 4.184 \text{ mL}$$

$$\text{Mass of Defoamer Required: } W_{defoamer} := V_{defoamer} \cdot \gamma_{def} = 3.892 \text{ gm}$$



**Batch #13:**

$$Defoamer\_content := 20 \frac{mL}{gal}$$

$$NanoFe_2O_3\_content := 7.5\%$$

$$wc := 0.40$$

Mass of Cement Required:  $W_{cement.total1} = 1560 \text{ gm}$

Mass of Water Required:  $W_{water.total1} = 624 \text{ gm}$

Mass of  $NanoFe_2O_3$  Required:  $W_{nano} := W_{cement.total1} \cdot NanoFe_2O_3\_content = 117 \text{ gm}$

Volume of Defoamer Required:  $V_{defoamer} := V_{water.total1} \cdot Defoamer\_content = 3.297 \text{ mL}$

Mass of Defoamer Required:  $W_{defoamer} := V_{defoamer} \cdot \gamma_{def} = 3.067 \text{ gm}$

**Batch #14:**

$$Defoamer\_content := 20 \frac{mL}{gal}$$

$$NanoFe_2O_3\_content := 7.5\%$$

$$wc := 0.45$$

Mass of Cement Required:  $W_{cement.total2} = 1500 \text{ gm}$

Mass of Water Required:  $W_{water.total2} = 675 \text{ gm}$

Mass of  $NanoFe_2O_3$  Required:  $W_{nano} := W_{cement.total2} \cdot NanoFe_2O_3\_content = 112.5 \text{ gm}$

Volume of Defoamer Required:  $V_{defoamer} := V_{water.total2} \cdot Defoamer\_content = 3.566 \text{ mL}$

Mass of Defoamer Required:  $W_{defoamer} := V_{defoamer} \cdot \gamma_{def} = 3.317 \text{ gm}$

**Batch #15:**

$$Defoamer\_content := 20 \frac{mL}{gal}$$

$$NanoFe_2O_3\_content := 7.5\%$$

$$wc := 0.50$$

$$\text{Mass of Cement Required: } W_{cement.total3} = 1440 \text{ gm}$$

$$\text{Mass of Water Required: } W_{water.total3} = 720 \text{ gm}$$

$$\text{Mass of } NanoFe_2O_3 \text{ Required: } W_{nano} := W_{cement.total3} \cdot NanoFe_2O_3\_content = 108 \text{ gm}$$

$$\text{Volume of Defoamer Required: } V_{defoamer} := V_{water.total3} \cdot Defoamer\_content = 3.804 \text{ mL}$$

$$\text{Mass of Defoamer Required: } W_{defoamer} := V_{defoamer} \cdot \gamma_{def} = 3.539 \text{ gm}$$

---

**Batch #16:**

$$Defoamer\_content := 20 \frac{mL}{gal}$$

$$NanoFe_2O_3\_content := 7.5\%$$

$$wc := 0.60$$

$$\text{Mass of Cement Required: } W_{cement.total4} = 1320 \text{ gm}$$

$$\text{Mass of Water Required: } W_{water.total4} = 792 \text{ gm}$$

$$\text{Mass of } NanoFe_2O_3 \text{ Required: } W_{nano} := W_{cement.total4} \cdot NanoFe_2O_3\_content = 99 \text{ gm}$$

$$\text{Volume of Defoamer Required: } V_{defoamer} := V_{water.total4} \cdot Defoamer\_content = 4.184 \text{ mL}$$

$$\text{Mass of Defoamer Required: } W_{defoamer} := V_{defoamer} \cdot \gamma_{def} = 3.892 \text{ gm}$$

**Batch #17:**

$$Defoamer\_content := 20 \frac{mL}{gal}$$

$$NanoFe_2O_3\_content := 10\%$$

$$wc := 0.40$$

$$\text{Mass of Cement Required: } W_{cement.total1} = 1560 \text{ gm}$$

$$\text{Mass of Water Required: } W_{water.total1} = 624 \text{ gm}$$

$$\text{Mass of } NanoFe_2O_3 \text{ Required: } W_{nano} := W_{cement.total1} \cdot NanoFe_2O_3\_content = 156 \text{ gm}$$

$$\text{Volume of Defoamer Required: } V_{defoamer} := V_{water.total1} \cdot Defoamer\_content = 3.297 \text{ mL}$$

$$\text{Mass of Defoamer Required: } W_{defoamer} := V_{defoamer} \cdot \gamma_{def} = 3.067 \text{ gm}$$

---

**Batch #18:**

$$Defoamer\_content := 20 \frac{mL}{gal}$$

$$NanoFe_2O_3\_content := 10\%$$

$$wc := 0.45$$

$$\text{Mass of Cement Required: } W_{cement.total2} = 1500 \text{ gm}$$

$$\text{Mass of Water Required: } W_{water.total2} = 675 \text{ gm}$$

$$\text{Mass of } NanoFe_2O_3 \text{ Required: } W_{nano} := W_{cement.total2} \cdot NanoFe_2O_3\_content = 150 \text{ gm}$$

$$\text{Volume of Defoamer Required: } V_{defoamer} := V_{water.total2} \cdot Defoamer\_content = 3.566 \text{ mL}$$

$$\text{Mass of Defoamer Required: } W_{defoamer} := V_{defoamer} \cdot \gamma_{def} = 3.317 \text{ gm} \quad 8$$

**Batch #19:**

$$Defoamer\_content := 20 \frac{mL}{gal}$$

$$NanoFe_2O_3\_content := 10\%$$

$$wc := 0.50$$

$$\text{Mass of Cement Required: } W_{cement.total3} = 1440 \text{ gm}$$

$$\text{Mass of Water Required: } W_{water.total3} = 720 \text{ gm}$$

$$\text{Mass of } NanoFe_2O_3 \text{ Required: } W_{nano} := W_{cement.total3} \cdot NanoFe_2O_3\_content = 144 \text{ gm}$$

$$\text{Volume of Defoamer Required: } V_{defoamer} := V_{water.total3} \cdot Defoamer\_content = 3.804 \text{ mL}$$

$$\text{Mass of Defoamer Required: } W_{defoamer} := V_{defoamer} \cdot \gamma_{def} = 3.539 \text{ gm}$$

**Batch #20:**

$$Defoamer\_content := 20 \frac{mL}{gal}$$

$$NanoFe_2O_3\_content := 10\%$$

$$wc := 0.60$$

$$\text{Mass of Cement Required: } W_{cement.total4} = 1320 \text{ gm}$$

$$\text{Mass of Water Required: } W_{water.total4} = 792 \text{ gm}$$

$$\text{Mass of } NanoFe_2O_3 \text{ Required: } W_{nano} := W_{cement.total4} \cdot NanoFe_2O_3\_content = 132 \text{ gm}$$

$$\text{Volume of Defoamer Required: } V_{defoamer} := V_{water.total4} \cdot Defoamer\_content = 4.184 \text{ mL}$$

$$\text{Mass of Defoamer Required: } W_{defoamer} := V_{defoamer} \cdot \gamma_{def} = 3.892 \text{ gm}$$

Totals: ORIGIN := 1

Cement :=	$\begin{bmatrix} 1560 \\ 1500 \\ 1440 \\ 1320 \\ 1560 \\ 1500 \\ 1440 \\ 1320 \\ 1560 \\ 1500 \\ 1440 \\ 1320 \\ 1560 \\ 1500 \\ 1440 \\ 1320 \end{bmatrix}$	Water :=	$\begin{bmatrix} 624 \\ 675 \\ 720 \\ 792 \\ 624 \\ 675 \\ 720 \\ 792 \\ 624 \\ 675 \\ 720 \\ 792 \\ 624 \\ 675 \\ 720 \\ 792 \end{bmatrix}$	Nano :=	$\begin{bmatrix} 0 \\ 0 \\ 0 \\ 0 \\ 39 \\ 37.5 \\ 36 \\ 33 \\ 78 \\ 75 \\ 72 \\ 66 \\ 117 \\ 112.5 \\ 108 \\ 99 \\ 156 \\ 150 \\ 144 \\ 132 \end{bmatrix}$	Defoamer :=	$\begin{bmatrix} 3.297 \\ 3.566 \\ 3.804 \\ 4.184 \\ 3.297 \\ 3.566 \\ 3.804 \\ 4.184 \\ 3.297 \\ 3.566 \\ 3.804 \\ 4.184 \\ 3.297 \\ 3.566 \\ 3.804 \\ 4.184 \end{bmatrix}$
	<b>gm</b>		<b>gm</b>		<b>gm</b>		<b>mL</b>

Defoamer Mass by Batch:

$$0.40 \text{ W/C Batches: } Def_{.40} := Defoamer_1 \cdot \gamma_{def} = 3.067 \text{ gm}$$

$$0.45 \text{ W/C Batches: } Def_{.45} := Defoamer_2 \cdot \gamma_{def} = 3.317 \text{ gm}$$

$$0.50 \text{ W/C Batches: } Def_{.50} := Defoamer_3 \cdot \gamma_{def} = 3.538 \text{ gm}$$

$$0.60 \text{ W/C Batches: } Def_{.60} := Defoamer_4 \cdot \gamma_{def} = 3.892 \text{ gm}$$

Total Material Requirements for Compression Testing:

$$Required.Cement := \sum Cement = 64.155 \text{ lb}$$

$$Required.Water := \sum Water = 30.986 \text{ lb}$$

$$Required.NanoFe_2O_3 := \sum Nano = 1455 \text{ gm}$$

$$Required.Defoamer.Volume := \sum Defoamer = 0.02 \text{ gal}$$

$$Required.Defoamer.Mass := \sum Defoamer \cdot \gamma_{def} = 69.072 \text{ gm}$$

**Resistivity Index (RI) Testing Required Material Quantities:**

Volume of RI Test Mold:  $V_{RI} := \frac{\pi \cdot (2 \text{ in})^2}{4} \cdot 1 \text{ in} = 3.142 \text{ in}^3$

Volume of Compression Test Cylinder:  $V_{compression} := \frac{\pi \cdot (2 \text{ in})^2}{4} \cdot 4 \text{ in} = 12.566 \text{ in}^3$

Ratio - RI Volume : Compression Volume:  $\frac{V_{RI}}{V_{compression}} = 0.25$

\*\*\* Material totals for compression testing are for 4 cylinders...

$$Cement_{RI} := \frac{Cement}{4} \cdot \frac{1}{4} = \begin{bmatrix} 97.5 \\ 93.75 \\ 90 \\ 82.5 \\ 97.5 \\ 93.75 \\ 90 \\ 82.5 \\ 97.5 \\ 93.75 \\ 90 \\ 82.5 \\ 97.5 \\ 93.75 \\ 90 \\ 82.5 \end{bmatrix} \text{ gm}$$

$$Water_{RI} := \frac{Water}{4} \cdot \frac{1}{4} = \begin{bmatrix} 39 \\ 42.19 \\ 45 \\ 49.5 \\ 39 \\ 42.19 \\ 45 \\ 49.5 \\ 39 \\ 42.19 \\ 45 \\ 49.5 \\ 39 \\ 42.19 \\ 45 \\ 49.5 \end{bmatrix} \text{ gm}$$

$$Nano_{RI} := \frac{Nano}{4} \cdot \frac{1}{4} = \begin{bmatrix} 0 \\ 0 \\ 0 \\ 0 \\ 2.438 \\ 2.344 \\ 2.25 \\ 2.063 \\ 4.875 \\ 4.688 \\ 4.5 \\ 4.125 \\ 7.313 \\ 7.031 \\ 6.75 \\ 6.188 \\ 9.75 \\ 9.375 \\ 9 \\ 8.25 \end{bmatrix} \text{ gm}$$

$$Defoamer_{RI} := \frac{Defoamer}{4} \cdot \frac{1}{4} = \begin{bmatrix} 0.206 \\ 0.223 \\ 0.238 \\ 0.262 \\ 0.206 \\ 0.223 \\ 0.238 \\ 0.262 \\ 0.206 \\ 0.223 \\ 0.238 \\ 0.262 \\ 0.206 \\ 0.223 \\ 0.238 \\ 0.262 \\ 0.206 \\ 0.223 \\ 0.238 \\ 0.262 \end{bmatrix} \text{ mL}$$

## Defoamer Mass by Batch:

$$0.40 \text{ W/C Batches: } Def_{.40} := Defoamer_{RI_1} \cdot \gamma_{def} = 0.192 \text{ gm}$$

$$0.45 \text{ W/C Batches: } Def_{.45} := Defoamer_{RI_2} \cdot \gamma_{def} = 0.207 \text{ gm}$$

$$0.50 \text{ W/C Batches: } Def_{.50} := Defoamer_{RI_3} \cdot \gamma_{def} = 0.221 \text{ gm}$$

$$0.60 \text{ W/C Batches: } Def_{.60} := Defoamer_{RI_4} \cdot \gamma_{def} = 0.243 \text{ gm}$$

## Total Material Requirements for RI Testing:

$$Required.Cement_{RI} := \sum Cement_{RI} = 4.01 \text{ lb}$$

$$Required.Water_{RI} := \sum Water_{RI} = 1.937 \text{ lb}$$

$$Required.NanoFe_2O_{3,RI} := \sum Nano_{RI} = 90.938 \text{ gm}$$

$$Required.Defoamer.Volume_{RI} := \sum Defoamer_{RI} = 0.001 \text{ gal}$$

$$Required.Defoamer.Mass_{RI} := \sum Defoamer_{RI} \cdot \gamma_{def} = 4.317 \text{ gm}$$

---

# **Appendix B**

## **Frequency Sweeps**



**Table B.1: 1 psi Frequency Sweep Capacitance vs. Frequency and Resistance vs. Frequency Tangent Line Intersection Values.**

Batch	Cylinder	NanoFe <sub>2</sub> O <sub>3</sub> (%)	Water- Cement Ratio	Curing Time (days)	Capacitance Intersection (kHz)	Resistance Intersection (kHz)
1	1	0	0.40	1	-	-
1	2	0	0.40	7	2757.23	167.72
1	3	0	0.40	28	3025.35	157.26
2	4	0	0.45	1	471.07	185.88
2	5	0	0.45	7	3761.13	194.52
2	6	0	0.45	28	3169.37	145.67
3	7	0	0.50	1	678.05	336.64
3	8	0	0.50	7	1821.18	270.07
3	9	0	0.50	28	3480.10	192.25
4	10	0	0.60	1	1049.27	266.50
4	11	0	0.60	7	1452.89	331.78
4	12	0	0.60	28	4362.32	235.51
5	13	2.5	0.40	1	3227.62	235.03
5	14	2.5	0.40	7	4951.05	199.35
5	15	2.5	0.40	28	3894.09	236.35
6	16	2.5	0.45	1	3158.10	188.39
6	17	2.5	0.45	7	4374.69	243.57
6	18	2.5	0.45	28	3818.03	187.19
7	19	2.5	0.50	1	2181.74	299.24
7	20	2.5	0.50	7	3716.57	320.03
7	21	2.5	0.50	28	3785.09	232.07
8	22	2.5	0.60	1	956.28	366.31
8	23	2.5	0.60	7	1670.29	308.91
8	24	2.5	0.60	28	2516.83	276.80
9	25	5	0.40	1	4406.46	364.91
9	26	5	0.40	7	3076.87	234.84
9	27	5	0.40	28	3450.68	232.64
10	28	5	0.45	1	695.54	304.75
10	29	5	0.45	7	4215.42	263.51
10	30	5	0.45	28	3506.08	234.50

**Table B.1 (Continued): 1 psi Frequency Sweep Capacitance vs. Frequency and Resistance vs. Frequency Tangent Line Intersection Values.**

Batch	Cylinder	NanoFe <sub>2</sub> O <sub>3</sub> (%)	Water- Cement Ratio	Curing Time (days)	Capacitance Intersection (kHz)	Resistance Intersection (kHz)
11	31	5	0.50	1	750.98	265.48
11	32	5	0.50	7	3152.65	317.31
11	33	5	0.50	28	3934.44	250.85
12	34	5	0.60	1	865.74	402.83
12	35	5	0.60	7	2156.18	281.47
12	36	5	0.60	28	2865.00	298.54
13	37	7.5	0.40	1	2726.21	343.20
13	38	7.5	0.40	7	3524.26	187.18
13	39	7.5	0.40	28	3335.56	229.85
14	40	7.5	0.45	1	5155.30	223.08
14	41	7.5	0.45	7	5543.75	192.09
14	42	7.5	0.45	28	4127.78	187.17
15	43	7.5	0.50	1	4556.06	205.97
15	44	7.5	0.50	7	1097.79	311.06
15	45	7.5	0.50	28	3825.26	260.65
16	46	7.5	0.60	1	1583.05	270.12
16	47	7.5	0.60	7	2941.63	216.17
16	48	7.5	0.60	28	750.00	312.08
17	49	10	0.40	1	2424.46	282.85
17	50	10	0.40	7	5115.07	183.36
17	51	10	0.40	28	3660.34	188.42
18	52	10	0.45	1	490.84	262.58
18	53	10	0.45	7	3877.39	204.40
18	54	10	0.45	28	4078.42	196.81
19	55	10	0.50	1	693.36	289.29
19	56	10	0.50	7	3608.79	199.35
19	57	10	0.50	28	3436.48	190.58
20	58	10	0.60	1	676.10	350.69
20	59	10	0.60	7	3427.72	263.17
20	60	10	0.60	28	5066.39	210.86

Frequency Sweep Capacitance Tangent Line Intersections Sorted by NanoFe<sub>2</sub>O<sub>3</sub> Content:

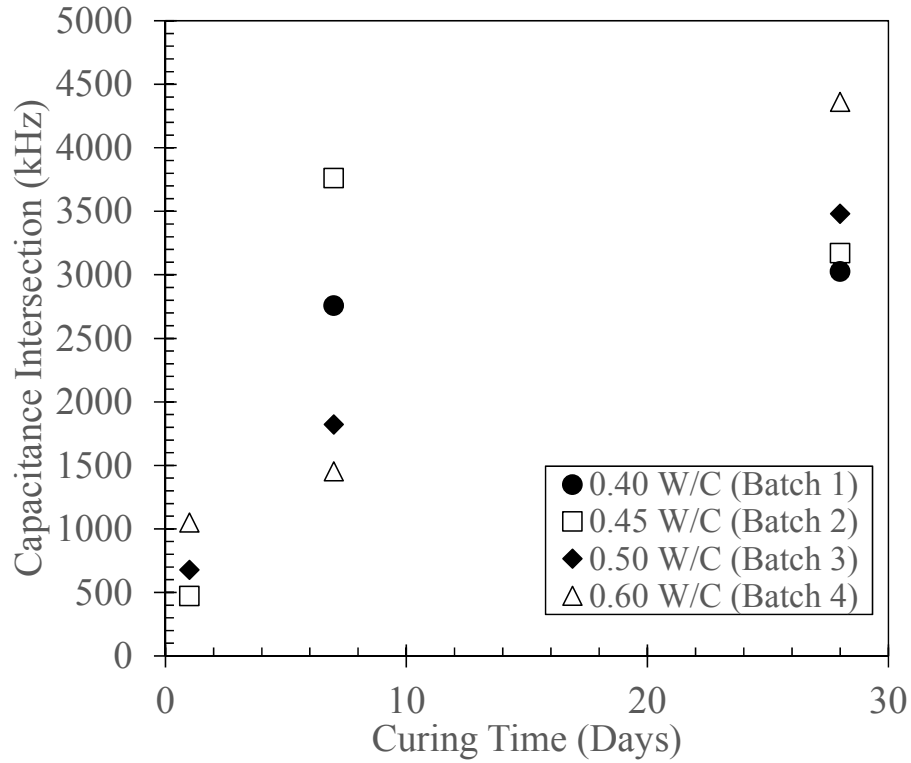


**Figure B.1: 0% NanoFe<sub>2</sub>O<sub>3</sub> - Capacitance Tangent Line Intersection.**

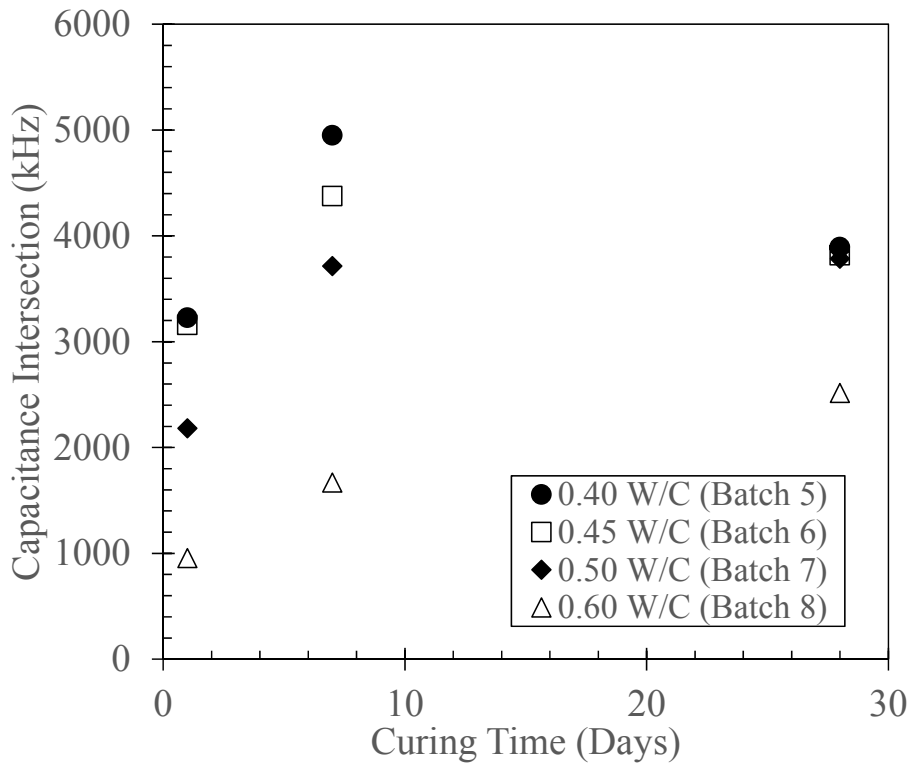


**Figure B.2: 2.5% NanoFe<sub>2</sub>O<sub>3</sub> - Capacitance Tangent Line Intersection.**

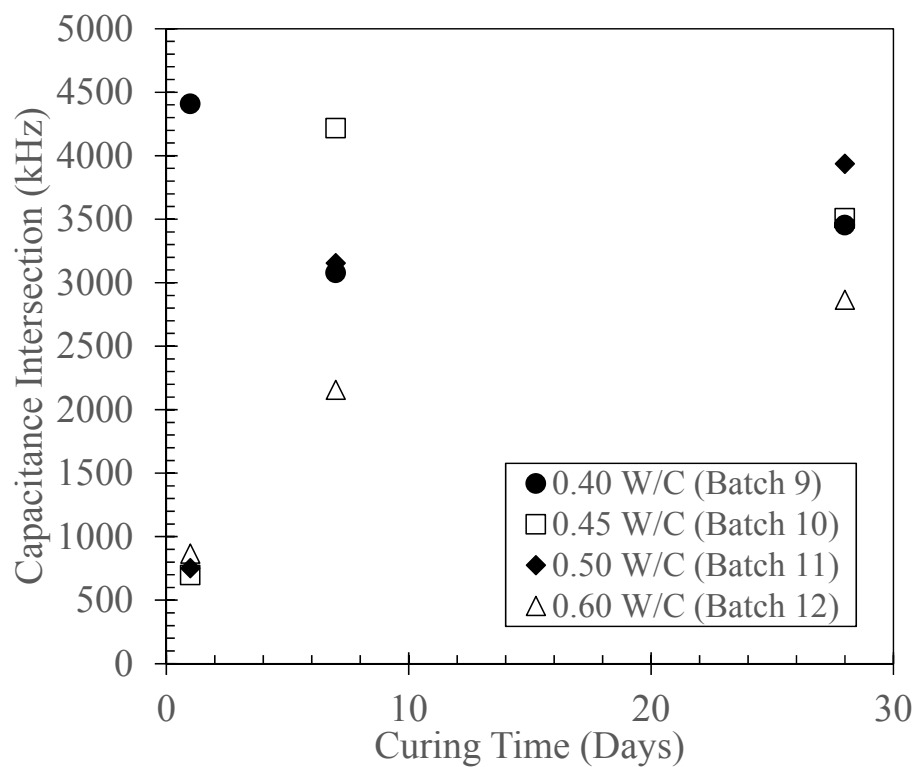


**Figure B.3: 5% NanoFe<sub>2</sub>O<sub>3</sub> - Capacitance Tangent Line Intersection.**

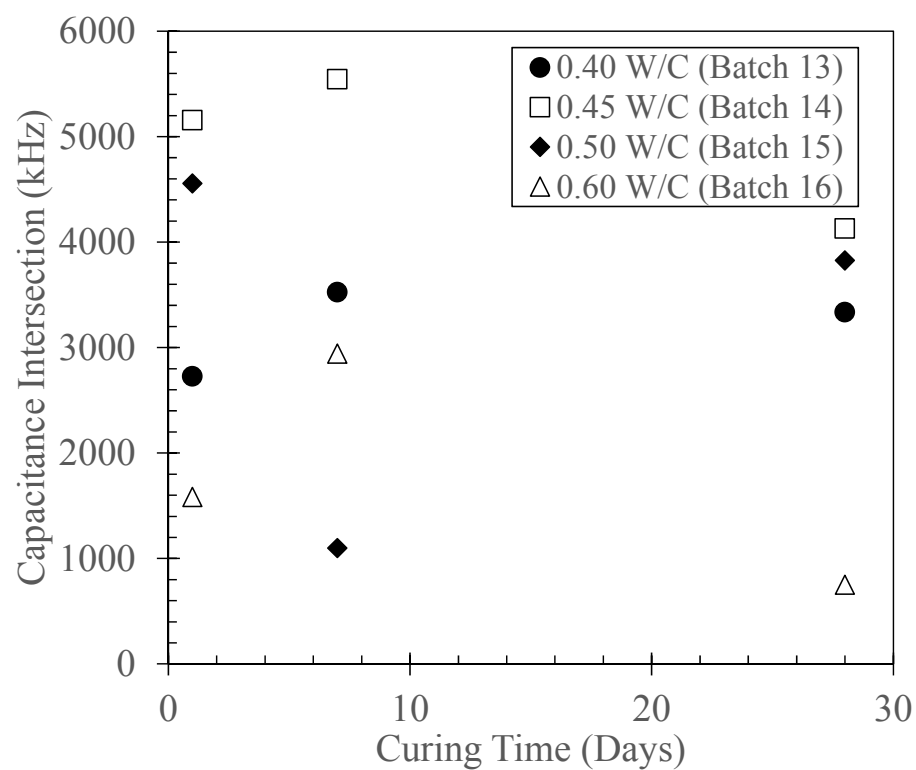


**Figure B.4: 7.5% NanoFe<sub>2</sub>O<sub>3</sub> - Capacitance Tangent Line Intersection.**

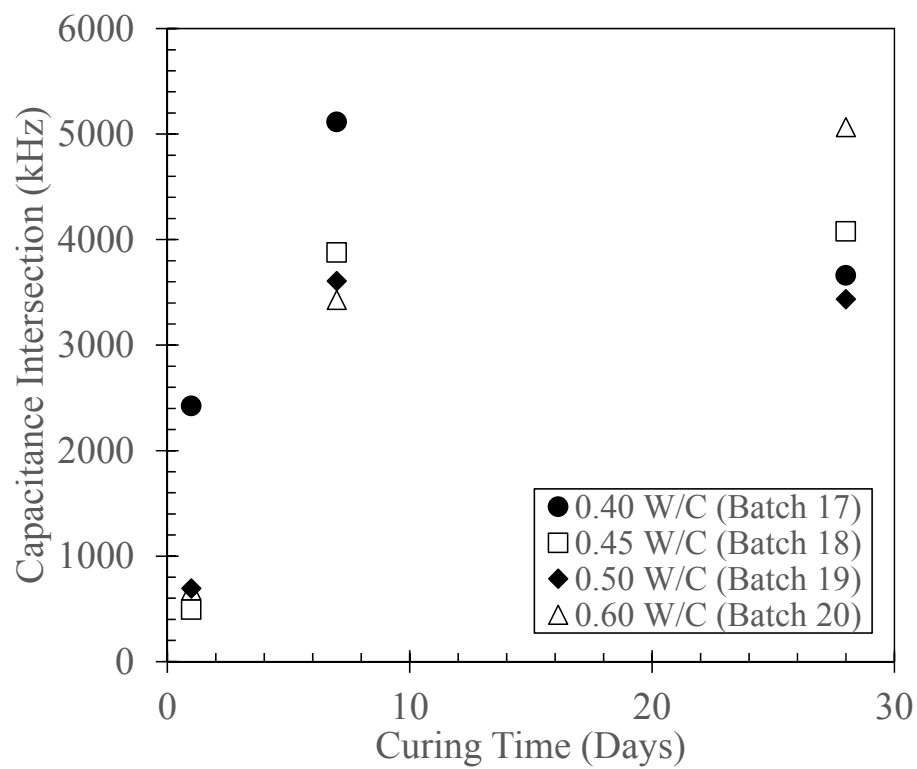


**Figure B.5: 10% NanoFe<sub>2</sub>O<sub>3</sub> - Capacitance Tangent Line Intersection.**

Frequency Sweep Resistance Tangent Line Intersections Sorted by NanoFe<sub>2</sub>O<sub>3</sub> Content:

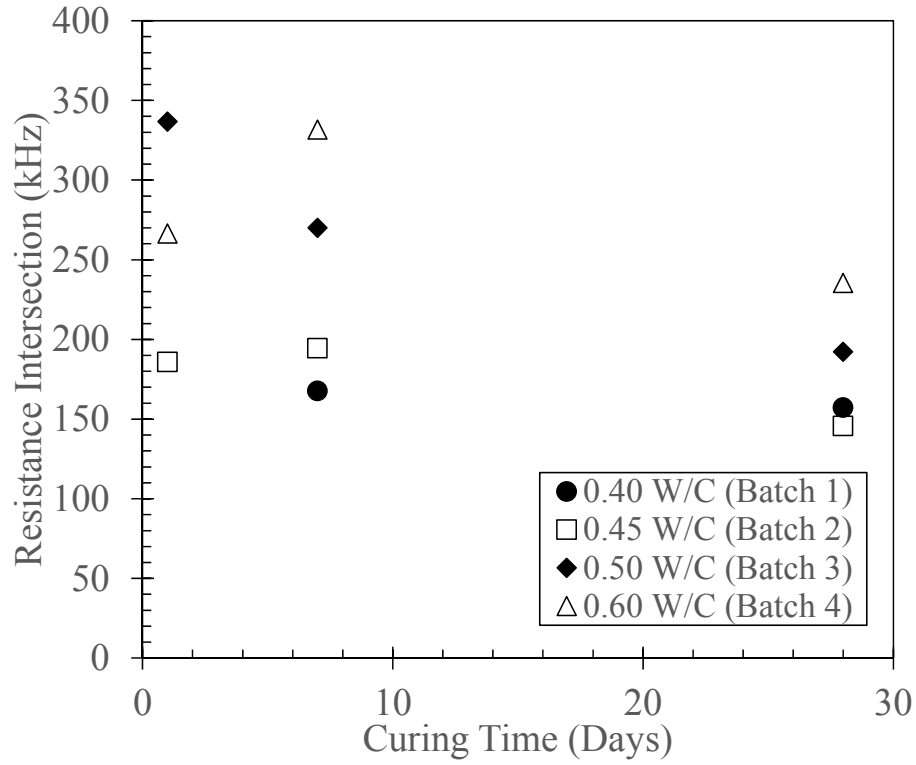


**Figure B.6: 0% NanoFe<sub>2</sub>O<sub>3</sub> - Resistance Tangent Line Intersection.**

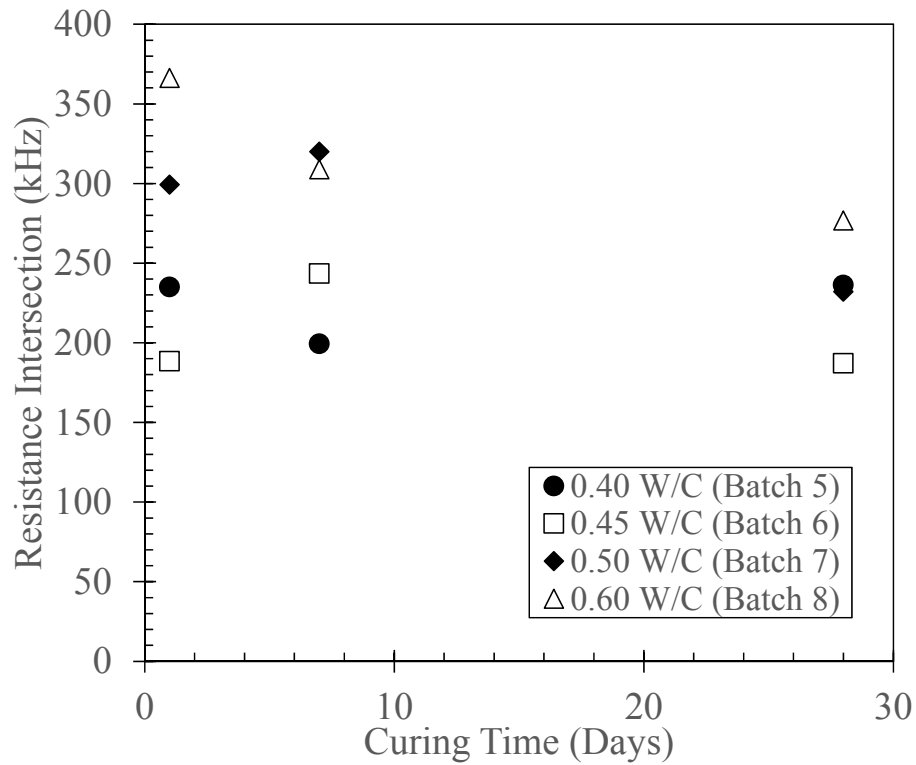


**Figure B.7: 2.5% NanoFe<sub>2</sub>O<sub>3</sub> - Resistance Tangent Line Intersection.**

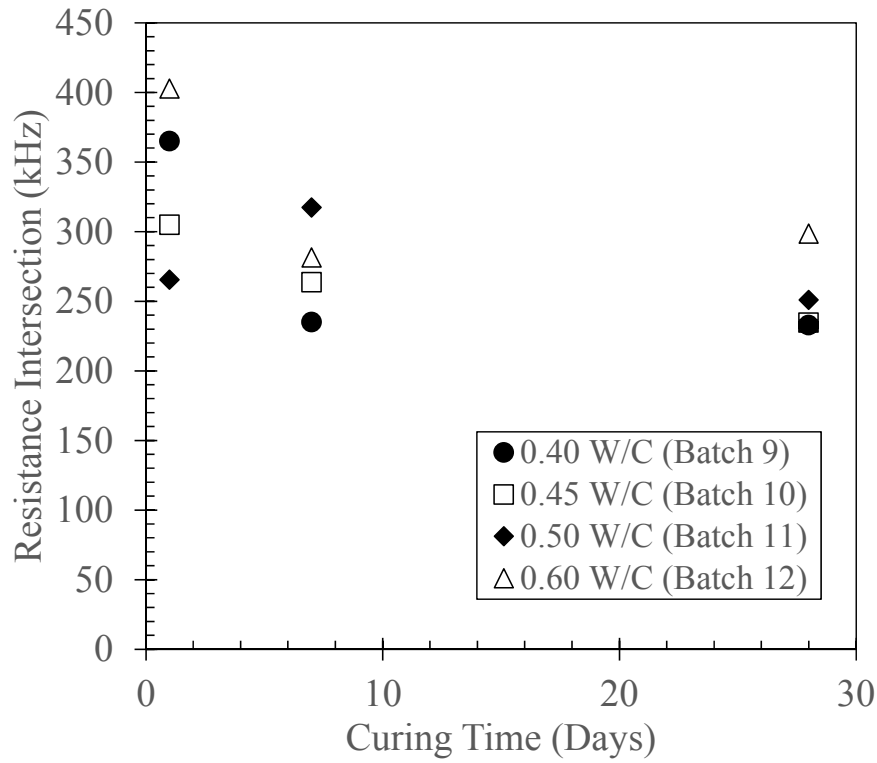


**Figure B.8: 5% NanoFe<sub>2</sub>O<sub>3</sub> - Resistance Tangent Line Intersection.**

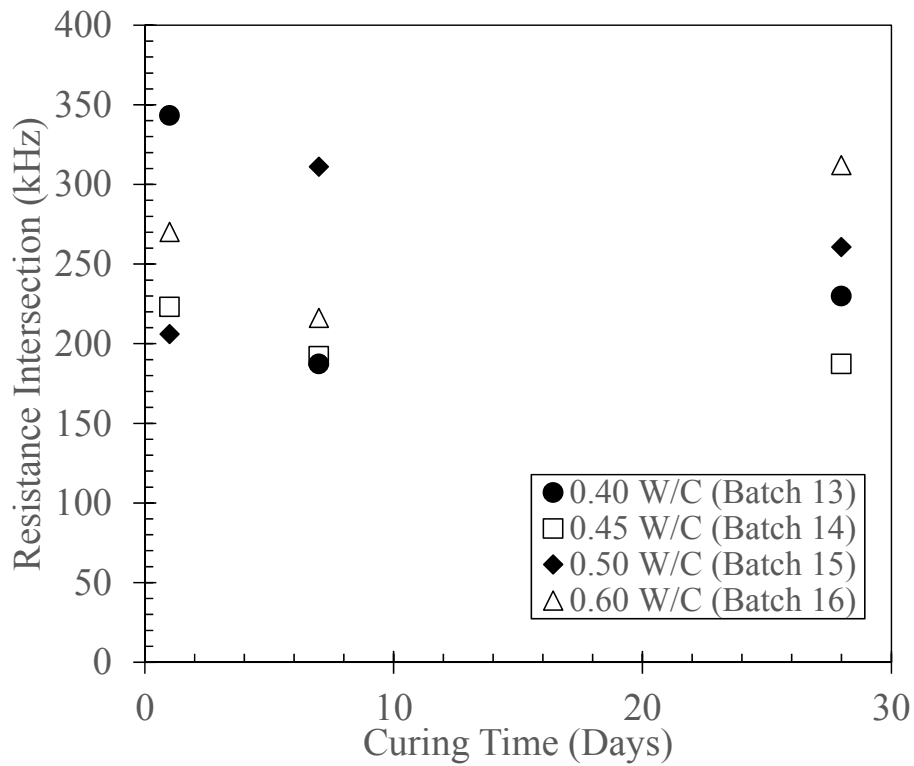


**Figure B.9: 7.5% NanoFe<sub>2</sub>O<sub>3</sub> - Resistance Tangent Line Intersection.**

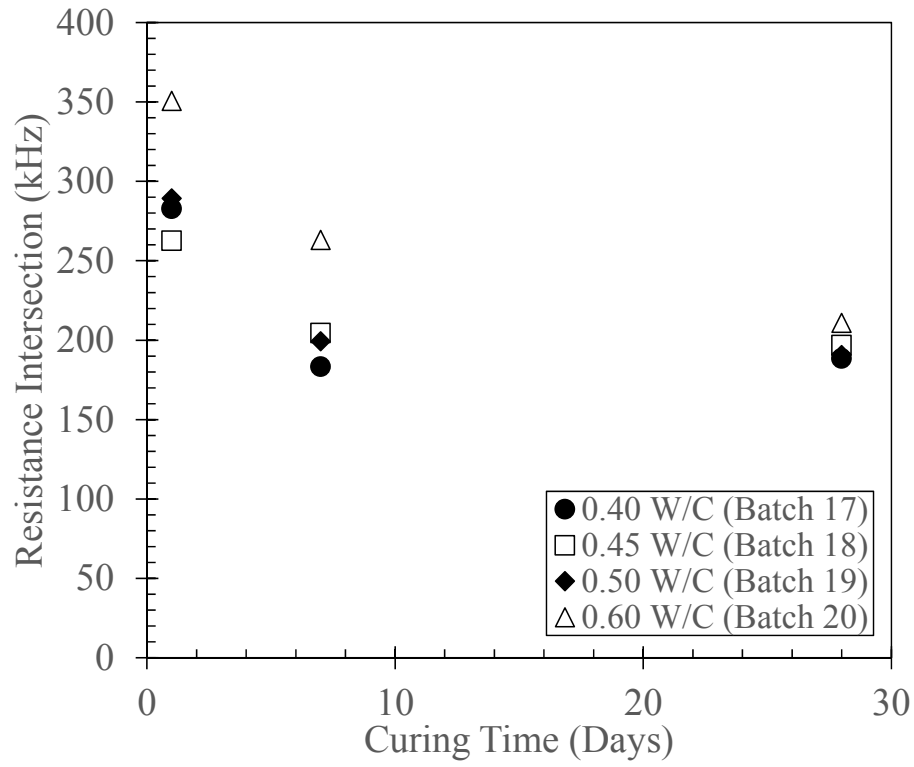


**Figure B.10: 2.5% NanoFe<sub>2</sub>O<sub>3</sub> - Resistance Tangent Line Intersection.**



Frequency Sweep Capacitance Tangent Line Intersections Sorted by Water-Cement Ratio:

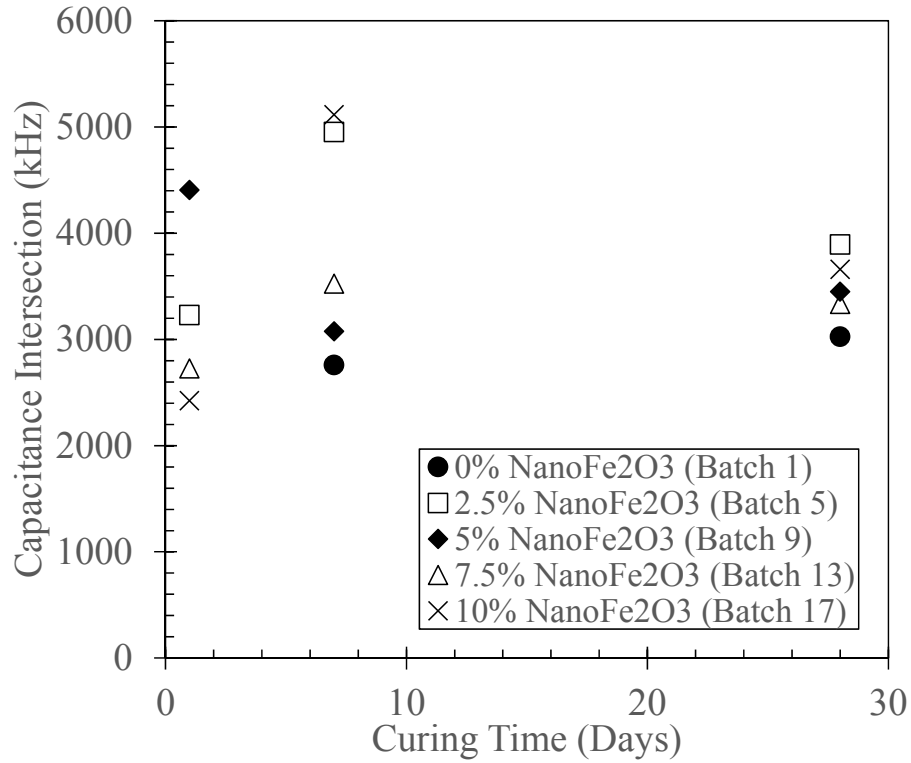


**Figure B.11: 0.40 Water-Cement Ratio - Capacitance Tangent Line Intersection.**

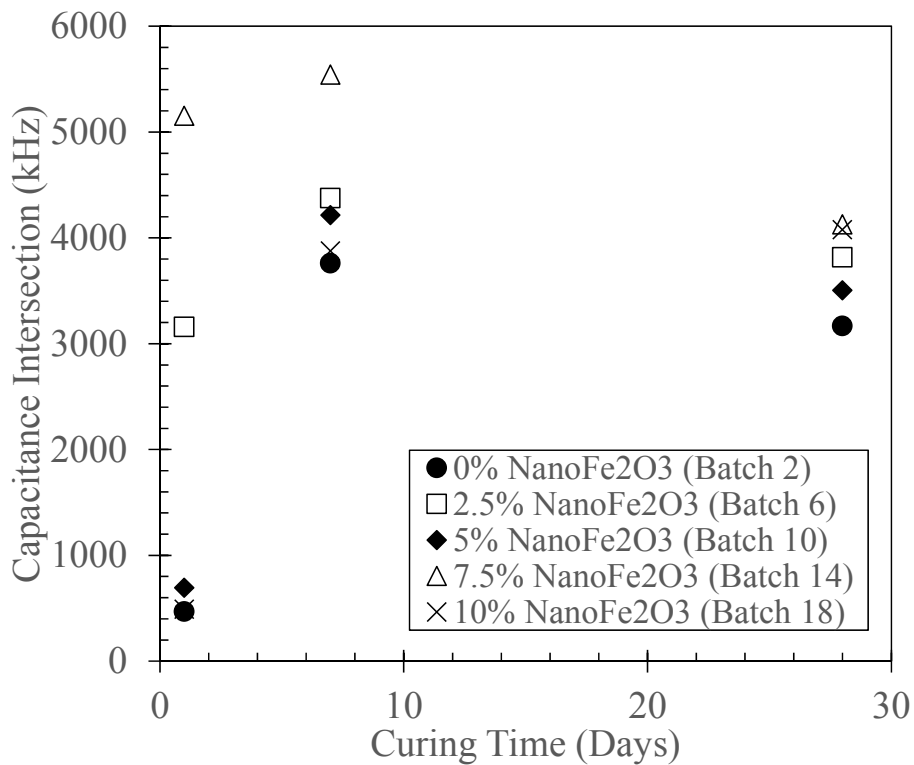


**Figure B.12: 0.45 Water-Cement Ratio - Capacitance Tangent Line Intersection.**

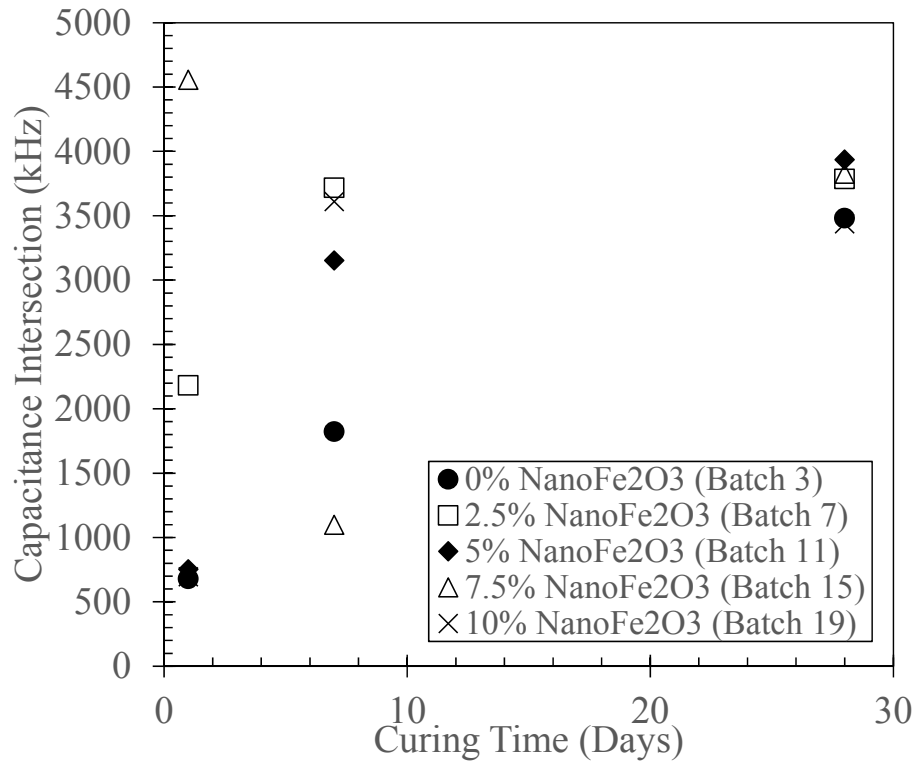


**Figure B.13: 0.50 Water-Cement Ratio - Capacitance Tangent Line Intersection.**

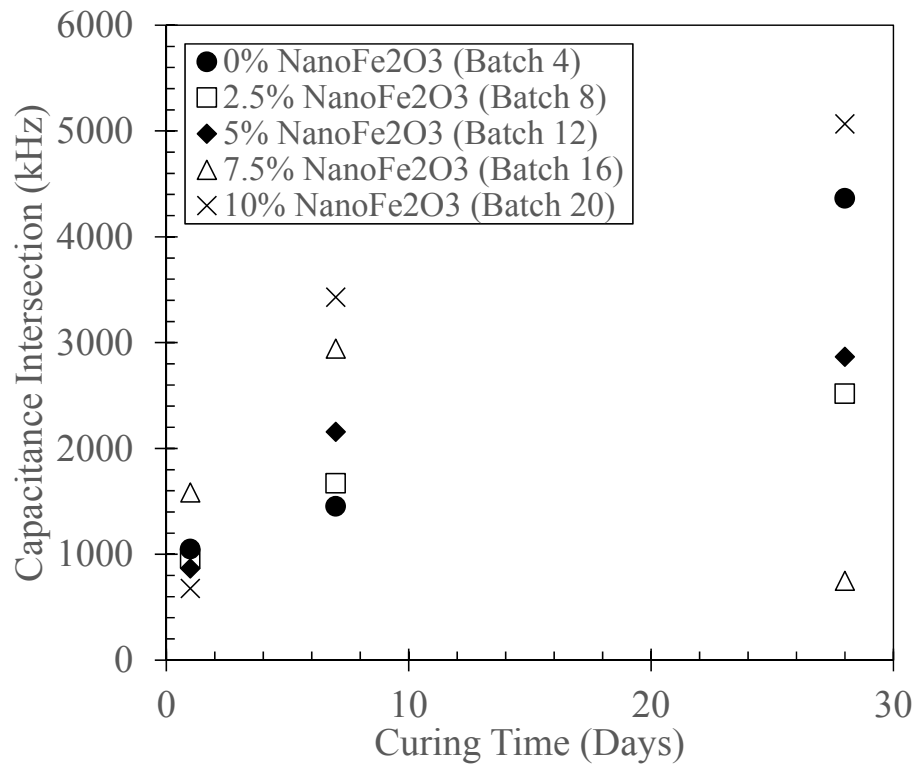


**Figure B.14: 0.60 Water-Cement Ratio - Capacitance Tangent Line Intersection.**

Frequency Sweep Resistance Tangent Line Intersections Sorted by Water-Cement Ratio:

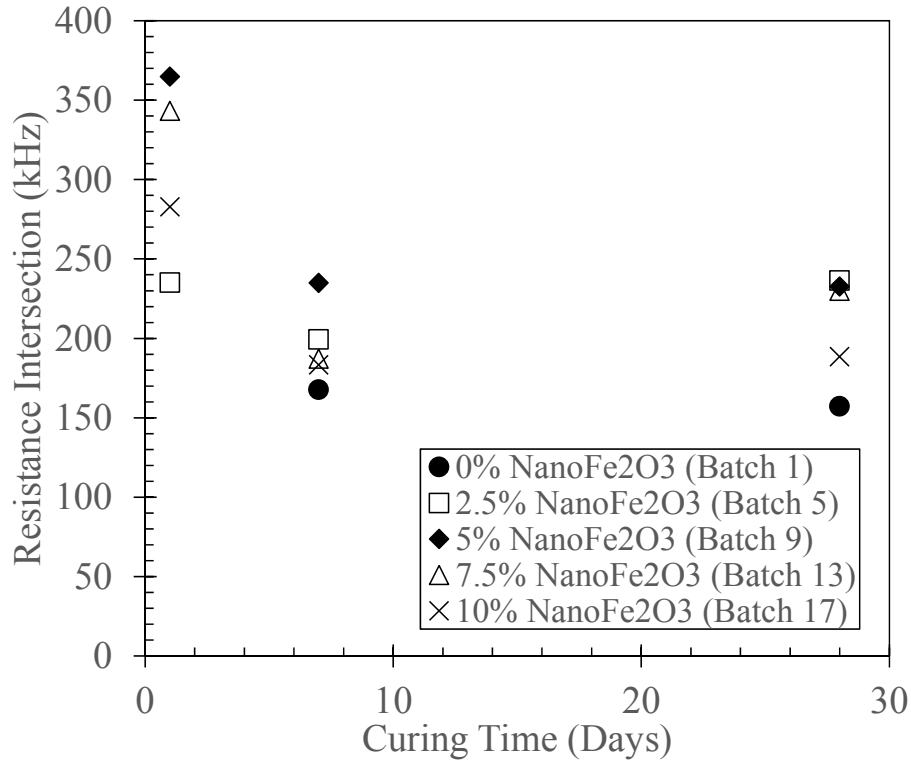


**Figure B.15: 0.40 Water-Cement Ratio - Resistance Tangent Line Intersection.**

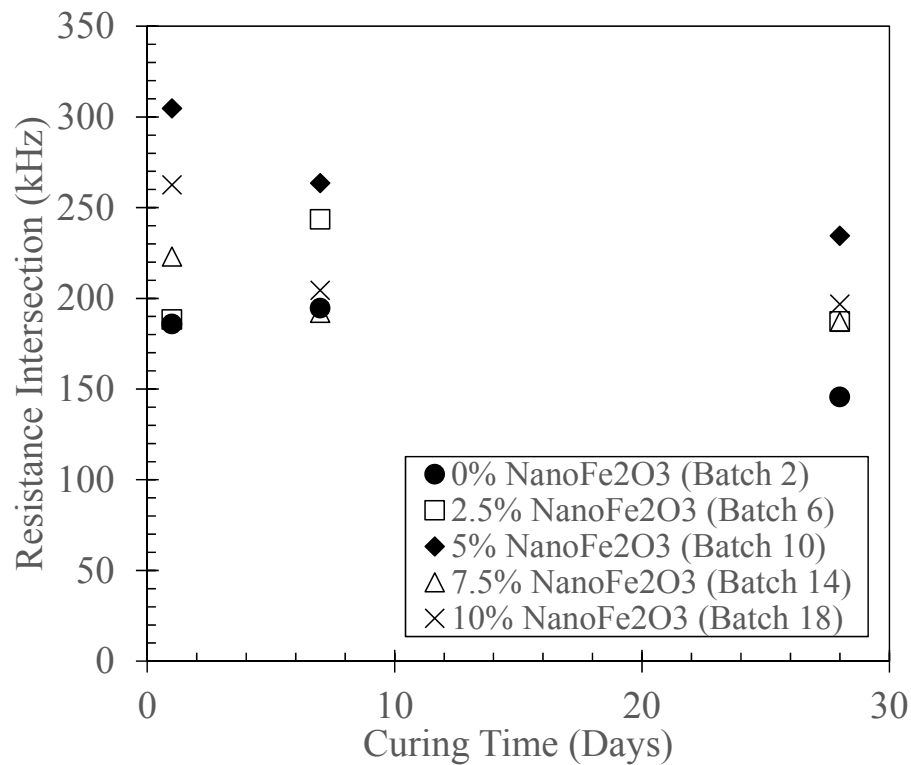


**Figure B.16: 0.45 Water-Cement Ratio - Resistance Tangent Line Intersection.**

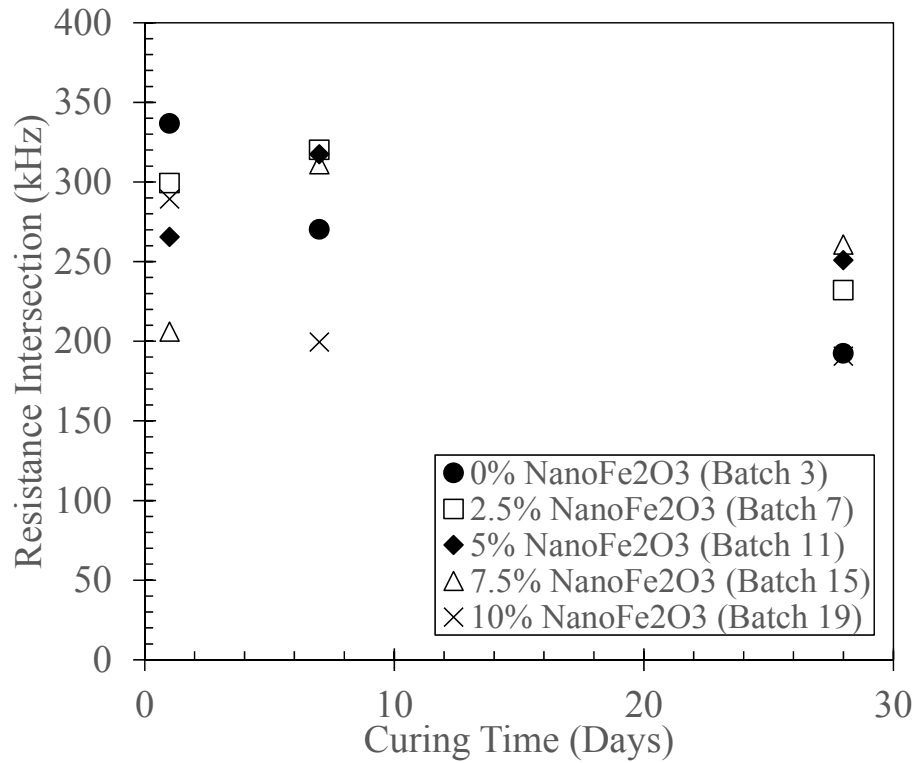


**Figure B.17: 0.50 Water-Cement Ratio - Resistance Tangent Line Intersection.**

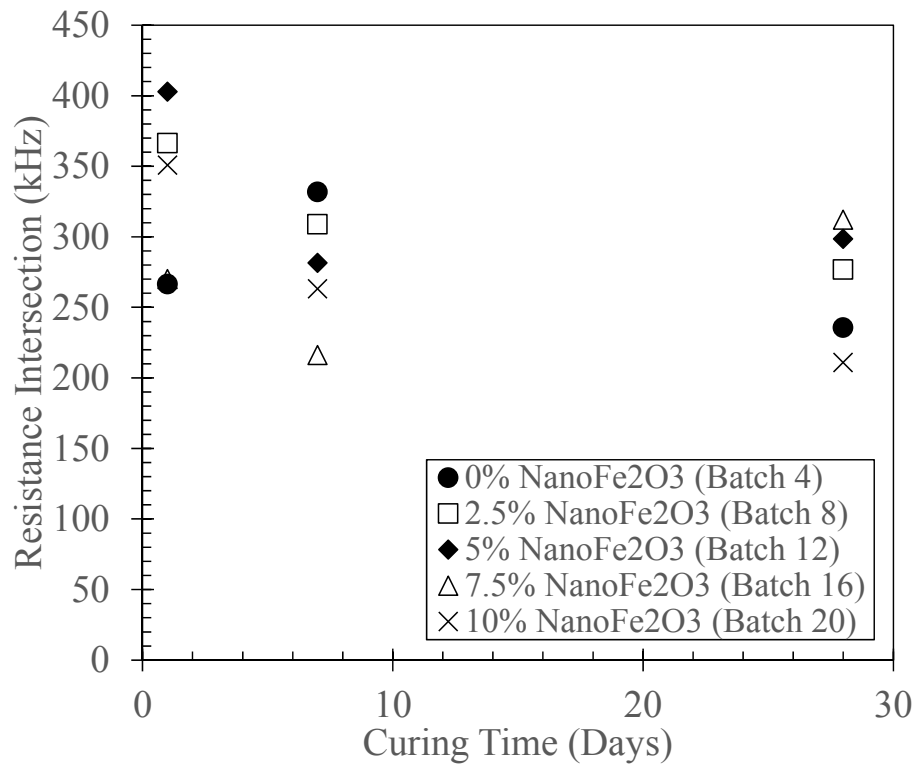


**Figure B.18: 0.60 Water-Cement Ratio - Resistance Tangent Line Intersection.**

Frequency Sweep Capacitance vs. Frequency Graphs:

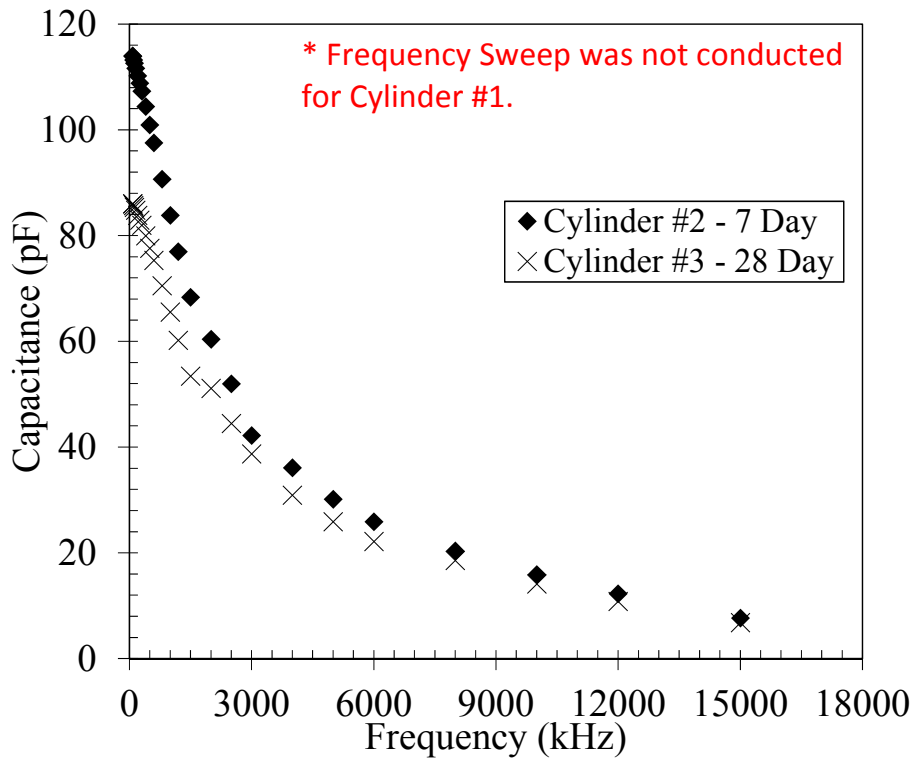


**Figure B.19: Capacitance vs. Frequency – Batch 1.**

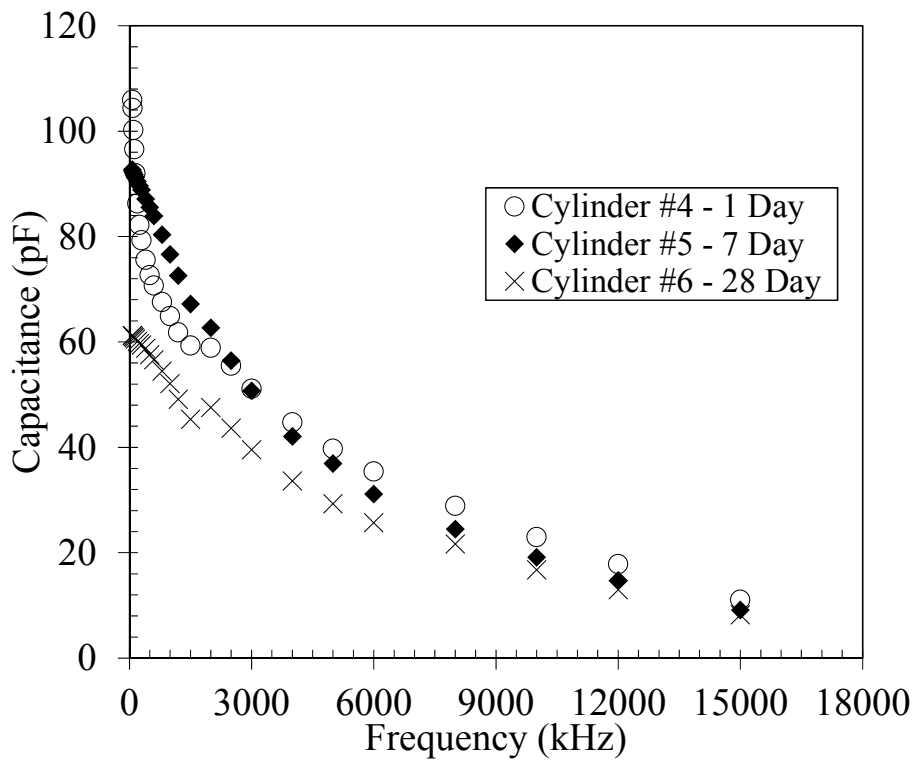


**Figure B.20: Capacitance vs. Frequency – Batch 2.**

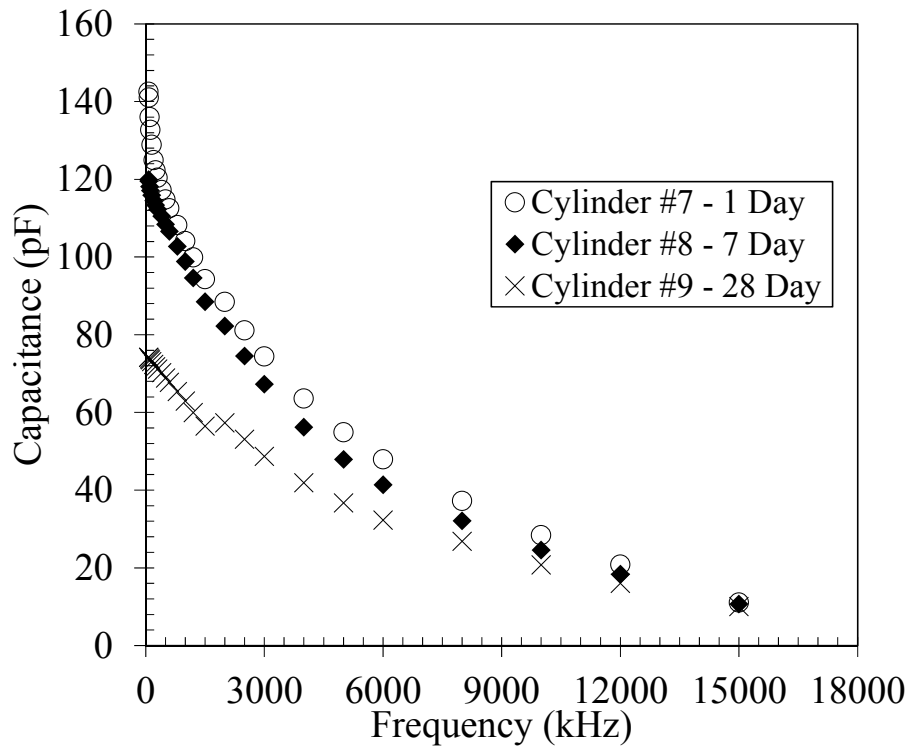


**Figure B.21: Capacitance vs. Frequency – Batch 3.**

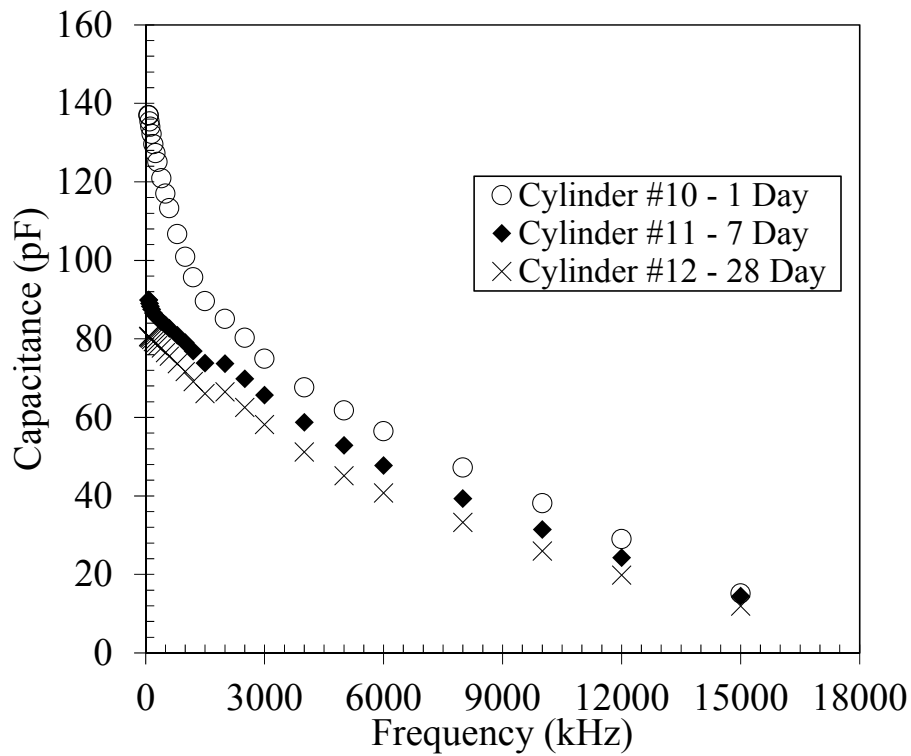


**Figure B.22: Capacitance vs. Frequency – Batch 4.**

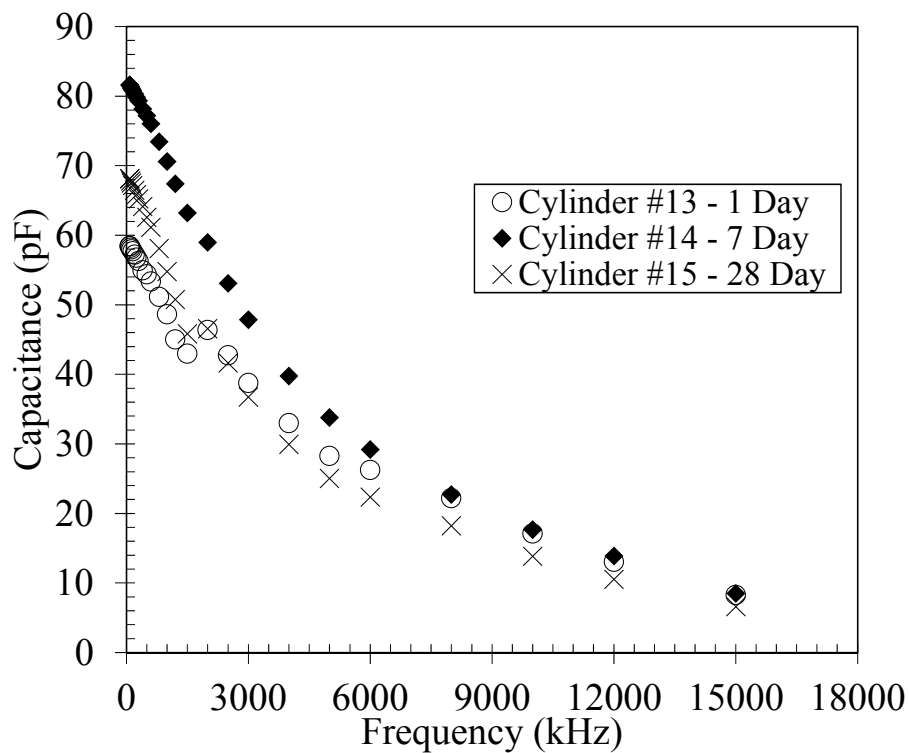


Figure B.23: Capacitance vs. Frequency – Batch 5.

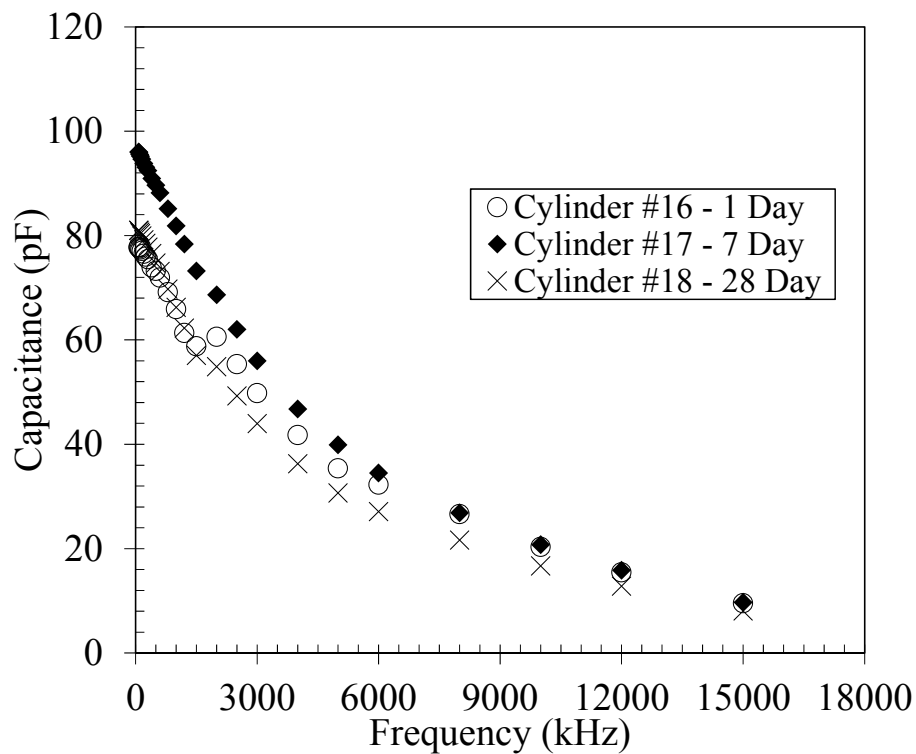


Figure B.24: Capacitance vs. Frequency – Batch 6.

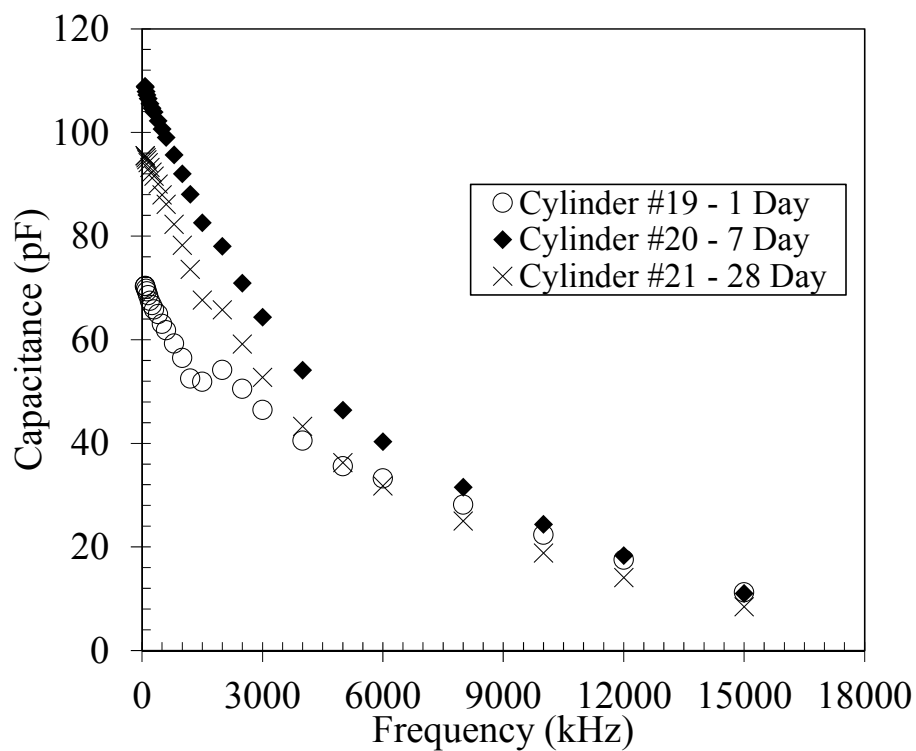


Figure B.25: Capacitance vs. Frequency – Batch 7.

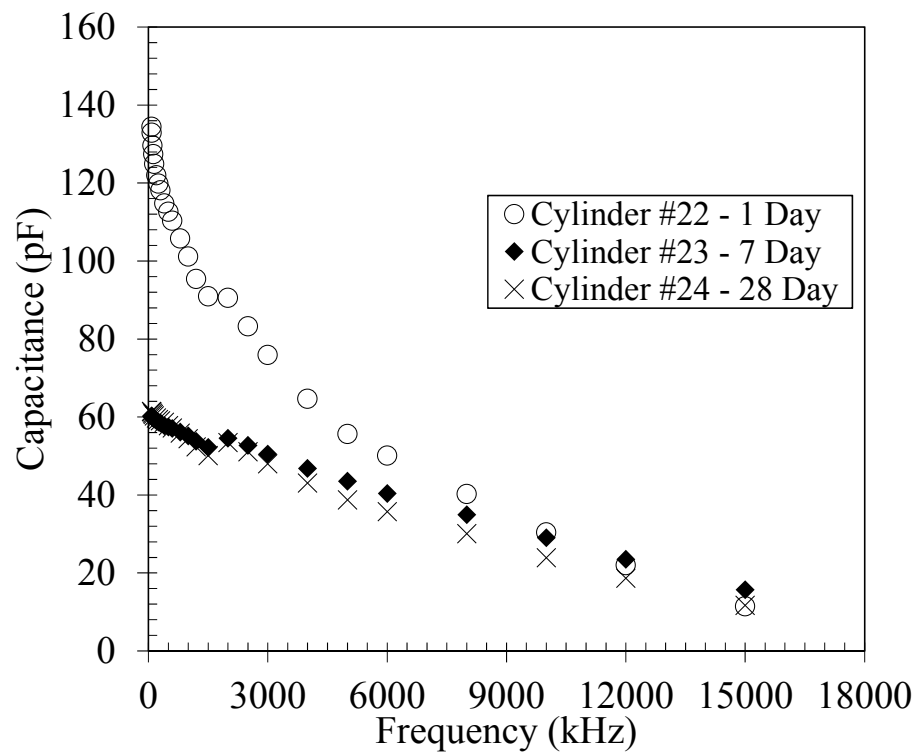


Figure B.26: Capacitance vs. Frequency – Batch 8.



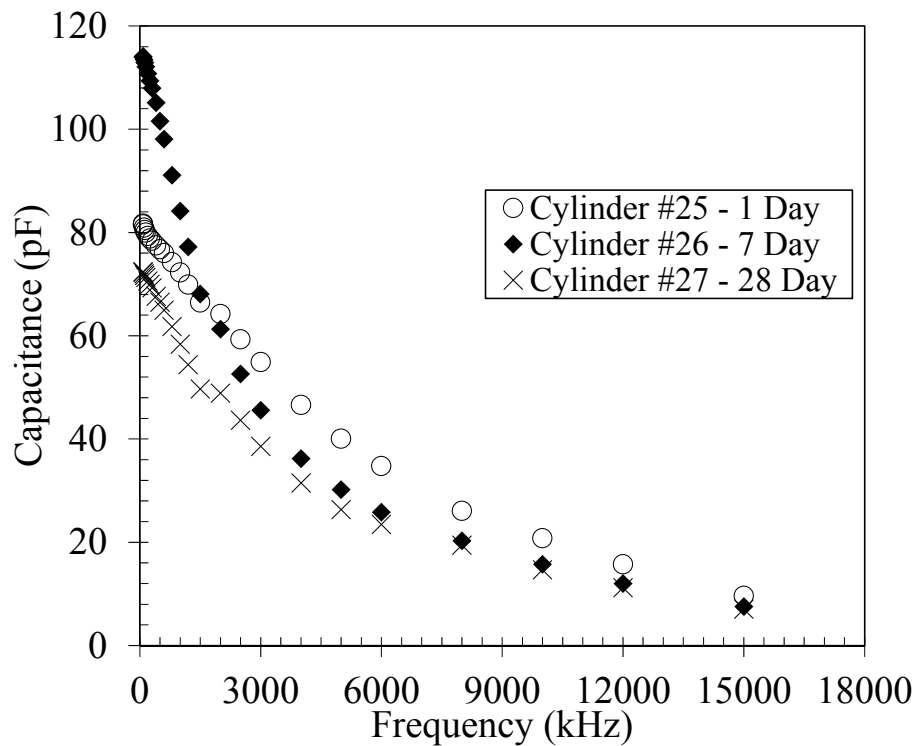


Figure B.27: Capacitance vs. Frequency – Batch 9.

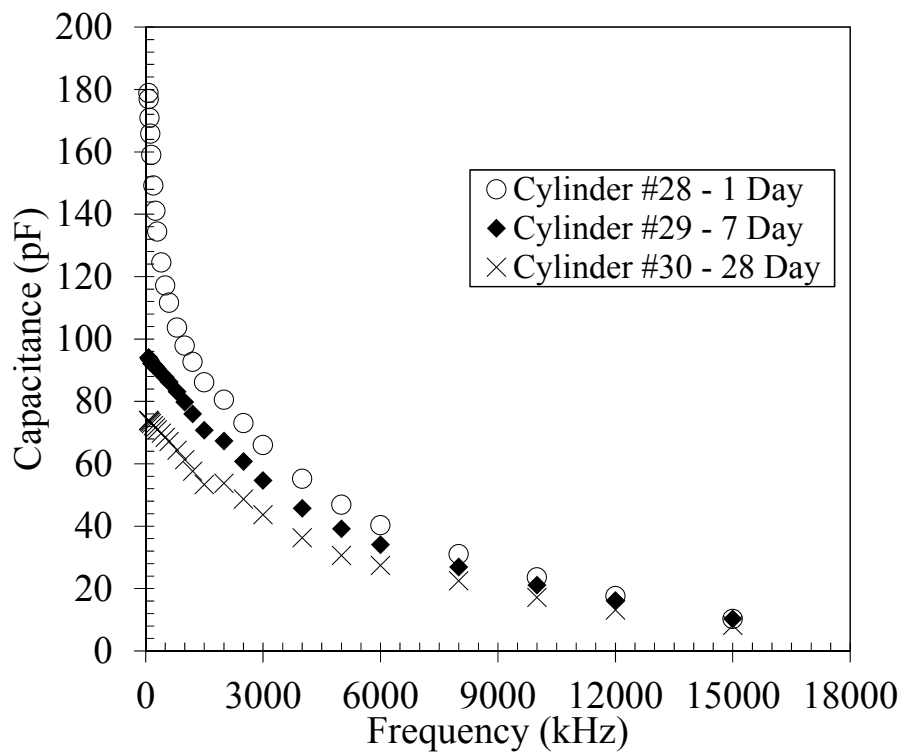


Figure B.28: Capacitance vs. Frequency – Batch 10.

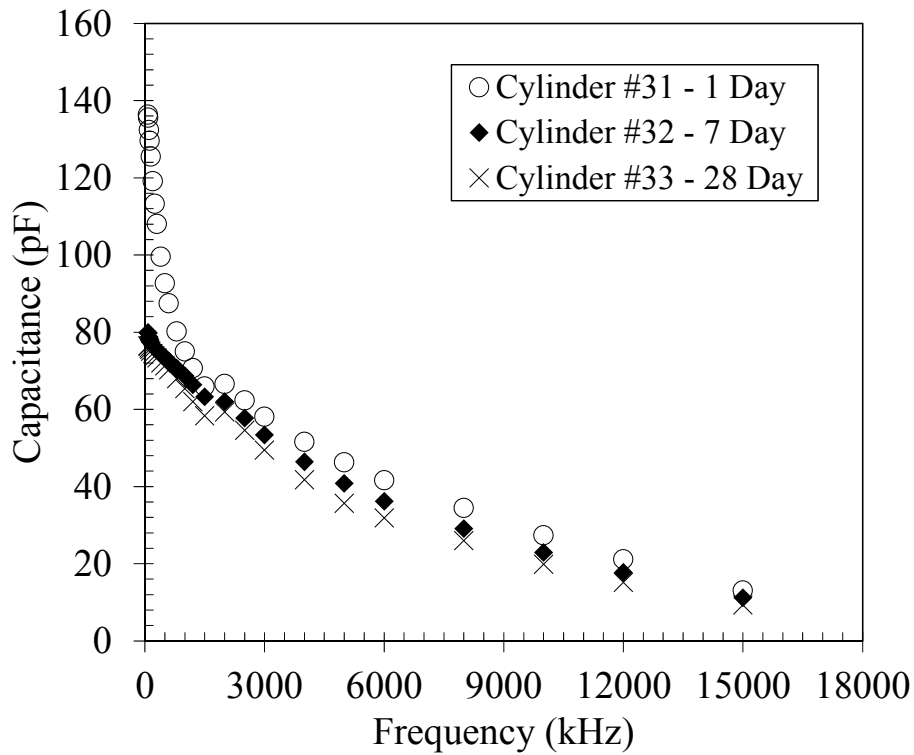


Figure B.29: Capacitance vs. Frequency – Batch 11.

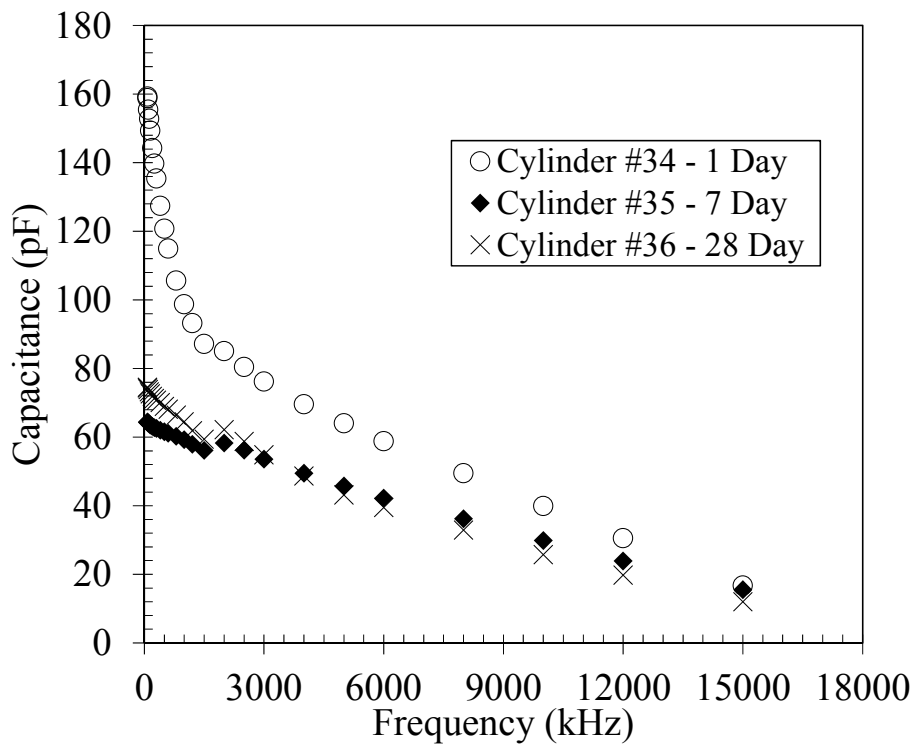


Figure B.30: Capacitance vs. Frequency – Batch 12.

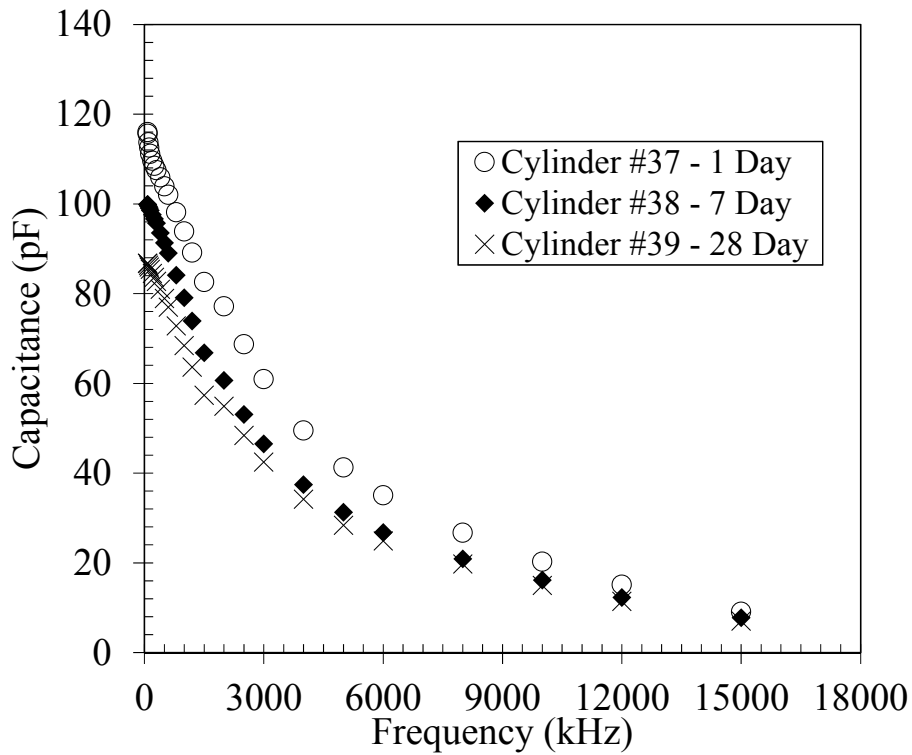


Figure B.31: Capacitance vs. Frequency – Batch 13.

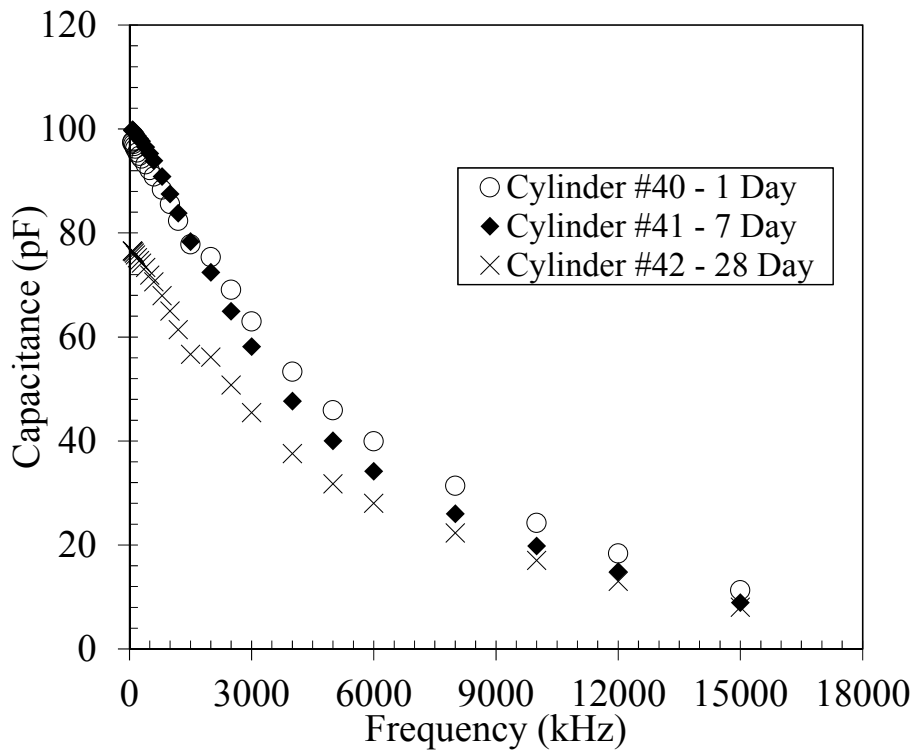


Figure B.32: Capacitance vs. Frequency – Batch 14.

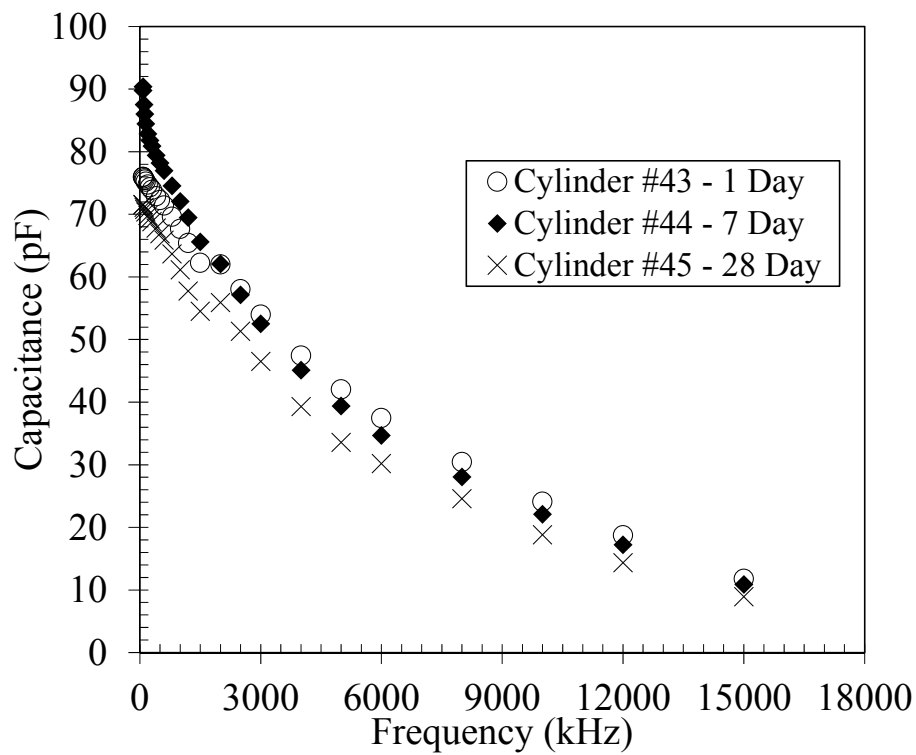


Figure B.33: Capacitance vs. Frequency – Batch 15.

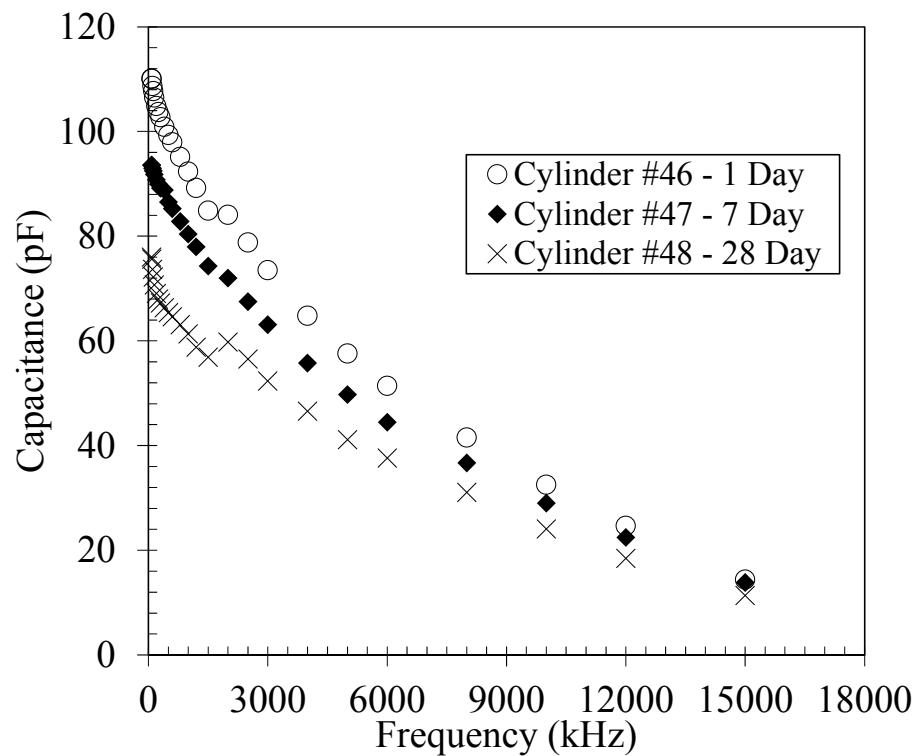


Figure B.34: Capacitance vs. Frequency – Batch 16.

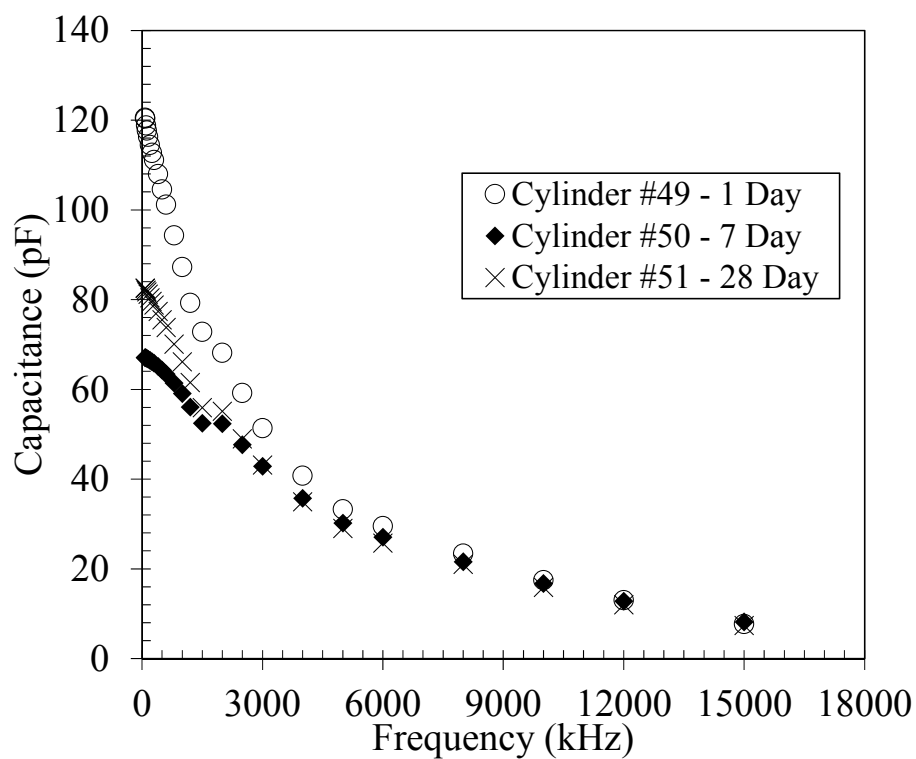


Figure B.35: Capacitance vs. Frequency – Batch 17.

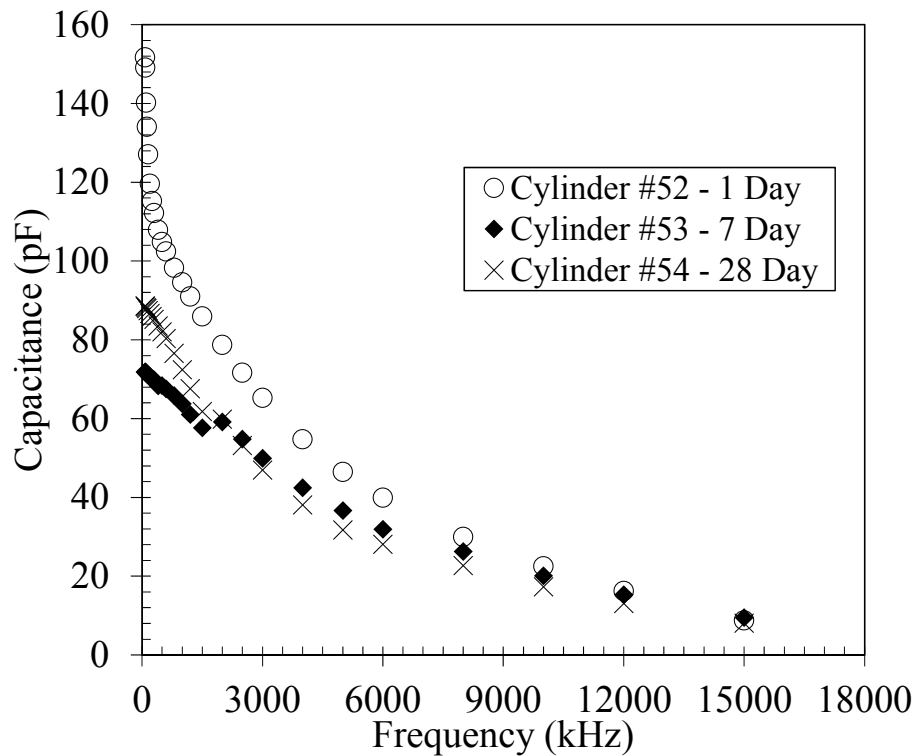
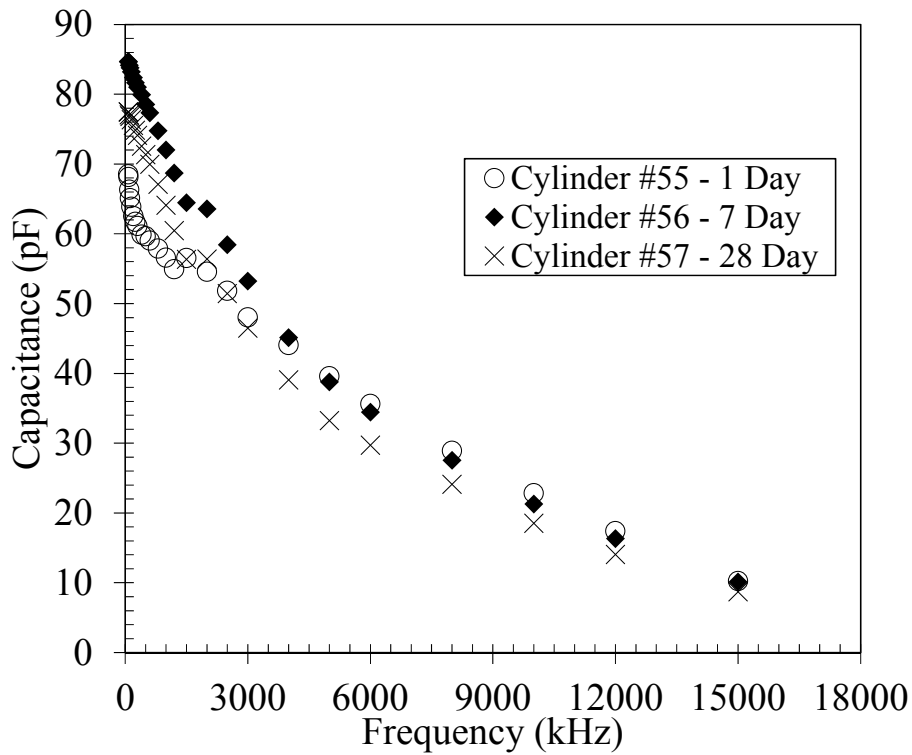
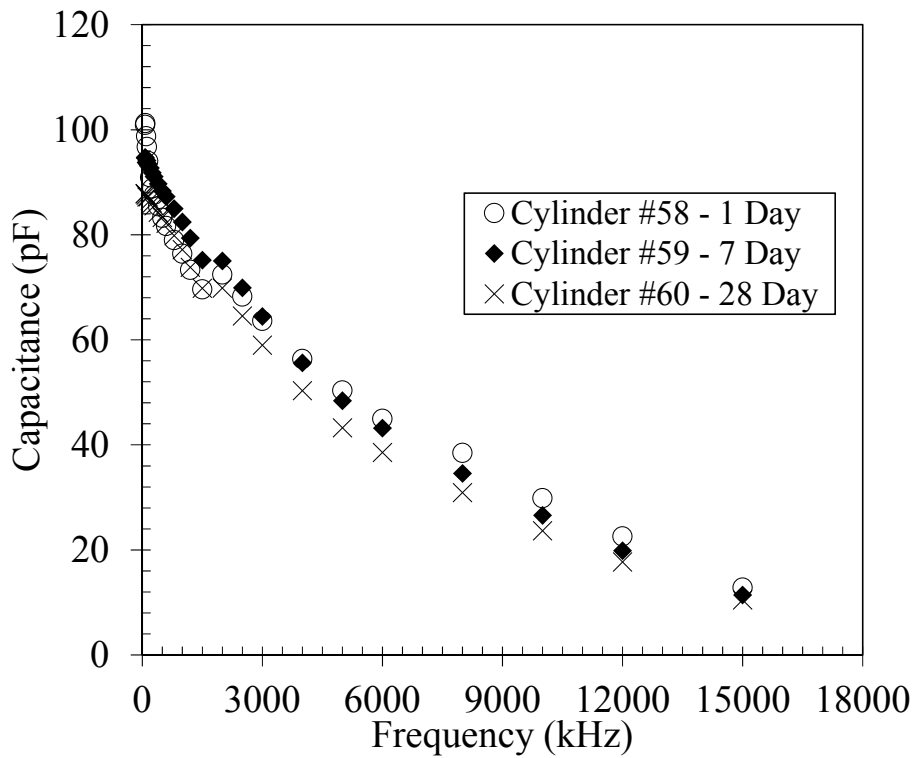


Figure B.36: Capacitance vs. Frequency – Batch 18.



**Figure B.37: Capacitance vs. Frequency – Batch 19.**



**Figure B.38: Capacitance vs. Frequency – Batch 20.**

Frequency Sweep Resistance vs. Frequency Graphs:

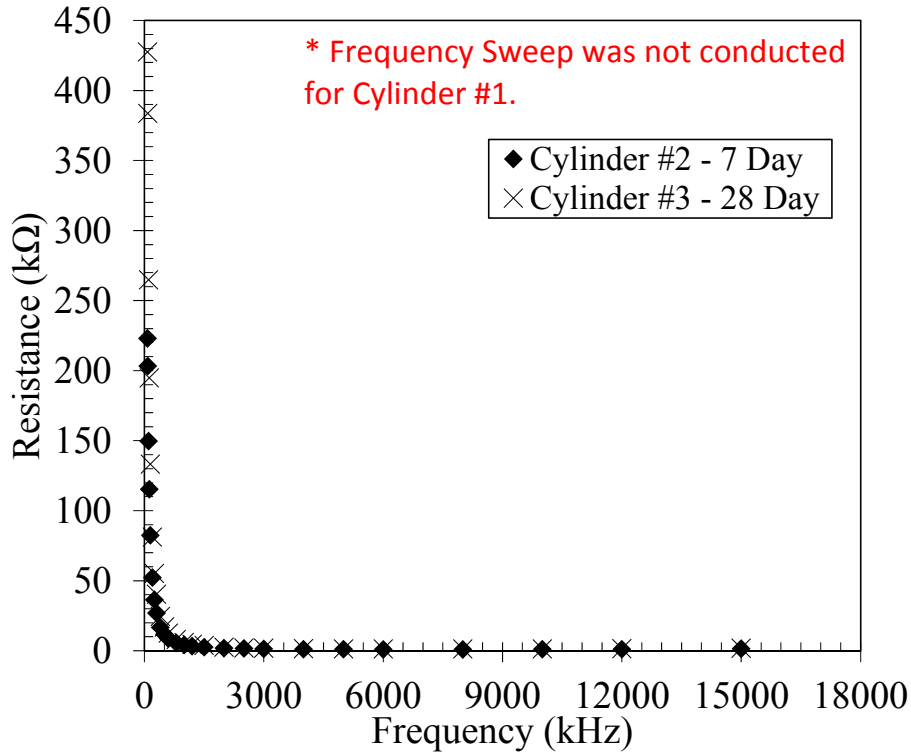


**Figure B.39: Resistance vs. Frequency – Batch 1.**

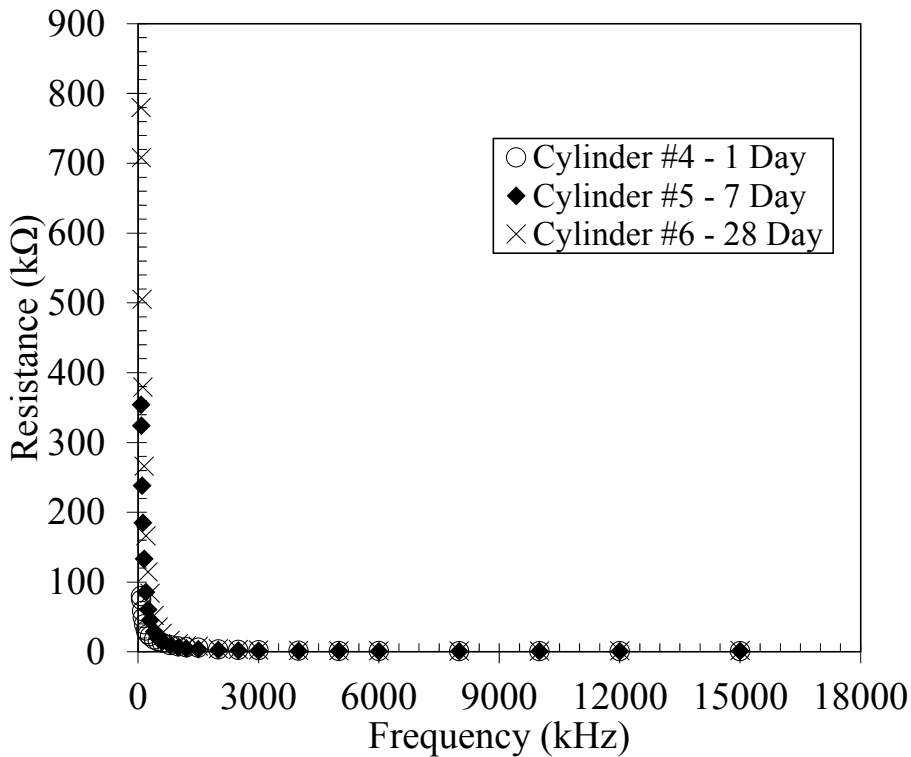


**Figure B.40: Resistance vs. Frequency – Batch 2.**

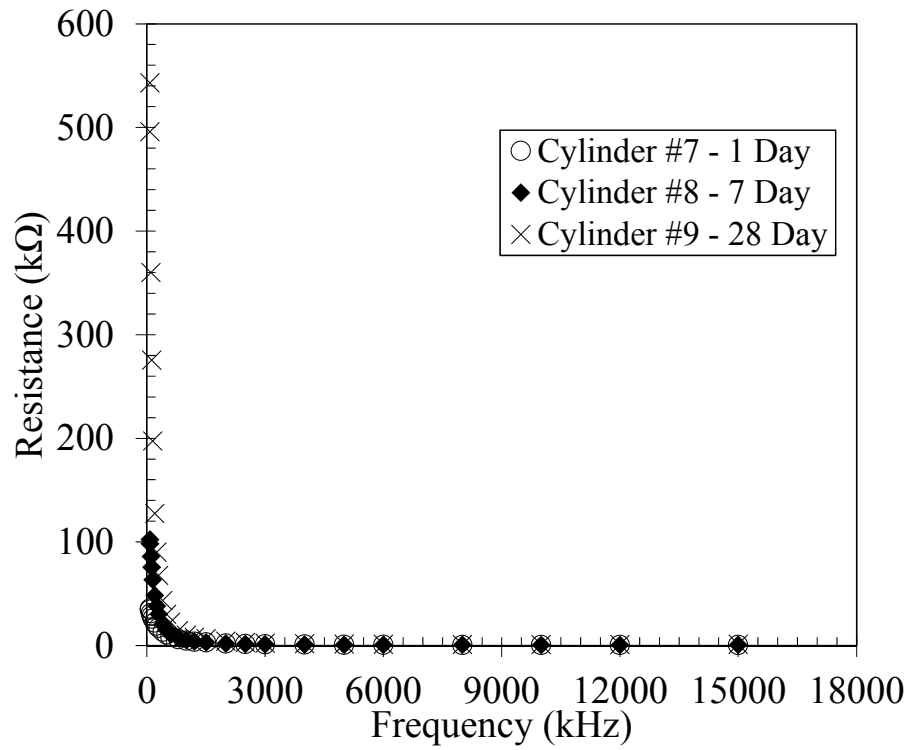


**Figure B.41: Resistance vs. Frequency – Batch 3.**

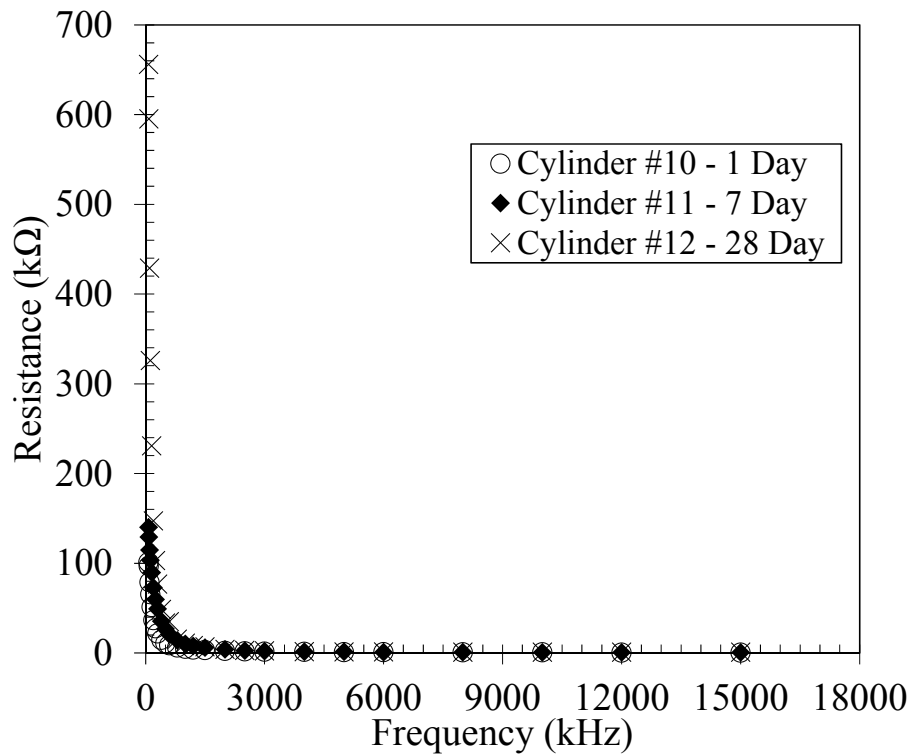


**Figure B.42: Resistance vs. Frequency – Batch 4.**



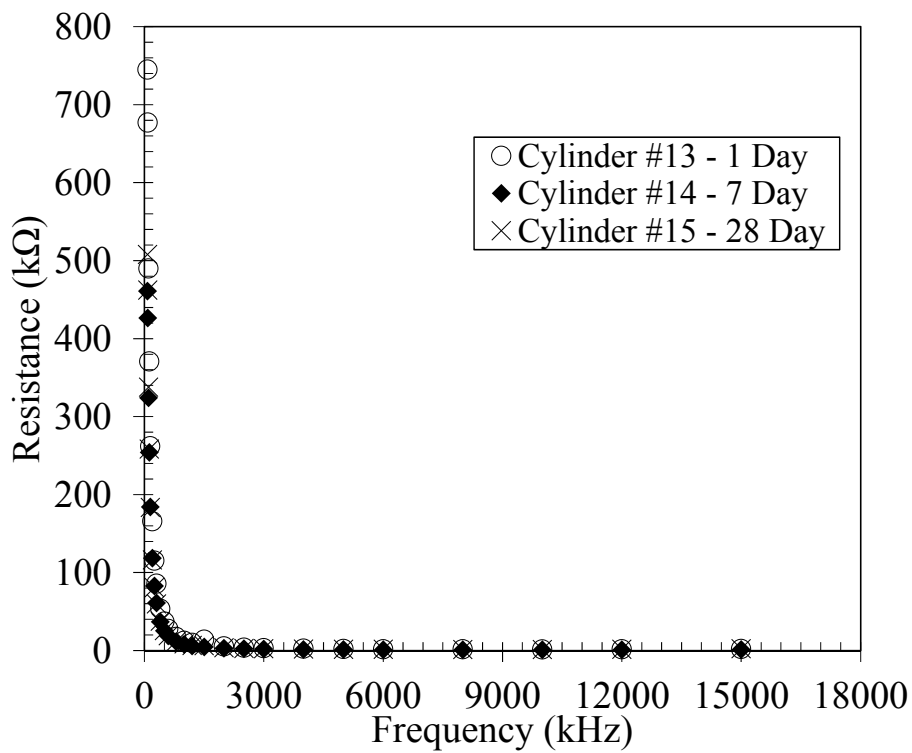


Figure B.43: Resistance vs. Frequency – Batch 5.

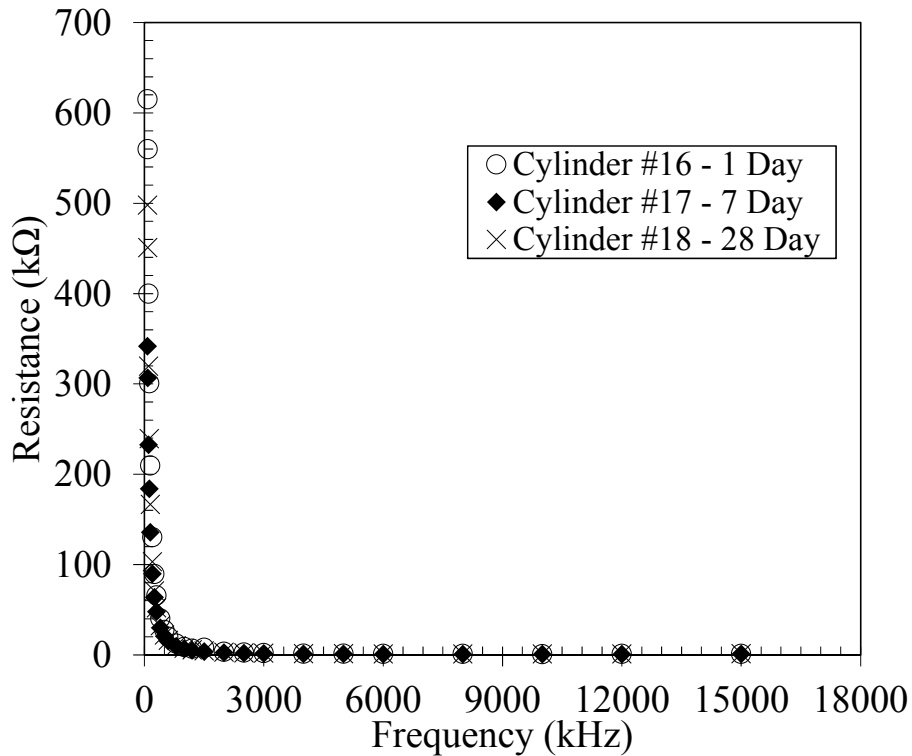


Figure B.44: Resistance vs. Frequency – Batch 6.

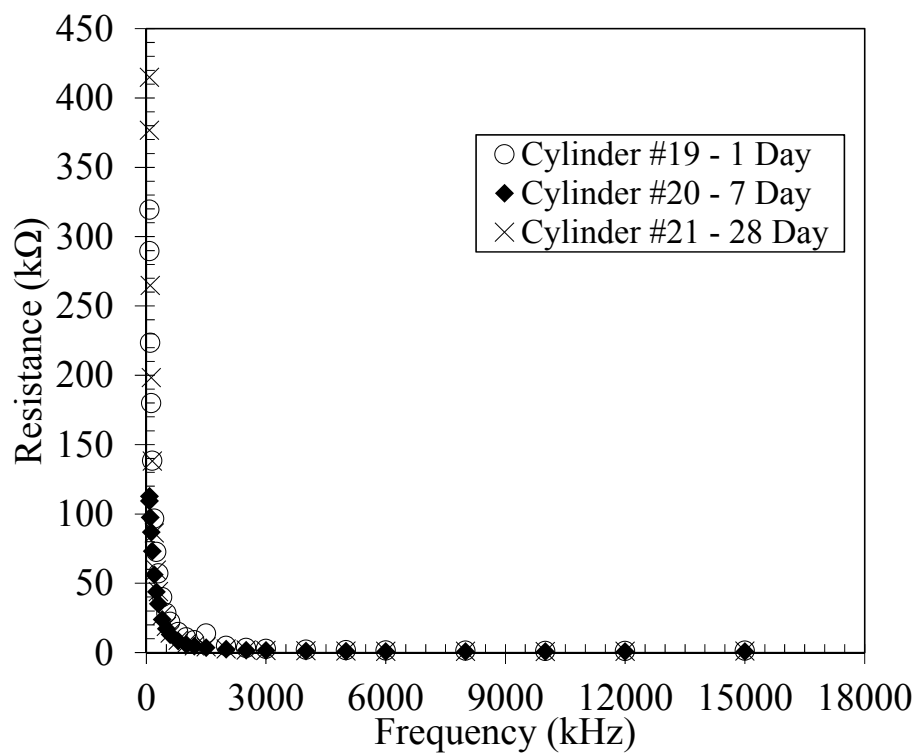


Figure B.45: Resistance vs. Frequency – Batch 7.

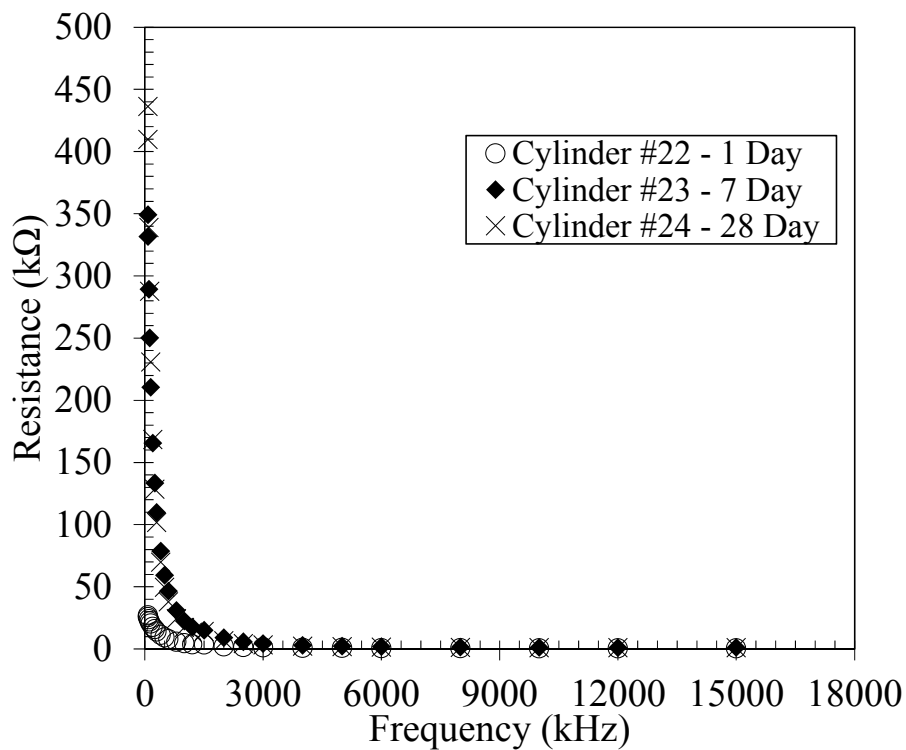


Figure B.46: Resistance vs. Frequency – Batch 8.

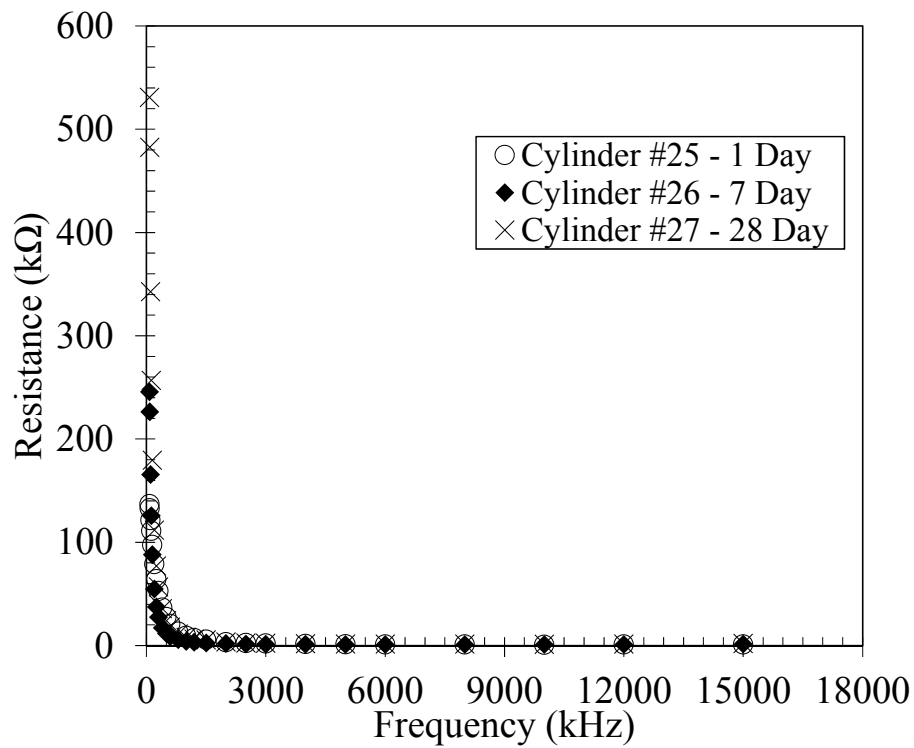


Figure B.47: Resistance vs. Frequency – Batch 9.

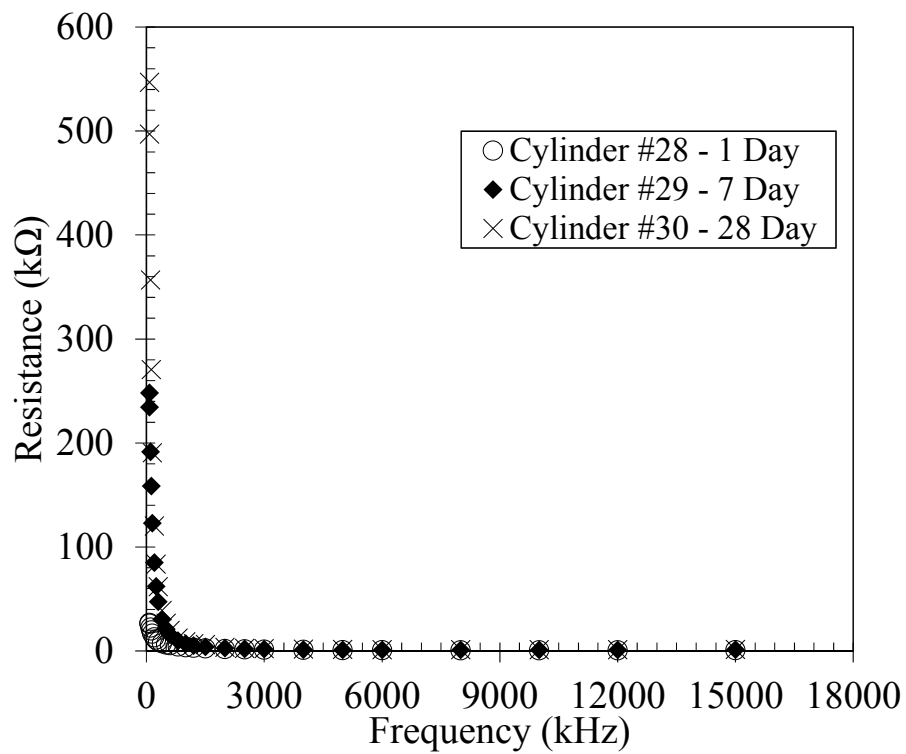


Figure B.48: Resistance vs. Frequency – Batch 10.

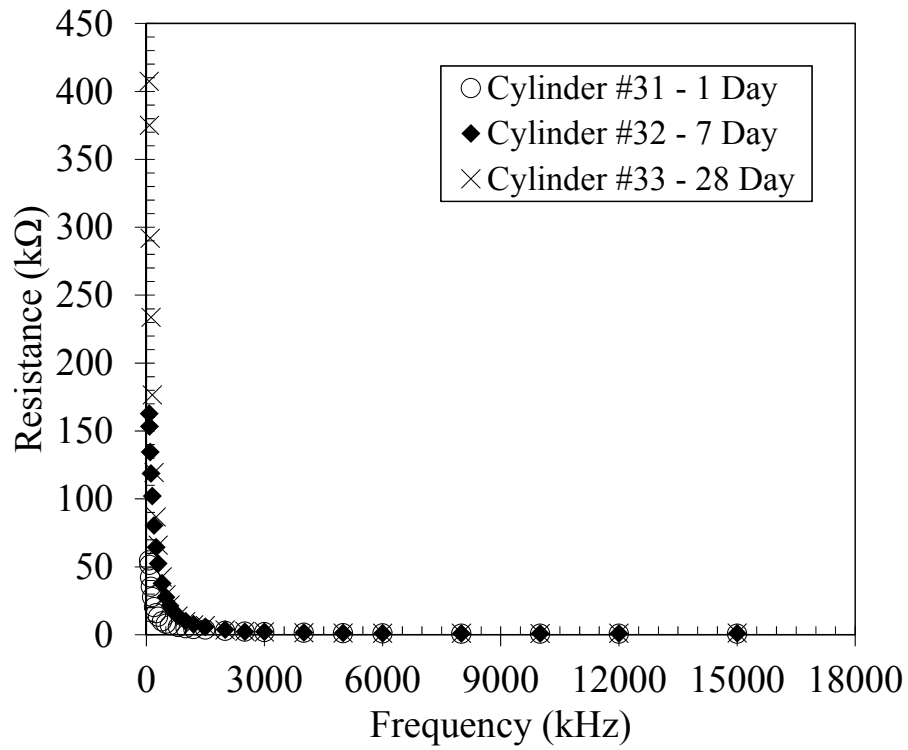


Figure B.49: Resistance vs. Frequency – Batch 11.

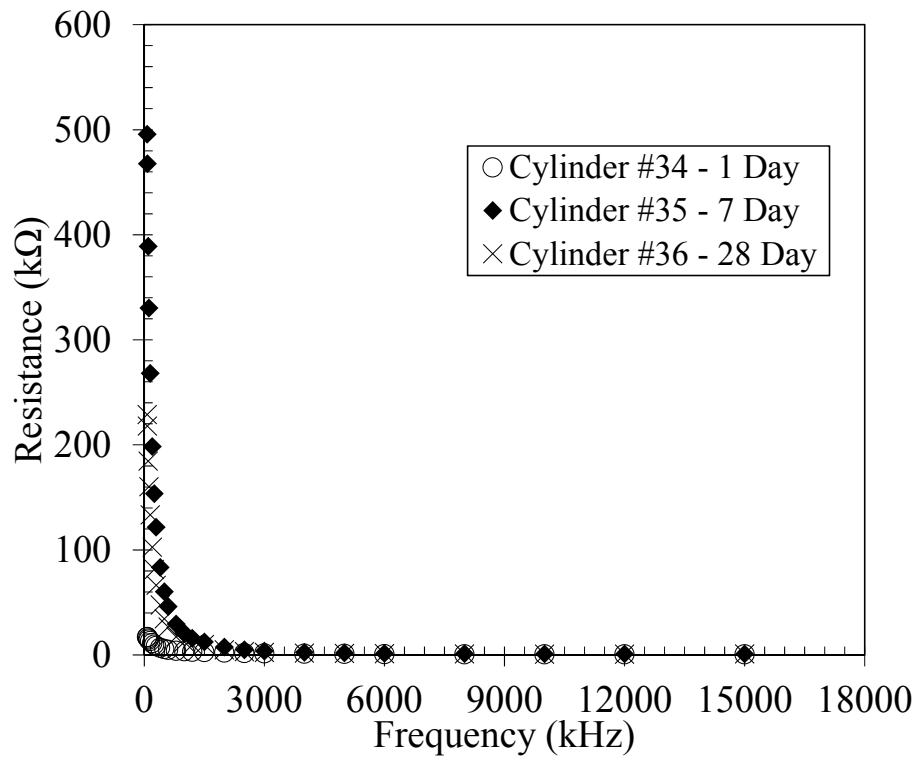


Figure B.50: Resistance vs. Frequency – Batch 12.

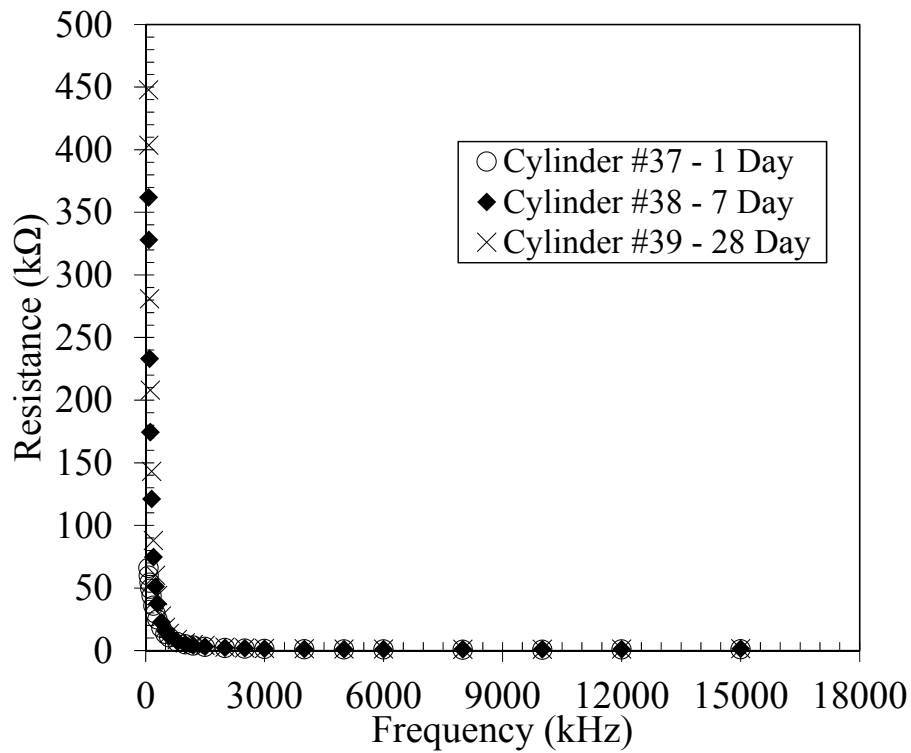


Figure B.51: Resistance vs. Frequency – Batch 13.

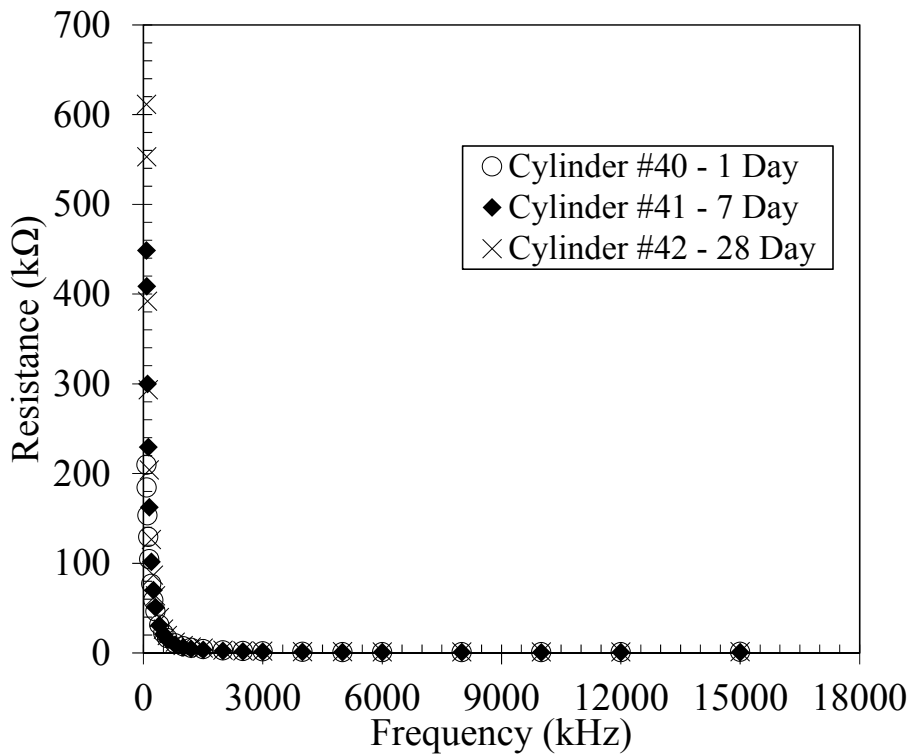


Figure B.52: Resistance vs. Frequency – Batch 14.

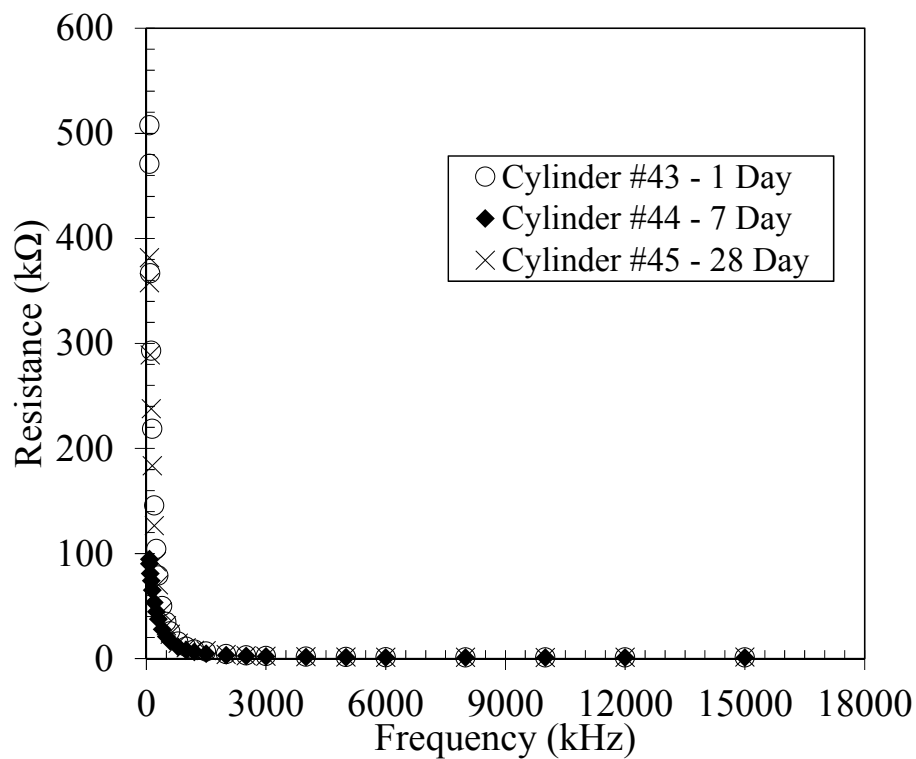


Figure B.53: Resistance vs. Frequency – Batch 15.

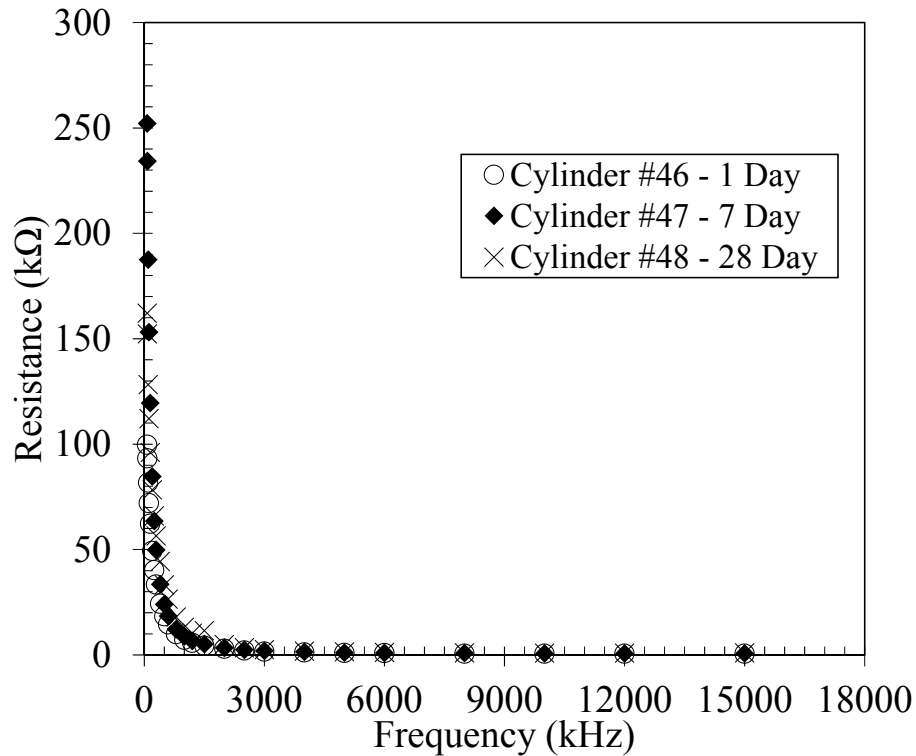


Figure B.54: Resistance vs. Frequency – Batch 16.

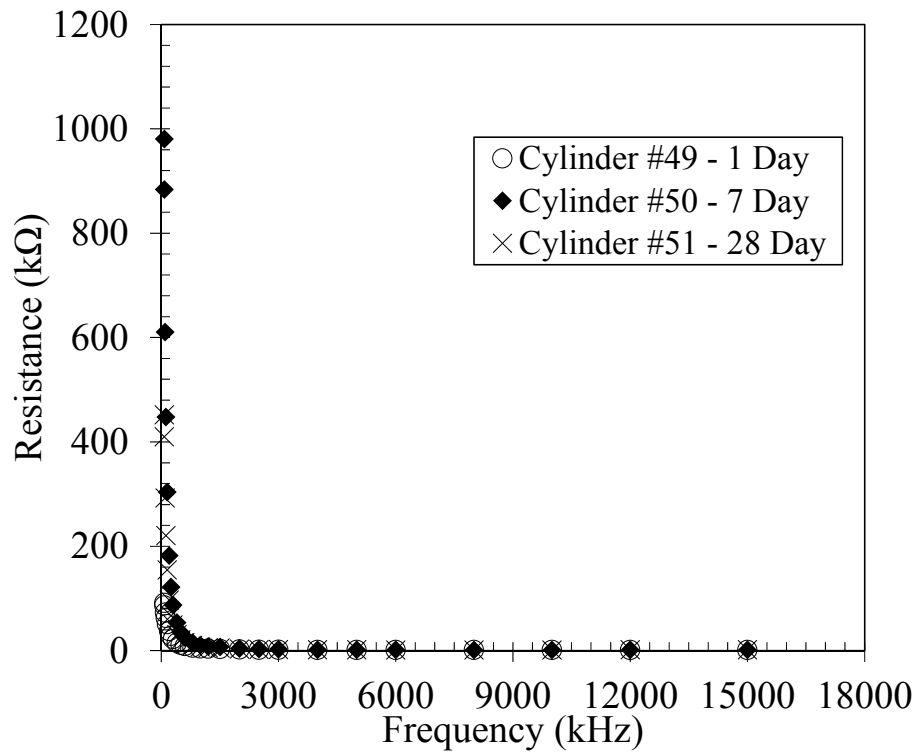


Figure B.55: Resistance vs. Frequency – Batch 17.

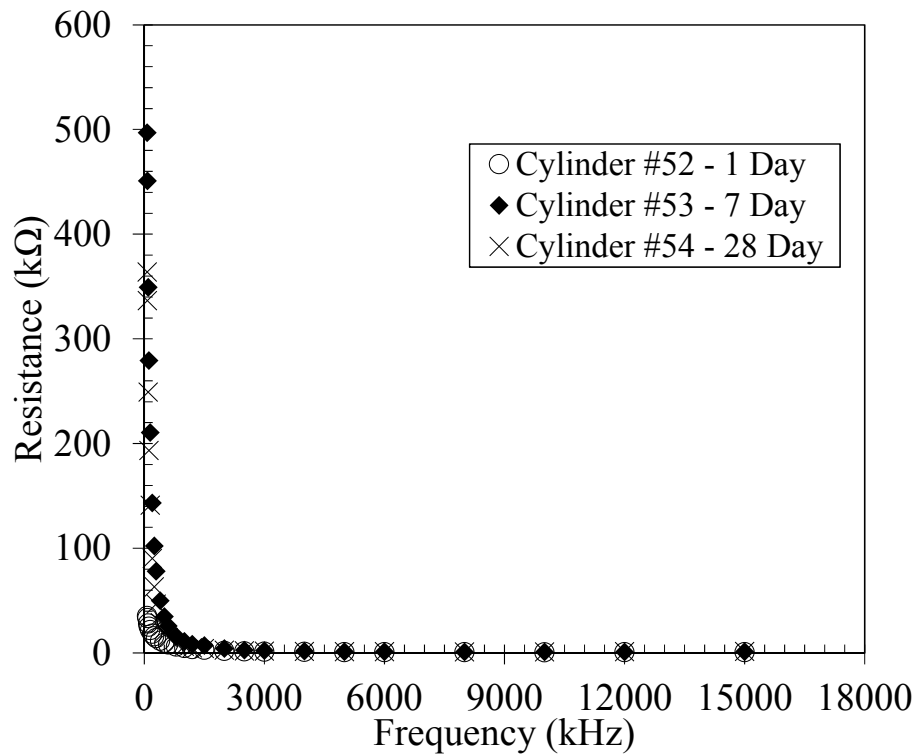


Figure B.56: Resistance vs. Frequency – Batch 18.

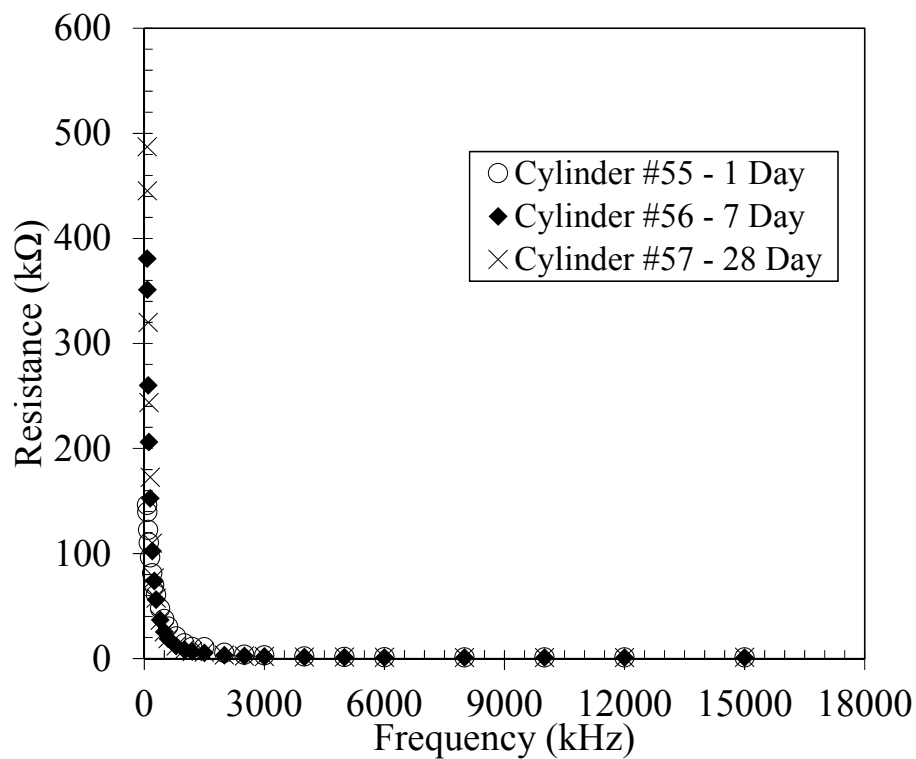


Figure B.57: Resistance vs. Frequency – Batch 19.

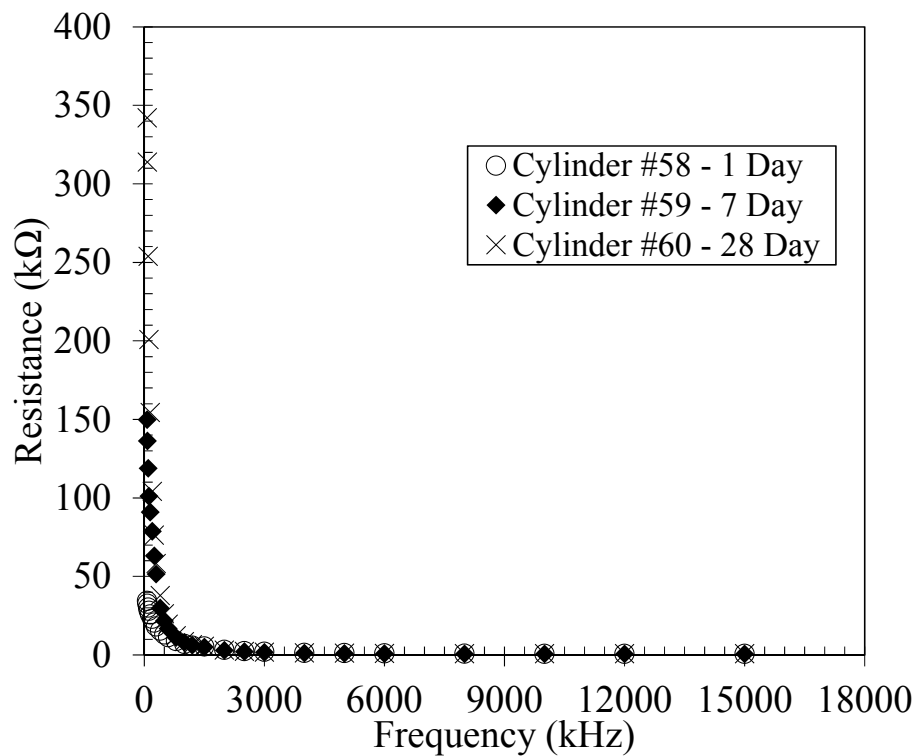


Figure B.58: Resistance vs. Frequency – Batch 20.



---

# **Appendix C**

## **Resistivity Index Testing**

Resistivity Index Testing Behavior over 24 Hours:

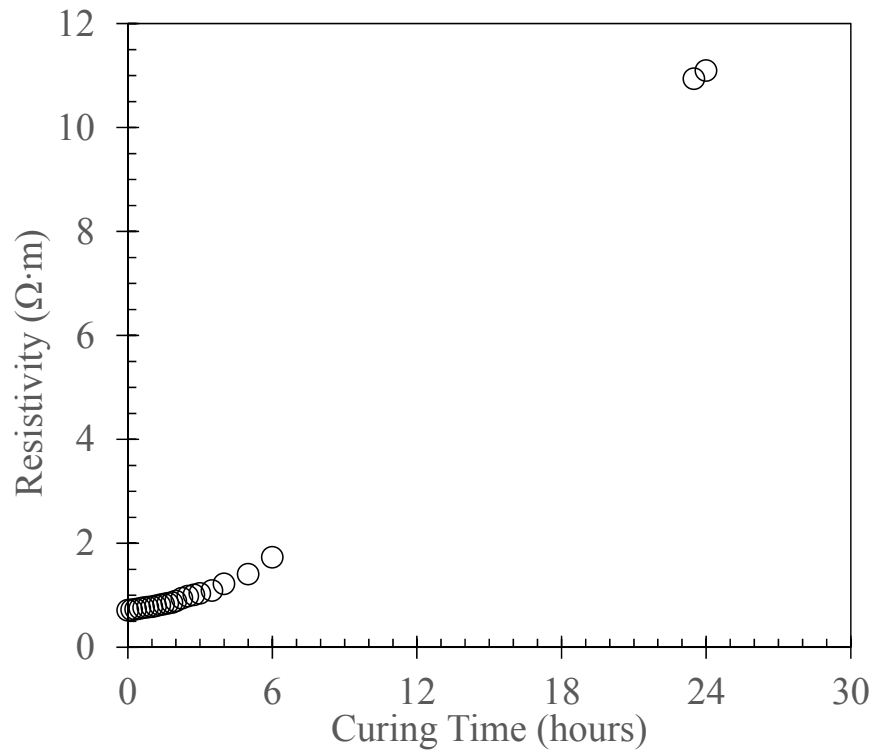


**Figure C.1: Resistivity vs. Curing Time Behavior – Batch 1.**

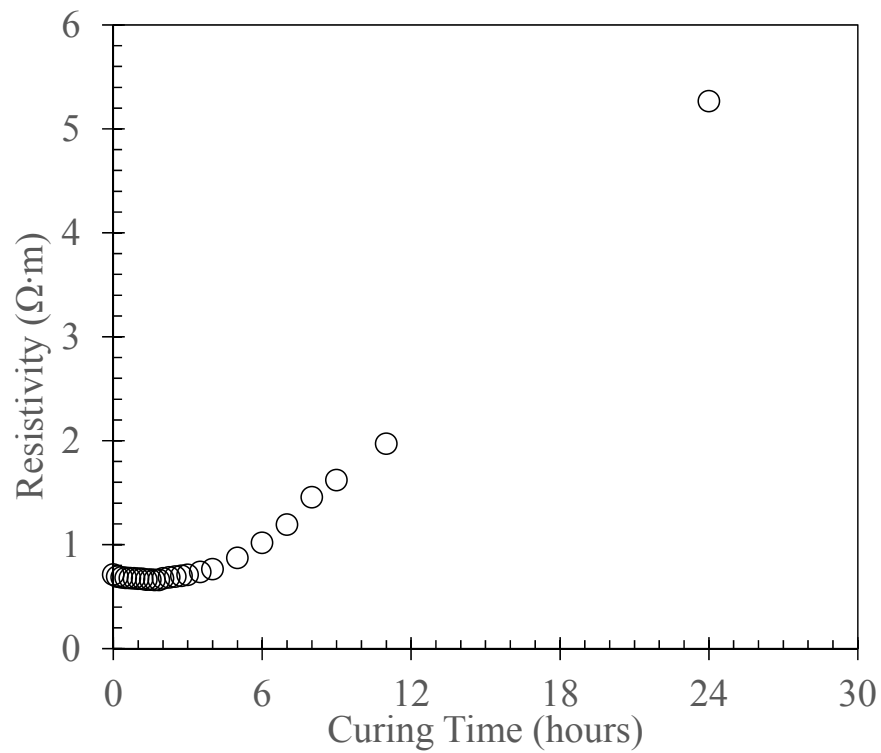


**Figure C.2: Resistivity vs. Curing Time Behavior – Batch 2.**

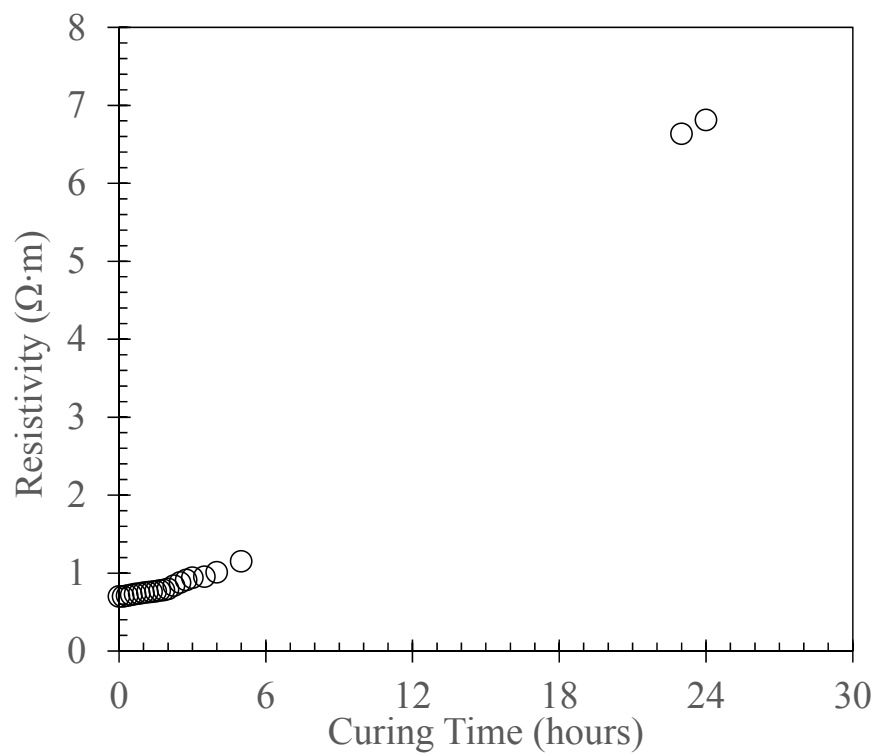


**Figure C.3: Resistivity vs. Curing Time Behavior – Batch 3.**

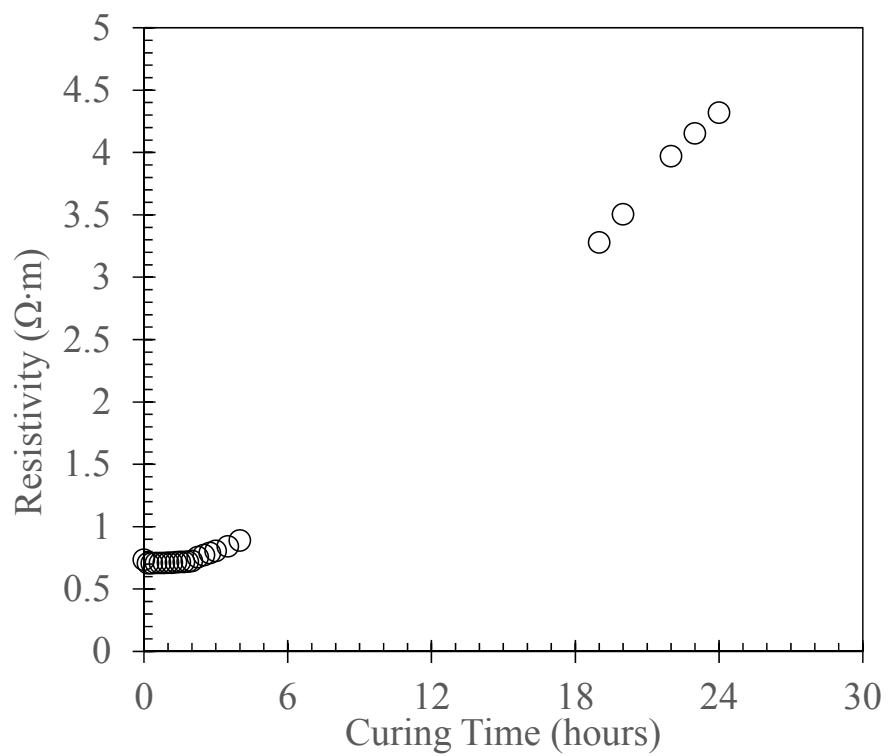


**Figure C.4: Resistivity vs. Curing Time Behavior – Batch 4.**

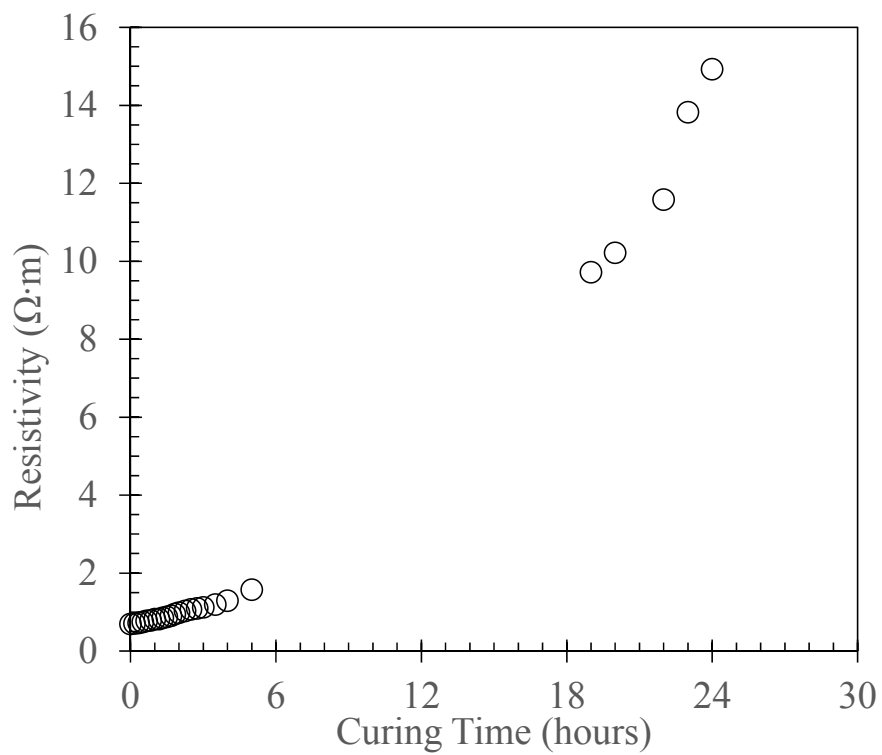


**Figure C.5: Resistivity vs. Curing Time Behavior – Batch 5.**

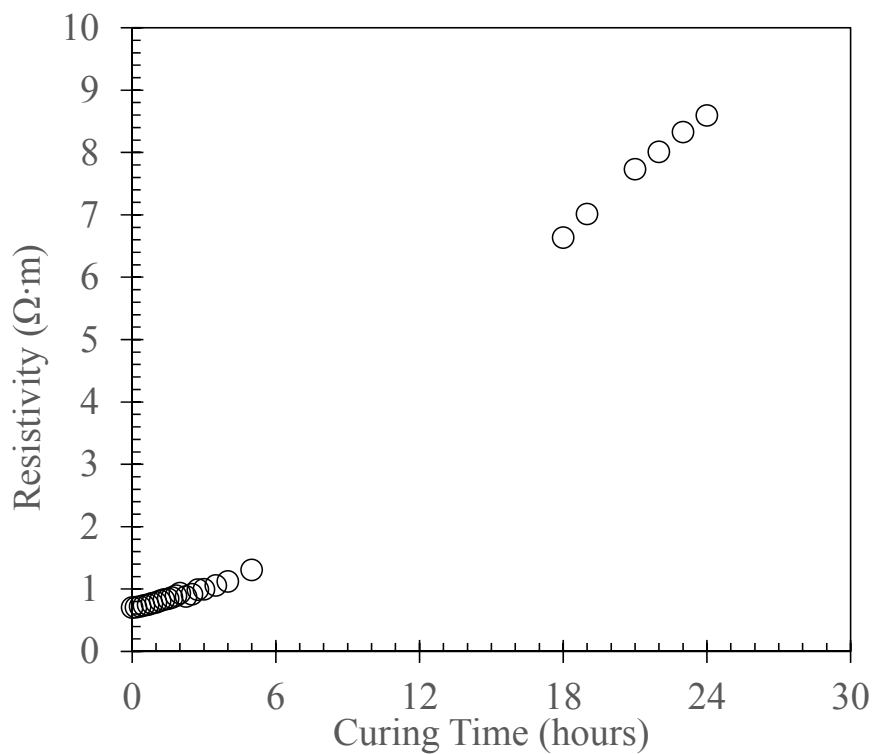


**Figure C.6: Resistivity vs. Curing Time Behavior – Batch 6.**

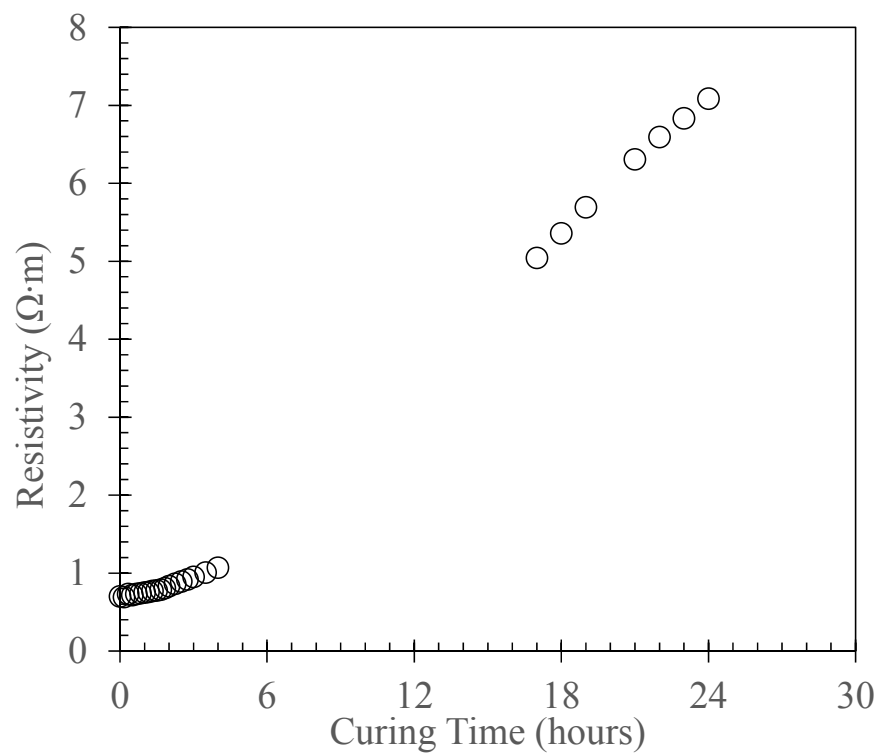


**Figure C.7: Resistivity vs. Curing Time Behavior – Batch 7.**

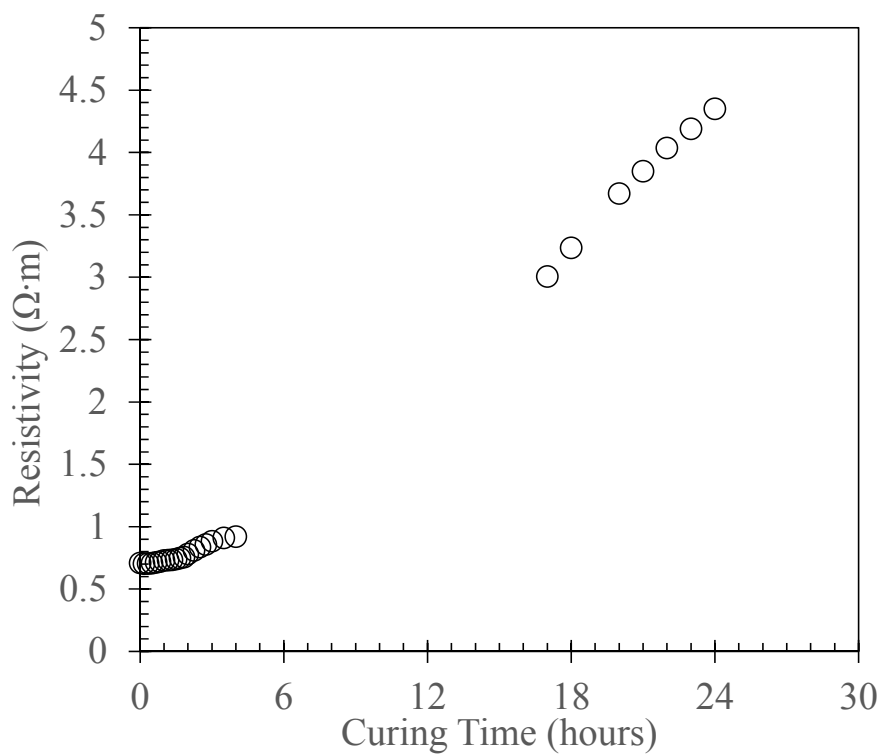


**Figure C.8: Resistivity vs. Curing Time Behavior – Batch 8.**

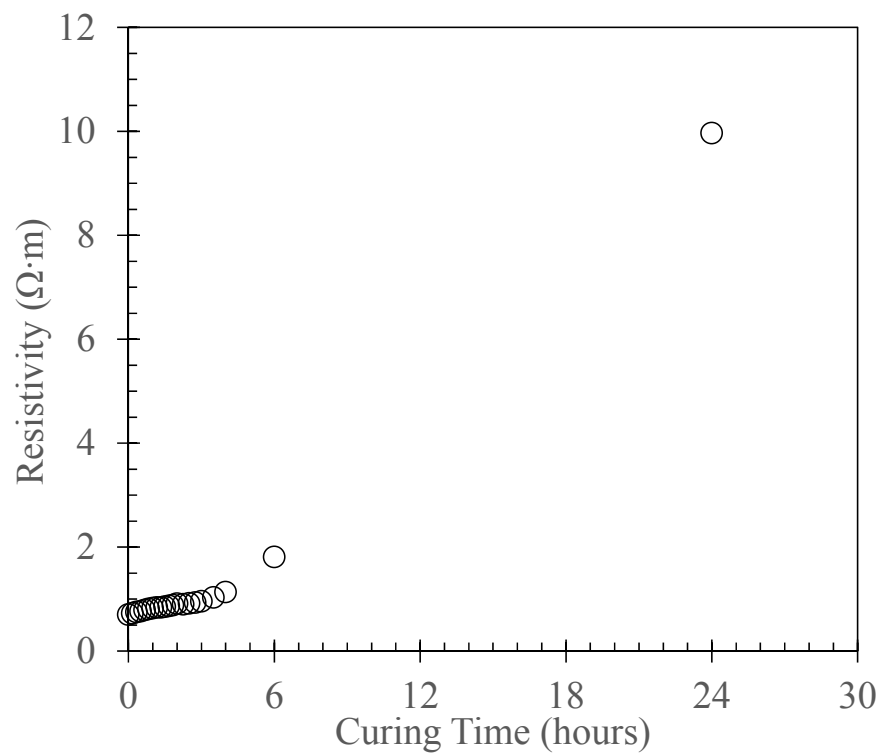


**Figure C.9: Resistivity vs. Curing Time Behavior – Batch 9.**

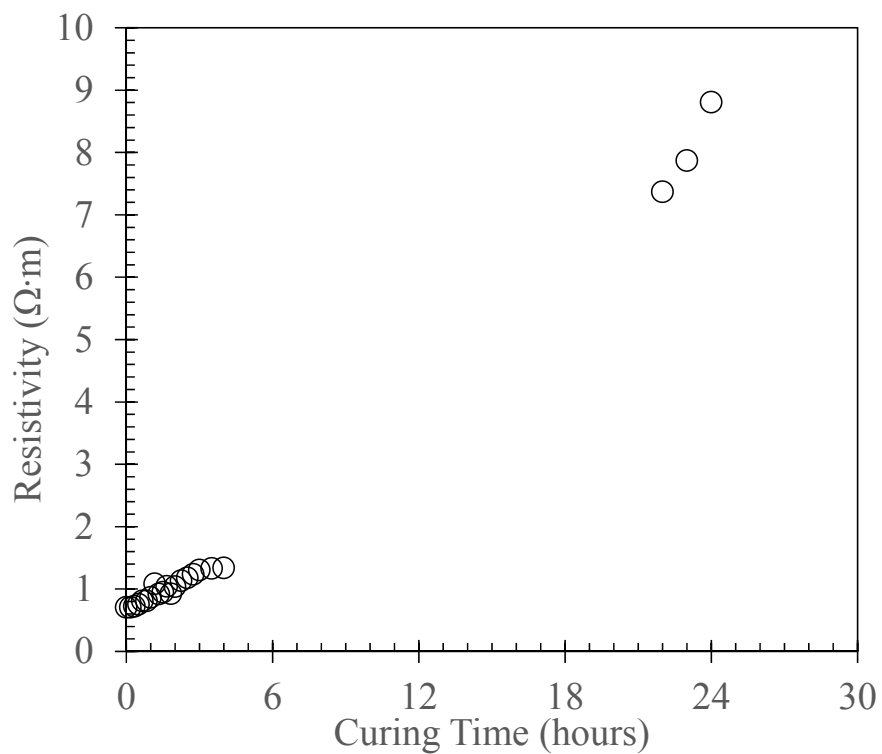


**Figure C.10: Resistivity vs. Curing Time Behavior – Batch 10.**

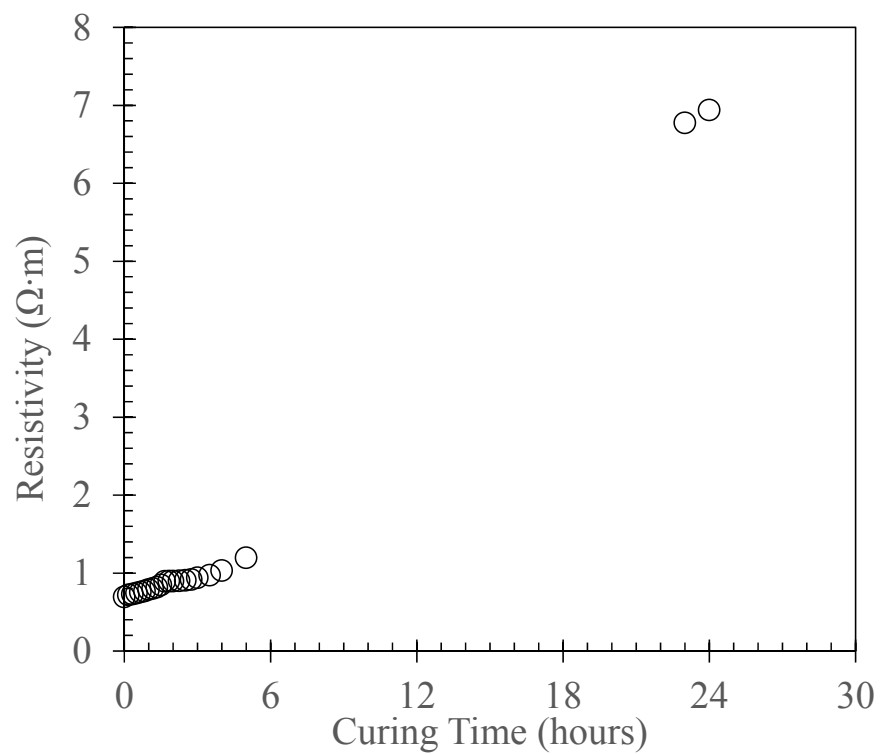


**Figure C.11: Resistivity vs. Curing Time Behavior – Batch 11.**

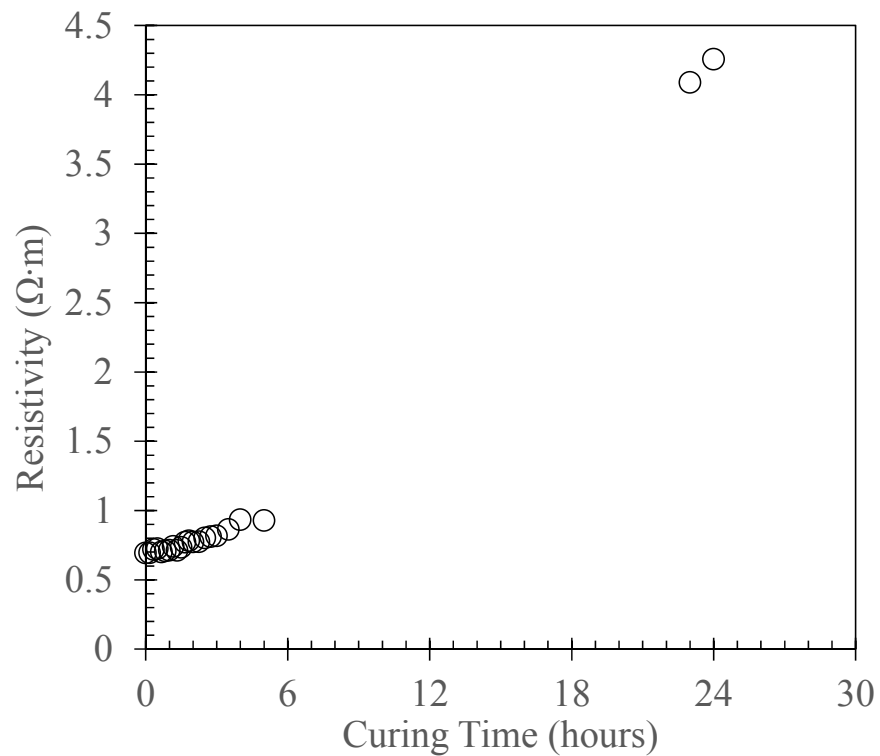


**Figure C.12: Resistivity vs. Curing Time Behavior – Batch 12.**

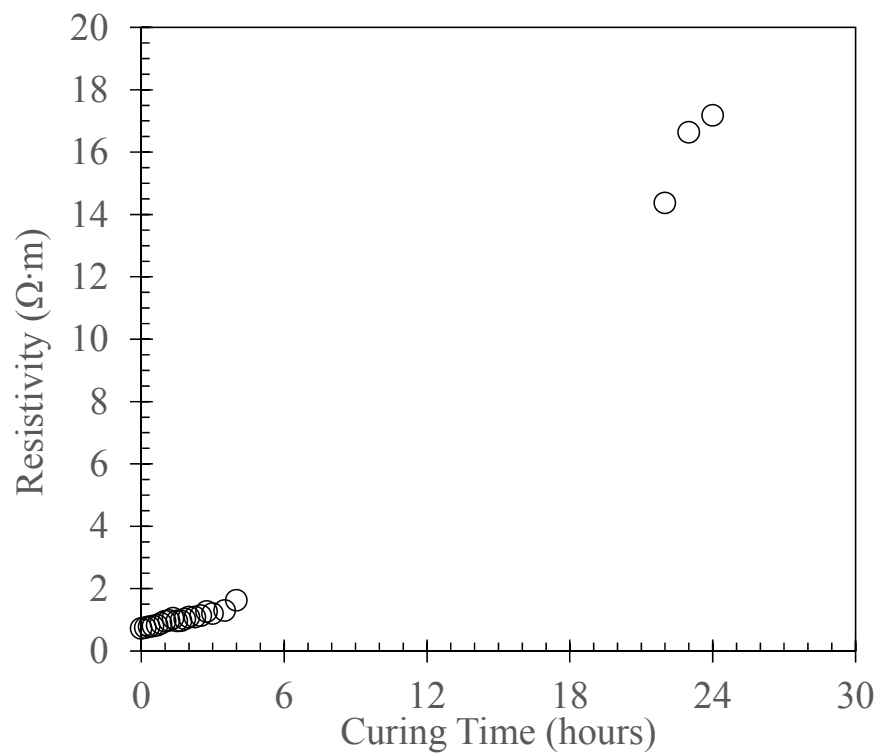


**Figure C.13: Resistivity vs. Curing Time Behavior – Batch 13.**

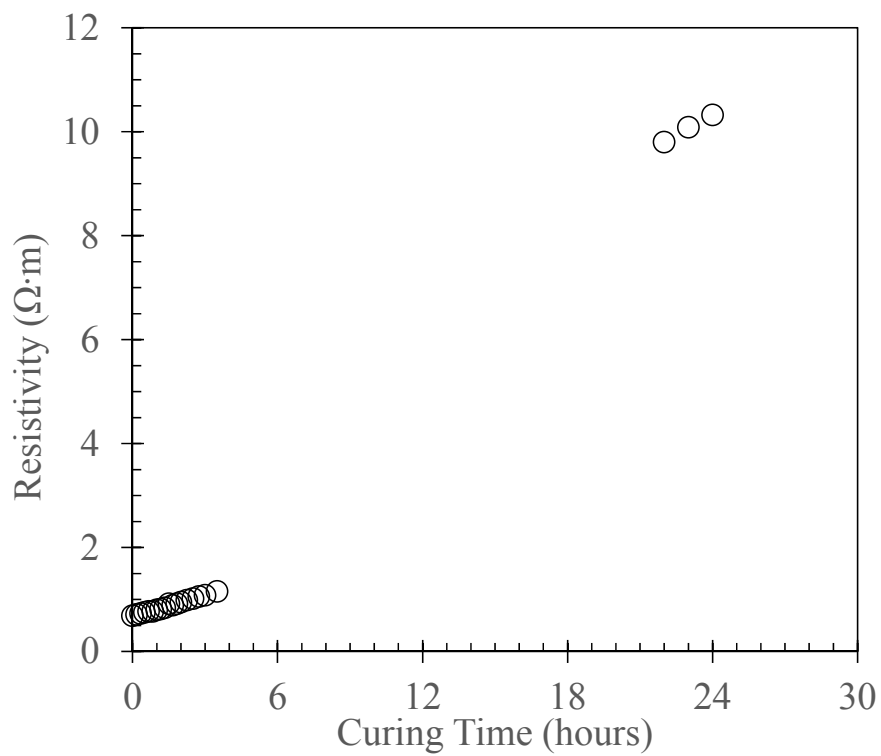


**Figure C.14: Resistivity vs. Curing Time Behavior – Batch 14.**



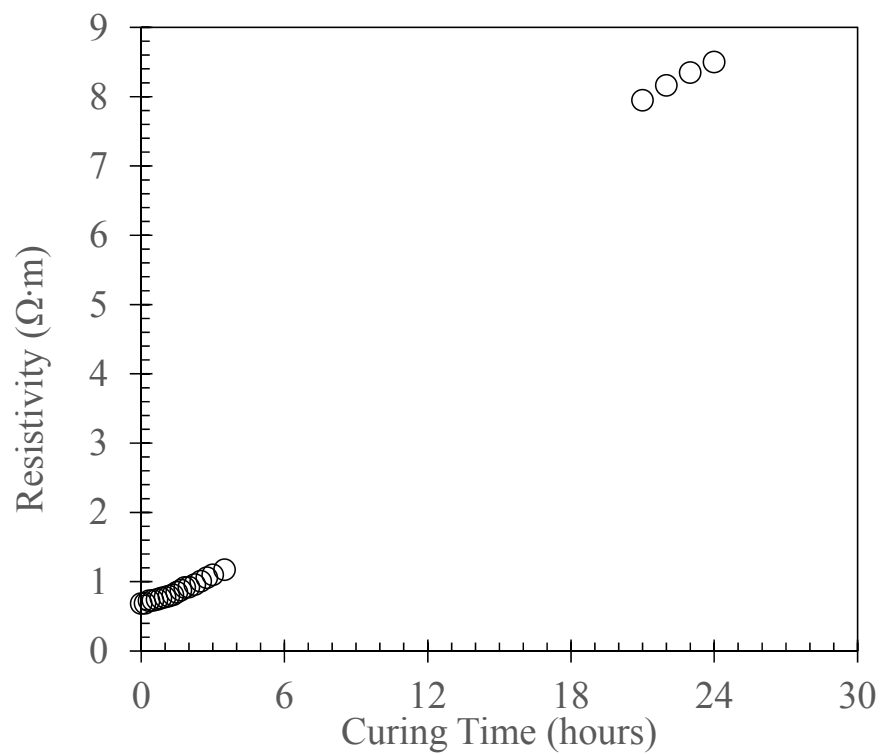


**Figure C.15: Resistivity vs. Curing Time Behavior – Batch 15.**

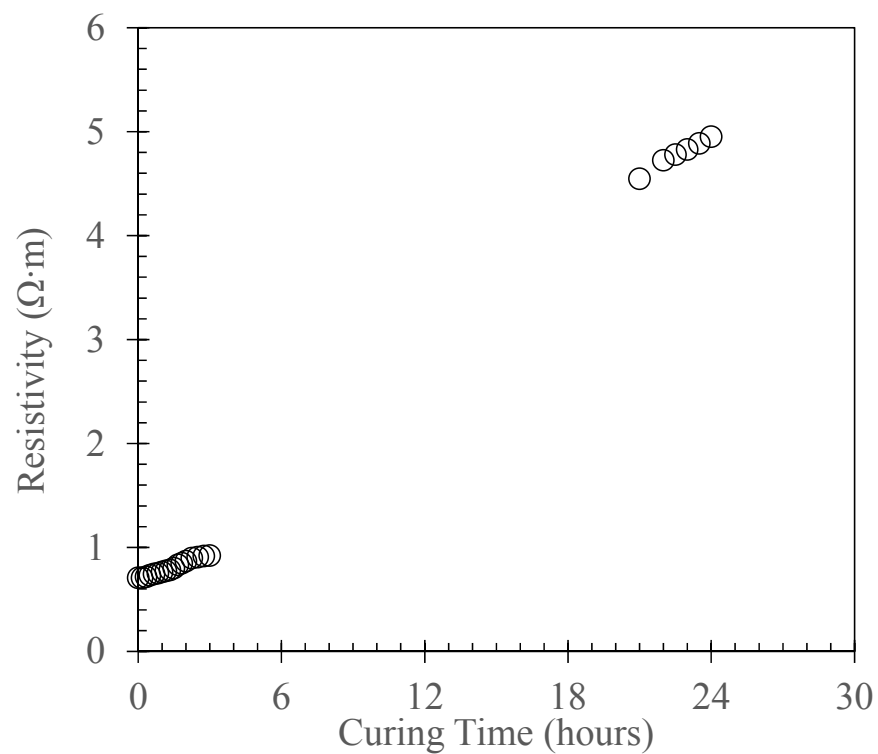


**Figure C.16: Resistivity vs. Curing Time Behavior – Batch 16.**

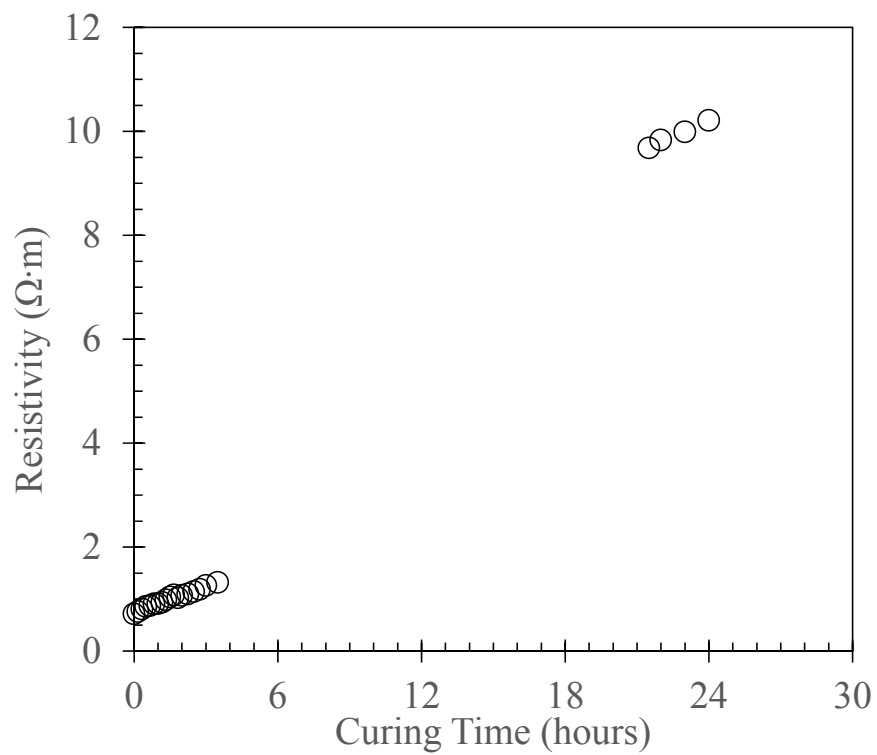


**Figure C.17: Resistivity vs. Curing Time Behavior – Batch 17.**

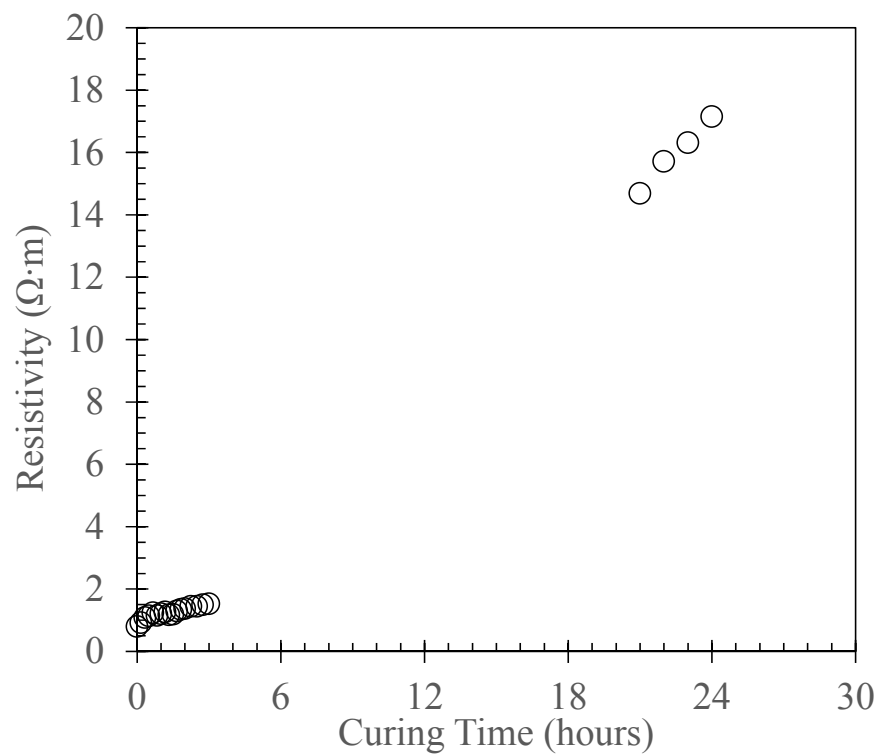


**Figure C.18: Resistivity vs. Curing Time Behavior – Batch 18.**

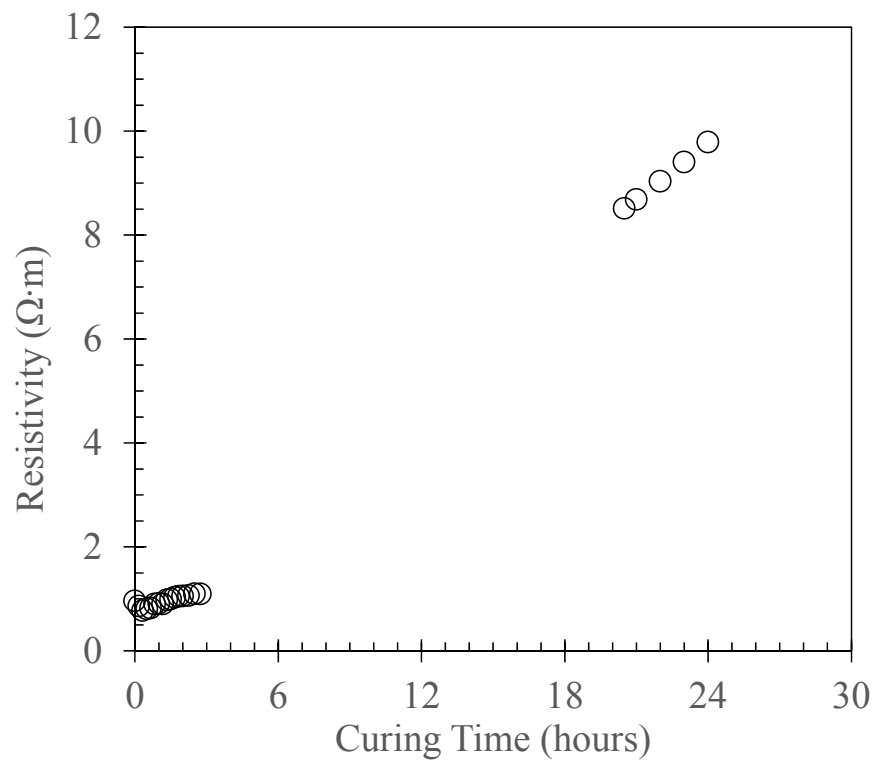


**Figure C.19: Resistivity vs. Curing Time Behavior – Batch 19.**

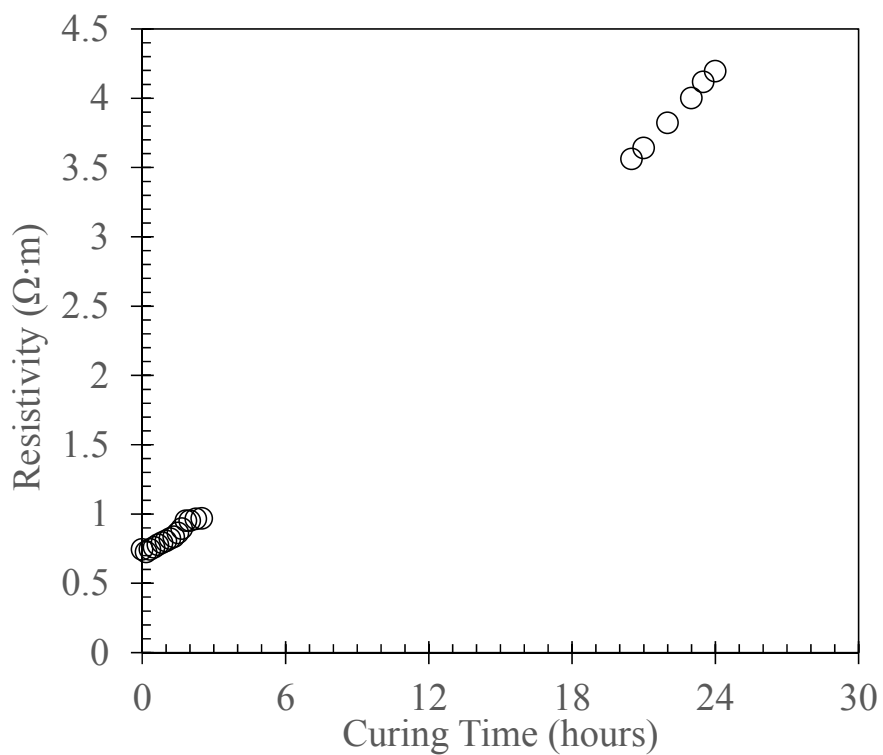


**Figure C.20: Resistivity vs. Curing Time Behavior – Batch 20.**

**Table C.1: Summary of Resistivity Index Testing Values for Each Batch.**

Batch	NanoFe <sub>2</sub> O <sub>3</sub> (%)	W/C Ratio	t <sub>min</sub> (hr)	ρ <sub>min</sub> (Ω·m)	ρ <sub>24</sub> (Ω·m)	RI <sub>24hr</sub>
1	0	0.40	0.00	0.709	11.094	14.659
2	0	0.45	1.83	0.660	5.265	6.977
3	0	0.50	0.17	0.699	6.812	8.749
4	0	0.60	0.33	0.707	4.319	5.112
5	2.5	0.40	0.00	0.692	14.926	20.578
6	2.5	0.45	0.00	0.703	8.593	11.222
7	2.5	0.50	0.17	0.690	7.083	9.263
8	2.5	0.60	0.17	0.701	4.349	5.201
9	5	0.40	0.00	0.702	14.952	20.306
10	5	0.45	0.00	0.704	8.808	11.505
11	5	0.50	0.00	0.693	6.939	9.007
12	5	0.60	0.00	0.694	4.257	5.137
13	7.5	0.40	0.00	0.725	17.173	22.702
14	7.5	0.45	0.00	0.686	10.320	14.035
15	7.5	0.50	0.00	0.684	8.498	11.426
16	7.5	0.60	0.00	0.706	4.951	6.013
17	10	0.40	0.00	0.716	15.318	36.700
18	10	0.45	0.00	0.799	17.151	20.456
19	10	0.50	0.33	0.774	9.787	11.650
20	10	0.60	0.17	0.726	4.196	4.778

\* Adjusted values explained in Chapter 4.2.

RI<sub>24hr</sub> Values Sorted by Both NanoFe<sub>2</sub>O<sub>3</sub> Content and Water-Cement Ratio:

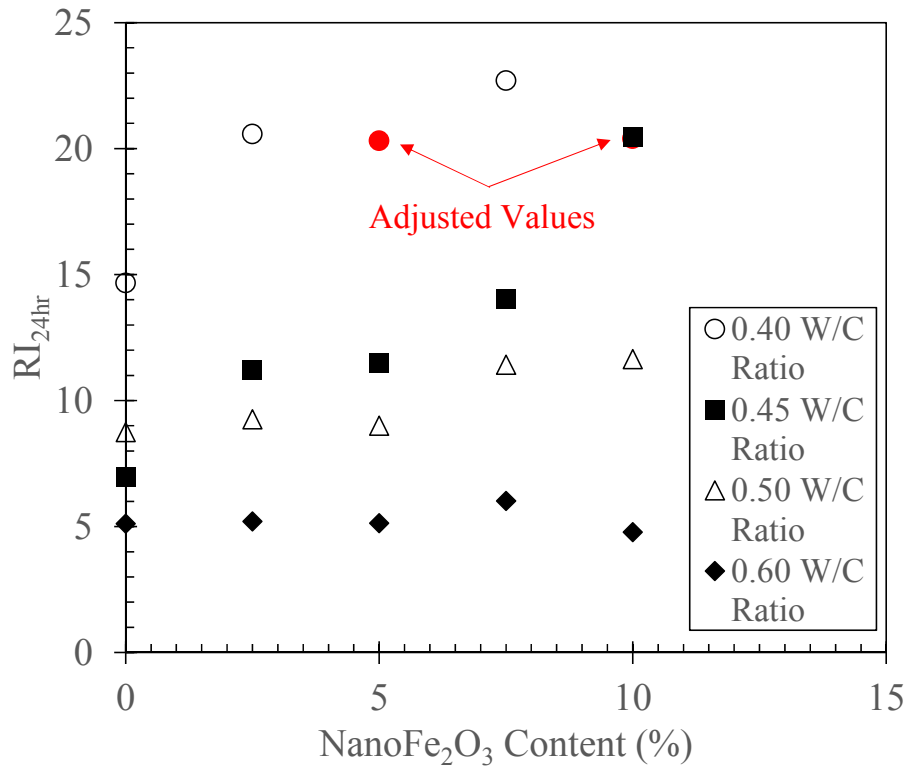


**Figure C.21: RI<sub>24hr</sub> values sorted by nanoFe<sub>2</sub>O<sub>3</sub> content.**

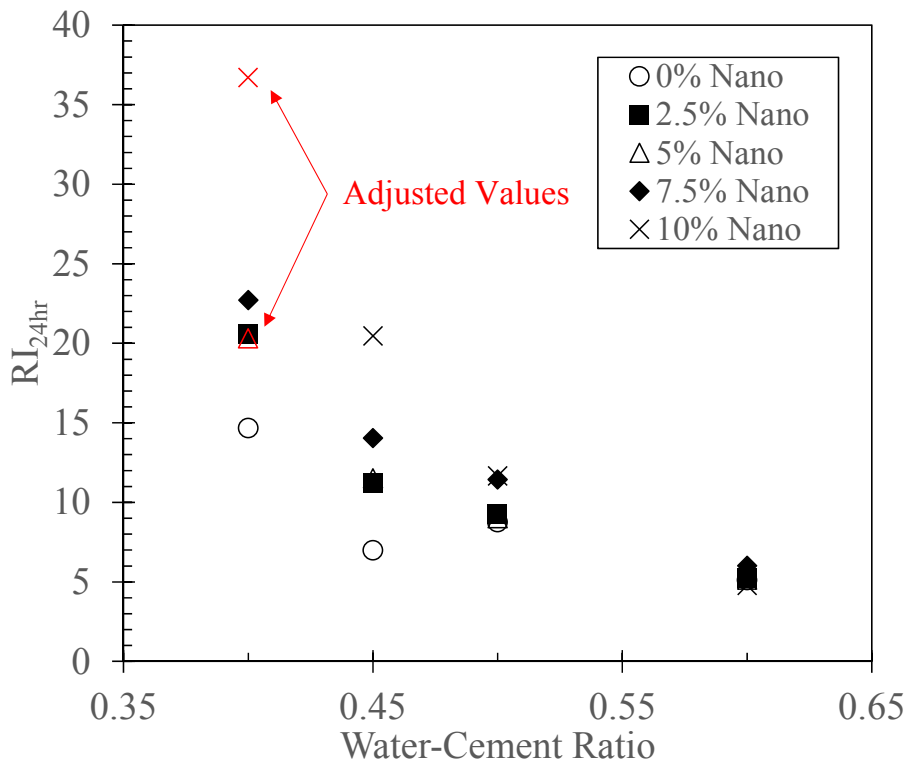


**Figure C.22: RI<sub>24hr</sub> values sorted by water-cement ratio.**

Average Resistivity Index Testing Values Sorted by NanoFe<sub>2</sub>O<sub>3</sub> Content:

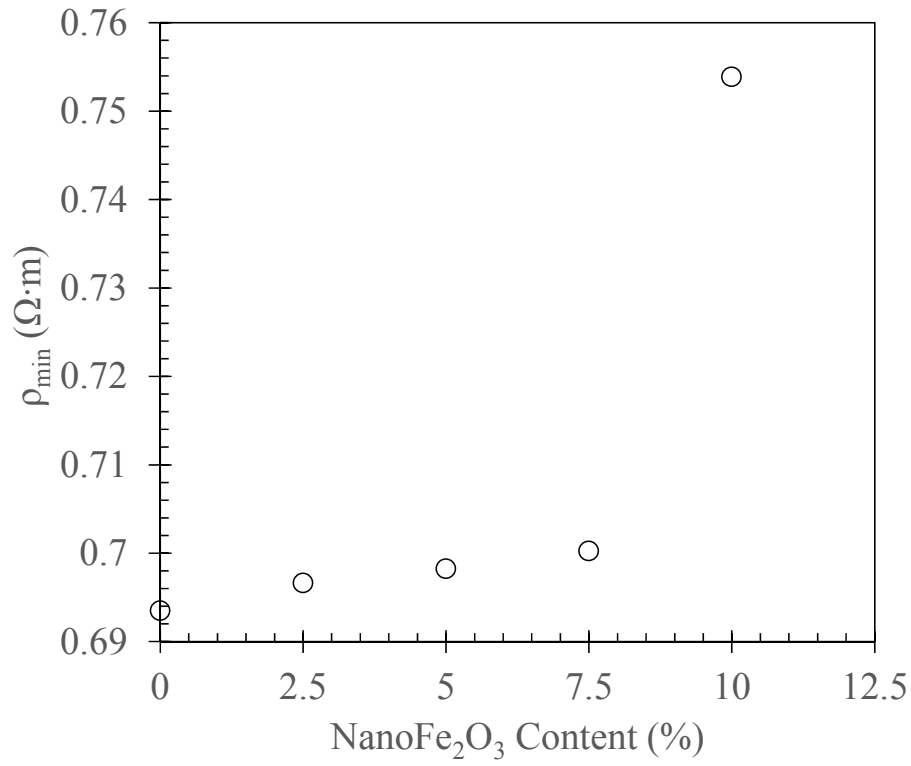


**Figure C.23: Average  $\rho_{\min}$  values of batches sorted by nanoFe<sub>2</sub>O<sub>3</sub> content.**

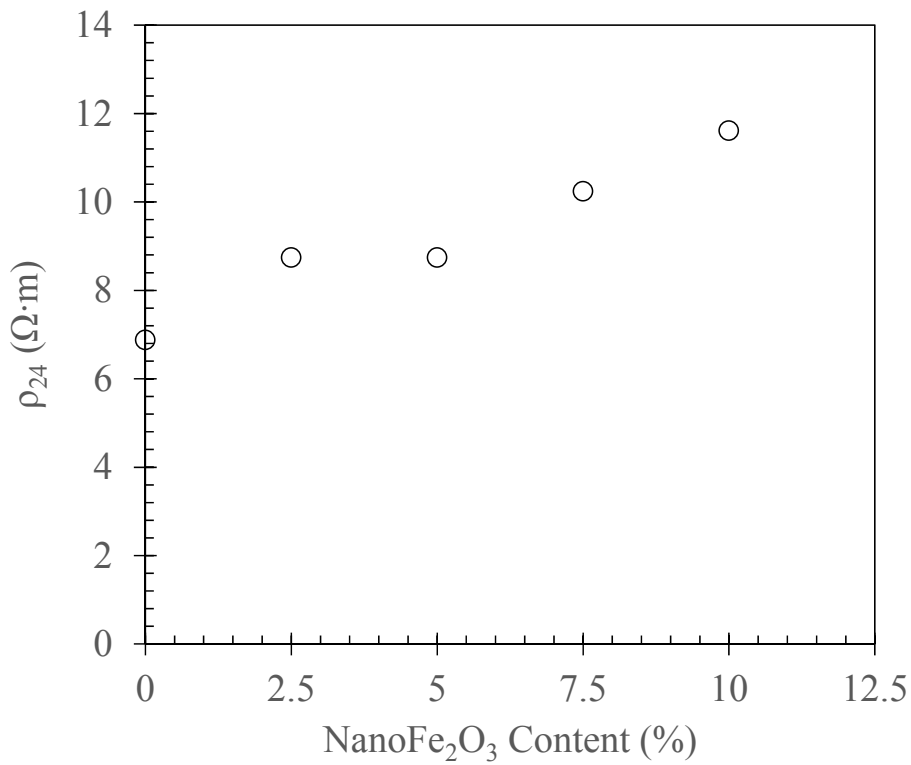


**Figure C.24: Average  $\rho_{24}$  values of batches sorted by nanoFe<sub>2</sub>O<sub>3</sub> content.**

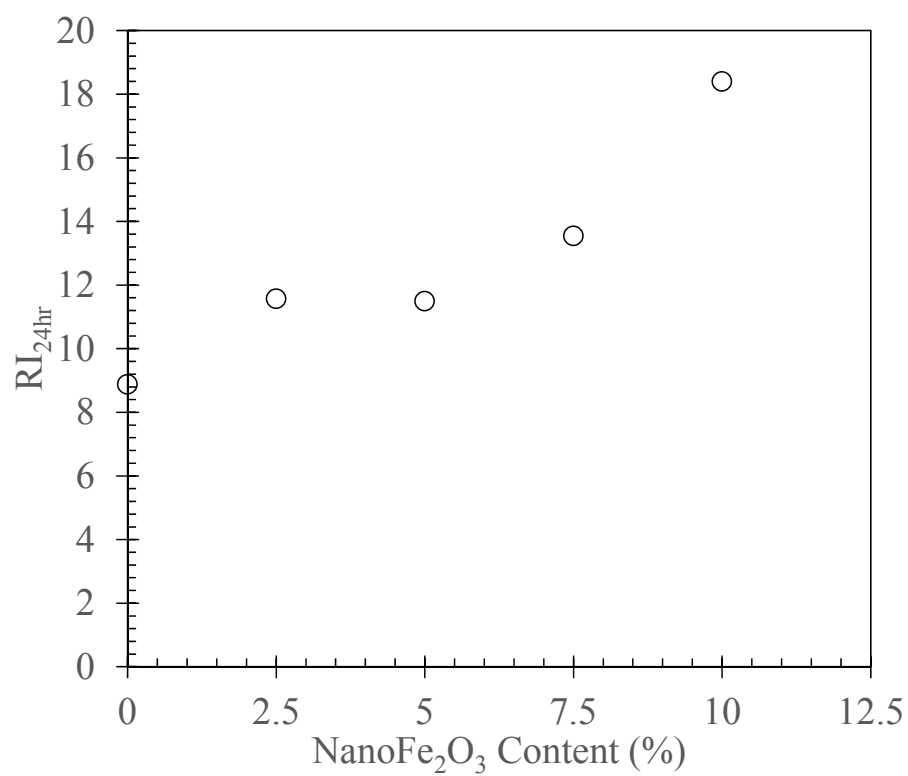


**Figure C.25: Average RI<sub>24hr</sub> values of batches sorted by nanoFe<sub>2</sub>O<sub>3</sub> content.**

Average Resistivity Index Testing Values Sorted by Water-Cement Ratio:

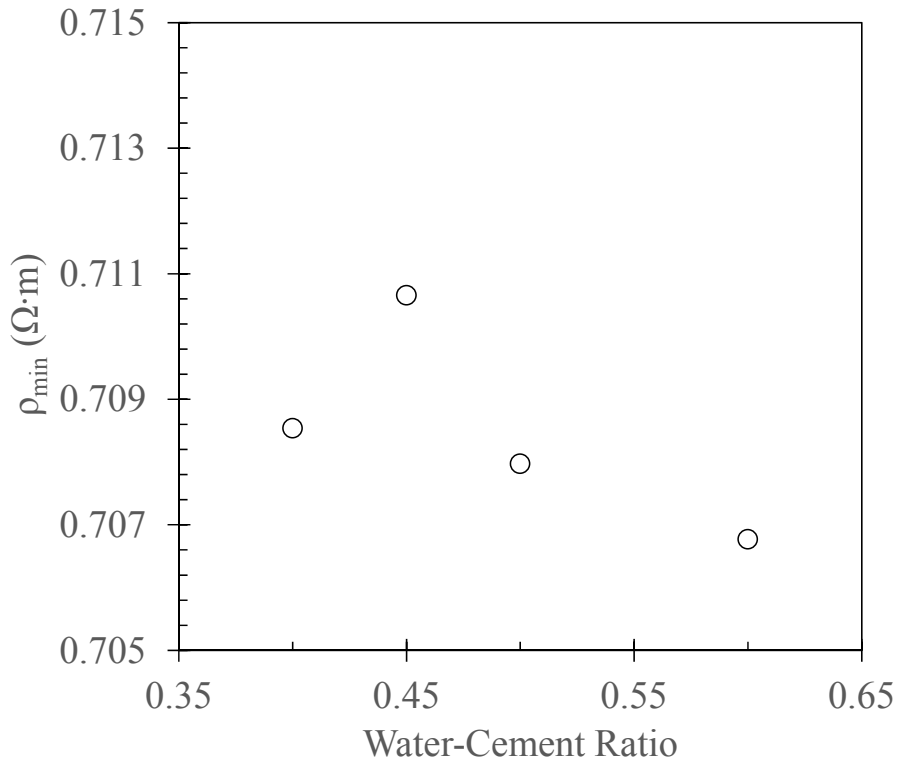


**Figure C.26: Average  $\rho_{\min}$  values of batches sorted by water-cement ratio.**

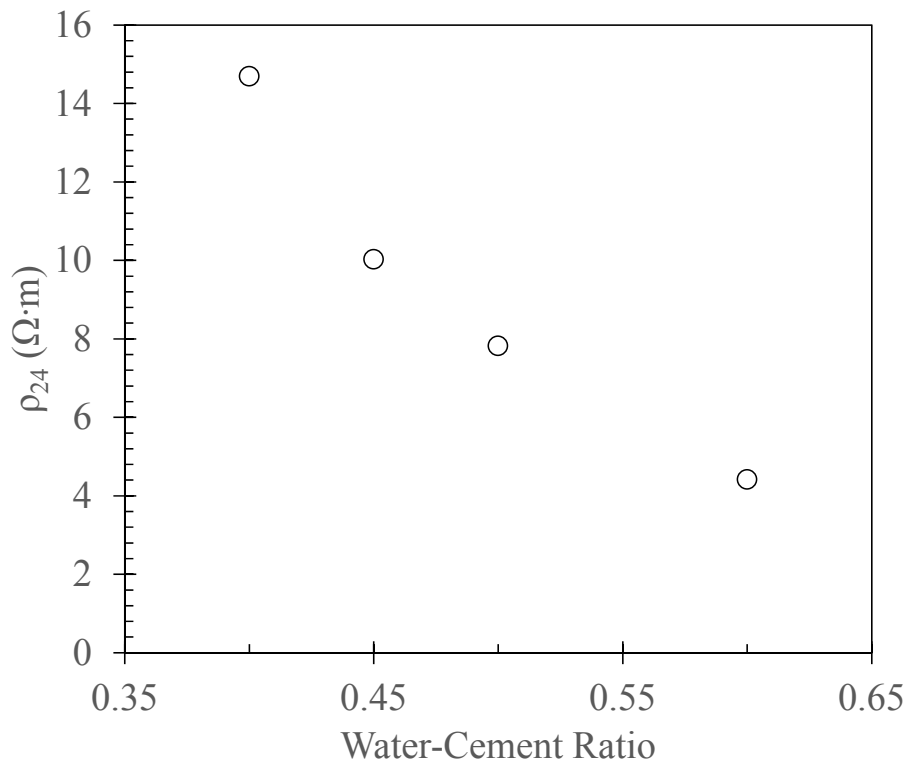


**Figure C.27: Average  $\rho_{24}$  values of batches sorted by water-cement ratio.**



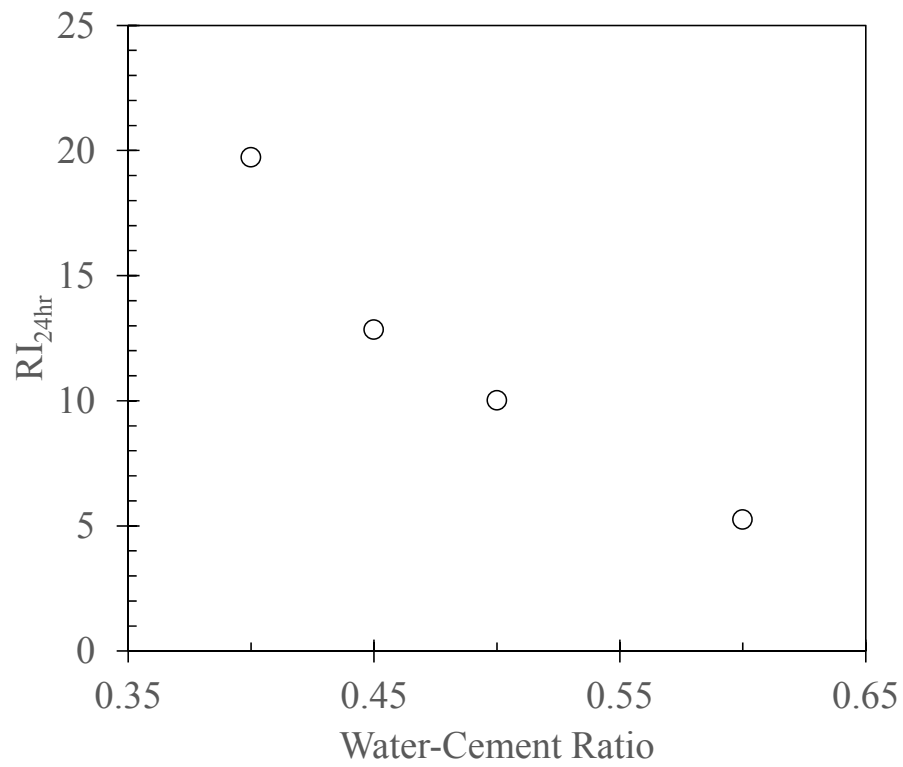


**Figure C.28: Average  $RI_{24hr}$  values of batches sorted by water-cement ratio.**

---

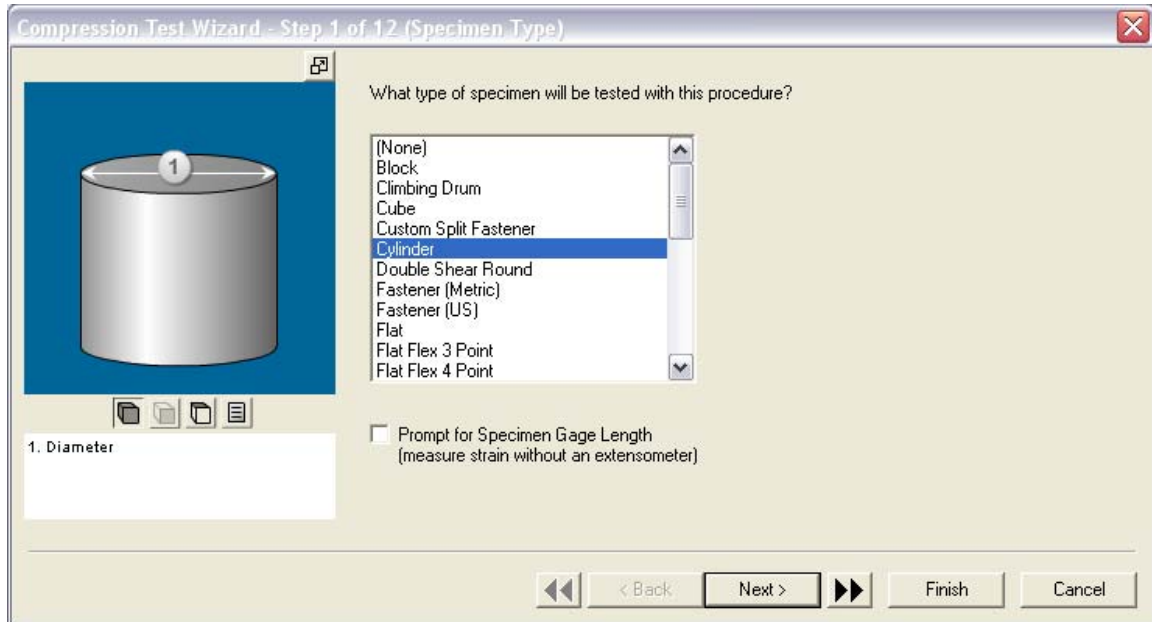
# **Appendix D**

## **Stress-Strain Testing**

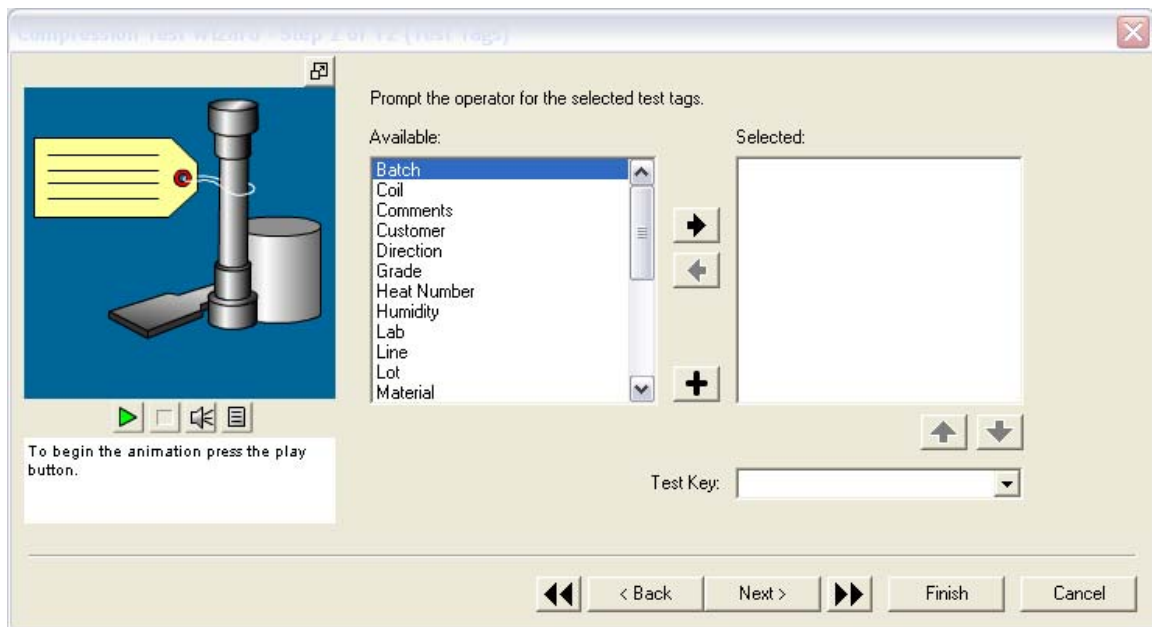
## Partner™ Software Procedure Setup:

The following steps were taken to develop the compression testing procedure.

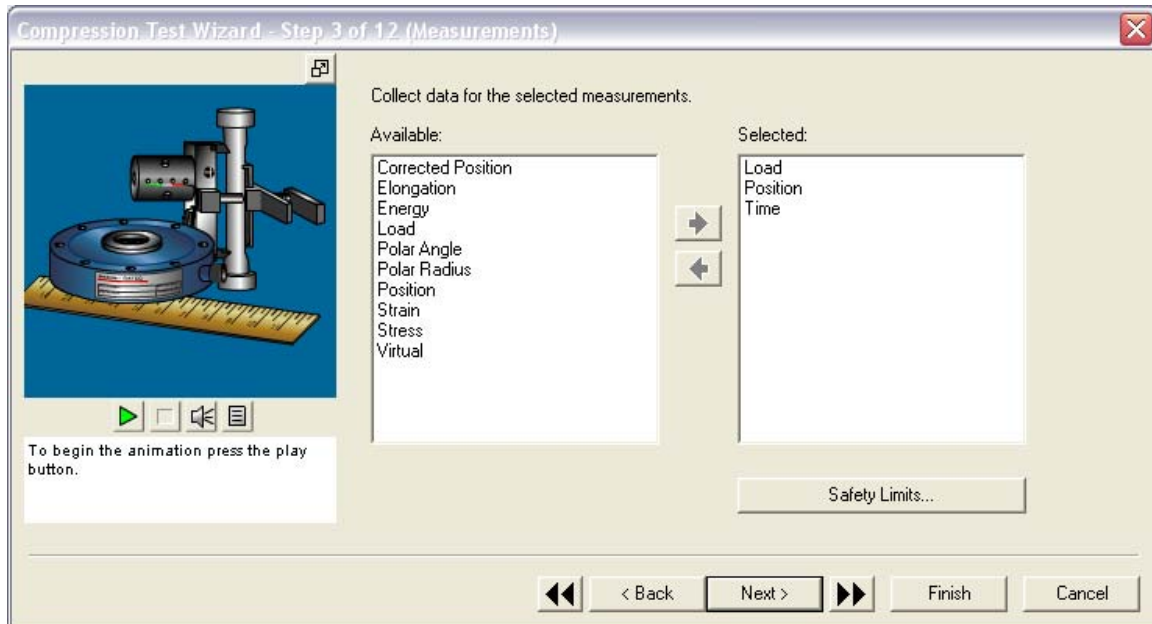
- Step 1: Select “Cylinder” as the specimen type. Click “Next”.



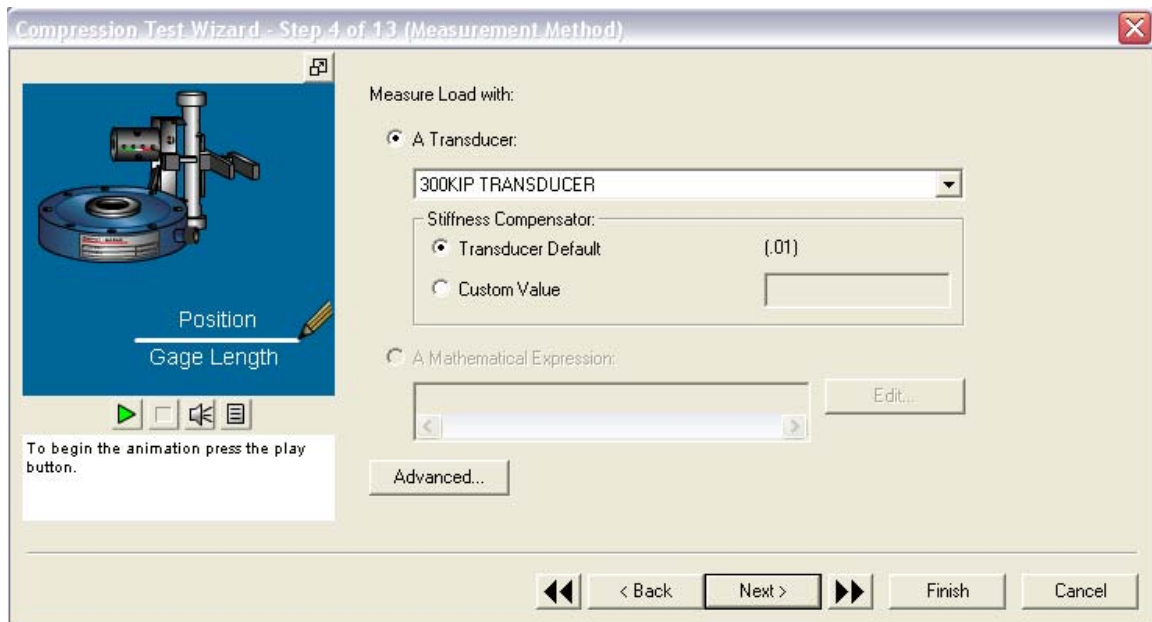
- Step 2: Do not select any options from this page. Click “Next”.



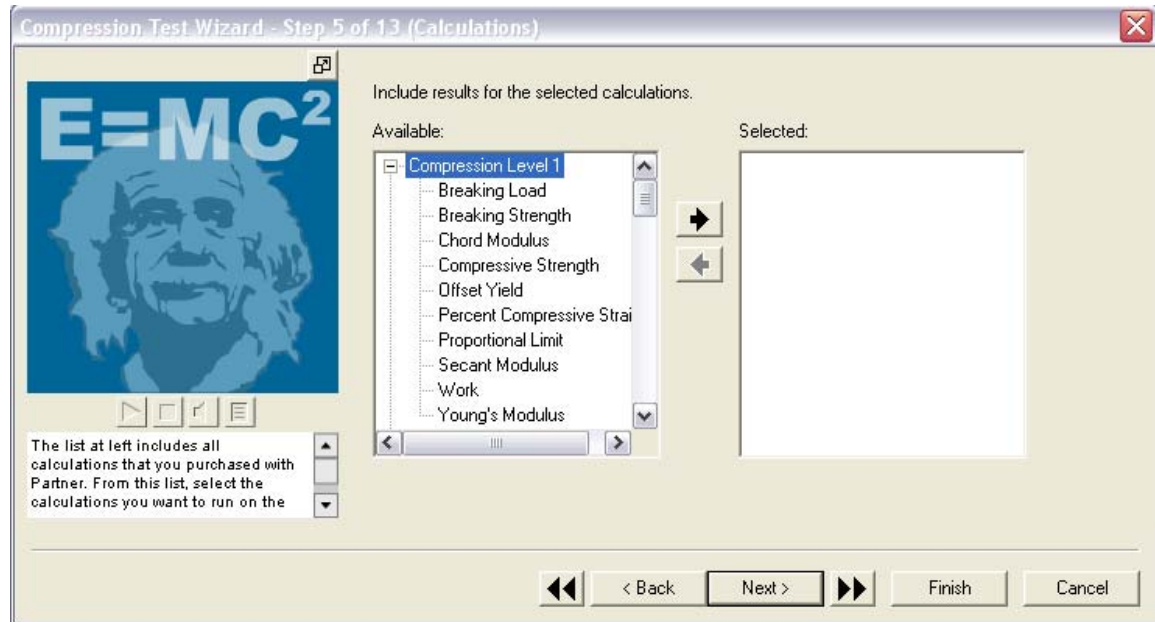
- Step 3: Select “Load”, “Position”, and “Time” from the selected measurements for data collection. Click “Next”.



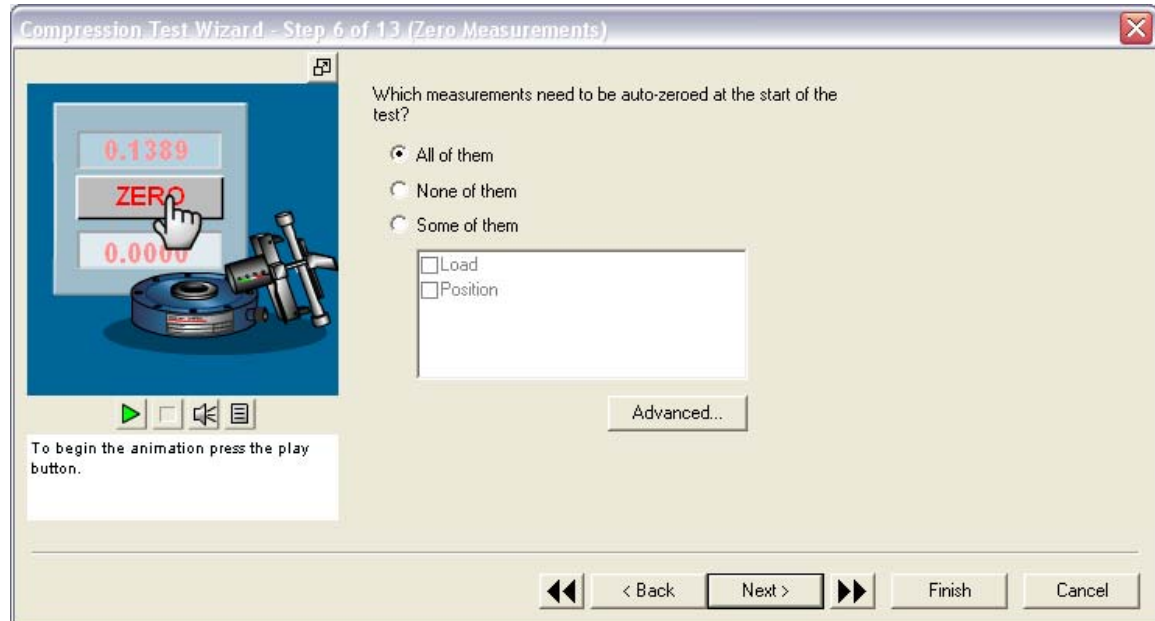
- Step 4: The load will be measured with a 300 kip transducer. Select the load to be measured with a transducer, then select the 300 kip transducer from the dropdown menu. Click “Next”.



- Step 5: Do not select any options from this page. Many of these results will be manually calculated after testing. Click “Next”.

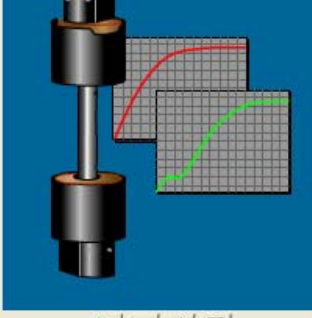


- Step 6: Select to auto-zero all measurements at the start of testing. Click “Next”.



- Step 7: Make sure that the Soft Start zone box is unchecked. Click “Next”.

Compression Test Wizard - Step 7 of 13 (Soft Start)



☐ Start test with a Soft Start zone

Control:

Zone Rate: Position 0.10 in/min

Zone End:

End Level: Load 100 lbf

Gain:

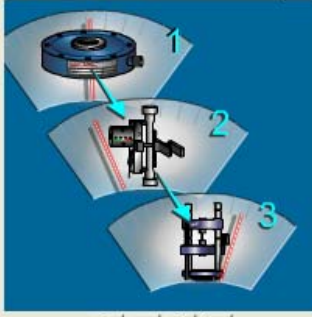
Multiplier: 1.0

To begin the animation press the play button.

<< < Back Next > >> Finish Cancel

- Step 8: Select “No” for the machine control changing during the test. Click “Next”.

Compression Test Wizard - Step 8 of 13 (Machine Control Setup)



Does the machine control need to change during the test ?

☒ No

☐ Yes

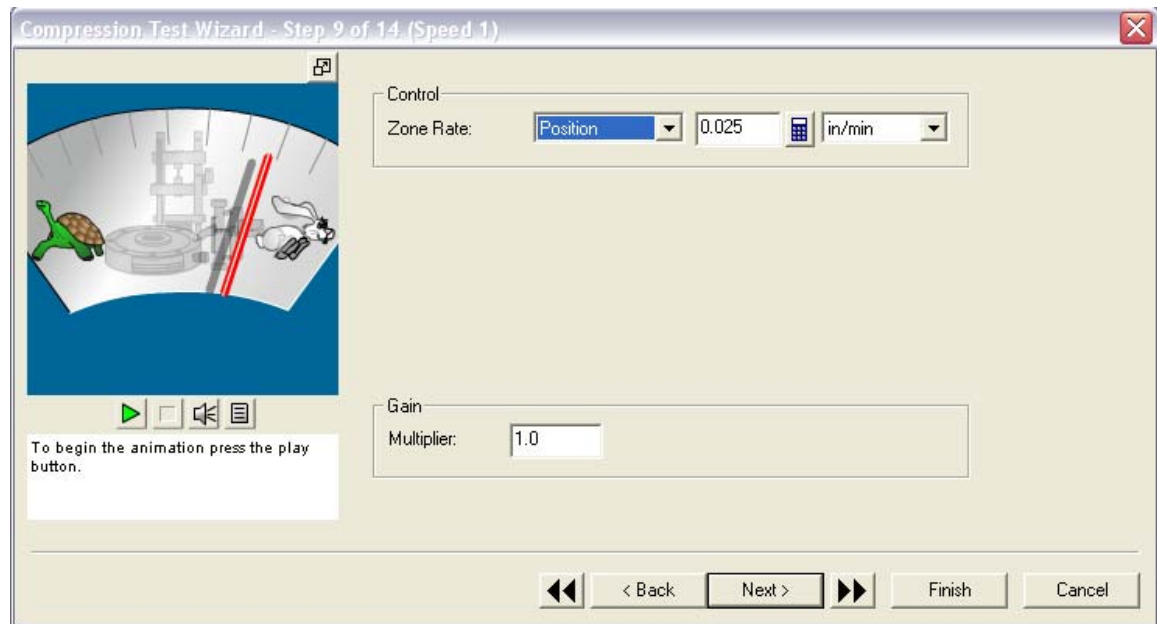
How many different zones of control are needed ?

1

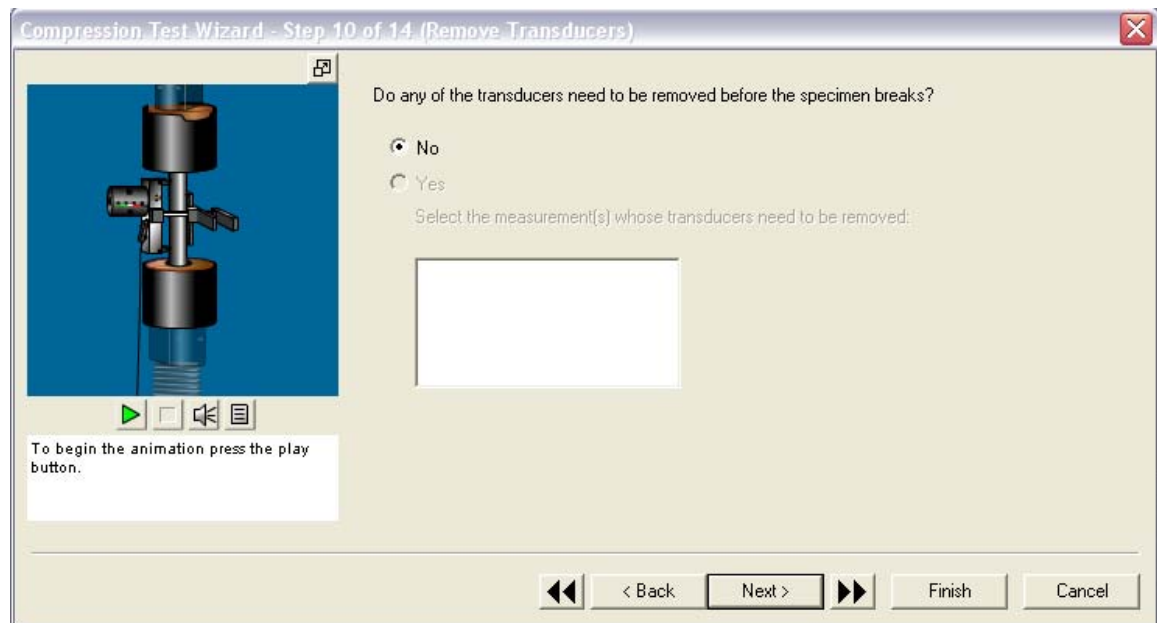
To begin the animation press the play button.

<< < Back Next > >> Finish Cancel

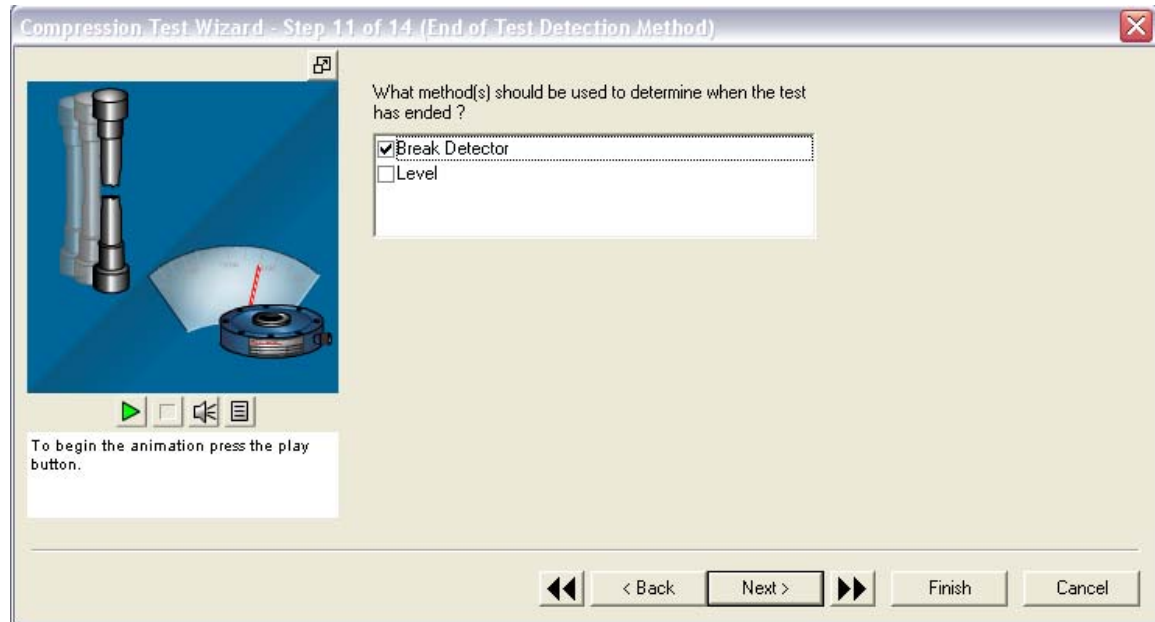
- Step 9: Set the compression test zone rate to be controlled by “Position” and set the rate to 0.025 in/min. This slow compression rate allows for easier manual electrical readings. Set the Gain Multiplier to 1.0. Click “Next”.



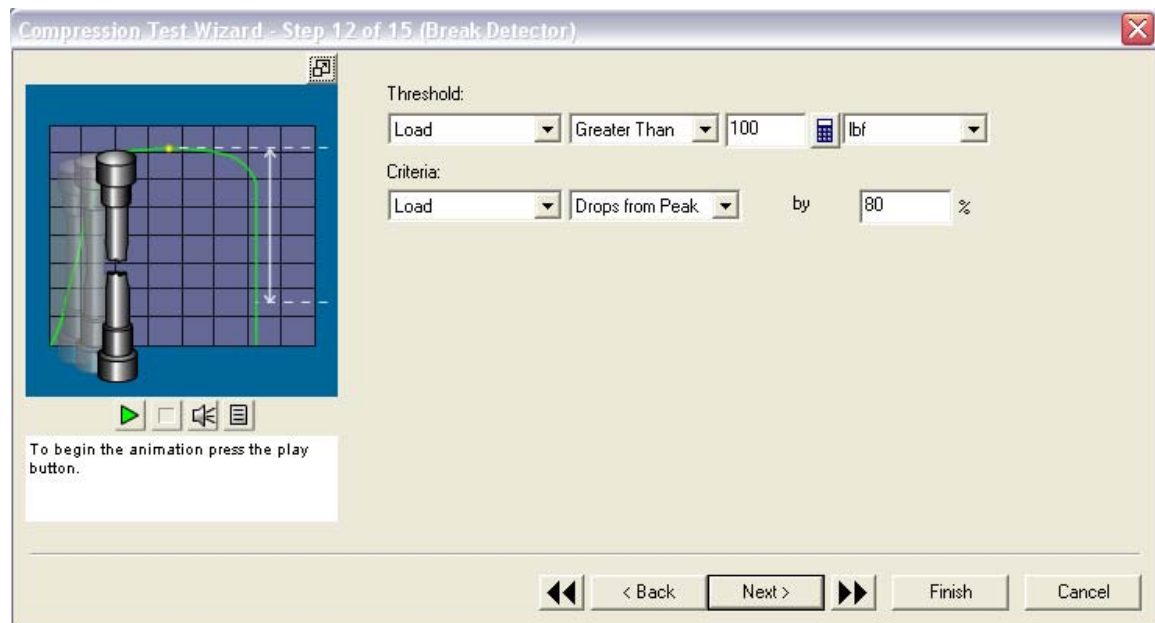
- Step 10: Select “No” for removing the transducer before the specimen breaks. Click “Next.”



- Step 11: Select the “Break Detector” for the method used to determine when the test has ended. Click “Next”.

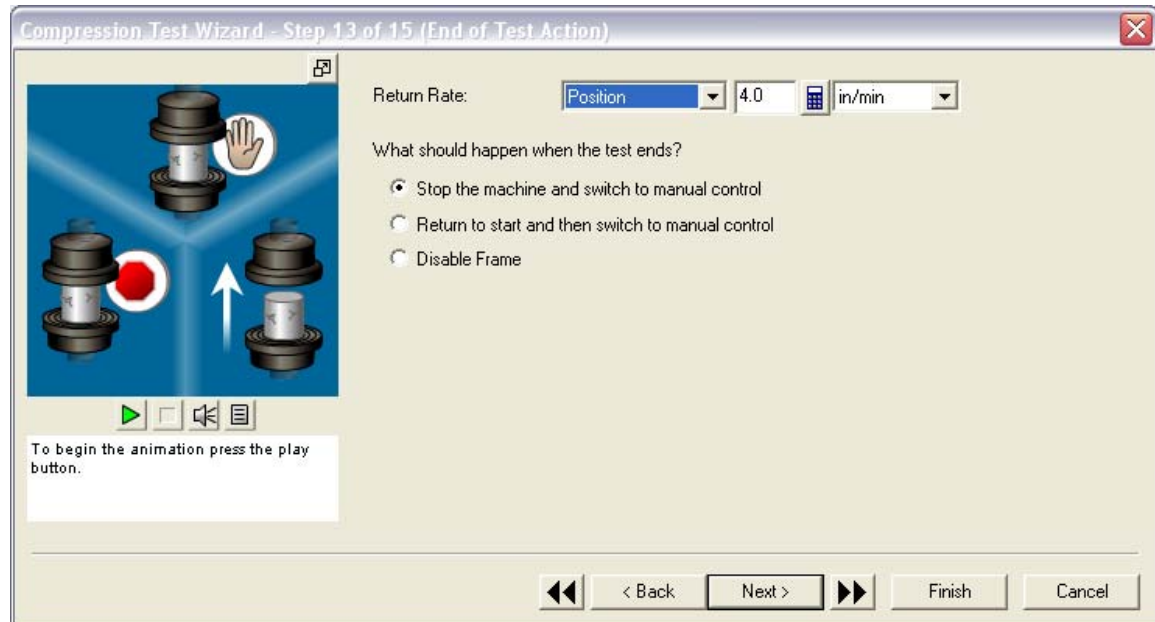


- Step 12: From the dropdown menu, select “Load” for the threshold and set it greater than 100 lbf. For the criteria, select “Load” and then drops from peak by 80%. Any unnecessary data can be cut after the conclusion of the test. Click “Next”.

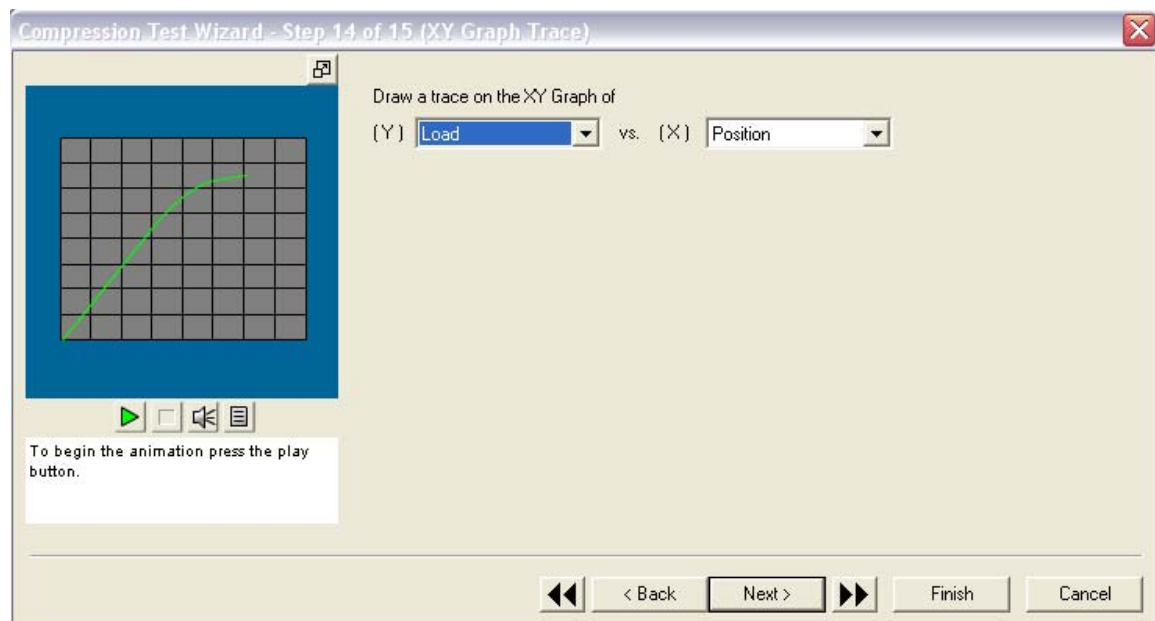




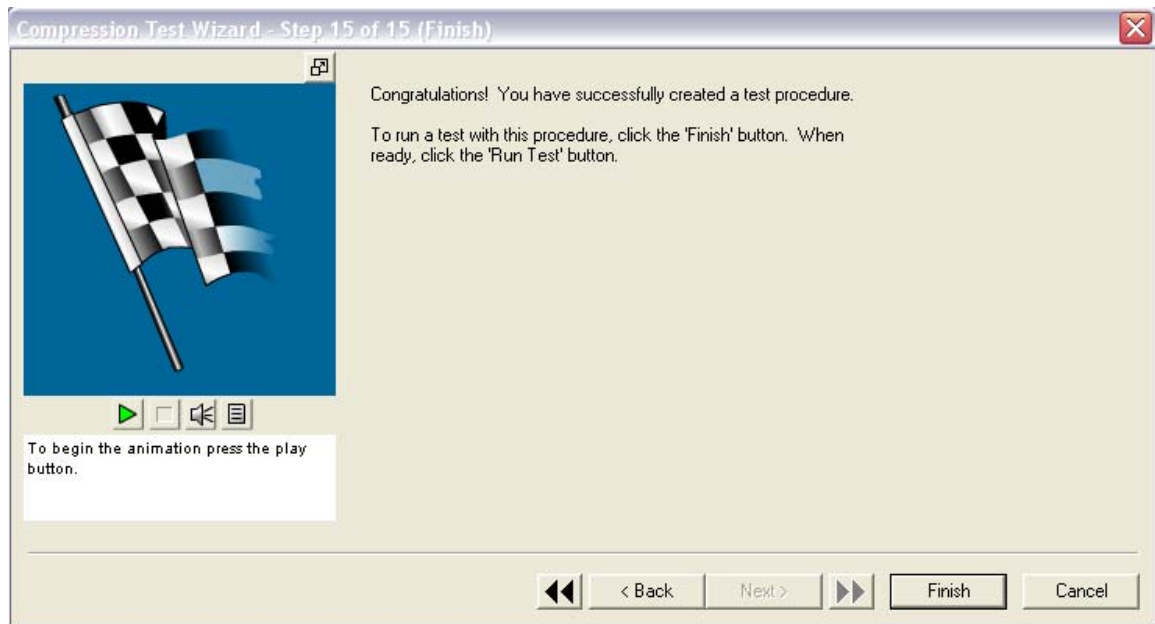
- Step 13: Select the return rate to “Position” and 4.0 in/min. The machine can also be switched to manual control at the conclusion of the test. Click “Next”.



- Step 14: Set the program to create an XY graph of “Load” (Y) vs. “Position” (X). Click “Next”.



- Step 15: Select “Finish”. Then rename the procedure and save.



- Step 16: Enter the cylinder diameter and click the “Run Test” button after the setup in Chapter 3.6 has been completed to begin the test.

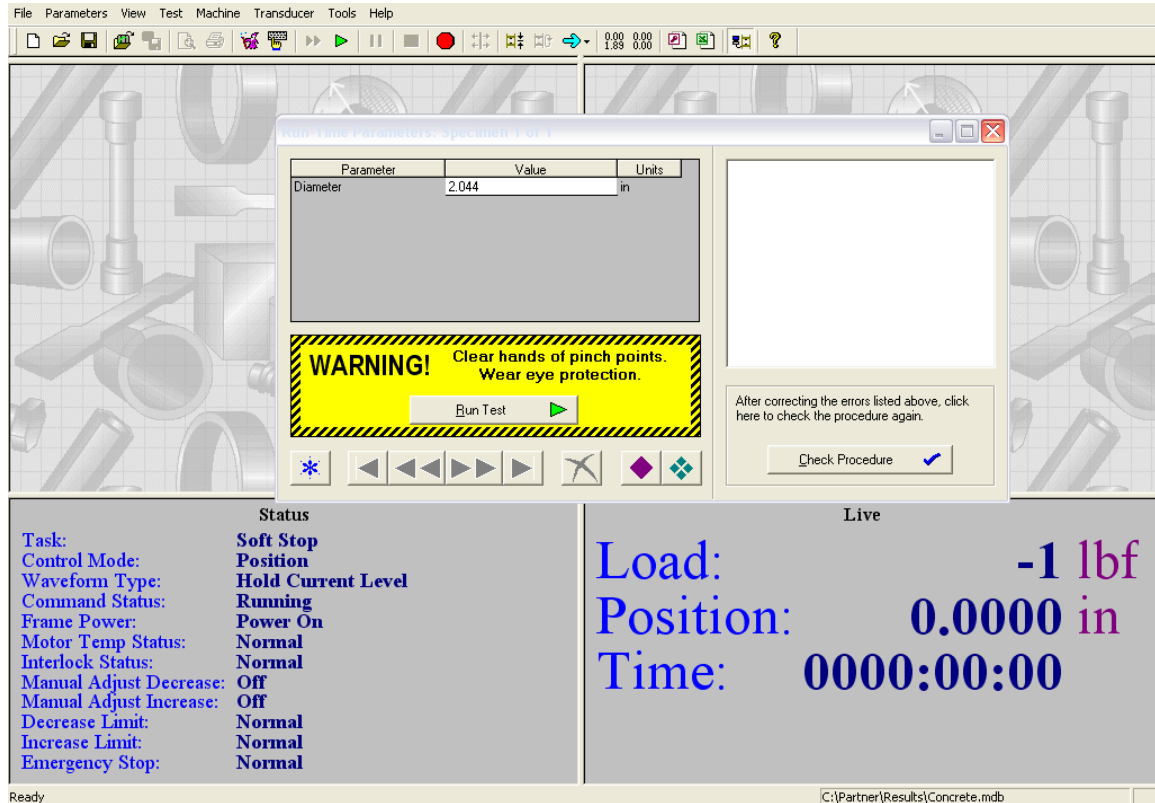


**Table D.1: Excel Personal Workbook Table Referenced in VBA Macro.**

Batch #	Cylinder #	NanoFe <sub>2</sub> O <sub>3</sub> (%)	Water-Cement Ratio	Curing Time (days)
1	1	0	0.40	1
	2	0	0.40	7
	3	0	0.40	28
2	4	0	0.45	1
	5	0	0.45	7
	6	0	0.45	28
3	7	0	0.50	1
	8	0	0.50	7
	9	0	0.50	28
4	10	0	0.60	1
	11	0	0.60	7
	12	0	0.60	28
5	13	2.5	0.40	1
	14	2.5	0.40	7
	15	2.5	0.40	28
6	16	2.5	0.45	1
	17	2.5	0.45	7
	18	2.5	0.45	28
7	19	2.5	0.50	1
	20	2.5	0.50	7
	21	2.5	0.50	28
8	22	2.5	0.60	1
	23	2.5	0.60	7
	24	2.5	0.60	28
9	25	5	0.40	1
	26	5	0.40	7
	27	5	0.40	28
10	28	5	0.45	1
	29	5	0.45	7
	30	5	0.45	28
11	31	5	0.50	1
	32	5	0.50	7
	33	5	0.50	28
12	34	5	0.60	1
	35	5	0.60	7
	36	5	0.60	28

**Table D.1 (Continued): Excel Personal Workbook Table Referenced in VBA Macro.**

Batch #	Cylinder #	NanoFe <sub>2</sub> O <sub>3</sub> (%)	Water-Cement Ratio	Curing Time (days)
13	37	7.5	0.40	1
	38	7.5	0.40	7
	39	7.5	0.40	28
14	40	7.5	0.45	1
	41	7.5	0.45	7
	42	7.5	0.45	28
15	43	7.5	0.50	1
	44	7.5	0.50	7
	45	7.5	0.50	28
16	46	7.5	0.60	1
	47	7.5	0.60	7
	48	7.5	0.60	28
17	49	10	0.40	1
	50	10	0.40	7
	51	10	0.40	28
18	52	10	0.45	1
	53	10	0.45	7
	54	10	0.45	28
19	55	10	0.50	1
	56	10	0.50	7
	57	10	0.50	28
20	58	10	0.60	1
	59	10	0.60	7
	60	10	0.60	28

## Excel VBA Macro Part 1 – Transforming Raw Data into Stress-Strain Prediction, Setting up Spreadsheet for Stress-Electrical Prediction (Macro Part 2):

```

Sub Reduction()
'
' Reduction Macro
'
' Performs 2 Tasks:
' (1) Converts Raw Data to Measured Stress-Strain Data
' (2) Converts Measured Stress-Strain Data to Predicted Stress-Strain Data
'
' * Macro is compatible for 10,001 data points = 1000 seconds
' at 10 Hz = 16.67 minutes
'
' Keyboard Shortcut: Ctrl+r
'
' Prompt for entering initial cement cylinder information
'
    Batch_Number = InputBox("Batch Number")
    Cyl_Number = InputBox("Cylinder Number")
    Cyl_Length = InputBox("Cylinder Length (in.)")
    Cyl_Diameter = InputBox("Cylinder Diameter (in.)")
'
'-----
' Begin Raw Data Reduction Portion of Macro
'-----
'
    ActiveWindow.Zoom = 90
    ActiveSheet.Name = "Sheet1"
    Rows("3:3").Insert Shift:=xlDown
'
' Initial Conditions
'
    Range("A1").FormulaR1C1 = "Batch Number:"
    Range("B1").Value = Batch_Number
    Range("A2").FormulaR1C1 = "Cylinder Number:"
    Range("B2").Value = Cyl_Number
    With Range("B1:B2")
        .HorizontalAlignment = xlCenter
    End With
    With Range("A1:B2")
        .Font.Bold = True
    End With
    Rows("4:10").Insert Shift:=xlDown
    Range("A4").FormulaR1C1 = "Length ( in ):"
    Range("B4").Value = Cyl_Length
    Range("A5").FormulaR1C1 = "Diameter ( in ):"
    Range("B5").Value = Cyl_Diameter
    Range("A6").FormulaR1C1 = "Length ( m ):"
    Range("B6").FormulaR1C1 = "=R[-2]C*0.0254"
    Range("A7").FormulaR1C1 = "Diameter ( m ):"
    Range("B7").FormulaR1C1 = "=R[-2]C*0.0254"
    Range("A8").FormulaR1C1 = "Initial Area ( m2 ):"
    With Range("A8").Characters(Start:=17, Length:=1).Font
        .Superscript = True
    End With
    Range("B8").FormulaR1C1 = "=PI()*R[-1]C^2/4"
    Columns("D:D").Delete Shift:=xlToLeft

    Range("D4").FormulaR1C1 = "Defoamer:"
    Range("E4").Value = 20
    Range("F4").FormulaR1C1 = "mL/gal H2O"
    With Range("F4")
        .Characters(Start:=9, Length:=1).Font.Subscript = True
    End With
    Range("D5").FormulaR1C1 = "NanoFe2O3 ( % ):"
    With Range("D5")
        .Characters(Start:=7, Length:=1).Font.Subscript = True
        .Characters(Start:=9, Length:=1).Font.Subscript = True
    End With
    Range("E5").FormulaR1C1 = _
        "=VLOOKUP(R2C2,[PERSONAL.XLSB]Sheet1!R2C2:R61C5,2,FALSE)"
    Range("D6").FormulaR1C1 = "W/C Ratio:"
    Range("E6").FormulaR1C1 = _
        "=VLOOKUP(R2C2,[PERSONAL.XLSB]Sheet1!R2C2:R61C5,3,FALSE)"
    Range("D7").FormulaR1C1 = "Curing Time:"
    Range("E7").FormulaR1C1 = _
        "=VLOOKUP(R2C2,[PERSONAL.XLSB]Sheet1!R2C2:R61C5,4,FALSE)"
    Range("F7").FormulaR1C1 =
    =IF(R7C5=1,"day","days")
    With Range("E4:E7")
        .HorizontalAlignment = xlCenter
    End With

    Range("H4").FormulaR1C1 = "Tangent Point"
    Range("H5").FormulaR1C1 = "1"
    Range("H6").FormulaR1C1 = "2"
    Range("I4").FormulaR1C1 = "Strain ( % )"
    Range("I5").FormulaR1C1 = "0.01"
    Range("I6").FormulaR1C1 = "0.25"
    Range("J4").FormulaR1C1 = "Stress ( MPa )"
    Range("J5").FormulaR1C1 =
    =VLOOKUP(RC[-1],R[7]C[-3]:R[10007]C,3,TRUE)
    Range("J6").FormulaR1C1 =
    =VLOOKUP(RC[-1],R[6]C[-3]:R[10006]C,3,TRUE)
    Range("H4:J6").HorizontalAlignment = xlCenter
    Range("J5:J6").NumberFormat = "0.000"

    Range("A10").Font.Bold = True
    Range("A10").FormulaR1C1 = "Raw Data:"
'
' Account for Dynamic Range:
'
' A Dynamic Range is a range that can be expanded or
' contracted in future versions of
' the spreadsheet. In other words, it is important when you
' cannot foresee the number
' of used cells in the range at the time of macro creation. It is
' a necessity when
' working with real data.
'
    Dim last As Double
    With ActiveSheet
        last = .Cells(.Rows.Count, "A").End(xlUp).Row
    End With
'
' Make all cells have row height = 18
'
    Cells.RowHeight = 18

```

```

'
' Position ( m )
'
    Range("D11").FormulaR1C1 = "Position ( m )"
    Range("D12").FormulaR1C1 = "=RC[-2]*0.0254"
    Range("D12").AutoFill Destination:=Range("D12:D" &
last)
'
' Load ( kN )
'
    Range("E11").FormulaR1C1 = "Load ( kN )"
    Range("E12").FormulaR1C1 = "=RC[-2]*4.44822/1000"
    Range("E12").AutoFill Destination:=Range("E12:E" &
last)
'
' Strain
'
    Range("F11").FormulaR1C1 = "Strain"
    Range("F12").FormulaR1C1 = "=RC[-2]/R6C2"
    Range("F12").AutoFill Destination:=Range("F12:F" &
last)
'
' Strain ( % )
'
    Range("G11").FormulaR1C1 = "Strain ( % )"
    Range("G12").FormulaR1C1 = "=RC[-1]*100"
    Range("G12").AutoFill Destination:=Range("G12:G" &
last)
'
' Corrected Area ( m^2 )
'
    Range("H11").FormulaR1C1 = "Corr. Area ( m2 )"
    With Range("H11").Characters(Start:=15, Length:=1).Font
        .Superscript = True
    End With
    Range("H12").FormulaR1C1 = "=R8C2/(1-RC[-2])"
    Range("H12").AutoFill Destination:=Range("H12:H" &
last)
'
' Stress ( MPa )
'
    Range("I11").FormulaR1C1 = "Stress ( MPa )"
    Range("I12").FormulaR1C1 = "=RC[-4]/RC[-1]/1000"
    Range("I12").AutoFill Destination:=Range("I12:I" & last)
'
' Tangent Modulus ( MPa )
'
    Range("J11").FormulaR1C1 = "Tan Modulus ( MPa )"
    Range("J12").FormulaR1C1 = "=RC[-1]/RC[-4]"
    Range("J12").AutoFill Destination:=Range("J12:J" & last)
'
' Autofit Data Columns
'
    Range("A11:J11").Columns.AutoFit
    Range("A8").Columns.AutoFit
    Range("F11").ColumnWidth = 10
    Range("D5").ColumnWidth = 14
    Range("A11:J11").Select
    Range(Selection, Selection.End(xlDown)).Select
    With Selection
        .HorizontalAlignment = xlCenter
        .VerticalAlignment = xlBottom
        .WrapText = False
        .Orientation = 0
        .AddIndent = False
        .IndentLevel = 0
        .ShrinkToFit = False
        .ReadingOrder = xlContext
        .MergeCells = False
    End With

```

```

Selection.Borders(xlDiagonalDown).LineStyle = xlNone
Selection.Borders(xlDiagonalUp).LineStyle = xlNone
With Selection.Borders(xlEdgeLeft)
    .LineStyle = xlContinuous
    .ColorIndex = xlAutomatic
    .TintAndShade = 0
    .Weight = xlThin
End With
With Selection.Borders(xlEdgeTop)
    .LineStyle = xlContinuous
    .ColorIndex = xlAutomatic
    .TintAndShade = 0
    .Weight = xlThin
End With
With Selection.Borders(xlEdgeBottom)
    .LineStyle = xlContinuous
    .ColorIndex = xlAutomatic
    .TintAndShade = 0
    .Weight = xlThin
End With
With Selection.Borders(xlEdgeRight)
    .LineStyle = xlContinuous
    .ColorIndex = xlAutomatic
    .TintAndShade = 0
    .Weight = xlThin
End With
With Selection.Borders(xlInsideVertical)
    .LineStyle = xlContinuous
    .ColorIndex = xlAutomatic
    .TintAndShade = 0
    .Weight = xlThin
End With
Selection.Borders(xlInsideHorizontal).LineStyle = xlNone
Range("A11:J11").Select
Selection.Borders(xlDiagonalDown).LineStyle = xlNone
Selection.Borders(xlDiagonalUp).LineStyle = xlNone
With Selection.Borders(xlEdgeLeft)
    .LineStyle = xlContinuous
    .ColorIndex = xlAutomatic
    .TintAndShade = 0
    .Weight = xlThin
End With
With Selection.Borders(xlEdgeTop)
    .LineStyle = xlContinuous
    .ColorIndex = xlAutomatic
    .TintAndShade = 0
    .Weight = xlThin
End With
With Selection.Borders(xlEdgeBottom)
    .LineStyle = xlContinuous
    .ColorIndex = 0
    .TintAndShade = 0
    .Weight = xlThin
End With
With Selection.Borders(xlEdgeRight)
    .LineStyle = xlContinuous
    .ColorIndex = xlAutomatic
    .TintAndShade = 0
    .Weight = xlThin
End With
With Selection.Borders(xlInsideVertical)
    .LineStyle = xlContinuous
    .ColorIndex = xlAutomatic
    .TintAndShade = 0
    .Weight = xlThin
End With
Selection.Borders(xlInsideHorizontal).LineStyle = xlNone
Range("A12:J12").Select
Range(Selection, Selection.End(xlDown)).NumberFormat
= "0.000"

```

```

With Range("B4:B8")
    .HorizontalAlignment = xlCenter
    .NumberFormat = "0.000"
End With
'
'-----
' Begin Prediction Portion of Macro
'-----
'
' Separate Raw and Predicted Data
'
Range("L1:L" & last).Select
Selection.ColumnWidth = 0.5
Selection.Borders(xlDiagonalDown).LineStyle = xlNone
Selection.Borders(xlDiagonalUp).LineStyle = xlNone
With Selection.Borders(xlEdgeLeft)
    .LineStyle = xlDouble
    .ColorIndex = xlAutomatic
    .TintAndShade = 0
    .Weight = xlThick
End With
Selection.Borders(xlEdgeTop).LineStyle = xlNone
Selection.Borders(xlEdgeBottom).LineStyle = xlNone
With Selection.Borders(xlEdgeRight)
    .LineStyle = xlDouble
    .ColorIndex = xlAutomatic
    .TintAndShade = 0
    .Weight = xlThick
End With
Selection.Borders(xlInsideVertical).LineStyle = xlNone
Selection.Borders(xlInsideHorizontal).LineStyle = xlNone
'
' Copy Data into Prediction Section
'
Range("G:G,I:I").Copy
Range("O1").Select
ActiveSheet.Paste
Columns("P:P").Select
Application.CutCopyMode = False
Selection.Cut
Range("N1").Select
ActiveSheet.Paste
Columns("N:Q").ColumnWidth = 12
Columns("S:V").ColumnWidth = 12
Range("P11,Q11").FormulaR1C1 = "Stress ( MPa )"
With Range("P11")
    .HorizontalAlignment = xlCenter
    .VerticalAlignment = xlBottom
    .WrapText = False
    .Orientation = 0
    .AddIndent = False
    .IndentLevel = 0
    .ShrinkToFit = False
    .ReadingOrder = xlContext
    .MergeCells = False
End With
Range("P11,Q11").Select
Selection.Borders(xlDiagonalDown).LineStyle = xlNone
Selection.Borders(xlDiagonalUp).LineStyle = xlNone
With Selection.Borders(xlEdgeLeft)
    .LineStyle = xlContinuous
    .ColorIndex = xlAutomatic
    .TintAndShade = 0
    .Weight = xlThin
End With
With Selection.Borders(xlEdgeTop)
    .LineStyle = xlContinuous
End With
With Selection.Borders(xlEdgeBottom)
    .LineStyle = xlContinuous
End With
With Selection.Borders(xlEdgeRight)
    .LineStyle = xlContinuous
End With
With Selection.Borders(xlInsideVertical)
    .LineStyle = xlNone
End With
With Selection.Borders(xlInsideHorizontal)
    .LineStyle = xlNone
End With
With Range("Q1:Q8,V1:V5")
    .HorizontalAlignment = xlCenter
    .NumberFormat = "0.0000"
End With
' Tangent Modulus (MPa)
'
    .ColorIndex = xlAutomatic
    .TintAndShade = 0
    .Weight = xlThin
End With
With Selection.Borders(xlEdgeBottom)
    .LineStyle = xlContinuous
    .ColorIndex = xlAutomatic
    .TintAndShade = 0
    .Weight = xlThin
End With
With Selection.Borders(xlEdgeRight)
    .LineStyle = xlContinuous
    .ColorIndex = xlAutomatic
    .TintAndShade = 0
    .Weight = xlThin
End With
With Selection.Borders(xlInsideVertical)
    .LineStyle = xlNone
End With
With Selection.Borders(xlInsideHorizontal)
    .LineStyle = xlNone
End With
Range("N1:P1,N2:P2,N3:P3,N4:P4,N5:P5,N6:P6,N7:P7,N8:
P8,S1:U1,S2:U2,S3:U3,S4:U4,S5:U5").Merge
With Selection
    .HorizontalAlignment = xlLeft
    .VerticalAlignment = xlBottom
    .WrapText = False
    .Orientation = 0
    .AddIndent = False
    .IndentLevel = 0
    .ShrinkToFit = False
    .ReadingOrder = xlContext
End With
Range("N1:P1,N2:P2,N3:P3,N4:P4,N5:P5,N6:P6,N7:P7,N8:
P8,S1:U1,S2:U2,S3:U3,S4:U4,S5:U5,Q1:Q8,V1:V5").Select
Selection.Borders(xlDiagonalDown).LineStyle = xlNone
Selection.Borders(xlDiagonalUp).LineStyle = xlNone
With Selection.Borders(xlEdgeLeft)
    .LineStyle = xlContinuous
    .ColorIndex = xlAutomatic
    .TintAndShade = 0
    .Weight = xlThin
End With
With Selection.Borders(xlEdgeTop)
    .LineStyle = xlContinuous
    .ColorIndex = xlAutomatic
    .TintAndShade = 0
    .Weight = xlThin
End With
With Selection.Borders(xlEdgeBottom)
    .LineStyle = xlContinuous
    .ColorIndex = xlAutomatic
    .TintAndShade = 0
    .Weight = xlThin
End With
With Selection.Borders(xlEdgeRight)
    .LineStyle = xlContinuous
    .ColorIndex = xlAutomatic
    .TintAndShade = 0
    .Weight = xlThin
End With
With Selection.Borders(xlInsideVertical)
    .LineStyle = xlNone
End With
With Selection.Borders(xlInsideHorizontal)
    .LineStyle = xlNone
End With
With Range("Q1:Q8,V1:V5")
    .HorizontalAlignment = xlCenter
    .NumberFormat = "0.0000"
End With
' Tangent Modulus (MPa)
'

```

```

Range("N1:P1").FormulaR1C1 = "Tangent Modulus ( MPa
)"
Range("Q1").FormulaR1C1 = "=(R6C10-R5C10)/(R6C9-
R5C9)*100"
'
' Secant Modulus (MPa)
'
Range("N2:P2").FormulaR1C1 = "Secant Modulus ( MPa
)"
Range("Q2").FormulaR1C1 =
"=VLOOKUP(MAX(R[10]C[-8]:R[10010]C[-
8]),R[10]C[-8]:R[10010]C[-7],2,FALSE)"
'
' Stress at Failure (MPa)
'
Range("N3:P3").FormulaR1C1 = "Stress at Failure ( MPa
)"
Range("Q3").FormulaR1C1 = "=MAX(R[9]C[-
3]:R[10009]C[-3])"
Range("S1:U1").FormulaR1C1 = "Stress at Failure ( MPa
)"
Range("V1").FormulaR1C1 = "=MAX(R[7]C[-
8]:R[10009]C[-8])"
'
' Strain at Failure (%)
'
Range("N4:P4,S2:U2").FormulaR1C1 = "Strain at Failure (
% )"
Range("Q4").FormulaR1C1 = "=VLOOKUP(R[-
1]C,R[8]C[-3]:R[10008]C[-2],2,FALSE)"
Range("S2:U2").FormulaR1C1 = "Strain at Failure ( % )"
Range("V2").FormulaR1C1 = "=VLOOKUP(R[-
1]C,R[6]C[-8]:R[10008]C[-7],2,FALSE)"
'
' q
'
Range("N5:P5").FormulaR1C1 = "q"
Range("Q5").FormulaR1C1 = "=R[-3]C/R[-4]C"
'
' p
'
Range("N6:P6").FormulaR1C1 = "p"
Range("Q6").FormulaR1C1 = "1"
'
' Beta
'
Range("S3:U3").FormulaR1C1 = "Beta"
Range("V3").FormulaR1C1 = "1.01"
'
' e^2
'
Range("N7:P7,S4:U4").FormulaR1C1 = "e2"
With Range("N7:P7,S4:U4").Characters(Start:=2,
Length:=1).Font
.Superscript = True
End With
'
' R^2
'
Range("N8:P8,S5:U5").FormulaR1C1 = "R2"
With Range("N8:P8,S5:U5").Characters(Start:=2,
Length:=1).Font
.Superscript = True
End With
'
' -----
' VIPULANANDAN Predicted Values
' -----
'
' Predicted Stress Values

```

```

'
Range("P12").FormulaR1C1 =
"=((RC[-1]/R4C17)/(R5C17+(1-R6C17-R5C17)*(RC[-
1]/R4C17)+R6C17*(RC[-
1]/R4C17)^((R6C17+R5C17)/R6C17)))*R3C17"
Range("P12").AutoFill Destination:=Range("P12:P" &
last)
Range("P12:P" & last).Select
With Selection
.HorizontalAlignment = xlCenter
.VerticalAlignment = xlBottom
.WrapText = False
.Orientation = 0
.AddIndent = False
.IndentLevel = 0
.ShrinkToFit = False
.ReadingOrder = xlContext
.MergeCells = False
End With
Selection.Borders(xlDiagonalDown).LineStyle = xlNone
Selection.Borders(xlDiagonalUp).LineStyle = xlNone
With Selection.Borders(xlEdgeLeft)
.LineStyle = xlContinuous
.ColorIndex = xlAutomatic
.TintAndShade = 0
.Weight = xlThin
End With
With Selection.Borders(xlEdgeTop)
.LineStyle = xlContinuous
.ColorIndex = xlAutomatic
.TintAndShade = 0
.Weight = xlThin
End With
With Selection.Borders(xlEdgeBottom)
.LineStyle = xlContinuous
.ColorIndex = xlAutomatic
.TintAndShade = 0
.Weight = xlThin
End With
With Selection.Borders(xlEdgeRight)
.LineStyle = xlContinuous
.ColorIndex = xlAutomatic
.TintAndShade = 0
.Weight = xlThin
End With
Selection.Borders(xlInsideVertical).LineStyle = xlNone
Selection.Borders(xlInsideHorizontal).LineStyle = xlNone
Selection.NumberFormat = "0.000"
'
' e^2 formula (performed after predicted stress values are
obtained for Vipulanandan Predictive Model)
'
Range("Q7").FormulaArray =
"=SUM(((R[5]C[-1]:R[10005]C[-1]-R[5]C[-
3]:R[10005]C[-3])/R3C17)^2)"
'
' R^2 formula (performed after predicted stress values are
obtained for Vipulanandan Predictive Model)
'
Range("Q8").FormulaArray =
"=1-(SUM((R[4]C[-3]:R[10004]C[-3]-R[4]C[-
1]:R[10004]C[-1])^2)/SUM((R[4]C[-3]:R[10004]C[-3]-
AVERAGE(R[4]C[-3]:R[10004]C[-3]))^2))"
'
' -----
' BETA Predicted Values
' -----
'
' Predicted Stress Values

```



```

Range("Q12").FormulaR1C1 = _
    "= (R3C22*(RC[-2]/R2C22)/(R3C22-1+(RC[-
2]/R2C22)^(R3C22)))*R1C22"
Range("Q12").AutoFill Destination:=Range("Q12:Q" &
last)
Range("Q12:Q" & last).Select
With Selection
    .HorizontalAlignment = xlCenter
    .VerticalAlignment = xlBottom
    .WrapText = False
    .Orientation = 0
    .AddIndent = False
    .IndentLevel = 0
    .ShrinkToFit = False
    .ReadingOrder = xlContext
    .MergeCells = False
End With
Selection.Borders(xlDiagonalDown).LineStyle = xlNone
Selection.Borders(xlDiagonalUp).LineStyle = xlNone
With Selection.Borders(xlEdgeLeft)
    .LineStyle = xlContinuous
    .ColorIndex = xlAutomatic
    .TintAndShade = 0
    .Weight = xlThin
End With
With Selection.Borders(xlEdgeTop)
    .LineStyle = xlContinuous
    .ColorIndex = xlAutomatic
    .TintAndShade = 0
    .Weight = xlThin
End With
With Selection.Borders(xlEdgeBottom)
    .LineStyle = xlContinuous
    .ColorIndex = xlAutomatic
    .TintAndShade = 0
    .Weight = xlThin
End With
With Selection.Borders(xlEdgeRight)
    .LineStyle = xlContinuous
    .ColorIndex = xlAutomatic
    .TintAndShade = 0
    .Weight = xlThin
End With
Selection.Borders(xlInsideVertical).LineStyle = xlNone
Selection.Borders(xlInsideHorizontal).LineStyle = xlNone
Selection.NumberFormat = "0.000"
'
' e^2 formula (performed after predicted stress values are
' obtained for Ezeldin & Balaguru Predictive Model)
'
Range("V4").FormulaArray = _
    "=SUM(((R[8]C[-5]:R[10008]C[-5]-R[8]C[-
8]:R[10008]C[-8])/R1C22)^2)"
'
' R^2 formula (performed after predicted stress values are
' obtained for Ezeldine & Balaguru Predictive Model)
'
Range("V5").FormulaArray = _
    "=1-(SUM((R[7]C[-8]:R[10007]C[-8]-R[7]C[-
5]:R[10007]C[-5])^2)/SUM((R[7]C[-8]:R[10007]C[-8]-
AVERAGE(R[7]C[-8]:R[10007]C[-8]))^2))"
'
' Show "Measured" as well as "Vipulanandan" and "Beta"
' above table
'
Range("N10:O10").Merge
With Range("N10:O10,P10,Q10")
    .HorizontalAlignment = xlCenter
    .Font.Bold = True
End With

```

```

Range("N10:O10").FormulaR1C1 = "Measured"
Range("P10").FormulaR1C1 = "Vipulanandan"
Range("Q10").FormulaR1C1 = "E & B"
Range("N1:P8").HorizontalAlignment = xlLeft
'
'
'-----
' Begin Chart Portion of Macro
'-----
'
'
Dim sh As Worksheet
Dim chrt As chart

Set sh = ActiveWorkbook.Worksheets("Sheet1")
Set chrt = sh.Shapes.AddChart.chart
With chrt
    .ChartType = xlXYScatter
    ' Data Collection - Measured Data
    .SeriesCollection.NewSeries
    .FullSeriesCollection(1).Name = """"Measured Data""""
    .FullSeriesCollection(1).XValues = _
        "=Sheet1!$O$12:$O$10012"
    .FullSeriesCollection(1).Values = _
        "=Sheet1!$N$12:$N$10012"
    ' Data Collection - Vipulanandan Predicted Data:
    .SeriesCollection.NewSeries
    .FullSeriesCollection(2).Name = """"Vipulanandan
Data""""
    .FullSeriesCollection(2).XValues = _
        "=Sheet1!$O$12:$O$10012"
    .FullSeriesCollection(2).Values = _
        "=Sheet1!$P$12:$P$10012"
    ' Data Collection - Ezeldin & Balaguru Predicted Data:
    .SeriesCollection.NewSeries
    .FullSeriesCollection(3).Name = """"Beta Model
Data""""
    .FullSeriesCollection(3).XValues = _
        "=Sheet1!$O$12:$O$10012"
    .FullSeriesCollection(3).Values = _
        "=Sheet1!$Q$12:$Q$10012"
    ' Chart Title
    .HasTitle = False
    ' X-Axis Name
    .Axes(xlCategory, xlPrimary).HasTitle = True
    .Axes(xlCategory, xlPrimary).AxisTitle.Characters.Text
    = "Strain ( % )"
    .Axes(xlCategory).AxisTitle.Select
    With Selection.Format.TextFrame2.TextRange.Font
        .NameComplexScript = "Times New Roman"
        .NameFarEast = "Times New Roman"
        .Name = "Times New Roman"
        .Size = 18
        .Bold = False
    End With
    With ActiveChart.Axes(xlCategory).TickLabels.Font
        .Name = "Times New Roman"
        .Size = 18
    End With
    ' Y-Axis Name
    .Axes(xlValue, xlPrimary).HasTitle = True
    .Axes(xlValue, xlPrimary).AxisTitle.Characters.Text =
    "Stress ( MPa )"
    .Axes(xlValue).AxisTitle.Select
    With Selection.Format.TextFrame2.TextRange.Font
        .NameComplexScript = "Times New Roman"
        .NameFarEast = "Times New Roman"
        .Name = "Times New Roman"
        .Size = 18
        .Bold = False
    End With

```

```

End With
With ActiveChart.Axes(xlValue).TickLabels.Font
    .Name = "Times New Roman"
    .Size = 18
End With
' Delete Minor and Major Gridlines
.Axes(xlCategory).HasMajorGridlines = False
.Axes(xlCategory).HasMinorGridlines = False
.Axes(xlValue).HasMajorGridlines = False
.Axes(xlValue).HasMinorGridlines = False
' Chart Height = 5" , Chart Width = 6"
.ChartArea.Height = 348
.ChartArea.Width = 427
' Add Legend
.HasLegend = True
' Add Minor and Major Tickmarks, "General" Number
Format
.Axes(xlCategory).MajorTickMark = xlCross
.Axes(xlCategory).MinorTickMark = xlInside
.Axes(xlCategory).TickLabels.NumberFormat =
"General"
    With .Axes(xlCategory).Format.Line
        .Visible = msoTrue
        .ForeColor.ObjectThemeColor =
msoThemeColorText1
        .ForeColor.TintAndShade = 0
        .ForeColor.Brightness = 0
        .Transparency = 0
    End With
.Axes(xlValue).MajorTickMark = xlCross
.Axes(xlValue).MinorTickMark = xlInside
.Axes(xlValue).TickLabels.NumberFormat = "General"
    With .Axes(xlValue).Format.Line
        .Visible = msoTrue
        .ForeColor.ObjectThemeColor =
msoThemeColorText1
        .ForeColor.TintAndShade = 0
        .ForeColor.Brightness = 0
        .Transparency = 0
    End With
' Add Border Around Plot Area
With .PlotArea.Format.Line
    .Visible = msoTrue
    .ForeColor.ObjectThemeColor =
msoThemeColorText1
    .ForeColor.TintAndShade = 0
    .ForeColor.Brightness = 0
    .Transparency = 0
End With
' Format Data Series:
' Measured Data:
With chrt.FullSeriesCollection(1)
    .MarkerStyle = 8
    .MarkerSize = 2
    .Format.Fill.Visible = msoFalse
    .MarkerForegroundColor = RGB(0, 0, 0)
    .Format.Line.Visible = msoFalse
End With
' Vipulanandan Predicted Data:
With chrt.FullSeriesCollection(2)
    .MarkerStyle = -4142
    .Format.Line.Visible = msoTrue
    .Format.Line.Weight = 1
End With
' Ezeldin and Balaguru Predicted Data:
With chrt.FullSeriesCollection(3)
    .MarkerStyle = -4142
    .Format.Line.Visible = msoTrue
    .Format.Line.DashStyle = msoLineDash
    .Format.Line.Weight = 1

End With
' Cleaning Up Chart...
chrt.FullSeriesCollection(4).Delete
With .Legend.Format.Line
    .Visible = msoTrue
    .ForeColor.RGB = RGB(0, 0, 0)
End With
ActiveChart.PlotArea.Select
Selection.Width = 425
.Legend.Left = 295
.Legend.Top = 235
.Legend.Format.TextFrame2.TextRange.Font.Size = 14
.Legend.Left = 250
.Legend.Width = 150
.Legend.Height = 50
End With

' Change Plot Area Dimensions
ActiveChart.PlotArea.Select
Selection.Left = 59.5
Selection.Height = 325
Selection.Width = 440
' Remove Border Around Chart
chrt.ChartArea.Border.LineStyle = xlNone

' Move chart to right of table
chrt.Parent.Cut
Range("S11").Select
ActiveSheet.Paste

' Begin Final Clean-Up

' Find last empty row, delete all blank cells below data to
ensure formulas use correct range
Range("N12").Select
Selection.End(xlToRight).Select
Selection.End(xlDown).Select
ActiveCell.Offset(1, 0).Select
Range(Selection, Selection.End(xlToLeft)).Select
Range(Selection, Selection.End(xlDown)).Delete
Shift:=xlUp

' Make all cells centered vertically
Cells.VerticalAlignment = xlCenter

' Begin Solver Portion of Macro to Optimize Curve

' Vipulanandan Predictive Model - Manipulates p to get lowest
e^2 value
SolverOk SetCell:="$Q$7", MaxMinVal:=2, ValueOf:=0,
ByChange:="$Q$6", Engine:=1,
, EngineDesc:="GRG Nonlinear"
SolverAdd CellRef:="$Q$6", Relation:=1,
FormulaText:="1"
SolverAdd CellRef:="$Q$6", Relation:=3,
FormulaText:="0.01"

```

```

SolverOk SetCell:="$Q$7", MaxMinVal:=2, ValueOf:=0,
ByChange:="$Q$6", Engine:=1 _
, EngineDesc:="GRG Nonlinear"
SolverOk SetCell:="$Q$7", MaxMinVal:=2, ValueOf:=0,
ByChange:="$Q$6", Engine:=1 _
, EngineDesc:="GRG Nonlinear"
SolverSolve
' Ezeldin & Balaguru Predictive Model - Manipulates beta to
get lowest e^2 value
'
SolverOk SetCell:="$V$4", MaxMinVal:=2, ValueOf:=0,
ByChange:="$V$3", Engine:=1 _
, EngineDesc:="GRG Nonlinear"
SolverOk SetCell:="$V$4", MaxMinVal:=2, ValueOf:=0,
ByChange:="$V$3", Engine:=1 _
, EngineDesc:="GRG Nonlinear"
SolverSolve
' Set to initial cell
'
Range("A1").Select
'
'-----
' Create Electrical Data Sheet
'-----
'
Sheets.Add After:=ActiveSheet
ActiveWindow.Zoom = 80
Cells.VerticalAlignment = xlCenter
Cells.HorizontalAlignment = xlCenter
Cells.RowHeight = 18

Sheets("Sheet1").Select
Columns("B:B").Select
Selection.Copy
Sheets("Sheet2").Select
Selection.PasteSpecial Paste:=xlPasteValues,
Operation:=xlNone, SkipBlanks _
:=False, Transpose:=False
Sheets("Sheet1").Select
Columns("I:I").Select
Application.CutCopyMode = False
Selection.Copy
Sheets("Sheet2").Select
Range("B1").Select
Selection.PasteSpecial Paste:=xlPasteValues,
Operation:=xlNone, SkipBlanks _
:=False, Transpose:=False
Sheets("Sheet1").Select
Columns("H:H").Select
Application.CutCopyMode = False
Selection.Copy
Sheets("Sheet2").Select
Range("C1").Select
Selection.PasteSpecial Paste:=xlPasteValues,
Operation:=xlNone, SkipBlanks _
:=False, Transpose:=False
Rows("1:10").Select
Application.CutCopyMode = False
Selection.Delete Shift:=xlUp
Columns("A:D").ColumnWidth = 15
Range("C1").Characters(Start:=15,
Length:=1).Font.Superscript = True
Range("D1").FormulaR1C1 = "Length ( m )"
Range("D2").FormulaR1C1 = "(Sheet1!R4C2-
Sheet2!RC[-3])*0.0254"
Range("D2").AutoFill Destination:=Range("D2:D10001")

```

```

Range("A2").Select
Range(Selection, Selection.End(xlToRight)).Select
Range(Selection, Selection.End(xlDown)).Select
Selection.NumberFormat = "0.000"
With Selection.Borders(xlEdgeLeft)
.LineStyle = xlContinuous
.ColorIndex = xlAutomatic
.TintAndShade = 0
.Weight = xlThin
End With
With Selection.Borders(xlEdgeTop)
.LineStyle = xlContinuous
.ColorIndex = xlAutomatic
.TintAndShade = 0
.Weight = xlThin
End With
With Selection.Borders(xlEdgeBottom)
.LineStyle = xlContinuous
.ColorIndex = xlAutomatic
.TintAndShade = 0
.Weight = xlThin
End With
With Selection.Borders(xlEdgeRight)
.LineStyle = xlContinuous
.ColorIndex = xlAutomatic
.TintAndShade = 0
.Weight = xlThin
End With
With Selection.Borders(xlInsideVertical)
.LineStyle = xlContinuous
.ColorIndex = xlAutomatic
.TintAndShade = 0
.Weight = xlThin
End With
Range("A1:D1").Font.Bold = True
Columns("F:O").ColumnWidth = 15
Range("F1:O1").Font.Bold = True
Range("F1").FormulaR1C1 = "Position ( in )"
Range("G1").FormulaR1C1 = "Cp ( pF )"
With Range("G1").Characters(Start:=2, Length:=1).Font
.Subscript = True
End With
Range("H1").FormulaR1C1 = "Rp ( k" & ChrW(&H3A9)
& " )"
With Range("H1").Characters(Start:=2, Length:=1).Font
.Subscript = True
End With
Range("I1").FormulaR1C1 = "Stress ( MPa )"
Range("J1").FormulaR1C1 = ChrW(&H394) & "R/Ro"
With Range("J1").Characters(Start:=5, Length:=1).Font
.Subscript = True
End With
Range("K1").FormulaR1C1 = "|" & ChrW(&H394) &
"R/Ro|"
With Range("K1").Characters(Start:=6, Length:=1).Font
.Subscript = True
End With
Range("L1").FormulaR1C1 = ChrW(&H3C1) & " ( " &
ChrW(&H3A9) & ChrW(8729) & " m )"
Range("M1").FormulaR1C1 = "|" & ChrW(&H394) &
ChrW(&H3C1) & "/" & ChrW(&H3C1) & "o|"
With Range("M1").Characters(Start:=6, Length:=1).Font
.Subscript = True
End With
Range("N1").FormulaR1C1 = ChrW(&H3BA) & " ( S/m )"
Range("O1").FormulaR1C1 = ChrW(&H394) &
ChrW(&H3BA) & "/" & ChrW(&H3BA) & "o"
With Range("O1").Characters(Start:=5, Length:=1).Font
.Subscript = True
End With

```

```

Range("F2").FormulaR1C1 = "0"
Range("F3").FormulaR1C1 = "0.005"
Range("F4").FormulaR1C1 = "0.01"
Range("F5").FormulaR1C1 = "0.015"
Range("F6").FormulaR1C1 = "0.02"
Range("F7").FormulaR1C1 = "0.025"
Range("F8").FormulaR1C1 = "0.03"
Range("F9").FormulaR1C1 = "0.035"
Range("F10").FormulaR1C1 = "0.04"
Range("F11").FormulaR1C1 = "0.045"
Range("F12").FormulaR1C1 = "0.05"
Range("F13").FormulaR1C1 = "0.055"
Range("F14").FormulaR1C1 = "0.06"
Range("F15").FormulaR1C1 = "0.065"
Range("F16").FormulaR1C1 = "0.07"
Range("F17").FormulaR1C1 = "0.075"
Range("F18").FormulaR1C1 = "0.08"
Range("F19").FormulaR1C1 = "0.085"
Range("F20").FormulaR1C1 = "0.09"
Range("F21").FormulaR1C1 = "0.095"
Range("F22").FormulaR1C1 = "0.1"
Range("F23").FormulaR1C1 = "0.105"
Range("F24").FormulaR1C1 = "0.11"
Range("F25").FormulaR1C1 = "0.115"
Range("F26").FormulaR1C1 = "0.12"
Range("F27").FormulaR1C1 = "0.125"
Range("F28").FormulaR1C1 = "0.13"
Range("F29").FormulaR1C1 = "0.135"
Range("F30").FormulaR1C1 = "0.14"
Range("F31").FormulaR1C1 = "0.145"
Range("F32").FormulaR1C1 = "0.15"
Range("F33").FormulaR1C1 = "0.155"
Range("F34").FormulaR1C1 = "0.16"
Range("F35").FormulaR1C1 = "0.165"
Range("F36").FormulaR1C1 = "0.17"
Range("F37").FormulaR1C1 = "0.175"
Range("F38").FormulaR1C1 = "0.18"
Range("F39").FormulaR1C1 = "0.185"
Range("F40").FormulaR1C1 = "0.19"
Range("F41").FormulaR1C1 = "0.195"
Range("F42").FormulaR1C1 = "0.2"
Range("F2:F42").NumberFormat = "0.000"

Range("I2").FormulaR1C1 = "=VLOOKUP(RC[-3],R2C1:R10001C2,2,TRUE)"
Range("I2").AutoFill Destination:=Range("I2:I42")
Range("J2").FormulaR1C1 = "=(RC[-2]-R2C8)/R2C8"
Range("J2").AutoFill Destination:=Range("J2:J42")
Range("K2").FormulaR1C1 = "=ABS(RC[-1])"
Range("K2").AutoFill Destination:=Range("K2:K42")
Range("L2").FormulaR1C1 = "=(RC[-4]*1000)*(VLOOKUP(RC[-6],R2C1:R10001C4,3,TRUE))/(VLOOKUP(RC[-6],R2C1:R10001C4,4,TRUE))"
Range("L2").AutoFill Destination:=Range("L2:L42")
Range("M2").FormulaR1C1 = "=ABS((RC[-1]-R2C12)/R2C12)"
Range("M2").AutoFill Destination:=Range("M2:M42")
Range("N2").FormulaR1C1 = "=1/RC[-2]"
Range("N2").AutoFill Destination:=Range("N2:N42")

Range("O2").FormulaR1C1 = "=(RC[-1]-R2C14)/R2C14"
Range("O2").AutoFill Destination:=Range("O2:O42")

With Range("A1:D1,F1:O1").Borders(xlEdgeLeft)
    .LineStyle = xlContinuous
    .ColorIndex = 0
    .TintAndShade = 0
    .Weight = xlThin
End With
With Range("A1:D1,F1:O1").Borders(xlEdgeTop)
    .LineStyle = xlContinuous
    .ColorIndex = 0
    .TintAndShade = 0
    .Weight = xlThin
End With
With Range("A1:D1,F1:O1").Borders(xlEdgeBottom)
    .LineStyle = xlContinuous
    .ColorIndex = 0
    .TintAndShade = 0
    .Weight = xlThin
End With
With Range("A1:D1,F1:O1").Borders(xlEdgeRight)
    .LineStyle = xlContinuous
    .ColorIndex = 0
    .TintAndShade = 0
    .Weight = xlThin
End With
With Range("A1:D1,F1:O1").Borders(xlInsideVertical)
    .LineStyle = xlContinuous
    .ColorIndex = 0
    .TintAndShade = 0
    .Weight = xlThin
End With
With Range("A1:D1,F1:O1").Borders(xlInsideHorizontal)
    .LineStyle = xlContinuous
    .ColorIndex = 0
    .TintAndShade = 0
    .Weight = xlThin
End With
Range("I2:O42").NumberFormat = "0.000"
'
'
'-----
' Begin Final Clean-Up
'-----
'
'
Range("A2").Select
Selection.End(xlDown).Select
ActiveCell.Offset(1, 0).Select
Range(Selection, Selection.End(xlToRight)).Select
Range(Selection, Selection.End(xlDown)).Delete
Shift:=xlUp

Range("G2").Select

End Sub

```

## Excel VBA Macro Part 2 – Stress-Electrical Prediction:

```
Sub Reduction_Part2()  
'  
' Reduction_Part2 Macro  
'  
' This macro picks up where the first macro stops. It begins  
after the user  
' manually enters the electrical data into the spreadsheet. The  
macro then  
' predicts the electrical response for different stresses on the  
cylinder.  
'  
' Keyboard Shortcut: Ctrl+g  
'  
'  
' Dynamic Range  
'  
    Dim last2 As Double  
    With ActiveSheet  
        last2 = .Cells(.Rows.Count, "A").End(xlUp).Row  
    End With  
'  
' Trim down data  
'  
    Range("G2").Select  
    Selection.End(xlDown).Select  
    ActiveCell.Offset(1, 0).Select  
    Range(Selection, Selection.End(xlToLeft)).Select  
    Range(Selection, Selection.End(xlDown)).Delete  
Shift:=xlUp  
    Range("H2").Select  
    Selection.End(xlDown).Select  
    ActiveCell.Offset(1, 1).Select  
    Range(Selection, Selection.End(xlToRight)).Select  
    Range(Selection, Selection.End(xlDown)).Delete  
Shift:=xlUp  
    Range("F2").Select  
    Range(Selection, Selection.End(xlToRight)).Select  
    Range(Selection, Selection.End(xlDown)).Select  
    Selection.Borders(xlDiagonalDown).LineStyle = xlNone  
    Selection.Borders(xlDiagonalUp).LineStyle = xlNone  
    With Selection.Borders(xlEdgeLeft)  
        .LineStyle = xlContinuous  
        .ColorIndex = 0  
        .TintAndShade = 0  
        .Weight = xlThin  
    End With  
    With Selection.Borders(xlEdgeTop)  
        .LineStyle = xlContinuous  
        .ColorIndex = 0  
        .TintAndShade = 0  
        .Weight = xlThin  
    End With  
    With Selection.Borders(xlEdgeBottom)  
        .LineStyle = xlContinuous  
        .ColorIndex = 0  
        .TintAndShade = 0  
        .Weight = xlThin  
    End With  
    With Selection.Borders(xlEdgeRight)  
        .LineStyle = xlContinuous  
        .ColorIndex = 0  
        .TintAndShade = 0  
        .Weight = xlThin  
    End With  
    With Selection.Borders(xlInsideVertical)  
        .LineStyle = xlContinuous  
        .ColorIndex = 0  
        .TintAndShade = 0  
        .Weight = xlThin  
    End With  
    Range("F1").Select  
'  
' Separate Raw and Predicted Data  
'  
    Range("Q1:Q" & last2).Select  
    Selection.ColumnWidth = 0.5  
    Selection.Borders(xlDiagonalDown).LineStyle = xlNone  
    Selection.Borders(xlDiagonalUp).LineStyle = xlNone  
    With Selection.Borders(xlEdgeLeft)  
        .LineStyle = xlDouble  
        .ColorIndex = xlAutomatic  
        .TintAndShade = 0  
        .Weight = xlThick  
    End With  
    Selection.Borders(xlEdgeTop).LineStyle = xlNone  
    Selection.Borders(xlEdgeBottom).LineStyle = xlNone  
    With Selection.Borders(xlEdgeRight)  
        .LineStyle = xlDouble  
        .ColorIndex = xlAutomatic  
        .TintAndShade = 0  
        .Weight = xlThick  
    End With  
    Selection.Borders(xlInsideVertical).LineStyle = xlNone  
    Selection.Borders(xlInsideHorizontal).LineStyle = xlNone  
  
    Columns("S:V").ColumnWidth = 12  
    Columns("X:AA").ColumnWidth = 12  
  
    Range("S2:U2,S3:U3,S4:U4,S5:U5,S6:U6,S7:U7,S8:U8,S9:  
U9,S12:U12,S13:U13,S14:U14,S15:U15,S16:U16,X2:Z2,X3:  
Z3,X4:Z4,X5:Z5,X6:Z6,X7:Z7,X8:Z8,X9:Z9,X12:Z12,X13:  
Z13,X14:Z14,X15:Z15,X16:Z16").Select  
    Selection.Merge  
    With Selection  
        .HorizontalAlignment = xlLeft  
        .VerticalAlignment = xlBottom  
        .WrapText = False  
        .Orientation = 0  
        .AddIndent = False  
        .IndentLevel = 0  
        .ShrinkToFit = False  
        .ReadingOrder = xlContext  
    End With  
  
    Range("S2:U2,S3:U3,S4:U4,S5:U5,S6:U6,S7:U7,S8:U8,S9:  
U9,S12:U12,S13:U13,S14:U14,S15:U15,S16:U16,V2:V9,V1  
2:V16,X2:Z2,X3:Z3,X4:Z4,X5:Z5,X6:Z6,X7:Z7,X8:Z8,X9:  
Z9,X12:Z12,X13:Z13,X14:Z14,X15:Z15,X16:Z16,AA2:AA  
9,AA12:AA16").Select  
    With Selection.Borders(xlEdgeLeft)  
        .LineStyle = xlContinuous  
        .ColorIndex = xlAutomatic  
        .TintAndShade = 0  
        .Weight = xlThin  
    End With  
    With Selection.Borders(xlEdgeTop)  
        .LineStyle = xlContinuous  
        .ColorIndex = xlAutomatic
```

```

        .TintAndShade = 0
        .Weight = xlThin
    End With
    With Selection.Borders(xlEdgeBottom)
        .LineStyle = xlContinuous
        .ColorIndex = xlAutomatic
        .TintAndShade = 0
        .Weight = xlThin
    End With
    With Selection.Borders(xlEdgeRight)
        .LineStyle = xlContinuous
        .ColorIndex = xlAutomatic
        .TintAndShade = 0
        .Weight = xlThin
    End With
    Range("S1,X1").FormulaR1C1 = "Vipulanandan"
    Range("S11,X11").FormulaR1C1 = "Ezeldin & Balaguru"
    With Range("S1,S11,X1,X11")
        .HorizontalAlignment = xlLeft
        .VerticalAlignment = xlBottom
        .Font.Bold = True
    End With
    ' Tangent Modulus ( MPa )
    Range("S2:U2,X2:Z2").FormulaR1C1 = "Tangent Modulus ( MPa )"
    Range("V2,AA2").FormulaR1C1 = "=R[21]C[-3]/R[21]C[-2]"
    ' Secant Modulus ( MPa )
    Range("S3:U3,X3:Z3").FormulaR1C1 = "Secant Modulus ( MPa )"
    Range("V3,AA3").FormulaR1C1 = "=R[1]C/R[2]C"
    ' Stress at Failure ( MPa )
    Range("S4:U4,S12:U12,X4:Z4,X12:Z12").FormulaR1C1 = "Stress at Failure ( MPa )"
    Range("V4,AA4").FormulaR1C1 = "=MAX(R[17]C[-3]:R[58]C[-3])"
    Range("V12,AA12").FormulaR1C1 = "=MAX(R[9]C[-3]:R[50]C[-3])"
    ' Resistivity at Failure
    Range("S5:U5,S13:U13").FormulaR1C1 = "Resistivity at Failure"
    Range("V5").FormulaR1C1 = "=VLOOKUP(R[-1]C,R[16]C[-3]:R[57]C[-2],2,FALSE)"
    Range("V13").FormulaR1C1 = "=VLOOKUP(R[-1]C,R[8]C[-3]:R[49]C[-2],2,FALSE)"
    ' Conductivity at Failure
    Range("X5:Z5,X13:Z13").FormulaR1C1 = "Conductivity at Failure"
    Range("AA5").FormulaR1C1 = "=VLOOKUP(R[-1]C,R[16]C[-3]:R[57]C[-2],2,FALSE)"
    Range("AA13").FormulaR1C1 = "=VLOOKUP(R[-1]C,R[8]C[-3]:R[49]C[-2],2,FALSE)"
    ' q
    Range("S6:U6,X6:Z6").FormulaR1C1 = "q"
    Range("V6,AA6").FormulaR1C1 = "=R[-3]C/R[-4]C"
    ' p

```

```

    Range("S7:U7,X7:Z7").FormulaR1C1 = "p"
    Range("V7,AA7").FormulaR1C1 = "1"
    ' Beta
    Range("S14:U14,X14:Z14").FormulaR1C1 = "Beta"
    Range("V14,AA14").FormulaR1C1 = "1.01"
    ' e^2
    Range("S8:U8,S15:U15,X8:Z8,X15:Z15").FormulaR1C1 = "e^2"
    With Range("S8:U8,S15:U15,X8:Z8,X15:Z15").Characters(Start:=2, Length:=1).Font
        .Superscript = True
    End With
    ' R^2
    Range("S9:U9,S16:U16,X9:Z9,X16:Z16").FormulaR1C1 = "R^2"
    With Range("S9:U9,S16:U16,X9:Z9,X16:Z16").Characters(Start:=2, Length:=1).Font
        .Superscript = True
    End With
    ' Copy Data into Prediction Section
    Range("S19:T19,X19:Y19").Merge
    Range("S19:T19,U19,V19,X19:Y19,Z19,AA19").Select
    With Selection
        .HorizontalAlignment = xlCenter
        .VerticalAlignment = xlBottom
        .Font.Bold = True
    End With
    Range("S19:T19,X19:Y19").FormulaR1C1 = "Measured"
    Range("U19,Z19").FormulaR1C1 = "Vipulanandan"
    Range("V19,AA19").FormulaR1C1 = "E & B"
    Range("I1:I42").Select
    Selection.Copy
    Range("S20").Select
    Selection.PasteSpecial Paste:=xlPasteValues, Operation:=xlNone, SkipBlanks _:=False, Transpose:=False
    Range("X20").Select
    Selection.PasteSpecial Paste:=xlPasteValues, Operation:=xlNone, SkipBlanks _:=False, Transpose:=False
    Range("M1:M42").Select
    Application.CutCopyMode = False
    Selection.Copy
    Range("T20").Select
    Selection.PasteSpecial Paste:=xlPasteValues, Operation:=xlNone, SkipBlanks _:=False, Transpose:=False
    Range("O1:O42").Select
    Application.CutCopyMode = False
    Selection.Copy
    Range("Y20").Select
    Selection.PasteSpecial Paste:=xlPasteValues, Operation:=xlNone, SkipBlanks _:=False, Transpose:=False
    Range("S21:T61,X21:Y61").Select
    Application.CutCopyMode = False
    Selection.NumberFormat = "0.000"
    Range("S20:V20,X20:AA20").Select

```

```

Selection.Font.Bold = True
With Selection.Borders(xlEdgeLeft)
    .LineStyle = xlContinuous
End With
With Selection.Borders(xlEdgeTop)
    .LineStyle = xlContinuous
End With
With Selection.Borders(xlEdgeBottom)
    .LineStyle = xlContinuous
End With
With Selection.Borders(xlEdgeRight)
    .LineStyle = xlContinuous
End With
With Selection.Borders(xlInsideVertical)
    .LineStyle = xlContinuous
End With
With Selection.Borders(xlInsideHorizontal)
    .LineStyle = xlContinuous
End With
Range("S20").Copy
Range("U20").Select
ActiveSheet.Paste
Range("V20").Select
ActiveSheet.Paste
Range("X20").Copy
Range("Z20").Select
ActiveSheet.Paste
Range("AA20").Select
ActiveSheet.Paste

'
'-----
' Prediction Portion
'-----
'
' Dim last3 As Double
' With ActiveSheet
'     last3 = .Cells(.Rows.Count, "S").End(xlUp).Row
' End With
'
'-----
' VIPULANANDAN Predicted Values
'-----
'
' Predicted Stress Values
'
' Range("U21").FormulaR1C1 = _
'     "=(RC[-1]/R5C22)/(R6C22+(1-R7C22-R6C22)*(RC[-1]/R5C22)+R7C22*(RC[-1]/R5C22)^(R7C22/(R7C22-R6C22))))*R4C22"
' Range("U21").AutoFill Destination:=Range("U21:U" & last3)
' Range("Z21").FormulaR1C1 = _
'     "=(RC[-1]/R5C27)/(R6C27+(1-R7C27-R6C27)*(RC[-1]/R5C27)+R7C27*(RC[-1]/R5C27)^(R7C27/(R7C27-R6C27))))*R4C27"
' Range("Z21").AutoFill Destination:=Range("Z21:Z" & last3)
'
' e^2 formula (performed after predicted stress values are
' obtained for Vipulanandan Predictive Model)
'
' Range("V8").FormulaArray = _
'     "=SUM(((R[13]C[-1]:R[54]C[-1]-R[13]C[-3]:R[54]C[-3])/R4C22)^2)"
' Range("AA8").FormulaArray = _
'     "=SUM(((R[13]C[-1]:R[54]C[-1]-R[13]C[-3]:R[54]C[-3])/R4C27)^2)"
'
' R^2 formula (performed after predicted stress values are
' obtained for Vipulanandan Predictive Model)
'
' Range("V9").FormulaArray = _
'     "=1-(SUM((R[12]C[-3]:R[53]C[-3]-R[12]C[-1]:R[53]C[-1])^2)/SUM((R[12]C[-3]:R[53]C[-3]-AVERAGE(R[12]C[-3]:R[53]C[-3])^2)))"
' Range("AA9").FormulaArray = _
'     "=1-(SUM((R[12]C[-3]:R[53]C[-3]-R[12]C[-1]:R[53]C[-1])^2)/SUM((R[12]C[-3]:R[53]C[-3]-AVERAGE(R[12]C[-3]:R[53]C[-3])^2)))"
'
'-----
' BETA Predicted Values
'-----
'
' Predicted Stress Values
'
' Range("V21").FormulaR1C1 = _
'     "=(R14C22*(RC[-2]/R13C22)/(R14C22-1+(RC[-2]/R13C22)^(R14C22)))*R12C22"
' Range("V21").AutoFill Destination:=Range("V21:V" & last3)
' Range("AA21").FormulaR1C1 = _
'     "=(R14C27*(RC[-2]/R13C27)/(R14C27-1+(RC[-2]/R13C27)^(R14C27)))*R12C27"
' Range("AA21").AutoFill Destination:=Range("AA21:AA" & last3)
'
' e^2 formula (performed after predicted stress values are
' obtained for Vipulanandan Predictive Model)
'
' Range("V15").FormulaArray = _
'     "=SUM(((R[6]C:R[47]C-R[6]C[-3]:R[47]C[-3])/R12C22)^2)"
' Range("AA15").FormulaArray = _
'     "=SUM(((R[6]C:R[47]C-R[6]C[-3]:R[47]C[-3])/R12C27)^2)"
'
' R^2 formula (performed after predicted stress values are
' obtained for Vipulanandan Predictive Model)
'
' Range("V16").FormulaArray = _
'     "=1-(SUM((R[5]C[-3]:R[46]C[-3]-R[5]C:R[46]C)^2)/SUM((R[5]C[-3]:R[46]C[-3]-AVERAGE(R[5]C[-3]:R[46]C[-3])^2)))"
' Range("AA16").FormulaArray = _
'     "=1-(SUM((R[5]C[-3]:R[46]C[-3]-R[5]C:R[46]C)^2)/SUM((R[5]C[-3]:R[46]C[-3]-AVERAGE(R[5]C[-3]:R[46]C[-3])^2)))"
'
'
' Clean up tables
'
Range("V2:V9,V12:V16,AA2:AA9,AA12:AA16").NumberFormat = "0.000"
Range("S21").Select
Range(Selection, Selection.End(xlDown)).Select
Range(Selection, Selection.End(xlToRight)).Select
With Selection.Borders(xlEdgeLeft)
    .LineStyle = xlContinuous
End With
With Selection.Borders(xlEdgeTop)
    .LineStyle = xlContinuous
End With
With Selection.Borders(xlEdgeBottom)
    .LineStyle = xlContinuous
End With

```

```

With Selection.Borders(xlEdgeRight)
    .LineStyle = xlContinuous
End With
With Selection.Borders(xlInsideVertical)
    .LineStyle = xlContinuous
End With
With Selection
    .NumberFormat = "0.000"
End With
Range("X21").Select
Range(Selection, Selection.End(xlDown)).Select
Range(Selection, Selection.End(xlToRight)).Select
With Selection.Borders(xlEdgeLeft)
    .LineStyle = xlContinuous
End With
With Selection.Borders(xlEdgeTop)
    .LineStyle = xlContinuous
End With
With Selection.Borders(xlEdgeBottom)
    .LineStyle = xlContinuous
End With
With Selection.Borders(xlEdgeRight)
    .LineStyle = xlContinuous
End With
With Selection.Borders(xlInsideVertical)
    .LineStyle = xlContinuous
End With
With Selection
    .NumberFormat = "0.000"
End With
'
'-----
' Chart Portion of Macro - Chart 1 = Stress vs. Resistivity
'-----
'
Dim sh As Worksheet
Dim chrt2 As chart

Set sh = ActiveWorkbook.Worksheets("Sheet2")
Set chrt2 = sh.Shapes.AddChart.chart
With chrt2
    .ChartType = xlXYScatter
' Data Collection - Measured Data
    .SeriesCollection.NewSeries
    .FullSeriesCollection(1).Name = """"Measured Data""""
    .FullSeriesCollection(1).XValues = "=Sheet2!$T$21:$T$61"
    .FullSeriesCollection(1).Values = "=Sheet2!$S$21:$S$61"
' Data Collection - Vipulanandan Predicted Data:
    .SeriesCollection.NewSeries
    .FullSeriesCollection(2).Name = """"Vipulanandan Data""""
    .FullSeriesCollection(2).XValues = "=Sheet2!$T$21:$T$61"
    .FullSeriesCollection(2).Values = "=Sheet2!$U$21:$U$61"
' Data Collection - Ezeldin & Balaguru Predicted Data:
    .SeriesCollection.NewSeries
    .FullSeriesCollection(3).Name = """"Beta Model Data""""
    .FullSeriesCollection(3).XValues = "=Sheet2!$T$21:$T$61"
    .FullSeriesCollection(3).Values = "=Sheet2!$V$21:$V$61"
' Chart Title
    .HasTitle = False
' X-Axis Name
    .Axes(xlCategory, xlPrimary).HasTitle = True
    .Axes(xlCategory, xlPrimary).AxisTitle.Characters.Text = "|" & ChrW(&H394) & ChrW(&H3C1) & "/" & ChrW(&H3C1) & "o"
    .Axes(xlCategory).AxisTitle.Select
    With Selection.Format.TextFrame2.TextRange.Font
        .NameComplexScript = "Times New Roman"
        .NameFarEast = "Times New Roman"
        .Name = "Times New Roman"
        .Size = 18
        .Bold = False
    End With
    With ActiveChart.Axes(xlCategory).TickLabels.Font
        .Name = "Times New Roman"
        .Size = 18
    End With
' Y-Axis Name
    .Axes(xlValue, xlPrimary).HasTitle = True
    .Axes(xlValue, xlPrimary).AxisTitle.Characters.Text = "Stress ( MPa )"
    .Axes(xlValue).AxisTitle.Select
    With Selection.Format.TextFrame2.TextRange.Font
        .NameComplexScript = "Times New Roman"
        .NameFarEast = "Times New Roman"
        .Name = "Times New Roman"
        .Size = 18
        .Bold = False
    End With
    With ActiveChart.Axes(xlValue).TickLabels.Font
        .Name = "Times New Roman"
        .Size = 18
    End With
' Delete Minor and Major Gridlines
    .Axes(xlCategory).HasMajorGridlines = False
    .Axes(xlCategory).HasMinorGridlines = False
    .Axes(xlValue).HasMajorGridlines = False
    .Axes(xlValue).HasMinorGridlines = False
' Chart Height = 5" , Chart Width = 6"
    .ChartArea.Height = 348
    .ChartArea.Width = 427
' Add Legend
    .HasLegend = True
' Add Minor and Major Tickmarks, "General" Number Format
    .Axes(xlCategory).MajorTickMark = xlCross
    .Axes(xlCategory).MinorTickMark = xlInside
    .Axes(xlCategory).TickLabels.NumberFormat = "General"
    With .Axes(xlCategory).Format.Line
        .Visible = msoTrue
        .ForeColor.ObjectThemeColor = msoThemeColorText1
        .ForeColor.TintAndShade = 0
        .ForeColor.Brightness = 0
        .Transparency = 0
    End With
    .Axes(xlValue).MajorTickMark = xlCross
    .Axes(xlValue).MinorTickMark = xlInside
    .Axes(xlValue).TickLabels.NumberFormat = "General"
    With .Axes(xlValue).Format.Line
        .Visible = msoTrue
        .ForeColor.ObjectThemeColor = msoThemeColorText1
        .ForeColor.TintAndShade = 0
        .ForeColor.Brightness = 0
        .Transparency = 0
    End With
' Add Border Around Plot Area

```



```

With .PlotArea.Format.Line
    .Visible = msoTrue
    .ForeColor.ObjectThemeColor = msoThemeColorText1
    .ForeColor.TintAndShade = 0
    .ForeColor.Brightness = 0
    .Transparency = 0
End With
' Format Data Series:
' Measured Data:
With chrt2.FullSeriesCollection(1)
    .MarkerStyle = 8
    .MarkerSize = 9
    .Format.Fill.Visible = msoFalse
    .MarkerForegroundColor = RGB(0, 0, 0)
    .Format.Line.Visible = msoFalse
End With
' Vipulanandan Predicted Data:
With chrt2.FullSeriesCollection(2)
    .MarkerStyle = -4142
    .Format.Line.Visible = msoTrue
    .Format.Line.Weight = 1
End With
' Ezeldin and Balaguru Predicted Data:
With chrt2.FullSeriesCollection(3)
    .MarkerStyle = -4142
    .Format.Line.Visible = msoTrue
    .Format.Line.DashStyle = msoLineDash
    .Format.Line.Weight = 1
End With
' Cleaning Up Chart...
chrt2.FullSeriesCollection(4).Delete
chrt2.FullSeriesCollection(5).Delete
With .Legend.Format.Line
    .Visible = msoTrue
    .ForeColor.RGB = RGB(0, 0, 0)
End With
ActiveChart.PlotArea.Select
Selection.Width = 425
.Legend.Left = 295
.Legend.Top = 30
.Legend.Format.TextFrame2.TextRange.Font.Size = 14
.Legend.Left = 85
.Legend.Width = 150
.Legend.Height = 50
End With

' Change Plot Area Dimensions
ActiveChart.PlotArea.Select
Selection.Left = 59.5
Selection.Height = 325
Selection.Width = 440
' Remove Border Around Chart
chrt2.ChartArea.Border.LineStyle = xlNone
'
' Move chart to right of table
'
chrt2.Parent.Cut
Range("AC2").Select
ActiveSheet.Paste
'
'-----
' Chart Portion of Macro - Chart 2 = Stress vs. Conductivity
'-----
'
'
Dim sh2 As Worksheet

```

```

Dim chrt3 As chart

Set sh2 = ActiveWorkbook.Worksheets("Sheet2")
Set chrt3 = sh2.Shapes.AddChart.chart
With chrt3
    .ChartType = xlXYScatter
    ' Data Collection - Measured Data
    .SeriesCollection.NewSeries
    .FullSeriesCollection(1).Name = """"Measured Data""""
    .FullSeriesCollection(1).XValues = "=Sheet2!$Y$21:$Y$61"
    .FullSeriesCollection(1).Values = "=Sheet2!$X$21:$X$61"
    ' Data Collection - Vipulanandan Predicted Data:
    .SeriesCollection.NewSeries
    .FullSeriesCollection(2).Name = """"Vipulanandan Data""""
    .FullSeriesCollection(2).XValues = "=Sheet2!$Y$21:$Y$61"
    .FullSeriesCollection(2).Values = "=Sheet2!$Z$21:$Z$61"
    ' Data Collection - Ezeldin & Balaguru Predicted Data:
    .SeriesCollection.NewSeries
    .FullSeriesCollection(3).Name = """"Beta Model Data""""
    .FullSeriesCollection(3).XValues = "=Sheet2!$Y$21:$Y$61"
    .FullSeriesCollection(3).Values = "=Sheet2!$AA$21:$AA$61"
    ' Chart Title
    .HasTitle = False
    ' X-Axis Name
    .Axes(xlCategory, xlPrimary).HasTitle = True
    .Axes(xlCategory, xlPrimary).AxisTitle.Characters.Text = ChrW(&H394) & ChrW(&H3BA) & "/" & ChrW(&H3BA) & "o"
    .Axes(xlCategory).AxisTitle.Select
    With Selection.Format.TextFrame2.TextRange.Font
        .NameComplexScript = "Times New Roman"
        .NameFarEast = "Times New Roman"
        .Name = "Times New Roman"
        .Size = 18
        .Bold = False
    End With
    With ActiveChart.Axes(xlCategory).TickLabels.Font
        .Name = "Times New Roman"
        .Size = 18
    End With
    ' Y-Axis Name
    .Axes(xlValue, xlPrimary).HasTitle = True
    .Axes(xlValue, xlPrimary).AxisTitle.Characters.Text = "Stress ( MPa )"
    .Axes(xlValue).AxisTitle.Select
    With Selection.Format.TextFrame2.TextRange.Font
        .NameComplexScript = "Times New Roman"
        .NameFarEast = "Times New Roman"
        .Name = "Times New Roman"
        .Size = 18
        .Bold = False
    End With
    With ActiveChart.Axes(xlValue).TickLabels.Font
        .Name = "Times New Roman"
        .Size = 18
    End With
    ' Delete Minor and Major Gridlines
    .Axes(xlCategory).HasMajorGridlines = False
    .Axes(xlCategory).HasMinorGridlines = False
    .Axes(xlValue).HasMajorGridlines = False
    .Axes(xlValue).HasMinorGridlines = False
    ' Chart Height = 5" , Chart Width = 6"

```

```

.ChartArea.Height = 348
.ChartArea.Width = 427
' Add Legend
.HasLegend = True
' Add Minor and Major Tickmarks, "General" Number
Format
.Axes(xlCategory).MajorTickMark = xlCross
.Axes(xlCategory).MinorTickMark = xlInside
.Axes(xlCategory).TickLabels.NumberFormat = "General"
With .Axes(xlCategory).Format.Line
.Visible = msoTrue
.ForeColor.ObjectThemeColor = msoThemeColorText1
.ForeColor.TintAndShade = 0
.ForeColor.Brightness = 0
.Transparency = 0
End With
.Axes(xlValue).MajorTickMark = xlCross
.Axes(xlValue).MinorTickMark = xlInside
.Axes(xlValue).TickLabels.NumberFormat = "General"
With .Axes(xlValue).Format.Line
.Visible = msoTrue
.ForeColor.ObjectThemeColor = msoThemeColorText1
.ForeColor.TintAndShade = 0
.ForeColor.Brightness = 0
.Transparency = 0
End With
' Add Border Around Plot Area
With .PlotArea.Format.Line
.Visible = msoTrue
.ForeColor.ObjectThemeColor = msoThemeColorText1
.ForeColor.TintAndShade = 0
.ForeColor.Brightness = 0
.Transparency = 0
End With
' Format Data Series:
' Measured Data:
With chrt3.FullSeriesCollection(1)
.MarkerStyle = 8
.MarkerSize = 9
.Format.Fill.Visible = msoFalse
.MarkerForegroundColor = RGB(0, 0, 0)
.Format.Line.Visible = msoFalse
End With
' Vipulanandan Predicted Data:
With chrt3.FullSeriesCollection(2)
.MarkerStyle = -4142
.Format.Line.Visible = msoTrue
.Format.Line.Weight = 1
End With
' Ezeldin and Balaguru Predicted Data:
With chrt3.FullSeriesCollection(3)
.MarkerStyle = -4142
.Format.Line.Visible = msoTrue
.Format.Line.DashStyle = msoLineDash
.Format.Line.Weight = 1
End With
' Cleaning Up Chart...
With .Legend.Format.Line
.Visible = msoTrue
.ForeColor.RGB = RGB(0, 0, 0)
End With
ActiveChart.PlotArea.Select
Selection.Width = 425
.Legend.Left = 295
.Legend.Top = 30
.Legend.Format.TextFrame2.TextRange.Font.Size = 14

.Legend.Left = 85
.Legend.Width = 150
.Legend.Height = 50
End With

' Change Plot Area Dimensions
ActiveChart.PlotArea.Select
Selection.Left = 59.5
Selection.Height = 325
Selection.Width = 440
' Remove Border Around Chart
chrt3.ChartArea.Border.LineStyle = xlNone
' Move chart to right of table
chrt3.Parent.Cut
Range("AM2").Select
ActiveSheet.Paste

' Begin Final Clean-Up
Range("S20").Select
Selection.End(xlDown).Select
ActiveCell.Offset(1, 0).Select
Range(Selection, Selection.End(xlToRight)).Select
Range(Selection, Selection.End(xlDown)).Delete
Shift:=xlUp

' Begin Solver Portion of Macro to Optimize Curve
' Vipulanandan Predictive Model - Manipulates p to get lowest
e^2 value (RESISTIVITY PREDICTION)
SolverOk SetCell:="$V$8", MaxMinVal:=2, ValueOf:=0,
ByChange:="$V$7", Engine:=1,
, EngineDesc:="GRG Nonlinear"
SolverAdd CellRef:="$V$7", Relation:=1,
FormulaText:="1"
SolverAdd CellRef:="$V$7", Relation:=3,
FormulaText:="0.01"
SolverOk SetCell:="$V$8", MaxMinVal:=2, ValueOf:=0,
ByChange:="$V$7", Engine:=1,
, EngineDesc:="GRG Nonlinear"
SolverOk SetCell:="$V$8", MaxMinVal:=2, ValueOf:=0,
ByChange:="$V$7", Engine:=1,
, EngineDesc:="GRG Nonlinear"
SolverSolve
' Ezeldin & Balaguru Predictive Model - Manipulates beta to
get lowest e^2 value (RESISTIVITY PREDICTION)

```

```

    SolverOk SetCell:="$V$15", MaxMinVal:=2, ValueOf:=0,
ByChange:="$V$14", Engine:=1 _
    , EngineDesc:="GRG Nonlinear"
    SolverOk SetCell:="$V$15", MaxMinVal:=2, ValueOf:=0,
ByChange:="$V$14", Engine:=1 _
    , EngineDesc:="GRG Nonlinear"
    SolverSolve
'
' Vipulanandan Predictive Model - Manipulates p to get lowest
e^2 value (CONDUCTIVITY PREDICTION)
'
    SolverOk SetCell:="$AA$8", MaxMinVal:=2,
ValueOf:=0, ByChange:="$AA$7", Engine:=1 _
    , EngineDesc:="GRG Nonlinear"
    SolverAdd CellRef:="$AA$7", Relation:=1,
FormulaText:="1"
    SolverAdd CellRef:="$AA$7", Relation:=3,
FormulaText:="0.01"
    SolverOk SetCell:="$AA$8", MaxMinVal:=2,
ValueOf:=0, ByChange:="$AA$7", Engine:=1 _

```

```

    , EngineDesc:="GRG Nonlinear"
    SolverOk SetCell:="$AA$8", MaxMinVal:=2,
ValueOf:=0, ByChange:="$AA$7", Engine:=1 _
    , EngineDesc:="GRG Nonlinear"
    SolverSolve
'
' Ezeldin & Balaguru Predictive Model - Manipulates beta to
get lowest e^2 value (CONDUCTIVITY PREDICTION)
'
    SolverOk SetCell:="$AA$15", MaxMinVal:=2,
ValueOf:=0, ByChange:="$AA$14", Engine:=1 _
    , EngineDesc:="GRG Nonlinear"
    SolverOk SetCell:="$AA$15", MaxMinVal:=2,
ValueOf:=0, ByChange:="$AA$14", Engine:=1 _
    , EngineDesc:="GRG Nonlinear"
    SolverSolve

End Sub

```

**Table D.2: Compression Testing Stress-Strain Results.**

<b>Cylinder #</b>	<b>NanoFe<sub>2</sub>O<sub>3</sub> (%)</b>	<b>W-C Ratio</b>	<b>Curing Time (days)</b>	<b>Tangent Modulus (MPa)</b>	<b>Secant Modulus (MPa)</b>	<b>Stress at Failure (MPa)</b>	<b>Strain at Failure (%)</b>
1	0	0.40	1	407.072	435.031	13.859	3.186
2	0	0.40	7	1446.503	1080.482	21.428	1.983
3	0	0.40	28	1497.904	2116.769	15.437	0.729
4	0	0.45	1	648.247	712.893	13.098	1.837
5	0	0.45	7	969.727	1214.430	12.747	1.050
6	0	0.45	28	1327.535	2369.483	25.112	1.060
7	0	0.50	1	852.227	503.389	8.895	1.767
8	0	0.50	7	1697.251	1588.267	21.116	1.330
9	0	0.50	28	1762.794	1996.505	28.792	1.442
10	0	0.60	1	783.942	739.469	8.061	1.090
11	0	0.60	7	865.296	1061.721	10.600	0.998
12	0	0.60	28	1104.921	882.134	13.288	1.506
13	2.5	0.40	1	1848.620	1567.078	19.296	1.231
14	2.5	0.40	7	1738.158	1325.532	23.467	1.770
15	2.5	0.40	28	1581.463	1922.787	16.333	0.849
16	2.5	0.45	1	898.774	896.037	12.223	1.364
17	2.5	0.45	7	1082.111	1182.065	19.484	1.648
18	2.5	0.45	28	1417.976	1788.552	16.366	0.915
19	2.5	0.50	1	483.165	497.066	7.681	1.545
20	2.5	0.50	7	1280.379	1735.134	23.246	1.340
21	2.5	0.50	28	1150.879	1562.957	16.094	1.030
22	2.5	0.60	1	1069.350	308.601	6.553	2.123
23	2.5	0.60	7	913.953	892.574	14.892	1.668
24	2.5	0.60	28	772.072	938.902	16.102	1.715
25	5	0.40	1	2064.368	1361.689	24.351	1.788
26	5	0.40	7	1403.443	1225.165	22.276	1.818
27	5	0.40	28	1897.354	2143.382	23.864	1.113
28	5	0.45	1	1481.738	1234.362	19.865	1.609
29	5	0.45	7	1825.678	1879.692	27.263	1.450
30	5	0.45	28	1789.223	2190.564	30.780	1.405

**Table D.2 (Continued): Compression Testing Stress-Strain Results.**

<b>Cylinder #</b>	<b>NanoFe<sub>2</sub>O<sub>3</sub> (%)</b>	<b>W-C Ratio</b>	<b>Curing Time (days)</b>	<b>Tangent Modulus (MPa)</b>	<b>Secant Modulus (MPa)</b>	<b>Stress at Failure (MPa)</b>	<b>Strain at Failure (%)</b>
31	5	0.50	1	1343.327	926.897	11.626	1.254
32	5	0.50	7	1011.362	1093.531	17.467	1.597
33	5	0.50	28	1441.138	1171.761	20.418	1.743
34	5	0.60	1	837.307	649.234	7.554	1.163
35	5	0.60	7	740.569	515.173	9.540	1.852
36	5	0.60	28	969.893	1539.813	17.718	1.151
37	7.5	0.40	1	2884.255	1856.388	23.691	1.276
38	7.5	0.40	7	1317.195	968.526	14.270	1.473
39	7.5	0.40	28	2837.863	1913.841	27.629	1.444
40	7.5	0.45	1	1265.184	1075.116	13.593	1.264
41	7.5	0.45	7	2435.012	1869.550	32.276	1.726
42	7.5	0.45	28	525.751	753.533	13.064	1.734
43	7.5	0.50	1	1139.240	892.124	14.194	1.591
44	7.5	0.50	7	1724.831	1639.826	22.411	1.367
45	7.5	0.50	28	1740.626	1378.778	16.597	1.204
46	7.5	0.60	1	1619.482	811.190	8.559	1.055
47	7.5	0.60	7	1098.508	628.617	10.315	1.641
48	7.5	0.60	28	1240.345	855.665	15.312	1.789
49	10	0.40	1	1286.236	1921.633	16.969	0.883
50	10	0.40	7	1048.218	494.891	10.099	2.041
51	10	0.40	28	2187.403	1967.463	26.503	1.347
52	10	0.45	1	1591.903	1080.581	17.538	1.623
53	10	0.45	7	1424.708	1380.246	22.839	1.655
54	10	0.45	28	1485.467	1870.138	25.681	1.373
55	10	0.50	1	1772.766	1350.396	21.817	1.616
56	10	0.50	7	1585.570	1297.253	22.218	1.713
57	10	0.50	28	2321.574	1961.523	32.894	1.677
58	10	0.60	1	1139.988	945.861	12.444	1.316
59	10	0.60	7	1018.342	758.048	10.645	1.404
60	10	0.60	28	1234.944	1094.894	15.874	1.450

**Table D.3: Vipulanandan  $p$  and  $q$  Parameters and Predictive Results.**

Cylinder #	NanoFe <sub>2</sub> O <sub>3</sub> (%)	W-C Ratio	Curing Time (days)	q	p	e <sup>2</sup>	R <sup>2</sup>
1	0	0.40	1	1.069	0.010	4.203	0.961
2	0	0.40	7	0.747	0.147	2.098	0.974
3	0	0.40	28	1.413	0.044	0.022	0.999
4	0	0.45	1	1.100	0.025	1.120	0.985
5	0	0.45	7	1.252	0.088	0.112	0.998
6	0	0.45	28	1.785	0.214	0.304	0.993
7	0	0.50	1	0.591	0.049	0.546	0.992
8	0	0.50	7	0.936	0.031	0.122	0.998
9	0	0.50	28	1.133	0.528	0.087	0.999
10	0	0.60	1	0.943	0.035	0.256	0.994
11	0	0.60	7	1.227	0.011	0.213	0.994
12	0	0.60	28	0.798	0.395	1.070	0.983
13	2.5	0.40	1	0.848	0.157	0.082	0.999
14	2.5	0.40	7	0.763	1.102	0.665	0.993
15	2.5	0.40	28	1.216	0.241	0.105	0.997
16	2.5	0.45	1	0.997	0.010	0.552	0.990
17	2.5	0.45	7	1.092	0.015	0.191	0.997
18	2.5	0.45	28	1.261	0.033	0.026	0.999
19	2.5	0.50	1	1.029	0.010	5.197	0.898
20	2.5	0.50	7	1.355	0.751	0.255	0.997
21	2.5	0.50	28	1.358	0.124	0.086	0.998
22	2.5	0.60	1	0.289	3.962	1.368	0.981
23	2.5	0.60	7	0.977	0.249	0.185	0.998
24	2.5	0.60	28	1.216	0.022	1.355	0.977
25	5	0.40	1	0.660	0.109	2.734	0.961
26	5	0.40	7	0.873	0.073	0.333	0.996
27	5	0.40	28	1.130	0.046	0.114	0.998
28	5	0.45	1	0.833	0.857	2.577	0.964
29	5	0.45	7	1.030	0.261	0.268	0.996
30	5	0.45	28	1.224	0.147	0.127	0.998

**Table D.3 (Continued): Vipulanandan  $p$  and  $q$  Parameters and Predictive Results.**

Cylinder #	NanoFe <sub>2</sub> O <sub>3</sub> (%)	W-C Ratio	Curing Time (days)	q	p	e <sup>2</sup>	R <sup>2</sup>
31	5	0.50	1	0.690	0.072	0.131	0.998
32	5	0.50	7	1.081	0.153	0.321	0.996
33	5	0.50	28	0.813	0.105	1.122	0.984
34	5	0.60	1	0.775	0.092	0.584	0.988
35	5	0.60	7	0.696	0.010	1.614	0.973
36	5	0.60	28	1.588	0.274	0.086	0.998
37	7.5	0.40	1	0.644	0.265	0.034	0.999
38	7.5	0.40	7	0.735	0.010	1.652	0.971
39	7.5	0.40	28	0.674	0.013	2.344	0.959
40	7.5	0.45	1	0.850	0.213	0.303	0.995
41	7.5	0.45	7	0.768	0.090	0.618	0.991
42	7.5	0.45	28	1.433	0.010	1.486	0.966
43	7.5	0.50	1	0.783	0.317	0.673	0.991
44	7.5	0.50	7	0.951	0.065	0.085	0.999
45	7.5	0.50	28	0.792	0.048	0.693	0.986
46	7.5	0.60	1	0.501	0.103	0.136	0.997
47	7.5	0.60	7	0.572	0.051	0.167	0.997
48	7.5	0.60	28	0.690	0.661	1.948	0.974
49	10	0.40	1	1.494	0.508	0.116	0.997
50	10	0.40	7	0.472	0.010	10.766	0.773
51	10	0.40	28	0.899	0.189	0.272	0.996
52	10	0.45	1	0.679	0.490	0.382	0.995
53	10	0.45	7	0.969	0.561	0.244	0.997
54	10	0.45	28	1.259	0.167	0.297	0.995
55	10	0.50	1	0.762	0.085	0.135	0.998
56	10	0.50	7	0.818	0.339	0.232	0.997
57	10	0.50	28	0.845	0.030	0.257	0.997
58	10	0.60	1	0.830	0.080	0.067	0.999
59	10	0.60	7	0.744	0.912	0.548	0.992
60	10	0.60	28	0.887	0.066	1.152	0.980

**Table D.4: Ezeldin & Balaguru  $\beta$  Parameter and Predictive Results.**

Cylinder #	NanoFe <sub>2</sub> O <sub>3</sub> (%)	W-C Ratio	Curing Time (days)	$\beta$	e <sup>2</sup>	R <sup>2</sup>
1	0	0.40	1	1192.452	5.177	0.951
2	0	0.40	7	4.420	2.253	0.972
3	0	0.40	28	181.187	1.150	0.965
4	0	0.45	1	470.138	1.676	0.978
5	0	0.45	7	3.04E+08	0.452	0.990
6	0	0.45	28	485.037	1.911	0.959
7	0	0.50	1	4.008	1.106	0.985
8	0	0.50	7	22.802	0.135	0.998
9	0	0.50	28	7.116	0.514	0.993
10	0	0.60	1	18.633	0.279	0.993
11	0	0.60	7	3.97E+08	0.264	0.993
12	0	0.60	28	3.785	1.101	0.983
13	2.5	0.40	1	6.670	0.082	0.999
14	2.5	0.40	7	2.665	1.040	0.988
15	2.5	0.40	28	22.062	0.242	0.994
16	2.5	0.45	1	187.242	0.540	0.990
17	2.5	0.45	7	829.926	0.433	0.994
18	2.5	0.45	28	2.12E+08	0.677	0.983
19	2.5	0.50	1	786.827	5.362	0.895
20	2.5	0.50	7	9.841	0.784	0.990
21	2.5	0.50	28	143.228	0.675	0.986
22	2.5	0.60	1	1.360	1.526	0.979
23	2.5	0.60	7	7.576	0.456	0.994
24	2.5	0.60	28	1362.131	1.656	0.972
25	5	0.40	1	3.466	3.114	0.955
26	5	0.40	7	9.993	0.407	0.995
27	5	0.40	28	419.603	0.332	0.993
28	5	0.45	1	3.159	2.573	0.964
29	5	0.45	7	8.670	0.269	0.996
30	5	0.45	28	59.597	0.356	0.995



**Table D.4 (Continued): Ezeldin & Balaguru  $\beta$  Parameter and Predictive Results.**

Cylinder #	NanoFe <sub>2</sub> O <sub>3</sub> (%)	W-C Ratio	Curing Time (days)	$\beta$	e <sup>2</sup>	R <sup>2</sup>
31	5	0.50	1	5.279	0.174	0.997
32	5	0.50	7	18.497	0.379	0.995
33	5	0.50	28	6.102	1.256	0.982
34	5	0.60	1	6.290	0.607	0.987
35	5	0.60	7	8.713	3.165	0.947
36	5	0.60	28	6.68E+09	1.217	0.977
37	7.5	0.40	1	3.027	0.049	0.999
38	7.5	0.40	7	11.919	2.583	0.954
39	7.5	0.40	28	4.255	3.428	0.939
40	7.5	0.45	1	5.609	0.303	0.995
41	7.5	0.45	7	5.529	0.924	0.987
42	7.5	0.45	28	2.79E+09	6.516	0.850
43	7.5	0.50	1	3.851	0.749	0.991
44	7.5	0.50	7	16.528	0.081	0.999
45	7.5	0.50	28	7.271	1.033	0.979
46	7.5	0.60	1	2.586	0.438	0.989
47	7.5	0.60	7	3.722	0.684	0.989
48	7.5	0.60	28	2.628	1.948	0.974
49	10	0.40	1	29.049	0.777	0.983
50	10	0.40	7	9.730	13.477	0.716
51	10	0.40	28	6.947	0.267	0.996
52	10	0.45	1	2.762	0.381	0.995
53	10	0.45	7	4.732	0.369	0.995
54	10	0.45	28	97.525	0.318	0.995
55	10	0.50	1	5.903	0.354	0.995
56	10	0.50	7	4.233	0.314	0.996
57	10	0.50	28	13.076	0.302	0.996
58	10	0.60	1	8.103	0.119	0.998
59	10	0.60	7	2.695	0.860	0.988
60	10	0.60	28	9.441	1.221	0.979

Stress-Strain Compression Testing Graphs:

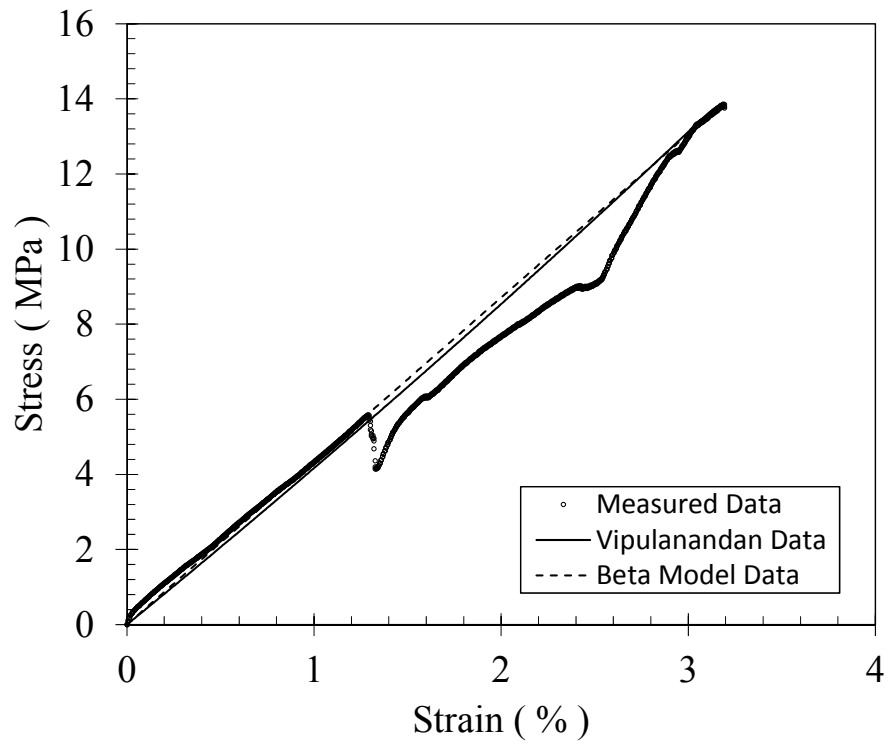


Figure D.1: Stress-Strain Data – Batch 1, Cylinder #1.

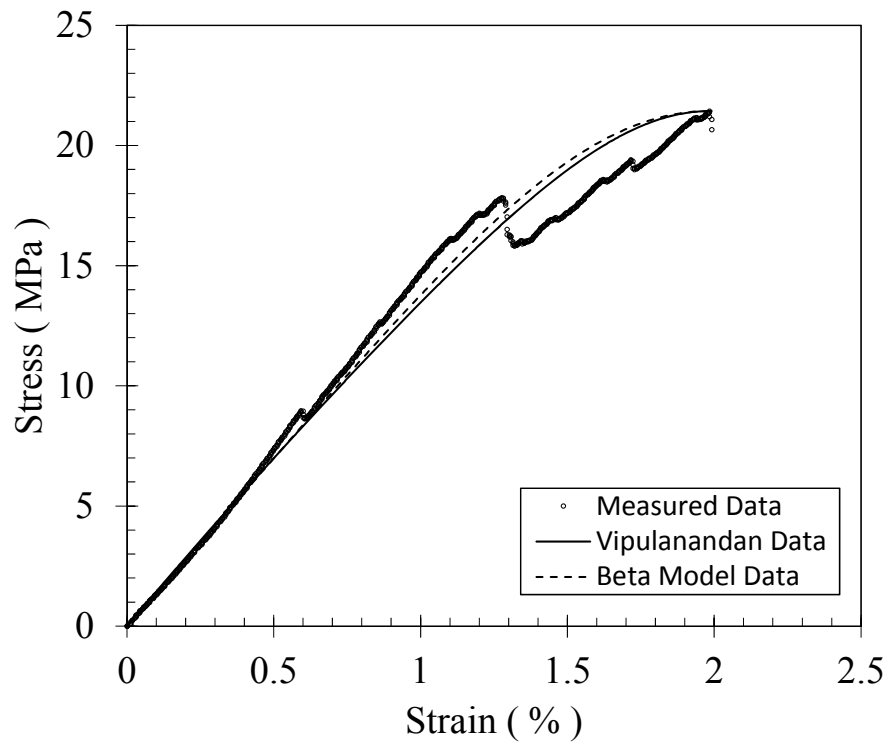
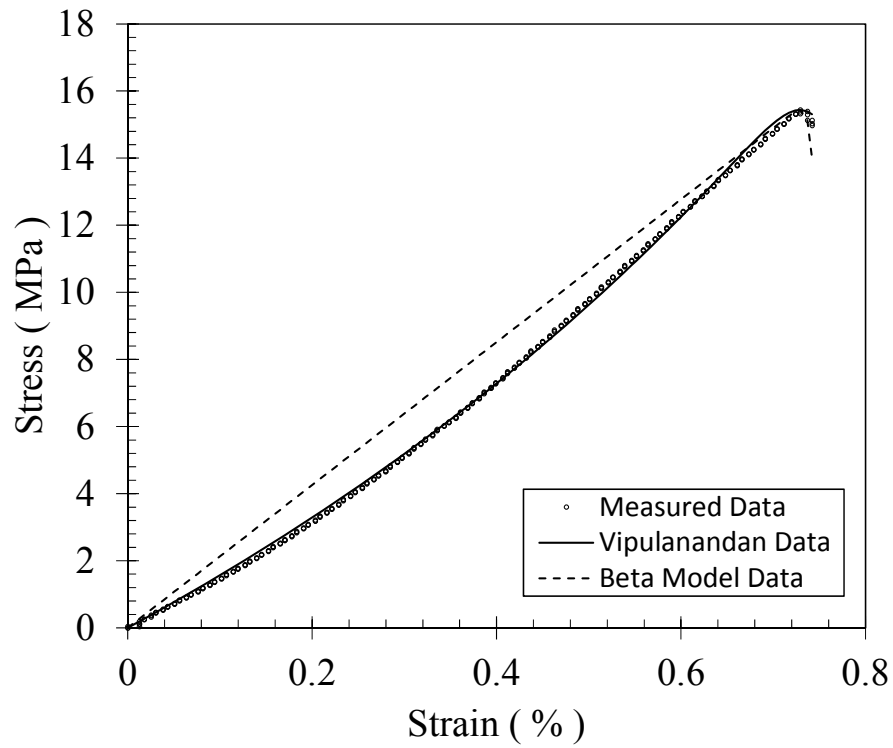
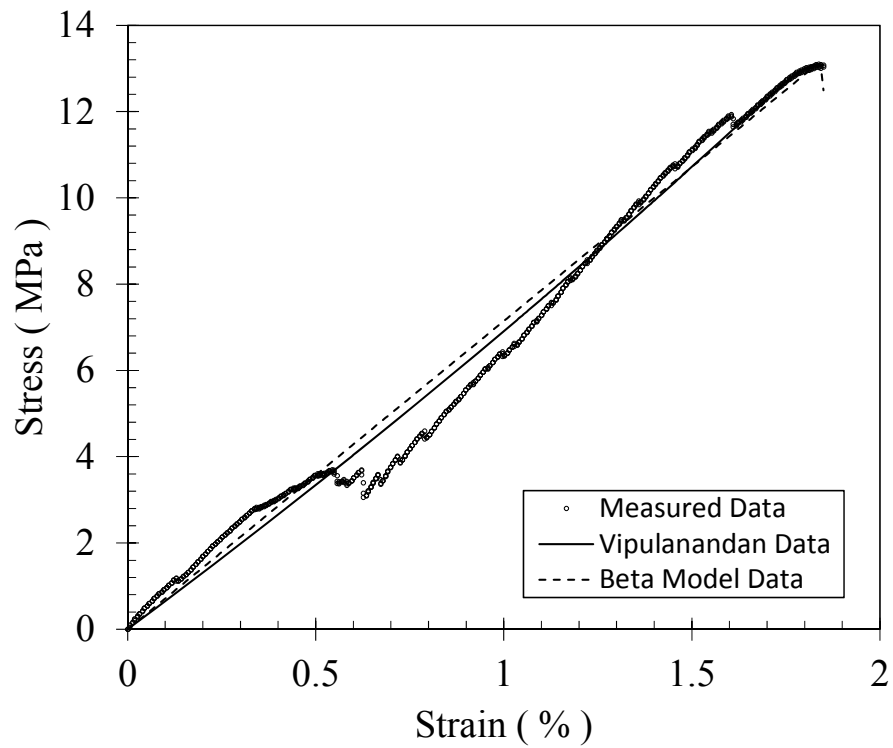


Figure D.2: Stress-Strain Data – Batch 1, Cylinder #2.



**Figure D.3: Stress-Strain Data – Batch 1, Cylinder #3.**



**Figure D.4: Stress-Strain Data – Batch 2, Cylinder #4.**

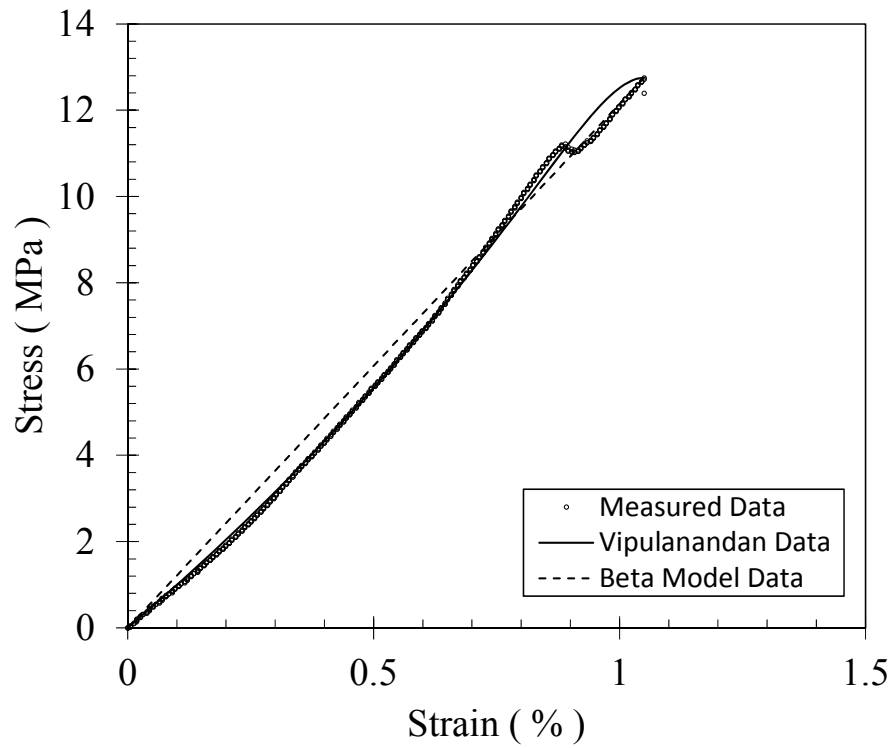


**Figure D.5: Stress-Strain Data – Batch 2, Cylinder #5.**

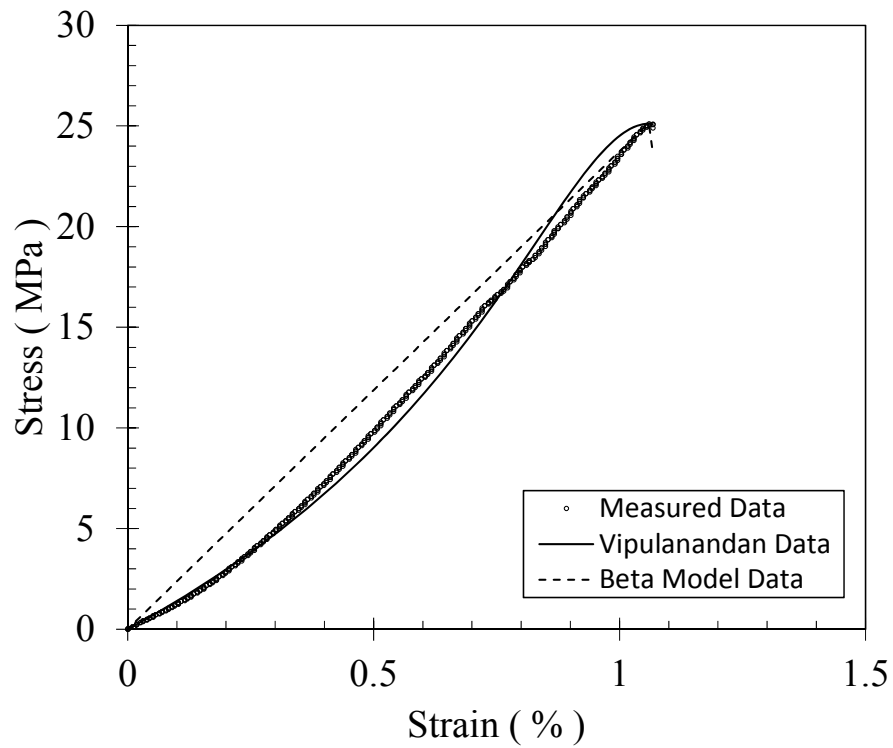


**Figure D.6: Stress-Strain Data – Batch 2, Cylinder #6.**

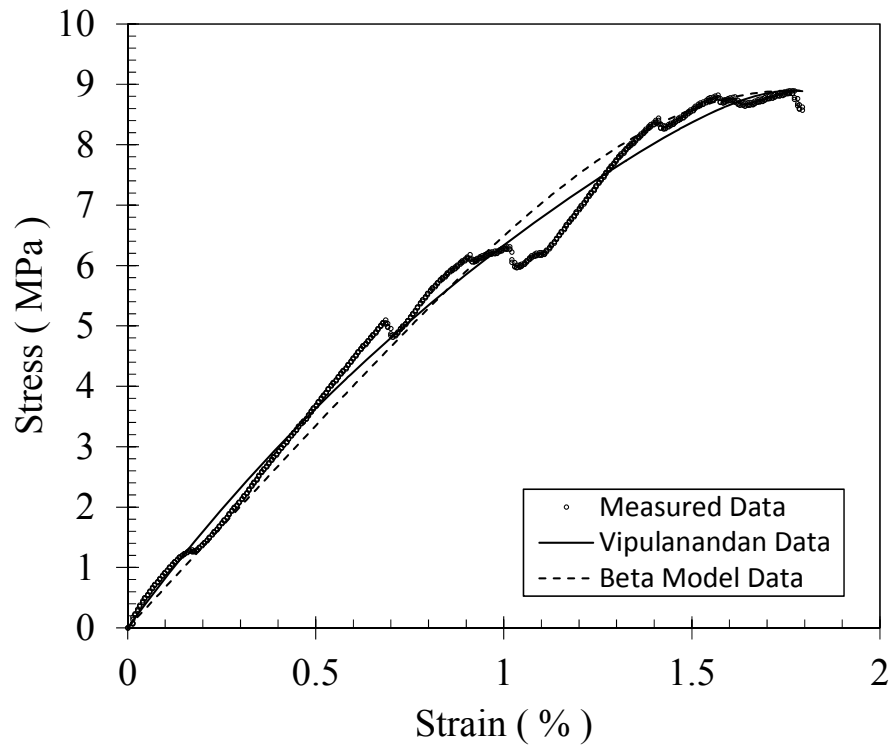


Figure D.7: Stress-Strain Data – Batch 3, Cylinder #7.

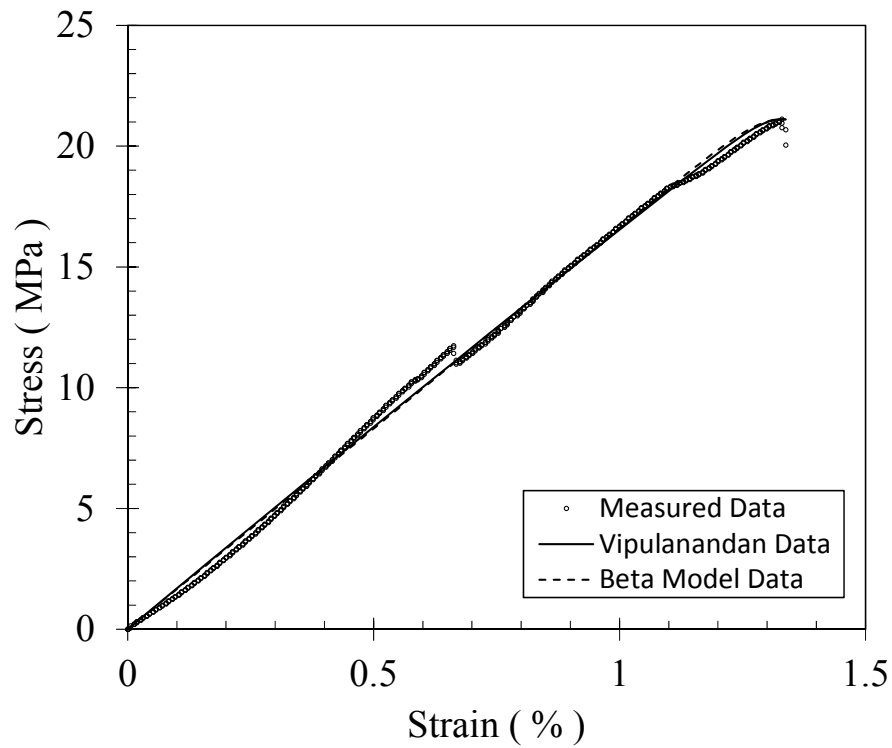


Figure D.8: Stress-Strain Data – Batch 3, Cylinder #8.

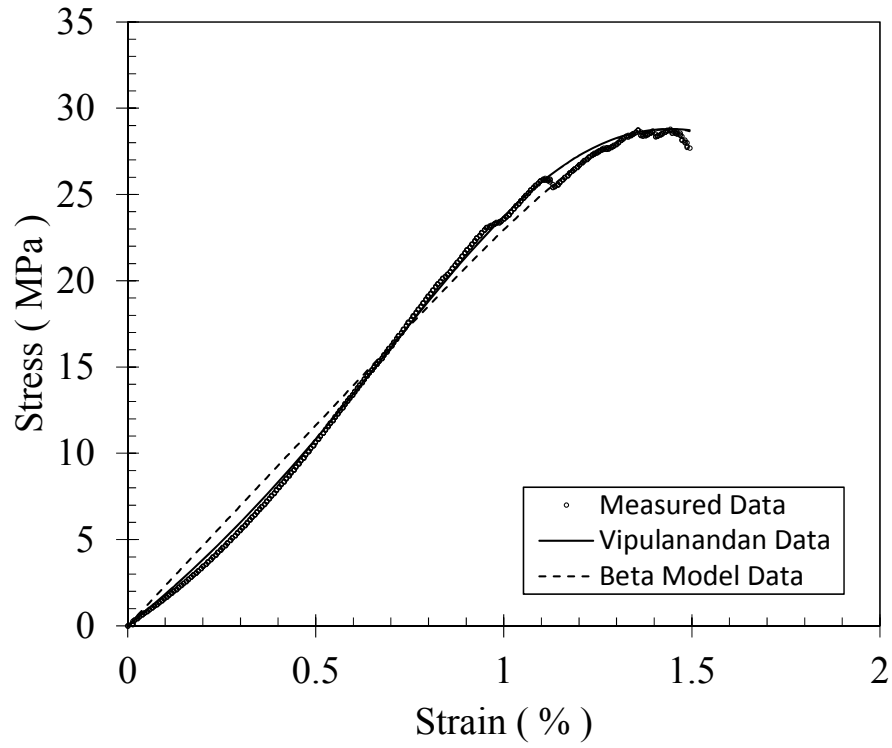


Figure D.9: Stress-Strain Data – Batch 3, Cylinder #9.

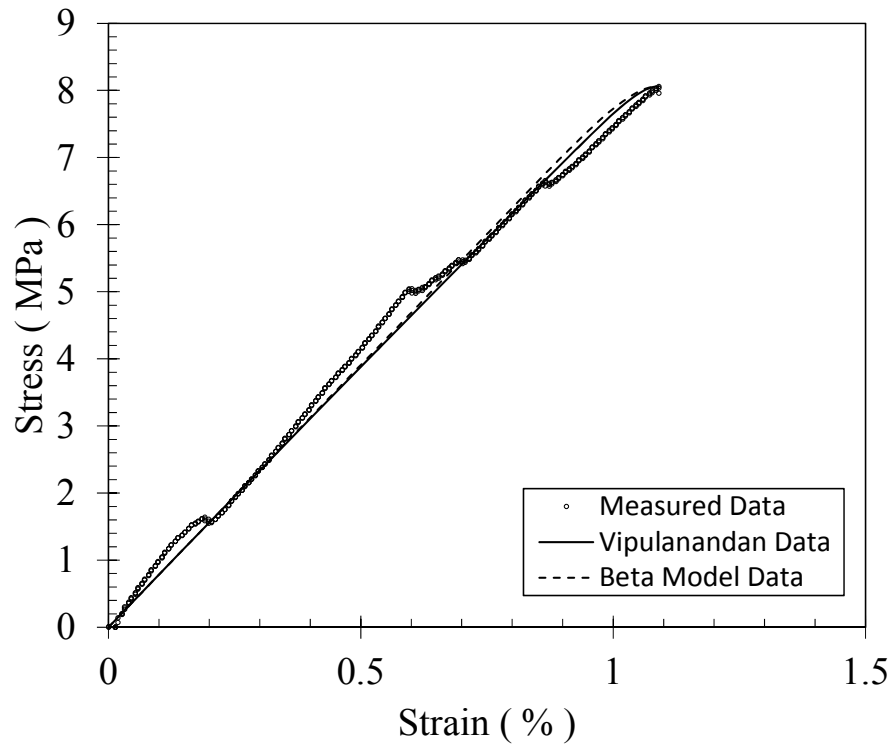


Figure D.10: Stress-Strain Data – Batch 4, Cylinder #10.

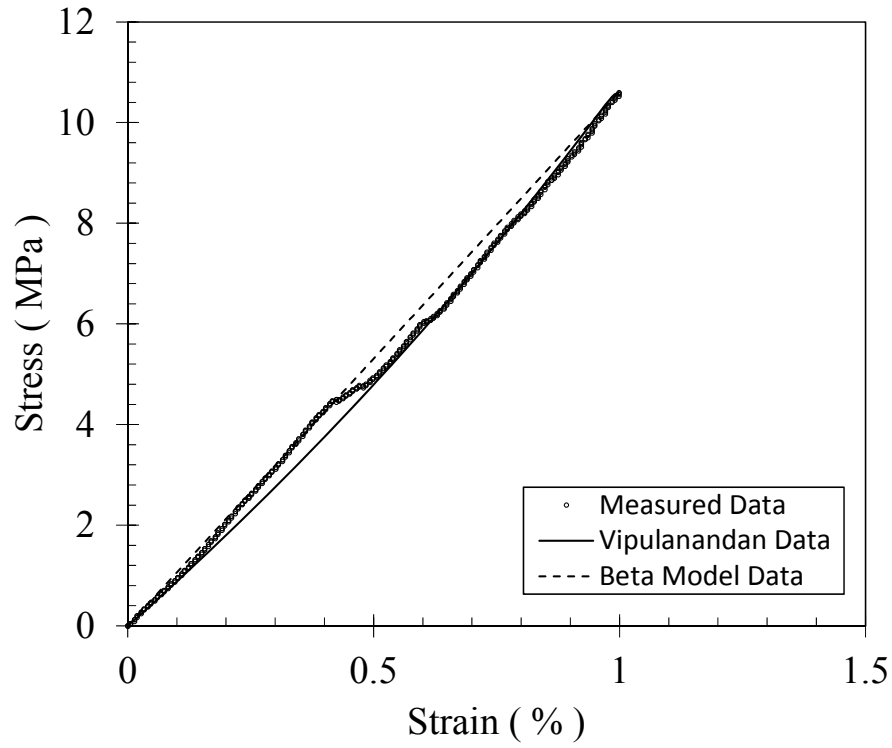


Figure D.11: Stress-Strain Data – Batch 4, Cylinder #11.

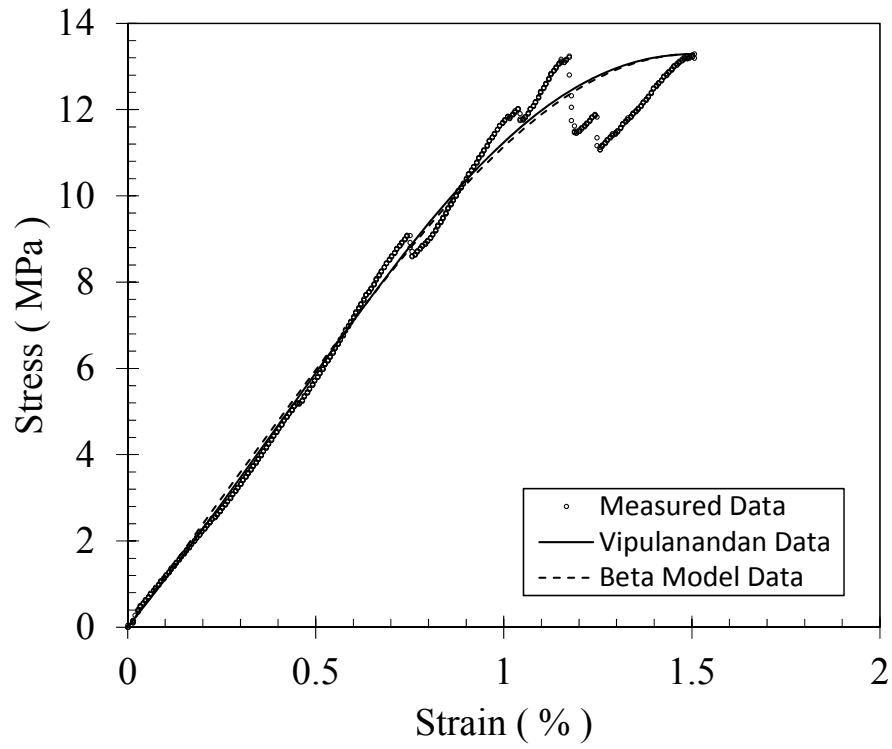


Figure D.12: Stress-Strain Data – Batch 4, Cylinder #12.

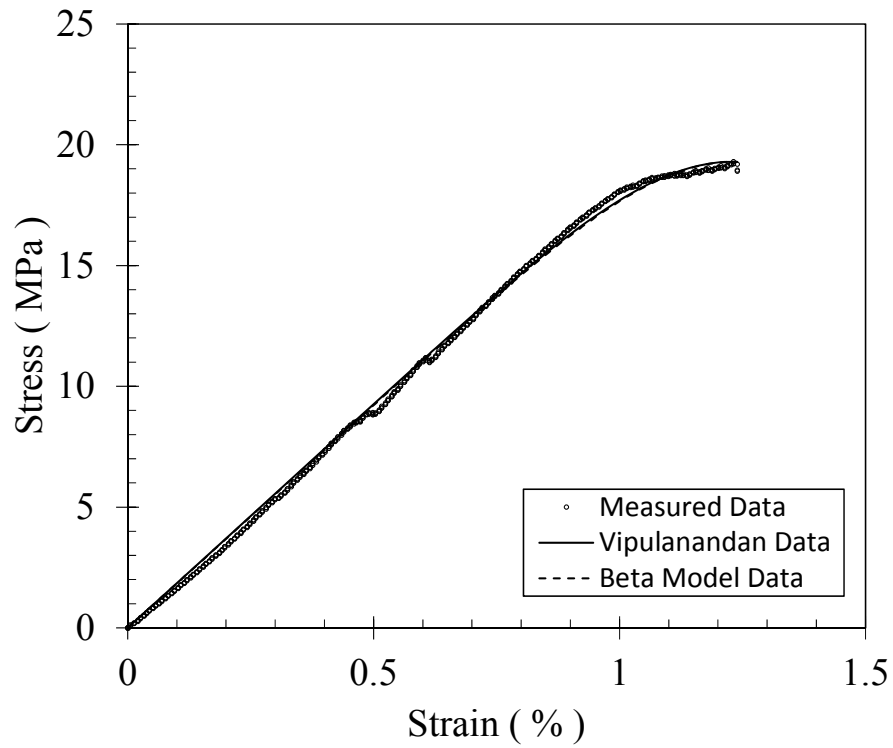


Figure D.13: Stress-Strain Data – Batch 5, Cylinder #13.

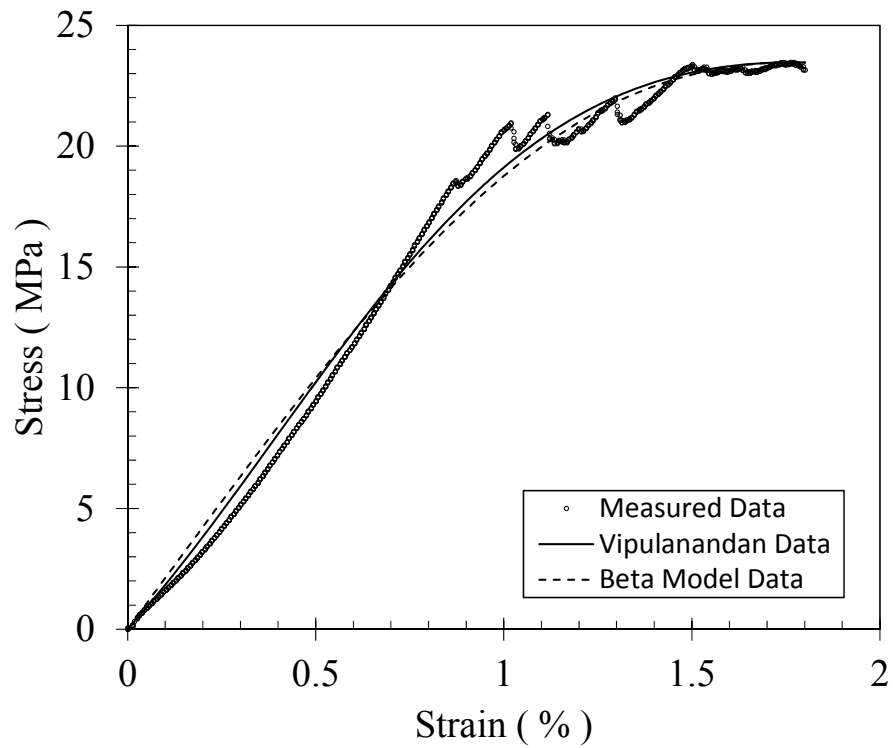


Figure D.14: Stress-Strain Data – Batch 5, Cylinder #14.



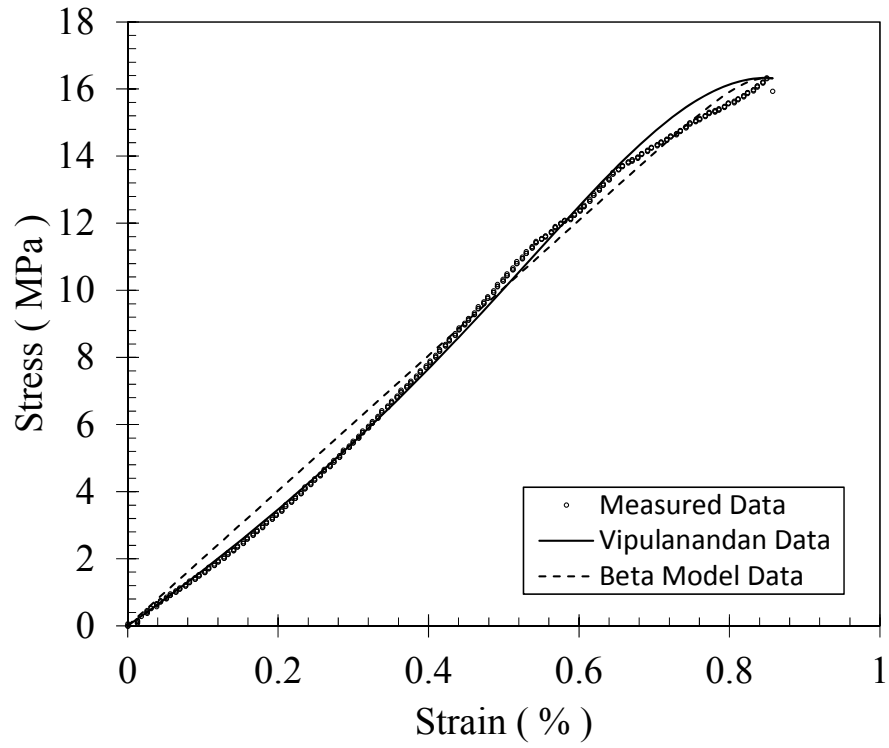


Figure D.15: Stress-Strain Data – Batch 5, Cylinder #15.

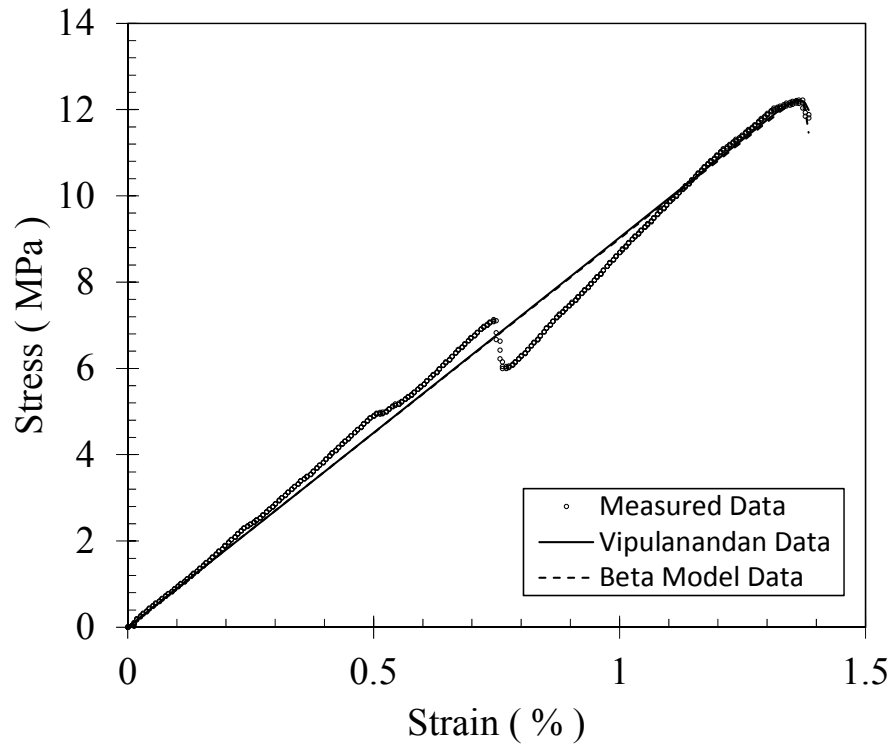


Figure D.16: Stress-Strain Data – Batch 6, Cylinder #16.

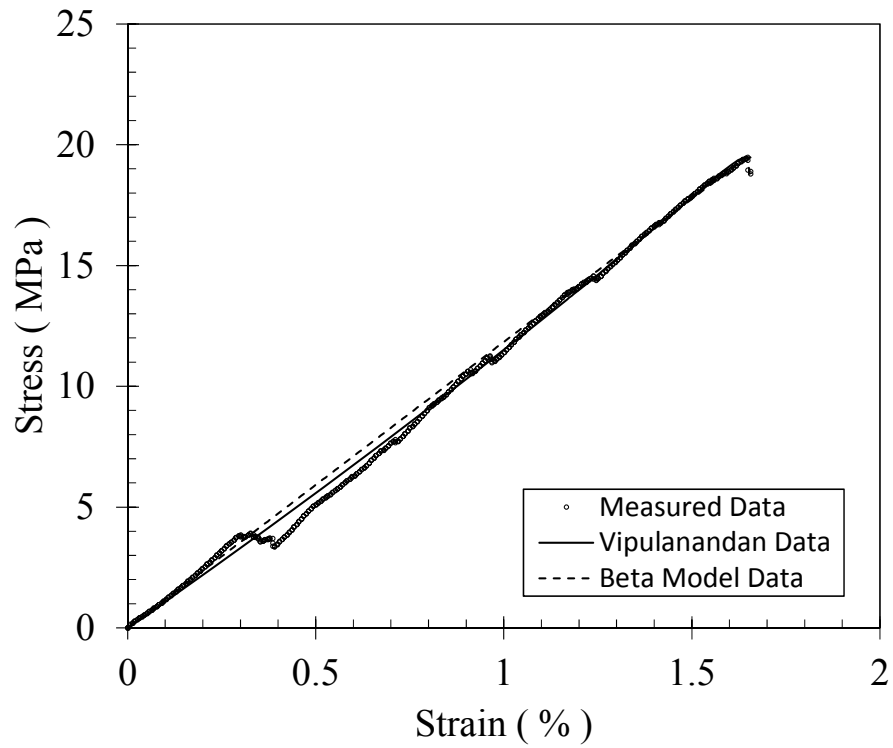


Figure D.17: Stress-Strain Data – Batch 6, Cylinder #17.

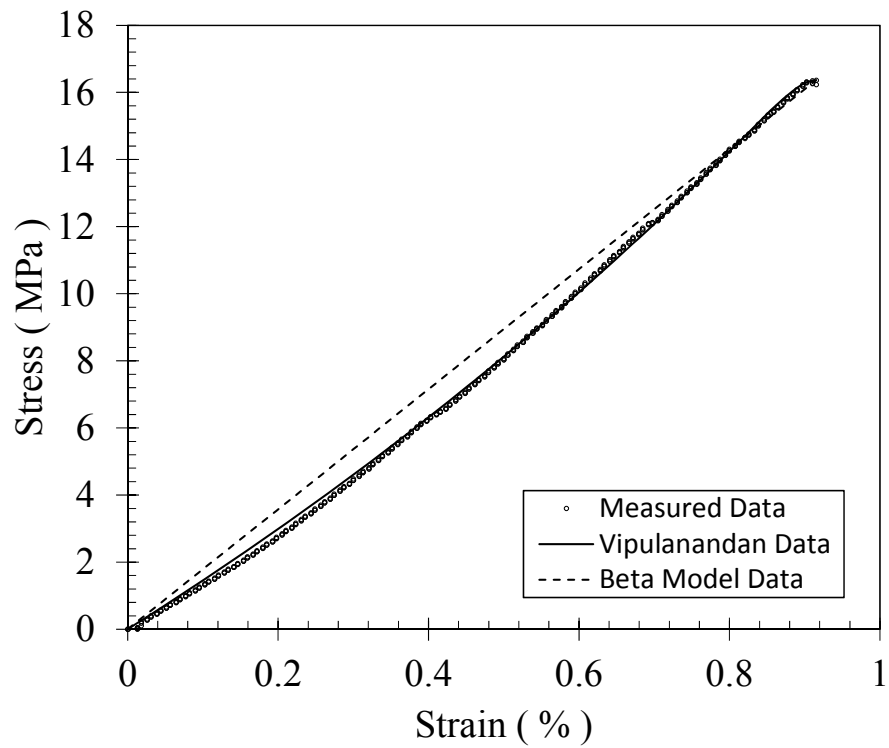


Figure D.18: Stress-Strain Data – Batch 6, Cylinder #18.

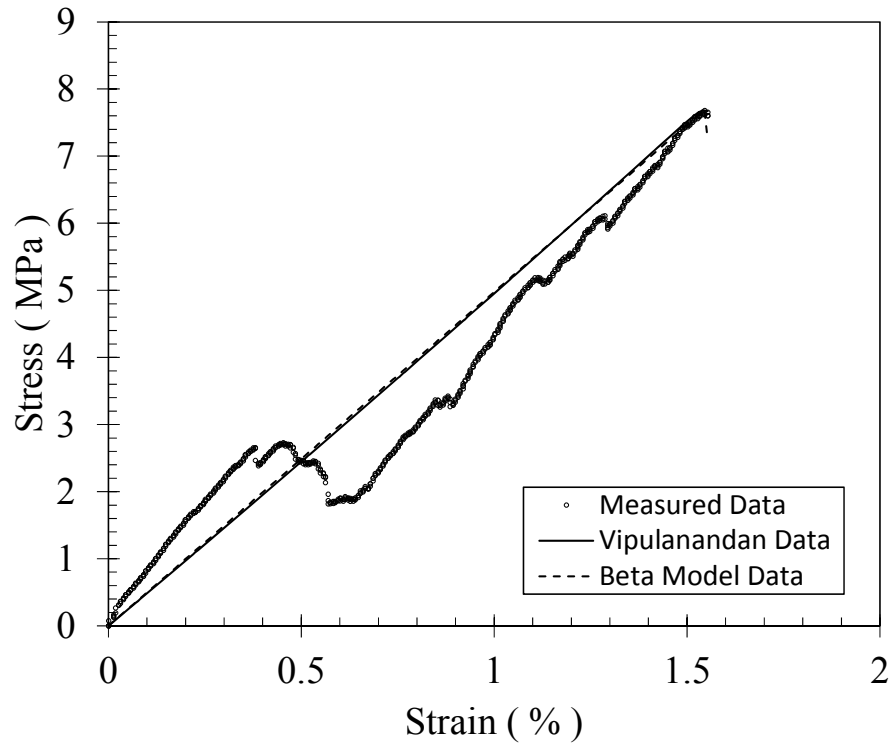


Figure D.19: Stress-Strain Data – Batch 7, Cylinder #19.

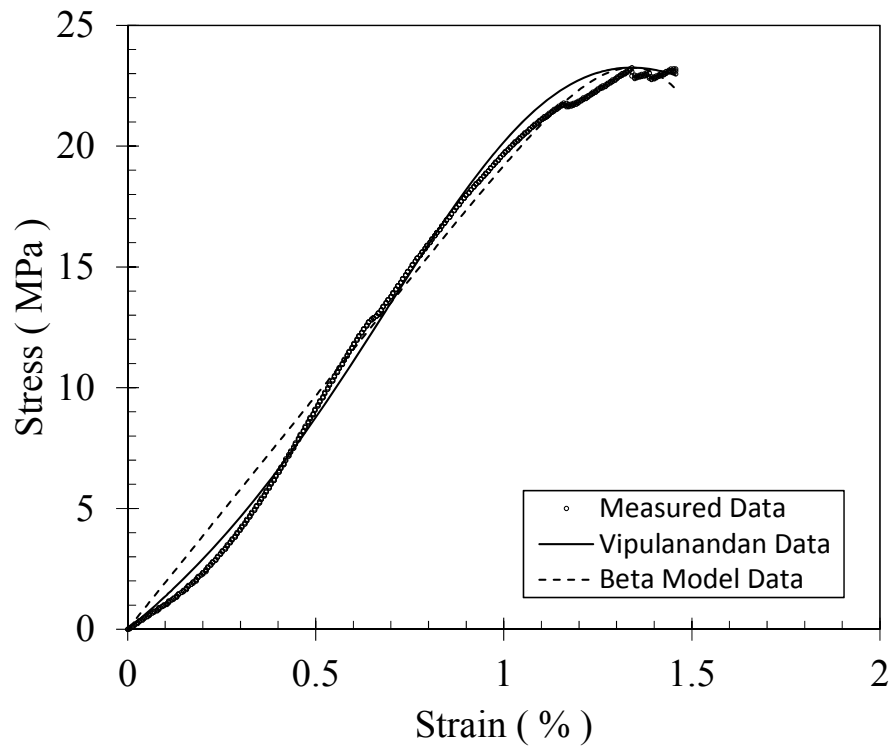


Figure D.20: Stress-Strain Data – Batch 7, Cylinder #20.

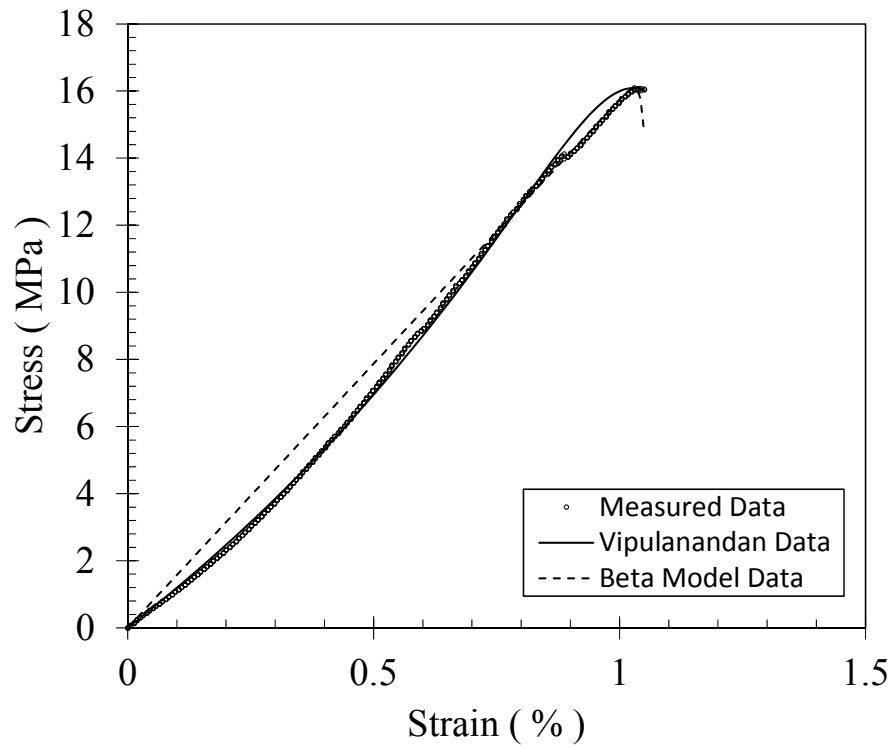


Figure D.21: Stress-Strain Data – Batch 7, Cylinder #21.

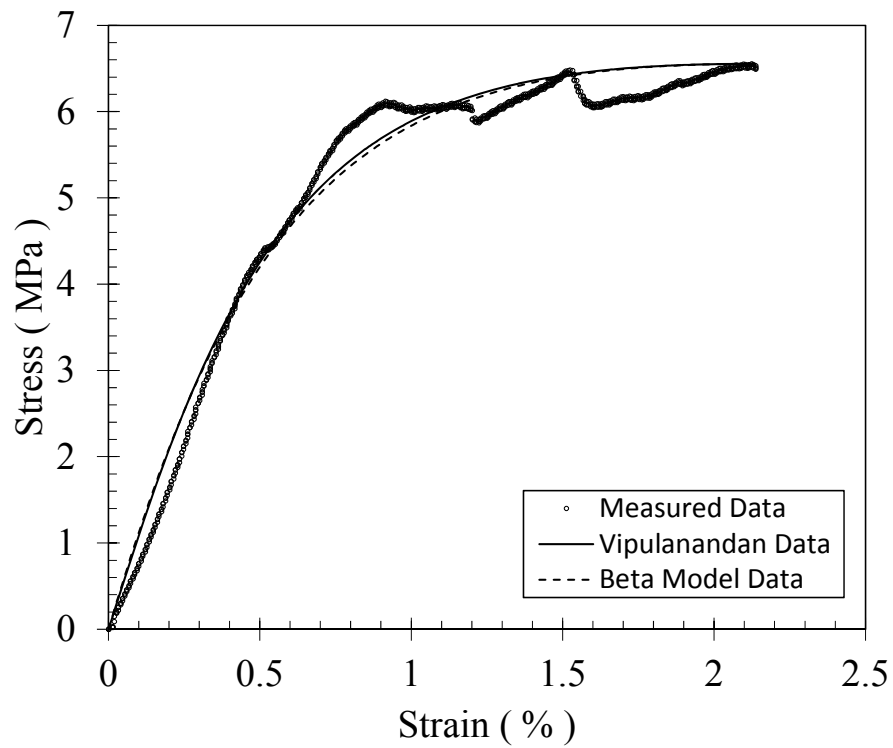


Figure D.22: Stress-Strain Data – Batch 8, Cylinder #22.

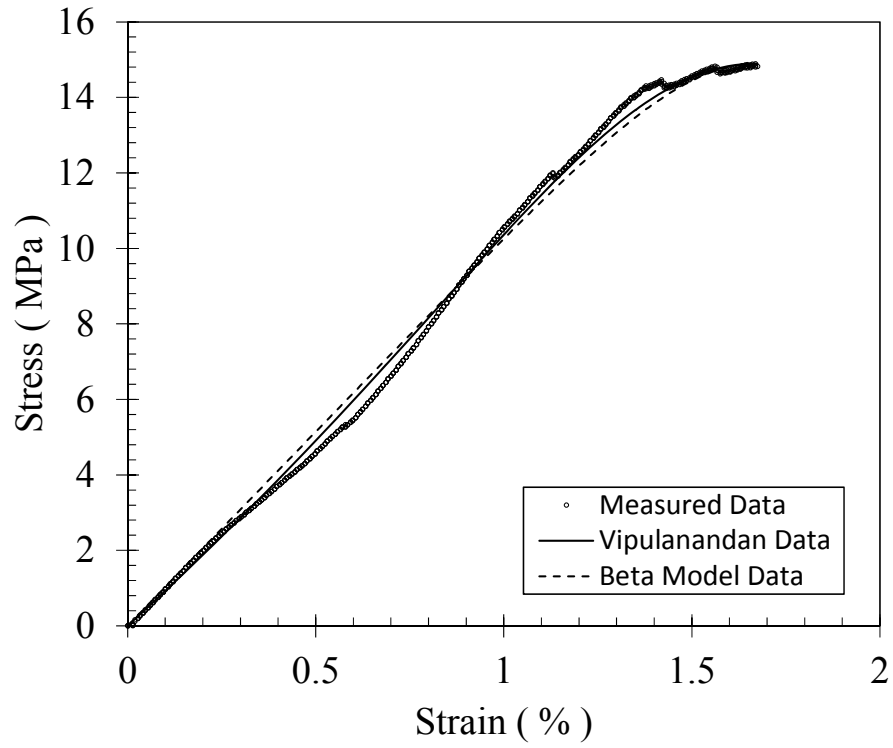


Figure D.23: Stress-Strain Data – Batch 8, Cylinder #23.

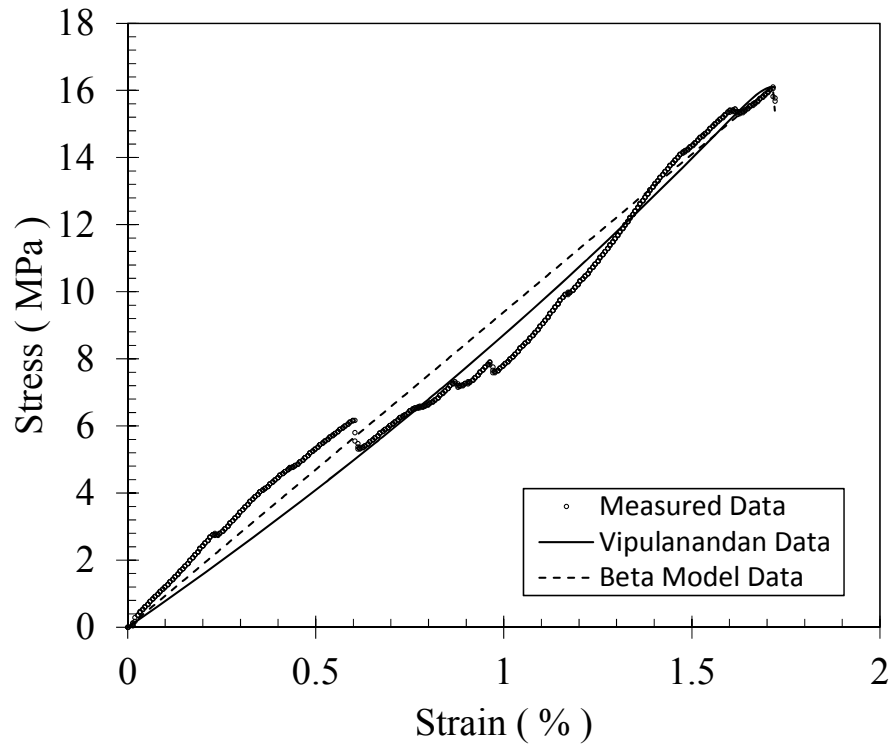


Figure D.24: Stress-Strain Data – Batch 8, Cylinder #24.

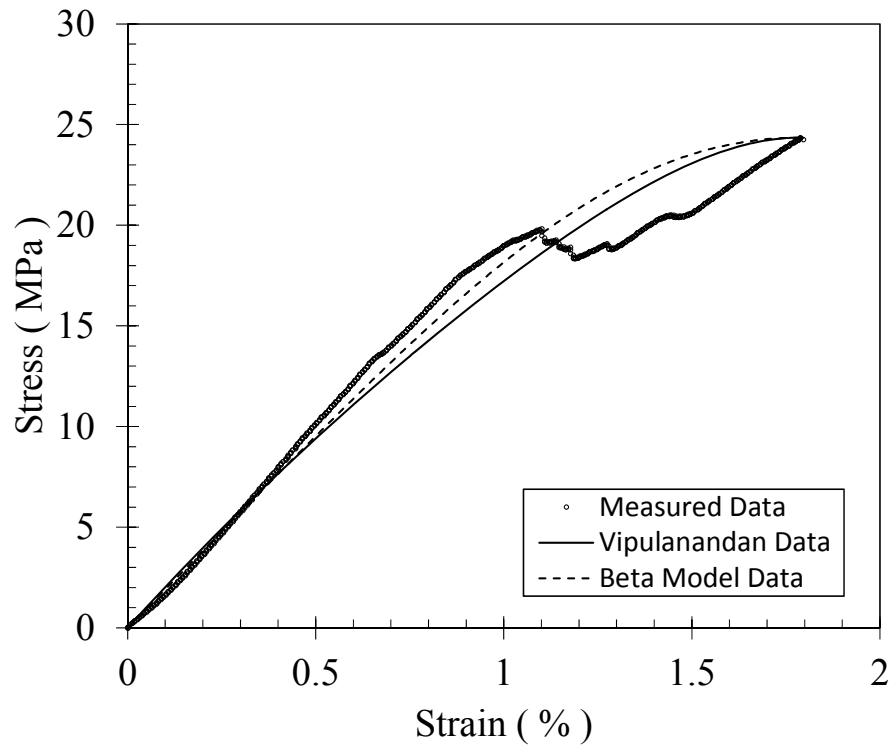


Figure D.25: Stress-Strain Data – Batch 9, Cylinder #25.

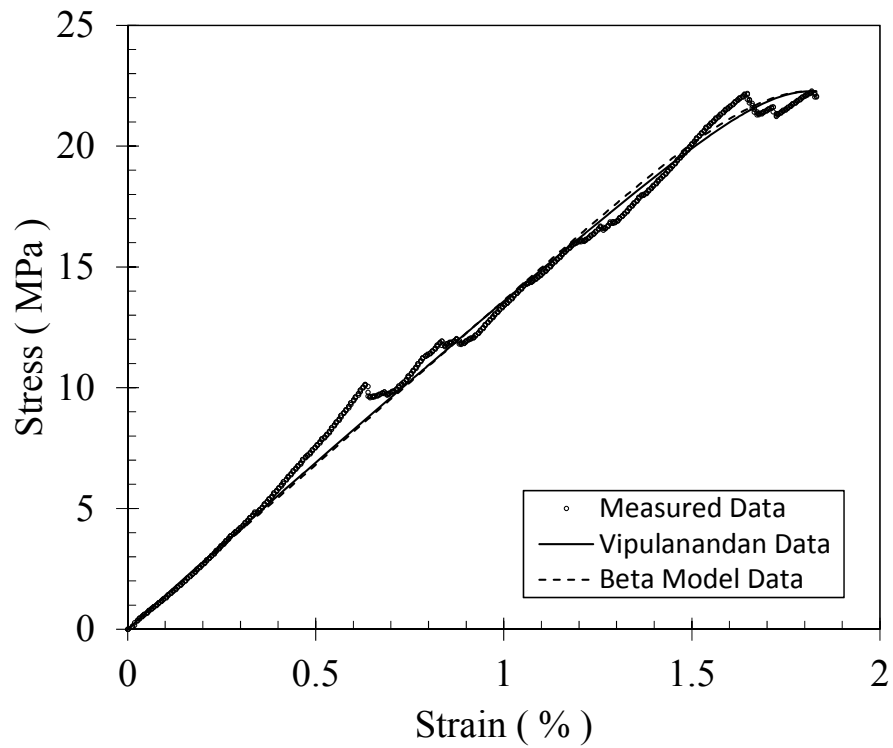


Figure D.26: Stress-Strain Data – Batch 9, Cylinder #26.

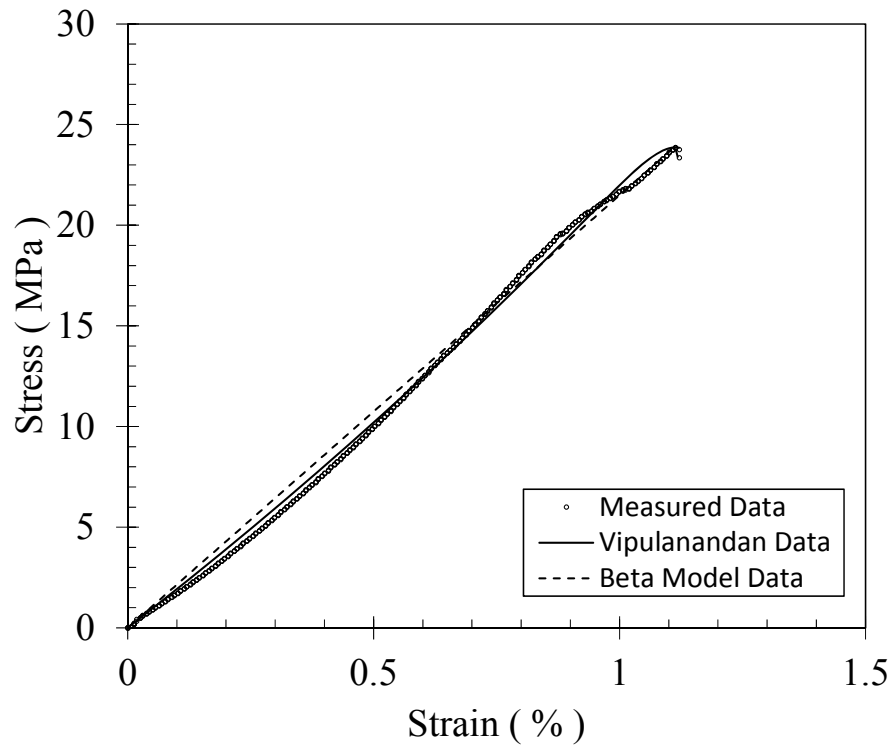


Figure D.27: Stress-Strain Data – Batch 9, Cylinder #27.

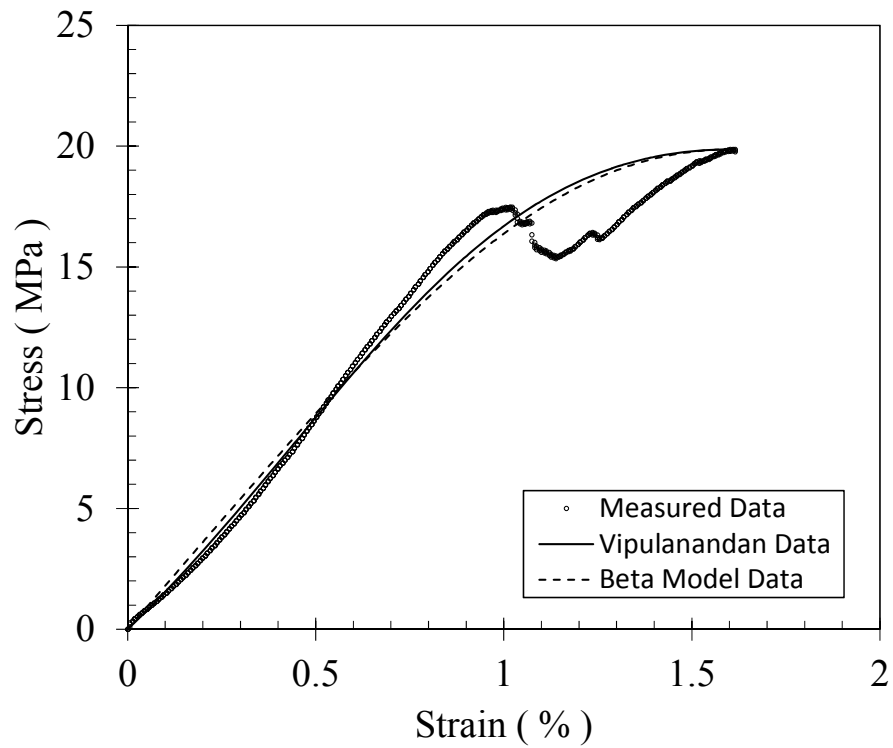


Figure D.28: Stress-Strain Data – Batch 10, Cylinder #28.

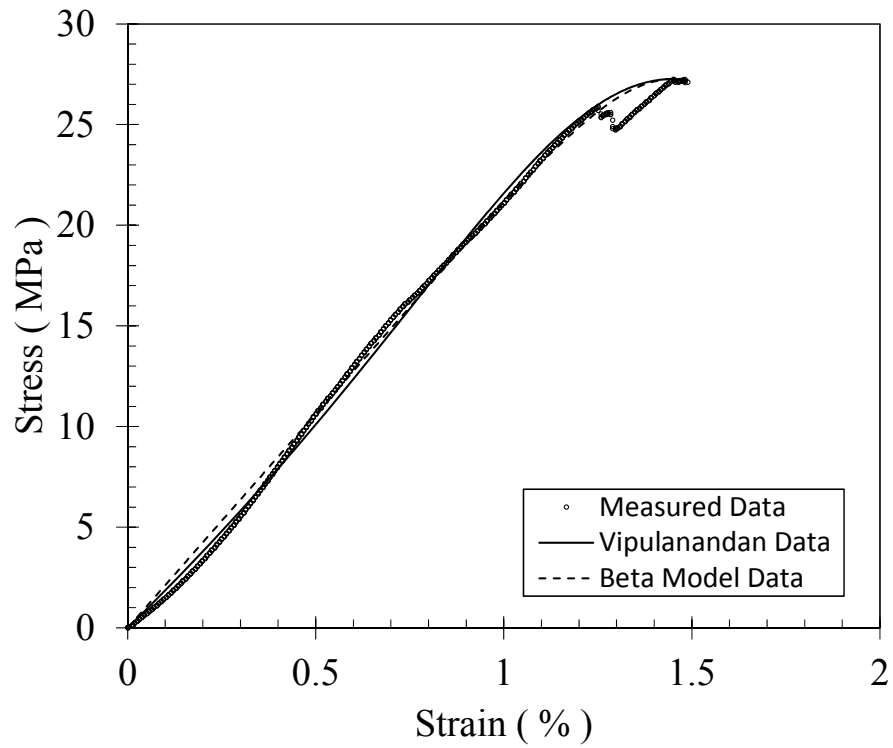


Figure D.29: Stress-Strain Data – Batch 10, Cylinder #29.

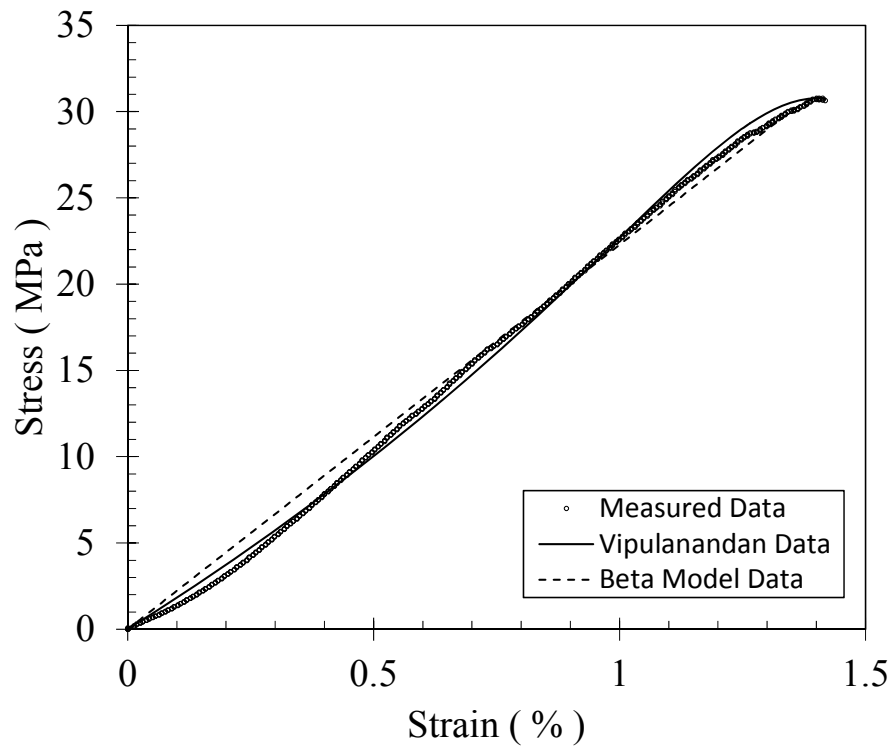


Figure D.30: Stress-Strain Data – Batch 10, Cylinder #30.



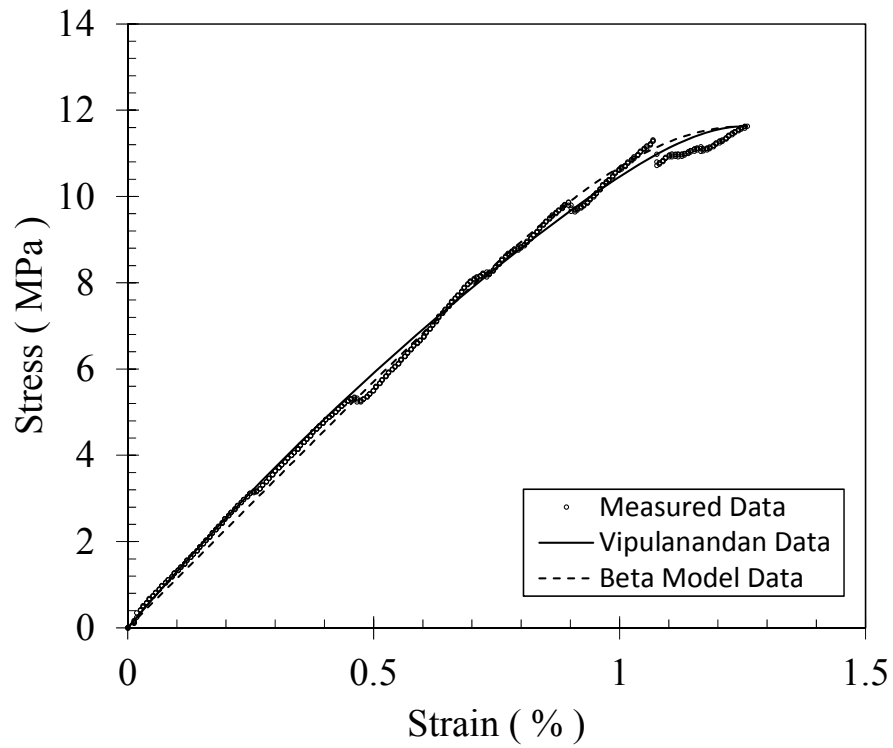


Figure D.31: Stress-Strain Data – Batch 11, Cylinder #31.

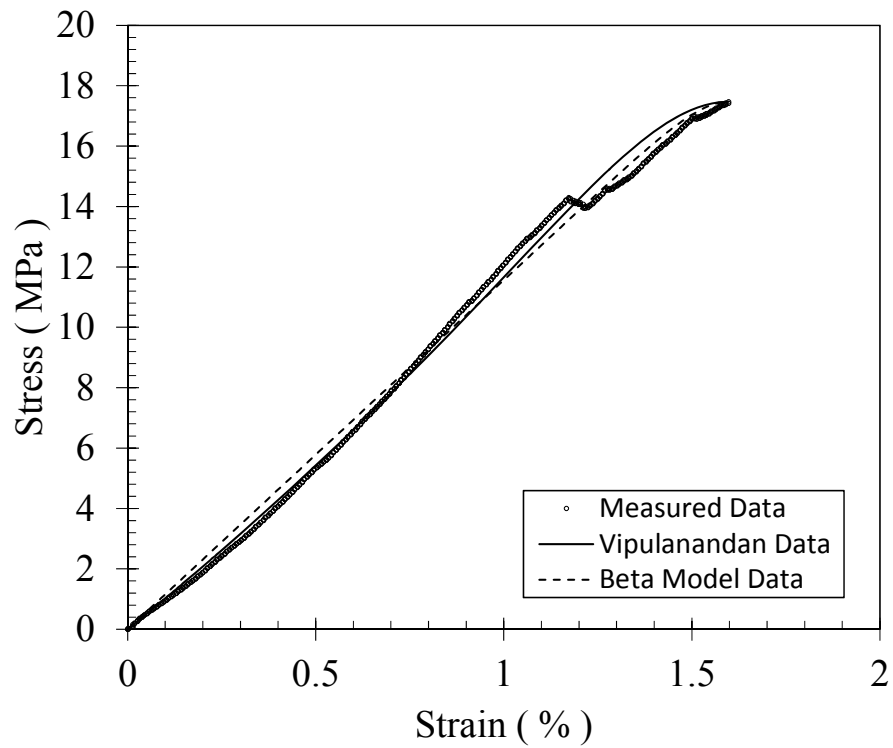


Figure D.32: Stress-Strain Data – Batch 11, Cylinder #32.

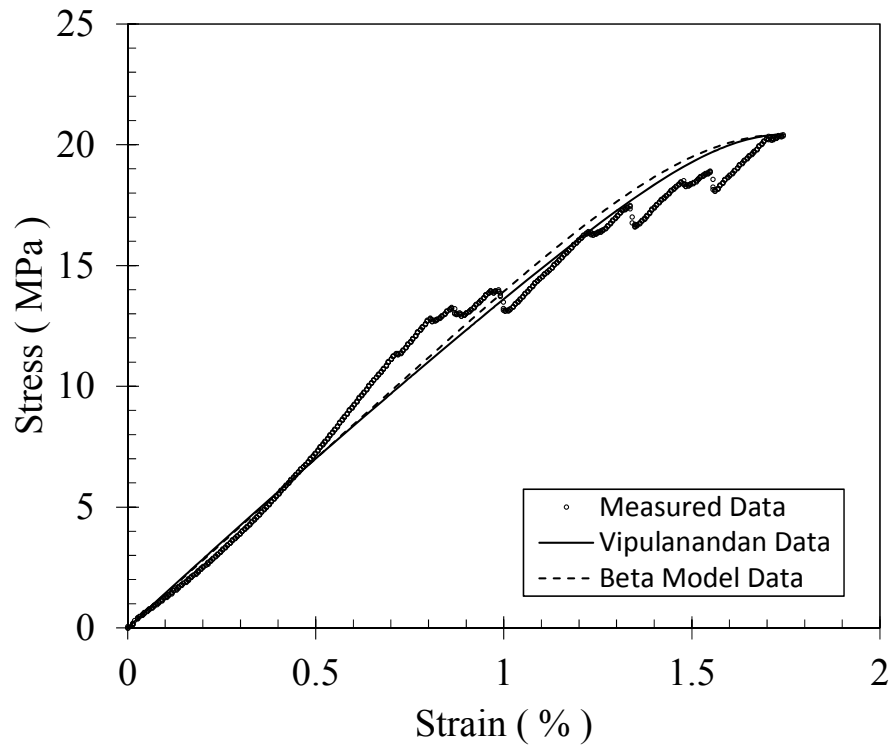


Figure D.33: Stress-Strain Data – Batch 11, Cylinder #33.

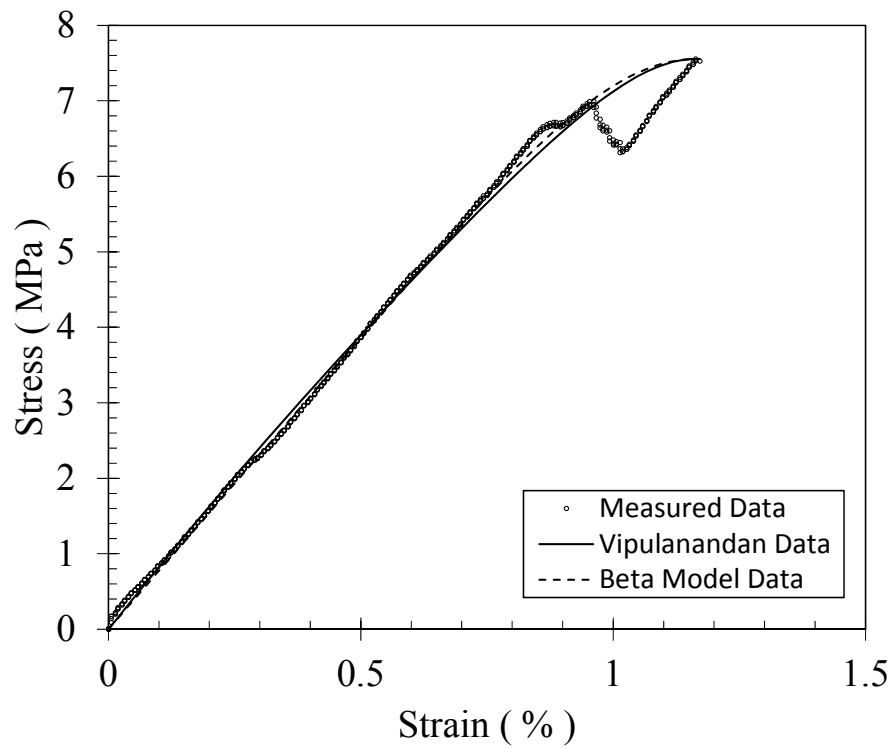


Figure D.34: Stress-Strain Data – Batch 12, Cylinder #34.

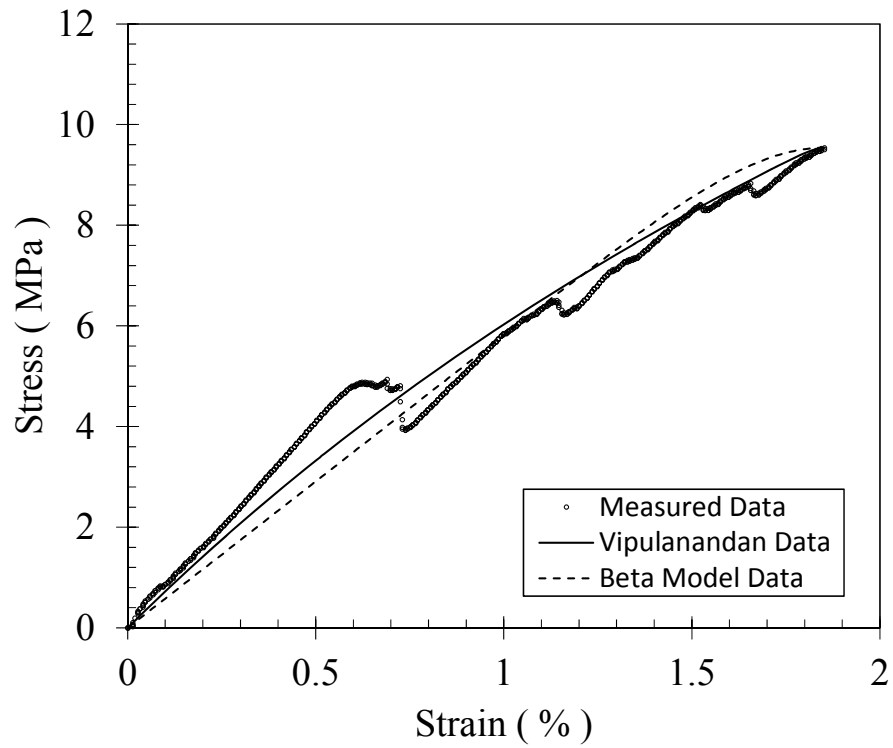


Figure D.35: Stress-Strain Data – Batch 12, Cylinder #35.

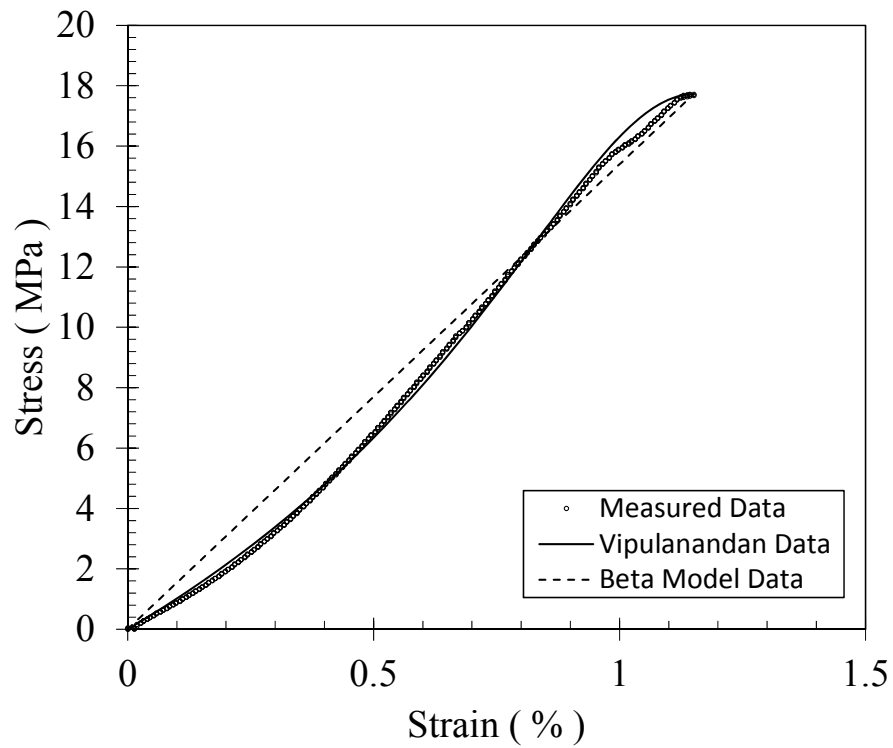


Figure D.36: Stress-Strain Data – Batch 12, Cylinder #36.

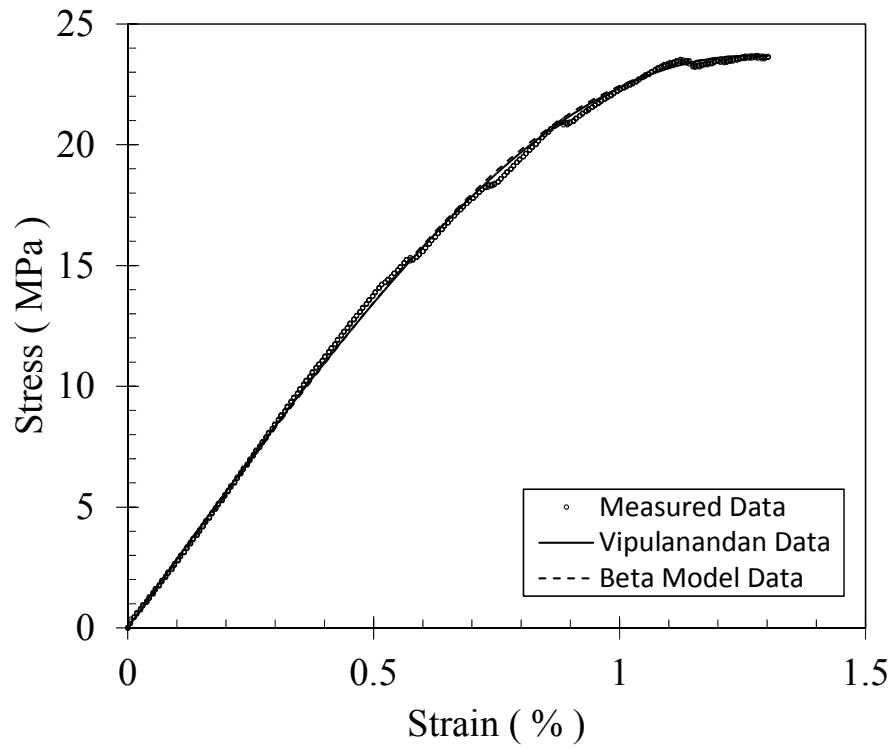


Figure D.37: Stress-Strain Data – Batch 13, Cylinder #37.

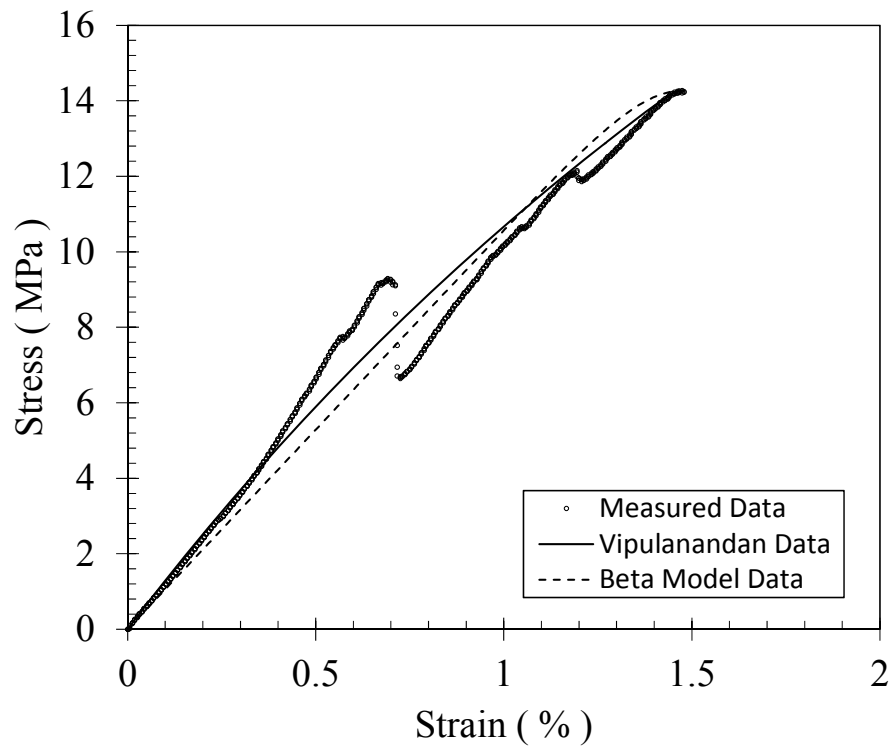


Figure D.38: Stress-Strain Data – Batch 13, Cylinder #38.

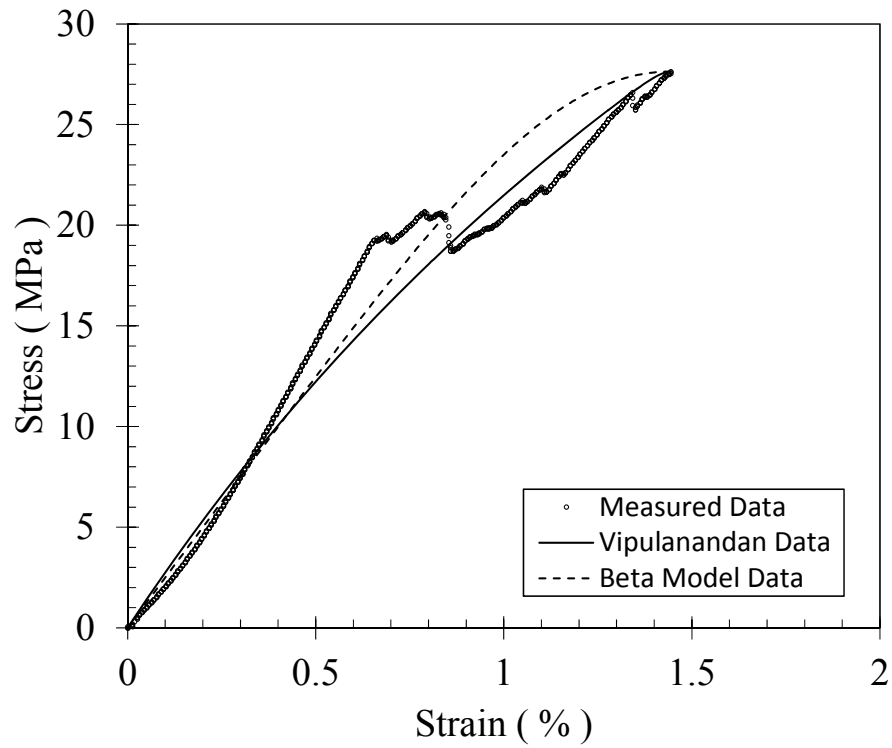


Figure D.39: Stress-Strain Data – Batch 13, Cylinder #39.

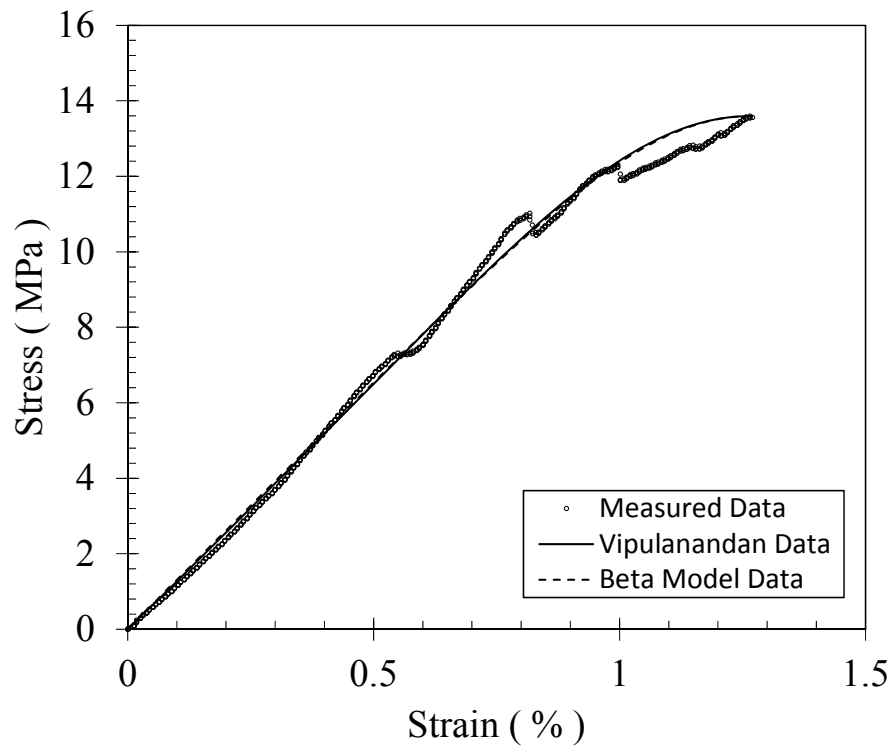


Figure D.40: Stress-Strain Data – Batch 14, Cylinder #40.

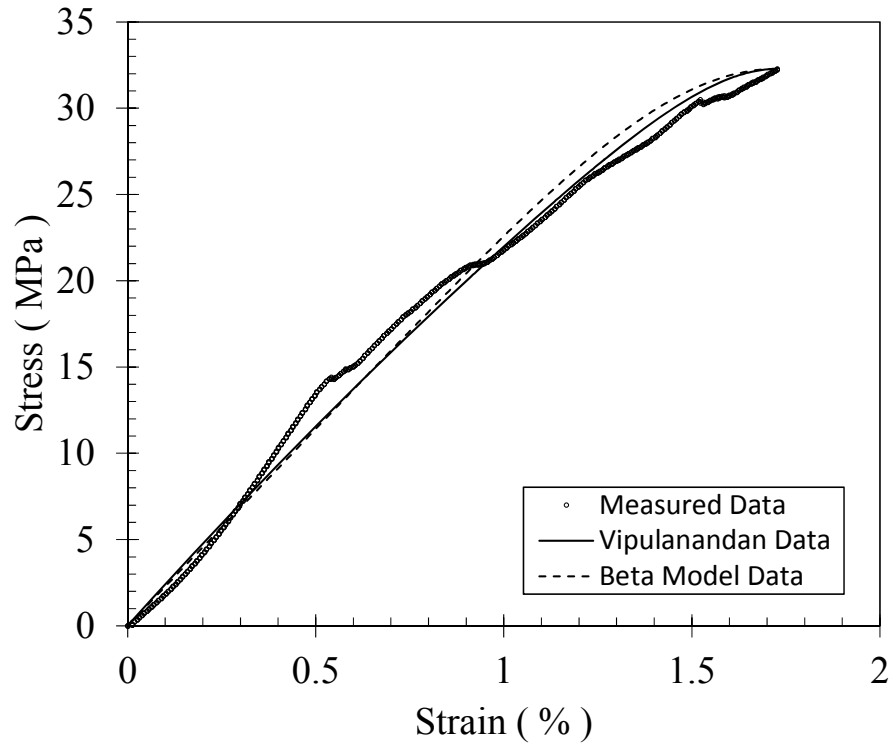


Figure D.41: Stress-Strain Data – Batch 14, Cylinder #41.

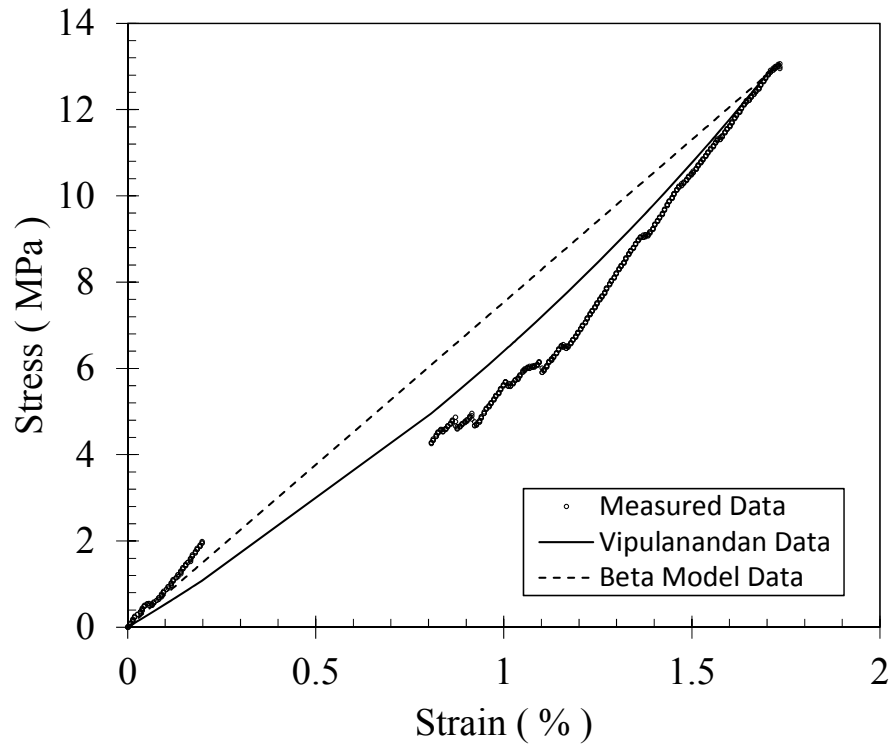


Figure D.42: Stress-Strain Data – Batch 14, Cylinder #42.

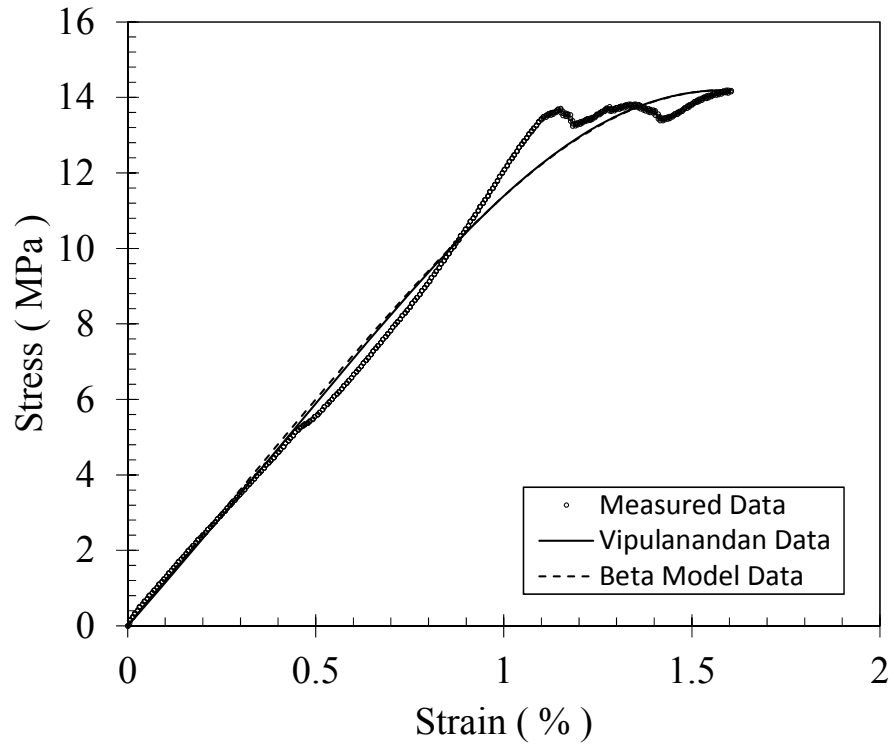


Figure D.43: Stress-Strain Data – Batch 15, Cylinder #43.

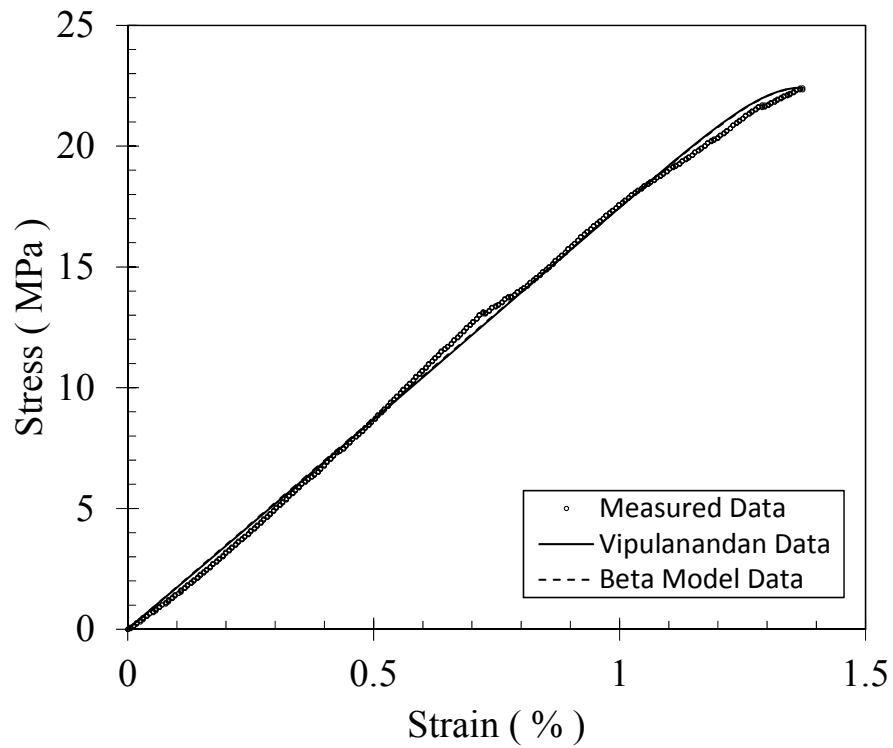


Figure D.44: Stress-Strain Data – Batch 15, Cylinder #44.

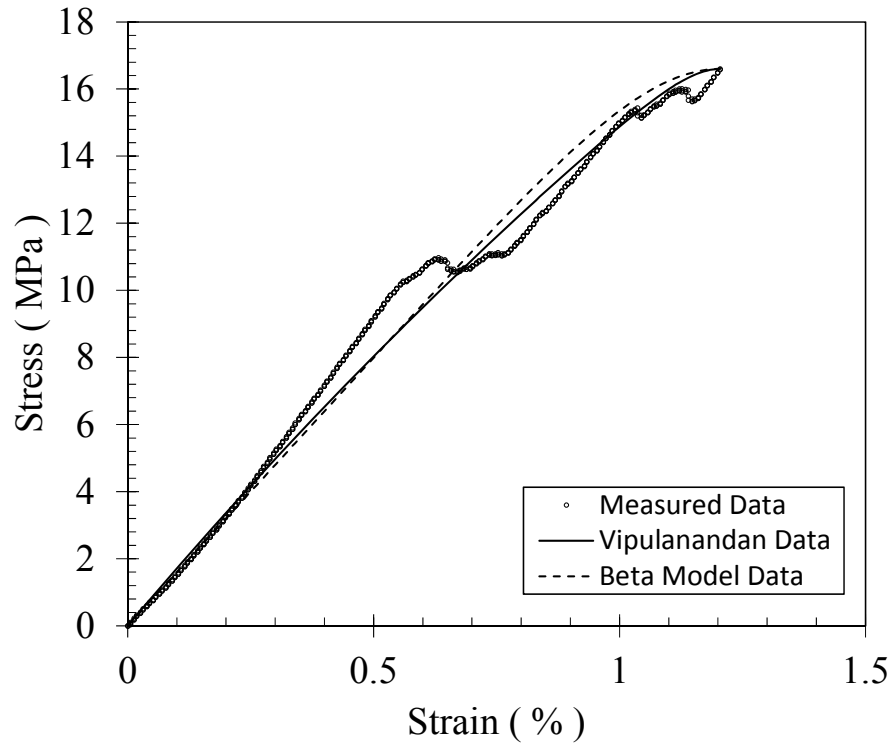


Figure D.45: Stress-Strain Data – Batch 15, Cylinder #45.

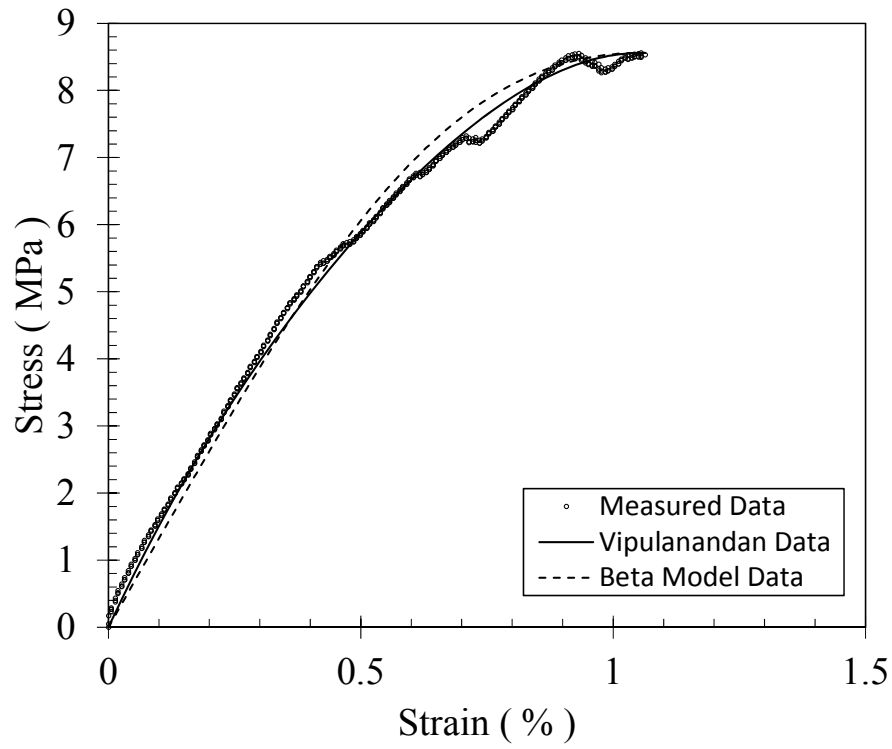


Figure D.46: Stress-Strain Data – Batch 16, Cylinder #46.



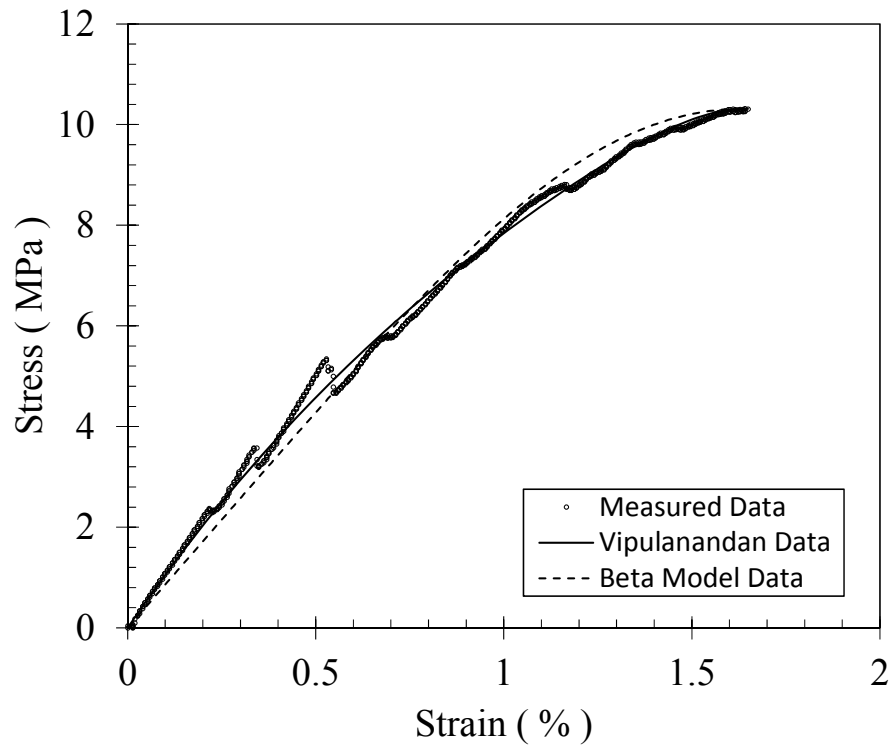


Figure D.47: Stress-Strain Data – Batch 16, Cylinder #47.

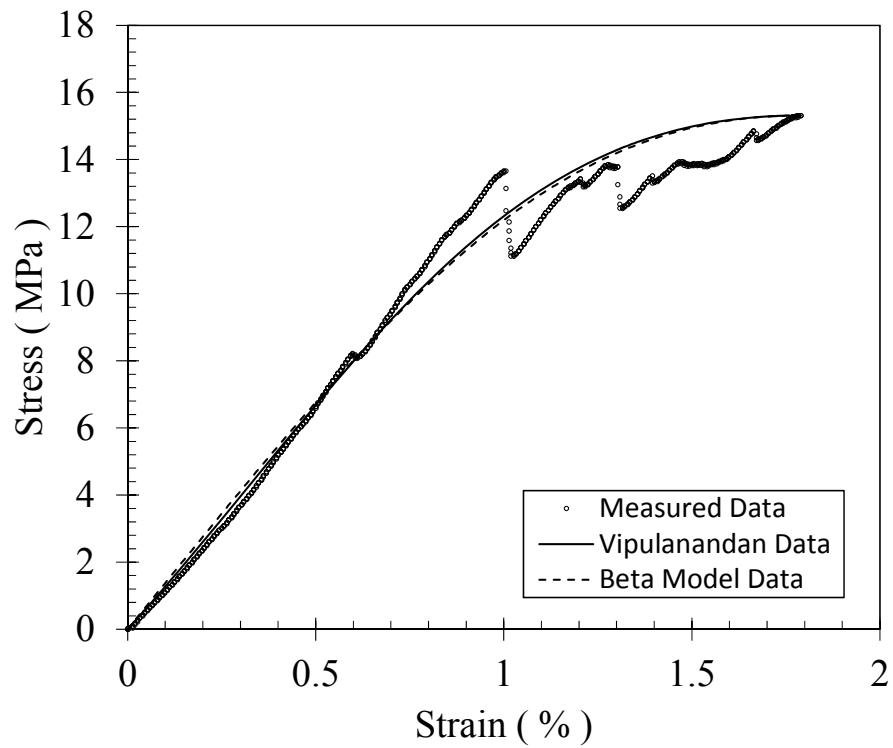


Figure D.48: Stress-Strain Data – Batch 16, Cylinder #48.

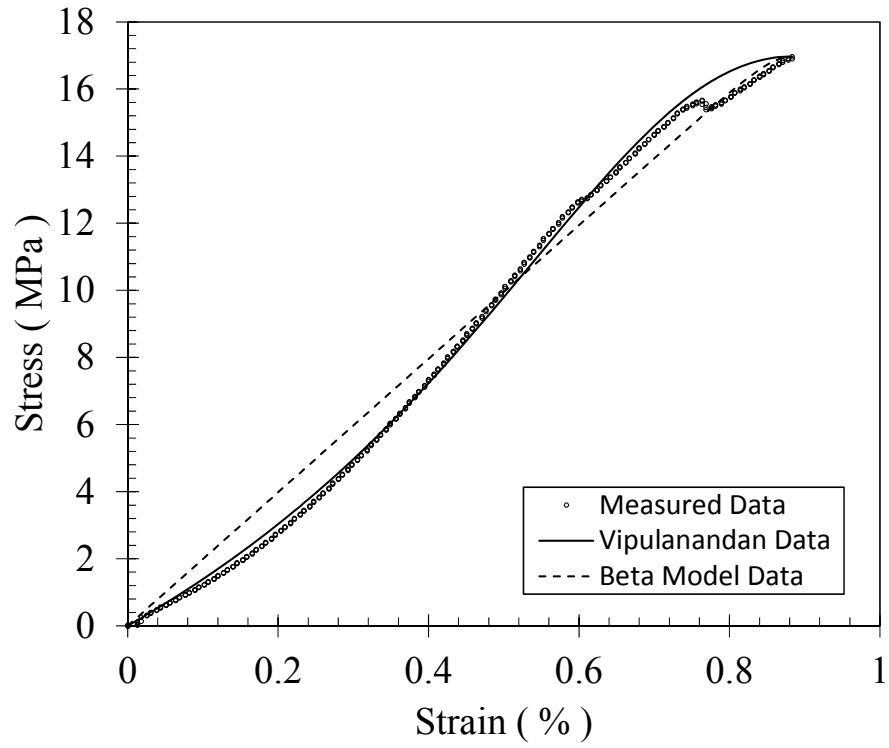


Figure D.49: Stress-Strain Data – Batch 17, Cylinder #49.

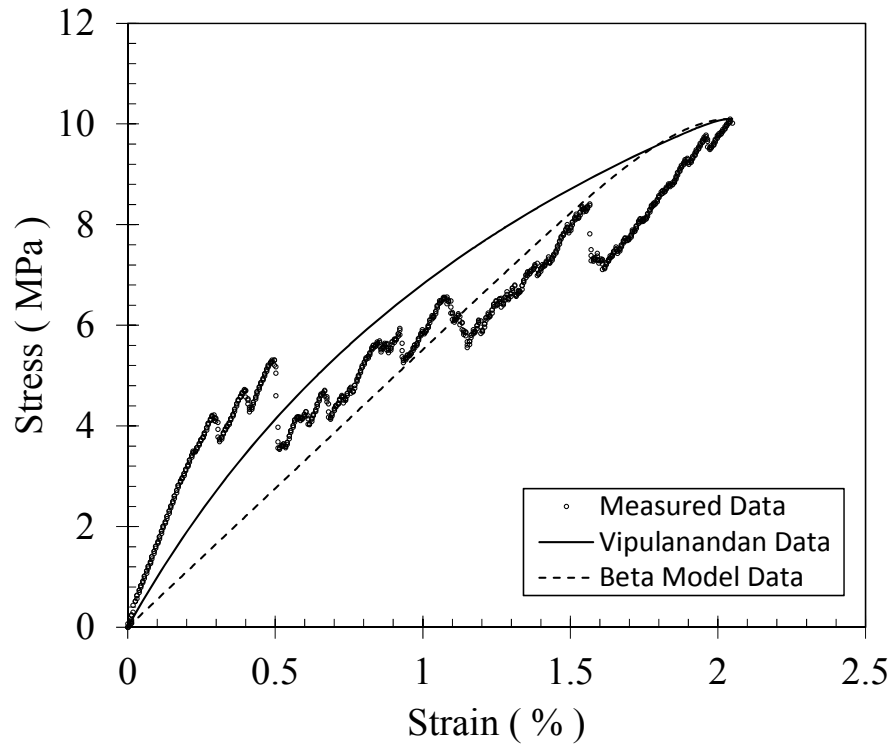


Figure D.50: Stress-Strain Data – Batch 17, Cylinder #50.

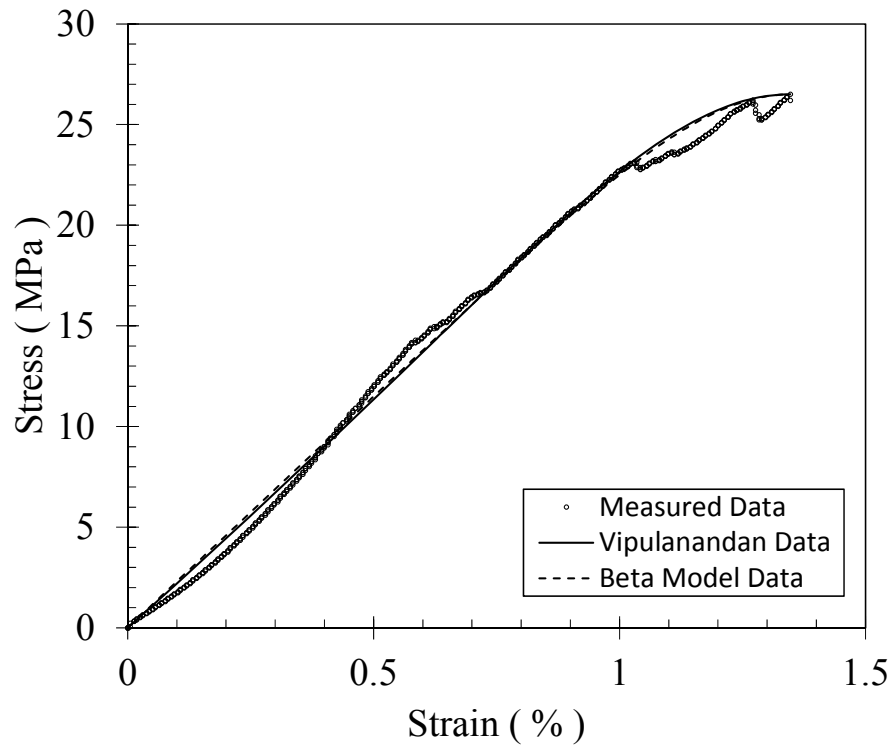


Figure D.51: Stress-Strain Data – Batch 17, Cylinder #51.

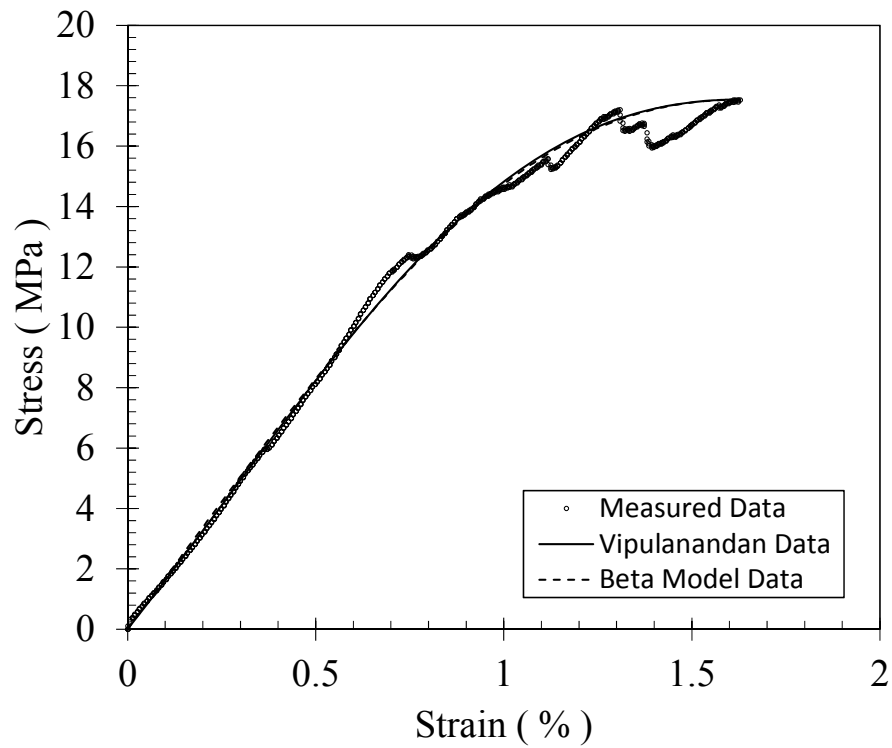


Figure D.52: Stress-Strain Data – Batch 18, Cylinder #52.

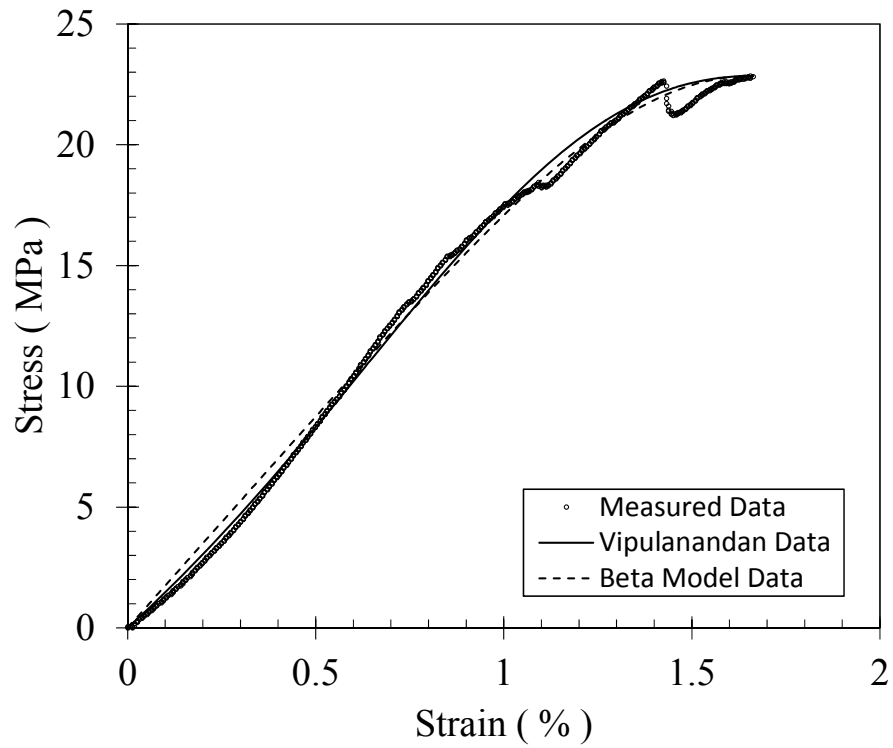


Figure D.53: Stress-Strain Data – Batch 18, Cylinder #53.

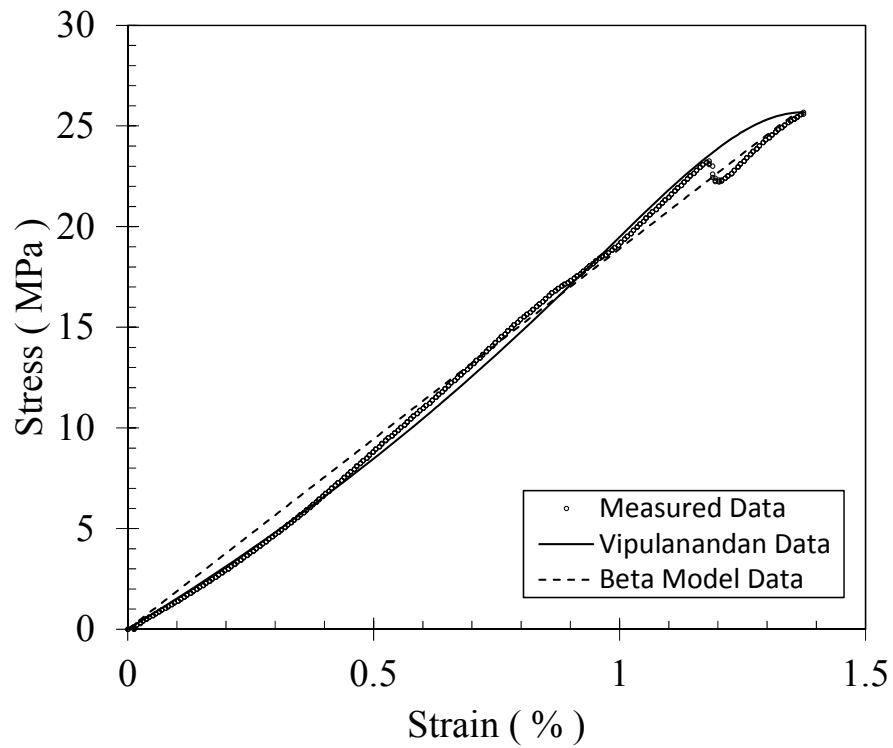


Figure D.54: Stress-Strain Data – Batch 18, Cylinder #54.

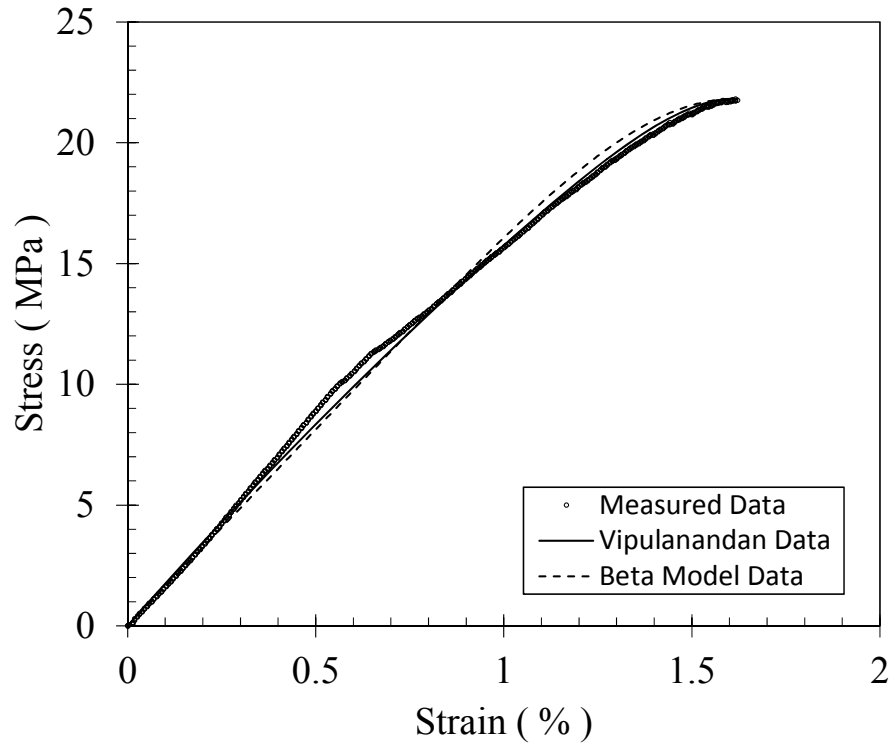


Figure D.55: Stress-Strain Data – Batch 19, Cylinder #55.

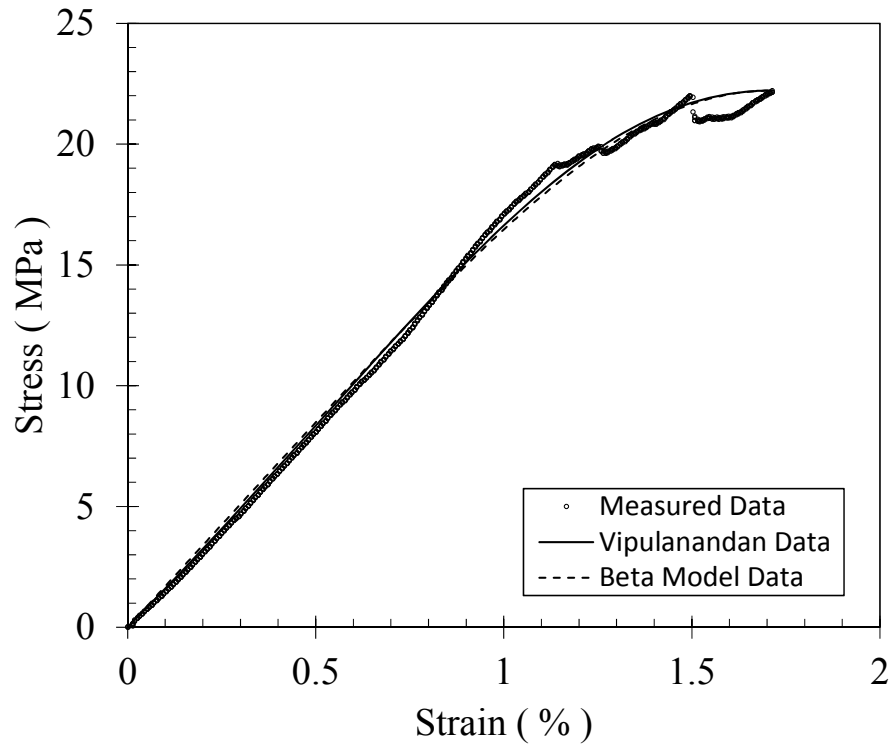


Figure D.56: Stress-Strain Data – Batch 19, Cylinder #56.

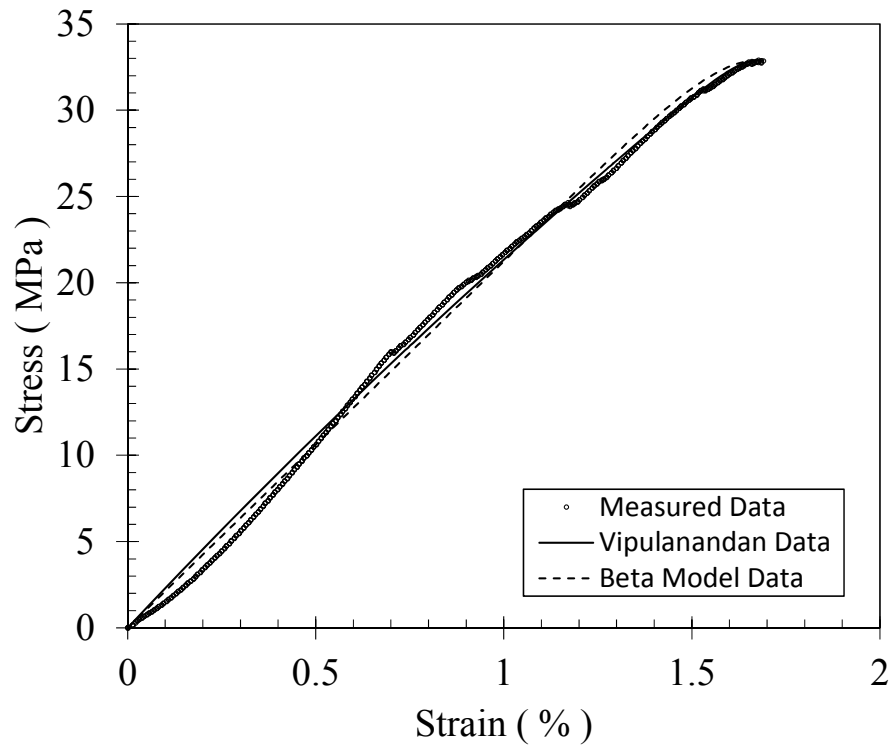


Figure D.57: Stress-Strain Data – Batch 19, Cylinder #57.

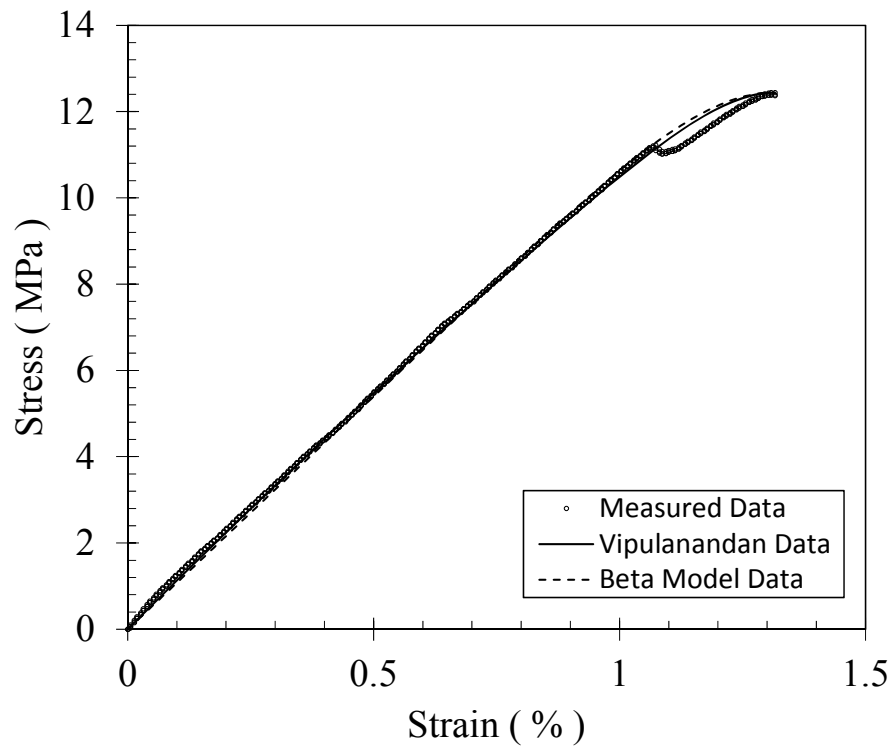


Figure D.58: Stress-Strain Data – Batch 20, Cylinder #58.

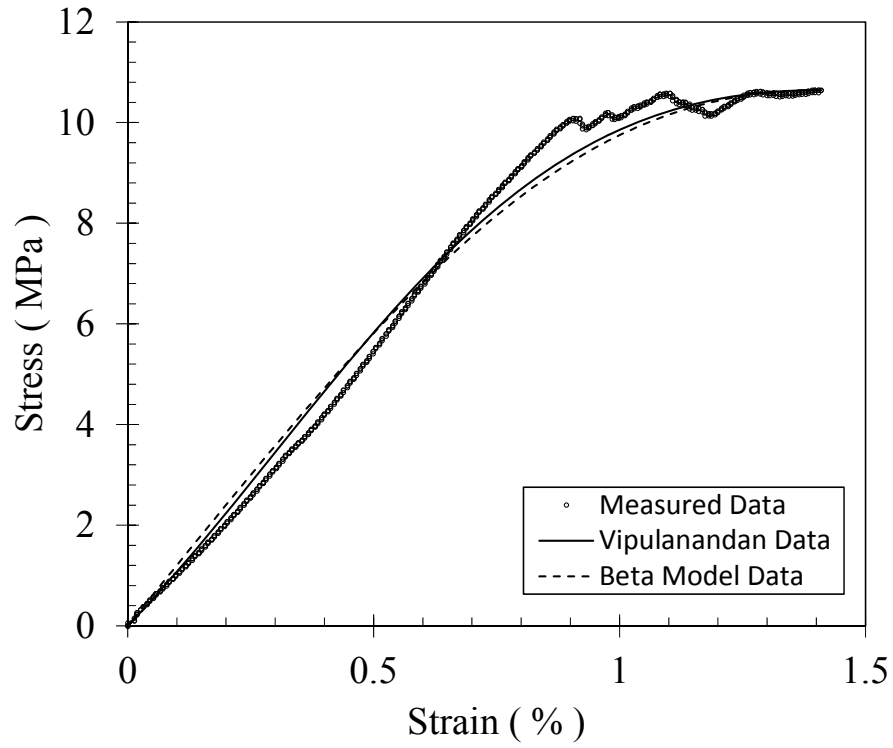


Figure D.59: Stress-Strain Data – Batch 20, Cylinder #59.

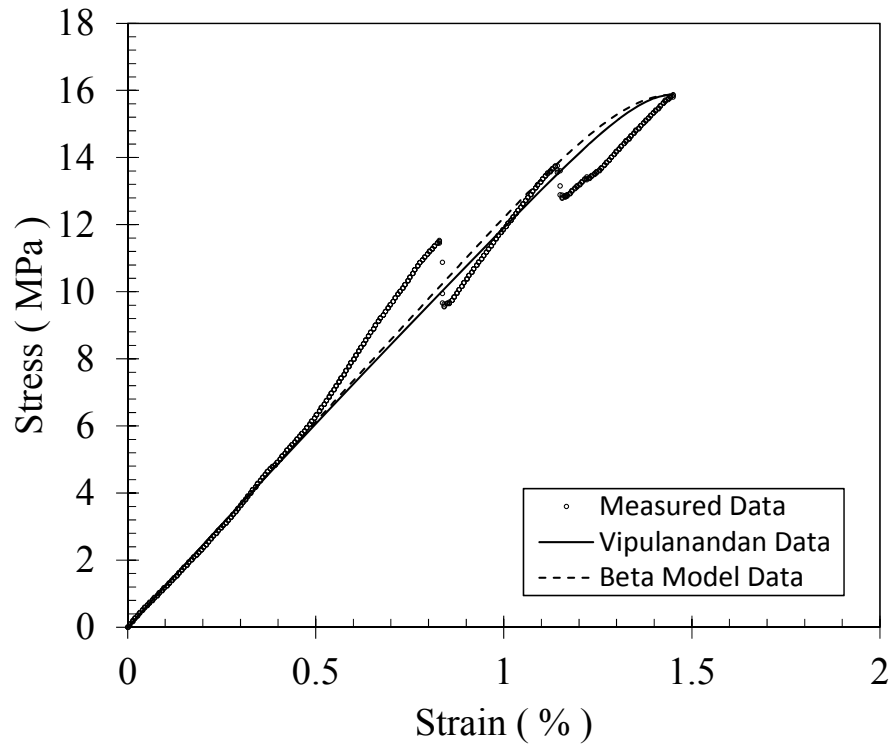
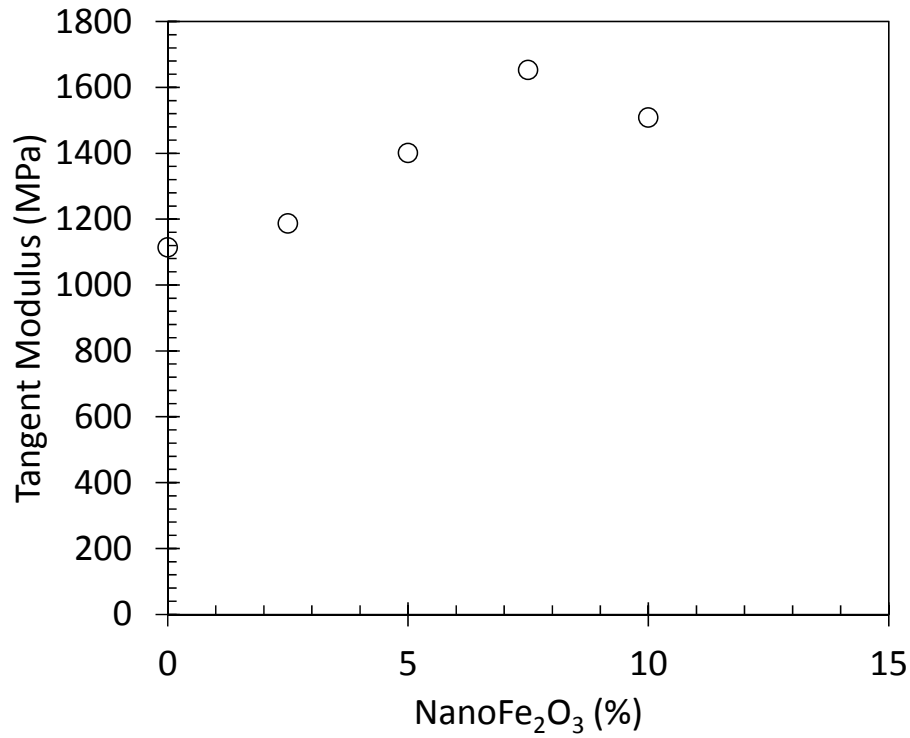
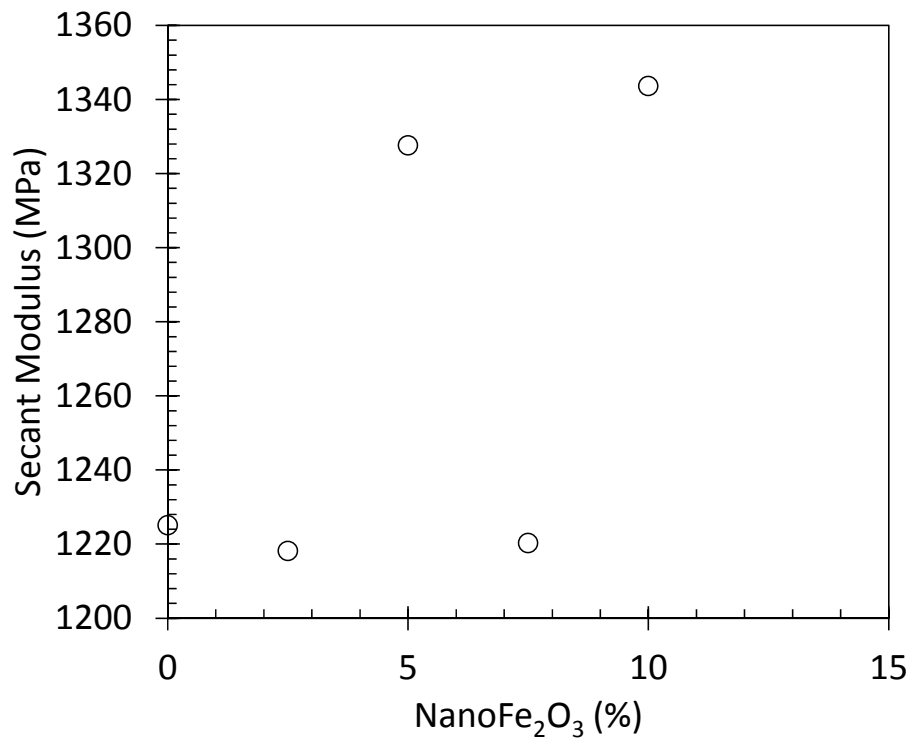


Figure D.60: Stress-Strain Data – Batch 20, Cylinder #60.

Averages of Stress-Strain Parameters Sorted by NanoFe<sub>2</sub>O<sub>3</sub> Content:



**Figure D.61: Tangent Modulus vs. NanoFe<sub>2</sub>O<sub>3</sub> Content.**



**Figure D.62: Secant Modulus vs. NanoFe<sub>2</sub>O<sub>3</sub> Content.**



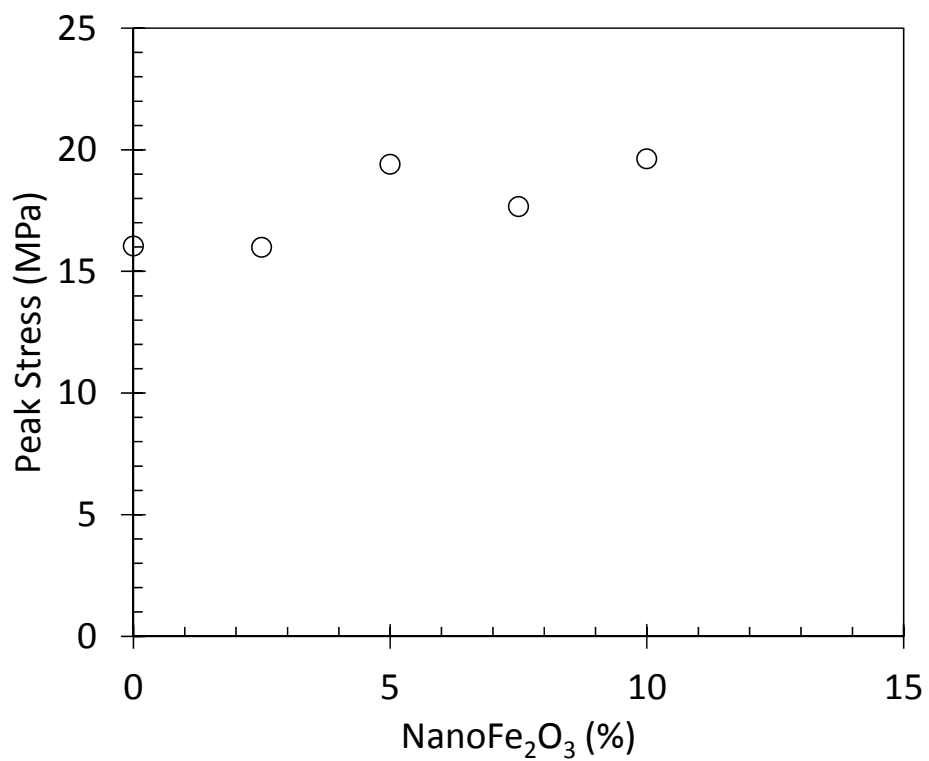


**Figure D.63: Peak Stress vs. NanoFe<sub>2</sub>O<sub>3</sub> Content.**

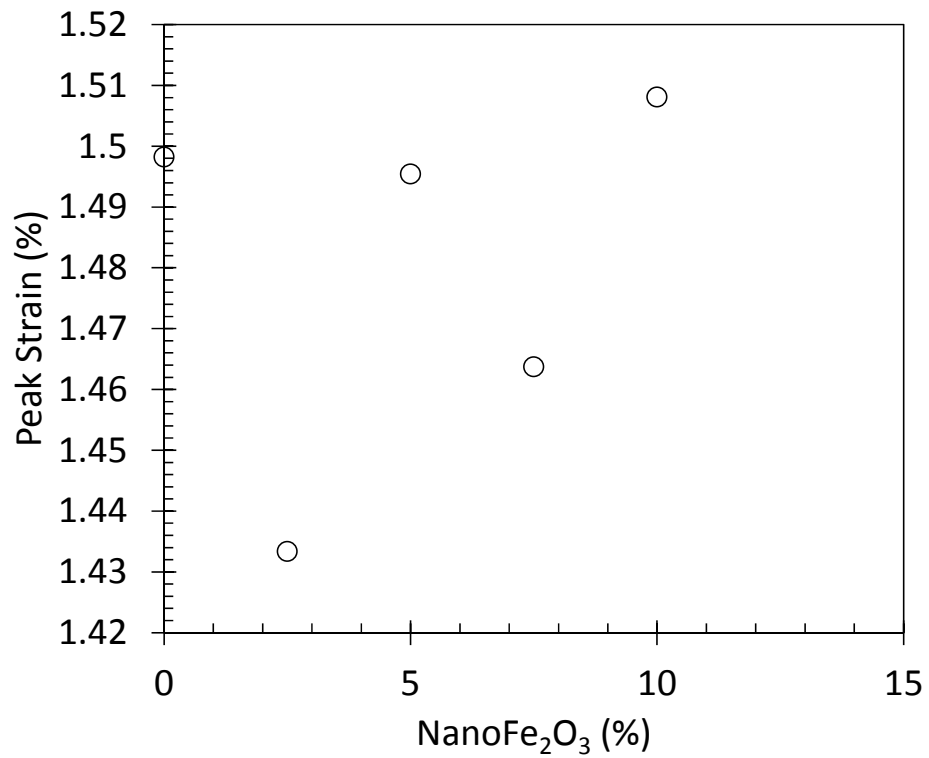


**Figure D.64: Peak Strain vs. NanoFe<sub>2</sub>O<sub>3</sub> Content.**

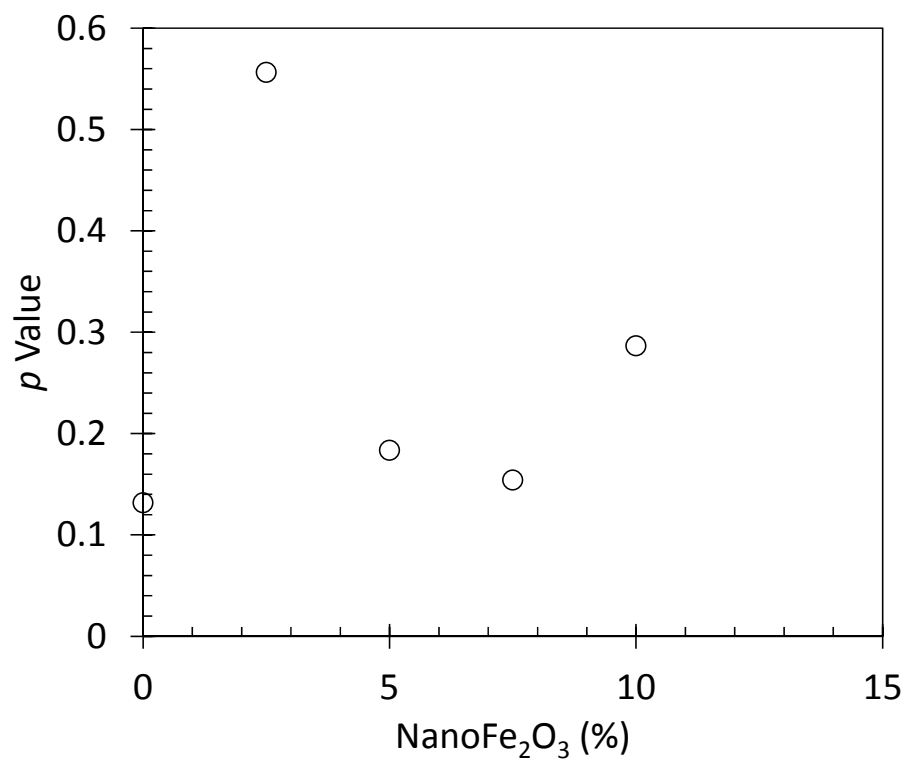


Figure D.65: *p* Value vs. NanoFe<sub>2</sub>O<sub>3</sub> Content.

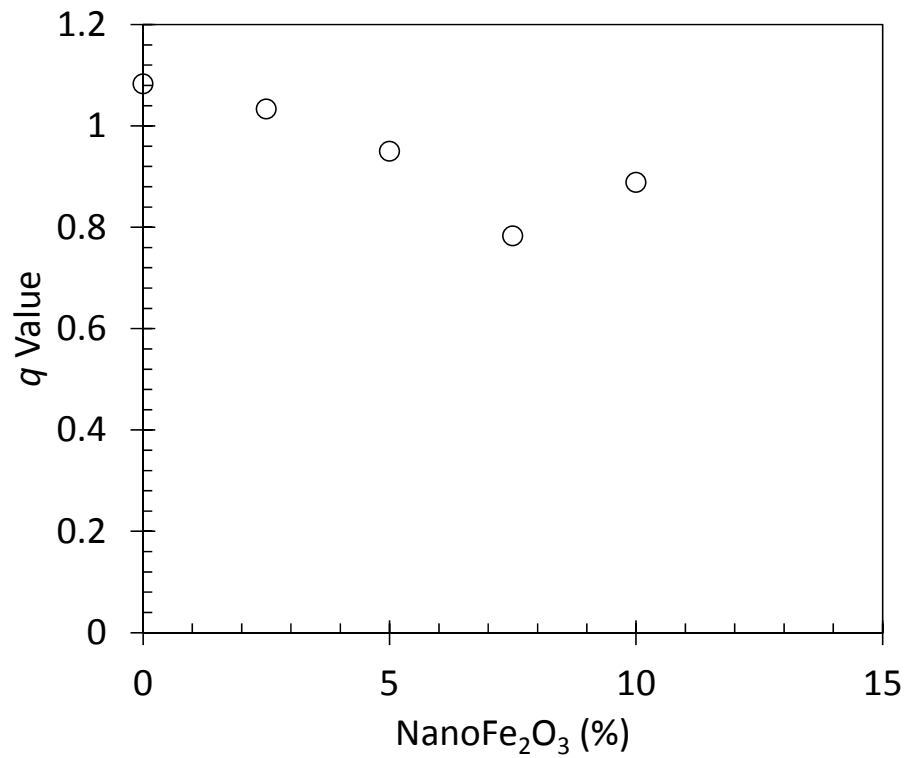
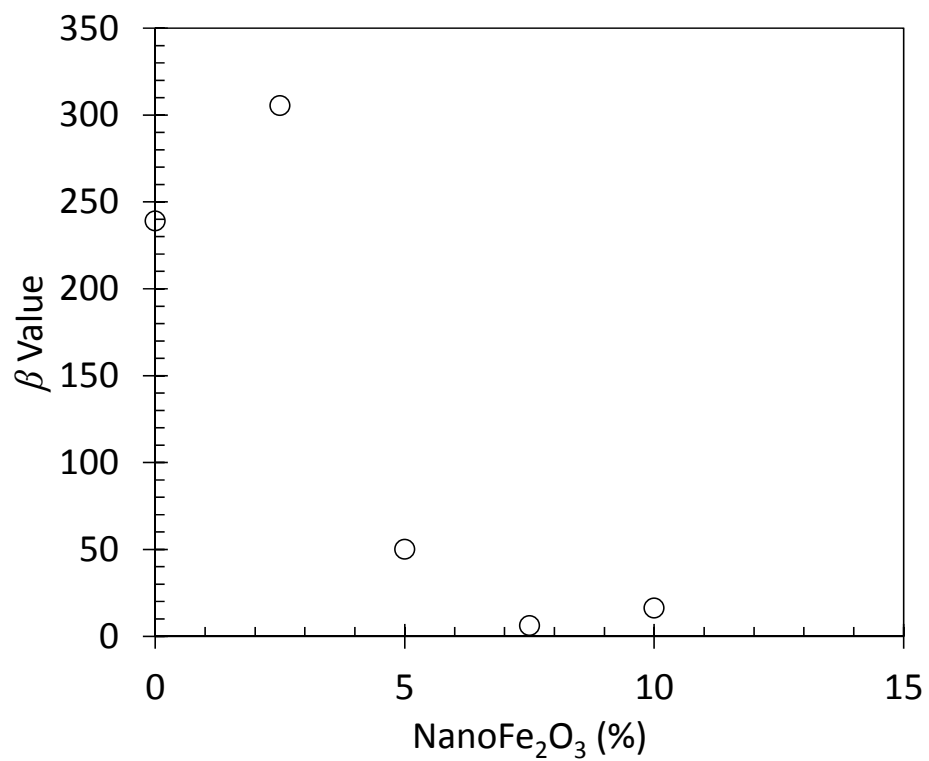
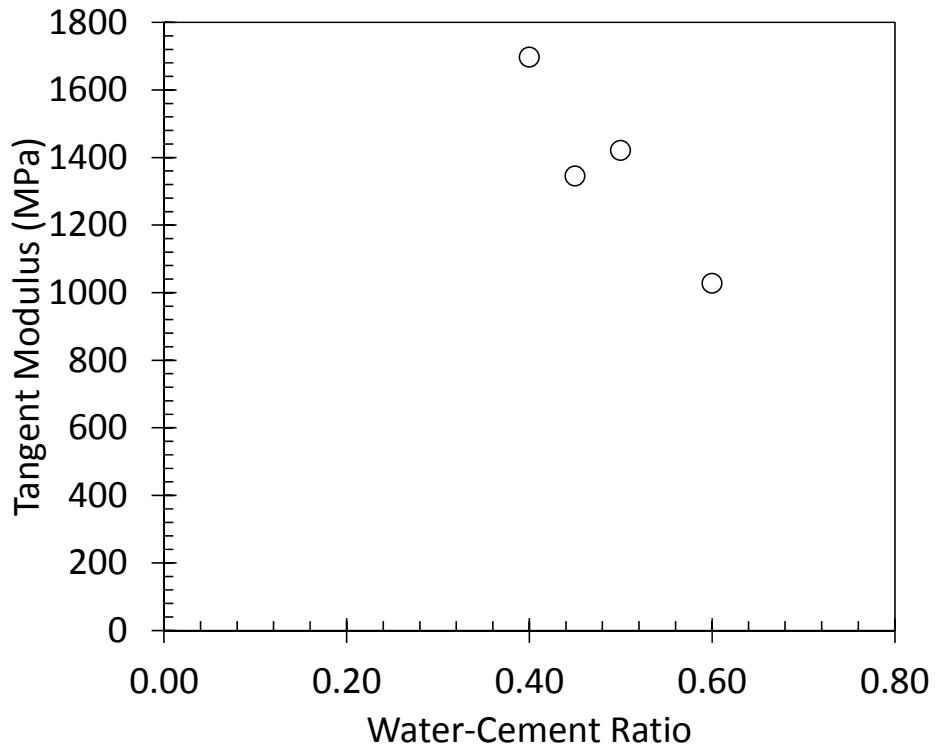


Figure D.66: *q* Value Modulus vs. NanoFe<sub>2</sub>O<sub>3</sub> Content.



**Figure D.67:  $\beta$  Value Modulus vs. NanoFe<sub>2</sub>O<sub>3</sub> Content.**

Averages of Stress-Strain Parameters Sorted by Water-Cement Ratio:



**Figure D.68: Tangent Modulus vs. Water-Cement Ratio.**

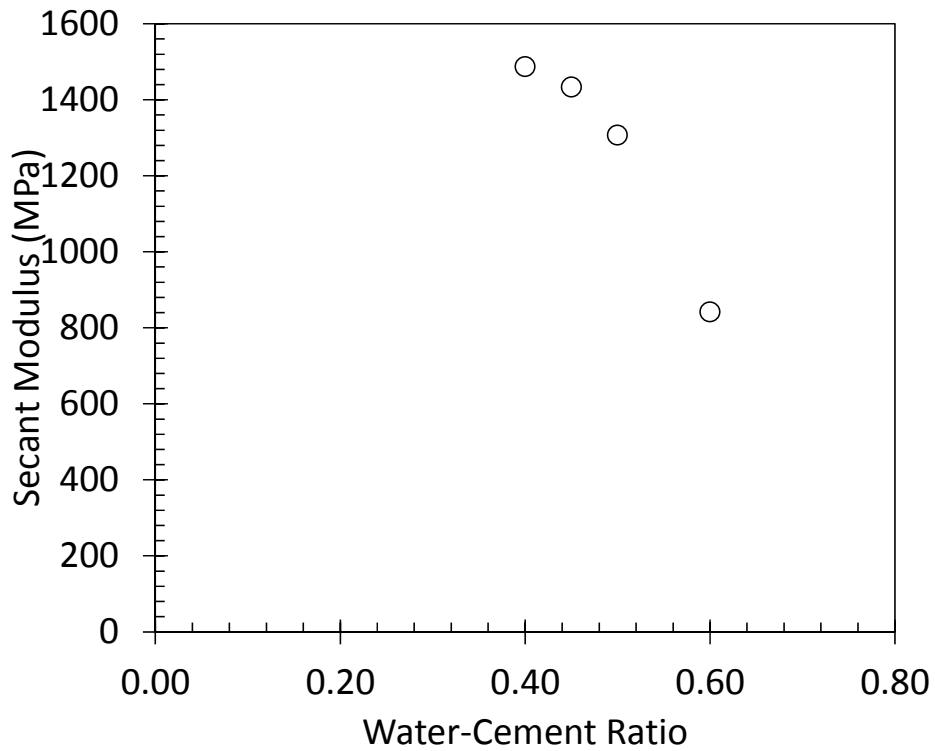


**Figure D.69: Secant Modulus vs. Water-Cement Ratio.**

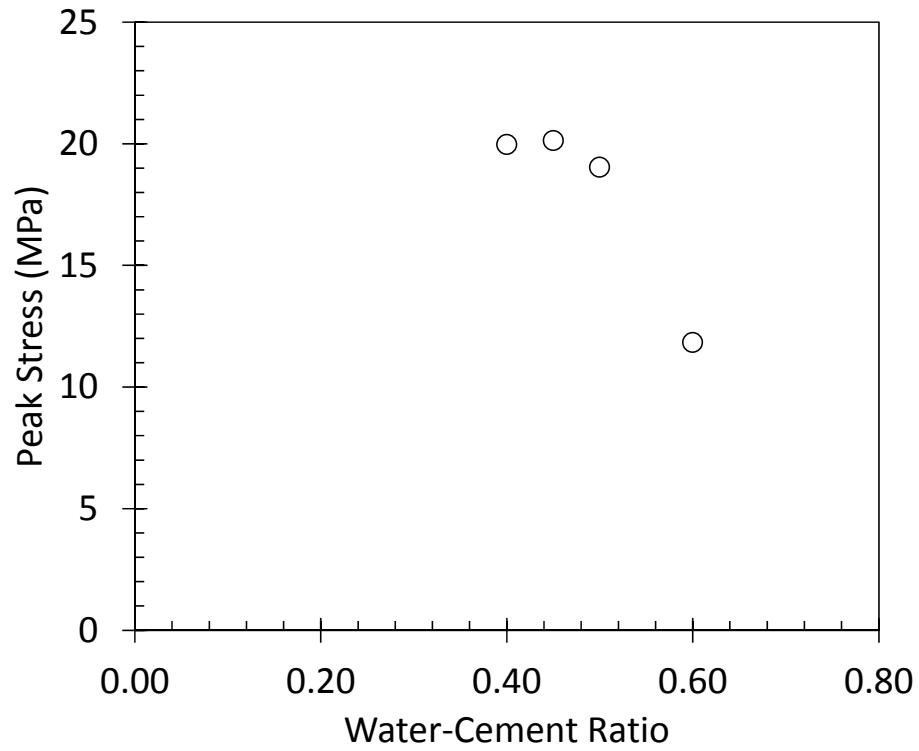


Figure D.70: Peak Stress vs. Water-Cement Ratio.

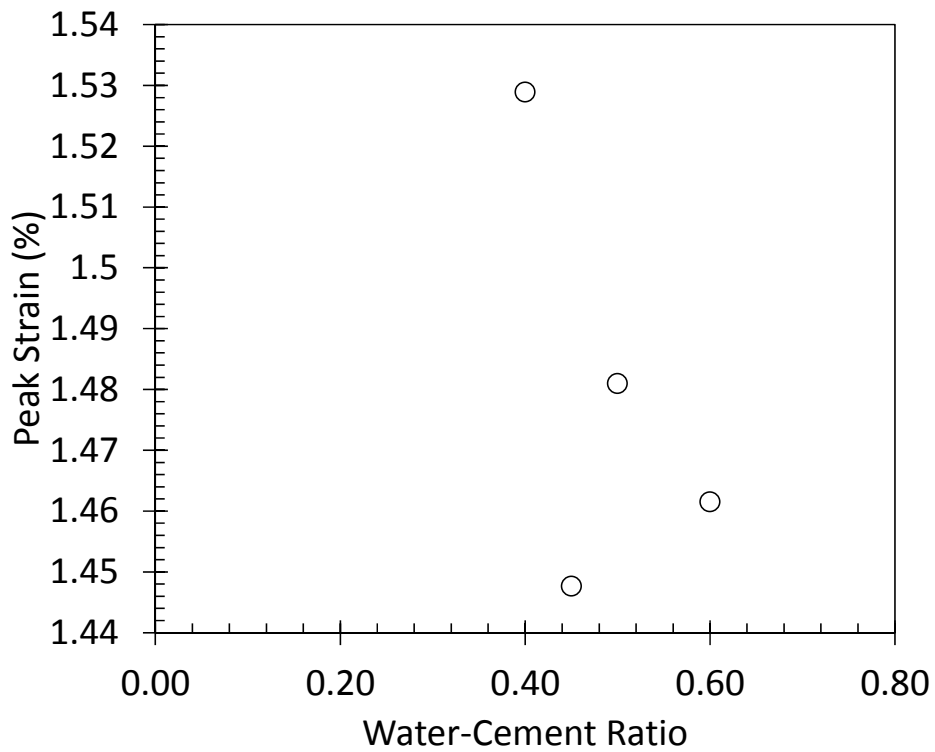


Figure D.71: Peak Strain vs. Water-Cement Ratio.

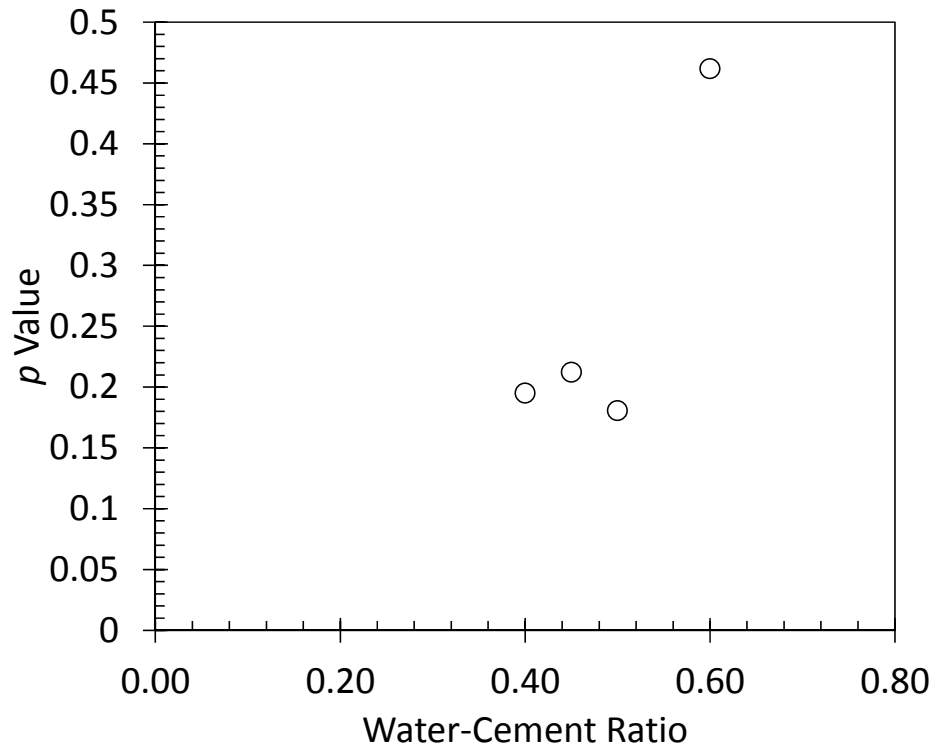


Figure D.72:  $p$  Value vs. Water-Cement Ratio.

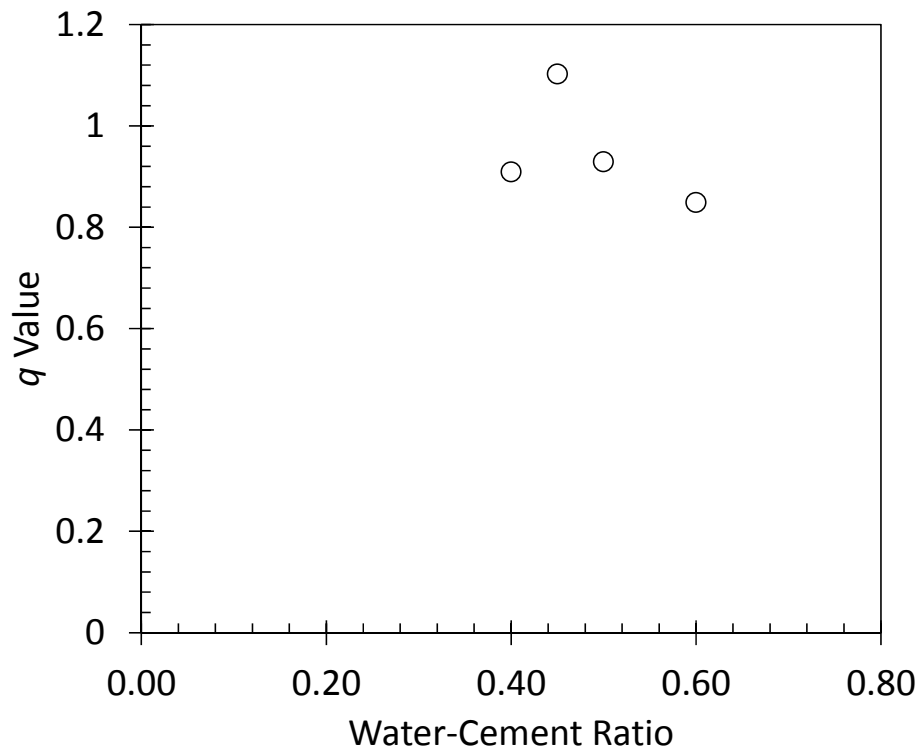
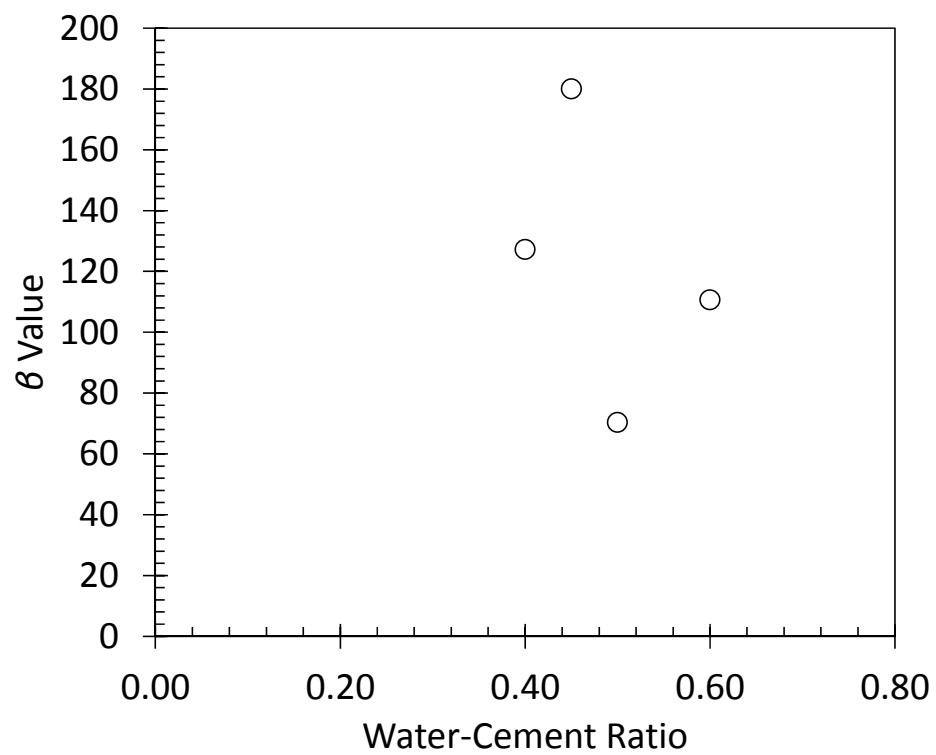
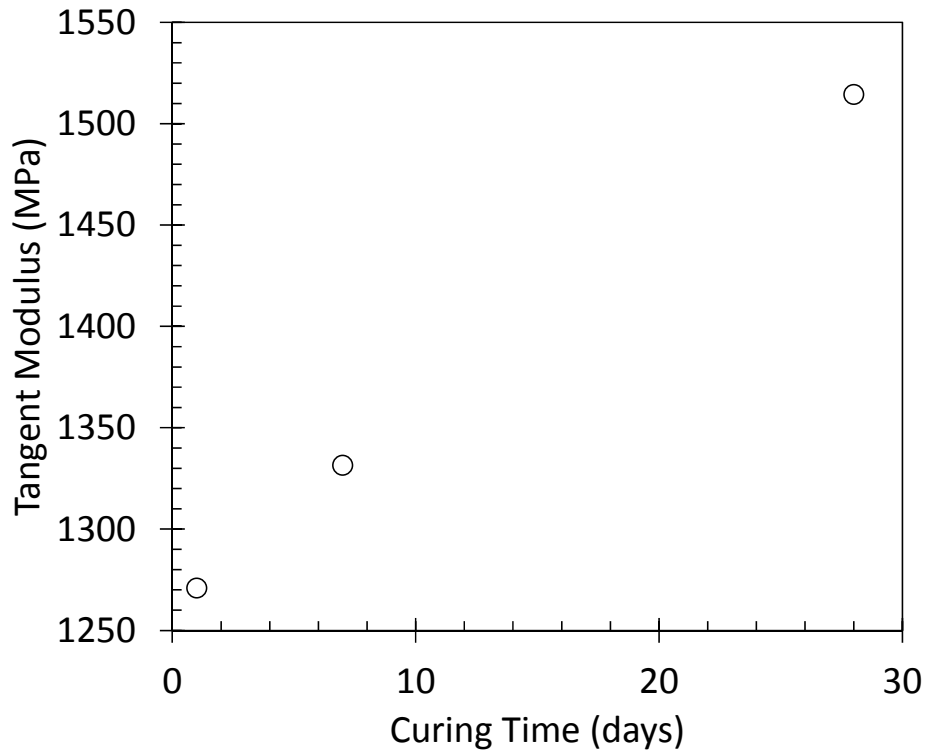


Figure D.73:  $q$  Value vs. Water-Cement Ratio.



**Figure D.74:  $\beta$  Value vs. Water-Cement Ratio.**

Averages of Stress-Strain Parameters Sorted by Curing Time:



**Figure D.75: Tangent Modulus vs. Curing Time.**

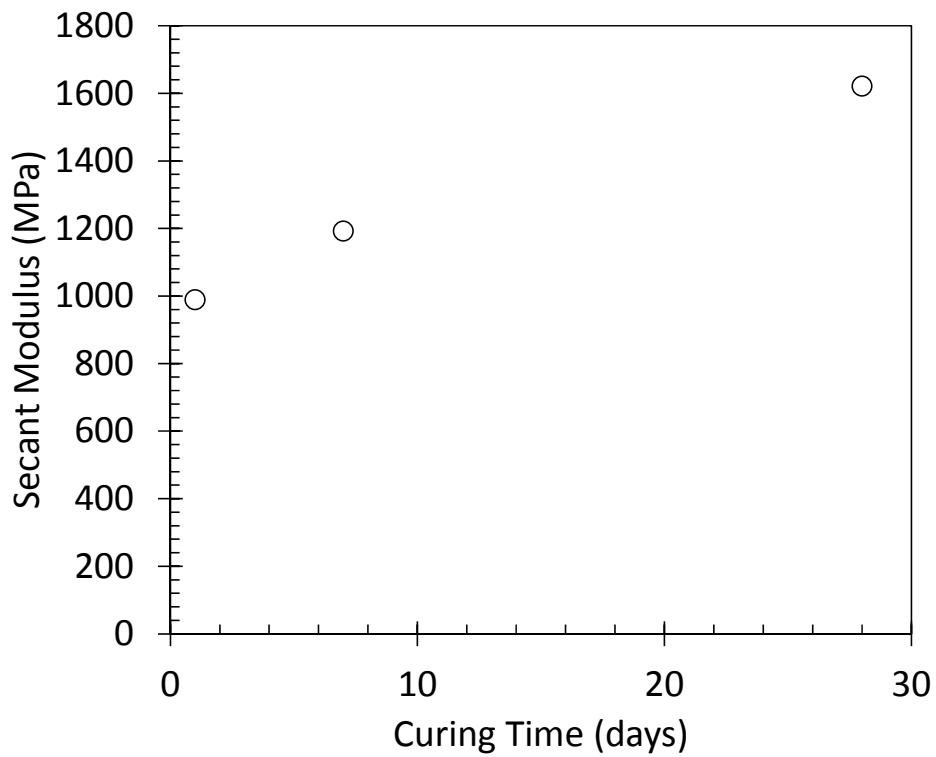


**Figure D.76: Secant Modulus vs. Curing Time.**



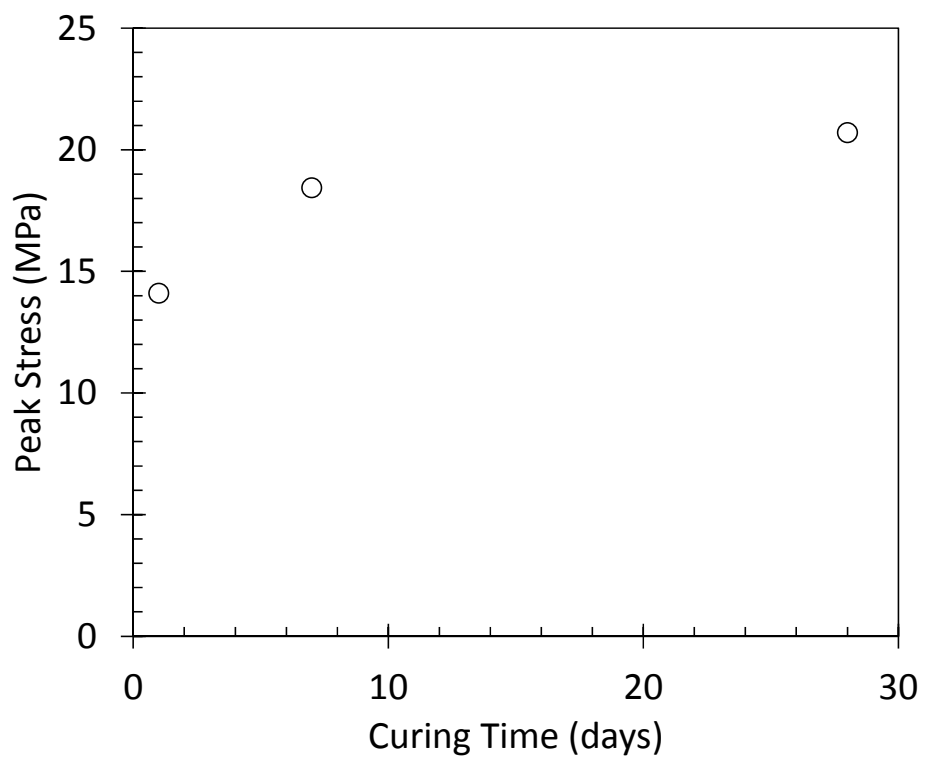


**Figure D.77: Peak Stress vs. Curing Time.**

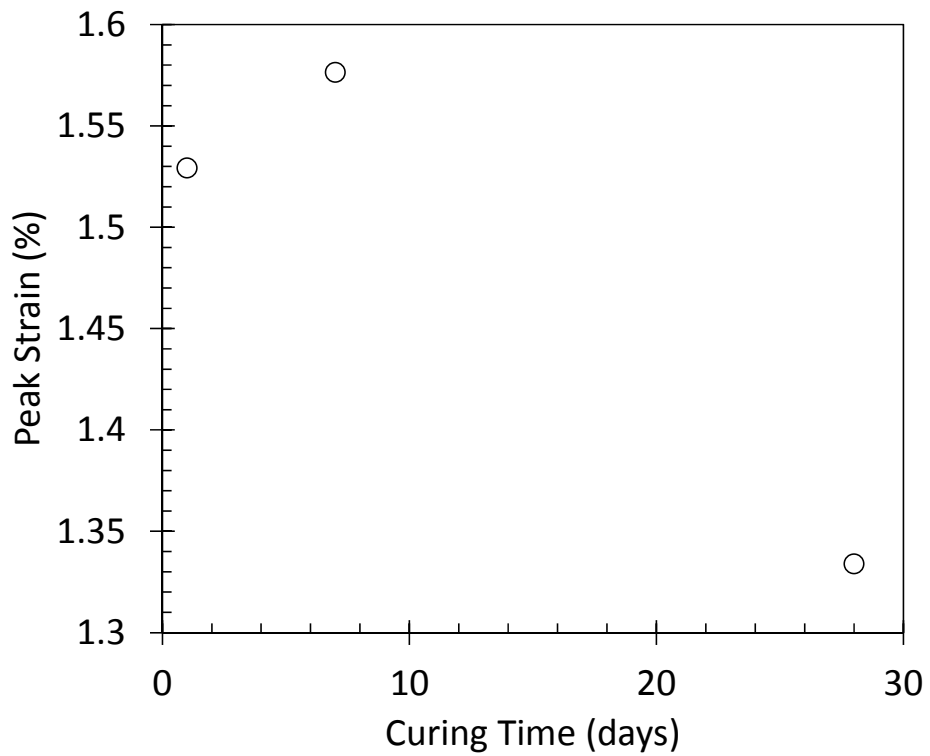


**Figure D.78: Peak Strain vs. Curing Time.**

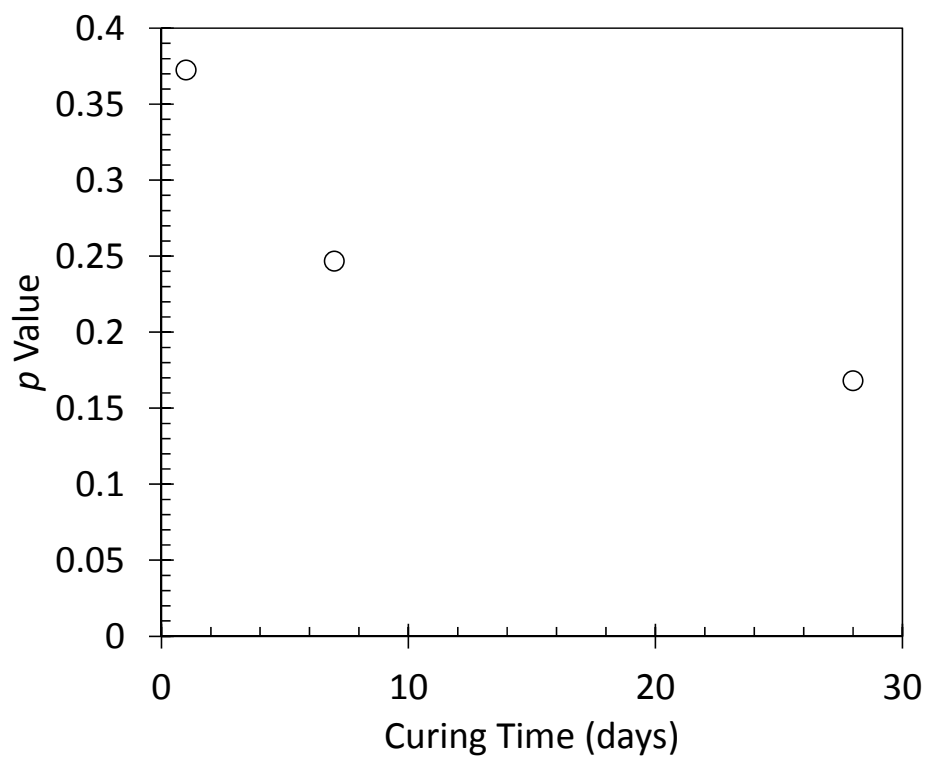


Figure D.79:  $p$  Value vs. Curing Time.

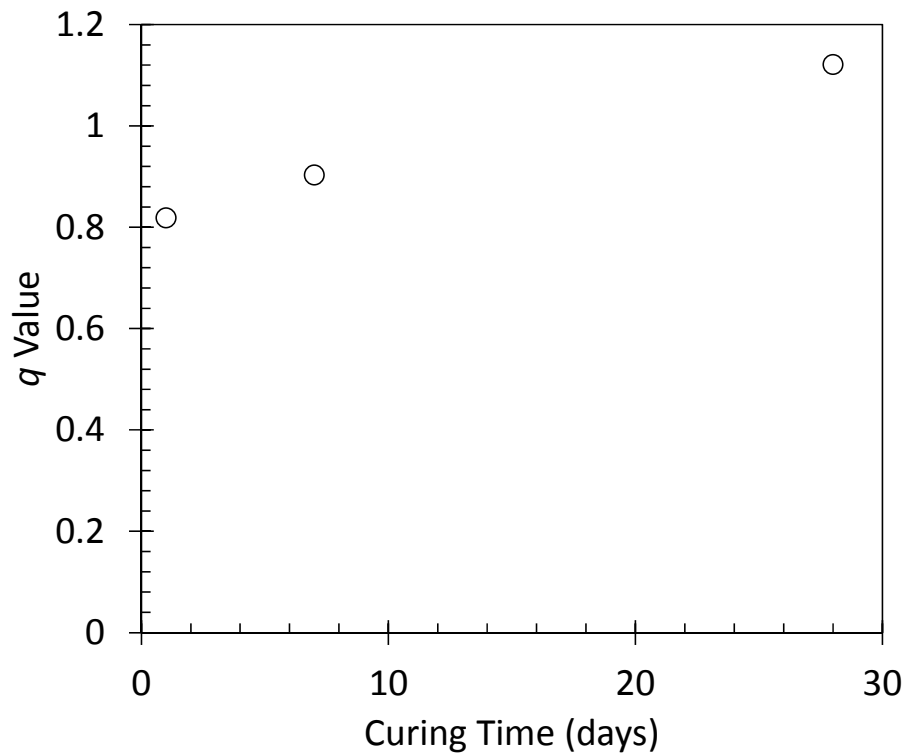
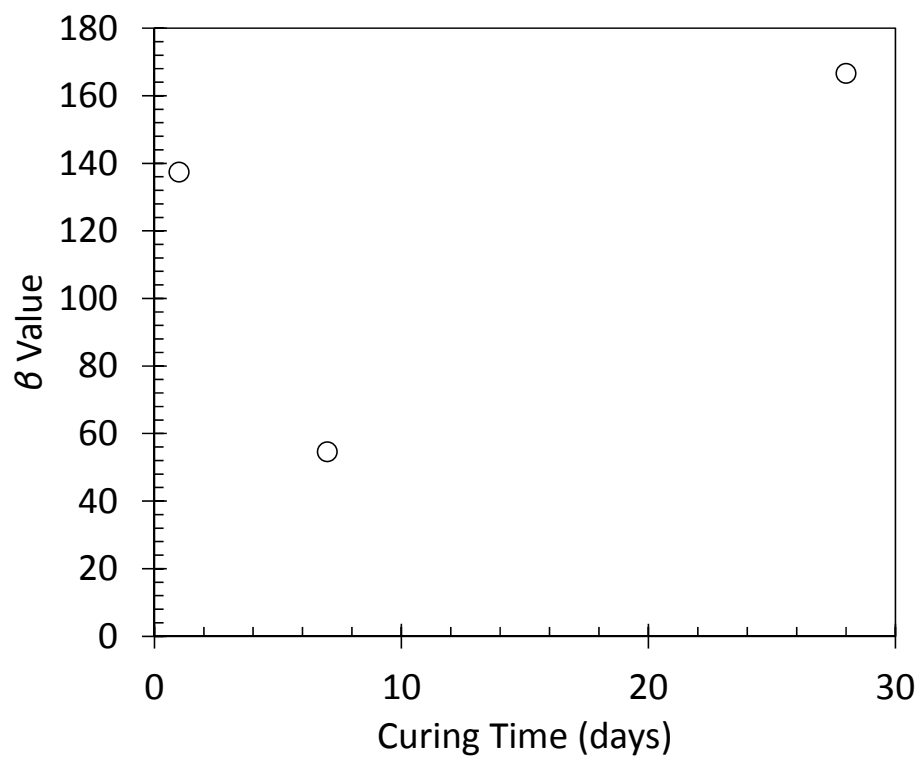


Figure D.80:  $q$  Value vs. Curing Time.



**Figure D.81:  $\beta$  Value vs. Curing Time.**

---

# **Appendix E**

## **Stress-Electrical Testing**

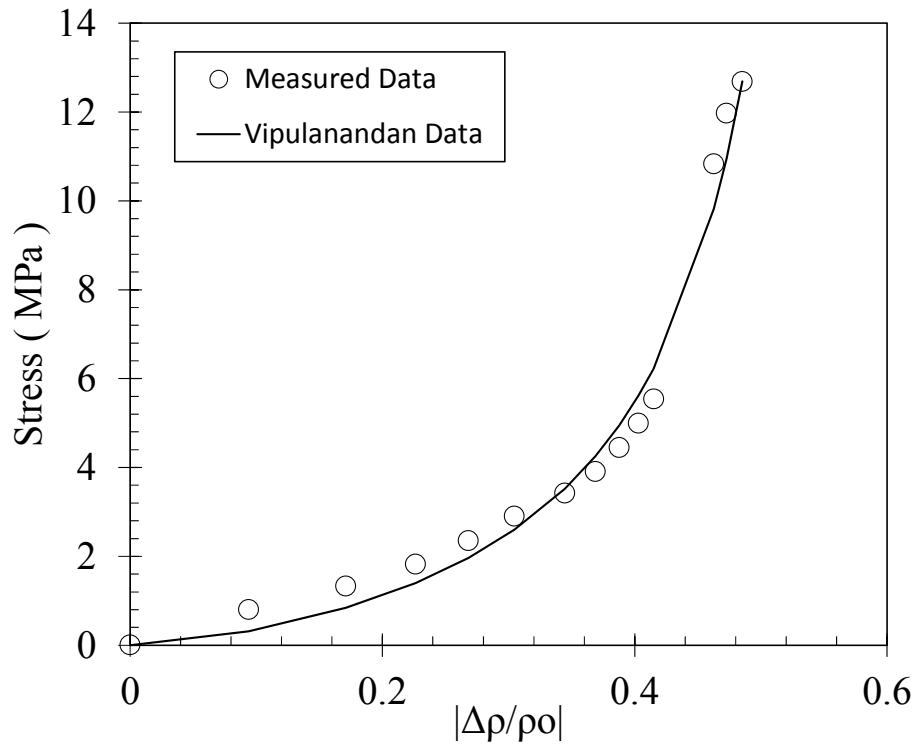


Figure E.1: Stress-Resistivity Data – Batch 1, Cylinder #1.

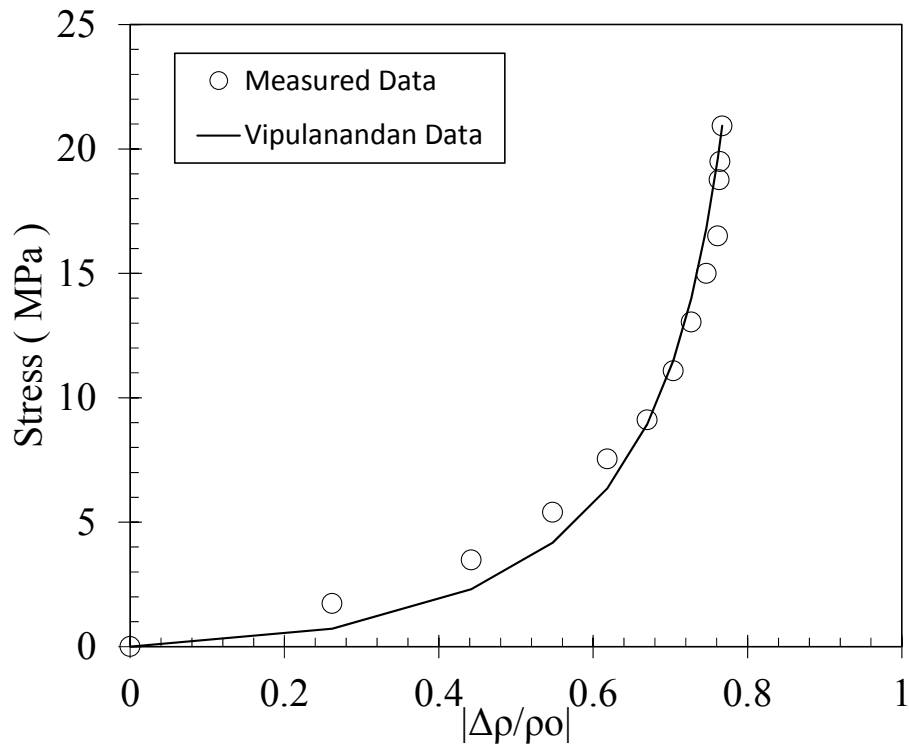


Figure E.2: Stress-Resistivity Data – Batch 1, Cylinder #2.

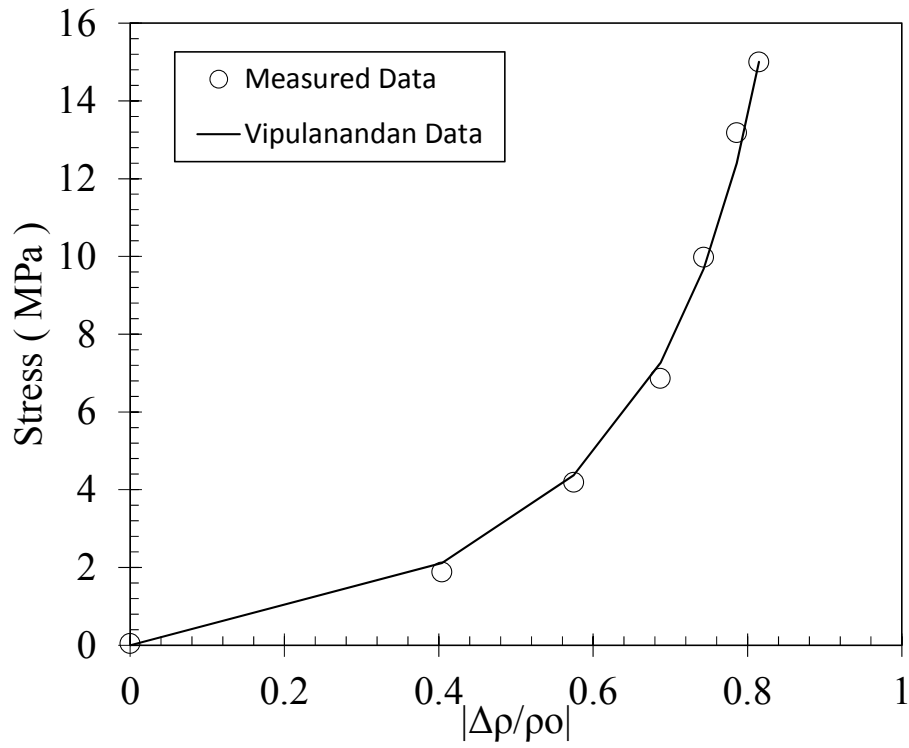


Figure E.3: Stress-Resistivity Data – Batch 1, Cylinder #3.

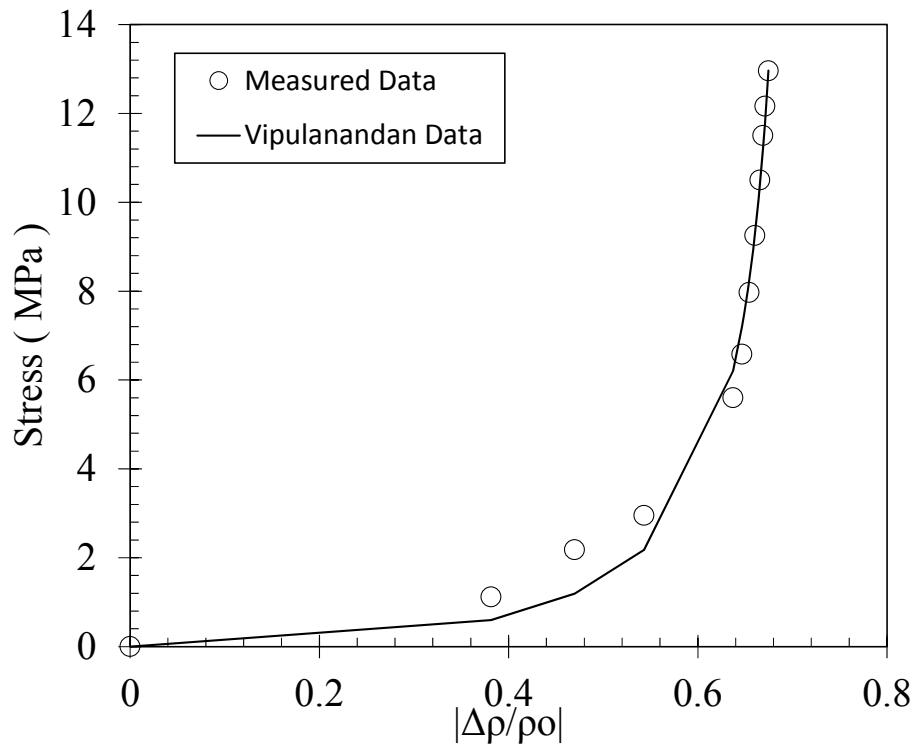


Figure E.4: Stress-Resistivity Data – Batch 2, Cylinder #4.

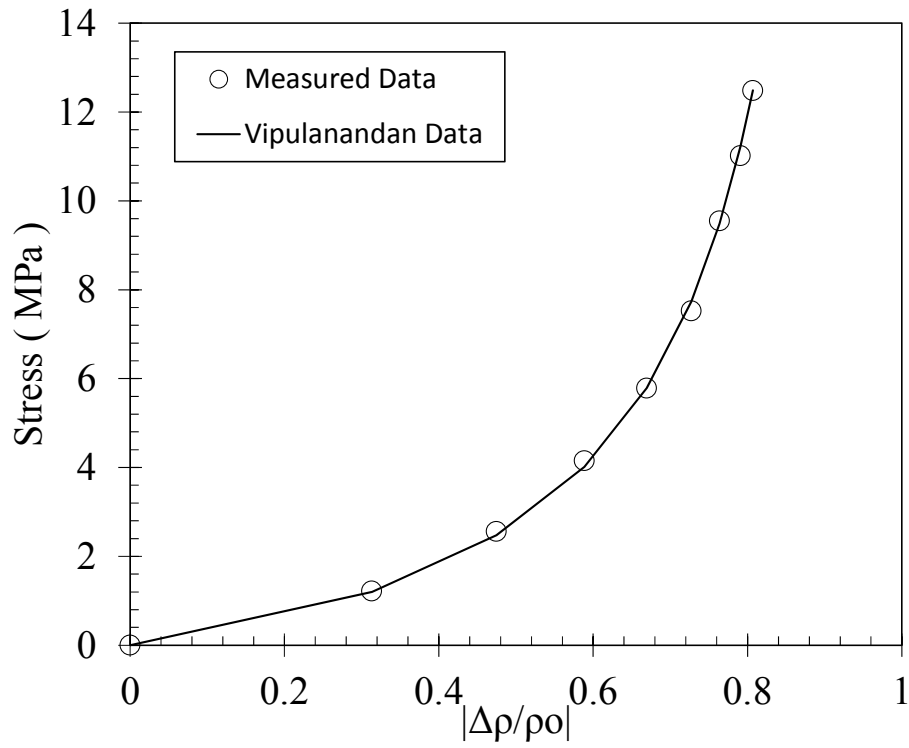


Figure E.5: Stress-Resistivity Data – Batch 2, Cylinder #5.

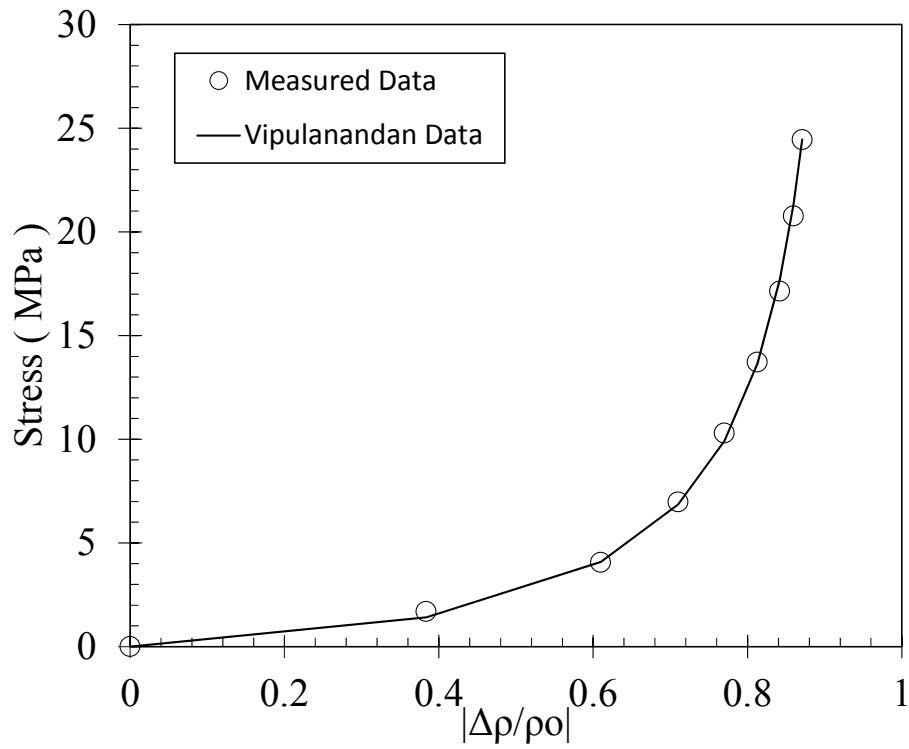


Figure E.6: Stress-Resistivity Data – Batch 2, Cylinder #6.

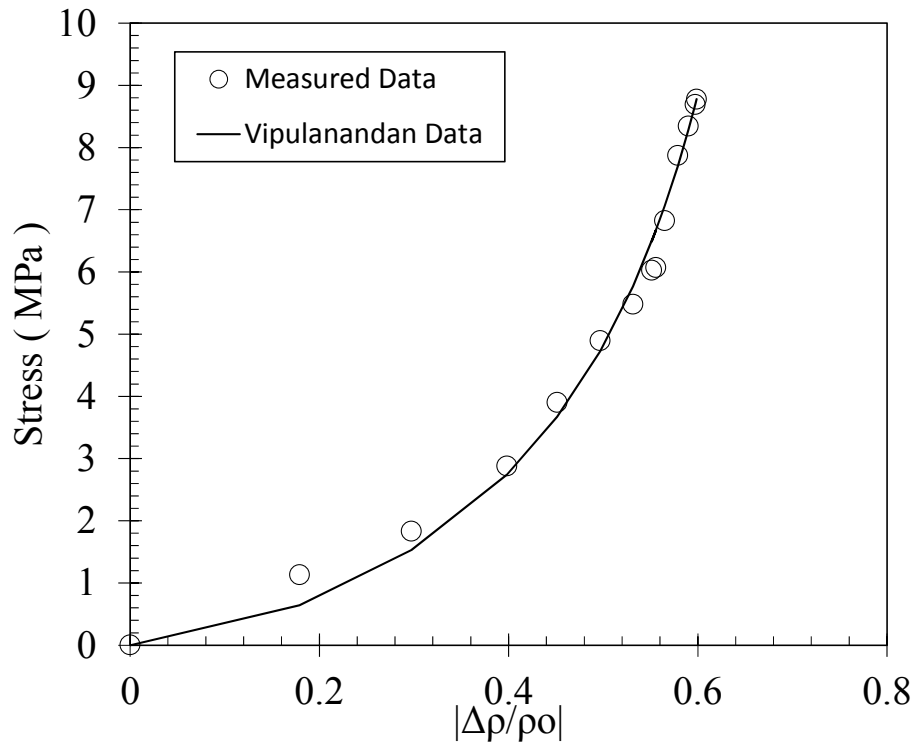


Figure E.7: Stress-Resistivity Data – Batch 3, Cylinder #7.

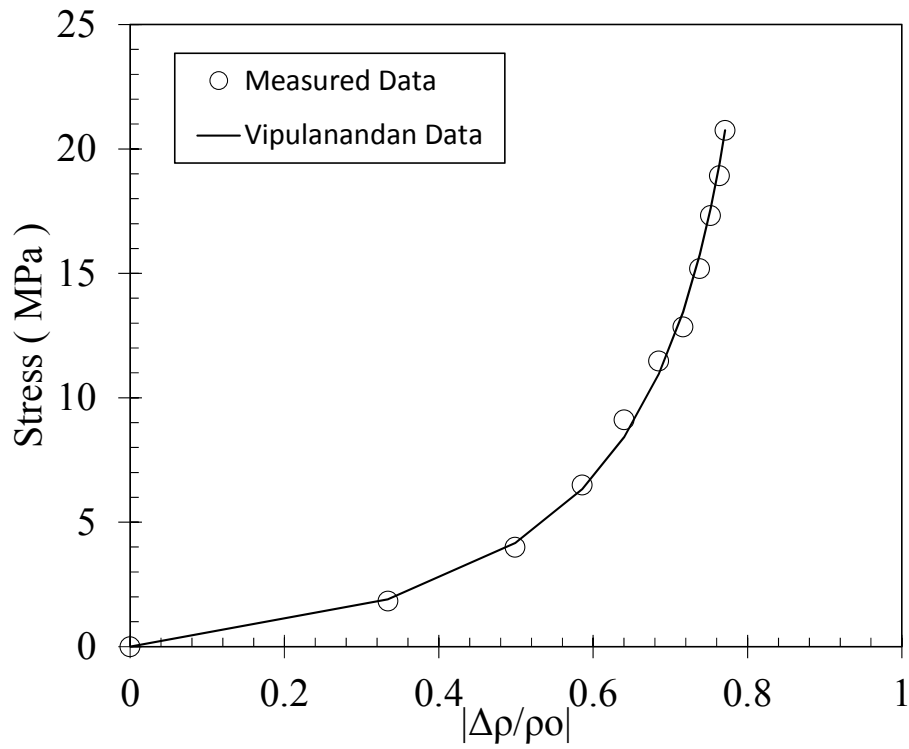
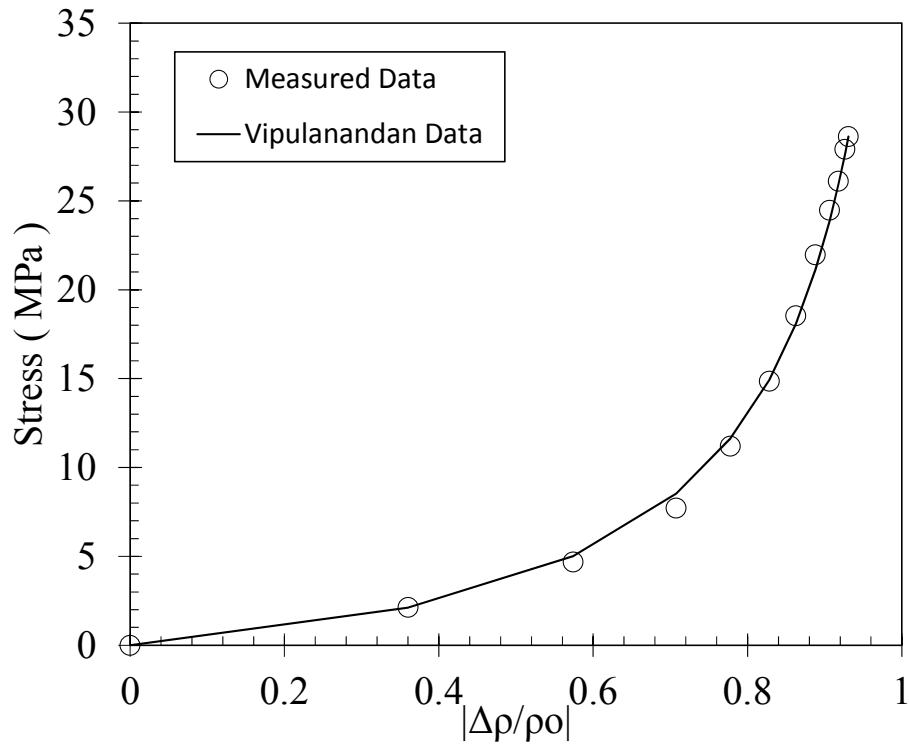
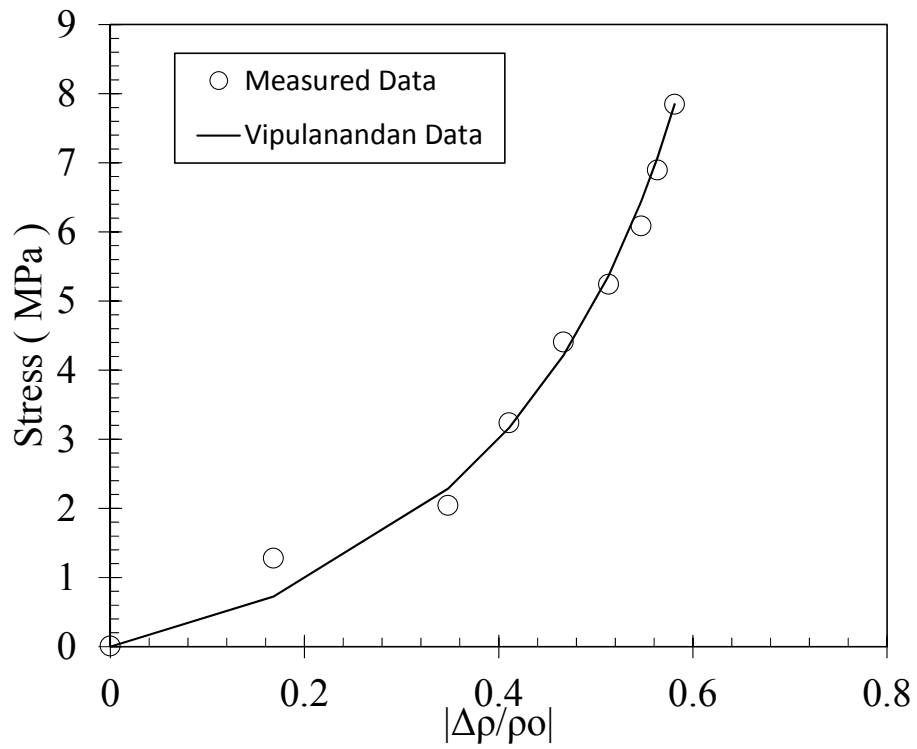


Figure E.8: Stress-Resistivity Data – Batch 3, Cylinder #8.





**Figure E.9: Stress-Resistivity Data – Batch 3, Cylinder #9.**



**Figure E.10: Stress-Resistivity Data – Batch 4, Cylinder #10.**

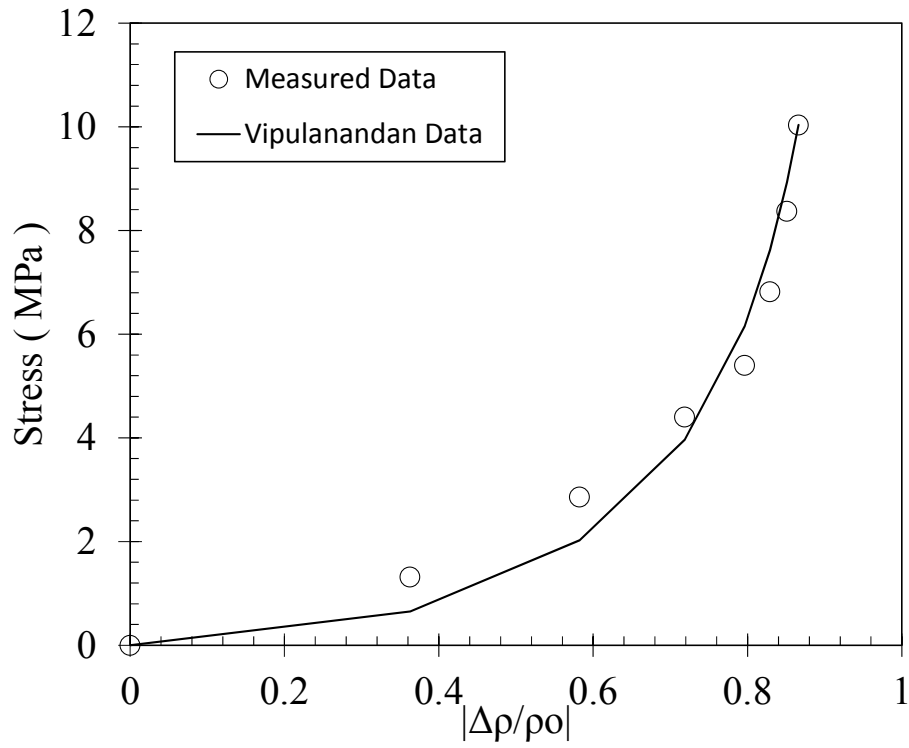


**Figure E.11: Stress-Resistivity Data – Batch 4, Cylinder #11.**

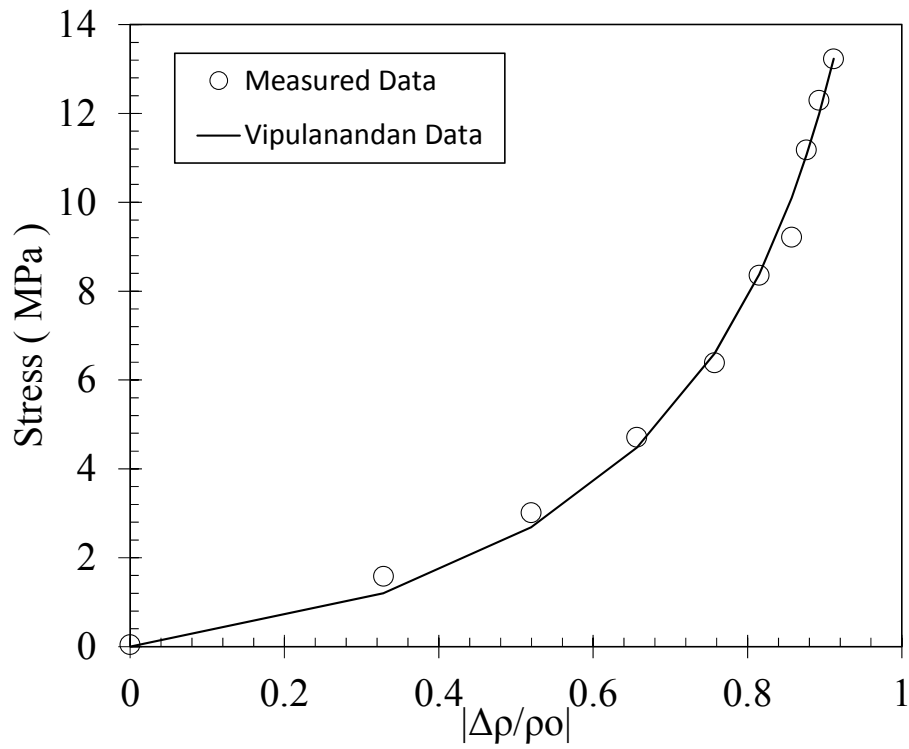


**Figure E.12: Stress-Resistivity Data – Batch 4, Cylinder #12.**

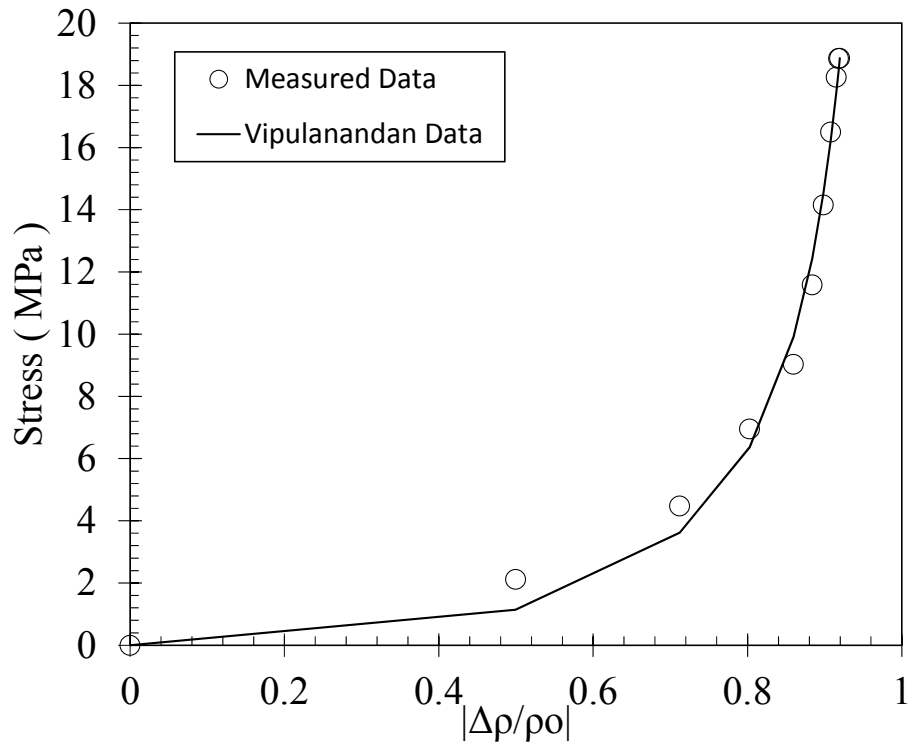


**Figure E.13: Stress-Resistivity Data – Batch 5, Cylinder #13.**

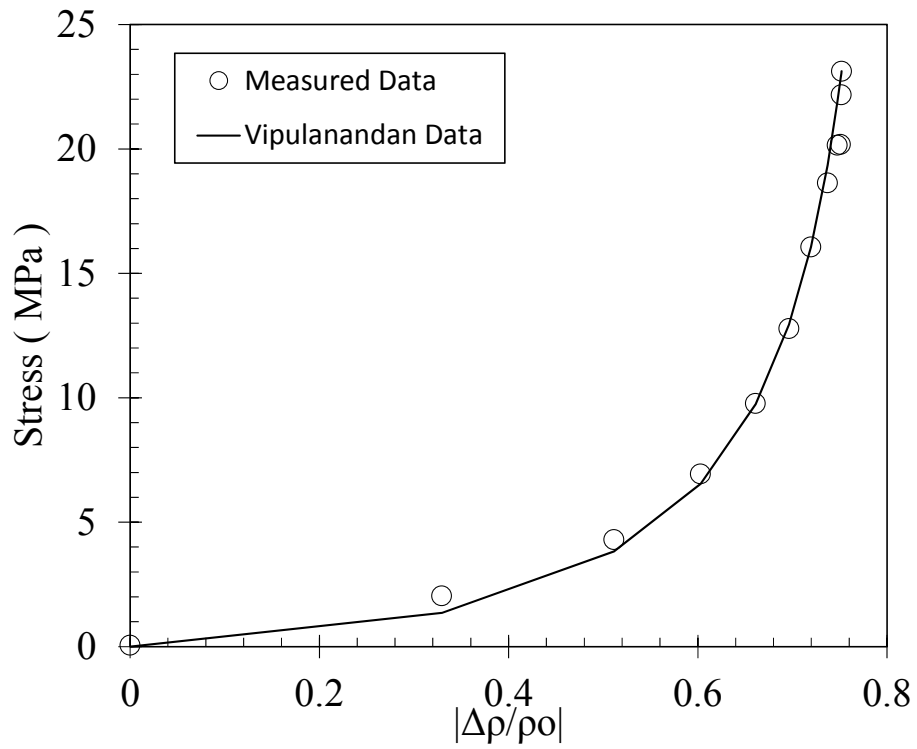


**Figure E.14: Stress-Resistivity Data – Batch 5, Cylinder #14.**

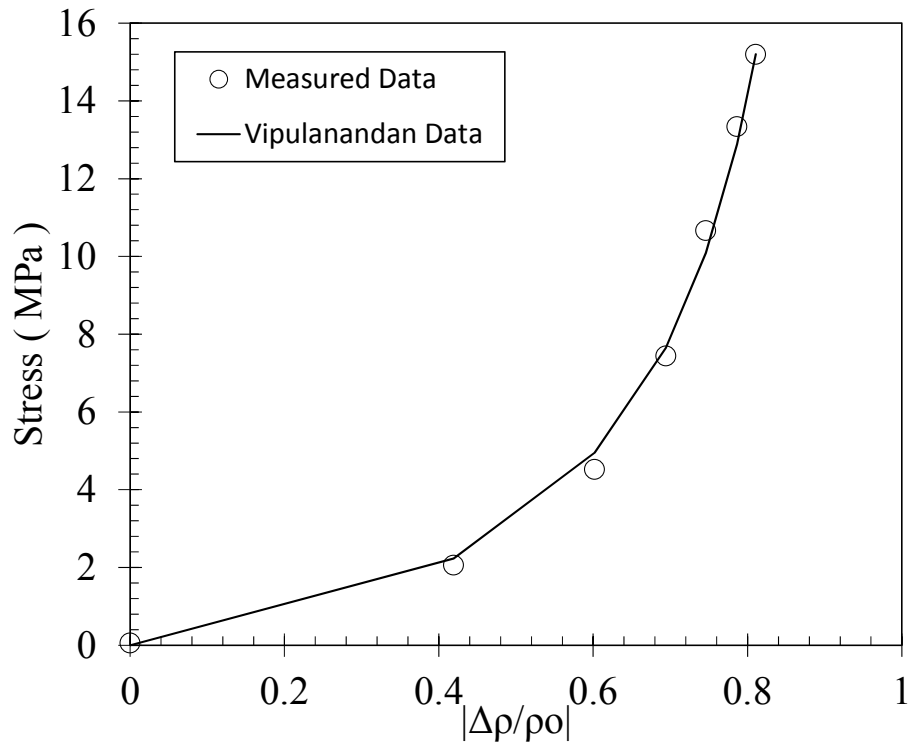


Figure E.15: Stress-Resistivity Data – Batch 5, Cylinder #15.

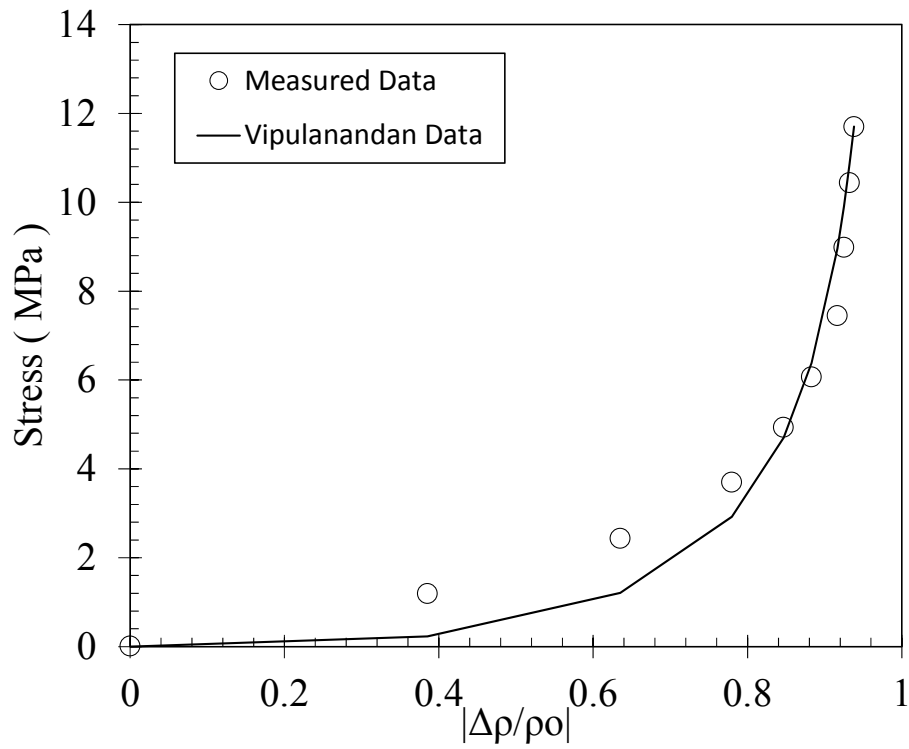


Figure E.16: Stress-Resistivity Data – Batch 6, Cylinder #16.

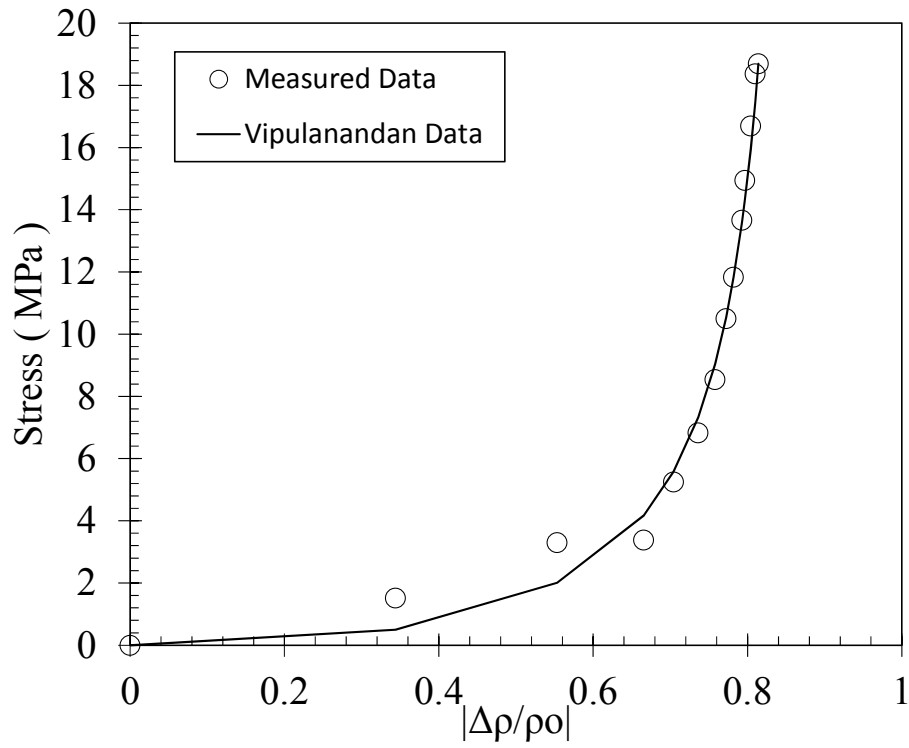


Figure E.17: Stress-Resistivity Data – Batch 6, Cylinder #17.

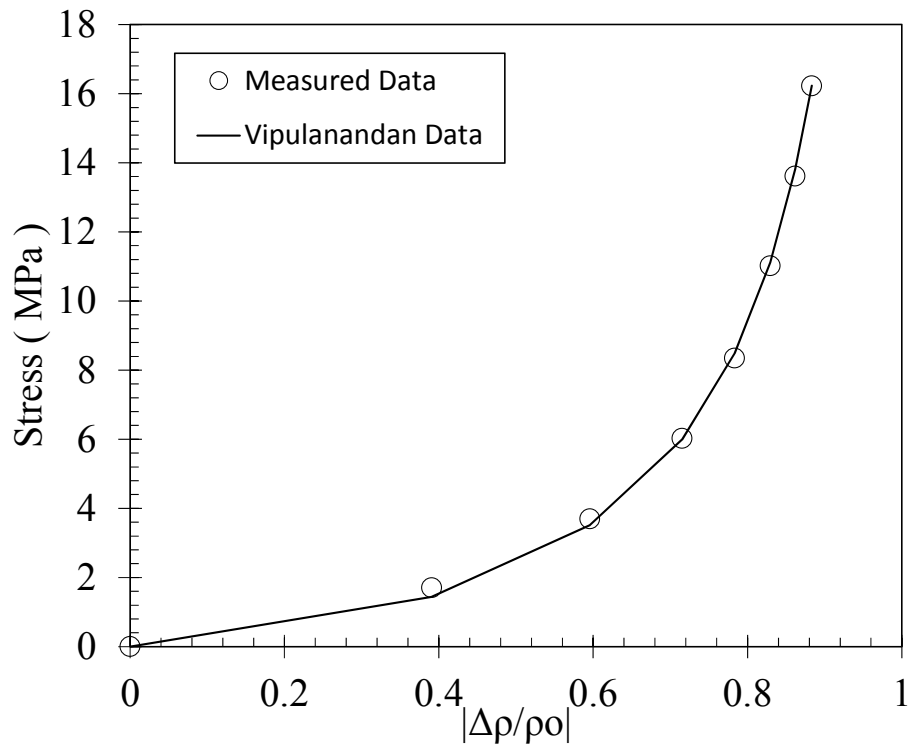
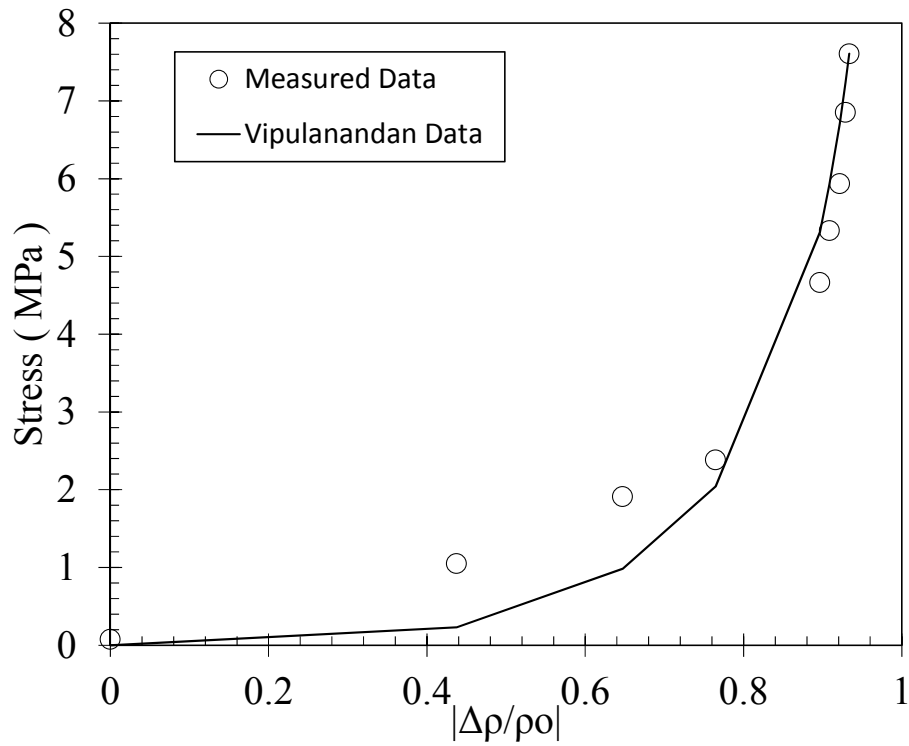
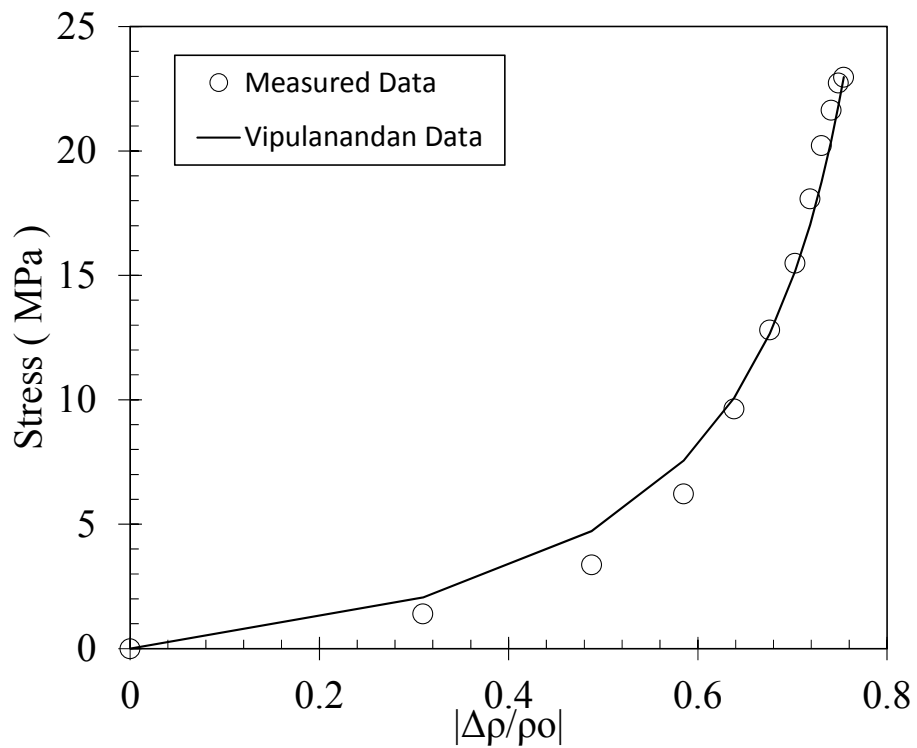


Figure E.18: Stress-Resistivity Data – Batch 6, Cylinder #18.



**Figure E.19: Stress-Resistivity Data – Batch 7, Cylinder #19.**



**Figure E.20: Stress-Resistivity Data – Batch 7, Cylinder #20.**

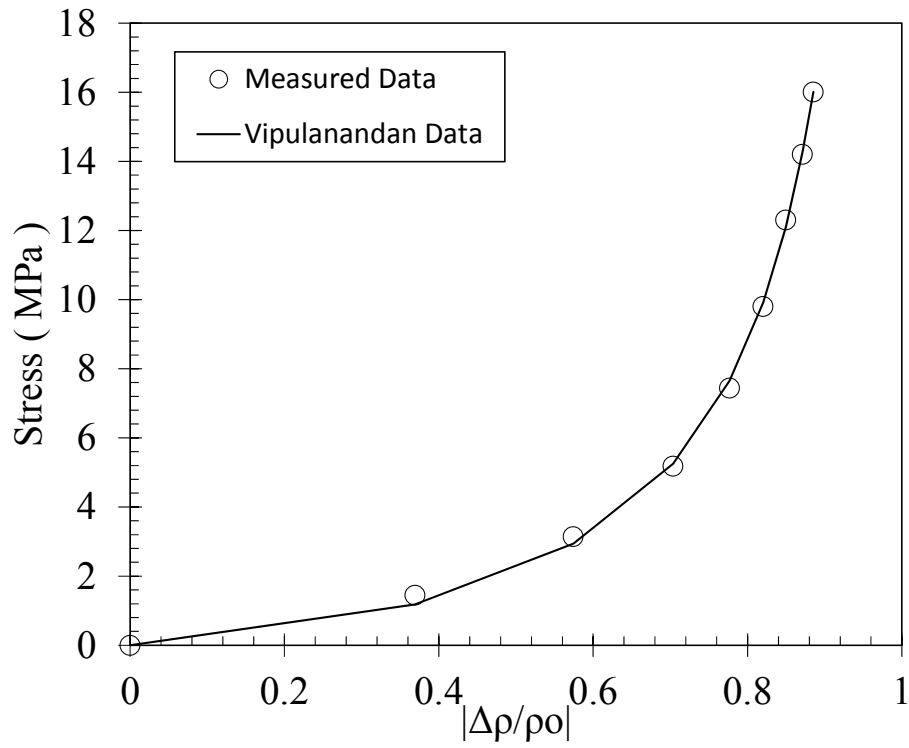


Figure E.21: Stress-Resistivity Data – Batch 7, Cylinder #21.

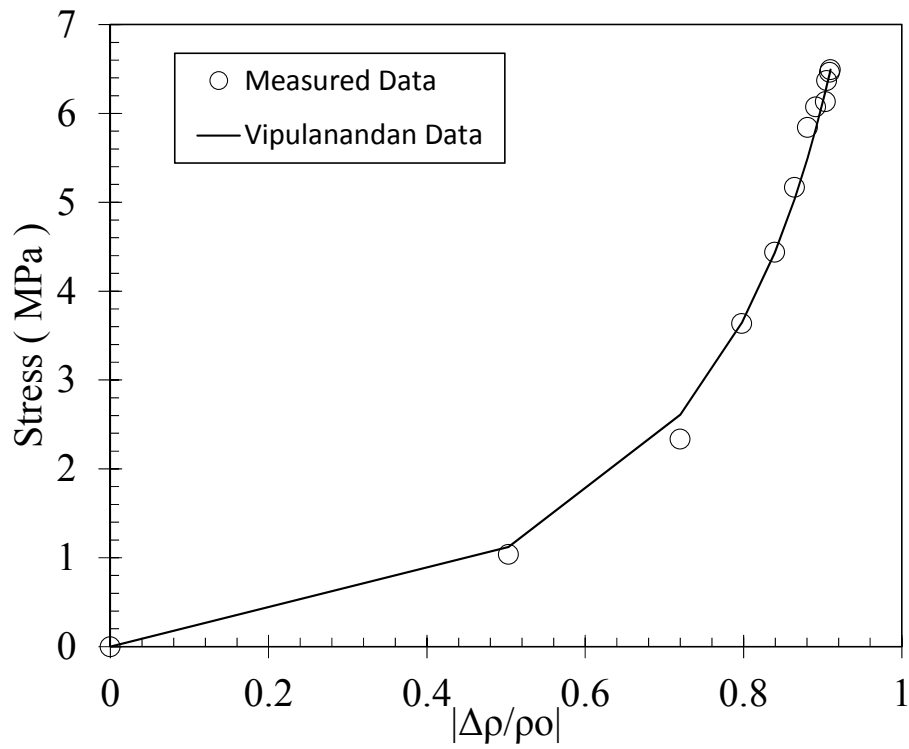


Figure E.22: Stress-Resistivity Data – Batch 8, Cylinder #22.

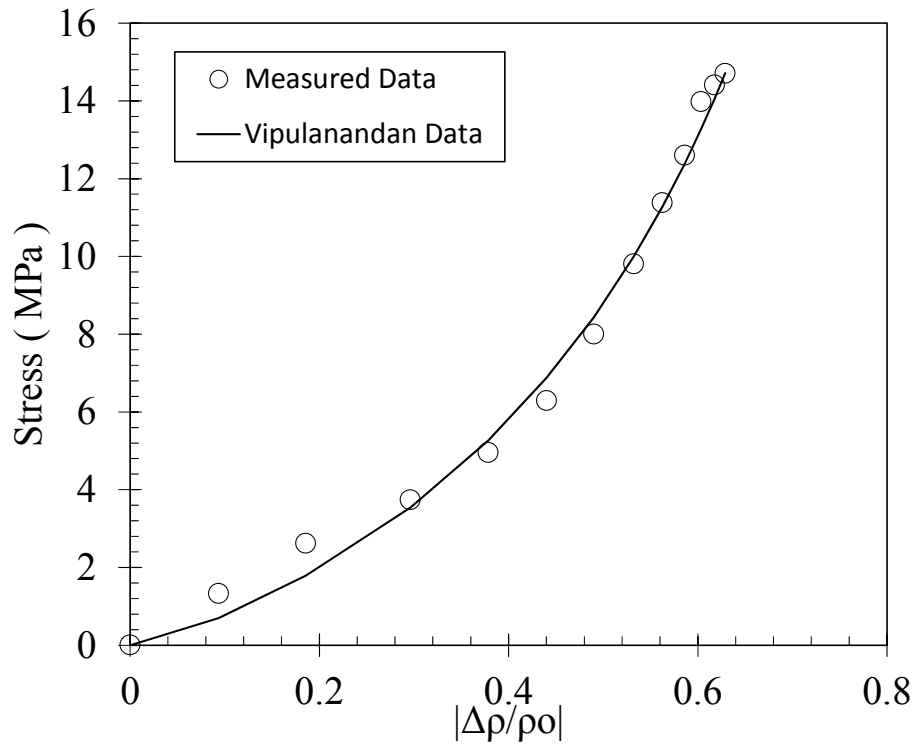


Figure E.23: Stress-Resistivity Data – Batch 8, Cylinder #23.

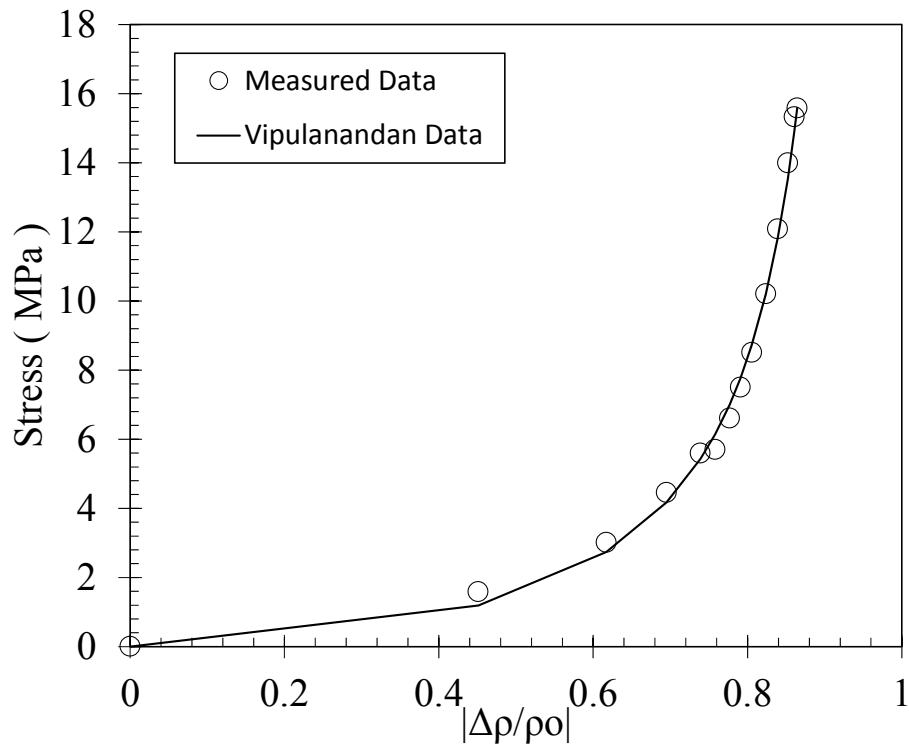


Figure E.24: Stress-Resistivity Data – Batch 8, Cylinder #24.



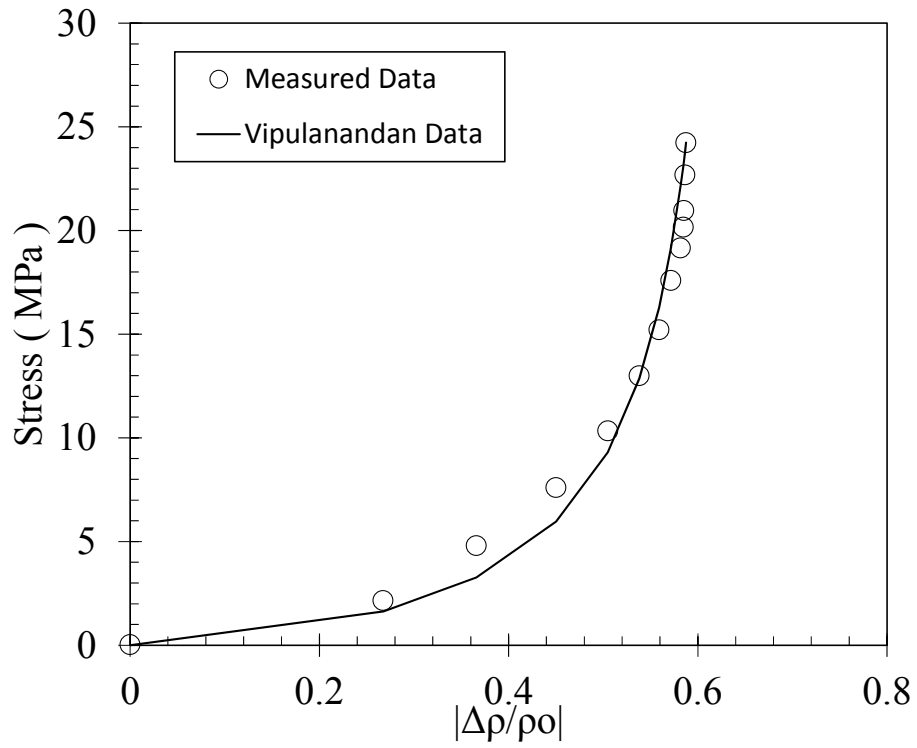


Figure E.25: Stress-Resistivity Data – Batch 9, Cylinder #25.

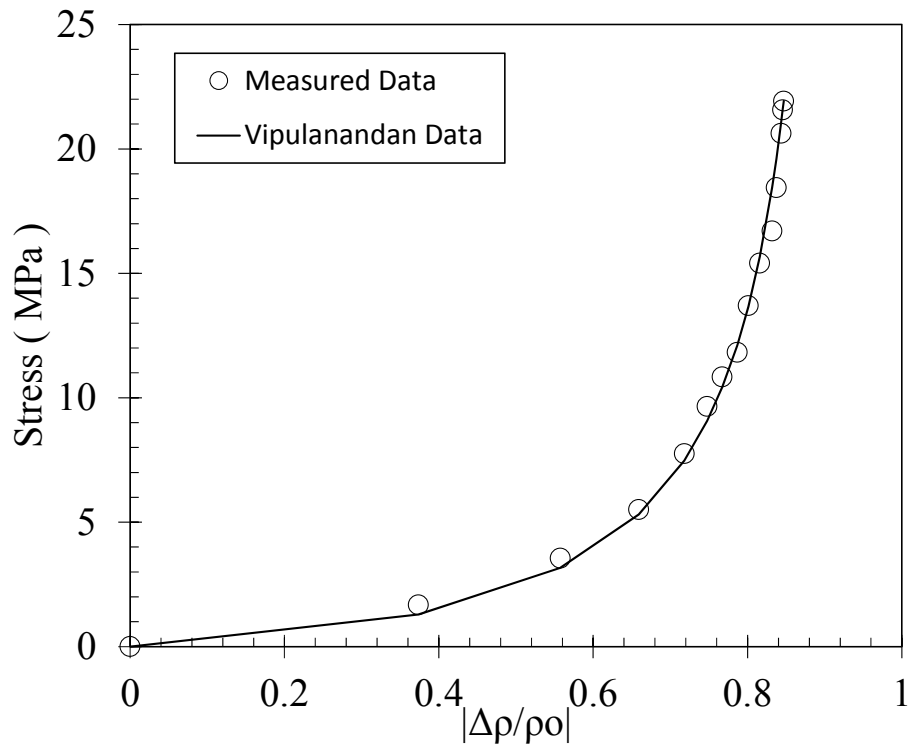


Figure E.26: Stress-Resistivity Data – Batch 9, Cylinder #26.

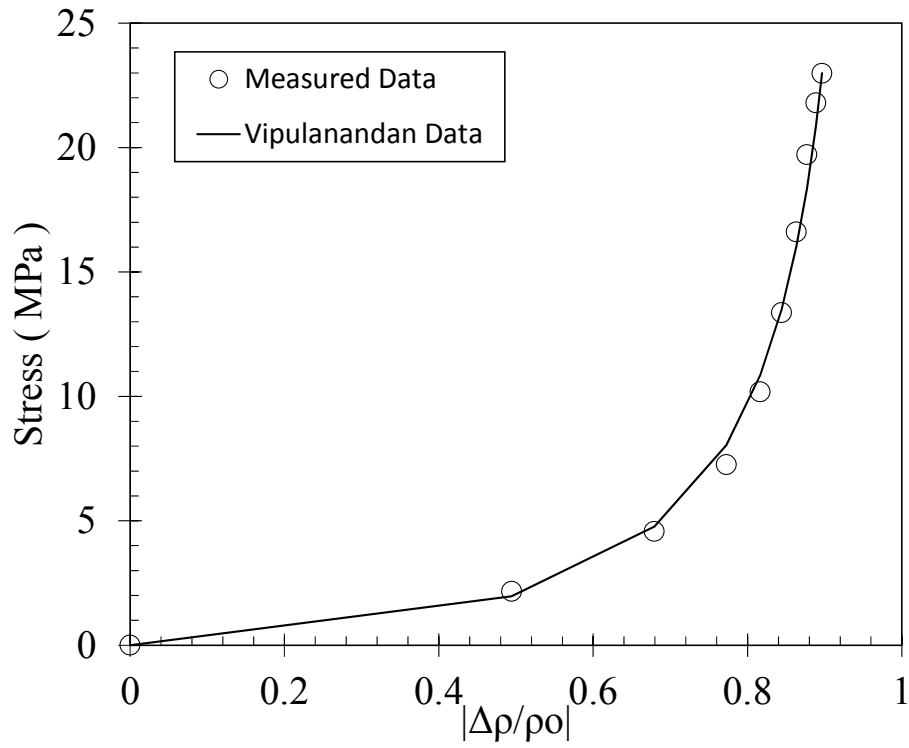


Figure E.27: Stress-Resistivity Data – Batch 9, Cylinder #27.

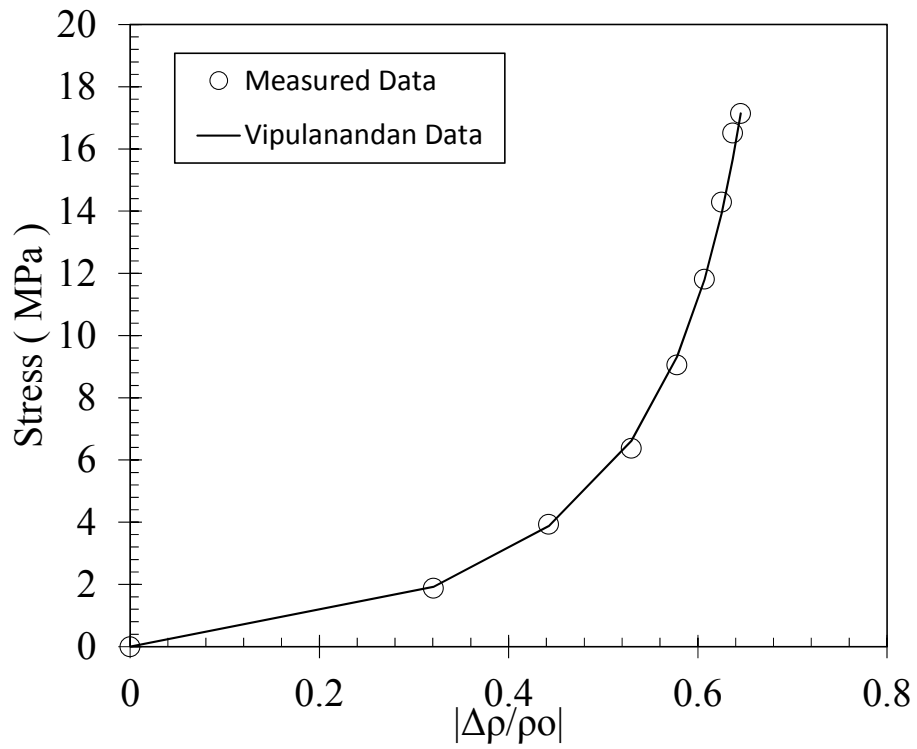
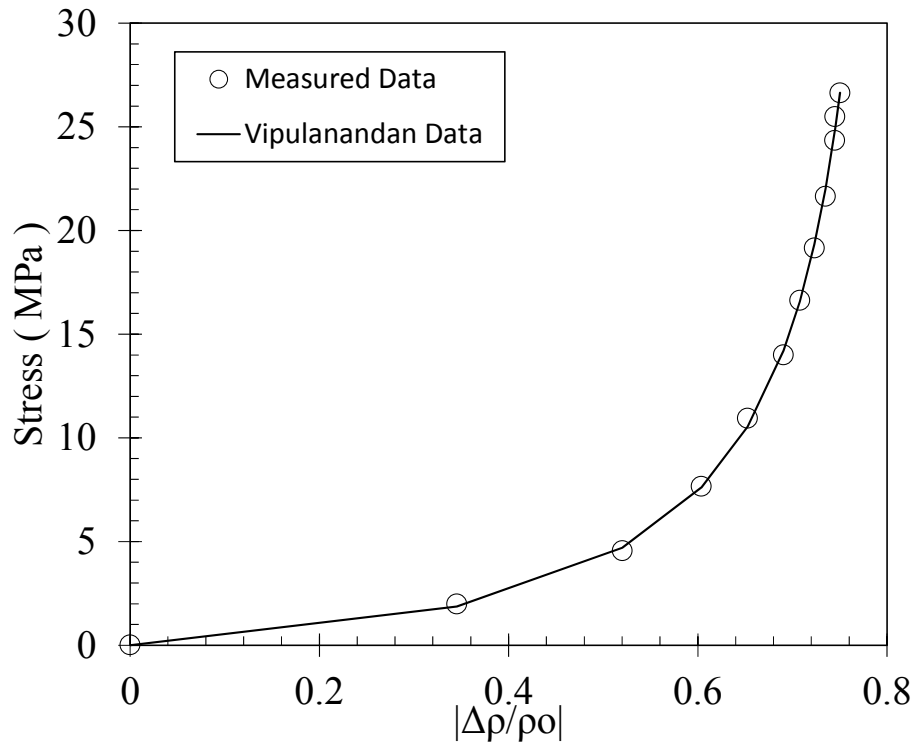
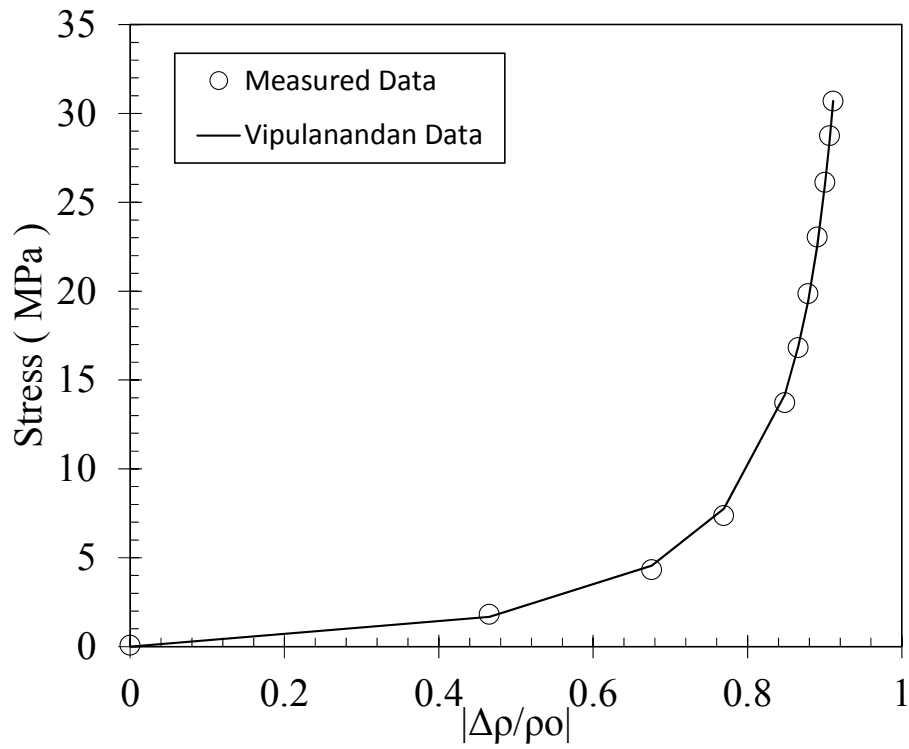


Figure E.28: Stress-Resistivity Data – Batch 10, Cylinder #28.



**Figure E.29: Stress-Resistivity Data – Batch 10, Cylinder #29.**



**Figure E.30: Stress-Resistivity Data – Batch 10, Cylinder #30.**

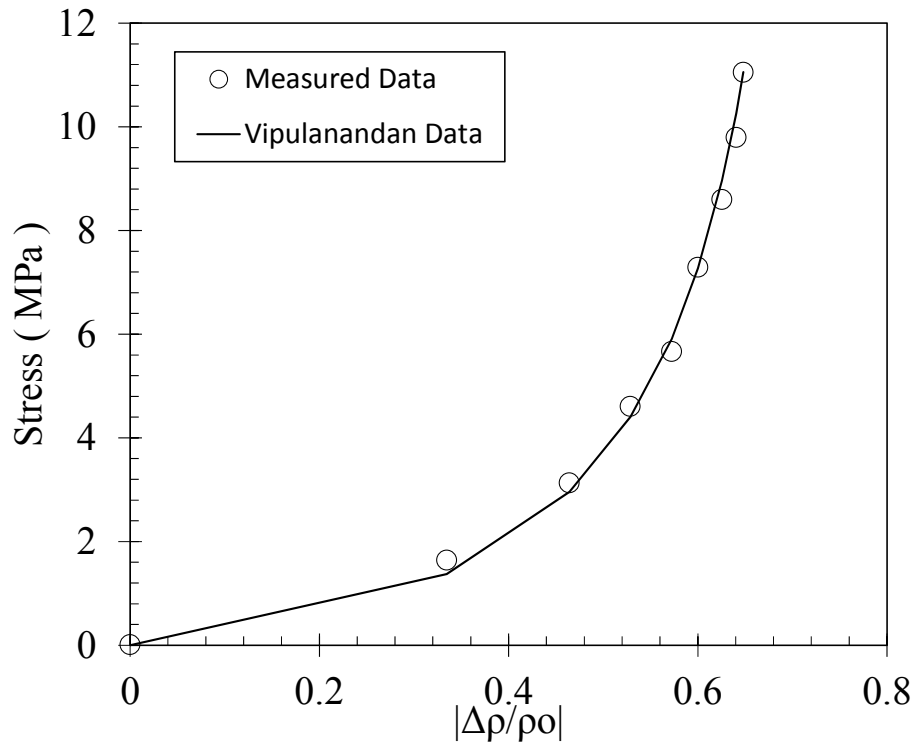


Figure E.31: Stress-Resistivity Data – Batch 11, Cylinder #31.

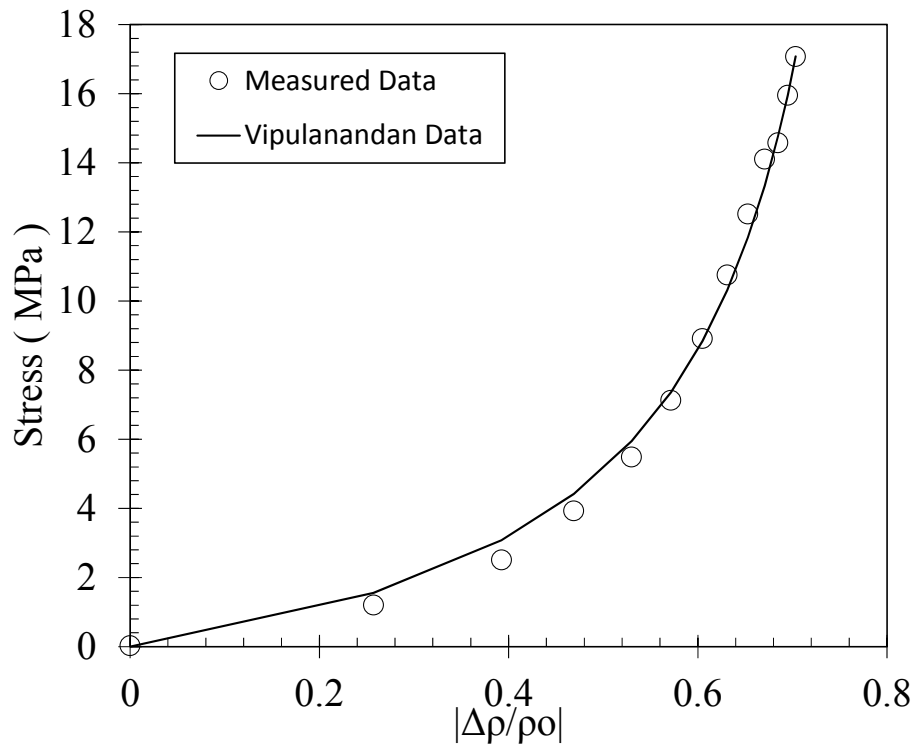


Figure E.32: Stress-Resistivity Data – Batch 11, Cylinder #32.

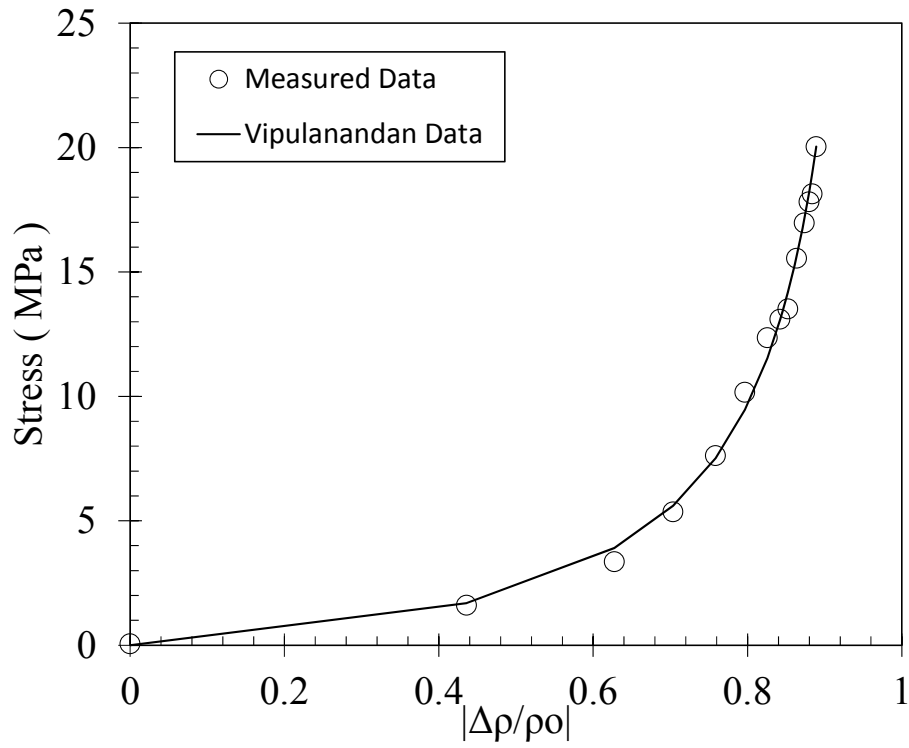


Figure E.33: Stress-Resistivity Data – Batch 11, Cylinder #33.

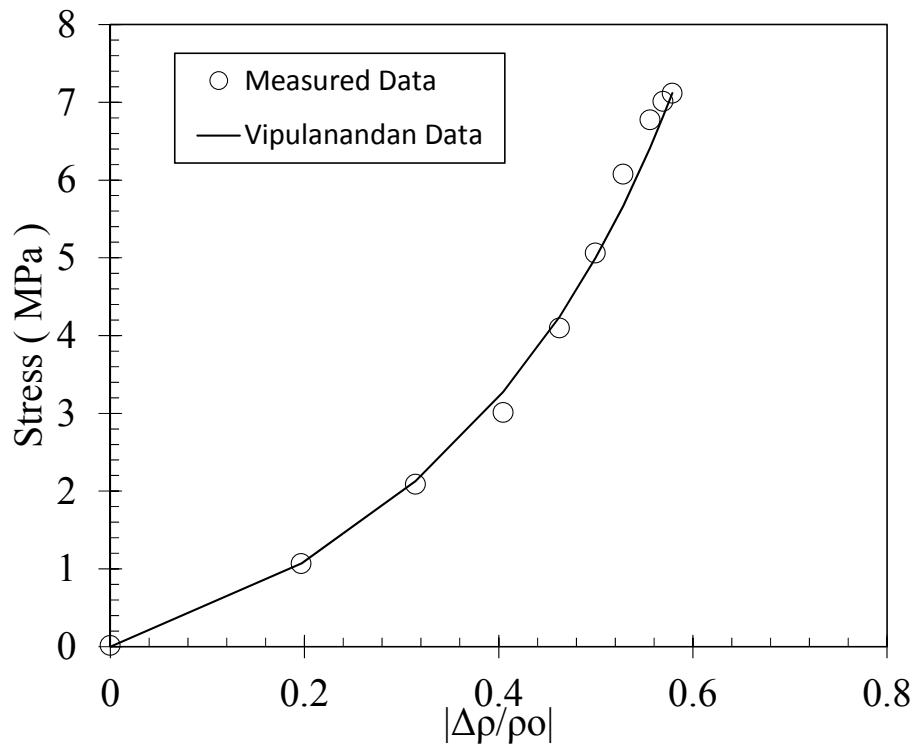


Figure E.34: Stress-Resistivity Data – Batch 12, Cylinder #34.

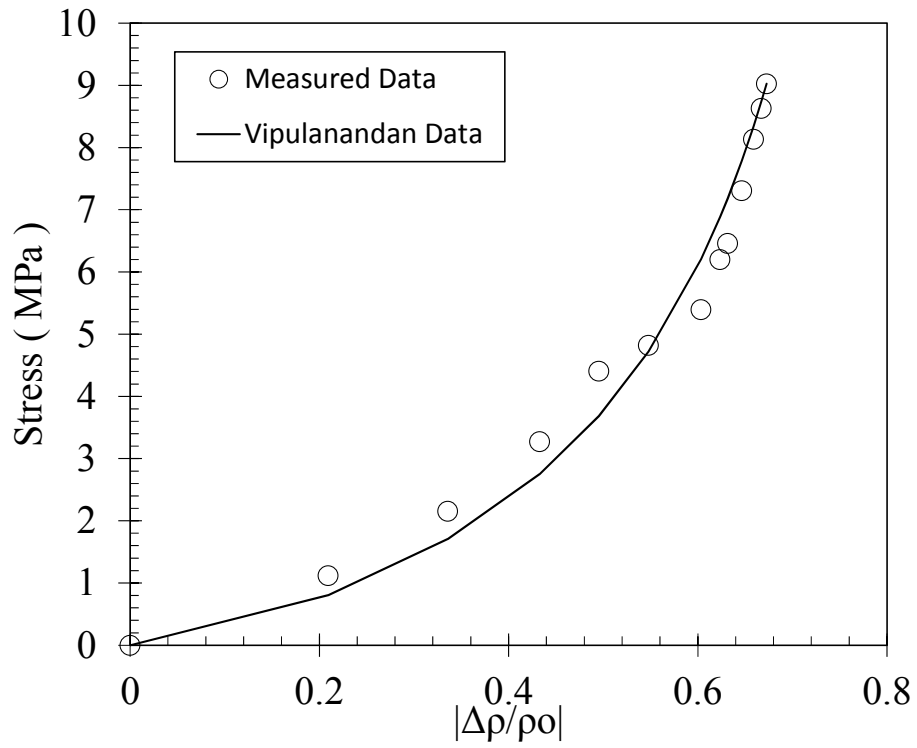


Figure E.35: Stress-Resistivity Data – Batch 12, Cylinder #35.

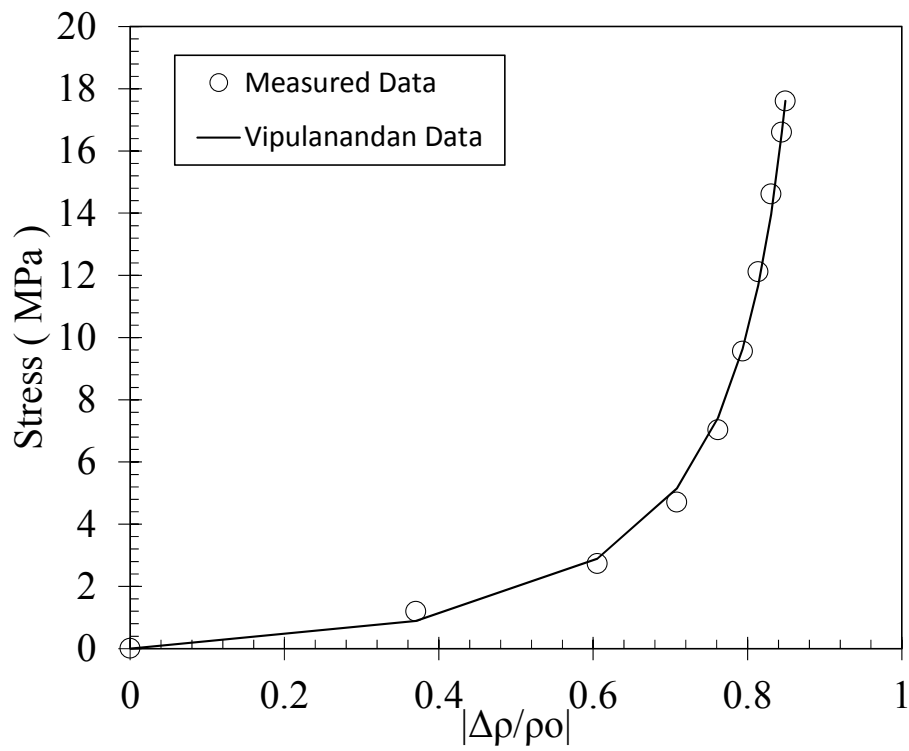


Figure E.36: Stress-Resistivity Data – Batch 12, Cylinder #36.

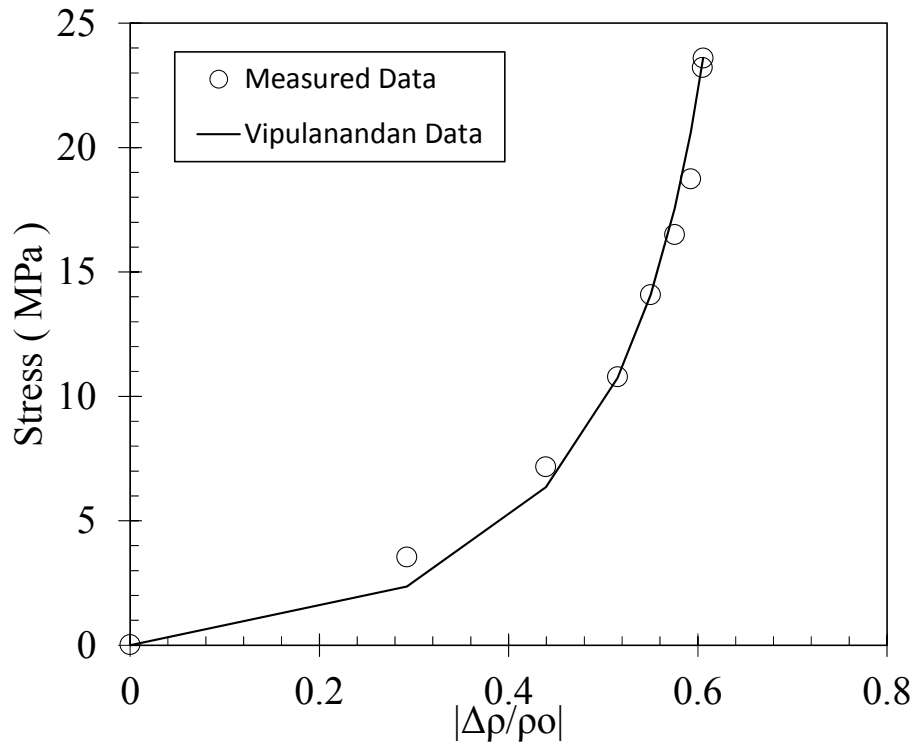


Figure E.37: Stress-Resistivity Data – Batch 13, Cylinder #37.

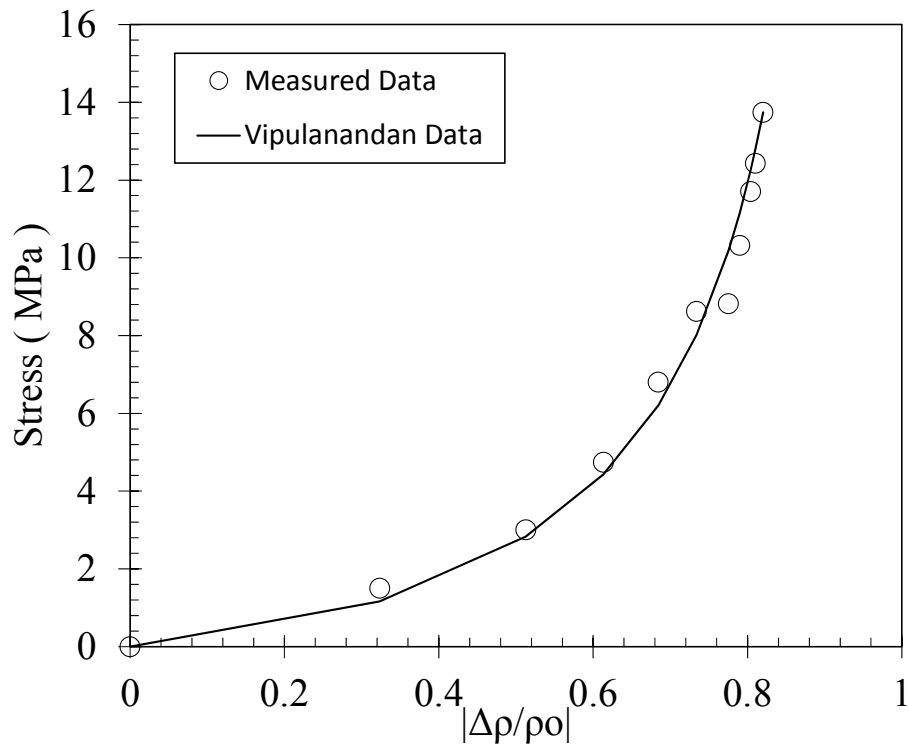


Figure E.38: Stress-Resistivity Data – Batch 13, Cylinder #38.

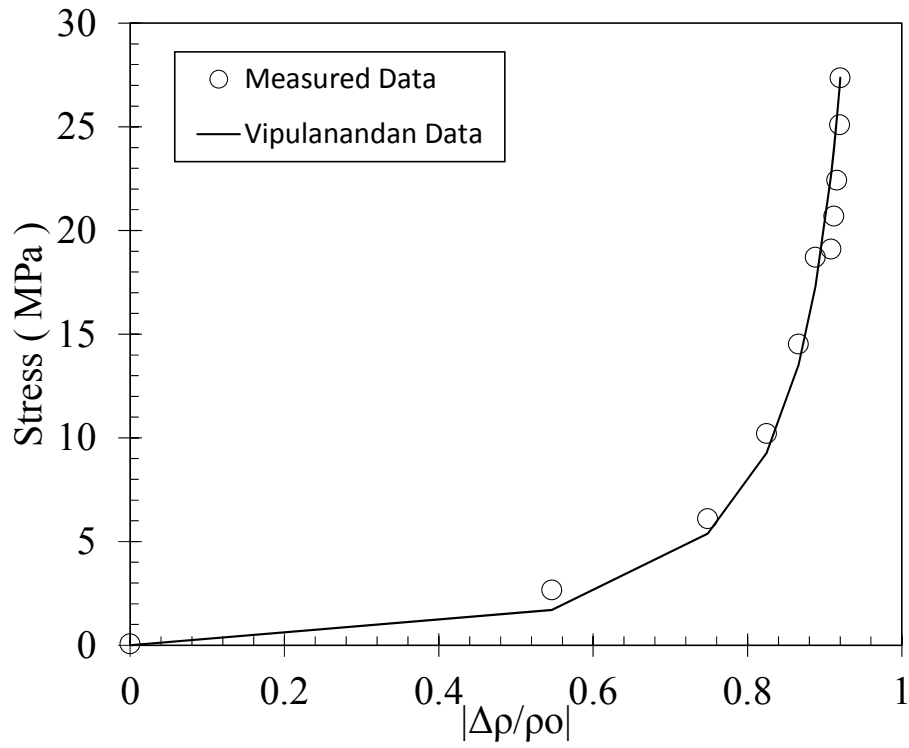


Figure E.39: Stress-Resistivity Data – Batch 13, Cylinder #39.

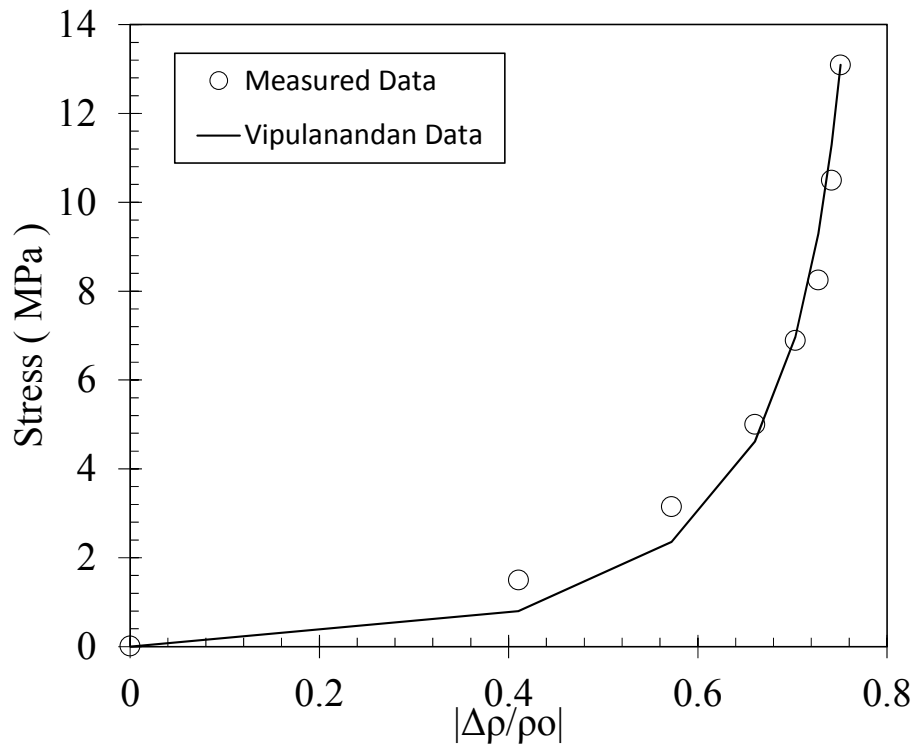


Figure E.40: Stress-Resistivity Data – Batch 14, Cylinder #40.



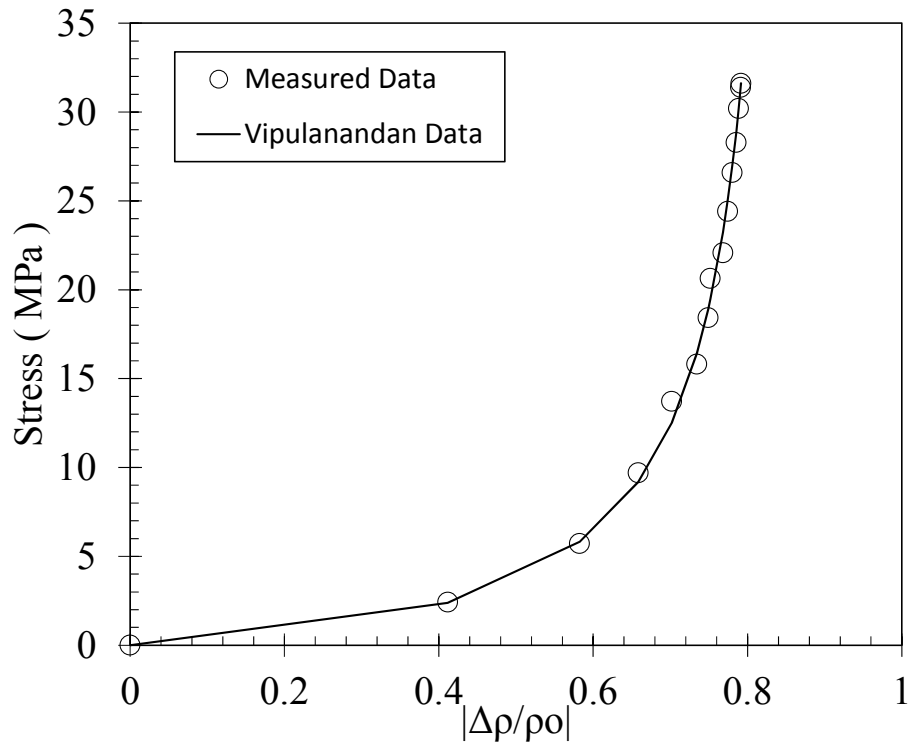


Figure E.41: Stress-Resistivity Data – Batch 14, Cylinder #41.

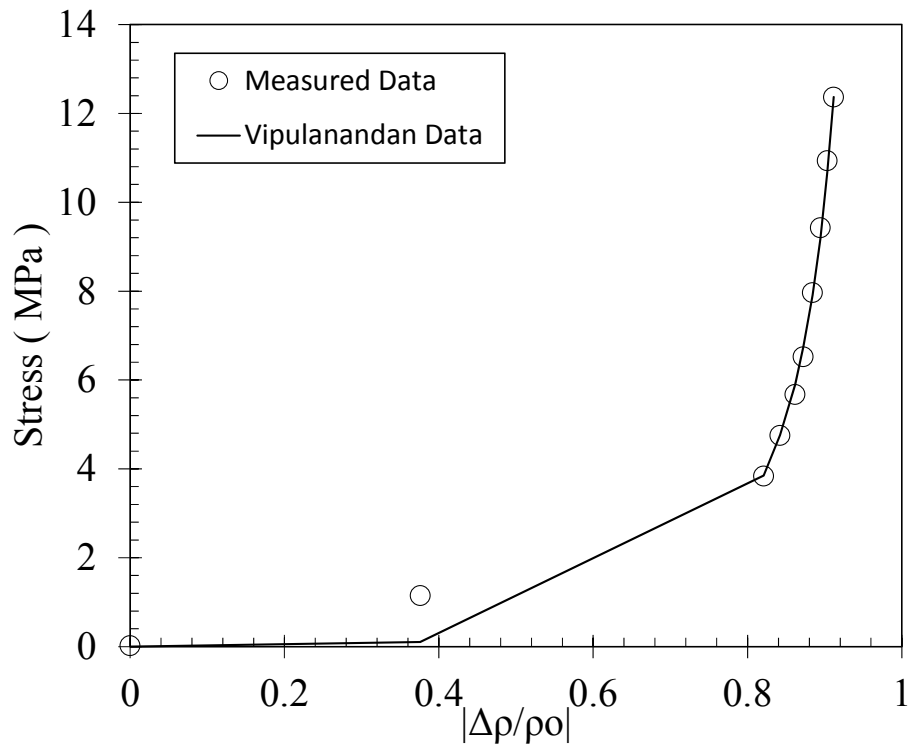


Figure E.42: Stress-Resistivity Data – Batch 14, Cylinder #42.

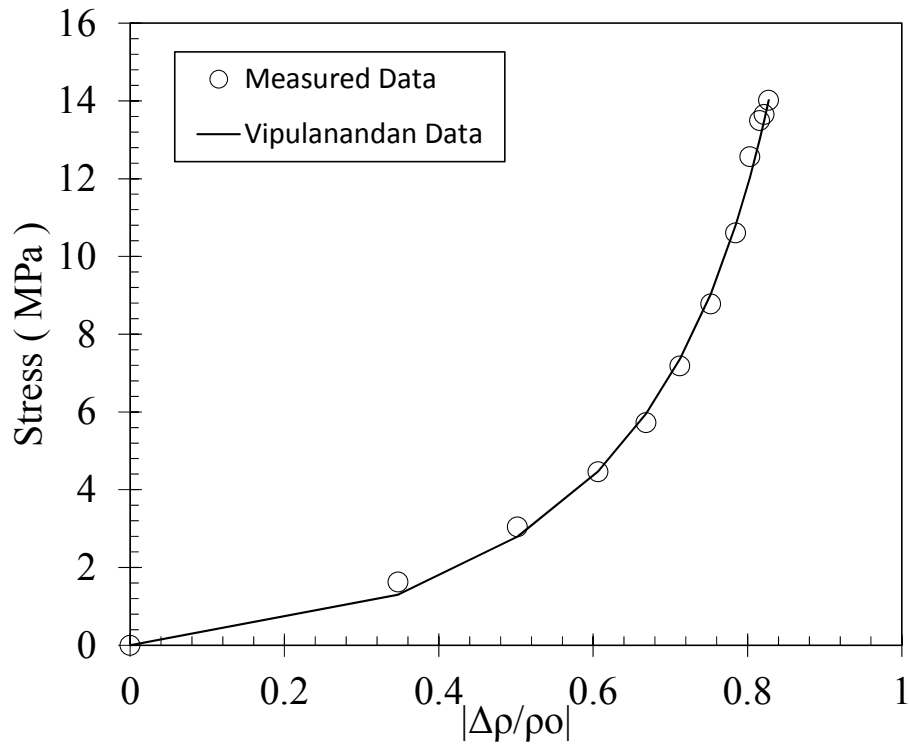


Figure E.43: Stress-Resistivity Data – Batch 15, Cylinder #43.

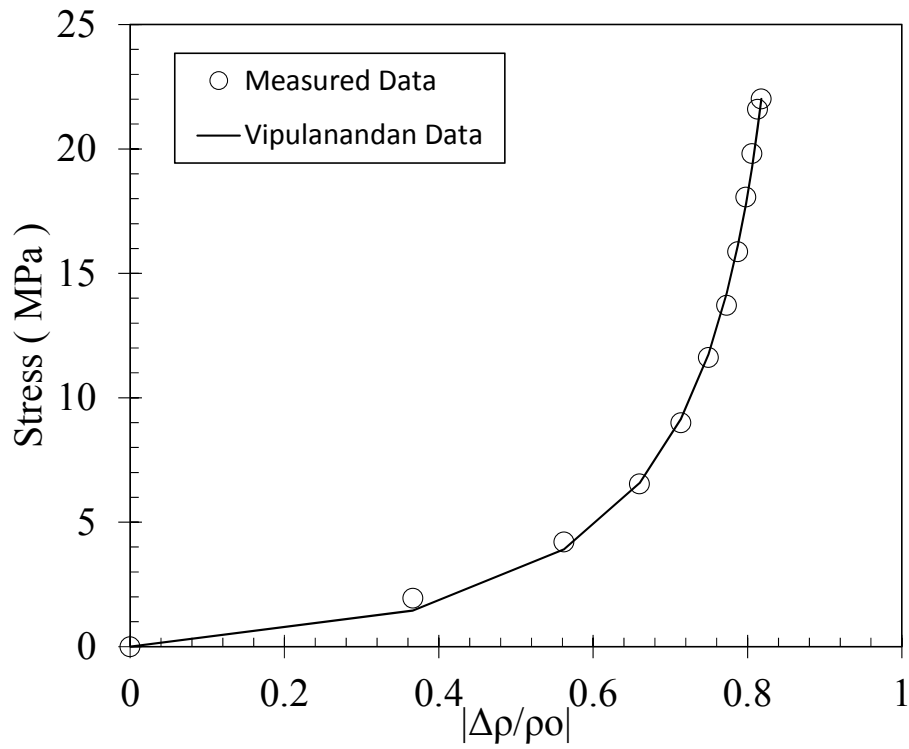


Figure E.44: Stress-Resistivity Data – Batch 15, Cylinder #44.

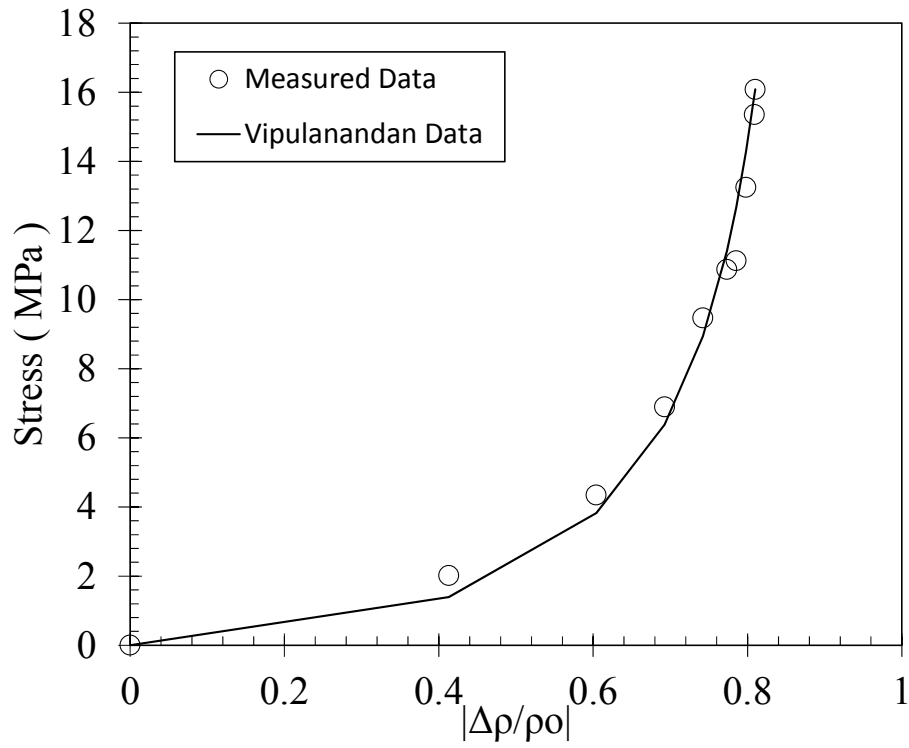


Figure E.45: Stress-Resistivity Data – Batch 15, Cylinder #45.

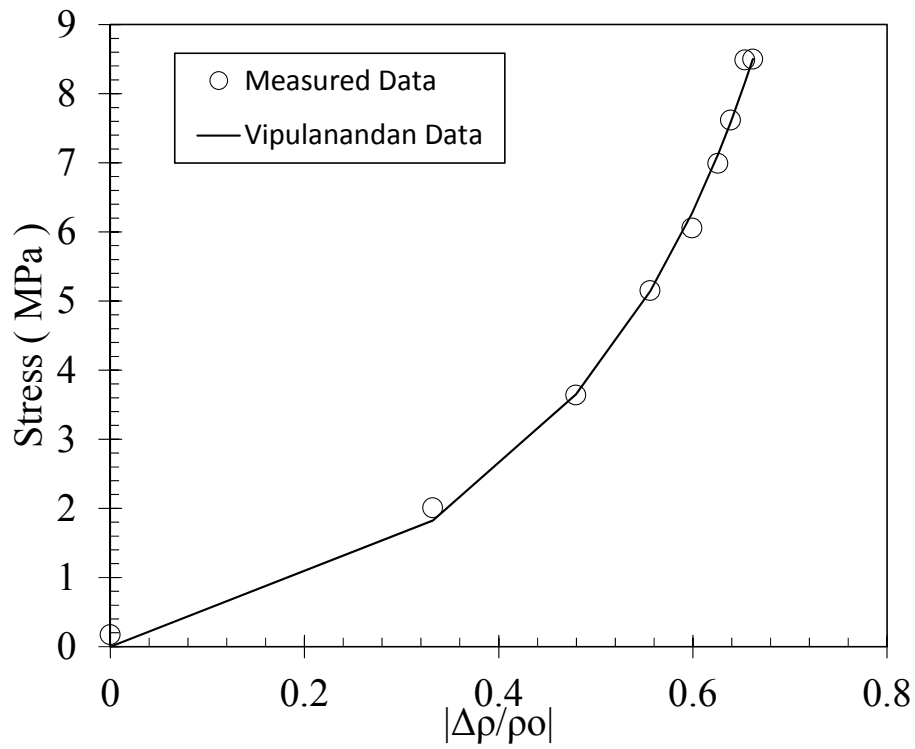


Figure E.46: Stress-Resistivity Data – Batch 16, Cylinder #46.

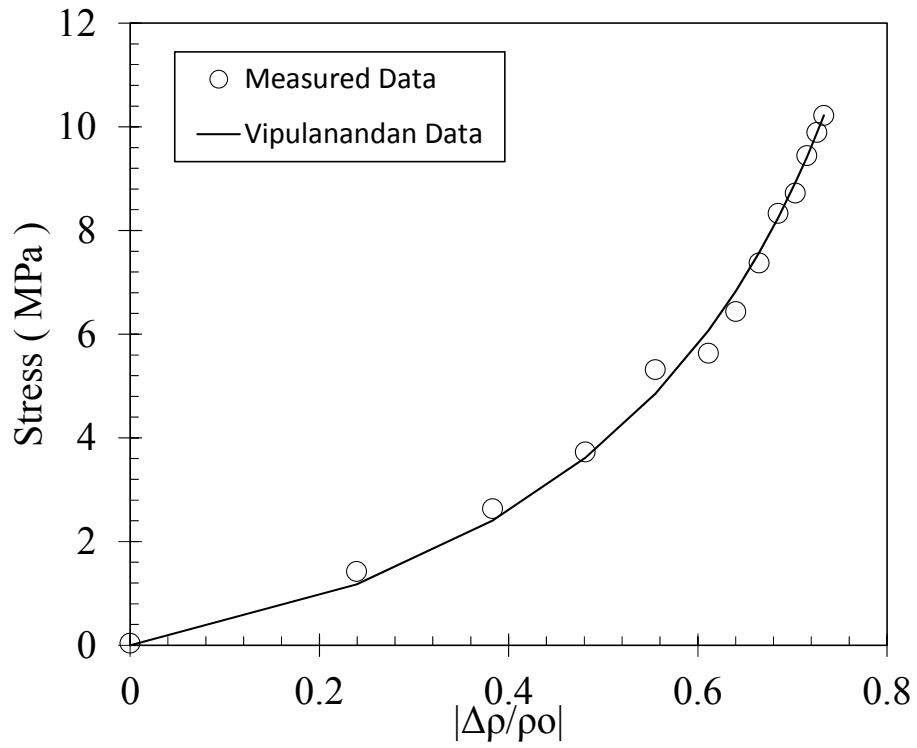


Figure E.47: Stress-Resistivity Data – Batch 16, Cylinder #47.

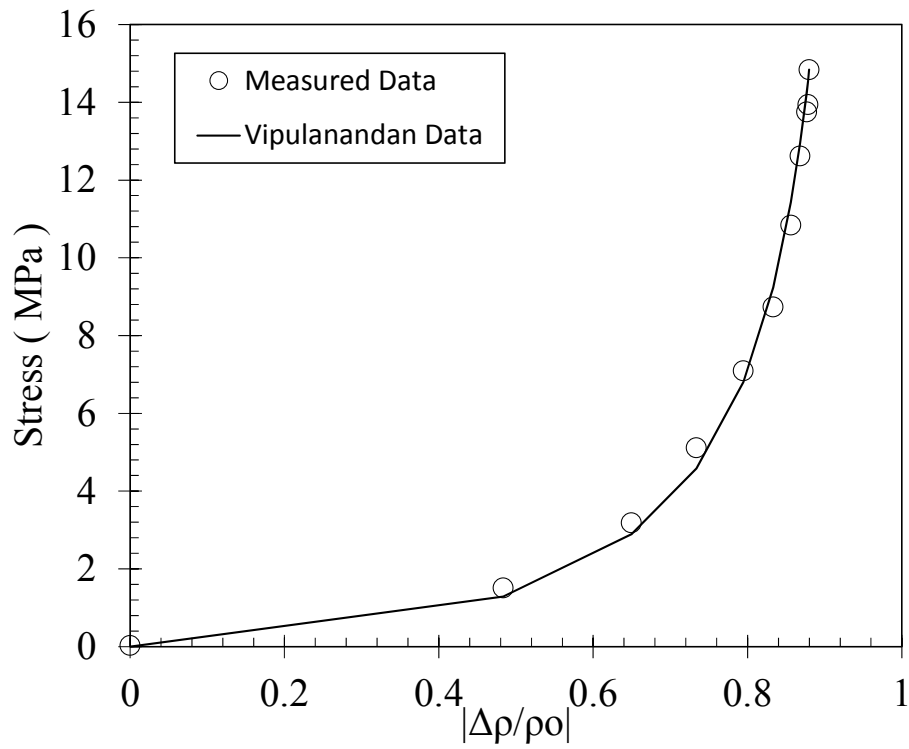
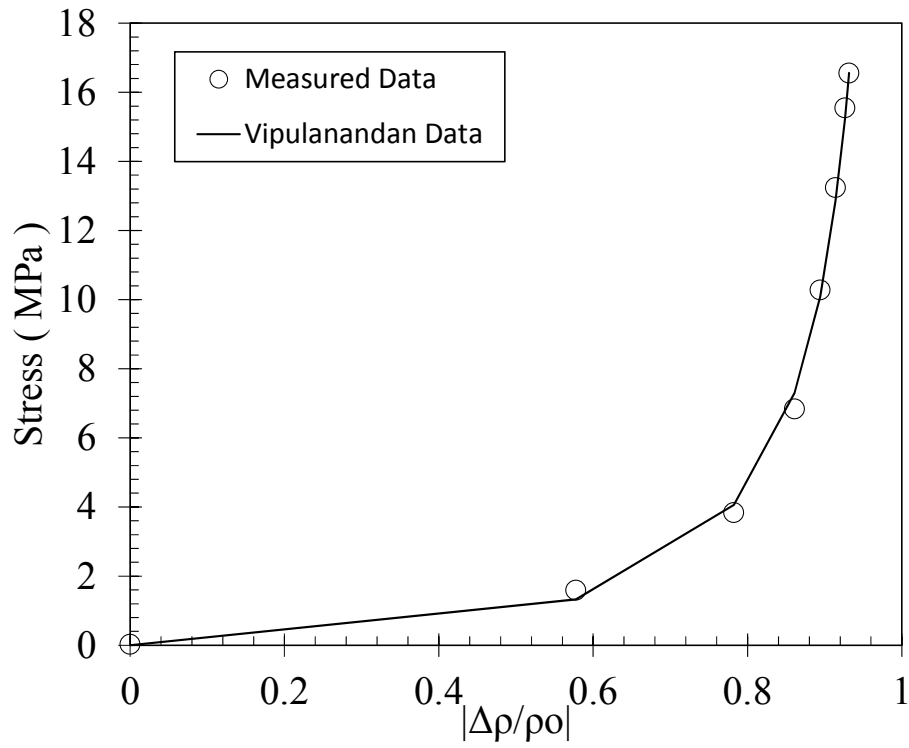
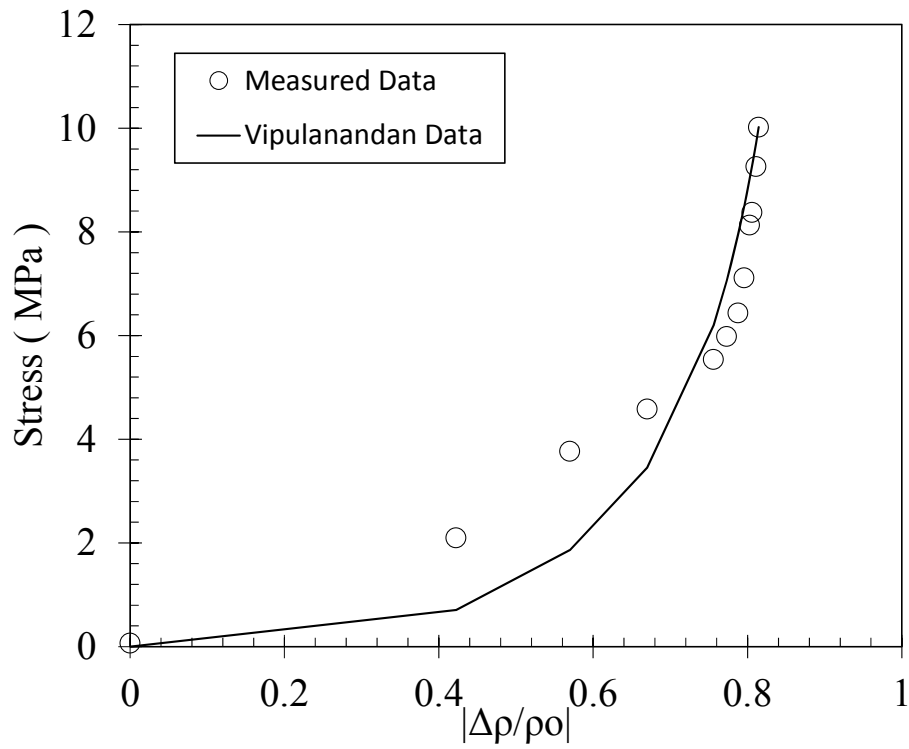


Figure E.48: Stress-Resistivity Data – Batch 16, Cylinder #48.



**Figure E.49: Stress-Resistivity Data – Batch 17, Cylinder #49.**



**Figure E.50: Stress-Resistivity Data – Batch 17, Cylinder #50.**

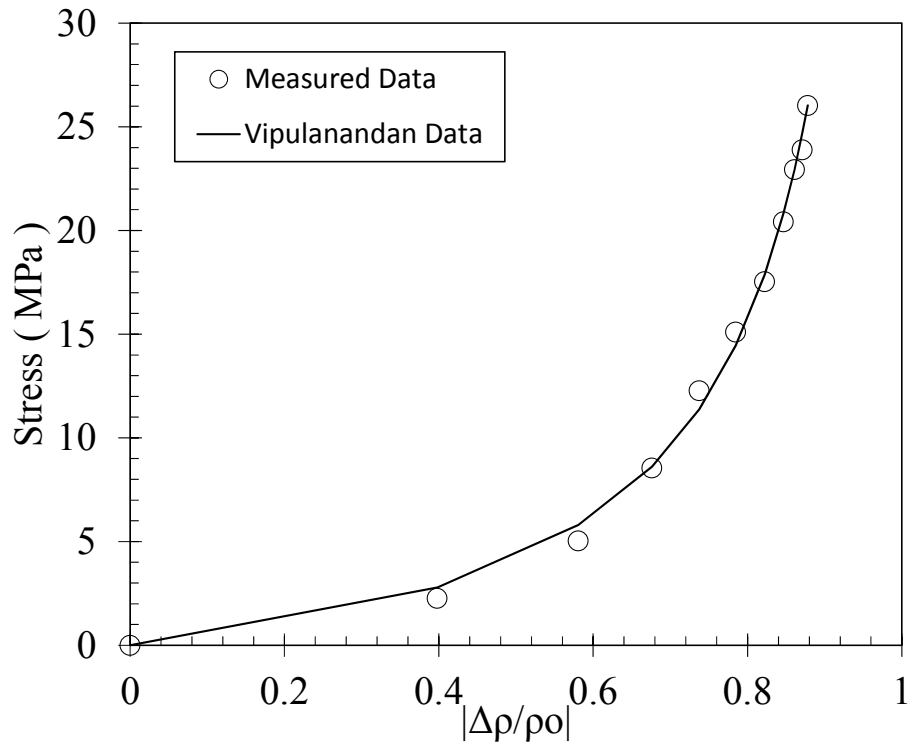


Figure E.51: Stress-Resistivity Data – Batch 17, Cylinder #51.

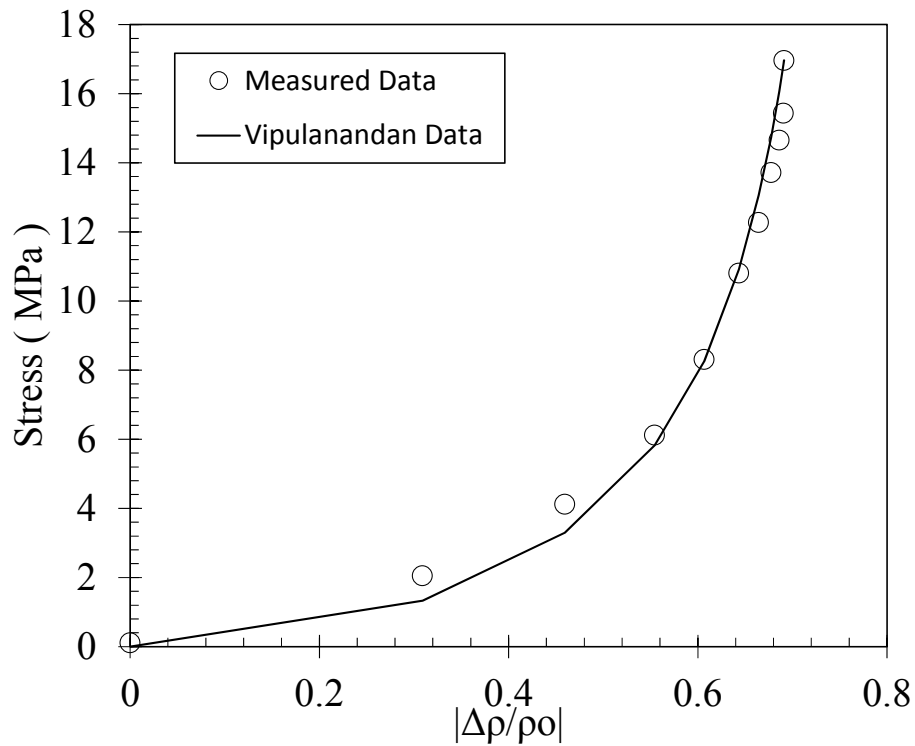


Figure E.52: Stress-Resistivity Data – Batch 18, Cylinder #52.

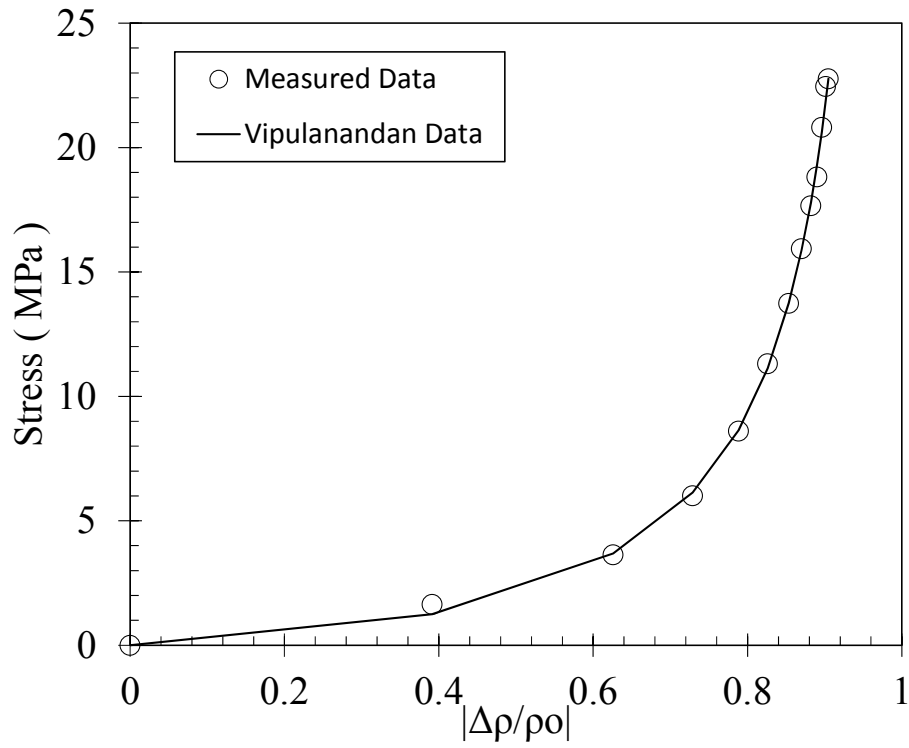


Figure E.53: Stress-Resistivity Data – Batch 18, Cylinder #53.

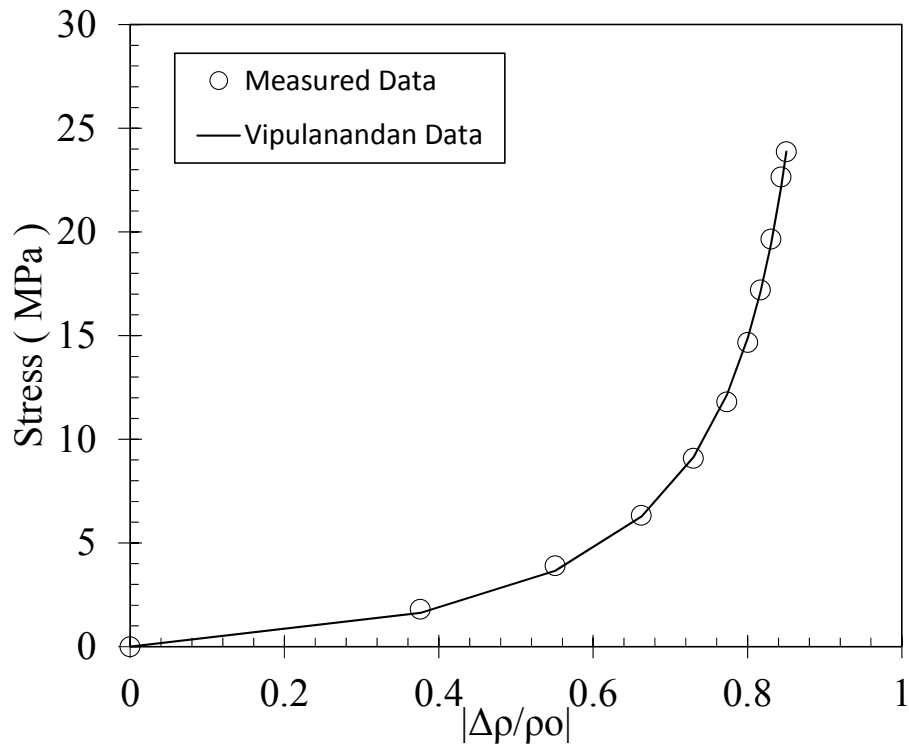


Figure E.54: Stress-Resistivity Data – Batch 18, Cylinder #54.

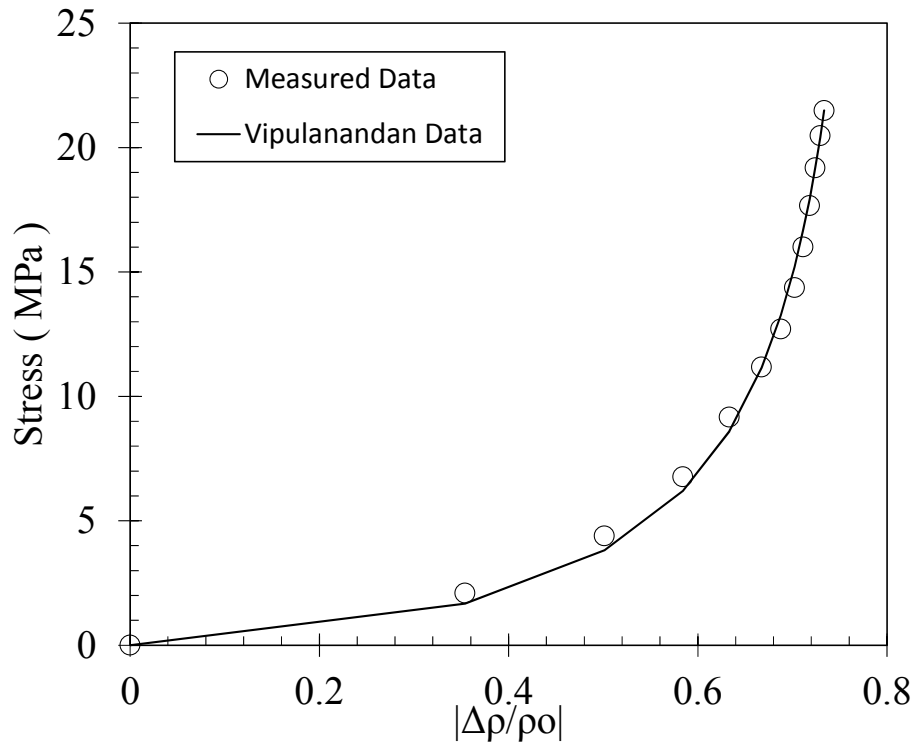


Figure E.55: Stress-Resistivity Data – Batch 19, Cylinder #55.

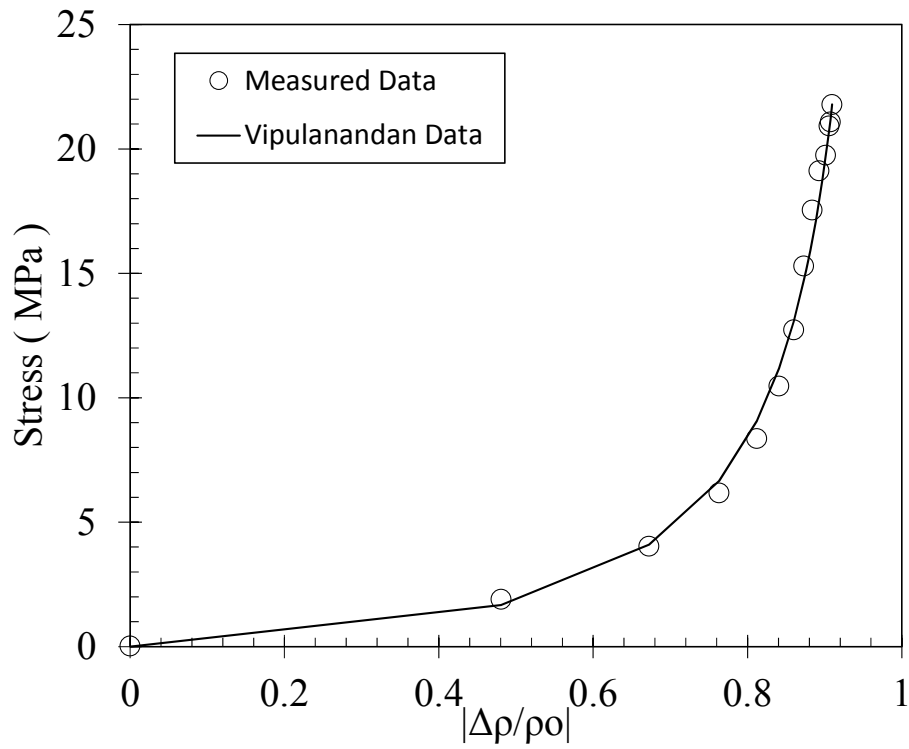


Figure E.56: Stress-Resistivity Data – Batch 19, Cylinder #56.



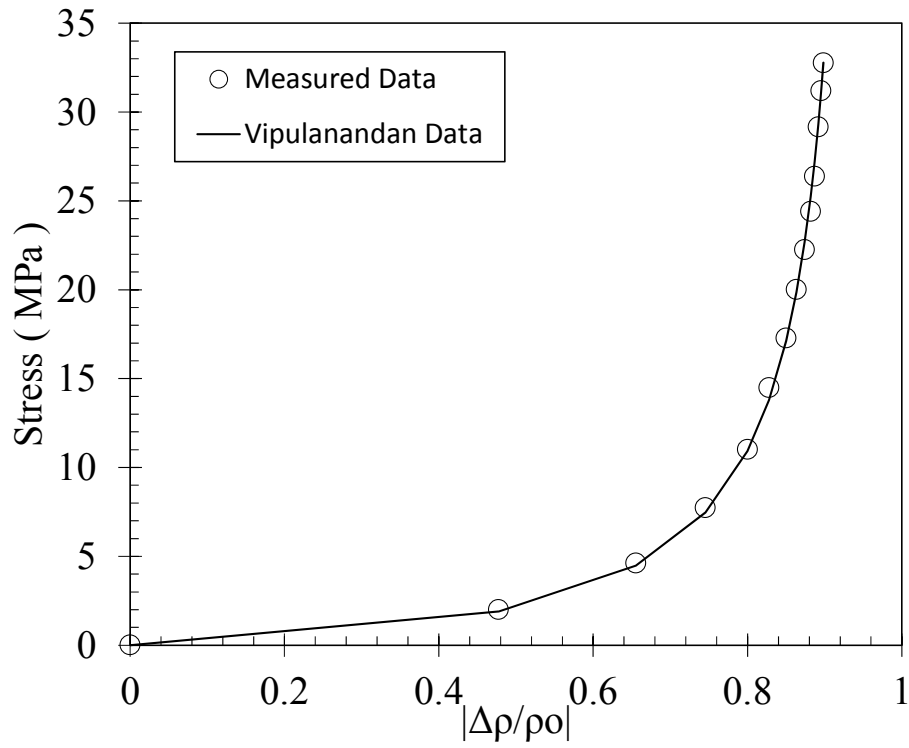


Figure E.57: Stress-Resistivity Data – Batch 19, Cylinder #57.

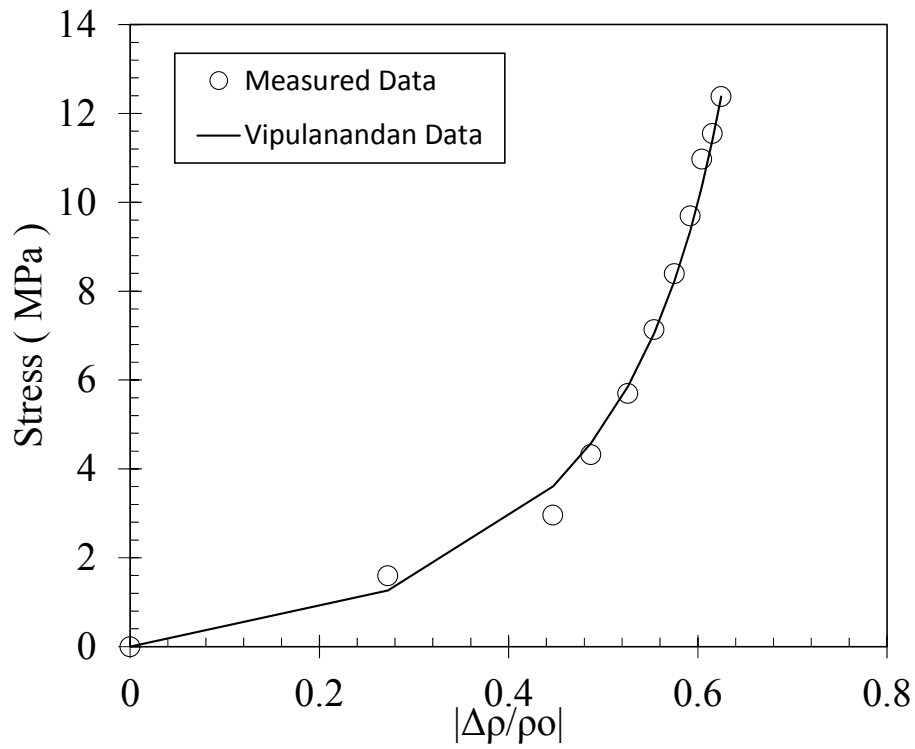
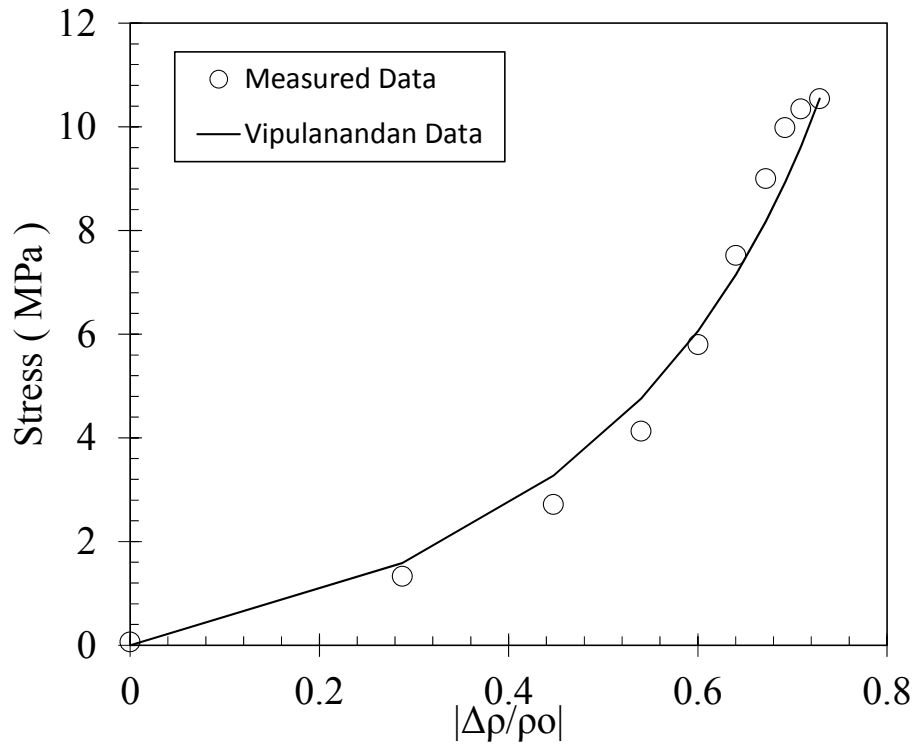
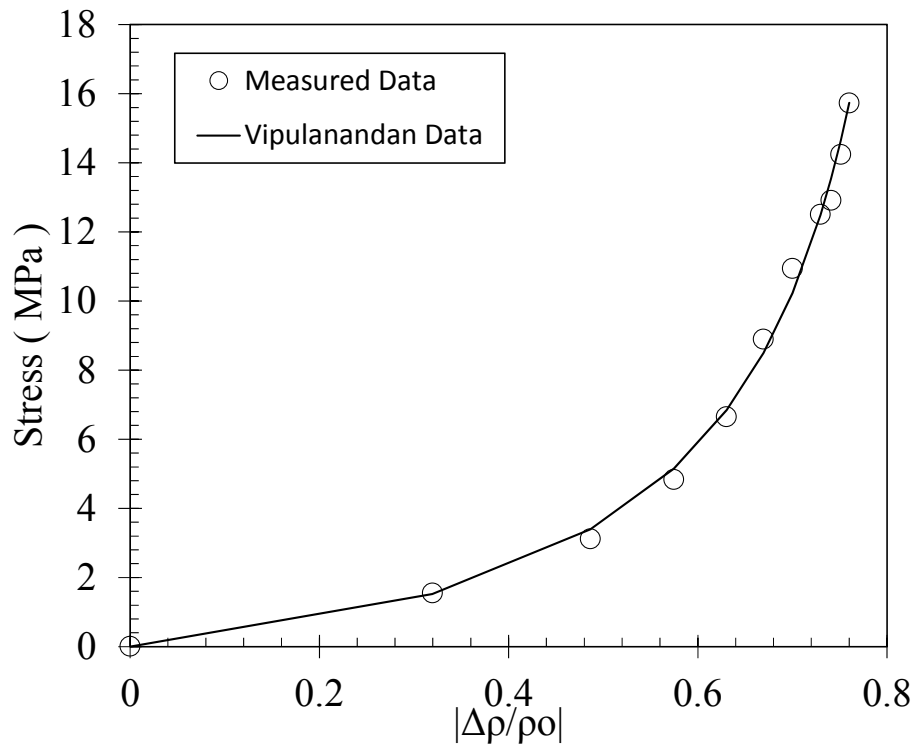


Figure E.58: Stress-Resistivity Data – Batch 20, Cylinder #58.



**Figure E.59: Stress-Resistivity Data – Batch 20, Cylinder #59.**



**Figure E.60: Stress-Resistivity Data – Batch 20, Cylinder #60.**

Averages of Stress-Resistivity Parameters Sorted by NanoFe<sub>2</sub>O<sub>3</sub> Content:

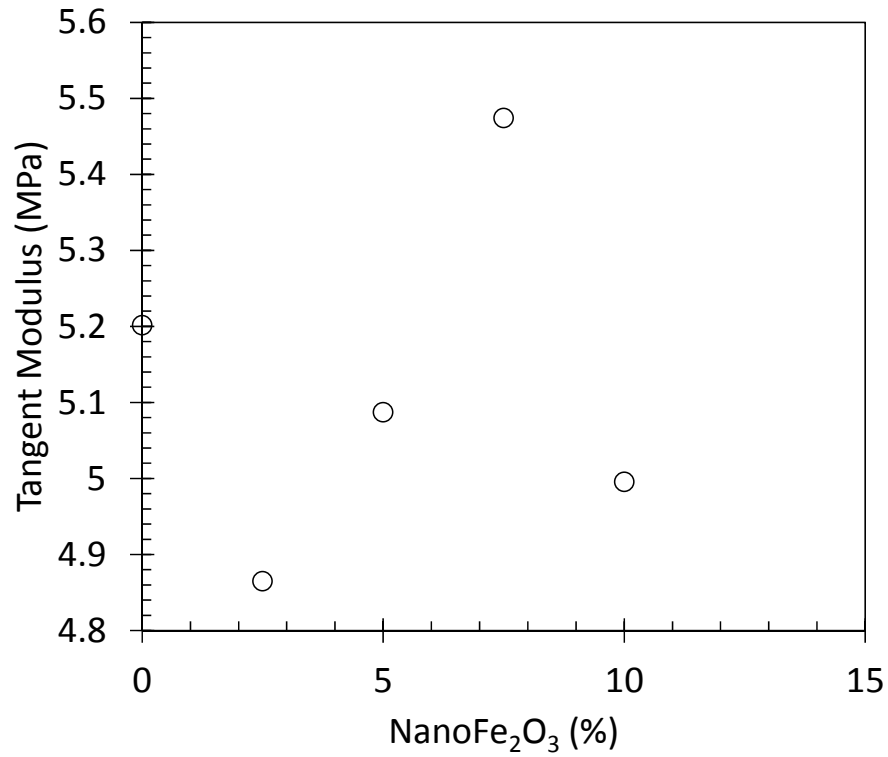


**Figure E.61: Tangent Modulus vs. NanoFe<sub>2</sub>O<sub>3</sub> Content.**

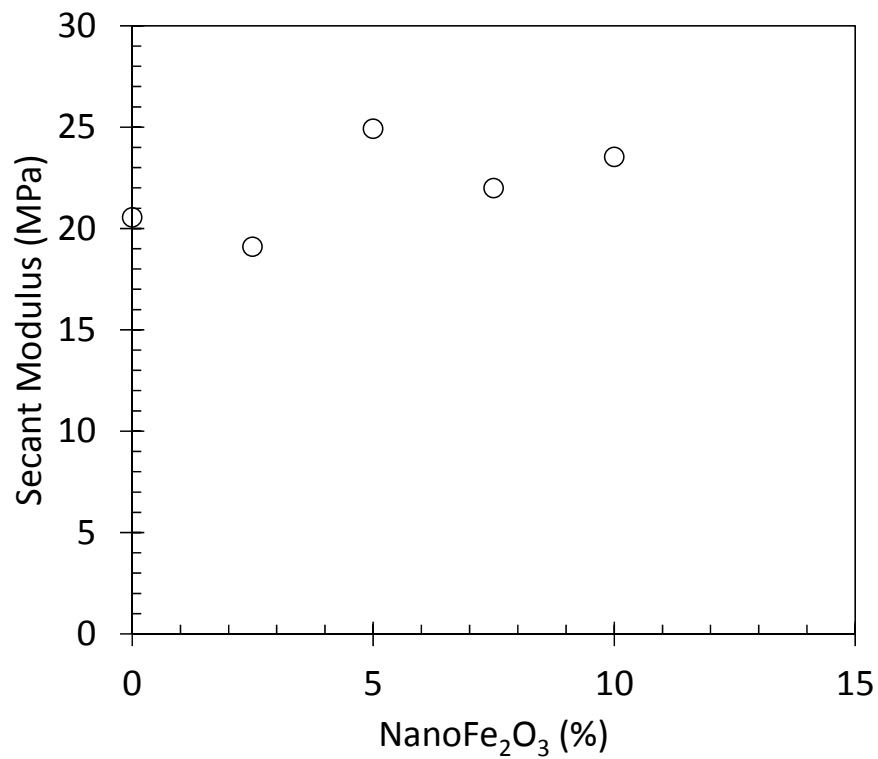


**Figure E.62: Secant Modulus vs. NanoFe<sub>2</sub>O<sub>3</sub> Content.**

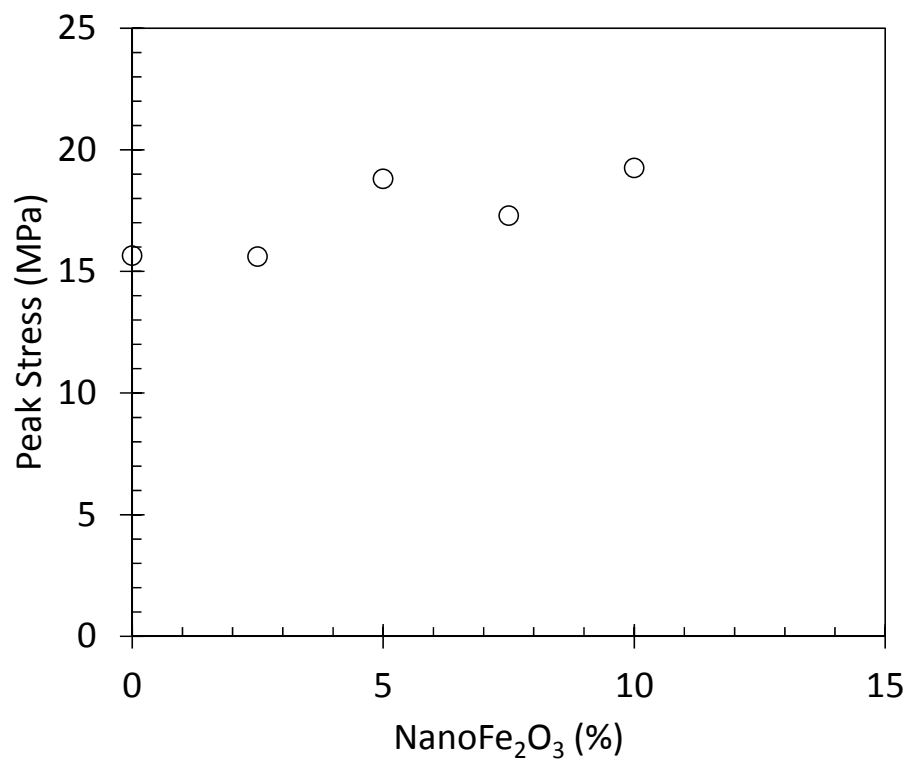


Figure E.63: Peak Stress vs. NanoFe<sub>2</sub>O<sub>3</sub> Content.

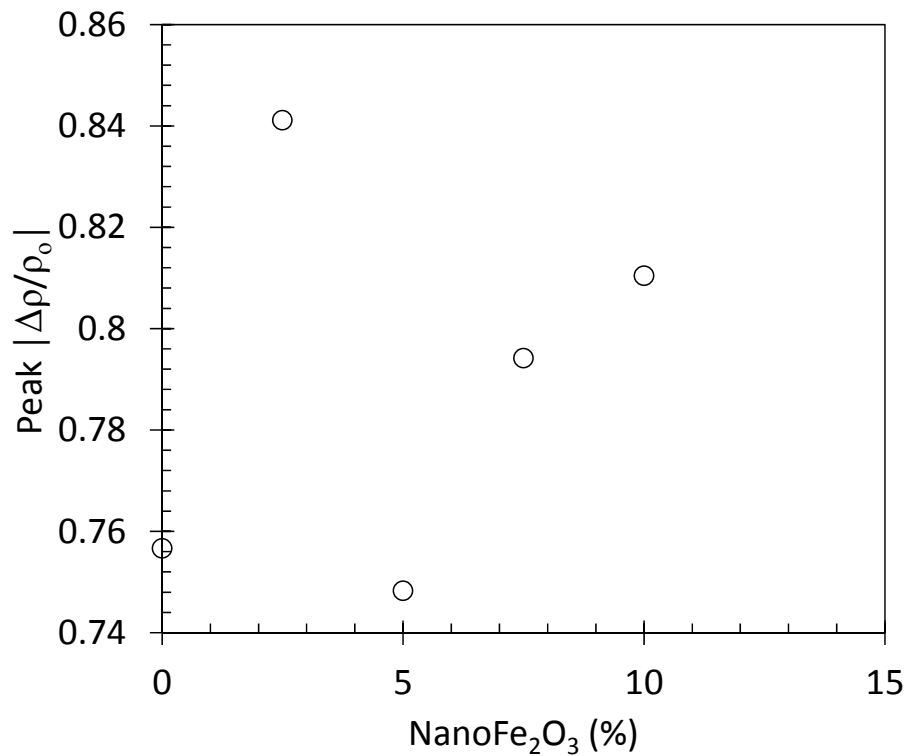


Figure E.64: Peak Change in Resistivity vs. NanoFe<sub>2</sub>O<sub>3</sub> Content.

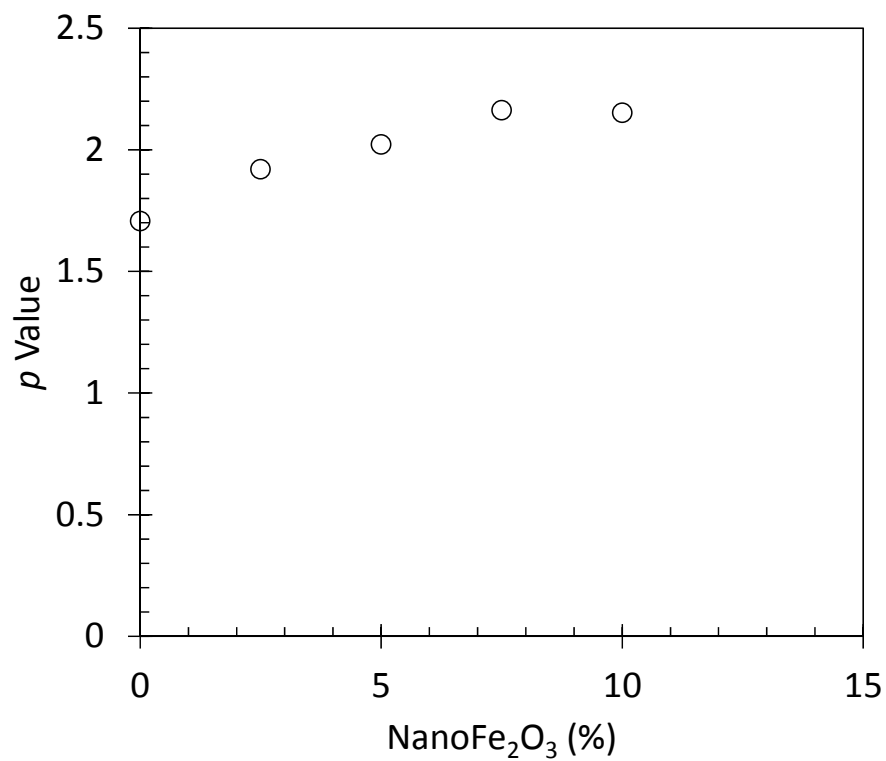


Figure E.65: *p* Value vs. NanoFe<sub>2</sub>O<sub>3</sub> Content.

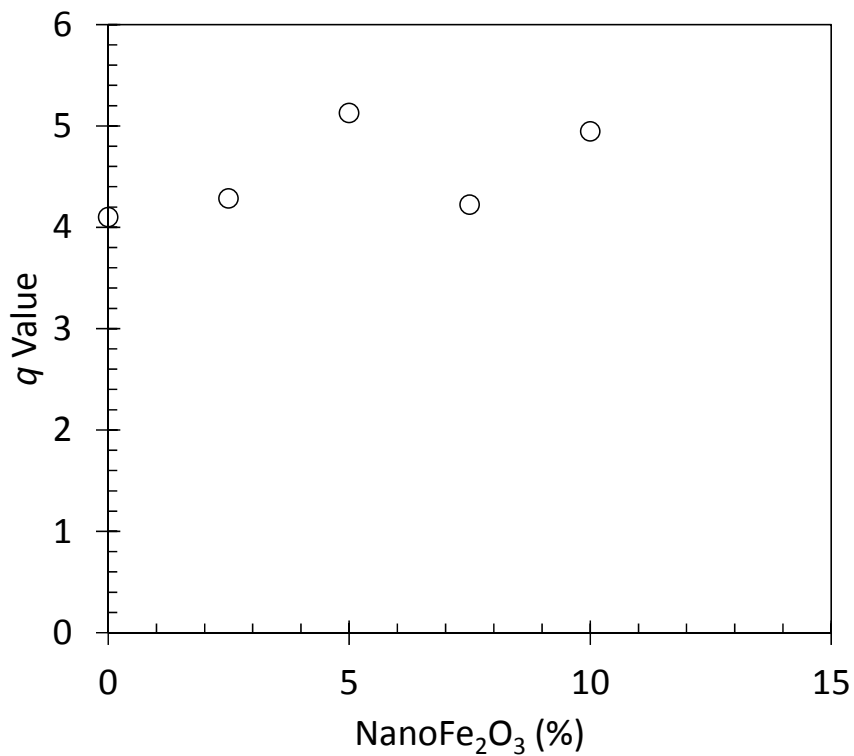
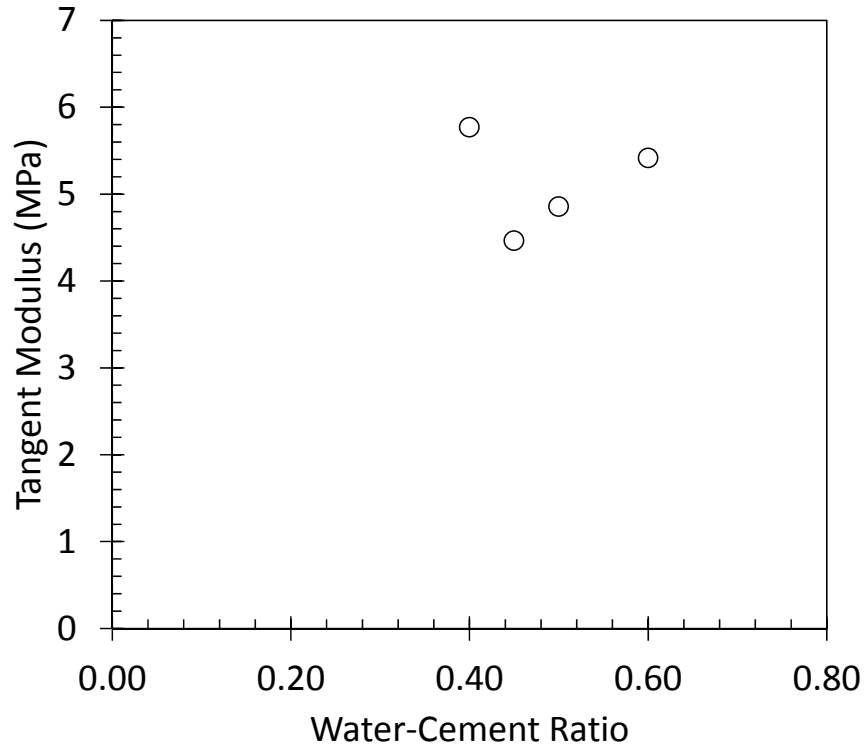
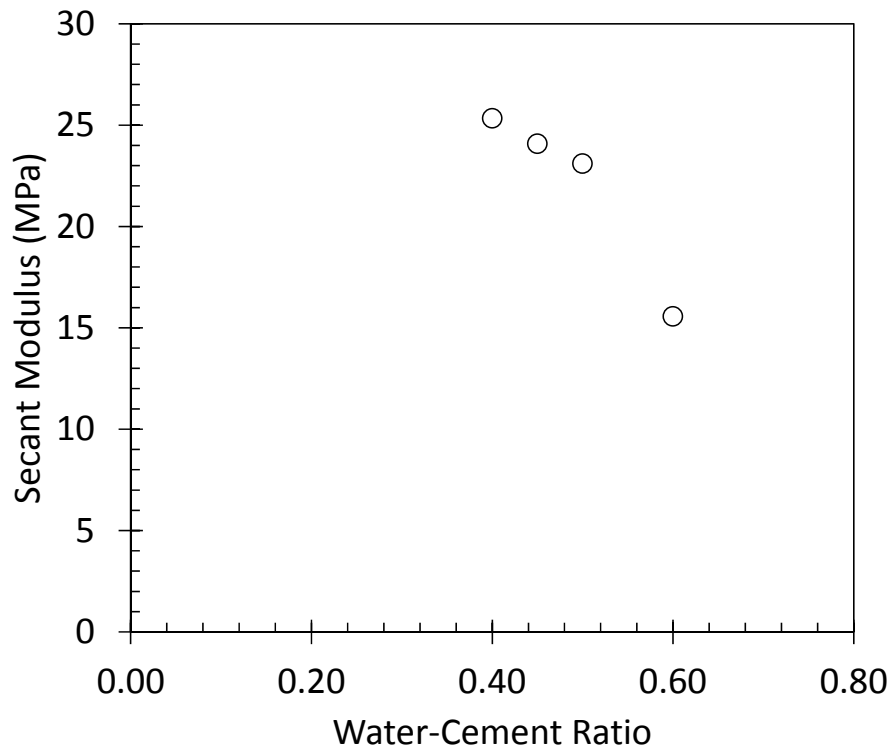


Figure E.66: *q* Value vs. NanoFe<sub>2</sub>O<sub>3</sub> Content.

Averages of Stress-Resistivity Parameters Sorted by Water-Cement Ratio:



**Figure E.67: Tangent Modulus vs. Water-Cement Ratio.**



**Figure E.68: Secant Modulus vs. Water-Cement Ratio.**

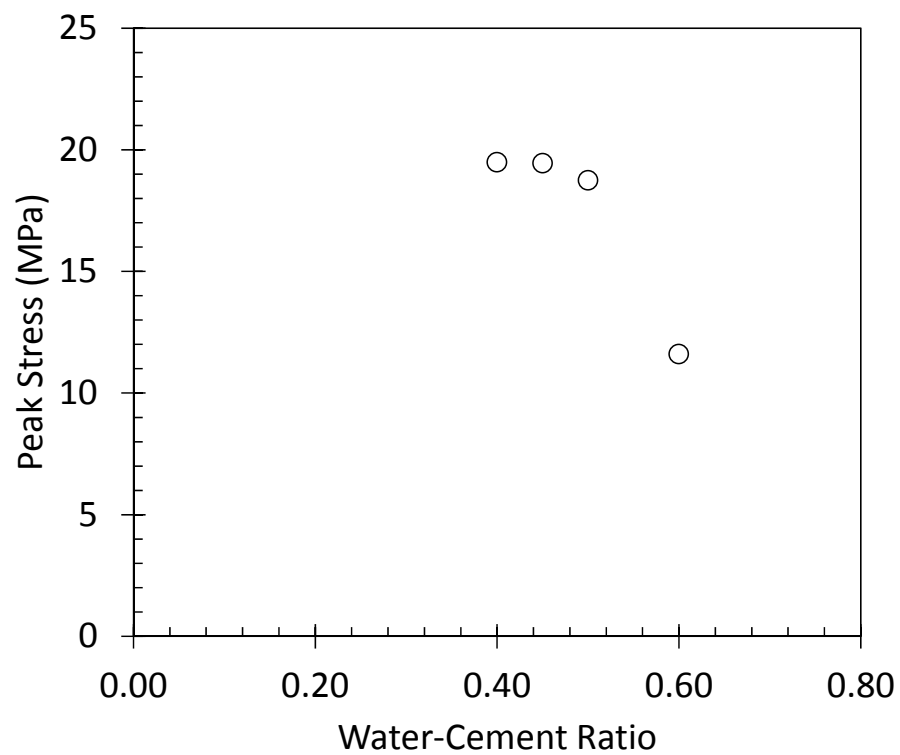


Figure E.69: Peak Stress vs. Water-Cement Ratio.

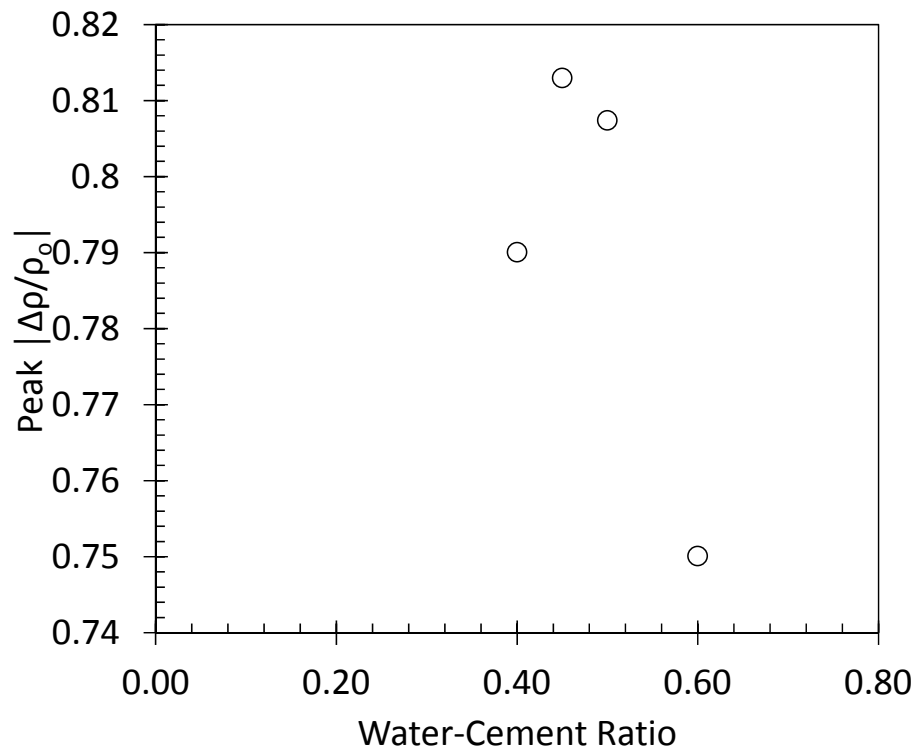


Figure E.70: Peak Change in Resistivity vs. Water-Cement Ratio.

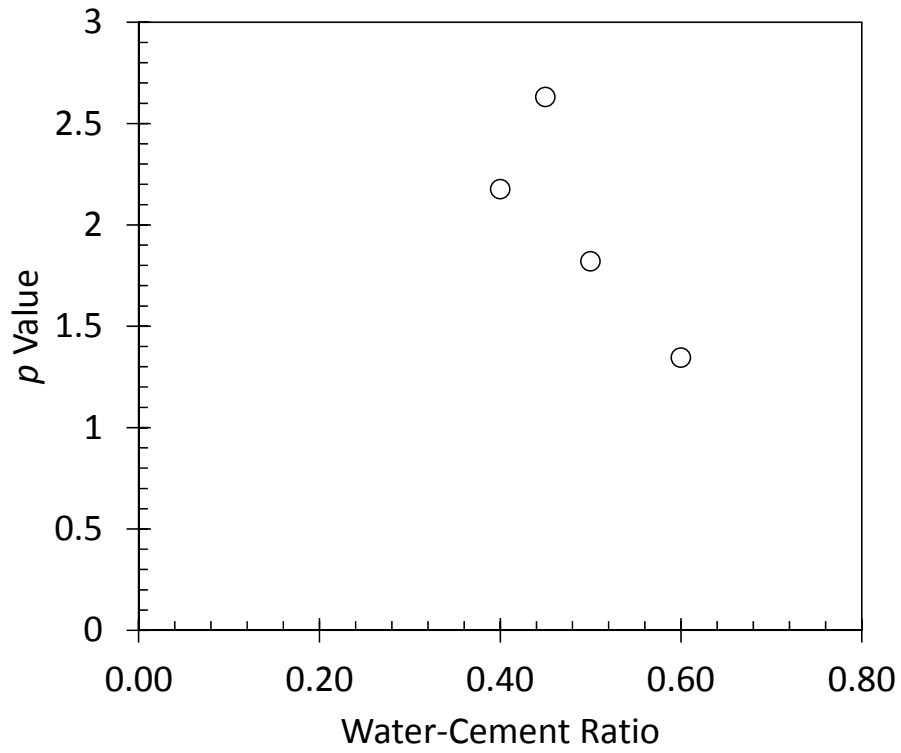


Figure E.71:  $p$  Value vs. Water-Cement Ratio.

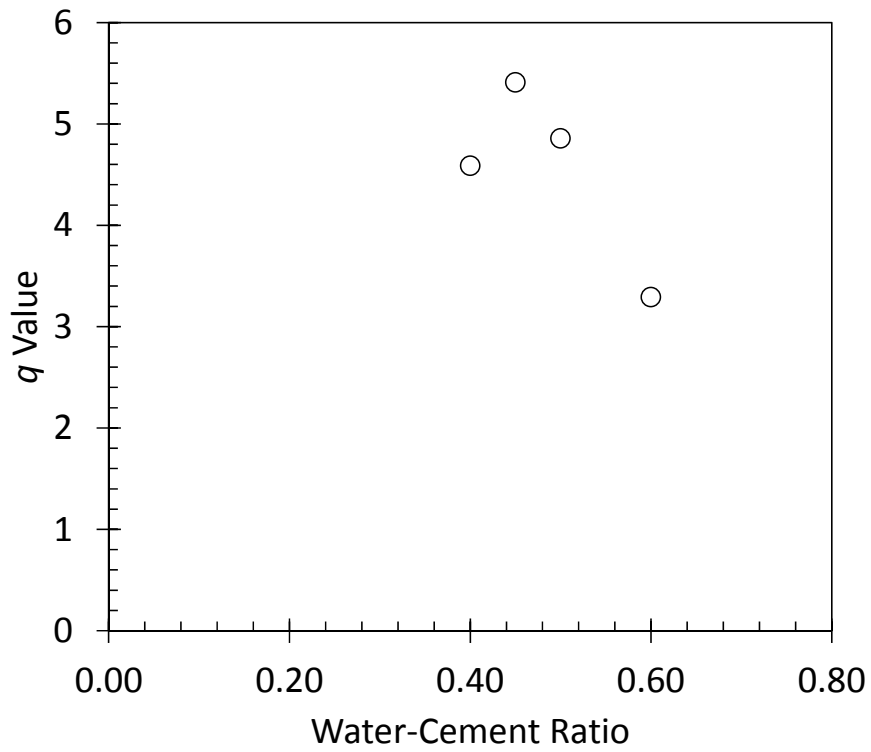
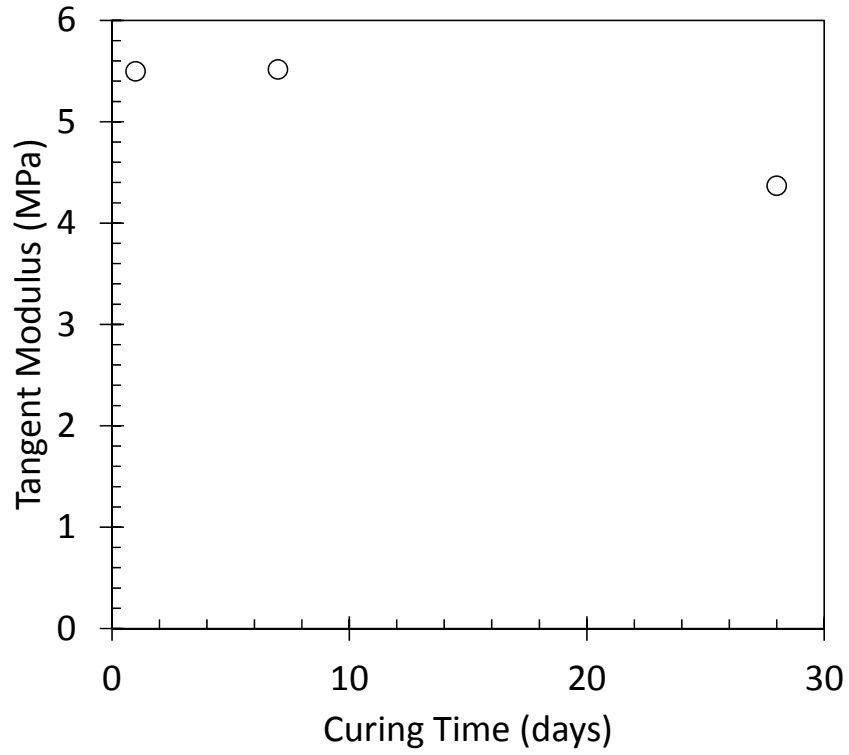


Figure E.72:  $q$  Value vs. Water-Cement Ratio.



Averages of Stress-Resistivity Parameters Sorted by Curing Time:



**Figure E.73: Tangent Modulus vs. Curing Time.**

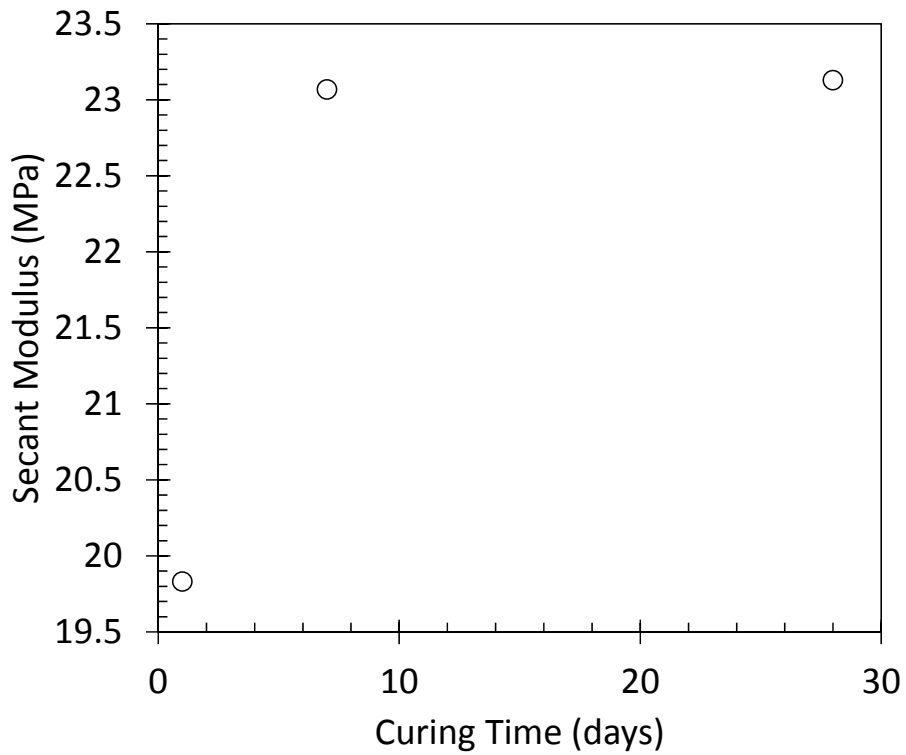


**Figure E.74: Secant Modulus vs. Curing Time.**

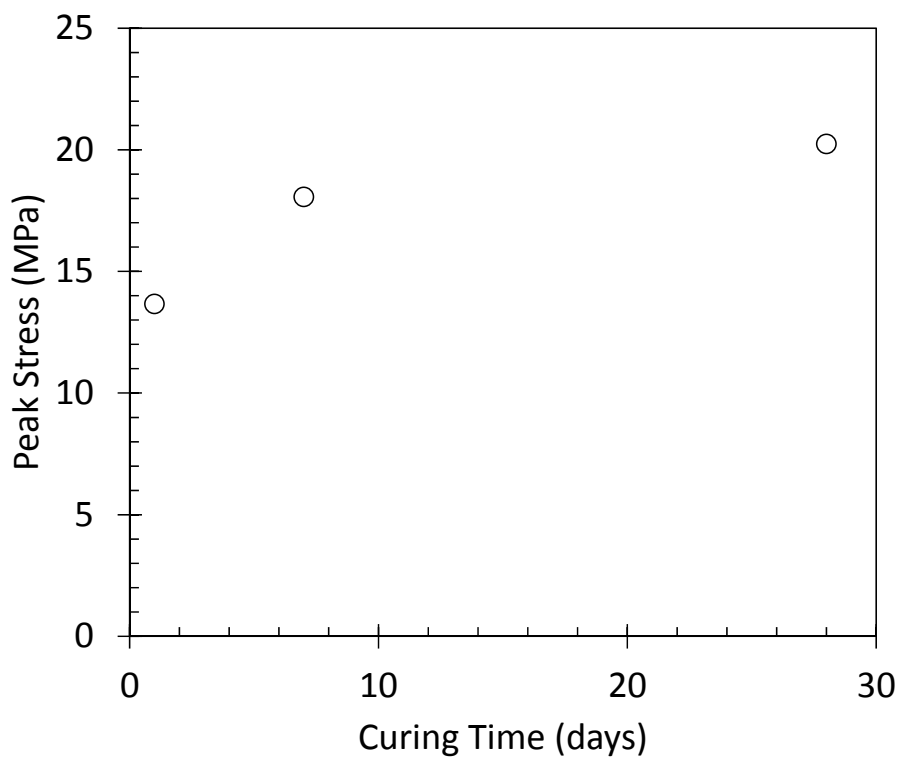


**Figure E.75: Peak Stress vs. Curing Time.**

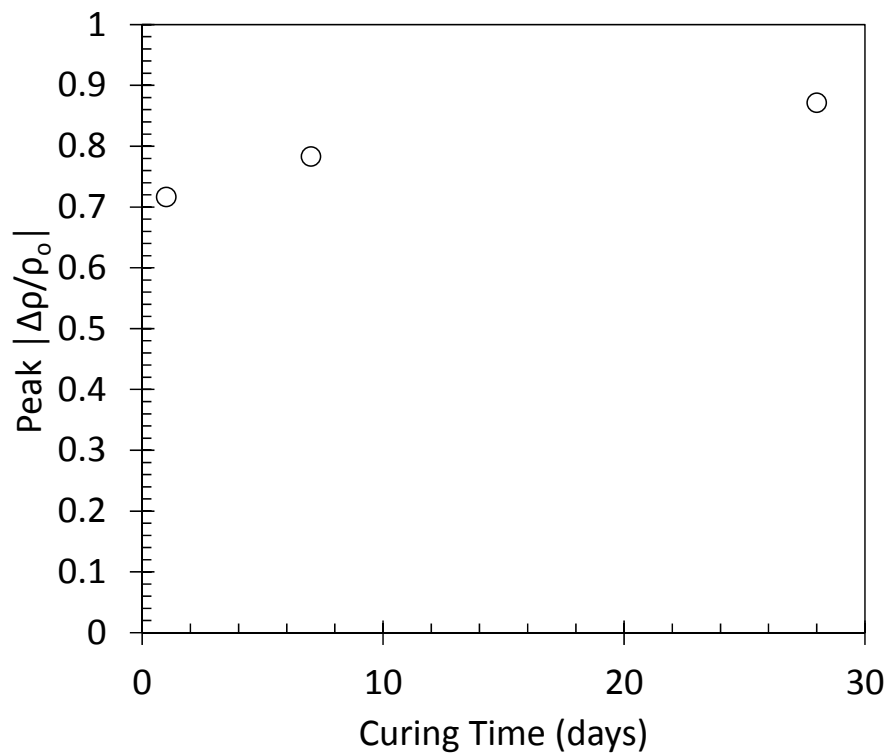


**Figure E.76: Peak Change in Resistivity vs. Curing Time.**

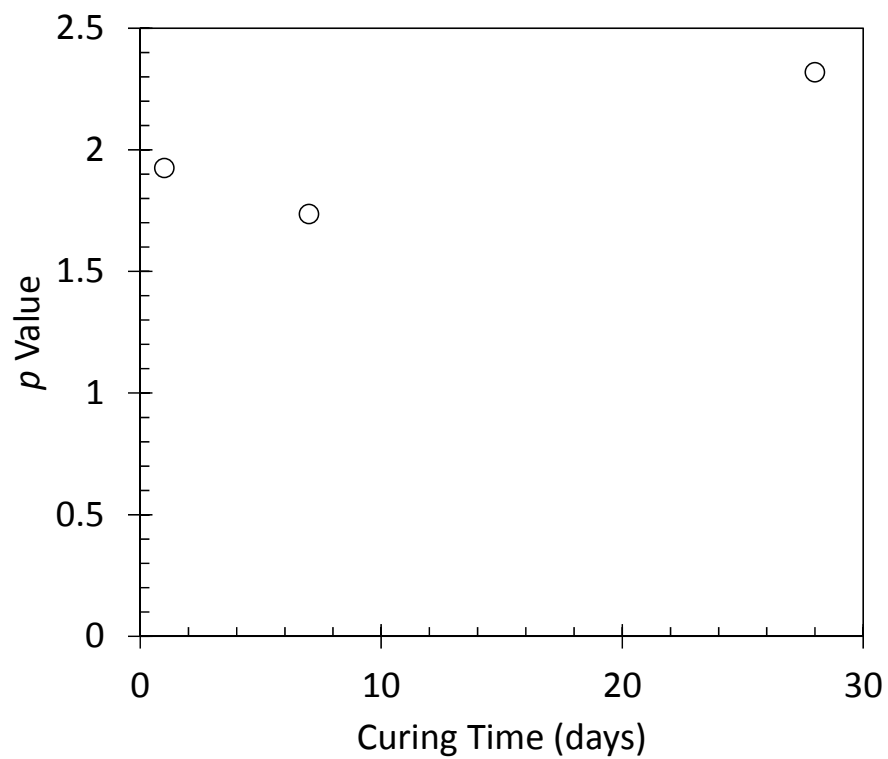


Figure E.77:  $p$  Value vs. Curing Time.

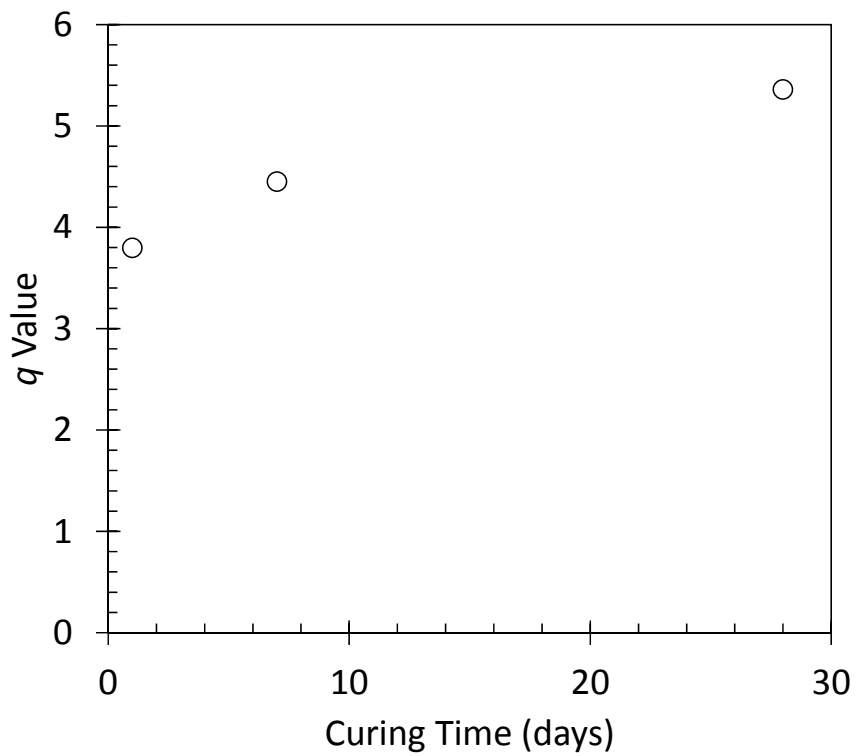


Figure E.78:  $q$  Value vs. Curing Time.

---

# **Appendix F**

## **Predictive Model**

Nonlinear Model Parameter Values for Each Predictive Model Parameter:

**Table F.1: Nonlinear model parameter values for  $\sigma_f$ .**

<b>Water-Cement Ratio</b>	<b>NanoFe<sub>2</sub>O<sub>3</sub> (%)</b>	<b>a</b>	<b>b</b>	<b>c</b>	<b>d</b>	<b>e</b>
0.40	0	1.408	0.710	1.000	1.000	1.000
	2.5	1.654	0.473	2.129	0.203	0.592
	5	0.888	0.226	1.662	0.632	0.269
	7.5	0.741	0.000	1.073	0.662	0.498
	10	0.980	0.932	0.761	0.202	0.449
0.45	0	0.985	0.964	1.000	1.000	1.000
	2.5	1.402	0.466	1.893	0.304	0.669
	5	0.900	0.506	0.920	0.632	0.764
	7.5	1.169	0.684	0.585	0.000	0.233
	10	0.967	0.905	0.760	0.201	0.447
0.50	0	1.002	1.006	1.000	1.000	1.000
	2.5	1.417	0.465	1.906	0.295	0.662
	5	0.954	0.847	0.761	0.202	0.614
	7.5	0.946	0.820	0.698	0.000	0.393
	10	0.727	0.000	1.082	0.733	0.412
0.60	0	0.962	0.787	1.000	1.000	1.000
	2.5	1.492	0.489	2.106	0.231	0.610
	5	0.941	0.800	0.763	0.207	0.616
	7.5	0.931	0.798	0.696	0.000	0.390
	10	0.944	0.816	0.697	0.000	0.305

**Table F.2: Nonlinear model parameter values for  $|\Delta\rho/\rho_o|_f$ .**

<b>Water-Cement Ratio</b>	<b>NanoFe<sub>2</sub>O<sub>3</sub> (%)</b>	<b>a</b>	<b>b</b>	<b>c</b>	<b>d</b>	<b>e</b>
0.40	0	0.716	0.039	1.000	1.000	1.000
	2.5	0.446	0.093	0.148	0.000	0.343
	5	0.519	0.018	0.294	0.011	0.077
	7.5	0.513	0.004	0.396	0.003	0.002
	10	0.402	0.004	0.461	0.004	0.003
0.45	0	0.724	0.056	1.000	1.000	1.000
	2.5	0.469	0.010	0.256	0.008	0.456
	5	0.521	0.022	0.296	0.013	0.078
	7.5	0.511	0.002	0.395	0.001	0.001
	10	0.241	0.000	0.457	0.058	0.040
0.50	0	0.731	0.073	1.000	1.000	1.000
	2.5	0.469	0.010	0.256	0.008	0.456
	5	0.518	0.016	0.293	0.010	0.076
	7.5	0.377	0.020	0.371	0.020	0.012
	10	0.404	0.007	0.464	0.009	0.006
0.60	0	0.729	0.067	1.000	1.000	1.000
	2.5	0.467	0.006	0.252	0.005	0.455
	5	0.512	0.006	0.286	0.004	0.073
	7.5	0.466	0.009	0.386	0.007	0.004
	10	0.226	0.000	0.443	0.038	0.026

**Table F.3: Nonlinear model parameter values for  $q$ .**

<b>Water-Cement Ratio</b>	<b>NanoFe<sub>2</sub>O<sub>3</sub> (%)</b>	<b>a</b>	<b>b</b>	<b>c</b>	<b>d</b>	<b>e</b>
0.40	0	1.892	0.221	1.000	1.000	1.000
	2.5	0.980	0.319	0.541	0.004	0.626
	5	1.321	0.392	0.547	0.000	0.353
	7.5	0.848	0.503	0.690	0.013	0.382
	10	0.914	0.472	0.594	0.000	0.139
0.45	0	0.914	0.581	1.000	1.000	1.000
	2.5	0.873	0.376	0.612	0.003	0.670
	5	0.884	0.624	0.692	0.000	0.508
	7.5	1.057	0.394	0.457	0.000	0.053
	10	0.847	0.502	0.688	0.001	0.289
0.50	0	1.449	0.383	1.000	1.000	1.000
	2.5	0.818	0.416	0.685	0.007	0.715
	5	1.290	0.415	0.540	0.000	0.344
	7.5	1.148	0.346	0.422	0.000	0.000
	10	1.306	0.549	0.510	0.000	0.000
0.60	0	2.450	0.061	1.000	1.000	1.000
	2.5	0.829	0.447	0.691	0.020	0.719
	5	1.195	0.457	0.533	0.000	0.332
	7.5	0.841	0.470	0.671	0.002	0.355
	10	1.095	0.377	0.411	0.000	0.000

**Table F.4: Nonlinear model parameter values for  $p$ .**

<b>Water-Cement Ratio</b>	<b>NanoFe<sub>2</sub>O<sub>3</sub> (%)</b>	<b>a</b>	<b>b</b>	<b>c</b>	<b>d</b>	<b>e</b>
0.40	0	0.779	0.129	1.000	1.000	1.053
	2.5	0.516	0.081	0.325	0.068	0.472
	5	0.700	0.034	0.693	0.074	0.506
	7.5	1.219	0.306	0.374	0.000	0.000
	10	0.605	0.012	0.507	0.010	0.007
0.45	0	2.437	0.027	1.000	1.000	1.000
	2.5	0.627	0.010	0.555	0.016	0.636
	5	1.077	0.340	0.381	0.000	0.157
	7.5	1.296	0.252	0.327	0.000	0.000
	10	0.723	0.101	0.675	0.001	0.269
0.50	0	0.762	0.206	1.000	1.000	1.000
	2.5	0.653	0.009	0.604	0.016	0.665
	5	0.687	0.006	0.665	0.013	0.477
	7.5	0.692	0.006	0.671	0.011	0.355
	10	1.147	0.346	0.313	0.000	0.000
0.60	0	0.764	0.118	1.000	1.000	1.031
	2.5	0.697	0.049	0.691	0.092	0.716
	5	0.702	0.039	0.699	0.085	0.512
	7.5	0.722	0.094	0.688	0.042	0.377
	10	0.628	0.015	0.551	0.015	0.074



---

## References

- Azhari, F., and Banthia, N. (2012). "Cement-based sensors with carbon fibers and carbon nanotubes for piezoresistive sensing." *Cement and Concrete Composites*, 34(7), 866-873.
- Catalá, G., Ramos-Fernández, E., Zornoza, E., Andión, L., and Garcés, P. (2010). "Influence of the oxidation process of carbon material on the mechanical properties of cement mortars." *Journal of Materials in Civil Engineering*, 23(3), 321-329.
- Chen, L. (2007). "Experimental study of ultra-sharp silicon nano-tips." *Solid State Communications*, 143(11), 553-557.
- Chen, P.-W., and Chung, D.D.L. (1993). "Carbon fiber reinforced concrete for smart structures capable of non-destructive flaw detection." *Smart Materials and Structures*, 2(1), 22.
- Chung, D. (2000). "Cement-matrix composites for smart structures." *Smart materials and structures*, 9(4), 389.
- Chung, D. (2004). "Electrically conductive cement-based materials." *Advances in Cement Research*, 16(4), 167-176.
- Chung, D.D.L. (1998). "Self-monitoring structural materials." *Materials Science and Engineering: R: Reports*, 22(2), 57-78.
- Ezeldin, A. S., and Balaguru, P. N. (1992). "Normal-and high-strength fiber-reinforced concrete under compression." *Journal of materials in civil engineering*, 4(4), 415-429.
- Falvo, M. R., Clary, G., Taylor Ii, R., and Chi, V. (1997). "Bending and buckling of carbon nanotubes under large strain." *Nature*, 389(6651), 582.
- Fu, X., and Chung, D. (1997). "Effect of curing age on the self-monitoring behavior of carbon fiber reinforced mortar." *Cement and concrete Research*, 27(9), 1313-1318.
- Fu, X., Lu, W., and Chung, D. (1998). "Improving the strain-sensing ability of carbon fiber-reinforced cement by ozone treatment of the fibers." *Cement and concrete research*, 28(2), 183-187.
- Han, B., Ding, S., and Yu, X. (2015). "Intrinsic self-sensing concrete and structures: A review." *Measurement*, 59, 110-128.
- Han, B., Guan, X., and Ou, J. (2007). "Electrode design, measuring method and data acquisition system of carbon fiber cement paste piezoresistive sensors." *Sensors and Actuators A: Physical*, 135(2), 360-369.
- Han, B., Han, B., and Yu, X. (2010). "Effects of the content level and particle size of nickel powder on the piezoresistivity of cement-based composites/sensors." *Smart Materials and Structures*, 19(6), 065012.
- Han, B., and Ou, J. (2007). "Embedded piezoresistive cement-based stress/strain sensor." *Sensors and Actuators A: Physical*, 138(2), 294-298.
- Han, B., Yu, Y., Han, B., and Ou, J. (2008). "Development of a wireless stress/strain measurement system integrated with pressure-sensitive nickel powder-filled cement-based sensors." *Sensors and Actuators A: Physical*, 147(2), 536-543.
- Han, B., Zhang, K., Yu, X., Kwon, E., and Ou, J. (2011). "Fabrication of piezoresistive CNT/CNF cementitious composites with superplasticizer as dispersant." *Journal of Materials in Civil Engineering*, 24(6), 658-665.

- Hognestad, E. (1951). "Study of combined bending and axial load in reinforced concrete members." University of Illinois at Urbana Champaign, College of Engineering. Engineering Experiment Station.
- Hou, T.-C., and Lynch, J.P. "Conductivity-based strain monitoring and damage characterization of fiber reinforced cementitious structural components." *Proc., Proc. SPIE*, 419-429.
- Karasin, A., Günaslan, S. E., and Öncü, M. E. (2014). "Models for Confined Concrete Columns with Fiber Composites." *International Journal of Advanced Research in Engineering and Technology*, 5(12), 55-63.
- Kent, D. C., and Park, R. (1971). "Flexural members with confined concrete." *Journal of the Structural Division*.
- Li, G. Y., Wang, P. M., and Zhao, X. (2007). "Pressure-sensitive properties and microstructure of carbon nanotube reinforced cement composites." *Cement and Concrete Composites*, 29(5), 377-382.
- Li, H., Xiao, H.-g., and Ou, J.-p. (2004). "A study on mechanical and pressure-sensitive properties of cement mortar with nanophase materials." *Cement and Concrete research*, 34(3), 435-438.
- Lourie, O., Cox, D., and Wagner, H. (1998). "Buckling and collapse of embedded carbon nanotubes." *Physical Review Letters*, 81(8), 1638.
- Mebarkia, S., and Vipulanandan, C. (1992). "Compressive Behavior of Glass-Fiber Reinforced Polymer Concrete." *Journal of materials in civil engineering*, 4(1), 91-105.
- Ou, J., and Li, H. (2010). "Structural health monitoring in mainland China: review and future trends." *Structural Health Monitoring*, 9(3), 219-231.
- Ozbakkaloglu, T., Lim, J. C., and Vincent, T. (2013). "FRP-confined concrete in circular sections: Review and assessment of stress-strain models." *Engineering Structures*, 49, 1068-1088.
- Reza, F., Batson, G. B., Yamamuro, J. A., and Lee, J. S. (2003). "Resistance changes during compression of carbon fiber cement composites." *Journal of Materials in Civil Engineering*, 15(5), 476-483.
- Vaisman, L., Wagner, H. D., and Marom, G. (2006). "The role of surfactants in dispersion of carbon nanotubes." *Advances in colloid and interface science*, 128, 37-46.
- Vipulanandan, C., and Mohammed, A. (2014). "Hyperbolic rheological model with shear stress limit for acrylamide polymer modified bentonite drilling muds." *Journal of Petroleum Science and Engineering*, 122, 38-47.
- Vipulanandan, C., and Mohammed, A. (2015). "Smart cement modified with iron oxide nanoparticles to enhance the piezoresistive behavior and compressive strength for oil well applications." *Smart Materials and Structures*, 24(12), 125020.
- Wang, S., and Chung, D. (2006). "Self-sensing of flexural strain and damage in carbon fiber polymer-matrix composite by electrical resistance measurement." *Carbon*, 44(13), 2739-2751.
- Wen, S., and Chung, D. (2006). "The role of electronic and ionic conduction in the electrical conductivity of carbon fiber reinforced cement." *Carbon*, 44(11), 2130-2138.

Xin, C., Shoude, W., Lingchao, L., and Shifeng, H. (2011). "Influence of preparation process on piezo-conductance effect of carbon fiber sulfoaluminate cement composite." *Journal of Composite Materials*, 45(20), 2033-2037.

---

**Vita**

Alexander Nicholas Houk was born and raised in Louisville, Kentucky. He graduated from Trinity High School with honors in 2011. Alex attended the University of Kentucky with a full-tuition Presidential Scholarship, making the Dean's List each semester before earning a Bachelor's of Science in Civil Engineering and graduating *summa cum laude* in 2015. He obtained his Engineer in Training (EIT) Certificate in April of 2015 in the state of Kentucky. Alex continued his education at the University of Kentucky, receiving a W.L. Matthews Jr. Fellowship for his first year of graduate school. Alex has worked as a Bridge Structural EIT for Palmer Engineering in Winchester, Kentucky for a year, and will be working with the same job title for HDR, Inc. in Charleston, South Carolina upon graduation.